

UNCLASSIFIED

AD 257 992

*Reproduced
by the*

ARMED SERVICES TECHNICAL INFORMATION AGENCY
ARLINGTON HALL STATION
ARLINGTON 12, VIRGINIA



UNCLASSIFIED

NOTICE: When government or other drawings, specifications or other data are used for any purpose other than in connection with a definitely related government procurement operation, the U. S. Government thereby incurs no responsibility, nor any obligation whatsoever; and the fact that the Government may have formulated, furnished, or in any way supplied the said drawings, specifications, or other data is not to be regarded by implication or otherwise as in any manner licensing the holder or any other person or corporation, or conveying any rights or permission to manufacture, use or sell any patented invention that may in any way be related thereto.

CATALOGED BY ASTIA 257992
AS AD No. _____

DETERMINATION THROUGH
WIND-TUNNEL TESTS AND ANALYTICAL
METHODS OF THE OPTIMUM DEFLEC-
TION DEVICES SUITABLE FOR USE ON
JET-FLAP HELICOPTER ROTOR BLADES

EUROPEAN RESEARCH OFFICE
US. DEPARTMENT OF THE ARMY
CONTRACT No. DA-91-591-EUC-1203

Report No. DE.2013
30 December 1960

\$ 19.75

NOX



Engineering Division GIRAVIONS DORAND Co.
PARIS

DETERMINATION THROUGH
WIND-TUNNEL TESTS AND ANALYTICAL
METHODS OF THE OPTIMUM DEFLEC-
TION DEVICES SUITABLE FOR USE ON
JET-FLAP HELICOPTER ROTOR BLADES

EUROPEAN RESEARCH OFFICE
US. DEPARTMENT OF THE ARMY
CONTRACT No. DA-91-591-EUC-1203

Report No. DE.2013
30 December 1960

Engineering Division GIRAVIONS DORAND Co.
PARIS

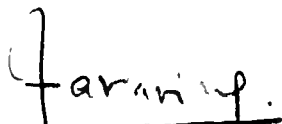
DETERMINATION THROUGH WIND-TUNNEL TESTS
AND ANALYTICAL METHODS OF THE OPTIMUM
DEFLECTION DEVICES SUITABLE FOR USE
ON JET-FLAP HELICOPTER ROTOR BLADES

EUROPEAN RESEARCH OFFICE
US. DEPARTMENT OF THE ARMY
CONTRACT No.DA-91-591-EUC-1203

Report No. DE.2013

30 December 1960

Head Engineer



S.TARARINE

Principal Investigator



R.DORAND
(Technical Director)

Engineering Division GIRAVIONS DORAND Co.

P A R I S

TABLE OF CONTENTS

(Pages of text are numbered from A.1 to A.98
Pages containing only Figures -- at the end of text --
are numbered from B.1 to B.221.)

	<u>Page number</u>
Unit Conversion Tables	:XIII to XV
Abstract	: XVI
List of Symbols	: A.1
<u>Introduction</u>	: A.2
<u>Apparatus and Test Methods</u>	: A.3
<u>Preliminary study of jet-flap configurations</u>	: A.4
<u>Tests in ONERA Wind-Tunnels</u>	: A.14
Tests in S ₁ Ch Wind-Tunnel	: A.14
Static tests in S ₃ Ch Wind-Tunnel	: A.19
Dynamic tests in S ₃ C' Wind-Tunnel	: A.24
<u>Additional tests and Corrections</u>	: A.32
Induced velocity corrections for tests in S ₁ Wind-Tunnel	: A.32
Second test series in S ₃ Ch Wind-Tunnel	: A.33
- Mechanical flap	: A.34
- Pneumatic flap	: A.35
<u>General discussion of the tests</u>	: A.36
<u>Effect of blowing on lift</u>	: A.36
Mach influence	: A.40
Influence of boundary layer. Supercirculation	: A.41
Empirical expressions for lift	: A.43
<u>Effect of blowing on drag</u>	: A.47
Mach influence	: A.50
	/.

	<u>Page number</u>
Optimum combination of section angle of attack and jet-flap deflection (advancing blade)	A.51
Propulsive effect of blown part of blade	A.52
Jet thrust recovery	A.53
Optimum section angle of attack and jet-flap deflection combination for fixed wing aircraft	A.55
<u>Practical test conclusions</u>	A.57
Analysis of test results	A.57
Influence of blowing flow characteristics	A.57
True deflection compared to theoretical deflection	A.58
Deflector matching and utilization spectrum	A.59
Effect of jet stall on lift	A.62
Effect of jet stall on drag	A.64
<u>General conclusions and Synopsis</u>	A.65
Data summarizing graphs	A.66
Control efficacy by deflector	A.69
Shift in Center of thrust	A.70
Deflector classification and final conclusions	A.70

APPENDIX

Page numb.

ANALYTICAL DETERMINATION OF THE
AERODYNAMIC TORSION MOMENTS ACTING
ON A JET-FLAPPED ROTOR BLADE AND METHODS
OF DEALING WITH SUCH MOMENTS ON A BLOWN
BLADE STRUCTURE

<u>Introduction</u>	A.72
Structural Requirements	A.72
Determining the torsion rigidity and the shear center in airfoil section models with a trailing edge slit	A.75
Aerodynamic torsion moments and Inertia torsion moments	A.79
<u>Analysis of test results</u>	A.79
<u>Analytical study of torsion moments due to inertia forces</u>	A.84
<u>Analytical study of torsion moments due to aerodynamic forces</u>	A.91
Comparative table of different patterns of variation of θ_j	A.96
Conclusions	A.97

LIST OF FIGURES

(Pages of the last part of Report containing
the Figures are numbered from B.1 to B.221)

PRELIMINARY TESTS OF JET-FLAPS

	<u>Fig. number</u>
Test installation in STAé. Wind-tunnel	1
Test of mechanical (solid) flaps	3 to 8
Tests of cylindrical flaps	9 to 12
Required slit width versus pressure ratio for avoiding flow separation	13
Tests of pneumatic deflectors	14 to 23
Tests of spoiler type deflectors	24 & 25
Tests of deflectors incorporating an auxiliary transverse jet	26 & 27

TESTS IN S1 Ch WIND-TUNNEL

General view	28
Set up in the passage	29
Characteristic features of model	30
Schematic drawings of flaps	31

Results for the mechanical flap :

Fig.number

Curves $C_z (i)$, $C_z (C_m)$, $C_z (C_x)$ for $\theta_j = 3^\circ, 15^\circ, 37.5^\circ, 52.5^\circ$, with $C_\mu = 0$ $V_o = 22$ m/s	32
same with $C_\mu = 0.09$, $V_o = 22$ m/s	33
same with $C_\mu = 0.22$, $V_o = 22$ m/s	34
same with $C_\mu = 0.70$, $V_o = 15$ m/s	35
Curve $R_j (q_m \cdot V_j)$	36
Local pressure coefficients K_p	37 to 45

Results for the spoiler-type flap :

Curves $C_z (C_\mu)$, $C_x (C_\mu)$, $C_m (C_\mu)$ for $\theta_j = 0^\circ, 20^\circ, 24^\circ, 32^\circ$, with $i = 0^\circ$	46
Curve $R_j (q_m \cdot V_j)$	47
Local pressure coefficients K_p	48

Results for the pneumatic flap

Curves $C_z (i)$, $C_z (C_m)$, $C_z (C_x)$ for $\theta_j = 4^\circ, 45^\circ, 47^\circ$, with $C_\mu = 0$ $V_o = 22$ m/s	49
same for $\theta_j = 4^\circ, 27^\circ, 32^\circ$, with $C_\mu = 0.08$ $V_o = 22$ m/s	50
same for $\theta_j = 4^\circ, 42^\circ, 45^\circ$, with $C_\mu = 0.22$ $V_o = 22$ m/s	51
same for $\theta_j = 4^\circ, 47^\circ, 48^\circ$, with $C_\mu = 0.81$ $V_o = 15$ m/s	52 & 53
Curves $C_z (C_\mu)$, $C_x (C_\mu)$, $C_m (C_\mu)$ for $\theta_j = 4^\circ, 47^\circ$, with $i = 0$	54
Curve $R_j (q_m \cdot V_j)$	55
Local pressure coefficient K_p	56 to 66
Static and dynamic pressure coefficients of the passage	67

STATIC TESTS IN S₃ Ch WIND-TUNNEL

Fig. number

Tests with mechanical flap

Characteristic features of the Model 68

Diagrammatic view of set-up in the passage 69

Curve R_j (q_m , V_j) 70

C_z (C_μ) $M_0 = 0.10$ $i = 0$ 71

Variable θ_j

C_z (C_x); C_z (C_m), C_z (1) $M_0 = 0.10$, $C_\mu = 0$ 72

" " " " $C_\mu = 0.02$ 73

" " " " $C_\mu = 0.06$ 74

" " " " $C_\mu = 0.19$ 75

Variable C_μ

C_z (C_x), C_z (C_m), C_z (1) $M_0 = 0.10$, $\theta_j = 22.5^\circ$ 76

" " " " $\theta_j = 41.5^\circ$ 77

" " " " $\theta_j = 59^\circ$ 78

" " " " $M_0 = 0.60$, $\theta_j = 22.5^\circ$ 79

" " " " $\theta_j = 30^\circ$ 80

" " " " $\theta_j = 37.5^\circ$ 81

" " " " $M_0 = 0.70$, $\theta_j = 22.5^\circ$ 82

" " " " $\theta_j = 30^\circ$ 83

" " " " $\theta_j = 37.5^\circ$ 84

" " " " $M_0 = 0.80$, $\theta_j = 22.5^\circ$ 85

" " " " $\theta_j = 30^\circ$ 86

" " " " $\theta_j = 37.5^\circ$ 87

Natural circulation

88

Tests with pneumatic flapFig. number

Characteristic features of the Model

89

Curve $R_j(q_\infty V_j)$

90

 $C_z(C_\mu) M_0 = 0.10, \alpha = 0$

91

Variable θ_j $C_z(C_x), C_z(C_m), C_z(\alpha) M_0 = 0.10, C_\mu = 0$

92

" " " " = 0.03

93

" " " " = 0.10

94

" " " " = 1.03

95 - 96

" " " " = 0.50, = 0

97

" " " " = 0.013

98

" " " " = 0.12

99

" " " " = 0.60 = 0

100

" " " " = 0.012

101

" " " " = 0.087

102

" " " " = 0.70 = 0

103

" " " " = 0.012

104

" " " " = 0.071

105

" " " " = 0.80 = 0

106

" " " " = 0.011

107

" " " " = 0.066

108

 $C_z(C_\mu), C_x(C_\mu), C_m(C_\mu) M_0 = 0.80$
(Tridimensional tests)

109

Natural Circulation

110

/.

DYNAMIC TESTS IN S₃ Ch WIND-TUNNEL

Fig. number

Characteristic features of Model	111
Arrangement of the measuring equipment	112
Variations of the aerodynamic derivatives $\frac{1}{q} \left(\frac{\partial p}{\partial \alpha} \right) \cos \varphi$ $\frac{1}{q} \left(\frac{\partial p}{\partial \alpha} \right) \sin \varphi$ and φ as a function of ω_R for $\alpha_0 = 3.25^\circ$, $C_\mu = 0$, $M = 0.5$	113
Evolution of the aerodynamic derivatives and φ as a function of C_μ for $\alpha_0 = 3.25^\circ$, $M = 0.5$	114
Evolution of the aerodynamic derivatives and φ as a function of ω_R for $\alpha_0 = -2.5^\circ$, $C_\mu = 0$, $M = 0.5$	115
Evolution of the aerodynamic derivatives and φ as a function of C_μ :	
1) for $\alpha_0 = -2.5^\circ$, $\omega_R = 0.096$, $M = 0.5$	116
2) for $\alpha_0 = -2.5^\circ$, $\omega_R = 0.134$, $M = 0.5$	117
3) for $\alpha_0 = -2.5^\circ$, $\omega_R = 0.192$, $M = 0.25$	118
4) for $\alpha_0 = -2.5^\circ$, $\omega_R = 0.272$, $M = 0.25$	119
Evolution of the aerodynamic derivatives as a function of ω_R (Summing up of the results):	
1) for $x/l = 0.037$	120
2) for $x/l = 0.537$	121
Evolution of φ as a function of ω_R for $x/l = 0.037$ and $x/l = 0.537$ (Summing up of the results)	122

ADDITIONAL TESTSTESTS IN S₁ Ch WIND-TUNNEL CORRECTED
FOR INFINITE ASPECT RATIO

Schematic representation of rheo-electric analogy assembly	123
Curves $\frac{\Delta I_0}{C_z}$ and $\frac{C_{xi}}{C_z^2}$ versus $\frac{dC_z}{dI_0}$	124
<u>Mechanical flap</u>	
C_z (i) and C_z (C_x) with $\theta_j = 3^\circ, 15^\circ, 37.5^\circ, 52.5^\circ$	

	Fig. number
$C_{\mu} = 0$	125
$C_{\mu} = 0.09$	126
$C_{\mu} = 0.22$	127
$C_{\mu} = 0.70$	128

Pneumatic flap

C_z (i) and C_x (C_x) with variable θ_j

$C_{\mu} = 0$	129
$C_{\mu} = 0.08$	130
$C_{\mu} = 0.22$	131
$C_{\mu} = 0.81$	132

Spoiler type deflector and pneumatic flap

C_x (C_{μ}) with variable θ_j	133
--	-----

All three types of deflectors

Variation of C_{μ} versus $\frac{P_o}{P_{ij}}$	134
--	-----

SECOND TEST SERIES IN S₃ Ch WIND-TUNNEL

- Mechanical flap:

Curves C_z (i) without blowing ($0.1 < M < 0.8$)	135
--	-----

Lift-drag curves without blowing ($0.10 < M < 0.8$)	136
---	-----

Lift-drag curves with blowing	137
-------------------------------	-----

C_z and C_x variations with blowing

$i = 0 \quad \alpha = -17.5^\circ \quad \theta_j = 5^\circ$	138
---	-----

$i = 0 \quad \alpha = 0 \quad \theta_j = 22^\circ 5'$	139
---	-----

Curve R_j ($q_m V_j$)	140
---------------------------	-----

Curve C_{μ} (P_o/P_{ij}) $M = 0.2$	141
--	-----

$M > 0.5$	142
-----------	-----

$M = 0.1$ (complements	143
------------------------	-----

$M > 0.2$ (to 1 st test series)	144
--	-----

- Pneumatic flap :

$\frac{dC_z}{d\epsilon}$ versus M_0 , A, $m_{i\infty}$ curve	145
$\Delta C_z (C_\mu)$ and $\Delta C_x (C_\mu)$ for $M = 0.2$ and variable θ_j	146
" " " " $M = 0.5$ " "	147
$C_z (\theta_j)$ and $C_x (\theta_j)$ for $M = 0.2$ and 0.5	148
Visualization of the deflected flow	149
$\theta_j (\frac{p_v - p_0}{p_0})$ and $\theta_j (\frac{p_0}{p_{ij}})$ for $M = 0$	150
True deflection θ_j' versus θ_j (variable p_{ij} and M)	151
$C_\mu (\frac{p_0}{p_{ij}})$ curve	152
$R_j (q_m \cdot V_j)$ curve	153

Complementary figures for 1st test series

$C_\mu (p_0/p_{ij})$ for $M = 0.1$	154
$C_\mu (p_0/p_{ij})$ for $M = 0.2$	155

GENERAL DISCUSSION OF THE TESTS.

EFFECT OF BLOWING ON LIFT.

Comparison of $C_z (C_\mu)$ for first and second test series in S_3 Ch w.t. (A_1 type flap)	156
Section lift coefficients versus M and C_μ (A_1 and A_2 flaps) 2 ^d test series S_3 Ch w.t.	157 to 160
Tests in S_3 Ch wind-tunnel α_j and K coefficients	161
Tests with Mechanical flap. Effect of C_μ on lift.	162 - 163
Variation of K coefficient	164
Spence theory coefficients	165
Comparison between test results and Spence theory	166 to 175

EFFECT OF BLOWING ON DRAG

Summary of lift-drag curves with blowing as resulting from tests	176 to 184
C_{xc} versus C_μ for advancing blade	185 - 186

Lift-drag curves for advancing blade and blade in symmetry plane 187

Lift-drag curves for retreating blade 188

Blowing pseudo-efficiency 189

Optimum combination of blade angle of attack and flap deflection 190 - 191

Optimum combination of i and C_j versus C_μ for a fixed-wing aircraft 192

PRACTICAL TEST RESULTS

Boundary of deflected jet stall.
Adaptation curves of pneumatic flap 193

Calibration at $V_0 = 0$ 194

Limit values of C_μ and pressure ratio 195 - 196

Effect of jet stall on lift coefficient 197 - 198

Effect of jet stall on drag 199 - 200

Section lift coefficient versus C_μ 201 - 202

Control efficiency 203

Flow circulation by centrifugal pumping 204

Effect of blowing alone on lift 205

APPENDIX

ANALYTICAL DETERMINATION OF THE AERODYNAMIC TORSION MOMENTS ACTING ON A JET-FLAPPED ROTOR BLADE

Blade model main duct average cross section 206

Schematic drawing of test assembly 207

Mechanical blade model characteristics 208

Variation of stiffness 209

Variation of shear center 210

Test results in S_1 Ch Wind-Tunnel 211

" " S_3 Ch " " 212 to 216
/.

Axes and References	217
Blowing parameters for a typical jet-flapped , jet-driven rotor, in forward flight	218
Blade air loads and flapping moments	219
Air loads on blown blade outer portion for a given deflection pattern	220
Max. pitching moments due to blowing and theoretical blade plan form with θ_j pattern giving zero flapping moments	221

UNIT CONVERSION TABLE

CONVERSION OF LINEAR DIMENSIONS

Multiply	by	to obtain
Inches	2.54	centimètres
Centimètres	0.3937	inches
Feet	30.48 0.3048 0.333	centimètres mètres yards
Yards	0.9144 3	mètres feet
Miles	5280 1.609 1760 0.868	feet kilomètres yards nautical miles
Mètres	39.37 3.281 1.094	inches feet yards
Degrés	0.01745	radians

CONVERSION OF SQUARE DIMENSIONS

Multiply	by	to obtain
Square inches	6.452	centimètres carrés
Centim. carrés	0.1550	square inches
Square feet	929 144 0.0929 0.111	centim. carrés square inches mètre carré square yards
Square yards	9.0 0.8361	square feet mètre carré
Mètres carrés	10.76 1.196	square feet square yards
Kilomètre carré	0.3861	square miles

CONVERSION OF SPEEDS

-XIV-

Multiply	by	to obtain
Feet/minute	0.01667 0.01136	feet/second miles/hour
Feet/second	1.097 0.5921 0.6818	kilomètres/heure knots miles/hour
Miles/hour	0.447 1.467 1.609 0.9684	mètre/seconde feet/second kilomètres/heure knots
R P M	0.1047	radian/second
Knots	1.689 1.853 1.152 0.5148	feet/second kilomètres/heure miles/hour mètres/seconde
Kilomètres/heure	0.9113 0.5396 0.6214 0.2778	feet/second knots miles/hour mètres/seconde
Mètres/seconde	3.281 2.237 3.6	feet/second miles/hour kilomètres/heure

CONVERSION OF WEIGHTS

Multiply	by	to obtain
Onces (Avoir du poids)	0.0625 28.35 0.9115	pounds grammes onces (troy)
Pounds (Avoir du poids)	16.0 0.454 1.21528	ounces kilogramme pounds (troy)
Tons	2000 907.18 0.9072	pounds kilogrammes tons (metric)
Tons (metric)	1000 2205	kilogrammes pounds (Avoir du poids)
Kilogrammes	2.205	pounds
Grammes	980.7	dynes
Dynes	2.248×10^{-6}	pounds

CONVERSION OF PRESSURES

Multiply	by	to obtain
Pounds/square inch	0.06804 2.036 703.1	atmospheres inches of mercury Kg/mètre carré
Pounds/square foot	0.19242 4.883	inches of water Kg/mètre carré
Atmospheres	29.92 1.033 14.7 2116	inches of mercury Kg/centimètre carré pounds/square inches pounds/square foot
Inches of water	0.07349 5.198 25.38	inches of mercury pounds/square foot Kg/mètre carré
Kg/mètre carré	0.2048	pounds/square foot
Kg/centimètre carré	14.22	pounds/square inches

CONVERSION OF POWERS

Multiply	by	to obtain
Foot.pounds/sec	0.07717 1.356 0.01945	BTU/minute Watts kg/calories/minute
BTU/minute	12.96 0.02356 17.56	foot.pounds/second Horsepower Watts
Horsepower	42.44 550.0 0.7457	BTU/minute Foot-pounds/sec kilowatts
Kg.calories/minute	51.43 0.0935	foot-pounds/second horsepower
Horsepower/hour	2545 641.7	BTU kilogr/calories
Foot-pounds	0.1383	kilogrammes mètre
Ergs	7.376×10^{-8}	foot-pounds

DETERMINATION THROUGH WIND-TUNNEL TESTS
AND ANALYTICAL METHODS OF THE OPTIMUM
DEFLECTION DEVICES SUITABLE FOR USE
ON JET-FLAP HELICOPTER ROTOR BLADES

ABSTRACT

Tests of various jet-flap configurations were carried out in the ONERA (Office Nationale d'Etudes et de Recherches Aéronautiques) wind tunnels, with Mach numbers, blade pitch angles, jet deflections and C_{μ} blowing coefficients approaching those encountered on helicopter blade rotors.

Despite some limitations in test conditions (use of laminar airfoils and compressed air characteristics), results proved largely satisfactory and the analysis of the test data showed that jet-flaps can be effectively used for control and propulsion of helicopter rotors, providing some precautions are taken concerning the compressed air characteristics and jet-flap design.

The various types of deflectors tested were classified by order of efficacy, the pneumatic flap showing to be the best.

This type of deflector provides universal possibilities and represents an instantaneous-response slaved control, devoid of play and inertia, capable of reproducing multicyclic control patterns over the azimuth of the swept disc and making it possible to insure constancy of the air loads acting on the blades by creating suitably high lift on the retreating blade.

The leading blade tip Mach number can be increased without fear of compressibility effects.

The tests showed also that control by jet-flaps is effective even in case of engine failure when "natural" blowing is used.

The Report includes, in Appendix, an analytical determination of the aerodynamic torsion moments acting on a jet-flap rotor blade.

SYMBOLS

- i Angle of attack of blade section
- α Angle of deflection of mechanical (solid) flap
- θ_j Angle of deflection of the jet stream with respect to the blade section chord line (In the case of the mechanical blown flap, when the jet stream follows the upper surface of the flap the angle of deflection of the jet stream is : $\theta_j = \alpha + \beta$.

with $\beta = 15^\circ$ for the blade model tested in the S_1 wind-tunnel

$\beta = 22.5^\circ$ for the blade model tested in the S_3 wind-tunnel).

C_z Section lift coefficient

C_x Section drag coefficient

C_m Section moment coefficient about quarter chord

V_o Wind speed

M Mach number

V_j Jet exhaust velocity

$q = \frac{\rho v^2}{2}$ dynamic pressure

q_m mass flow of the compressed air used for blowing

P_{1j} total pressure in blowing slit distribution chamber

R_j Resulting aerodynamic force originated by blowing in stationary conditions ($V_o = 0$)

$\dot{C}_m = \frac{q_m V_j}{\frac{1}{2} \rho V_o^2} k$ with $k = \frac{R_j}{q_m V_j}$

l blade chord

R Reynolds number

S Reference model surface

INTRODUCTION

The research reported in this document has been made possible through the support and sponsorship of the U.S. Department of Army, through its European Research Office. (*)

The object of this Report which forms the second phase of the research program relevant to the application of jet-flap principles to large helicopter rotors, is a two-dimensional wind-tunnel test program on helicopter rotor blade elements, tested in conditions approaching as closely as possible the operating conditions of helicopter rotors.

This experimental work is accompanied by a theoretical analysis of the torsional moments acting on the jet flapped rotor blades.

The test program covers static and dynamic experimental studies of optimum jet-flap deflectors and their control systems to be used in the recommended crane helicopter rotor configurations (see Report No.1088, GIRAVIONS DORAND. Design Study of the Feasibility of Flying-Crane Type Helicopters Incorporating the Jet-Flap Control System. E.R.O.,US. Departement of the Army. Contract No.DA-91-591-EUC-987).

The work performed includes the study of the behaviour of various jet-flap configurations in real tip-speed Mach conditions with blade pitch angles, jet deflections and C_{μ} coefficients as defined in the design study mentioned above.

The main objectives of the research are :

- selection of the optimum jet deflector, efficient up to a 60° deflection at low Mach numbers (retreating blade),
- investigation of jet-flap efficiencies at high Mach numbers (approx. 0.85) for small deflections (approx 10°) corresponding to the advancing blade conditions,
- determination of the aerodynamic response time (phase angle) of jet-flaps operating in a frequency band of 0.5 to 20 cycles per second,
- analytical determination of the aerodynamic torsional moments acting on the blade for various jet-flap deflections and C_{μ} values.

..... /.

(*) The monitoring and funding Agency in the Department of the Army was the Transportation Research Command, Fort Eustis, Virginia.

The French Government contributed to the program through its "Service Technique de l'Aéronautique" in funding half of the wind-tunnel expenses involved.

APPARATUS AND TEST METHODS

The experimental investigations reported herein were conducted in the O.N.E.R.A. (°) S_1^{Ch} and S_3^{Ch} Wind-tunnels.

Preliminary tests on deflectors were carried out in the ISSY Wind-tunnel belonging to the SERVICE TECHNIQUE AERONAUTIQUE (STAé.)

Characteristics of the Wind-tunnels :

The main characteristics of the wind-tunnels are indicated hereafter :

Name	Working Section		Max Velocity	Type
	Form	Dimension		
ONERA S_1^{Ch}	elliptical	16 x 8 m	50 m/sec	Open-throat
ONERA S_3^{Ch}	circular	1.0 m	$M = 1.0$	Return-flow
STAé. ISSY	"	2.0 m	58 m/sec	Open-throat

Description of blade models

Two blade models were used in the ONERA Wind-Tunnel tests. Each model specially designed according to the characteristics of the wind-tunnel in which it was to be tested in order to yield useful data at various Reynolds and Mach numbers.

Both blade models were of dural construction and had removable trailing edges so as to permit the testing of various jet-flap configurations.

They had both NACA 66011 Sections.

Their main dimensions are given hereafter and in Fig 30 and 68.

The wind-tunnel mountings and testing procedures are indicated in the following text.

Designation	chord	span	Ref. Area	Ref. Volume
S_1 Ch Blade model	1.1 m	2.01 m	2.21 m^2	2.431 m^3
S_3 Ch " "	0.35 m	0.44 m	0.154 m^2	0.0539 m^3

O.N.E.R.A. : OFFICE NATIONAL D'ETUDES ET DE RECHERCHES AERONAUTIQUES

Classification of the tested jet-flap configurations

During the course of the investigation the following types of jet-flap were studied :

- a) - Mechanical (solid) tangentially blown flap.
- b) - Pneumatic deflector.
- c) - Deflector incorporating an obstacle (spoiler) in the jet stream, associated with a convex wall,
- d) - Deflector incorporating a pilot jet associated with a convex wall.

Schematic drawings of the tested jet-flap configurations as a result of several changes to the basic configurations are given in Fig 31, 68, and 89 for the first three types of deflectors.

Preliminary study and tests of jet-flaps

Prior to construction of jet-flaps for testing on blade models in the ONERA wind-tunnels, preliminary studies and tests have been carried-out on various jet-flap configurations.

The elementary theory of jet reattachment along a flap contour (convex wall) is reminded hereafter.

Let us consider a jet element $d\ell$ moving along a wall (see Fig. 26) and write its equilibrium conditions.

The centrifugal force of this element, having a width x and a height h is

$$\int_j \frac{V^2}{R} h x d\ell$$

The negative pressure (suction) acting on the side $a' b'$ is $x \Delta p d\ell$.

In equilibrium conditions one gets :

$$\int_j \frac{V^2}{R} h x d\ell = x \Delta p d\ell$$

The required pressure along the wall is thus :

$$\Delta p = \frac{1}{2} \rho_j V^2 \frac{2h}{R}$$

Δp is created in a natural way.

In order to decrease Δp locally it is necessary :

- to decrease V or h
- to increase R

Variation of R along the convex wall.

On the basis of pressure distribution along the upper surface of an airfoil section it may be said that R must increase towards the trailing edge.

Different curvature distributions have been tested during the preliminary tests.

Various disturbances occurring in the boundary layer (modification of Δp) may cause the stalling of the flow.

In a similar way to the case of a sphere (PRANDTL) two flow conditions (one laminar and one turbulent) may exist. The existence of such two working conditions and of the critical pressure ratio separating them has been made evident during the tests (see further). The influence of the rate of variation of the pressure along the section contour (Schlichting) has also been made evident.

An experimental curve has been established (see Fig.13) which gives, in function of such parameters as slit width, radius of curvature of flap and up-stream pressure ratio, the line of separation between laminar and turbulent flow conditions.

A small amount of suction along the wall near the leading edge (see Fig.7) has but a little effect.

Theoretically it should be possible to delay stall by the means of a homogenous suction along the entire wall contour.

This method has not been applied for technological reasons (complexity).

The preliminary tests on the various jet-flap configurations have been performed in the STA wind-tunnel.

The testing installation is indicated in Fig.1.

Preliminary tests of mechanical tangentially blown flaps

These tests consisted in studying the effects of slit width, pressure ratio, position of slit edges with respect to flap and flap surface, aspect and geometrical characteristics.

The testing assembly is shown in Fig.2.

Flap deflections were achieved by means of a specially designed push-pull cardan type device connected to the control rod.

/.

Fig.3 to 12 present the results of these preliminary tests which are discussed in the sections which follow.

A schematic drawing of the blade trailing edge slit position with respect to the flap leading edge is given in Fig.3.

The blowing jet stream arrives tangentially on the flap upper surface.

If the flap is deflected in a continuous way, the jet stream follows the flap until a certain limit deflection when it starts quivering and suddenly stalls and returns to its initial direction (flap not deflected).

If the deflection of the flap is then decreased the jet stream will eventually return back towards the flap but only at a flap deflection which is generally smaller than the previous stalling limit.

This effect may be visualized by means of a thread placed in the jet stream (see Fig. 2) and, if the flap is deviated by hand, the variation of the pitching moment, when stall appears, may be felt quite well.

In order to investigate the dynamic response, flap deviations were controlled by a motor having an eccentric drive, and an electronic speed regulation.

Tests have been carried out at frequencies of 8, 10, 12 and 15 cycles per second.

a) Effect of slot width δ and of pressure ratio (Fig.4)

For narrow slits there appear to exist two different flow working conditions, functions of the pressure ratio.

For low pressure ratios the first condition is characterized by jet deviations which may exceed 90 degrees (the jet stream may return in the backward direction).

The flow is very even and the jet stream follows closely the flap over all its surface.

The second working condition is characterized by a limit angle of deviation of about 50 degrees. It appears for higher pressure ratios.

In this case the thread, placed in the jet stream, follows the flap up to a deviation of approximately 20 or 25 degrees. After that the flow shows a lump at the leading edge of the flap and the thread quivers and does not follow closely the flap any more. When stalling occurs the jet stream returns to its initial direction as if the flap were not deflected.

For the critical pressure ratio, which is fairly "peaky", the two working conditions exist simultaneously : the second condition is obtained easily, whilst the first condition is obtained when the flap is deflected in a slow and even way.

When the width of the slit is increased up to 2.5 mm it becomes difficult to determine the critical pressure ratio, though the two working conditions subsist.

When the width of the slit reaches 3.5 mm the first working condition disappears.

These tests have also brought to evidence effects of parameters such as :

- radius of the flap leading edge,
- position of the point of maximum neg. pressure over the flap airfoil,

Curve in Fig.13 gives, in terms of the blowing pressure ratio, the limit value of the ratio between slit width and flap leading edge radius in order to avoid the second working condition indicated above and stalling of the jet sheet.

b) Effect of the position of the upper edge of the slot relative to the flap axis of rotation (Fig.5).

In order to get negative jet stream deviations (upwards) it is necessary to cut off the upper edge of the slit.

With slit upper edges shortened by 3 to 7 mm. the efficiency of the system was not noticeably modified.

It must be noted however that the shortening of the slit upper edge modifies the width of the slit,

c) Effect of the flap surface aspect and effect of the distance h between the flap and the slit lower edge (Fig.6)

Flap surface aspect (polishing) has little effect on performance, but the latter are very sensitive to variations of h .

An increase of h from 1.3 mm. to 1.8 mm. may cause the disappearance of the first flow working condition described previously .

d) Effect of apertures designed for communication with atmospheric pressure (Fig.7)

The presence of apertures such as indicated in sketch n°.1 has no effect on the critical pressure ratio.

/.

On the contrary an aperture configuration such as shown in sketch No.2 decreases the critical pressure ratio.

In this last case, when communication with atmospheric pressure is suppressed, the initial critical pressure is practically restored.

e) Effect of concave flap sections (Fig.8)

These sections have been tested for technological purposes.

Decrease of efficiency is evident but not prohibitive.

f) Effect of tubular flaps

Tubular flaps (see Fig.9 to 12) have also been tested. Tube radii were comprized between 20 and 58 mm.

The width of the slit was given three different values :

$$s_j = 1.8 \text{ mm.} \quad s_j = 4.3 \text{ mm.} \quad \text{and} \quad s_j = 7.3 \text{ mm.}$$

Figures 10 and 11 show the compared performances of tubular and conventional flaps.

It may be seen on Fig. 10 that the first flow working condition subsists for higher pressure ratios in the case of tubular flaps.

On the other hand, when the ratio of the slit width to the flap tube radius exceeds 0.18 the jet stream does not follow the tubular flap any more.

The mechanical flap characteristics selected for the wind-tunnel tests at ONERA are indicated in Fig.3/ and 68.

The distance between flap trailing edge and its hinge axis has been fixed approximately at 16 % of blade chord.

Preliminary tests of pneumatic deflectors

The preliminary series of tests have been carried out on 3 types of rubber membranes:

- a) - Pure rubber, 1 mm. thick,
- c) - Fabric reinforced rubber, 0.65 mm. thick,
- c) - Fabric reinforced rubber, 2.3 mm. thick,

The object of the first series of tests was to study the behaviour (vibration) of a plan rubber membrane submitted to the action of a tangential jet stream.

The variable parameters were :

- width of the jet stream (slit)
- pressure of the jet stream
- initial tension of the membrane.

The test assembly is shown in Fig. 14.

The second series of tests has been carried out in order to study the behaviour of the rubber membrane when distorted by swelling up of a boot.

The test assembly is shown in Fig. 15.

Membranes of types a) and b) were selected for these tests.

Pure rubber and fabric reinforced rubber boots were both used.

The variable parameters were the same as in the first series of tests.

The results showed to be satisfactory with jet deflections over 60 degrees.

The results of these tests are summarized in Table 1.

An initial tension of 13 % and the b) type membrane were then selected for testing a jet-flap configuration as shown in Fig 16.

This type of deflector was tested with slits of 1 mm. and 1.5 mm. thickness and various jet stream pressures.

Curves in Fig.19 show, as a function of pressure in the rubber boot :

- the angle of deflection α of the flap
- the angle of deflection θ_j of the jet stream.

A second type of deflector, as shown on Fig. 17, was also tested.

Test results are given in Fig.20.

These tests indicated that the tension of the membrane did not remain constant and that a flexible hinge favoured vibration of the metal blade.

the
Following tests carried out on flexible rubber deflectors, a new type of deflector, as shown in Fig.18 and made up of thin steel blades and a rubber boot was tested.

TABLE I

Type a)	Type b)	Type c)	Tension	Slot width
Distorts at 1.3 pressure ratio	Vibrates at 2.7 pressure ratio	Vibrates at 4.0 pressure ratio	3 %	1.3 mm.
Distorts at 2.5 vibrates at 2.7 pressure ratio	Vibrates at 2.9 pressure ratio		13 %	
Vibrates at 3.0 pressure ratio	Vibrates at 2.6 pressure ratio		23 %	
	Vibrates at 3.1 pressure ratio	Vibrates at 2.85 pressure ratio	3 %	4.3 mm.
Vibrates at 4.0 pressure ratio		Vibrates at 4.3 pressure ratio	13 %	
Distorts at 2.4 pressure ratio			23 %	2.3 mm.
Vibrates at 2.6 pressure ratio			23 %	

Jet pressure Kg/cm ²	Type b) Tension 2 % pure rubber boot			Type b) Tension 12 % Fabric-rubber boot	Type a) pure rubber boot
	2,5 mm slot	1,9 slot	0,9 slot	1,5 slot	2,5 slot
1.65	Correct $\theta > 60^\circ$	Correct	Correct	Correct	Correct $\theta > 60^\circ$
1.8	"	"	"	"	"
2.15	Correct	"	"	"	Correct for $\theta < 30^\circ$
2.4	Obstacle in jet stream	Correct but noisy	"	"	
2.7		Vibrates	"	"	
3.5				Deflection stops	
	Pressure in boot : 0.45 Kg/cm ² max.			Pressure in boot : 1.3 Kg/cm ² (For lower pressures there appears a high pitched noise	

Fig.21 to 23 indicate, as a function of the pressure in the rubber boot:

- the angle of deflection α of the flap
- the angle of deflection θ_j of the jet stream
- the jet stream pressure.

Such a deflector gives a combination of solid and fluid flap effects.

Its operation is effected by means of the rubber boot inflation which simultaneously controls the deflection of the flap and its curvature.

The proportion between solid flap deflection and jet deflection may be adjusted at will.

This type of deflector was selected for the wind-tunnel tests to be carried out on the rotor blade models.

Preliminary tests of deflectors incorporating a spoiler (screen) associated with a convex wall (YOUNG-COANDA effect)

A schematic configuration of this type of deflector is indicated in Fig. 24.

The preliminary tests consisted in studying the influence of such parameters as :

- vertical (Y) and horizontal (X) distances of the convex wall with respect to slit edge,
- location of spoiler (screen) with respect to slit edge,
- height h of spoiler (portion emerging in jet stream),
- curvature of convex wall.

The results of these tests are presented in Fig. 25 where jet deflections are plotted in function of the height h of spoiler,

The selected values of X and Y were :

$$X = 5 \quad Y = -1 \quad (\text{see Fig.25}).$$

The curvature of the convex wall was designed in such a way that no high pressure zone appears at the leading edge and a correct pressure distribution is obtained along the entire section.

These pressure distribution for different values of h are also indicated in Fig.25.

Study of deflectors incorporating a pilot jet associated with a convex wall.

A preliminary study of such deflectors has been made in collaboration with the PERTIN Co. (specialists of reverse jet techniques).

Fig.26 shows a schematic presentation of a deflector incorporating a transverse auxiliary jet and reattachment along a convex wall.

Fig.27 indicates the deflections which may be obtained with a deflector of this type as a function of the momentum ratio δ of the main and auxiliary flows.

ϵ is the contraction coefficient which for practical applications should be small (around 0.7 to 0.8), in order to avoid up-stream unacceptable excess pressures.

This Fig.27 shows that for deflections larger than 20 degrees the auxiliary jet mass flow becomes prohibitive.

For this reason this type of deflector was not retained for wind-tunnel tests.

Discussion of the preliminary tests and studies conducted on the various jet-flap configuration

The preliminary tests and systematic studies conducted on the various types of jet deflector configurations described above indicated a possible design criterion that may be used to select jet deflectors which can be efficiently operated for any given type of rotor-blade.

The following conclusions may be suggested :

- the first two types of deflectors (mechanical blown flaps and pneumatic deflector) are better adapted for use with narrow ejection slits (width of slit to blade chord ratio under 1/3).

The field of application of these two types of deflectors may tentatively be indicated as follows :

- for wide rotor blades (chord over two ft.) either of these deflectors may be used,
- for narrow rotor blades the pneumatic deflector is preferable.

Jet deflections obtained with these two types of deflectors exceed 50 degrees and their dynamic behaviour (up to 20 cycles per second) is satisfactory. /.

The mechanical blown flap appears to give larger values of drag than the pneumatic deflector.

The configuration selected for the pneumatic type of deflector associates an inflatable boot with a solid flexible covering permitting a variation of curvature of the upper surface of the flap together with its deflection.

The last two types of deflectors (spoiler type and auxiliary pilot jet type) are characterized by wide ejection slits and are mainly applicable for use with wide chord, jet-driven, rotor blades and high temperature, low pressure ratio, air flow.

Jet deflections obtained with the spoiler type deflector are almost comparable to those obtained with the first two types of deflectors.

Jet deflections obtained with the deflector incorporating a pilot jet reach a maximum of approximately 20 degrees. Its efficiency is limited by the amount of mass flow required for the auxiliary high pressure pilot jet.

The deflectors which have finally been selected for testing in the ONERA wind tunnels belong to the first three types described above.

The following configurations were used in these tests:

1.- 2.01×1.10 blade model (Tests in S_1 Ch Wind-tunnel) :

- Mechanical blown flap
- Pneumatic deflector
- Spoiler type deflector.

Static tests only were carried-out in this wind-tunnel for these three types of deflectors.

2.- 0.44×0.35 blade model (Tests in S_3 Ch Wind-tunnel)

- Mechanical blown flap
- Pneumatic deflector

Static tests were carried-out for the two types of deflectors.

Dynamic tests were carried-out for the mechanical blown flap only.

(Previous dynamic tests performed outside of the wind-tunnel with the three types of deflectors showed that their behaviour was comparable).

TESTS IN O.N.E.R.A. WIND-TUNNELS

TEST PROCEDURE AND PRESENTATION OF RESULTS

General considerations

Before giving a description of the test procedures and presenting the test results it has been thought of interest to indicate the assumed domain of variation of the different parameters involved, such as applicable to helicopter flight conditions.

Table 2 indicates this domain of variation for :

- Jet exhaust velocity (at slit) ,
- C_{μ} coefficient
- Blade lift coefficient C_z (section coefficient)
- Required jet-flap deflection

and for different helicopter design configurations.

TESTS IN S₁ Ch WIND-TUNNELDescription of the model

The model was a rectangular helicopter blade member (airfoil section NACA 66011), comprising a front portion (up to about 70 % of the chord) and a removable rear portion adapted to receive three flap configurations (see Fig.31):

- a mechanical flap
- a spoiler-type flap
- a pneumatic flap, deformable under the action of a rubber boot.

References :

Blade chord : $\ell = 1.10 \text{ m}$

Span : $2b = 2.01 \text{ m}$

Reference surface : $S = 2.21 \text{ m}^2$

Reference volume : $V = 2.431 \text{ m}^3$.

The origine of the reference axes was located at the intersection between the symmetry plane of the blade and the rotation axis of the front attachments (see Fig.30). /.

Item	Type of helicopter				
	Case of power failure (centrifug. circulat.)	Mechanically driven with partial blowing	Jet driven		High speed helicopter
			Low speed (cold cycle)	Hot cycle	
Blowing power comp. to total power	0	15	100	100	100
Pressure ratio	0	1.6 to 1.7	2 to 2.5	1.6 to 1.8	3 to 4
Jet exhaust velocity m/s	0.8 Ωr	275 to 300	300 to 350	350 to 450	400 to 500
C_p	0.004/0.006 0.006/0.01 0.03/0.05	0.01/0.014 0.015/0.02 0.08/0.12	0.014/0.018 0.02/0.03 0.10/0.12	0.05/0.07 0.06/0.08 0.25/0.30	0.06/0.08 0.12/0.18 0.5/0.8
Flap deflection θ_f (degrees)	5 to 20 5 to 10 30 to 35	10 to 20 5 to 10 50 to 60	10 to 20 5 to 10 40 to 45		10 to 15 5 to 10 40 to 45
Mean blade section lift coefficient C_z				0.2 to 0.3 0.5 to 0.8 2.0 to 3.5	

Mach number of blade tip
 (Advancing blade) $0.6 < M < 0.9$
 (Symetry plane) $0.35 < M < 0.6$
 (Retreating blade) $0.1 < M < 0.35$

The flap blowing compressed air, supplied through two centered elbows on the front attachments, fed both ends of a distributing duct located in a distributing box extending along the whole span-length.

Wind-tunnel test procedure

The blade was secured between panels. Two protecting plates, provided to avoid interaction in the boundary layer of the panels, were integral therewith.

Figures 28 & 29 show the set up in the wind-tunnel section.

The front attachments of the blades defined the rotation axis for incidence variations; they were pivoted on two dynamometer spindles. Two air-tight rotary joints permitted rotation of the blade.

The rear attachment was articulated, through a dynamometer ring about the end of a telescopic strut (incidence adjustment).

Apparatus and instruments

The air loads were determined by means of extensometer gauge dynamometers.

The local pressures were measured in a blade section parallel to the symmetry plane (see Fig.30).

The distribution of the pressures on the blade (wall pick-up's) were measured by means of an alcohol multi-manometer.

The measures have been recorded photographically.

The air rates of flow were measured by means of an AFNOR diaphragm.

Test Results

The test results are presented in Fig. 32 to 67 as follows:

Tests with mechanical flap

- Curves $C_z (i)$, $C_z (C_m)$, $C_z (C_x)$ with

$\theta_j = 3^\circ, 15^\circ, 37.5^\circ, 52.5^\circ$ for $C_\mu = 0, 0.09, 0.22$ and $V_0 = 22$ m/s
Fig.32 to 34.

- Curves $C_z (i)$, $C_z (C_m)$, $C_z (C_x)$ with

$\theta_j = 3^\circ, 15^\circ, 37.5^\circ, 52.5^\circ$ for $C_\mu = 0.70$ and $V_0 = 15$ m/s Fig.35

- Curves $K_p (z/l)$ for $\theta_j = 3^\circ, 15^\circ, 37.5^\circ, 52.5^\circ$ with

$i = -5^\circ, 0^\circ, 6^\circ, 15^\circ$ and $C_\mu = 0, 0.075, 0.22, 0.61$ Fig.37 to 45

Tests with spoiler-type flap

- Curves $C_z(C_\mu)$, $C_x(C_\mu)$, $C_m(C_\mu)$ with $\theta_j = 0^\circ, 20^\circ, 24^\circ, 32^\circ$ and $i = 0$ with $V_0 = 22$ m/s for $C_\mu < 0.2$ and $V_0 = 15$ m/s for $C_\mu > 0.2$ Fig. 46

- Variations of K_p for limit values of $\theta_j = 0^\circ$ and 32° , and $C_\mu = 0$ and 0.39 (The variations of K_p are small for the intermediate values of C_μ and θ_j) Fig. 48

Tests with pneumatic flap

- Curves $C_z(i)$, $C_z(C_m)$, $C_z(C_x)$ for three values of θ_j and $C_\mu = 0, 0.08, 0.22$ and $V_0 = 22$ m/s Fig. 49 to 51
- Curves $C_z(i)$, $C_z(C_m)$, $C_z(C_x)$ for $\theta_j = 4^\circ, 47^\circ, 48^\circ$ with $C_\mu = 0.81$ and $V_0 = 15$ m/s Fig. 52 and 53
- Curves $\dot{C}_z(C_\mu)$, $\dot{C}_x(C_\mu)$, $\dot{C}_m(C_\mu)$ with $\theta_j = 0^\circ, 46^\circ$ and $i = 0$ $V_0 = 22$ m/s for $C_\mu < 0.2$ and $V_0 = 15$ m/s for $C_\mu > 0.2$ Fig. 54
- Variations of K_p ($^\circ/e$) with $i = -5^\circ, 0^\circ, 6^\circ, 15^\circ$ and $C_\mu = 0, 0.087, 0.36, 0.8$, $\theta_j = 4^\circ$ and other values comprised between 34° and 48° . Fig. 56 to 66

- Stationary conditions ($V_0 = 0$)

- Curves $R_j(q_m V_j)$ for the three types of flaps Fig. 36, 47 and 55

RemarksCorrections

The tunnel section ascending correction has been effected.

The aspect-ratio corrections resulting from the speeds induced by the panel, the protecting plates, and the tunnel

/.

section limitation have been the object of a study by means of rheo-electric analogy methods.

The correction for parasite loads introduced by the rear strut, the three attachments and the air-tight joints (drag and friction) has also been effected.

Measuring of loads and pressures have been effected separately in order to eliminate the parasite stresses of the pressure captor pipings.

Measuring accuracy

Load measuring accuracy : approx. 1 %

Blowing Coefficient C_μ

The blowing coefficient is defined as follows :

$$C_\mu = \frac{q_m V_j}{\frac{1}{2} \rho_0 V_0^2} \cdot k \quad : \quad \text{with} \quad k = \frac{R_j}{q_m V_j}$$

R_j is the resultant aerodynamical force measured in stationary conditions ($V_0 = 0$) for different values of $q_m V_j$

Figures 36, 47 and 55 show a comparison between R_j as measured and $q_m V_j$ determined :

- by measuring q_m ,
- by computing V_j , assuming that the expansion is isentropic from P_{1j} to p_0 ; the difference between this curve and the theoretical straight line $R_j = q_m V_j$ results, in particular :
- from the head losses inside the blowing box,
- from the fact that the pressure P_{1j} is not uniform in said box.

Deflection of the jet

The angle θ_j was computed from $\tan \theta_j = R_z / R_x$, R_z and R_x being measured in stationary conditions, for the spoiler type flap and the pneumatic flap.

Reference speed

Exploration has shown the distribution of the static and dynamic pressures in the passage in the presence of the panels and protecting plates.

Fig.67 shows, as a function of x and z , the evolution :

/.

- of the dynamic pressure coefficient defined by :

$$K = \frac{q \text{ (exploration)}}{q \text{ (reference)}}$$

- of the static pressure coefficient :

$$= \frac{p \text{ (reference)} - p \text{ (exploration)}}{q \text{ (reference)}}$$

TESTS IN S₃ Ch WIND-TUNNEL

STATIC TESTS

Description of the model

The model was a rectangular helicopter blade member, designed to be set along the tunnel wall.

It was machined with airfoil section NACA 66011, i.e. with a relative thickness of 11 % for a theoretical chord $\ell = 0.350$ m. The deflecting flap did not exactly fit with the shape of the theoretical airfoil trailing edge; it was shorter by 33 mm, which, for a chord of 0.317 m, leads to a relative thickness of 12.2 %.

The general shape and main dimensions are defined in Fig. 68 and Fig.69.

length of the blade member : $b = 0.440$ m

width of the slit : 1.5 mm,

pitching-moment axis : 25 % of the chord .

For the set of tests performed in tridimensional flow a wing-tip bay was added at the free end of the blade-model.

References

Chord : $\ell = 0.350$ m

Surface : $S = \ell \cdot b = 0.154$ m²

Volume : $V = S \cdot \ell = 0.0539$ m³ .

Configurations of the tested jet-flaps

Two types of deflecting flaps were tested :

Type A1 - Rigid mechanical flap (Fig.68). It comprises a mechanical control system enabling it to pivot about an axis located inside the blade airfoil.

/.

Type A2 - Pneumatic flap, controlled by compressed air (Fig.89). The deflection of the jet is obtained by curving an elastic metal part, the curvature variation of which is produced by means of an inflatable boot, made of rubber textile.

Both flap types act as jet flaps as well as solid flaps and therefore keep a certain amount of efficiency when blowing is stopped.

Wind-tunnel test procedure

The tests were performed in passage No.1 incorporating perforated walls and equipped with a remotely controlled wall balance support.

Two-dimensionnal tests were conducted between panels, the passage being divided into two compartments, along its vertical symmetry plane by means of a duralumin panel (Fig.69). A fairing having the same shape as the model was disposed symmetrically therewith in respect to the panel so as to balance the obstruction of the passage. The links controlling the angular motion of the flap during dynamic tests were passing through this fairing.

This fairing was removed during tests at high Mach numbers in order to reduce the obstruction.

Tridimensional tests have also been carried-out. During these tests the symmetry panel and the fairing were removed.

The tests program included :

- static tests with A1 and A2 flap configurations ,
- dynamic tests with A2 flap configuration (see test procedure in next section).

Modification of the flap deflections during the static tests could only be made with the wind-tunnel stopped. The value of the deflection was read on a graduated scale segment connected with the model.

In all cases, the reference value was angle α .

STATIC TESTS

Apparatus and equipment

The balance used was the wall balance n°41, designed and developed by the ONERA Measuring Department.

For dynamic tests, this balance was replaced by a rigid disc fast with the wall balance support.

The measures have been effected with standard OA gauge balance equipment, for several Mach numbers, with variable incidence angles, flap deflections and C_μ values.

Determination of the mass flow q_m , was effected by means of an AFNOR diaphragm, the blowing jet speed V_j was derived from pressures p_{1j} measured in the blade upstream the slit and p_0 measured in the airstream.

For high Mach numbers, the cross-sections in the flow-meter, proved to be too small, thus requiring pressures inconsistent with safe working of the plant. The flow-meter was therefore replaced by a diaphragmless piping, of larger and uniform cross-section.

$q_m V_j$ was computed by extrapolating the results measured on the flow-meter, from pressure p_{1j} (diagram $q_m(p_{1j})$).

The reference dynamic pressure and the Mach number were derived from the generating and static pressures, in the case of an isentropic flow.

The readings recorded on perforated tapes have been studied by the Central Computing Department OPca.

Test Results

The test results are presented in Fig.71 to 110 as follows:

Tests with A1 type flap (mechanical flap)

- Curves $C_z(C_\mu)$ with $i=0$, for $M_0=0.10$ Fig.71
- Curves $C_z(C_x)$, $C_z(C_m)$, $C_z(i)$ for $M_0=0.10$:
 - with variable θ_j and $C_\mu=0, 0.02, 0.06, 0.19$ Fig.72 to 75
 - with variable C_μ and $\theta_j=22.5^\circ, 41.5^\circ, 59^\circ$ Fig.76 to 78
- Curves $C_z(C_x)$, $C_z(C_m)$, $C_z(i)$ for $\theta_j=22.5^\circ, 30^\circ, 37.5^\circ$:
 - with variable C_μ :

$M_0 = 0.60$ Fig. 79 to 81

$M_0 = 0.70$ Fig. 82 to 84

$M_0 = 0.80$ Fig. 85 to 87

- Curves $C_z (\theta_j)$ and $C_m (\theta_j)$ with natural circulation (centrifugal pumping, the model being in the same internal pressure conditions as the rotor blade with no blowing)

Fig.88

Tests with $\Lambda 2$ type flap (pneumatic deflector)

- Curves $C_z (C_\mu)$ with $i=0$, for $M_0 = 0.10$

Fig.91

- Curves $C_z (C_x)$, $C_z (C_m)$ and $C_z(i)$ with variable

θ_j and C_μ :

$M_0 = 0.10$

Fig.92 to 96

$M_0 = 0.50$

Fig.97 to 99

$M_0 = 0.60$

Fig.100 " 102

$M_0 = 0.70$

Fig.103 " 105

$M_0 = 0.80$

Fig.106 " 108

- Curves $C_x (C_\mu)$, $C_z (C_\mu)$ and $C_m (C_\mu)$ for $M_0=0.80$ (tridimensional tests)

Fig.109

- Curves $C_x (\theta_j)$, $C_z (\theta_j)$ and $C_m (\theta_j)$ with natural circulation (centrifugal pumping)

Fig. 110

Remarks

Corrections

The wall correction, in the case of a passage provided with perforated walls, cannot be determined correctly by means of the rheo-electric-analogy. Furthermore it is estimated as having a comparatively low value. Therefore no correction have been effected for the wall effect.

Measuring accuracy

Incidence angle : $|\Delta i| < 0.10^\circ$

Lift coefficient: $|\Delta C_z| < 0.005$

Drag coefficient: $|\Delta C_x| < 0.001$

Moment coefficient: $|\Delta C_m| < 0.001$

Mach number : $|\Delta M_0| < 0.005$

/.

Blowing coefficient C_μ

Coefficient $k = R_j / q_m V_j$, used for computing C_μ was determined in stationary state, i.e. with the wind-tunnel stopped. The jet reaction R_j was measured by means of the balance for various blowing conditions $q_m V_j$. Curve $R_j (q_m V_j)$ ought to be linear with a slope equal to unity; the deviation visible in Fig.70, is to be imputed to a non-isentropic expansion due to lamination in the feeding duct between that cross-section in which p_{1j} has been measured and the nozzle.

Comments

The compressed air required for blowing was supplied under a pressure of 220 Kg/cm² at room temperature. Before use, this pressure had to be reduced down to values varying, within the model, from about 0 to 8 Kg/cm².

This expansion caused a cooling down of the balance, resulting in considerable temperature gradients as well as thermal drifts altering the readings of the dynamometers.

The behaviour of these drifts is not well known; thus the corrections can be but comparatively coarse, which does not permit figuring out the accuracy of the aerodynamic coefficient measuring. This explains the dispersion which may be observed on certain curves (small air loads in the tests effected with $M=0.1$).

In order to reduce to a minimum the thermal drifts the tests conducted with B2 type flap were carried-out in the following way:

Between every test-point the wind-tunnel was stopped and a zero correction was effected.

The reference static pressure (p_0) tapping used for determining the Mach number, was located in the lower tank of the passage, beneath the perforated wall. Its indications were checked up by detailed examination of the flow in the presence of the model. The measures proved to be consistent up to $M_0 = 0.7$, whereabove they led to a somewhat too high M_0 .

The Reynolds number of the flow, computed with the reference chord, varies from 800,000 to 4,100,000.

For certain high values of M_0 and θ_j the loads would have overcome the maximum acceptable loads for the balance; this is why no experiment has been effected at such values. When certain measuring points appeared as aberrant, the corresponding curves have been drawn in dotted lines (tests effected with $M = 0.1$).

For deviation $\alpha = 7.5$ ($\theta_j = 30^\circ$) with $M_o = 0.60, 0.7, 0.8$ a systematic positional anomaly of curve C_z (1) with $C_{\mu} = 0$ has been observed (this anomaly is illustrated in Fig. 88).

Some anomalies are also to be noted in Fig. 91 for $\theta_j = 20^\circ$ and in Fig. 98 for $\theta_j = 15.5^\circ$.

A systematic study of θ_j in function of M and C_{μ} has been carried-out in a series of additional tests (see further).

DYNAMIC TESTS

Particular Notations

Readings of the amplitude of the flap oscillating angle :

1) d_s : for static tests

2) d_d : for dynamic tests

$\mathcal{L}(p)$: reading of the pressure amplitude

Calibrating coefficients of the resisting pressure-gauges:

1) $k_s(p)$: for static tests

2) $k_d(p)$: for dynamic tests

α : $\bar{\alpha} \sin \omega t$

f : frequency

$\omega_R = \frac{\pi f l}{V}$: reduced frequency

Δp : pressure differential between upper and lower surface

$\Delta \varphi$: phase-shift introduced by the response delay of a pressure pick-up.

φ : phase relationship between the local pressure on the model and the flap position.

$\Delta p \cos \varphi$
 $\Delta p \sin \varphi$: Amplitudes of Δp variation in-phase and in-quadrature with α .

$\left(\frac{\partial p}{\partial \alpha}\right) \cos \varphi$
 $\left(\frac{\partial p}{\partial \alpha}\right) \sin \varphi$: aerodynamic derivatives

Dimensionless coefficients ;

$$\frac{1}{q} \left(\frac{\partial p}{\partial x} \right) \cos \varphi, \quad \frac{1}{q} \left(\frac{\partial p}{\partial x} \right) \sin \varphi, \quad C_{\mu} = \frac{q_m V_j^2}{\rho/2 V^2}$$

Object of the dynamic tests

The rapid deflection of the blown jet stream may serve two purposes :

- a) to obtain a multicyclic control of the flap in forward flight, in order to make the lift uniform across the disc,
- b) to control the rotor.

The pattern of the multicyclic jet deflection, over azimuth, for a forward speed of 300 Km/h was evaluated.

Its harmonic analysis gives :

$$\theta_j = 15.4 + 13.8 \cos (\omega t + \varphi_1) + 10.7 \cos (2\omega t + \varphi_2) + 0.83 \cos (3\omega t + \varphi_3) + 1.1 \cos (4\omega t + \varphi_4) + 1.0 \cos (5\omega t + \varphi_5) \text{ which leads to frequencies of the order of } 20 \text{ to } 22 \text{ c.p.s.}$$

Rotor control leads to somewhat lower frequencies :

stick motion 0.5 to 2 c.p.s.

rotational speed $\omega = \frac{2\pi}{T}$

frequencies $f = 4\pi \pm \omega < 20 \text{ c.p.s.}$

These rapid deflections can not be considered as static and non stationary aerodynamic forces must be introduced .

The non stationary state modifies the gain (amplitude) and the phase angle (lag) of the stationary forces.

The important factor for rotor control being the aerodynamic lag the object of the tests consists in measuring this lag in blowing conditions.

Apparatus and equipment

The blade model was the same as the one used for static tests. Its general shape and dimensions are defined in Fig.III.

The airfoil chord, provided with a "mechanical" flap was reduced by 10.4 % with respect to the theoretical airfoil chord. The pivoting axis of the flap was located 1.43 % under the mid-plane of the airfoil and 83.6 % from the actual airfoil chord.

The sinusoidal rotation of the flap took place about its pivoting axis. The amplitude α was constant and equal to 12.25° on either side of a mean angle α_0 of $+ 3.25^\circ$ (first testing series) or $- 2.5^\circ$ (second testing series).

The energising frequency of the flap was about 5 to 21 cycles.

A compressed air duct housed within the model and terminating along the span by a slit of 1.5 mm thickness permitted blowing an air jet on the upper surface of the flap.

During the tests, pressure measurements were substituted to load weighings.

The blade member was equipped with two pressure pick-up's located in the symmetry plane at 3.7 % (pressure gauge 1.) and 53.7 % (pressure gauge 2.) of the theoretical chord $c = 0.350$ m (Fig.III).

Operating Apparatus

A motor provided with a speed variator ensured driving of the model flap through a connecting-rod crank system.

Pressure pick-up's

The pressure pick-up's used were OPa, 20 H 60 type manometers with resisting gauges.

Their measuring range is 200 g/cm² and their bandwidth is about 200 cycles.

Their dimensions are : diameter 10 mm, height 2mm.

The pressure pick-up pipes had a diameter of 0.8 mm.

The pick-up's were mounted differentially between the inner and upper surfaces of the airfoil.

Measuring method and Means

The measuring method was based on a direct harmonic analysis (multiplying method).

The gauges of the pressure pick-up's were fed with a pure sinusoidal current of same frequency as the imparted motion and
/.

the phase of which was adjustable. By multiplying the sinusoidal intensity of this current by the resistance variation of same frequency undergone by the pick-up's, a direct current component was obtained in the measuring diagonal arms of the gauge bridges.

During the test, the sinusoidal current was successively set in-phase and then in-quadrature with the flap motion. The galvanometer readings respectively corresponded to the in-phase and quadrature components.

The measuring equipment is diagrammatically shown in Fig. 112.

Calibratings

The pressure and amplitude calibrating coefficients were determined by static measurements, the gauge being fed with a direct current:

$$k_s(p) = \frac{\text{Height of the water column}}{\text{Reading of the gauge manometer.}}$$

$$d_s = \text{Reading of the amplitude of the flap scanning angle.}$$

The gauge alternating current feeding voltage (dynamic tests) being different from the gauge direct current feeding voltage (static tests), the pressure amplitude readings were multiplied by the flap displacement amplitude readings ratio, said readings being proportional to the dynamic and static feeding voltages. The calibrating coefficient of the resisting gauge manometer permitted direct translation of the readings into pressure units.

$$k_s(p) \times \frac{d_s}{d_d} \times \mathcal{L}(\partial p \cos \varphi) = \partial p \cos \varphi \quad (1)$$

$$k_s(p) \times \frac{d_s}{d_d} \times \mathcal{L}(\partial p \sin \varphi) = \partial p \sin \varphi \quad (2)$$

Use of the results

The aerodynamic coefficients per angle unit are given by :

$$\frac{1}{q} \left(\frac{\partial p}{\partial x} \right) \cos \varphi, \quad \frac{1}{q} \left(\frac{\partial p}{\partial x} \right) \sin \varphi$$

The ratio between these two relations permits obtaining the phase-shift φ between the local pressure on the model and the deflection of the flap.

Test Results

The constant test parameters were :

- the blade member incidence angle $i = 6^\circ$
- the flap angular stroke $\alpha = 12.25^\circ$
- the variable parameters were :
- the Mach number ($M = 0.25$ and 0.5 , $R = 2.2 \times 10^6$ and 3.5×10^6)
- the blowing coefficient C_μ ($C_\mu = 0$ to 0.07)
- the flap deflection in mean position α_0
- the operating frequency of the flap f (hence $\omega_R = \frac{\pi f \ell}{V}$)

The test result diagrams (see Fig.113 to 119) which are enlisted in the following table, show the variations of

$\frac{1}{q} \left(\frac{\partial p}{\partial x} \right) \cos \varphi$, $\frac{1}{q} \left(\frac{\partial p}{\partial x} \right) \sin \varphi$ and φ as a function of ω_R or C_μ , for the various variable parameters.

	α_0	M	C_μ	f	ω_R	Figure
First test run	$+ 3.25^\circ$	0.5	0	5.3/9.7 Hz	0.034/0.062	113
			0.02/0.05	5.3	0.0336	114
				9.7	0.0620	
Second test run	$- 2.5^\circ$	0.5	0	10 to 20	0.063/0.128	115
			0.01/0.04	15.05	0.096	116
			0.015/0.04	21	0.134	117
		0.25	0.025/0.100	15.05	0.192	118
				21.25	0.272	119

Figures 120, 121 and 122 summarise the test results effected with or without blowing on the flap upper surface: For the tests with blowing, the selected values of C_μ substantially correspond to the saturating rate of the measured variables, the lag reaching rapidly, in function of C_μ , an asymptotic value.

/.

RemarksCorrections

- A correction relating to the phase-shift $\Delta\varphi$ resulting from the response delay of the pressure pick-up's has been effected. The value of $\Delta\varphi$ as measured on similar pressure pick-up's used in the same manner was :

$$\Delta\varphi^\circ = - 0.094 \text{ f}$$

- No wall correction has been effected.

Frequency range

It is to be noted that during the first test run, the frequencies used varied only from 5 to 10 cycles approximately. A mechanical incident did not permit operating the flap at higher frequencies. After repair, a second test run has been undertaken, during which the frequencies used were comprised between about 10 and 21 cycles.

To obtain high reduced frequencies, a part of these tests was effected at a speed corresponding to $M = 0.25$.

The sensitivity of the pressure pick-up's was too low, due to the small values of Δp measured with blowing at this speed (2 % of the measuring range in phase and 0.2 %/° in quadrature) to permit using the wind-tunnel at a lower Mach number.

Measuring accuracy

Calibrating of the frequency-meter by means of a low frequency generator and a two-curved oscilloscope and the high stability of the speed variator lead to a 0.1 cycle accuracy of the frequency measuring.

- The higher sensitivity of the pressure measuring apparatus permitted (with a reading error of one-fourth of a scale division) to evaluate pressure differentials of 0.4 mm water, i.e. 0.2 %/° of the pressure pick-up's measuring range.
- The reading of the flap stroke amplitude could be effected with an approximation of one-tenth of a degree.
- Phase adjustment : the shift corresponding to twice the phase error was 0.5 % on the tangent line. Thus the phase error reaches about one-tenth of a degree.

Aerodynamic coefficient $\frac{1}{q} \left(\frac{\partial p}{\partial x} \right) \cos \varphi$:

- Without blowing, this coefficient, which is substantially constant with ω_R , varies with the parameters α_0 and M .
- With blowing, this coefficient decreases as a function of ω_R .

(except for the rear pick-up at $M = 0.5$ and $\alpha_o = -2.5^\circ$).

It also varies with α_o and M .

- The blowing has the result of increasing $\frac{1}{q} \left(\frac{\partial p}{\partial x} \right) \cos \varphi$. The value of coefficient K_1 in the various testing conditions, with

$$K_1 = \frac{\left[\frac{1}{q} \left(\frac{\partial p}{\partial x} \right) \cos \varphi \right]_{C_\mu}}{\left[\frac{1}{q} \left(\frac{\partial p}{\partial x} \right) \cos \varphi \right]_{C_\mu = 0}}$$

is given hereunder for the pick-up's 1 and 2 :

α_o	M	C_μ	ω_R	K_1	K_1
				Front pick-up	Rear pick-up
3.25°	0.5	0.04	0.05	5.5	2.58
-2.5°	0.5	0.03	0.011	1.87	2.96
	0.25	0.07	0.24	2.15	2.2

Aerodynamic coefficient $\frac{1}{q} \left(\frac{\partial p}{\partial x} \right) \sin \varphi$:

This coefficient increases with ω_R and varies with α_o and M .

The blowing results in increasing the value of $\frac{1}{q} \left(\frac{\partial p}{\partial x} \right) \sin \varphi$.

The value of coefficient K_2 which is defined in the same manner as K_1 , in the various testing conditions, is given hereafter :

α_o	M	C_μ	ω_R	K_2	K_2
				Front pick-up	Rear pick-up
3.25°	0.5	0.04	0.05	11.8	12
-2.5°	0.5	0.03	0.11	1.8	6.4
	0.25	0.07	0.24	3.9	13

/.

Phase φ between the local pressure on the model and the flap angular position :

The building-up of the local pressure on the model, at the level of the two pick-up's used, lags with respect to the flap displacement.

The phase lag increases with ω_R and varies with α_o and M at $x/l = 0.537$; it remains small for $C_\mu = 0$, whatever may be the value of the reduced frequency.

For the rear pick-up ($x/l = 0.537$) a slight phase advance (1.2 to 1.8 degrees) has been observed in the following testing conditions : $C_\mu = 0$, $\alpha_o = -2.5^\circ$, $M = 0.25$. However, since the values to be measured in quadrature in these conditions were very small, it is possible that the measured phase advance be a result of possible unaccuracies in the evaluation of the pick-up response delay.

The phase-shift [$\Delta\bar{\varphi}^\circ = \varphi_{C_\mu=0} - \varphi_{C_\mu}$] resulting from the blowing on the flap upper surface is given in the following table in the various cases :

α_o	M	C_μ	ω_R	$\Delta\bar{\varphi}^\circ$	$\Delta\bar{\varphi}^\circ$
				Front pick-up	Rear pick up
3.25°	0.5	0.04	0.05	4	2.6
-2.5°	0.5	0.03	0.11	0	2.1
	0.25	0.07	0.24	11	9.5

Conclusive remarks pertaining to the dynamic tests

The main purpose of these tests was to measure the phase between the local pressure on the blade and study the variations of said phase under blowing upon the flap. The observation of the measuring apparatus has shown no discontinuity in the amplitude and phase variation as a function of the frequency and C_μ .

In the testing conditions defined in the report, φ substantially varies linearly as a function of the reduced frequency, with or without blowing.

The phase-shift tends towards a limit value that seems to be reached rapidly with the blowing, in particular for tests effected at $M = 0.5$ and $\alpha_o = -2.5^\circ$. It is to be noted that ...

in this configuration, ψ is practically independant from C_{μ} at $x/\ell = 0.037$ for flap deflection frequencies comprised between 15 and 21 cycles ($\omega_R = 0.096$ and 0.134).

It may be concluded that circulation takes a longer time to reach an established state in the case of blowing.

The difference however does not exceed 20 degrees and for the practical application to multicyclic deflection and rotor control there seems to be no major difficulty.

ADDITIONAL TESTS AND CORRECTIONS

- INDUCED VELOCITY CORRECTIONS

In the previous text (pages 14 to 18) and in Figures 32 to 67 were presented the test procedure and the test results obtained for the three selected flap configurations at the S₁ Ch Wind-tunnel.

These results were presented without aspect ratio corrections.

It is the object of this section to give these same results corrected for infinite aspect ratio.

These corrections were performed by means of rheo-electric analogy (See fig.123) and take into account the velocities induced by the panels, the protecting plates and the transverse boundary of the wind-tunnel section.

They permit to evaluate the section angle of attack and the profile drag for an infinite aspect ratio.

Angle of attack

The angle of attack i_0 , for an aspect ratio $A = \infty$, defined by:

$i_0 = I_0 + \Delta I_0$

and was computed from $\left(\frac{\Delta I}{C_z}\right)$ for every of $\left(\frac{dC_z}{dI_0}\right)$. See Fig.124.

Induced drag

The induced drag was obtained with $\left(\frac{C_{xi}}{C_z^2}\right)$ evaluated for every value of $\left(\frac{dC_z}{dI_0}\right)$. See Fig.124.

In the case of the spoiler type deflector the tests were carried out at $i = 0$ and the $\left(\frac{dC_z}{dI_0}\right)$ was taken equal to the $\left(\frac{dC_z}{dI_0}\right)$ determined for the mechanical flap at $\alpha = 0$.

The results are presented in Fig.123 to 134 as follows :

- Mechanical flap

Curves $C_z(1)$, C_z (C_x) with

$$\theta_j = 3^\circ, 15^\circ, 37.5^\circ \text{ and } 52.5^\circ$$

for $C_\mu = 0, 0.09, 0.22 \text{ and } 0.70$

Fig.125 to 128

- Pneumatic flap

Curves $C_z(1)$, C_z (C_x) with

$$\theta_j \text{ variable for } C_\mu = 0, 0.08, 0.22 \text{ and } 0.81$$

Fig.121 - 132

- Spoiler type deflector and pneumatic flap

C_x (C_μ) with θ_j variable

Fig.133

These results are completed by Fig.134 which gives the variations of C_μ versus P_o/P_{ij} ratio for the three types of deflectors .

$$\frac{P_o}{P_{ij}} = \frac{\text{pressure in Wind-tunnel section}}{\text{pressure in blowing box}}$$

ADDITIONAL TESTS

(SECOND TEST SERIES IN S3 Ch WIND-TUNNEL)

These second series tests complete the tests of the first series for $i = 0$ and variable M .

The results presented hereafter also incorporate calibration curves for C_μ (versus P_o/P_{ij}), for the two test series and a study of aspect ratios for the two types of flaps considered (A_1 and A_2).

Test procedure. Apparatus and Equipment.

These additional tests were carried out in the same conditions and with the same blade model as the first test run.

The upper lip of the slit was however thinned-down (see Fig.156).

In order to reduce to a minimum the influence of the thermic drifts mentioned previously (see page A.23) the tests were performed as follows :

- Measurements without blowing :
point after point tests, i.e., after each test the wind tunnel was stopped and zero corrections were performed.
- Measurements with blowing :
variation method : uninterrupted operation of the wind-tunnel, adjustment of the desired blowing conditions for every test point and measurement of the variations of the aerodynamic forces due to blowing by sudden interruption of the latter. The aerodynamic coefficients of the lift and drag forces with blowing are obtained by algebraic sommation of the corresponding coefficients without blowing and of their variations due to blowing.

Aspect ratios

The study of the compressible flow leads to consider the expression :

$$\frac{m A \sqrt{1 - M_o^2}}{A \pi - m} = \frac{m_{i\infty}}{\pi} = \text{Const.}$$

m being the slope of the lift in compressible flow, and

$m_{i\infty}$ the slope of the lift in non-compressible flow of the same airfoil for an infinite aspect ratio.

This expression gives :

$$m = \frac{dC_z}{di} = f(M_o, A, m_{i\infty})$$

The values of m are given in Fig.145.

For the experimental results of the first test runs the aspect ratio is comprised between 6 and 7. The opening made in the central panel in order to reach extreme values of the mechanical flap (A_1 type) deflections gave way to a noticeable decrease of the $\frac{dC_z}{di}$ slope (see Fig.145).

Test Results

The test results are presented in Figures 135 through 155 as follows :

- Mechanical flap (A_1 type)

C_z (i) and lift-drag curves without blowing Fig.135 - 136

Lift-drag curves with blowing Fig.137

C_z and C_x variations with blowing	Fig.138 - 139
R_j versus $q_m V_j$ curves	Fig.140
C_μ versus p_o/p_{1j} for different M	Fig.141 to 144
- <u>Pneumatic flap (A_2 type)</u>	
$\frac{d C_z}{d i}$ curve versus $M_o, A, m_{1\infty}$ (complement to 1st test runs)	Fig.145
Variations of the aerodynamic coefficients versus C_μ for $i = 0, M_o = 0.2$ and 0.5 and variable θ_j	Fig.146 to 148
Variation of θ_j determined at $V_o=0$ versus p_o/p_{1j} (for a constant pressure in boot)	Fig.150
Calibration curve for θ_j versus pressure ratio $\frac{p_v - p_o}{p_o}$ in boot	Fig.150
Variation of true deflection θ_j' versus θ_j determined at $V_o = 0$ with variable	
p_{ij} and M_o (Obtained by visualization).	Fig.151
C_μ versus p_o/p_{1j} curves	Fig.152
R_j versus $q_m V_j$ curve	Fig.153
C_μ versus p_o/p_{1j} curves (complements to first test j run)	Fig.154 - 155

GENERAL DISCUSSION OF THE TESTS

EFFECT OF BLOWING ON LIFT

GENERAL

It is proposed to examine in this section the results obtained, first from the point of view of overall application to jet flap helicopter rotors, following which a detailed examination will be made of the primary effects.

The tests were performed on laminar airfoil sections of 11% thickness ratio; therefore general conclusions relevant to the blowing cannot be made.

A laminar section was chosen in order to obtain high Mach numbers for the advancing blade.

All airfoil sections were provided either with the mechanical flap, the jet-flap, or the spoiler type flap.

During the additional tests performed in the S_3 Ch wind-tunnel, the thickness of the upper lip of the blowing slit (upper surface) was reduced. In all cases, the lip to which the results refer is specified.

APPLICATION OF BLOWING TO HELICOPTER ROTORS

One of the important factors is the C_μ , a non-dimensional parameter for the jet momentum referred to the value :

$$\frac{\rho}{2} (\omega r + V \sin \psi)^2 l dr$$

It may be noted that if the intensity of blowing remains constant regardless of the blade azimuth ψ , the value of C_μ varies to a significant extent with ψ .

Thus in the case of a rotor in which all the power is used for blowing, then for an advance ratio $\mu = 0.4$, the values of C_μ vary in the following manner :

For the advancing blade, the value of C_μ is measured in hundredths.

For the retreating blade, the value of C_μ is measured in tenths and seldom exceeds 1.0.

For the blade lying on the centerline, the value of C_μ fluctuates around 0.15.

If very little power is devoted to blowing (to improve performance only, say), the values mentioned above may be divided by 10.
/.

Should it be desired to equalize blade lift at different azimuths, or, better still, to equalize the aerodynamic flapping moments at the blade root, the local C_z may be defined as follows in terms of the rotor's mean C_z :

- Blade lying on centerline : the local C_z is of the same order of magnitude as the rotor's mean C_z
- Advancing blade : 1/4 to 1/6th of the rotor's C_z
- Retreating blade : five to ten times the rotor's C_z

The C_μ variation takes place in the right direction; however, a θ_j jet deflection variation is necessary, for although the direction of the variation of C_μ is correct, it may prove inadequate from the amplitude standpoint. For this reason the retreating blade is associated to high deflections ($\theta_j = 30^\circ$ to 60°), small Mach numbers ($M < 0.5$) and high C_μ values.

The advancing blade is associated to low C_μ values, high Mach numbers (0.76 to 0.8) and small θ_j values.

In cases where all the power is used for blowing, it is necessary to insure rotor control in addition to equalizing blade loads and restoring the retreating blade's lift, which in turn implies that such control must remain effective in the event of a power failure. This means that one must use flaps of substantial chord as well as "natural" blowing (the blade ducts act as a centrifugal compressor).

Wind-Tunnel Results

Mechanical Flap

Region of Advancing Blade

The advancing blade operates at high Mach number (0.7, 0.8), at small angle of attack, at low C_z (0.4, 0.5) and at a C_μ comprised between 0.025 and 0.7.

The first S₃ Ch wind-tunnel tests give, for $M = 0.80$ (Figure 85), undisturbed C_z (1) curves for a range of small C_μ values.

A second test run in the S₃ Ch wind-tunnel (Fig. 145 to 155) using a thinned-down upper lip, provided results for higher C_μ values. Thus, for $C_\mu = 0.075$, $C_z = 0.4$ is obtained for $i = 2^\circ$. The C_z (1) curve is perfectly straight, so that a satisfactory utilization margin is provided in angle of attack.

Region with Blade on Centerline

This blade operates at a moderate Mach number (0.4, 0.6), at /.

a small angle of incidence of the order of 4° to 5° , and with a mean C_z of 1.0, the C_μ being of the order of 1.15.

The results of the second run in the S_3 Ch wind-tunnel gave for $M = 0.5$, $C_\mu = 0.095$, a $C_z(i)$ curve which was perfectly straight for $-3 < i < 4$. An overall C_z of 0.6 was obtained for $i = 2^\circ$. For a test performed with a higher C_μ , say 0.15, it would be justifiable to expect a C_z of the order of unity.

The utilization margin is a wide one and, here again, one may envisage a helicopter blade operating in this zone.

Region of Retreating Blade

The retreating blade may be said to be demanding from the standpoint of C_z , θ_j , C_μ and angle of incidence. Orders of magnitude for these parameters are as follows :

$$\theta_j = 40^\circ \quad C_\mu = 0.6, 0.8 \quad C_z = 4 \text{ to } 4.5 \text{ for } i = 6 \text{ to } 8^\circ.$$

The Mach number attains 0.2 to 0.3.

The S_1 Ch wind-tunnel tests (Figure 35) gave a maximum overall C_z of 3.7 for $i = 10^\circ$, $C_\mu = 0.70$ and $\theta_j = 52.5^\circ$ at $V_0 = 15$ m/sec.

In the S_3 Ch wind-tunnel (Figure 71), and for $M = 0.10$ at $i = 0$, $\theta_j = 59^\circ$, $C_\mu = 0.90$, the overall C_z reaches 4. For a larger angle of incidence it would be justifiable to expect a higher C_z , though it will be noted that the C_z obtained is already quite adequate.

The tests results are thus acceptable also for the retreating blade region.

To summarize, the various test results obtained for the mechanical flap provide a good utilization envelope from the lift standpoint for application to the helicopter with blown rotor.

Deflection by Spoiler type Deflector

The S_1 Ch wind-tunnel tests (Figure 46) gave C_z values which did not exceed 0.7 for C_μ values of up to 0.4 and for a θ_j deflection of 32° . These results are therefore very inadequate for the blade requirements of a blown rotor, and high C_z values would necessitate much larger C_μ values (which would in turn call for prohibitive power). Furthermore, the jet deflections measured in the tunnel proved less than those obtained outside the tunnel. This solution will therefore be rejected for the time being insofar as application to a helicopter with blown rotor is concerned.

This type of deflector was envisaged for the case of high temperature mixed flows (hot cycle), though here again the use of a /.

mechanical flap or a pneumatic flap may be envisaged instead of the spoiler type deflector, subject to certain technical precautions being taken for which provision has been made.

(Yet another solution would consist in not mixing the two flows within the blade and in causing the hot flow layer to emerge above the cold layer, the latter alone affecting the flap. On exit from the nozzle, expansion of the jet lowers its temperature)

Pneumatic flap

Region of Advancing Blade

The S₃ Ch wind-tunnel tests gave, for $M = 0.80$ at $C_{\mu} = 0.066$ (Figure 108) $C_z(i)$ curves which are quite straight. By producing the straight line relevant to $\theta_j = 29^\circ$, a C_z value of 0.4 is obtained for $i = 3, 5^\circ$.

For $M = 0.70$ at $C_{\mu} = 0.071$ (Figure 105) a C_z value of 0.4 is obtained for $i = 3^\circ$.

For $M = 0.60$, $C_{\mu} = 0.087$ (Figure 102) at $\theta_j = 29^\circ$, a C_z value of 0.5 is obtained for $i = 3^\circ$.

These results are amply sufficient for application to a helicopter with blown rotor.

Region with Blade on Centerline

Let us revert to the S₃ Ch wind-tunnel tests for $M = 0.50$, $C_{\mu} = 0.12$ (Figure 99). For $\theta_j = 27^\circ$ and an angle of incidence of 4° , $C_z = 0.63$. Taking a larger θ_j of the order of 40° , there is every reason to expect a C_z of close to 0.9 or 1.0. The $C_z(i)$ curves reveal no irregularity, which leaves a wide angle of incidence margin.

Region of Retreating Blade

The S₃ Ch wind-tunnel tests for $M = 0.10$, $C_{\mu} = 0.90$ (Figure 94) give a C_z in excess of 3 for $i = 5^\circ$ and $\theta_j = 50^\circ$. A C_z value of 4 could be obtained for a much higher and consequently unacceptable C_{μ} value (1.7 to 1.8).

The S₁ Ch wind-tunnel tests at $V_0 = 15$ m/sec and $C_{\mu} = 0.81$ (Figure 52) give, for $\theta_j = 48^\circ$, a maximum C_z of 3.6 for $i = 10^\circ$. (The constant slope of the $C_z(i)$ curves should be noted). To reach a C_z of 4 to 4.5 for $\theta_j = 48^\circ$, a C_{μ} of the order of 0.9 would be needed.

The tests results pertaining to the pneumatic flap are satisfactory and provide utilization envelopes, from the lift standpoint, revealing no irregularities. In consequence, this type of flap may be envisaged for use on the helicopter with blown rotor.

Note : The pneumatic flap's relative chord is less than that of the mechanical flap (7.45 % against 16.6 %).

MACH INFLUENCE

In what follows, a study will be made of the C_z variations in terms of the Mach number for different C_μ values.

Mechanical Flap

Figure 156 shows the variations of ΔC_z in terms of C_μ for different Mach numbers and for two test runs in the S₃ Ch wind-tunnel (first test run made with thick lip, second run with thinned-down lip).

The following effects were observed :

at $M = 0.1$, the thick lip increased the lift

at $M = 0.8$, the thick lip proved detrimental

at $M = 0.5, 0.6$, the two types of ^{lip} gave comparable lift.

Figure 157 gives the variations in the overall C_z in terms of Mach number at constant C_μ . The lift drops markedly from Mach 0.9 onwards for large C_μ values: for small C_μ values the drop in lift does not appear before Mach 0.95. No account was taken of the results relevant to Mach 0.76, and since no results were available for Mach values comprised between 0.5 and 0.76 the curves were interpolated.

Pneumatic flap

Figure 159 shows the evolution of the C_z in terms of Mach number for a constant C_μ value.

The aspect of the curves resulting from measurement interpolations is somewhat different from that of the curves pertaining to the mechanical flap. The drop in lift is initiated at as low as Mach 0.7 for $C_\mu = 0.05$.

For both flaps, the C_z decreases as the Mach number increases, the rate of decrease being all the greater as the C_μ value is higher.

The question of Mach number influence is dealt with more specifically in the general conclusions, in conjunction with the effect of the characteristics of the compressed air and a study of the adaptability range of a deflector.

Figures 158 and 160 show that the drop in the coefficient of lift C_z which accompanies an increase in the Mach number is not reflected by a drop in the lift, the value of the latter being proportional to $M^2 C_z$.

/.

To within a factor of 0.340^2 , the scale graduations are proportional to the jet thrust $M^2 C_\mu$ and to the blade lift $M^2 C_z$, both being referred to unit blade area.

The abscissae on these figures are used to represent the values of $M^2 C_\mu$ for different crane type helicopter projects and for a high speed helicopter, respectively.

The broken vertical lines indicate the specific adaptability limits envisaged for each deflector.

The hatched zone is seldom exceeded in practice, and the absolute maximum value of $10^2 M^2 C_\mu$ is of the order of 11.

In Figure 158, the ordinates represent the variation $\Delta C_z M^2$ due to blowing alone. The solid flap effect is not included.

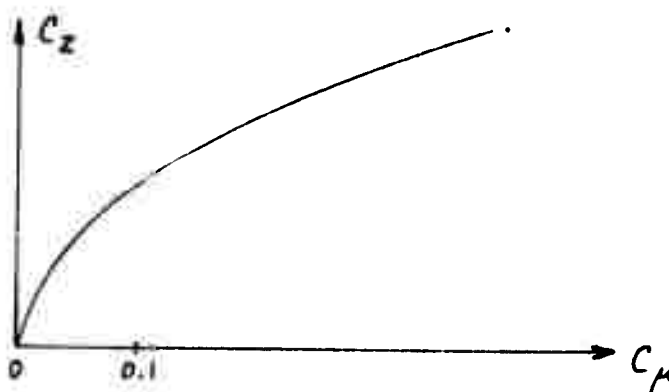
In Figure 160, the ordinates represent the overall variation in $\Delta C_z M^2$ when the deflection changes from $\theta = 0^\circ$ (negative lift) to $\theta = 22^\circ$. The favorable effect resulting from the solid flap becomes apparent when the two graphs are compared.

The ratio of the thrust variation due to flap deflection to the jet thrust, which is of the order of 7 for mechanically-driven helicopters, is of little significance in the case of jet-driven helicopters since the major part of the jet thrust serves to propel the unblown parts of the blade.

INFLUENCE ON BOUNDARY LAYER. SUPERCIRCULATION

Introduction

On the $C_z (C_\mu)$ curves, two regions will be noted : one in which the C_μ values are small and in which the slope decreases, the other extending from small to big C_μ values, in which the slope varies very little.



These two regions determine two flow regimes :

/.

- the first representing the influence on the boundary layer
- the second representing the supercirculation.

Expression for the Lift

The transition point between these two regimes is not clearly defined by the $C_z(C_\mu)$ curve. It is proposed to place it in evidence by expressing the C_z as follows :

$$C_z = C_z(i) + \frac{dC_z}{d\alpha} \alpha + K C_\mu^{\alpha_1} (\theta_j + i) + C_\mu \sin(\theta_j + i)$$

where $C_z(i)$ is the incidence effect without blowing,

$\frac{dC_z}{d\alpha}$ the flap lift for a flap deflection α ,

C_μ the momentum coefficient,

θ_j the jet deflection

and α_1 and K coefficients which it is proposed to determine.

To simplify the expression for C_z , it is proposed to proceed for $i = 0$ and $\alpha = 0$, whence

$$K C_\mu^{\alpha_1} = \frac{C_z - C_z(i) - C_\mu \sin \theta_j}{\theta_j}$$

Taking $K.C_\mu^{\alpha_1}$ in terms of C_μ in logarithmic coordinates, we have

$$\log K.C_\mu^{\alpha_1} = \log K + \alpha_1 \log C_\mu ,$$

thereby providing an equation representing a straight line of slope α_1 having an ordinate value at the origin of $\log K$; whence α_1 and K are determined.

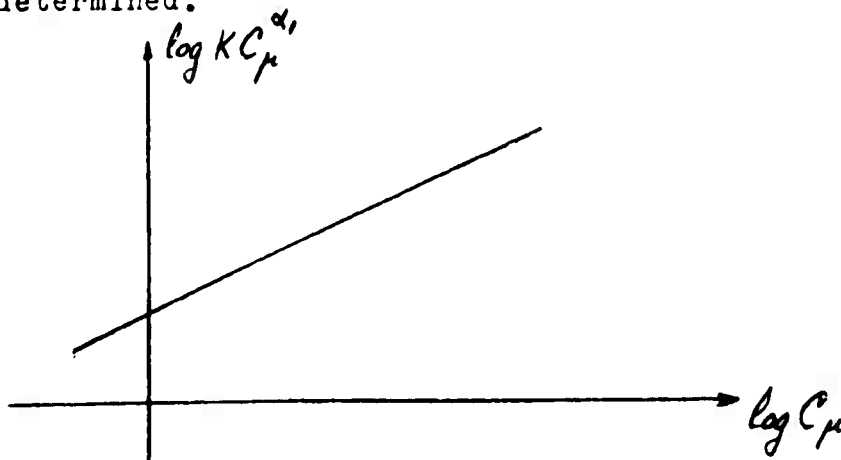
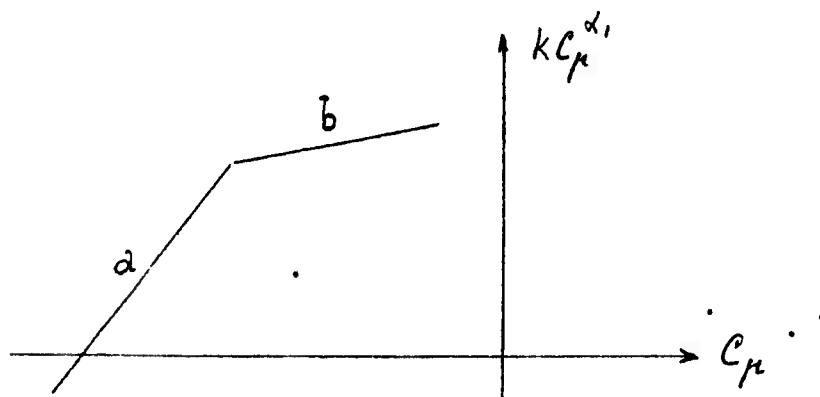


Figure 161 represents these straight lines for different Mach numbers.

For a given Mach number, two straight sections may be noted; these sections are of different slope and different ordinate values at the origin. Thus the two regimes are clearly dissociated.



a = restoration of the boundary layer

b = supercirculation.

EMPIRICAL EXPRESSIONS FOR THE LIFT

Malavart's Expression

The lift is a function only of the blowing momentum C_μ and of the orientation of the jet with respect to the relative flow:

$$\Delta C_z = F(C_\mu)(i + \theta_j)$$

This function $F(C_\mu)$ can be broken down into two functions:

$f(C_\mu)(i + \theta_j)$ representing the influence of the jet on the surrounding fluid

$C_\mu(i + \theta_j)$ representing the vertical projection of the jet reaction.

The lift may be expressed by :

$$C_z = C_z(i) + \frac{dC_z}{d\alpha} \alpha + k \sqrt{C_\mu} \sin(i + \theta_j) + C_\mu \sin(i + \theta_j)$$

where $C_z(i)$ is the influence of incidence on the airfoil section without blowing,

$\frac{dC_z}{d\alpha} \alpha$ the lift on the flap deflected through α ,

C_μ the momentum coefficient,

and K a coefficient to be determined.

/.

Determination of K

Assuming zero incidence for given θ_j and α values, then as long as C_μ remains small, the term $C_\mu \sin \theta_j$ may be neglected.

The expression for C_z may then be written in the form :

$$\frac{C_z - C_z(i)}{\sin \theta_j} = K \sqrt{C_\mu} + \frac{dC_z}{d\alpha} \cdot \frac{\alpha}{\sin \theta_j}$$

If the variations in this expression be plotted against $\sqrt{C_\mu}$, a straight line of slope K and of ordinate value at the origin $\frac{dC_z}{d\alpha} \cdot \frac{\alpha}{\sin \theta_j}$ is obtained.

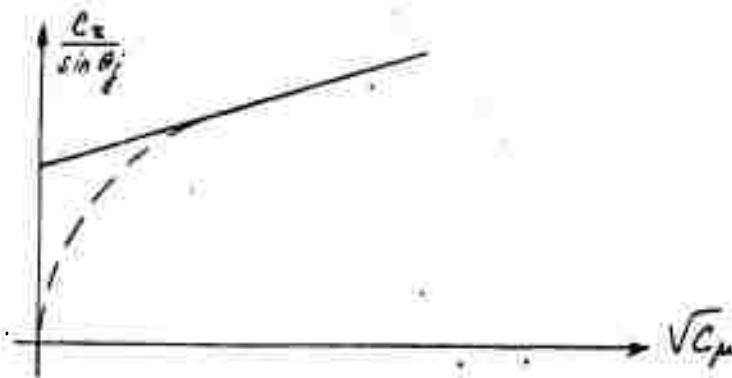


Fig.162 and 163 show the values of the coefficient K and also the flap lift slope for the S₁ Ch and S₃ Ch wind-tunnel tests, for different θ_j values and at constant speed.

From this, the following may be deduced :

- a) For different θ_j values, the straight lines have the same slope

$K = 2.88$ for S₁ Ch tests and 3.86 for S₃ Ch tests.

- b) In the zone of small C_μ values, the values of $\frac{dC_z}{d\alpha} \cdot \frac{\alpha}{\sin \theta_j}$ determine a curve which joins onto the straight line of slope K. In this zone, the slope is steep but then flattens out till it reaches the K slope of the straight line. This is the zone of restoration of the boundary layer, where flap efficiency is low.

Influence of Incidence and Mach Number

This coefficient K determined for zero incidence remains constant in terms of $\sqrt{C_\mu}$ for different θ_j values. With changing incidence, this property is retained, but the value of K is reduced, while with changing Mach number the coefficient K alters in terms of $\sqrt{C_\mu}$ for different θ_j values. Figure 164 shows the evolution of the coefficient K in terms of Mach number; the curves have been extrapolated between Mach 0.10 and Mach 0.60, due to the fact that no test results in this region were available.

Conclusion

The expression given does not seem satisfactory, as the influence of the parameters C_μ , i , M , θ_j lead to fluctuations in the values of K . However, this representation in $K\sqrt{C_\mu}$ form is capable of providing useful indications so long as the speed, the incidence and the values of C_μ remain low.

Spence's Expression

Spence's Theory leads to an expression for the lift of a flapless airfoil section with trailing edge blowing slot that may be written :

$$C_z = \frac{\partial C_z}{\partial i} i + \frac{\partial C_z}{\partial \theta_j} \theta_j$$

The terms $\frac{\partial C_z}{\partial i}$ and $\frac{\partial C_z}{\partial \theta_j}$ are series developments of C_μ , but which will be restricted here to the third term only. Figure 165 gives the values of these coefficients.

$$\frac{\partial C_z}{\partial i} = 2\pi + 1.152 C_\mu^{1/2} + 1.106 C_\mu + 0.051 C_\mu^{3/2} + \dots$$

$$\frac{\partial C_z}{\partial \theta_j} = 3.54 C_\mu^{1/2} + 0.325 C_\mu + 0.156 C_\mu^{3/2} + \dots$$

This expression is valid for non-compressible flows only.

Application to Test Results

This theory was applied to the $C_z(i)$ curves pertaining to the test results obtained from the S_1 Ch and S_3 Ch wind-tunnels. On adding the flap effect at zero incidence to the Spence curves, a comparison may be made between the slopes of the experimental curves and these obtained theoretically.

Figure 166 shows this comparison made in the case of the S_1 Ch wind-tunnel tests.

Figures 167 through 170 show the comparison for the first test run in the S_3 Ch wind-tunnel.

Figures 171 through 175 show the comparison for the second test run in the S_3 wind-tunnel.

These lead to the following conclusions :

- a) So long as the C_μ values remain small (zone of influence on the boundary layer), the slopes match even at high Mach numbers (Figures 165, 166 and 167).
- b) For higher C_μ values, of the order of 0.1 (supercirculation), there is disparity between the slopes (Figures 171 through 175).

/.

Spence's theory agrees with the test results so long as small C_μ values are used (measured in hundredths); for higher C_μ values (measured in tenths) this agreement vanishes.

CONCLUSION

The results of the wind-tunnel tests made on models equipped with a mechanical or a pneumatic flap show that there is adequate lift in the zones of the advancing blade, the centerline and the retreating blade^{and} hence make it possible to envisage the use of such deflector devices on a helicopter rotors provided even with partial blowing only.

EFFECT OF BLOWING ON DRAG

INTRODUCTION

Let us designate by C_{x_s} the horizontal component of the drag coefficient measured with blowing and mark it off on the coefficient of drag C_x .

This component is propulsive and hence negative in the case of jet-flapped, jet-driven helicopters. It is zero in the case of a rotor provided with suitable mechanical assistance to drive the unblown part of the blades. In such cases, the blown airfoil sections are self-propulsive. The component is positive in the case of a mechanically-driven helicopter rotor provided with complementary blowing or utilizing centrifugal circulation of the air in the blades to supply the ejection slits.

To estimate the effect of the blowing on the lift/drag ratio of a jet-flapped blade it is convenient to plot lift/drag curves in which the expression $C_{x_c} = C_{\mu} + C_{x_s}$, where C_{x_c} represents a conventional drag. In this way, practical lift/drag curves may be obtained enabling performance calculations to be made on the basis of the jet thrust without resorting to calculations into which the jet deflection θ_j enters.

EFFECT OF BLOWING (PNEUMATIC FLAP)

Figure 176 gives an example of a practical lift/drag curve (curve I). This lift/drag curve is obtained by offsetting the lift/drag curve with blowing in a positive direction by the value C_{μ} .

The effect of the blowing, in the case of a small jet deflection $\theta_j = 4^\circ$, improves the lift/drag curve as compared to the lift/drag curve without blowing, even in the case where only light blowing is used (curve II) ($C_{\mu} = 0.08$).

Figure 177, which is complementary to Figure 176, shows, expressed as a percentage of the drag without blowing, the evolution in the improvement derived from the drag due to the blowing.

JET DRIVEN ROTOR CONTROLLED BY JET-FLAPS

Schematic Example of the Aerodynamic Behaviour of a High Speed Helicopter Rotor Controlled by Jet-Flaps, in accordance with a periodic pattern of jet deflection whereby the thrust is maintained constant in all azimuths.

Speed : 340 k.p.h. Tip speed : 200 m/sec = ωR

(Slit located at $\bar{r} = 0.7$ to $\bar{r} = 1$).

/.

The table below gives, for $\bar{r} = 0.8$, the azimuthal evolution of C_z for a constant air load :

Blade	Advancing	Centerline	Retreating	Remarks
Mach Number M	0.75	0.47	0.192	
C_μ	0.067	0.17	1.01	
$10^2 M^2 C_\mu$	3.75	3.75	3.75	Jet thrust is constant
C_z	0.196	0.5	3	Constant lift
$10^2 M^2 C_z$	11	11	11	

Optimum Conditions for Aerodynamic Adaptation

Based on Figures 180 to 186, Figures 178 and 179 show the lift/drag curves relevant to the blade elements at $\bar{r} = 0.8$ as they cross the principal azimuth regions (advancing blade, centerline, retreating blade), for the case of the mechanical and pneumatic flaps respectively and jet driven rotors.

It will be seen that, for the C_z values indicated in the table and for C_μ values close to those indicated in the table, the conventional coefficient of drag $C_{x_c} = C_{x_s} + C_\mu$ is near of its minimum both with the mechanical flap and the pneumatic flap.

The conventional drag C_{x_c} of the pneumatic flap is distinctly less than that of the mechanical flap particularly for large θ_j values. This can be ascribed to the following :

- a) Smaller relative chord of pneumatic flap :

$$\frac{l_v}{l} = 0.07 \text{ instead of } 0.16 ,$$

where l_v is the flap chord, and

l the blade chord.

- b) Elastic deformation of the trailing edge, causing uniform alteration of the flap frame curvature in the case of the pneumatic flap.

Moreover, jet deflection is obtained by a swelling of the flap's upper surface. On the other hand in the case of the mechanical flap, the break caused by flap deflection affects the drag.

CASE OF CONVENTIONAL CYCLIC CONTROL (θ_f' constant)

Control via θ_f' serves only to modify the lift.

Cyclic control can be obtained by tilting the hub, the pitch remaining fixed. (Direct control).

Figures 180a and 180b give the lift/drag curves for an aspect ratio of 6.

In order to estimate the profile drag C_{xp} to be used in rotor draft project calculations, the lift/drag curve for an aspect ratio of 6 has been plotted (C_{xi} = induced drag).

$$C_{xp} = C_{xc} - C_{xi} = C_{xs} + C_{\mu} - C_{xi}$$

C_{xp} varies between the following values, for the pneumatic and mechanical flaps respectively :

C_z	Conventional drag	Mechanical flap	Pneumatic flap
0	$C_{xp} = C_{xs} + C_{\mu} - C_{xi}$	0.025	0.01
1.8	" " " "	0.035	0.03

The value of C_{xp} at zero lift ($C_z = 0$) is very high in the case of the mechanical flap due to the fact the latter is deflected upward through 19° .

CASE OF SELF-PROPULSION (Helicopter with mixed power drive)

The lift/drag curve O, A, B, C, D, in Figure 181 (curve I), applying to the mechanical flap, produces junctions between sections of lift/drag curves plotted for θ_f' values increasing from 15° to $52,5^\circ$ when C_z increases from 0.8 to 3.

Curve III gives, by way of indication, the evolution in the incidence i (aspect ratio 6) for each lift/drag curve section.

Curve II gives, for comparison purpose, the improved lift/drag curve in the case of the pneumatic flap.

Curves IV and V give, for the mechanical and the pneumatic flaps respectively, the profile drag value C_{xp} to be adopted in calculations, compared to the induced lift/drag curve for an aspect ratio of 6.

Remarks :

- a) The lift/drag curve is applicable to all blade positions,

from advancing blade (zone OA), through hovering and ascending flight (zone A B) to retreating blade (zone B D).

- b) For large values of C_z , self-propulsion results in less favorable aerodynamic adaptability than propulsion (Figure 178 and 179).

LIFT/DRAG CURVE, AT ZERO INCIDENCE AND VARIABLE θ_j'

Fig.182 gives the lift/drag curves plotted for $i = 0$ by suitably varying θ_j' and C_{μ} .

Curve I relates to the mechanical flap and curve II to the pneumatic flap.

Curves III and IV give the practical drag coefficients C_{xp} to be adopted for draft project calculations in the case of mechanical and pneumatic flaps respectively.

INFLUENCE OF MACH NUMBER

Mach Number Below 0.5 (Pneumatic flap)

The lift/drag curve plotted in Fig.183 for Mach 0.5 is comparable to the preceding lift/drag curves from the practical profile drag standpoint. The tests were performed in the S_3 Ch wind-tunnel with pneumatic flap.

This lift/drag curve relates to the blade as it crosses the centerline.

Mach Number in Excess of 0.8 (Pneumatic Flap)

The graph in Figure 184 compares the lift/drag curves for the blown blade (curves for the blown blade--continuous lines--and the unblown blade--broken lines). The coefficient of drag is lower with blowing than without. In the lift/drag curve relevant to the unblown blade, the C_z max diminishes as M increases while in the case of the lift/drag curve with blowing, the C_z continues to increase. For $C_z = 0.2$ in the case of the advancing blade, $C_{xp} = C_{xc} - C_{xi}$ increases with M as shown below :

M	0.5	0.6	0.7	0.8
C_{xp}	0.012	0.013	0.017	0.021

For $M = 0.8$, the C_{xp} gain is 10% in favor of blowing.

/.

OPTIMUM COMBINATION OF AIRFOIL INCIDENCE i AND
JET-FLAP DEFLECTION θ_j IN THE CASE OF THE ADVANCING
BLADE (Pneumatic flap)

Usefulness of Deflection

High Mach number tests on jet-flapped airfoils have shown that, in order to set back the critical Mach number, it is preferable to operate at a low incidence i and an appropriate flap deflection θ_j . This deflection, however, must not be excessive. This question will now be examined.

Figures 185 and 186 relating to the pneumatic flap give, in terms of C_μ , the evolution in the conventional profile drag coefficient $C_{x_c} = C_{x_s} + C_\mu$ ($A = 6$), for different values of M and θ_j and for $C_z = 0.2$.

The Mach number value $M = 0.8$ relates to the tip of the advancing blade (Fig. 185) while $M = 0.6$ is relevant to the blade section at $\bar{r} = 0.75$ (Figure 186).

Clearly, there is every reason to choose the combination giving minimum values for C_x .

Tip of Advancing Blade

In the case of the tip of the advancing blade, it will be seen it would be appropriate to choose i close to 2° and θ_j included between 5° and 10° . The deflection $\theta_j = 20^\circ$ is excessive.

Flap Adaptation

The pneumatic flap in the tests was studied to simulate a mechanically-driven, jet-flap-assisted helicopter rotor having narrow slits in view of the small extent of blowing used. Since the slots were of small depth the pressure ratio was too high to permit transposition to the case of jet-driven rotors through which large adiabatic power streams in the form of compressed air. (The air pressure ratio P_1/P_0 attained 6).

Jet Stall (See also "General Conclusions")

It may be useful to note the points at which jet stall takes place; these are designated by the letters E (Fig. 185). Stall occurs at higher pressure ratios when the deflection θ_j decreases, due to the fact that the radius of curvature of the guiding surface increases ($4 < P_1/P_0 < 6$).

Despite the fact that the pneumatic flap was not adapted to the jet-driven rotors, its functioning characteristics from the drag point of view remain acceptable.

Section at $\bar{r} = 0.75$

Figure 186 shows that the best combination is

$$0 < i < 1.5^\circ \quad 16^\circ < \theta_j < 21^\circ.$$

A deflection $\theta_j = 29^\circ$ remains permissible despite the fact that it introduces drag due to the flap deflection.

Drag increment ΔC_{x_c} relative to the unblown airfoil section

The optimum is obtained for $C_\mu = 0.04$.

$$0.002 < \Delta C_{x_c} < 0.003$$

$$5\% < \frac{\Delta C_{x_c}}{C_\mu} < 7.5\%$$

This relative advantage will affect the power.

PROPULSIVE EFFECT OF BLOWN PART OF BLADE TIPInfluence of slit depth

It is interesting to examine, for the particular case of the deflectors envisaged, the propulsive effect of the jet emerging from the ejection slits. The jet takes up only the outer part of the blade radius and should in general contribute to propulsion of the unblown blade sections, particularly in the case of jet-driven rotors.

The relative depth s/l of the slit will depend upon the helicopter design, where s is the slit depth and l the airfoil chord.

$s/l = 0.43$ was chosen for the tests, as this seemed a reasonable compromise value between the case of a mechanically-driven helicopter and that of a jet-driven one.

Net drag of a jet-driven helicopter blade airfoil section

Using the tests results and for different azimuthal blade positions and corresponding values for the parameters C_μ , θ_j , i , C_z and Mach number, the drag coefficients and the net drag $\Delta C_{x_s} + C_\mu \cos \theta_j$, were determined in order to show that a gain is obtained which is capable of propelling the unblown part of the blade.

Advancing blade

$$M = 0.8 \quad C_\mu = 0.075 \quad \theta_j = 22.5^\circ \quad i = 2^\circ \quad C_z = 0.4$$

(See Figure 187, curve I),

The ΔC_{x_s} due to blowing is equal to - 0.072.

ΔC_{x_s} is negative, showing that the section is propulsive.

The quantity $\Delta C_{x_s} + C_{\mu} \cos \theta_j$ is also negative (- 0.003); thus a gain is obtained which contributes to propelling the unblown part of the blade.

Blade over centerline (Figure 187, curve II).

$$M = 0.05 \quad C_{\mu} = 0.095 \quad \theta_j = 22,5^\circ \quad i = 4^\circ \quad C_z = 0.60$$

ΔC_{x_s} is again negative (- 0.083).

$\Delta C_{x_s} + C_{\mu} \cos \theta_j = + 0.007$, the net drag, is positive. In this case the section is not propulsive, so that it would be necessary to increase the slit depth in the proportion

$$\frac{\Delta C_{x_s} + C_{\mu} \cos \theta_j}{C_{\mu}} = \frac{0.0077}{0.095} = 0.0812$$

The slit depth would therefore to be 1.63 mm instead of 1.5 mm.

Retreating blade (Figure 188)

$$M = 0.1 \quad C_{\mu} = 0.89 \quad \theta_j = 50^\circ \\ C_z = 2.84 \text{ at } i = 0$$

$$\Delta C_{x_s} = - 0.585$$

$$\Delta C_{x_s} + C_{\mu} \cos \theta_j = - 0.015, \text{ thereby providing a notable gain.}$$

To conclude, it may be said that, in the case of a high-speed, jet-driven helicopter utilizing ^{blowing} over part of the blade, a negative net drag $\Delta C_{x_s} + C_{\mu} \cos \theta_j$ will be obtained for certain azimuthal positions which will contribute to propelling the unblown part of the blade.

JET THRUST RECOVERY

Definition

The concept of jet thrust recovery is defined as the ratio of the net reduction in drag resulting from the blowing to the intensity of the blowing (denoted by C_{μ}):

$$e = - \frac{\Delta C_{x_N}}{C_{\mu}}$$

/.

Conventionally, the value of ΔC_{x_N} is obtained by subtracting, from the drag variation ΔC_{x_B} measured on the balance (with and without blowing), the induced drag resulting from the increased lift due to super-circulation :

$$\Delta C_{x_N} = \Delta C_{x_B} - k_i (\Delta C_z - C_{\mu} \sin \theta_j)^2$$

The value $k_i = 1/\pi A$ of the lift/drag curve coefficient appertains to the aspect ratio used for the test without blowing ($A = 6$).

This defines a pseudo blowing efficiency $(1 + e)$, which is the ratio of the useful jet thrust F_{jv} to the real jet thrust F_{jR} that would be furnished by a conventional nozzle insuring the same fluid momentum but not serving for blowing purposes.

In the calculation pertaining to rotor driving torque, the useful thrust will be given by the relation :

$$F_{jv} = (1 + e) F_{jR} = (1 + e) \frac{\rho}{2} \Delta S V_a^2 C_{\mu}$$

where ΔS is the blade element of area S affected by the blowing, and

V_a the local aerodynamic velocity.

The pseudo efficiency is in certain cases greater than unity, in particular for $\theta_j = 0$, due to the fact that the blowing reduces the profile drag.

Zero incidence

For the sake of simplicity, it is advisable to examine the case of zero incidence ($i = 0$) when plotting the evolution of the pseudo blowing efficiency $(1 + e)$ in terms of C_{μ} . In general, this particular case is at variance with the actual optimum conditions of adaptation.

Figure 189, based on the test run made with the mechanical and the pneumatic flaps in the S3 Ch wind-tunnel, shows the evolution of $(1 + e)$ for different Mach numbers over a range of C_{μ} values, for the advancing blades ($0.5 < M < 0.8$ and $0.01 < C_{\mu} < 0.007$) and the blades crossing the centerline ($0.2 < M < 0.5$ and $0.01 < C_{\mu} < 0.20$).

According to this graph, the pseudo efficiency $(1 + e)$ is not affected by high Mach numbers, particularly in the case of $M = 0.8$ (This is the well known favorable effect of blowing on the drag critical Mach number).

/.

Again according to this graph, the pseudo efficiency $(1 + e)$ varies between 0.9 and 1.0 for the mechanical flap and reaches 1.05 for the pneumatic flap.

Optimum adaptation

The S₁ Ch wind-tunnel test results ($M = 0.1$) were used transposed for infinite aspect ratio, thereby simplifying calculations since there is then no call to introduce the induced drag. The evolution in the pseudo efficiency $(1 + e)$ for the complete range of C_{μ} values was established for both pneumatic and mechanical flaps (Figures 190 and 191, respectively).

Since the tests were performed at a low Mach number, the graphs do not apply to the advancing blade under transonic conditions and are especially relevant to the retreating blade.

For this latter blade, the $(1 + e)$ values are as follows :

	Flap	
	Mechanical	Pneumatic
$1 + e$	0.98	1.02

The upper curves give the best incidence i and jet deflection θ_j combinations in terms of C_{μ} capable of giving these results.

OPTIMUM i AND θ_j COMBINATION FOR A FIXED WING (aspect ratio 6)

Figure 180 defines such a combination, which may serve for guidance purposes when seeking optimum adaptation to a fixed aircraft wing.

In the case of a helicopter rotor, the optimum adaptation referred to before ($A = \infty$) differs from this. Evidently, the rotor's induced drag will have to be taken into account.

CONCLUSION

- Use of jet-flaps at the trailing edge of lifting airfoils provide improved profile drag.

- On the other hand, the propulsive component of the jet is reduced in the proportion $\cos \theta_j$.

- Deflection of the flap may also give rise to an additional
/.

profile drag due to the break in the flap, particularly in the case of the mechanical type.

Simple rules are first proposed to permit rapid performance estimates to be made without laborious calculations.

The power supplied to the rotor is assumed to be that supplied by the non-deflected jet.

In order to take due account of the effects discussed above, an imaginary profile drag varying with the C_z is proposed for each type of rotor and defined for each of the following particular cases :

- Mechanically driven helicopter with partial blowing but jet-flap control

Fig.180a - mechanical flap

Fig.180b - Jet-flap.

The profile drag coefficient C_{x_p} for an infinite aspect ratio is obtained by measuring the difference between the abscisse on lift/drag curves I and II.

- Mixed-drive helicopter

The profile drag coefficient C_{x_p} is given in Figure 181 by curve IV for the mechanical flap and curve V for the pneumatic flap.

- Jet driven helicopters (Fig.182).

Curves III and IV give the coefficient C_{x_p} for the mechanical flap and the pneumatic flap respectively.

In the case of the advancing blades, due account must be taken of the favorable effect provided by blowing on the critical Mach number (Figure 184). The optimum incidence and jet deflection combinations are given in Figures 185 and 186.

In the case of rotors equipping high speed helicopters, the powerful effect of the blowing results in optimum utilization being made, with maximum benefit derived from the blowing (Figure 178 and 179).

Another way of looking at the question is that whereby, in the calculations, the profile drag is adopted without blowing and a pseudo efficiency factor $1/\epsilon$ (which may be greater than unity) is applied to the jet thrust.

/.

Figures 189, 190 and 191 give, in terms of C_{μ} , and for different Mach numbers, the evolution in the pseudo efficiency $1+e$ (which varies from 0.90 to 1.0 in the case of the mechanical flap and from 0.90 to 1.1 in that of the pneumatic flap).

Comparison between mechanical flap and pneumatic flap

The pneumatic flap has a shorter chord length and the deformation of its trailing edge is progressive; this explains why its profile drag is lower than that of a conventional flap and its pseudo efficiency higher.

PRACTICAL TEST CONCLUSIONS

ANALYSIS OF TEST RESULTS

An analysis of the test results has shown that, over a limited working range (moderate Mach number and C_{μ} values), it is possible to apply certain theories to the tangentially blown flaps.

The theory, however, takes no account of the influence of the Mach number and the fluid characteristics. This will be discussed in detail in what follows.

INFLUENCE OF BLOWING-FLOW CHARACTERISTICS

Influence of pressure ratio $\frac{p_1}{p_0}$

All three types of deflector are based on a well-known principle :

A fluid layer meeting a convex cylindrical surface tangentially will, under certain conditions defined below, follow the cylinder wall and leave it after sustaining a certain deflection θ_j .

If the ratio s_j/R_j of the ejection slit width to the cylindrical leading edge radius of curvature R_j exceeds a certain value which depends upon the characteristics of the fluid supplying the slits, the jet splits (stalls) and no longer follows the cylindrical surface.

Curve I in Figure 193 gives, for compressed air at a temperature of 15°C and for different air pressure ratios $\frac{p_1}{p_0}$, the maximum permissible value of s_j/R_j to insure that splitting does not occur.

Influence of compressed air temperature

In applications to real helicopter rotors supplied by air compressors, the air temperature is high ($T = 180^\circ\text{C}$, for $\frac{p_1}{p_0} = 3.8$).

In the case of the tests dealt with in this report, however, the air temperature in the blade plenum chamber was of the order of -30°C .

The compressed air was stored in high pressure reservoirs (300 Kg/sq.cm) close to the wind tunnel and was subsequently decompressed to a working pressure of $1.2 < \frac{p_1}{p_0} < 7$.

By reason of time schedule it was not possible to supplement this specially rigged installation with a heating system for the decompressed air.

The use of icy air instead of hot air in no way affects the validity of the tests, the coefficient C_{μ} being defined by the measured jet thrust F_j :

$$F_j = q S C_{\mu}$$

where S is the area of the model and

q the dynamic wind pressure in the tunnel.

However, the use of icy air brings nearer the point at which the laminar layer is transformed into a turbulent layer, owing to the reduced coefficient of kinematic viscosity.

Thus in the case of air at -30°C , and for a jet-flap geometrical deflection of 45° , the deflection limit at which the jet still follows the deflector is only 22° , whereas it is as much as 45° in the case of the hot flow.

TRUE DEFLECTION θ'_j COMPARED TO THEORETICAL DEFLECTION θ_j FOR COLD AIR

Case of zero wind $V_0 = 0$

For deflection ranging from 0 to 35° , the real deflection is equal to the geometrical deflection, irrespective of what the pressure ratio may be between 1.2 and 4 .

For a subcritical pressure ratio $\frac{p_1}{p_0} = 1.8$, the real deflection θ'_j very closely follows the geometrical deflection (Figure 194).

Influence of wind velocity V_0

Wind velocity, even when moderate ($M=0.1$), provokes a notable reduction in the deflection :

$$\theta'_j = 20^{\circ} \text{ for } \theta_j = 40^{\circ} \text{ (with } 1.75 < \frac{p_1}{p_0} < 3)$$

$$\theta'_j = 10^{\circ} \text{ for } \theta_j = 40^{\circ} \text{ (at } \frac{p_1}{p_0} = 1.25).$$

Increasing the wind velocity V_0 beyond $M = 0.1$ has a less marked effect on the real deflection.

For example, for $M = 0.8$,

$$\theta_j' = 12^\circ \text{ for } \theta_j = 40^\circ \text{ (for } \frac{p_1}{p_0} = 3 \text{ and } \frac{p_1}{p_v} = 4.55)$$

where p_1/p_0 is measured relative to the surrounding atmosphere, and p_1/p_v is measured relative to the wind in the tunnel test section.

For $M = 0.5$ and $\theta_j = 40^\circ$, θ_j' decreases from 22° to 12° when p_1/p_0 decreases from 3 to 1.25 (with p_1/p_v decreasing from 3.45 to 1.44).

As anticipated, for $p_1/p_0 = 4$ and $p_1/p_v = 4.63$, the deflection diminishes suddenly, due to jet stall, and drops to the value $\theta_j' = 12^\circ$.

This systematic reduction in the jet deflection depends essentially upon deflector compatibility and utilization spectrum.

DEFLECTOR MATCHING AND UTILIZATION SPECTRUM

Pneumatic flap matching

The jet-flap tested had been more specifically matched to suit mechanically driven helicopters providing blowing assistance (low pressure ratio : $1.6 < \frac{p_1}{p_0} < 2$; low mass flow; low C_μ).

The aim was to obtain a high $dC_z/d\theta_j$ value for low C_μ values. This aim was fully achieved by taking the following precaution :

The deflecting surface consisted of a sheet-metal cylinder of radius R_j terminating in a trailing edge surface of small curvature forming a solid flap. Total relative chord of the deflecting surface was 7.45 % of the airfoil's theoretical chord

The measurements were pursued up to high pressure ratios ($p_1/p_0 = 6$) and high C_μ values accompanying high M values, the aim being to study the effect of anticipated jet stall in the region of $p_1/p_0 = 4$.

The test results given later show that the blowing effect passes through a maximum for the pressure ratio corresponding to jet stall and then gradually diminishes.

Principle of deflector matching

Technological possibilities

In the case of high pressure ratios it is necessary to increase the flap leading edge radius R_j and, if necessary, reduce the length of the rear part of the flap, thereby enabling /.

the same relative chord to be retained. It is in general preferable to increase the flap chord to over 7 %. It would be possible to go up to 16 % (relative chord of mechanical flap) should it be desired to increase control efficacy.

Matching calculations

It will be required to calculate the minimum radius R_j (corresponding to maximum flap deflection).

Let us consider a jet-driven helicopter rotor supplied by an air compressor feeding air under a pressure ratio p_1/p_0 , at a temperature determined by the compressor's efficiency.

Compressor shaft power per unit area of nozzle cross-section ($\frac{HP}{S_j}$) is defined by the pressure ratio (Curve VI in Fig. 193).

The nozzle area is given by $S_j = s_j \cdot L$ where L is the length of the slit and s_j its width.

The jet thrust per unit area of nozzle cross-section ($\frac{F_j}{S_j}$) is defined by Curve III in Fig. 193.

In the case of a truncated nozzle, the momentum of the ejected fluid $q_m V_j$ is less than F_j , where q_m is the mass flow and V_j the throat velocity. In this case a definition of $\frac{q_m V_j}{S_j}$ is given (Curve II, Fig. 193).

Depending on whether the nozzle provides total expansion or is truncated, C_μ will be calculated on the basis of F_j or $q_m V_j$, respectively.

In the case of the deflector under test, the nozzle was truncated.

Since the length of the blowing slit is imposed by blade design project requirements, and the nozzle area S_j by the power in HP and the pressure ratio, s_j is consequently also imposed.

It now becomes necessary to define the radius of curvature R_j of the flap leading edge.

If we let ℓ be the airfoil chord, then we may write :

$$\begin{array}{ll} \text{Nozzle} & \text{Truncated : } \frac{q_m V_j}{L s_j} = 0.725 M^2 C_{\mu t} \\ & \text{Total expansion : } \frac{F_j}{L s_j} = 0.725 M^2 C_{\mu} \end{array}$$

leading to :

$$\begin{array}{l} \frac{q_m V_j}{L s_j} \cdot \frac{s_j}{R_j} \cdot \frac{R_j}{\ell} = 0.725 M^2 \cdot C_{\mu t} \\ \frac{F_j}{L s_j} \cdot \frac{s_j}{R_j} \cdot \frac{R_j}{\ell} = 0.725 M^2 \cdot C_{\mu} \end{array}$$

whence :

$$M^2 C_{\mu} \frac{l}{R_j} = 1.385 \frac{q_m V_{jt}}{S_j} \cdot \frac{b_j}{R_j}$$

$$M^2 C_{\mu} \frac{l}{R_j} = 1.385 \frac{F_j}{S_j} \cdot \frac{b_j}{R_j}$$

By combining Curves II and III with Curve I of Fig. 193, it is possible to plot the curves V_a and V_b representing $M^2 C_{\mu} \frac{l}{R_j}$ in the case of a truncated nozzle and a total expansion nozzle respectively.

Since, further, $M^2 C_{\mu}$ is imposed, $\frac{R_j}{l}$ can be deduced from it, and hence also R_j .

Pneumatic flap tested at S₃ Ch wind-tunnel

Curves I and II of Fig. 194 represent the calibration performed in the wind tunnel at $V_0 = 0$, to give the correspondence between geometrical flap deflection and jet deflection.

By combining Curve IV of Fig. 194 with Curve V of the Fig. 193, it is possible to plot the graph given in Figure 195 which in turn defines the C_{μ} values corresponding to deflector jet stall for different values of M , as well as the pressure ratios corresponding to jet stall in terms of θ_j .

As an example, this graph shows that for $M = 0.8$ and $\theta_j = 15^\circ$, the jet will split if $C_{\mu} > 0.054$.

For $\theta_j = 50^\circ$ and $M = 0.5$, the jet will split if $C_{\mu} > 0.07$.

Thus, at the limit, the pneumatic flap is still applicable to the cold cycle jet-driven helicopter.

The curves in Figure 195 enable the onset of jet stall to be pinpointed for each test.

Pneumatic flap for high-speed jet-driven helicopter rotor

A pneumatic flap adapted to a high-speed jet-driven helicopter is currently undergoing testing. The pressure ratio considered is $p_1/p_0 = 3.7$.

Compressed air mass flow : 2.8 Kg/sec per linear meter of slit length.

Adiabatic power : 500 GHP per meter of slit length

$M^2 C_{\mu}$ values adopted: $\left\{ \begin{array}{l} 0.04 \text{ for } \bar{r} = 1 \\ 0.025 \text{ for } \bar{r} = 0.7 \end{array} \right.$

Curve I in Figure 196 gives the evolution of R_j in terms of θ_j .

Curves II and III, plotted as before for the case of the truncated nozzle, give the maximum admissible pressure ratio and C_μ values for different values of M in terms of θ_j .

Slit depth is $s_j = 3.5$ mm

Flap chord is $l_v = 45$ mm

This deflector amply covers the working range of the high speed helicopter rotor as defined at the beginning of this report.

In hovering flight, for $M = 0.5$, $C_\mu = 0.16$ (predicted) is attained without difficulty and without jet stall with $\theta_j = 60^\circ$.

In the case of forward flight and for the advancing blade, for $M = 0.8$, the predicted $C_\mu = 0.07$ is attained with $\theta_j = 22^\circ$ (predicted maximum).

EFFECT OF JET STALL ON LIFT COEFFICIENT, IN TERMS OF MACH NUMBER

Figure 197 gives, in terms of C_μ and for $\theta_j = 30^\circ$, the C_z values for five different Mach number values ($M = 0.1, 0.5, 0.6, 0.7, 0.8$).

From Fig.19, the points identifying jet stall have been plotted in and are located along the dotted E_j line. The pressure ratio P_i/P_o corresponding to jet stall is given by $P_i/P_o = 4$ (relative to surrounding atmosphere). Taken in relation to the pressure p_v in the wind-tunnel test section, the ratio P_i/P_v varies from 4.8 to 5.2.

The real deflection θ'_j in the relative wind is substantially half the deflection θ_j (no relative wind).

The points A, B, C, D, E, F, indicate the values of C_μ pertaining to the following types of helicopter rotor :

- (A) natural circulation (NC measurement points)
- (B,C) mechanically driven rotors with partial blowing
- (D,E) jet-driven rotors with total blowing (crane types)
- (F) high speed helicopter jet-driven rotors.

The lift coefficient increment ΔC_z , for a deflection $\theta_j = 30^\circ$ at the instant of jet stall retains the values indicated in the table below :

/.

M	0.5	0.6	0.7	0.8
C_μ	0.075	0.06	0.042	0.035
ΔC_z	0.65	0.5	0.375	0.27
$10^2 \cdot M^2 \cdot \Delta C_z$	16	18	18	16

The corresponding increase in thrust, represented by $M^2 \Delta C_z$, remains unaffected by the Mach number.

The graph in Figure 198 relates specifically to the case of Mach 0.5 relevant to vertical flight.

The points corresponding to jet stall are represented by E_j .

The points A, B, C, D, E, appertain to the rotor types defined above.

It will be observed that within the deflector compatibility spectrum (Projects A, B, C), the efficacy of the piloting effect remains excellent.

As an example, taking the case of natural circulation (points NC), a 30-degree flap deflection θ_j provides a ΔC_z increase of 0.35,

while a deflection $\theta_j = 50^\circ$ results in a corresponding increment of 0.6, which is adequate for deflector-controlled autorotative flight.

Once the zone of lesser jet stability is reached, the curve giving C_z in terms of C_μ for $M = 0.5$ detaches itself from the corresponding curve plotted for $M = 0.1$ and passes through a maximum at the onset of jet stall when a pressure ratio $P/P_v = 4.8$ is reached.

Note

In the case of helicopter rotors with total blowing, it is advantageous to shift the jet stall curve E_j toward the right.

Two methods of achieving this are respectively defined by Curve Va (Fig.193) for truncated nozzle deflectors and by Curve Vb for total expansion nozzles.

The aim is to seek to increase the value of the product $M^2 \cdot C_\mu$ at which jet stall takes place.

Two methods of achieving this are visible on Fig.193.

/.

- A reduction in the pressure ratio from 4.8 (tests) to 3.8 (real rotor) causes the value of the product $M^2 C_\mu \frac{\ell}{R_j}$ to rise from 0.1 to 0.3 (truncated nozzle).

If the radius R_j of the flap leading edge is left unaltered, $M^2 C_\mu$ will be multiplied by 3 when the geometrically similar real deflector is substituted for the test deflector, due to the reduction in the pressure ratio.

- If it is required to still further increase $M^2 C_\mu$ a second method would consist in increasing the radius R_j by modifying the profile of the tested deflector : to this end, the circular portion would be extended almost up to the trailing edge instead of using a circular leading edge followed by a curved rear portion (case of deflector tested for rotor with partial blowing).
- A third possibility would consist in increasing the flap chord, which can be raised from 7 % to 16 % without unfavorable effects.

EFFECT OF JET STALL ON DRAG

Fig.199 and 200 give, in terms of C_μ , the values of the coefficient of drag in a direction parallel to the relative wind, measured with blowing.

Fig.199 was plotted for $C_z = 0.2$ (advancing blade tip, $M = 0.8$).

By way of comparison, the case corresponding to $M = 0.5$ has been plotted on this graph.

Fig.200, which refers to the blade as it crosses an intermediate azimuth between the advancing blade and centerline azimuth, has been plotted for different C_z values between 0.1 and 0.4 and for $M = 0.6$.

On all the graphs, the points E_j corresponding to jet stall, defined by Fig.195, have been marked in.

It was observed that, in all cases, as long as the jet stall condition was not reached, the effect of blowing on the drag obeyed the laws set forth precedingly.

Beyond the stalling points, the drag increases, as is indicated by the sag in the curves.

Note 1

These graphs show that, up to the jet stalling point, the reduction in drag due to blowing offsets the reduction in the propulsive force due to deflection of the jet.

/.

An analysis of the tests has shown that a reduction in drag could be expected as compared to the unblown helicopter.

Note 2

Fig.200 shows that, for $C_z = 0.4$ and $\theta_1 = 25^\circ$, blowing improves drag as compared to the unblown rotor and that it provides the same C_z up to $C_\mu = 0.075$, i.e. beyond jet stall.

GENERAL CONCLUSIONS AND SYNOPSIS

An analysis and interpretation of the measurement data have shown that control by jet flap deflector can be effectively applied to the various helicopter rotor projects as classified below :

- Mechanically-driven helicopters with natural (A) or partial (B) (C) blowing
- Jet-driven crane helicopters (D) (E)
- High-speed jet-driven helicopters (F).

The analysis brought the following to light in particular :

Control by jet flap makes it possible to insure constancy of the thrust exerted on the blades over all azimuths, by creating suitably high lift coefficient values for the retreating blade.

The leading blade Mach number can be increased thanks to blowing, without fear of compressibility effects.

Piloting by jet deflector is effective even when natural blowing is used.

Recapitulative graphs

The conclusions reached from the analysis are contained in the various sections of this report. By way of conclusion, an overall picture of the main results obtained is presented in the form of recapitulative graphs.

The analysis dealt in particular with the more classic question of the mechanical flap type of deflector. The synthesis graphs, however, will be based on the test results obtained with the pneumatic flaps.

Despite the small relative chord (7 %), the pneumatic flap offers a degree of efficiency, from the standpoint of increased lift, comparable with that of the mechanical flap, the relative chord of which is 16 %.

In addition, it offers reduced profile drag.

It provides accurate, virtually instantaneous pneumatically slaved control at the cost of a small mass flow of compressed air employed at a pressure below ejection slit feed pressure.

It has virtually no inertia and is capable of faithfully reproducing the patterns of multicyclic control to insure azimuthal constancy of thrust.

Its universal utilization possibilities makes it applicable to all the rotor projects enumerated previously.

A number of results which were not placed in evidence in the sections dealing with the analysis of the tests are grouped together below in systematic fashion.

Preliminary remark concerning the characteristics of the fluid feeding the ejection slits and their effect on the results.

In the case of flying rotors, the pressure ratio of the feed air varies from 1.5 to 3.8 and the temperature from 80° to 180°C in the case of the cold cycle. In the case of the hot cycle, the temperature attains 450° C.

In the case of the tests performed in the S₃ Ch wind-tunnel, the air temperature was of the order of - 30° C, while the pressure ratio p/p_0 had to exceed 6 in order to achieve a C_{μ} value of 0.07 with $M = 0.8$ in the case of the high speed helicopter. Such abnormal fluid characteristics, which were imposed by circumstances, in no way affect measurement standards; however, they

/.

do influence the conditions under which the fluid layer follows the guiding surfaces, firstly due to the use of very cold air, secondly because of the high pressures.

The point of transition of the laminar flow into a turbulent flow moves closer to the ejection slit and entrainment of the fluid layer along the length of the curved surface becomes less stable, firstly due to the use of high pressures, secondly because of the increased centrifugal force exerted along the length of the guiding wall on particles of a fluid made denser by its very low temperature.

Contrarily to the warm layer, this extremely cold fluid layer is consequently in a state of almost indifferent stability similar to that which characterized the functioning principle of the spoiler type deflector which proved sensitive to external influences, for example to the wind-tunnel flow which caused a marked reduction in the deflection of the layer of air, thereby producing an effect opposite to the deflection effects of the spoiler.

The result of this substitution of an icy fluid (-30°C) for a hot fluid (180°C), in conjunction with a substantial increase in the pressure of the compressed air, is reflected by a reduction of the true jet deflection when the wind tunnel is started up. Due to the extent of the tests and the delays involved, it was not possible to perform tests with a slit of greater relative thickness (e.g. 0.75 % instead of 0.45 %, which would have lowered the pressure ratio).

True deflection θ_j' in the relative wind

The jet deflections θ_j marked on all graphs represent those obtained without relative wind and with a pressure ratio of 1.8 (See Fig.194). These experimental deflections are substantially equal to the predicted deflections θ_j , the jet emerging tangentially to the trailing edge of the deflecting surface.

By way of complementary data, the values of the true deflection θ_j' are shown on graphs of Fig.202. In this case, the real deflection value was markedly at variance with the theoretical deflection θ_j . This Figure illustrates that when the conditions for which the jet deflector is matched (partially blown rotors) are not observed, θ_j' comes out at approximately $\frac{\theta_j}{3}$.

Methods under development for increasing the deflection θ_j'

Notwithstanding the fact that the results obtained are satisfactory and applicable to different rotor projects, it is evidently preferable to increase the deflection θ_j' and oblige the jet to follow the guiding surface up to the latter's trailing edge, thereby enabling the blowing efficiency to be increased or the geometrical deflection angle θ_j to be reduced in cases where the blowing effects is more than ample.

Two methods are envisaged :

- To use warm fluid and restrict the pressure ratio to 3.8.
- To adapt the profile of the deflector to the aim sought in each project, on the basis of the data given above.

With a view to evolving total deflection deflectors ($\theta'_j = 0_j$), even in the case of high pressures, a test program was established in agreement with the O.N.E.R.A. and the Saclay Test Center. This program aims at using visualization techniques in a wind-tunnel being built specially for the purpose to permit the experimental testing in the near future, under conditions simulating reality, of a deflector designed for adaptation to a high speed helicopter rotor (*) supplied with compressed air at high pressure ($P/P_0 = 3.8$).

The compressed air is to be produced by two TURBOMECA "PALOUSTE" engines and the Mach number in the wind-tunnel is to reach 0.8.

Following these developments, aerodynamic measurements will be made in the O.N.E.R.A. S₃ Ch wind-tunnel, using compressed air at different temperatures.

Data summarizing graphs

Pneumatic flap (case of zero incidence $i = 0$)

Low C_μ values (Figure 201)

The A, B, C, D, E, indications given at the bottom of the graph refer to the different types of rotor defined precedingly, for the case of vertical flight or for that in which the blades cross the helicopter centerline.

Moderate and high C_μ values (Figure 202)

It is to be noted that θ'_j/θ_j begins to decrease when C_μ increases; for $C_\mu = 0.17$ its value drops to 0.75. This occurs in the case of the high speed helicopter, which falls outside the adaptation range of the deflector.

The C_μ values of the retreating blade, for each specific project, are given at the bottom of the graph.

In the case of Project F, which falls outside the adaptation range, θ'_j attains no more than half θ_j . The use of warm air instead of icy air, if necessary in conjunction with special /.

.....

(*) This rotor is an experimental model intended for testing in the big wind tunnel facility at the Ames Research Center and for which the U.S. Army has placed a contract.

matching of the deflector, will enable the measured value ($C_z = 3$) to be doubled for $C_\mu = 1$. Such matching will further enable flap angle of deflection θ_j and flap drag to be both reduced. ($C_z = 3$ was found adequate for $i = 0$ when the analysis was made, for if $i = 0$ with an infinite aspect ratio, then C_z reaches 3.6 for $\theta_j = 47^\circ$.)

Control efficacy by deflector

Efficacy varies to a small extent with θ_j . Fig.202 refers to control with a deflection of around $\theta_j = 30^\circ$. This Fig.203 gives the control efficacy defined by $dC_z/d\theta_j$ in terms of C_μ , for different Mach values.

$dC_z/d\theta_j$ diminishes little as M increases from 0.1 to 0.5 but then diminishes rapidly as M rises from 0.5 to 0.8.

No disadvantages are attached to this decrease, since the product $M^2 \cdot dC_z/d\theta_j$, which represents the effect on vertical thrust, practically does not vary as M increases from 0.5 to 0.8.

It is instructive to compare $dC_z/d\theta_j$ with dC_z/di . Without blowing, the experimentally measured value of dC_z/di is of the order of 0.08 for $C_\mu = 0$ and $M = 0.5$.

The aspect ratio of the model was in region of 6.

In hovering flight ($M = 0.5$), the ratio $\frac{dC_z/d\theta_j}{dC_z/di}$, which compares the efficacy of blade pitch control (without blowing) with that of flap control (with blowing), varies between 4 (Rotor A) and 2.5 (Rotor F).

This ratio varies between 3 (rotor A) and 1.3 (Rotor F) for the retreating blade.

Control efficacy in the event of engine failure and in the case of natural centrifugal circulation (Fig.204)

Pressure of the air feeding the slits was adjusted so as not to exceed 70 % of the dynamic pressure of the air flow in the wind-tunnel test section.

Control efficacy came out as follow :

M	0.5	0.7
$\frac{dC_z}{d\theta_j^\circ}$	0.014	0.013

To fix ideas, a flap deflection variation of $\Delta\theta_j = 5.5^\circ$ corresponds to blade pitch variation Δi of 1° .

Effect of blowing alone (without solid flap effect)

Comparison between flaps A1 and A2.

The graph in Fig.205 shows the difference in the measurements made, in the case of both types of flap A_1 and A_2 , for $i = 0$ and for different values of θ_j , with and without blowing (2nd test run).

The tests were performed for different values of M and refer to the mechanical flap A_1 and the pneumatic flap A_2 .

For the small C_μ value ($C_\mu < 0.03$) used for projects A, B, C, for which the flap was matched, Mach Number effects between 0.2 to 0.8 are not marked.

On the other hand, for higher C_μ values (high speed helicopter) the upper graph shows that the ΔC_z due to blowing, at $C_\mu = 0.11$, varies little as the Mach number increases from 0.2 to 0.5, but that it then drops abruptly and tends to vanish as M approaches unity.

It is important to note that the product $M^2 C_z$, representing the true thrust variation, changes little as M increases from 0.5 to 0.85.

SHIFT IN CENTER OF THRUST

As will be seen in Appendix, tests showed the existence of two centers, defined physically as follows :

- 1) With zero flap deflection and an airfoil section assumed symmetrical, if the incidence i is modified the thrust will be applied substantially at 25 % chord (measured from leading edge).
- 2) With zero incidence i , if flap deflection be modified, then regardless of the C_μ value, the thrust will be applied substantially at 50 % chord.

If operational needs require the center of thrust to remain stationary, then, starting from zero incidence and the given flap deflection, both the incidence and the flap deflection θ_j will have to be increased in equal proportions.

Even if blade pitch remains fixed in the case of a helicopter in forward flight, it will be appreciated that it is possible to combine direct control (by forward tilting of the rotor shaft) with control by jet-flap to achieve this end with a sufficient degree of approximation.

DEFLECTOR CLASSIFICATION AND FINAL CONCLUSIONS

Deflector classification by order of efficacy is as follows:

/.

- 1) Pneumatic flap (best lift/drag ratio and good efficacy).
- 2) Mechanical flap (good efficacy).
- 3) Deflectors using spoilers or auxiliary jets (limited efficacy).

The pneumatic flap provides universal utilization possibilities. It represents an instantaneous-response slaved control devoid of play or inertia, capable of reproducing all multicyclic control patterns.

In order to arrive at a valid comparison between the mechanical flap and the pneumatic flap--each tested in two wind tunnels (subsonic S_1 Ch and transonic S_3 Ch)--a unique relative slit depth was adopted ($\delta/l = 0.45\%$), providing compromise compatibility between the partially blown and the fully blown rotors.

In the case of the fully blown rotor, this resulted in the compressed air pressure ratio being roughly double the maximum value envisaged in practice ($P/P_0 = 3.8$). In addition, the compressed air was extremely cold, being at -30°C instead of 180°C .

Due to the characteristics of the compressed air supplied during the S_3 Ch transonic wind-tunnel tests, jet entrainment stability was affected.

At zero wind speed, the fluid layer followed the deflecting surface fairly closely and emerged from its trailing edge tangentially even when high pressure ratios were involved.

In the wind-tunnel relative flow, the jet sheet lifted quite considerably to the detriment of increased C_z , at high C_μ or Mach number values, or more precisely at high $M^2 \cdot C_\mu$ values corresponding to high pressures.

Despite the unfavorable test conditions (laminar airfoil section and compressed air characteristics) results proved excellent in the case of partially or naturally blown rotors, and good though perfectible, in the case of fully blown rotors notwithstanding the fact that jet-flap had been matched for moderate blowing only.

It is interesting to note that the slope of the lift/drag curves remains unaffected by jet lift as long as the pressure ratio of the compressed air remains below the critical value corresponding to the onset of jet stall.

The effect of blowing on the lift coefficient can be increased in the case of the high speed helicopter rotor by using a more favorable true compressed air temperature at a more moderate pressure ($P/P_0 = 3.8$) and by matching the flap accordingly.

Testing is being pursued along these lines.

/.

APPENDIX

ANALYTICAL DETERMINATION OF THE AERODYNAMIC TORSION MOMENTS ACTING ON A JET-FLAPPED ROTOR BLADE AND METHODS OF DEALING WITH SUCH MOMENTS ON A BLOWN BLADE STRUCTURE

INTRODUCTION

Jet-flap control and propulsion, on the one hand requires a modification of the blade structure which has to include a duct intended to carry the compressed air from the root of the blade towards its tip and a slit located in the trailing edge of the blade, generally along its outer portion and, on the other hand, introduces a modification of the air loads acting on the blade.

The blade torsional stiffness and the pitching aerodynamic moments are thus modified and it is the object of this section to study the effects of this double modification.

STRUCTURAL REQUIREMENTS

The width of the ejection slit which is located roughly along the outer 30 % of the blade, at its trailing edge, represents a few per cents of the blade chord.

This slit is situated at the upper part of the trailing edge of the blade member in front of the flap which has a depth of 4 to 20 % of the blade chord.

The flap has to be controlled from the rotor head and suitable controls have to be provided and located inside the blade structure.

The ejection slit is partly stopped by cross-members (braces) which increase the torsion stiffness of the blade and prevent deformation of the slit width which would lead to undesirable variations of the blown air mass flow.

However, this partial stopping of the slit gives rise to head losses and a compromise has thus to be found between the torsion stiffness requirements and the lifting capability of the system.

If l_s designates the stopped portion of the slit and l_o its open portion, the lifting efficiency of the slit as compared to a continuous open slit is given as follows :

l_s/l_o	0	25%	50%	75%
Lifting efficiency	100%	79%	63%	50%

Spanwise, two different structures are to be considered for the blown blade :

- the inner portion from $\bar{r} = 0$ to approximately $\bar{r} = 0.6$ or 0.7 ,
- the outer blown portion, beyond the previous limit, up to the tip.

Inner non-blown portion of the blade

The structure of this portion (Taken apart the blade root which, owing to the fact that the blown blade is fixed in pitch, is of simpler design) is not very different from the structure of a conventional blade.

This portion incorporates however a duct for the compressed air. This duct may be the hollow spar of the blade.

Compressed air characteristics and power requirements lead to the following considerations for the configurations of the duct :

- the cross section must be the larger possible in order to decrease head losses,
- for a given cross section of elliptical form head losses vary in a large way when the ratio between the two axes of the ellipse is in the range of 0.10 to 0.25.
- if the temperature of the compressed air is high there is an additional advantage to reduce losses by reverberation. Owing to this the duct cross section should be the closer possible to a circle, and this leads to increase the relative thickness of the blade airfoil section.

Pressure requirements and problems of dilatation due to temperature may also lead to consider :

- the use of several ducts instead of a single duct,
- the use of cylindrical ducts or at least approaching as closely as possible a circular cross section.

The consequences of these considerations may be summarized as follows :

- The relative thickness of a blown blade should be larger than that of a conventional blade.

Relative thicknesses of 15 to 20 % are to be considered.

- The torsion and bending stiffnesses of a blown blade are increased with respect to a conventional blade.
- The weight of a blown blade is also increased even if the compressed air duct is structurally active.
- The center of gravity of such a blade section (if no weight is added at the leading edge) is located between 30 and 35 % of the blade chord.
- The shearing center is located approximately between 25 and 35 % of the blade chord.
- The moment of inertia in torsion is increased.
- The torsion and bending natural frequencies of this portion of the blade are not noticeably modified with respect to a conventional blade structure.

Outer blown portion of the blade

This portion of the blade is a cylindrical box beam opened along one of its sides (slit) and its rigidity is thus largely decreased. The shearing center of such a section is located in front of its leading edge.

The presence of air deflectors (deflection of the air flow towards the ejection slit) and reinforcement of the edges of the slit permit to increase the initial rigidity of this portion of the blade and to bring the shearing center inside the section.

This leads however to push the c.g. of the blade section beyond the 25 % limit, unless a counterpoise is provided in the leading edge.

In any case the weight of this part of the blade is increased in comparison with a conventional structure and its natural bending and torsion frequencies are lowered.

DETERMINING THE TORSION RIGIDITY AND THE SHEAR CENTER IN AIRFOIL SECTION MODELS WITH A TRAILING EDGE SLIT

GENERAL

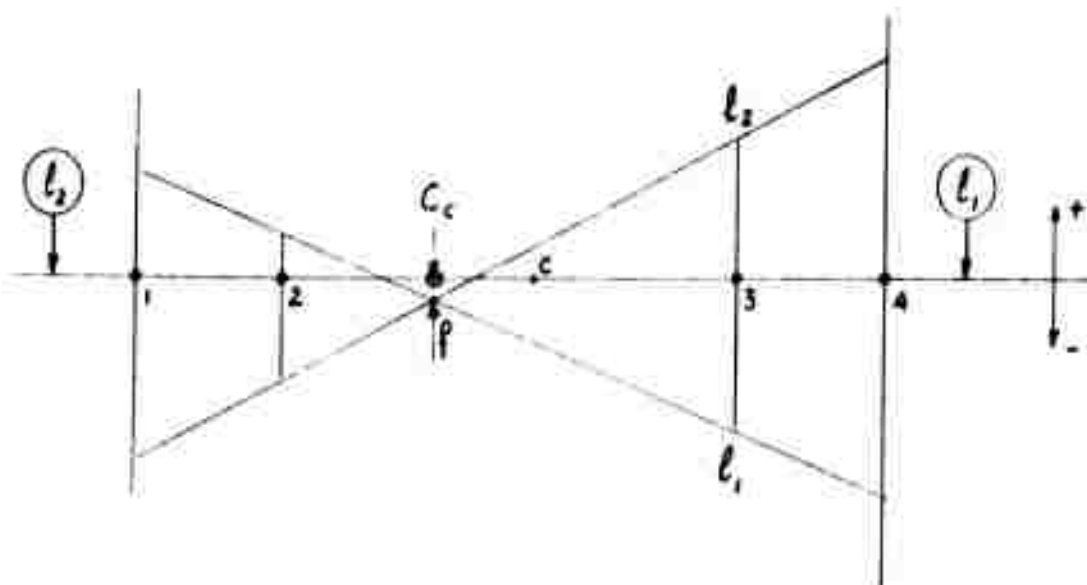
Torsional tests were performed on a steel blade spar model (see Figures 206 and 208) provided with a longitudinal slit strengthened by means of braces. Both the spacing of the braces and the inertia of the slit were varied in order to measure the influence of these two factors on the rigidity of the section and on the position of the shear center.

Method Used for Tests

One end of the model was clamped fast and the free end rendered integral with a rigid bar drilled with four holes arranged symmetrically in relation to the computed shear center of the closed section (see Figure 207). The twisting moments were applied by means of weights hung from the level of each hole in turn, so that the section was subjected to combined twisting and bending. A comparator placed at each end of the bar was used to measure the deflection.

Determination of the Shear Center and the Flexural Rigidity

The weights were hung from holes 1, 2, 3 and 4 in turn and the corresponding deflections at the two comparators plotted. The sag and the location of the shear center at the intersection of the two curves were then determined, as shown in the diagram below.



Knowing the sag, the flexural rigidity of the cantilever beam can be deduced as follows :

$$EI = \frac{PL^3}{3f}$$

Where P is the force applied to the section,

L the length of the beam,

I its moment of inertia

E the modulus of elasticity and f the sag.

Repeating these measurements for different weights enables the sag to be plotted against the weight, thereby furnishing a mean value for the flexural rigidity.

Determination of the torsional rigidity and the angular deflection

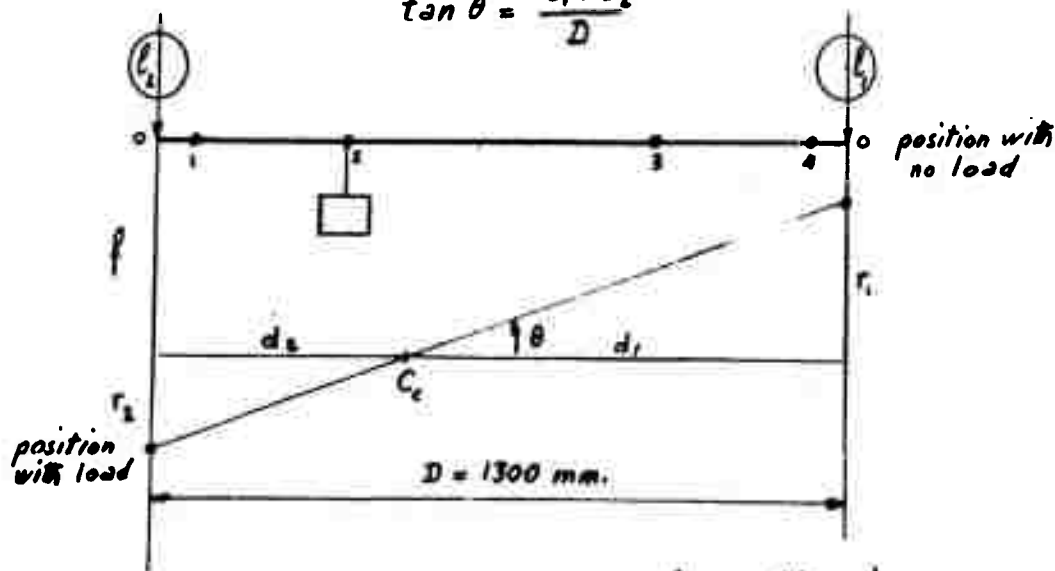
The angular deflection θ of the section was determined for each position of the weight.

Let l_1 and l_2 be the deflections read at each end of the bar, the sign + being used to designate upward deflection of the comparator feeler.

Let D be the distance between the two measurement points.

The angular deflection θ is then given by

$$\tan \theta = \frac{l_1 + l_2}{D}$$



f : sag
 r : twist

$$l_2 = -(f + r_2)$$

$$l_1 = -(f - r_1)$$

$$\tan \theta = \frac{r_1}{d_1} = \frac{-r_2}{d_2} = \frac{r_1 - r_2}{D} = \frac{l_1 + l_2}{D}$$

The torsional rigidity is defined by

$$GK = \frac{M}{\frac{d\theta}{dL}}$$

where M = twisting moment applied to the section

G = modulus of elasticity in shear

K = a torsional constant

$\frac{d\theta}{dL}$ = angle of twist per unit length.

The angle of twist θ of the section and the twisting moment were both computed for each weight and for each position of those weights. The curves obtained by plotting θ against M then enabled a mean value to be determined for GK.

During the tests, the spacing for the braces was varied as shown in Figure 206 and the inertia of the slit was increased in varying degrees by the use of reinforcement brackets of different size :

- 1) - bracket without flange, thickness 1.5 mm
- 2) - bracket with flange of : 10.5 mm wide
- 3) - bracket with flange of : 5.5 mm wide
- 4) - bracket as per (2) above boxed over with sheet metal.

The results obtained are tabulated in Figure 208.

Note

Some of the results are at variance with the overall pattern: it is clear that the rigidity of the beam and the value of the flexural rigidity must decrease :

- a) - with increasing spacing between the braces
- b) - with decreasing inertia of the slit.

The discrepancies in some of the results stem from , the fact that in order to alter the brace spacings and the degrees of strengthening used for the slit it was necessary to remove the beam from its housing and withdraw the fixing bolts used for the braces and the brackets; thus the conditions of assembly and tightening up varied from one test to the next, which in turn introduced minor errors into the measurements.

Variation in the Rigidity

The rigidities GK were correlated to the rigidity of the beam with full stiffening, so that the ordinates were used to represent the ratio GK/GK_0 , which varies between $+ \epsilon$ and 1.

In order to find a non-dimensional coefficient in terms of EI and α , and of the spacing between the braces ($\alpha = \ell_0/L$).

where ℓ_0 is the free length between two braces and

L is the distance between the free and clamped ends of the beam

the location of the shear center of an open section with braces along the length of the slit was expressed by calculation.

These calculations showed that the location of the shear center of such a section may be expressed in terms of :

1) - the ratio of the flexural inertia contributed by the strengthening means to the inertia of the open section without strengthening means,

2) - the cube of the lengths ratio $\alpha = \frac{\ell_0}{L}$,
where;

L is the total length of the beam and

ℓ_0 the free length between 2 braces .

The abscissae were used to represent the values of the non-dimensional coefficient.

$$\beta = \frac{\frac{\ell_0^3}{EI_c}}{\frac{L^3}{EI_t}} = \frac{EI_t}{EI_c} \cdot \alpha^3$$

where : EI_t total inertia of the section, determined experimentally

EI_c flexural inertia of the reinforcement (computed).

The curve representing the variations of GK/GK_0 in terms of β is given in (Figure 209).

Location of Shear Center

The locations of the shear center of the open section C_0 (no braces, no reinforcement) and of the closed section C_f (no reinforcement, but with braces) were determined by calculation. The value 1 was assigned to the distance $C_0 C_f$. The ordinate was used to represent the ratio C/C_0 , where C is the shear

center of an arbitrarily chosen section. The abscissa represented the coefficient β .

This gave the curve shown in Figure 210, which covers the results.

Conclusion

It is practically possible to insure a fairly equivalent torsional rigidity in a beam embodying a longitudinal slit as that provided by a closed beam, by means of braces disposed in the slit and reinforcements of the slit edges.

AERODYNAMICAL TORSION MOMENTS AND INERTIA FORCES TORSION MOMENTS

ANALYSIS OF AERODYNAMIC RESULTS IN CONNECTION WITH TORSION MOMENTS IN A BLOWN AIRFOIL SECTION

Procedure followed

An examination of the test results giving C_m in terms of C_z shows that the moments vary but little with the angle of incidence i .

The coefficient C_m is consequently proportional to the difference between the total C_z and the C_z that would be measured were the angle of deflection θ_j of the air jet to be zero, all other things being equal. Indeed this difference is independent of i in the regions of linear variation of C_z in terms of i .

This is tantamount to assuming the existence of a center of thrust for the forces resulting from $C_{z(t)} - C_z(\theta_j = 0)$, and of a center of thrust which is located in the neighborhood of the balance arm for the forces resulting from $C_z(\theta_j = 0)$ and which is analogous to an aerodynamic center located at quarter chord in a non-blown airfoil section.

Two methods were used for the analyses :

Method A

It was assumed that the coefficient C_m may be expressed by :

$$C_m = \bar{a} C_{z(\theta_j=0)} + \bar{b} [C_{z(t)} - C_{z(\theta_j=0)} - C_{z(r)}] + \bar{d} C_{z(r)}$$

where : $C_{z(\theta_j=0)}$ is the C_z that would be measured were θ_j to be zero, all other things being equal,

$C_{z(t)}$ the total C_z read off the diagram obtained from the measurements, and

$C_{z(r)}$ the fraction of the C_z due to the reaction of the jet.

In other words, the existence of three centers of thrust was assumed here, the jet reaction forces (considered separately) being applied to one of those centers (taken to be stationary in the middle of the flap).

The coefficients \bar{a} , \bar{b} , \bar{d} , are the non dimensional abscissae (related to the chord length ℓ) of the centers of thrust, the origin being the balance arm.

The corresponding value of \bar{d} was fixed at 0.64.

Method B

The coefficient C_m is given by the formula

$$C_m = \bar{a} C_{z(\theta_j=0)} + \bar{b} [C_{z(t)} - C_{z(\theta_j=0)}]$$

In other words, all the lift forces resulting from $C_{z(t)} - C_{z(\theta_j=0)}$ are assumed applied at a unique center of thrust.

Tests in S₁ Oh Wind Tunnel

These tests were performed on a model of laminar airfoil section with a chord length of 1 meter, a span of 2 meters and equipped with a blown flap extending over 16,5 % chord, the model being placed between panels. The balance arm was located at 25 % chord from the leading edge. The relative wind speeds (15 and 22 m/sec) corresponded to Mach Numbers below 0.10 and to Reynolds Numbers of 0.7 to 1.0×10^6 .

Analysis of results by Method A

The $C_m - \bar{d} C_z(\mu)$ curves were drawn for i , M , C_μ constant and θ_j variable. Neglecting measurement and reading errors, these curves can be regarded as straight lines. This means that the coefficient \bar{b} does not depend upon θ_j to any appreciable extent.

The coefficient \bar{b} is little dependent upon C_μ , as shown in the following table :

C_μ	\bar{b}
0.09	- 0.264
0.22	- 0.253
0.70	- 0.242

The values of the coefficient \bar{a} are given in the table below :

C_μ	\bar{a}
0.09	0.025
0.22	0.040
0.70	0.035

The formula :

$$C_m = \bar{a} C_{z(\theta_j=0)} + \bar{b} [C_{z(t)} - C_{z(\theta_j=0)} - C_{z(r)}] + \bar{a} C_{z(r)}$$

was applied for calculation of the moments from the lift forces.

All values for the various coefficients of lift entering into this formula are values read off the diagrams in the test reports.

It will be seen that the C_m values calculated in this way agree very well with the experimental values in the region limited by the $C_{z(t)}$ maxima.

The preceding method therefore remains valid outside the area of linearity of the C_z in terms of i .

By way of example, the moments pertaining to $C_\mu = 0.22$ and $V_o = 22$ m/sec were recomputed and entered onto diagram in Figure 211.

Analysis of results by Method B

The C_m curves were drawn for i, M, C_μ constant and θ_j variable. The curves obtained are again straight lines. The coefficient \bar{b}_i varies with the C_μ as shown in the table below :

C_μ	\bar{b}_i
0.09	- 0.285
0.22	- 0.30
0.70	- 0.33

The values of \bar{a} are the same as those calculated by the first method.

It may be noted that \bar{b}_i increases with C_μ , as opposed to the \bar{b} coefficients computed by method A,

This suggests that the coefficient \bar{d} is equal neither to 0 nor to 0.63, but to some intermediate value.

In both methods, \bar{b} does not depend upon θ_j . For a given C_μ , the lift forces ascribable to blowing and those due to the jet reaction are both proportional to $\sin \theta_j$. It is thus not surprising that the independance of the \bar{b} with respect to θ_j in one method should lead to independance of the \bar{b} with respect to θ_j in the other method.

The moments pertaining to $C_\mu = 0.22$, $V_0 = 22$ m/sec were also recomputed and entered onto diagram of Fig. 211.

Tests in S₃ Ch Wind-Tunnel

These tests refer to a model of laminar airfoil section having a chord length of 0.317 m and a span of 0.440 m and equipped with a flap over 16.5 % of chord length. The balance arm was located at 25 % chord from the leading edge. The model was placed between panels, and the relative wind speed ranged from Mach 0.10 to Mach 0.80, corresponding to Reynolds Numbers extending from 800,000 to 4,000,000.

Analysis of test results by Method A

At Mach 0.10 the curves $C_m - \bar{d} C_{z(r)}$ are straight lines which do not pass through the origin. According to method A the expression of the moment is :

$$C_m = C_{m_0} + \bar{d} C_{z(\theta_j=0)} + \bar{b} [C_{z(t)} - C_{z(\theta_j=0)} - C_{z(r)}] + \bar{d} C_{z(r)}$$

At all Mach Numbers, C_{m_0} comes close to 0.006.

The coefficient \bar{b} decreases as C_μ increases, for Mach 0.10. It increases with C_μ for Mach 0.70 and remains independant of C_μ for Mach 0.60 and Mach 0.80. In no case does it vary by more than 3 %.

The table below gives the mean values of \bar{b} in terms of the Mach Numbers :

Mach	0.1	0.6	0.7	0.8
\bar{b}	0.202	0.251	0.282	0.339

Figure 212 shows the shifts of the center of thrust \bar{b} in terms of Mach Number.

The coefficient \bar{a} is more often than not equal to zero or is slightly positive by a quantity that is difficult to appreciate.

The moments were calculated by this method for

$$M_o = 0.10 \quad \theta_j = 59^\circ \text{ (Figure 213) }$$

$$M_o = 0.70 \quad \theta_j = 30^\circ \text{ (Figure 214) }$$

Analysis of test results by Method B

The C_m curves are straight lines which do not pass through the origin. In all cases there exists a constant moment close to 0.006, probably due to a zeroing error.

The coefficient \bar{b} always increases with C_μ .

The table below gives the mean values of \bar{b} in terms of the Mach Number.

Mach	0.1	0.6	0.7	0.8
\bar{b}	0.231	0.262	0.228	0.336

Figure 212 shows the shifts in the center of thrust b in terms of Mach Number.

The moments were calculated by this method for the following values :

$$M_o = 0.10 \quad \theta_j = 59^\circ \text{ (Figure 213) }$$

$$M_o = 0.70 \quad \theta_j = 30^\circ \text{ (Figure 214) }$$

Conclusion

In the C_μ and C_z area explored, the most accurate formula for expressing the moment about the axis of suspension is :

$$C_m = C_{m_o} + \bar{a} C_{z(\theta_j=0)} + \bar{b} [C_{z(e)} - C_{z(\theta_j=0)} - C_{z(r)}] + \bar{d} C_{z(r)}$$

where $C_{m_o} = 0$ for the tests in S_1 Ch Wind-Tunnel

$C_{m_o} = 0.006$ for the tests in S_3 Wind-Tunnel

\bar{d} is difficult to state precisely but is probably in the neighborhood of 0.60; however it does not seriously affect the accuracy of the results.

The analyses consequently establish the existence of an aerodynamic center for the lift forces arising from blowing and from the flap effect.

Thus, blowing brings to light an aerodynamic center which is inexistent when the flap operates without blowing.

/...

Shifts in locations^{of} aerodynamic center of blowing lift forces as the result of a modification to the model

Additional tests were performed with the same model after the latter had been slightly modified by thinning down the upper lip of the blowing slit, the depth of the slit remaining unchanged (Figure 156).

Analyses were made, in accordance both with methods A and B, for a unique angle $\theta_i = 22^\circ,5$.

The locations of the aerodynamic center of the blowing lift forces were plotted in terms of the C_μ for different Mach Numbers (Fig. 215-216). (To permit comparison, the aerodynamic center locations pertaining to the previous tests have been indicated also, again for $\theta_i = 22^\circ,5$).

It may be noted that for this value of θ_i and for low values of C_μ , the corresponding values of C_m and C_z are relatively small; this accounts for the fluctuations in the location of the aerodynamic center.

ANALYTICAL STUDY OF TORSION (PITCHING) MOMENTS DUE TO INERTIA FORCES

It is the purpose of this section to proceed with a complete enumeration of the inertia torsion moments sustained by the blade, due to rotation about the rotor axis and also to oscillation about the flapping and drag hinges and about the feathering axis. The torsion moments arising from flap deflection were also studied.

System of Coordinates-Degrees of Freedom-Hypotheses

The OZ axis in the reference system is the rotor's conicity axis, i.e. such that the vertical flapping of the first order (frequency equal to the number of revolutions made by the rotor per second) shall be zero. The rotor mast's oscillations in roll and in pitch are reflected by a variation in the cyclic pitch. Vertical flapping, and hence also flapping about the drag hinge, are reduced to a minimum.

The rigid blade possesses four degrees of freedom (Figure 217-A)

- The rotation ψ about OZ
- The rotation β about the vertical flapping hinge perpendicular to OA and to the rotor mast
- The rotation δ about the drag hinge axis passing through E and lying parallel to the rotor mast
- The rotation θ about the feathering axis.

The moments of inertia considered subsequently are the following :

$$\begin{aligned} I_x &= \sum m y^2 \\ I_y &= \sum m x^2 \\ I_o &= I_x + I_y \end{aligned} \quad (\text{Fig. 217B})$$

The centers of gravity of all the blade sections are assumed to lie along the feathering axis.

Pitching moments sustained by the blade.

Restoring moments due to centrifugal forces.

The effect of centrifugal forces is to tend to pull all material points constituting the blade away from the axis of rotation. This is reflected by a couple which tends to cancel out θ if the rotation is through ψ or through δ , or to make it equal to $\frac{\pi}{2}$ if the rotation takes place through β .

If the angles β and δ are assumed to be small, the expression for these moments may be written :

$$M^t = (\dot{\psi}^2 + \dot{\delta}^2 - \dot{\beta}^2)(I_y - I_x)\theta$$

Numerical Example :

<u>Blade</u> :	mean chord	0.5 m
	length	6 m
	airfoil section	64. A. 018
I_x =		$7.3 \cdot 10^{-3} \text{ (Kg. m. sec}^2\text{)}$
I_y =		$54 \cdot 10^{-3} \text{ (" " ")}$

$$\dot{\psi}^2 = 1,000 \quad (\omega = \text{rotor angular velocity})$$

Variable	β	β	δ	θ
Pulsation	2ω	3ω	1.1ω	ω
Amplitude	5°	2°	2°	12°

On the basis of these values, the portion of the torsion moment due to the rotational speed through $\dot{\psi}$ is of the order of

/...

$M_0 = 24 \text{ m/Kg}$, and this will be the value with which the other portions of the torsion moments will be compared :

The portion due to motion about the drag hinge is :

$$0.03 \text{ m/Kg} = 0.001 M_0$$

The portion due to motion about the flapping hinge is :

$$0.73 \text{ m/Kg} = 0.03 M_0$$

Pitching moments due to Coriolis forces

Coupling the $\dot{\psi}$ and $\dot{\beta}r$ motions produces the moments :

$$M^t = 2 \dot{\psi} \dot{\beta} \cos \beta (I_y \sin^2 \theta + I_x \cos^2 \theta)$$

Coupling of the $\dot{\psi}$ and $\dot{\delta}r$ motions gives :

$$M^t = -2 \dot{\psi} \dot{\delta} (I_y - I_x) \sin \theta \cos \theta \cos \beta$$

Lastly, the β rotation coupled to the $\dot{\delta}r$ motion produces the moment :

$$M^t = -2 \dot{\beta} \dot{\delta} (I_y \cos^2 \theta + I_x \sin^2 \theta)$$

Numerical Example :

On the basis of the same numerical data, the moment due to $\dot{\beta}r$ and to $\dot{\psi}$ will be of the order of

$$2.5 \text{ m/Kg} = 0.1 M_0 .$$

The moment resulting from $\dot{\psi}$ and $\dot{\delta}r$ will be of the order of

$$0.020 \text{ m/Kg} = 0.001 M_0 ,$$

while that resulting from $\dot{\beta}$ and $\dot{\delta}r$ will be of the order of

$$0.63 \text{ m/Kg} = 0.025 M_0 .$$

Pitching moments due to flap deflection

In the case of blades equipped with flaps designed to provide blowing at the trailing edge, deflections of such a flap will produce twisting moments about the feathering axis.

The deflections of the flap may be such, for example, that they result in constancy of the moments resulting from the lift forces, as referred to the blade root. The variations in θ_j , the angle of deflection of the jet, are known. A breakdown into a Fourier series enables the first ^{harmonics} of the θ_j function to be obtained. The amplitude e_0 of the shift sustained by the flap's center of gravity will be assumed proportional to the amplitude of θ_j .

As an example, the results of the harmonic analysis for a given set of flight conditions emerge as follows :

Order of harmonics	Constant term	1	2	3	4	5
Amplitude	15.4°	13.8°	10.7°	0.83°	1.1°	1°

Displacement of center of gravity : 1 mm for $\theta_j = 5^\circ$

Mass of flap per running meter : $m = \frac{0.850 \text{ (Kg/m)}}{9.81 \text{ (m/sec}^2\text{)}} = 0.086 \text{ Kg.m}^{-2}\text{s}^2$

The inertia force due to flap deflection may be written :

$$F = m \sum_n l_n n^2 \omega^2 e^{in\omega t}$$

Taking the flap to be at a distance d from the feathering axis, the moment due to the inertia forces may be written :

$$M^t = m d \sum_n l_n n^2 \omega^2 e^{in\omega t}$$

Whence can be obtained the numerical values for the magnitudes of the blade moments.

Value of d : 0.20 m

Length of flap : 1.8 m.

Fundamental Term

$$0.086 \times 0.20 \times \frac{13.8}{5} \times 1.8 = 0.086 \text{ m.Kg} = 0.0036 M_0$$

2nd Order Harmonic

$$0.086 \left(\frac{2\omega}{\omega} \right)^2 \times \frac{10.7}{13.8} = 0.270 \text{ m Kg} = 0.011 M_0$$

3rd Order Harmonic

$$0.086 \times 9 \times \frac{0.83}{13.8} = 0.0465 \text{ mKg} = 0.002 M_0$$

4th Order Harmonic

$$0.086 \times 16 \times \frac{1.1}{13.8} = 0.110 \text{ mKg} = 0.0046 M_0$$

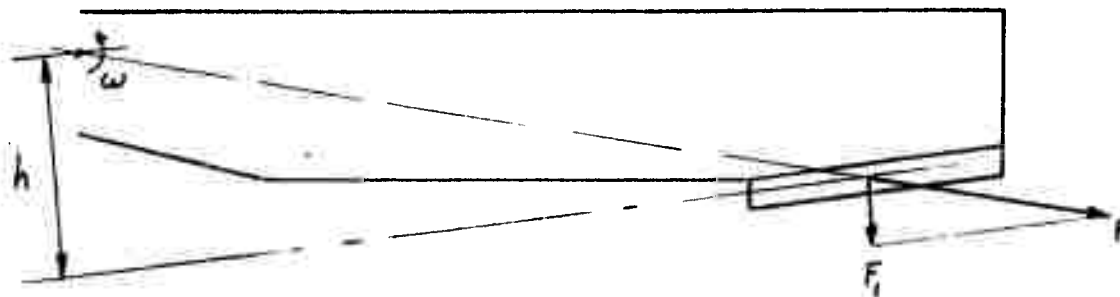
5th Order Harmonic

$$0.086 \times 25 \times \frac{1}{13.8} = 0.157 \text{ mKg} = 0.0065 M_0$$

Pitching moments sustained by flap.Restoring moments due to centrifugal forces

The flap rotates at a velocity ω and is the seat of a force F whose component F_1 resolved perpendicular to the flap's hinge line is given by

$$F_1 = m \omega^2 h$$



where m is the mass of the flap and h the distance of its longitudinal axis from the rotor's axis of rotation.

On the basis of the numerical data used precedingly, and taking $h = 0.90$ m, then we have

$$F = \frac{0.850 \times 1.8}{9.81} \times 1,000 \times 0.9 = 173 \text{ Kg}$$

If the distance of the center of gravity of the flap from the latter's hinge line be $k = 0.02$ m, then the restoring moment on the flap will be given by

$$\begin{aligned} M^t &= F \cdot k \sin \alpha = 173 \times 0.02 \sin \alpha \\ &= 3.5 \sin \alpha \cdot \text{mKg} = 0.15 M_0 \sin \alpha \end{aligned}$$

where α is the angle of deflection of the flap.

Moments due to the accelerating rotation of the blade through β .

$$F = m \sum_2^n f_n \eta^2 \omega^2 e^{i n \omega t}$$

Taking f_n as the linear flapping amplitude at the level of the flap's center of gravity, we have :

$$f_n = 0.85 R \times \beta$$

with $\beta = 5^\circ$, $n = 2$

$$F_{\max} = 1.8 \times 0.086 \times \frac{5 \times 6}{57.3} \times 0.85 \times 4,000 = 280 \text{ Kg.}$$

Whence may be obtained the moment referred to the flap's hinge line :

$$M^t = F \times k = 5.6 \text{ mKg} = 0.215 M_0 .$$

Moment on flap due to blade motion through θ .

This is given by

$$M^t = k m f \omega^2 e^{i\omega t}$$

where f is the amplitude of the flap displacement.

The amplitude of this Moment is of the order of
 $0.10 \text{ mKg} = 0.004 M_0 .$

Moments resultings from Coriolis forces

The angles of deflection of the flap about its hinge line are of the same order as the variations in the angle θ . The dimensional characteristics of the flap section are ten times less than those of the blade section. The length of the flap being 1.8 m and that of the blade 6 m, the moments of inertia of the flap are of the order of 1/300th of those of the blade. In consequence, the moments resulting from the Coriolis forces are likewise of the order of 1/300 of those sustained by the blade, and can therefore be neglected.

Conclusion

All results have been summarized in the table below which permits the effects of each moment to be assessed without difficulty. These effects are in all cases referred to the restoring moment M_0 due to the centrifugal force arising from the rotation

$$M_c = 24 \text{ mKg.}$$

./.

Nature of Moment	Pulsation	Relative Amplitude
<u>Pitching Moments sustained by the blade</u>		
Centrifugal forces		
ψ rotation	ω	1
δ rotation	1.1ω	0.001
β rotation	2ω	0.03
	3ω	0.01
Coriolis forces		
$\dot{\psi} \wedge \dot{\beta} r$	2ω	0.1
$\dot{\psi} \wedge \dot{\delta} r$	3ω	0.06
$\dot{\beta} \wedge \dot{\delta} r$	1.1ω	0.001
Flap deflections		
	ω	0.0036
	2ω	0.011
	3ω	0.002
	4ω	0.0046
	5ω	0.0065
<u>Pitching Moments sustained by the flap</u>		
Centrifugal forces		
ψ rotation	ω	$0.15 \sin \alpha$
$\ddot{\beta}$ Acceleration	2ω	0.215
	3ω	
Blade motion through θ	ω	0.004
Coriolis forces		< 0.0003

ANALYTICAL STUDY OF TORSION MOMENTS DUE TO AERODYNAMIC FORCES

Since in the case of a rotor with blown blades the position of the center of thrust of the aerodynamic forces depends upon the angle of incidence i , the blowing coefficient C_μ , the angle θ_j of jet deflection and the Mach number, calculations for the pitching moments cannot be conducted in the classic manner. The method used instead is set out below and is applied to a numerical example.

The pitching moments generally vary with blade azimuth and the problem of reducing the amplitude of these variations has been studied.

Principle underlying the analytical method of determining the aerodynamic pitching moments

The aerodynamic pitching moments are calculated with reference to the centers of gravity of the various blade sections; indeed, when referred to these points, the moments due to the inertia forces are at a minimum while those due to the aerodynamic forces are virtually the largest the blade will be called upon to sustain.

To this end, the moments are calculated with reference to the leading edge by the approximate method B described in previous Section, i.e. by assuming that the force arising from a C_z corresponding to $\theta_j = 0$ (all other things being equal) is applied at 25 % chord, and that the remainder of the forces are applied at a center of thrust given by Figure 215.

Next are deduced the locations of the centers of thrust. Knowledge of these, in conjunction with that of the corresponding lift forces, is sufficient to determine the locus of the centers of gravity relative to the blade's leading edge required to insure that the maximum moment during blade rotation is as small as possible. It is supposed that the center of gravity and the center of shear are located at the same point which means that there is only pure torsion.

The maximum moment is then computed with reference to this locus.

Numerical Example

This example is based on the following flight and rotor characteristics :

Number of blades	$b = 2$
Rotor radius	$R = 6 \text{ m}$
Length of blown section	$0.7 R \text{ to } 1.0 R$
Blade chord at $0.85 R$	$c = 0.455 \text{ m}$
Rotational speed	$n = 5 \text{ r.p.s.}$

/.

Lift $F_n = 3,000 \text{ Kg}$
 Forward speed $V = 300 \text{ k.p.h.}$
 Inclination of rotor shaft $\alpha_R = 10^\circ 5'$

The pattern governing the variation of the angle of deflection θ_j of the air jet is determined by the condition that the bending moments at the blade root due to the lift forces shall be zero.

Figure 218 shows, in terms of ψ , and at 0.85 R, the value of the jet deflection angle θ_j , of the blowing coefficient C_μ , and of:

the C_{z_s} due to the blowing

the $C_{z_{Ae}}$ due to the effect of $\frac{dC_z}{d\psi}$

the C_{z_v} due to the flap effect

the C_{z_r} due to the jet reaction.

Figure 219 indicates the moments M_{Ae} at the blade root due to effect of $\frac{dC_z}{d\psi}$ and the total moments M_t resulting from the lift forces. The figure also shows the variation in the blade lift P_{Ae} due to effect of $\frac{dC_z}{d\psi}$, the total lift P_t and the half sum of the total lift at ψ and $\psi + \pi$.

The diagram giving the air loads at 0.7 R, 1.0 R, is given in Figure 220. On this diagram are figured the vectors representing the air loads per meter of blade length at every azimuthal position of the blade and also their point of application along the blade chord.

The center of gravity of the blade outer portion was located so that the mean torsion moment in that section over a complete revolution of the blade should be zero. This location works out at approximately midway along the tip chord of the blade.

At 0.7 R, which is the boundary between the blown section of the blade (requiring a center of gravity at 42 % chord) and the unblown section (requiring a center of gravity at 25 % chord), a compromise was reached. The center of gravity was fixed at 36.4 % chord, as this gives equality between the maximum nose-down and nose-up pitching moments in absolute values.

The center of gravity then shifts progressively from 36.4 % at 0.7 R to 25 % at 0.5 R, and remains at this percentage value from 0.5 R to 0.

The corresponding theoretical blade shape is given in Figure 221.

A variable moment consequently subsists whose amplitude is of the order of 80 mKg and which is maximum at 0.7 R when it is a nose-down moment ($\psi = 270^\circ$) and maximum at 0.5 R when it is a nose-up

moment ($\psi = 30^\circ$) its spanwise variation being shown in Figure 221. The shift in the center of thrust at 0.85 R is $\pm 16.5\%$ of chord.

It may be noted that these results could be improved by decreasing the collective angle of attack of the blade and increasing the over-all deflection θ_j in order to take ^{advantage} of the favorable effect of the Mach number on the advancing blade.

It was seen in the previous sections that when the Mach number increases the center of thrust shifts towards the trailing edge for a given value of θ_j .

As the retreating blade has its center of thrust well at the rear, due to the high deflection θ_j , it is only necessary to moderately deflect the flap of the advancing blade to obtain an equivalent shift of the center of thrust in this area and, consequently, equalize the pitching moments.

It may also be noted that this moderate θ_j deflection in the advancing blade area is advantageous in terms of the critical Mach number.

Reducing the shift in the center of thrust of the lift forces on the blade

The method of calculating the moments, as applied to the preceding numerical example, shows the advantage of envisaging other solutions for reducing the amplitude of the torsion moments. The problem is first dealt with in its general aspects, following which particular cases are considered leading to practical embodiments.

Principle underlying the method

It was seen in a previous Section that the pitching moment due to the blowing forces, referred to a point F on the airfoil chord, takes the form :

$$M^t = F.A \left[\frac{dC_z}{di} + k\sqrt{C_\mu} \right] i - F.B \left[k\sqrt{C_\mu} \sin \theta_j + \frac{dC_z}{d\alpha} (\alpha - 22.5^\circ) \right]$$

"A" is the point at which the lift forces due to the effect of the incidence i are applied.

"B" is the point at which are applied the lift forces which vary with θ_j and which include the blowing and flap effects.

Whereas it is not easy to operate on the C_μ , it is on the other hand possible to cancel out M^t by making θ_j vary with respect to ψ in obedience to a suitable pattern.

Whence the method is derived as follows :

A pattern is adopted for the variation of the blade pitch

/.

with respect to ψ . From this i can be deduced and i , C_μ , F_A and F_B replaced by their values. From this in turn θ_j can be deduced in terms of ψ , the position of F being determined empirically on the basis of the requirement that, over a complete blade revolution, i and θ_j shall reach their maximum permissible values.

Approximate methods

The intent must in all cases be to seek to approach proportionality between the lift due to the incidence i and the lift due to jet deflection θ_j .

$\theta_j = 0$ pattern

With low C_μ values, this solution enables the C_z of the retreating blade to be improved at the cost of a minimum of modification to the blade; it also enables the critical Mach number to be raised and the rotor's lift/drag ratio to be improved. This in turn will be reflected by an increase in the helicopter's maximum speed. The centers of thrust are at 25 % chord as with conventional blades, so that blowing introduces no twisting moments.

$\theta_j = \text{constant}$ pattern

The numerical example was based on $\theta_j = 22.5^\circ$. The center of thrust shifts by about $\pm 10\%$ of chord at 0.85 R. In comparison with the previous method, the C_z of the retreating blade is increased, as is also the disc loading. The blade here requires to be more rigid in torsion owing to the pitching moments which arise.

$\theta_j = k \cdot i$ pattern

The law of variation of i taken "a priori" was that applying to the case of flight with a constant moment at the blade root, as indicated above.

Another example based on the $\theta_j = 4i$ pattern, gave moments of ± 30 mKg, i.e. of the order of one-third pitching moments set up if constant bending moments are applied to the blade root.

The center of thrust shift was $\pm 6.5\%$ of chord.

On Figure 22 are also indicated the lift forces in terms of ψ at 0.85 R for this $\theta_j = 4i$ pattern.

$$\theta_j = k \frac{i}{\sqrt{C_\mu}} \quad \text{pattern}$$

It is possible to still further reduce the twisting moments. $\theta_j = k \frac{i}{\sqrt{C_\mu}}$ particular pattern of variation of θ_j , when applied to the numerical example involving the flight conditions referred to previously, results in a center of thrust shift of less than ± 1 cm, i.e. $\pm 2\%$ of chord, in other words in pit-

ching moments of less than 10 mKg.

This establishes the possibility of reducing variable pitching moments to values that may be virtually as small as desired, by causing θ_i to vary in terms of ψ in obedience to a suitable pattern.

A compromise is to be made between the two extreme cases respectively involving a solution on the basis of $\theta_i' = 0$, which leads to moderately improved aerodynamic performance in comparison with conventional helicopters without giving rise to additional pitching moments, and the solution based on a constant bending moment at the blade root, which gives highly improved aerodynamic performance characteristics in conjunction with higher pitching moments.

The table below compares the consequences on aerodynamic performance and blade characteristics of the different patterns of variation of θ_i open to choice.

/.

COMPARATIVE TABLE OF DIFFERENT PATTERNS OF VARIATION OF θ_f

Pattern of variation of θ_f	Aerodynamic Performance		Blade Characteristics		
	C of retreating blade	Possibility of controlling the lift via θ_f	Center of thrust shift	Pitching moments	Required mechanical blade characteristics
1) Pattern giving constant bending moments at blade root	very high	yes	$\pm 16,5\%$ of chord	large	torsional rigidity greater than in a conventional blade
2) $\theta_f' = 0$	moderate	no	nil	nil	same torsional rigidity as with conventional blade
3) $\theta_f = \text{constant}$	high		$\pm 10\%$	fairly large	
4) $\theta_f = k \cdot i$	high		$\pm 6,5\%$	moderate	
5) $\theta_f = k \frac{i}{V C_p}$	moderate		$\pm 2\%$	very small	
(k = constant)					

CONCLUSION

The aerodynamic torsion (pitching) moments acting on a blown blade may be largely different from those which act on a conventional blade.

The tests carried out show the existence of two aerodynamic centers in the blown blade section.

The first aerodynamic center located approximately at quarter chord is the point of application of all the aerodynamic forces when the direction of the jet sheet is parallel to the section zero lift axis ($\theta_j' = 0$).

These lift forces include the conventional lift force due to airfoil non zero angle of attack and the lift force due to blowing at $\theta_j' = 0$.

The second aerodynamic center located approximately at half chord is the point of application of the aerodynamic lift force due to blowing at zero angle of attack of the blade section. This force includes the effects of C_{μ} and θ_j' and also the effect of the flap itself at zero angle of attack of the blade section.

A single aerodynamic center may thus be obtained only in the three following cases :

- a) - Blowing is maintained in a fixed direction with no deflection ($\theta_j' = 0$). In this case blowing is used only to improve performance, the rotor being driven and controlled by conventional means.

The aerodynamic center is located, in this case, at the blade section quarter chord.

- b) - The blown blade always operates at zero angle of attack. The totality of the lift is, in this case, produced by blowing ($i = 0$, $\theta_j' \neq 0$)

The aerodynamic center is located at half chord.

- c) - The pattern of the jet deflection over azimuth is such that there is a fixed proportion between the forces acting at the two aerodynamic centers.

Such a pattern is practically feasible and it is favorable for rotor control.

In this case all happens as if there was, a single fixed aerodynamic center located in an intermediary position between quarter and half chord.

For rotor control the variations of θ_j' move this aerodynamic center only in a transient way. Blade pitch may remain fixed.

The torsion moments acting on the blade being referenced with respect to the section shearing center, it is thus possible to find a combination of the section c.g., shearing center and aerodynamic center locations which would give a mean torsion moment as low desired, by means of :

- choosing a suitable jet deflection pattern over azimuth in order to obtain a fixed aerodynamic center ,
- putting on additional weight in the blade in order to move to the desired position the c.g. and the shearing center.

It must be noted here that in the case of a jet-flap driven and controlled rotor the blades are fixed in pitch and, therefore, the torsion moments acting at the root of the blade are directly taken by the rotor head structure, and no loads are transmitted to the blade controls.

The shearing stresses in the blade structure due to torsion are however to be taken into account and can be fairly high.

As far as the blade outer portion is considered, and though this part of the blade structure is opened along one of its sides (slit) the torsion rigidity may be made as high as desirable by increasing structure weight within limits required for a satisfactory operation of the rotor.

LIST OF REFERENCES

- P.CARRIERE, E.A.EICHELBRENNER et Ph.POISSON-QUINTON de l'ONERA (France).
"Contribution theorique et expérimentale à l'étude du contrôle de couche limite par soufflage".

1^{er} Congrès International des Sciences Aéronautiques
MADRID, 8 Septembre 1958.
- SPENCE.- "Lift coefficients of a thin blown airfoil".

Proceedings of the Royal Society of London. Series A.
Mathematical and Physical Sciences (vol.238, 29 january 1957).
- P.JOUSSERANDOT. "Contrôle de circulation par soufflage"
(Résumé des Résultats expérimentaux et comparaison avec la théorie).

Réunion d'étude sous le patronnage du Conseil Consultatif
23 Février 1955 - ONERA.
- L.MALAVARD. "Contribution à l'étude théorique du soufflage au bord de fuite d'un profil d'aile".

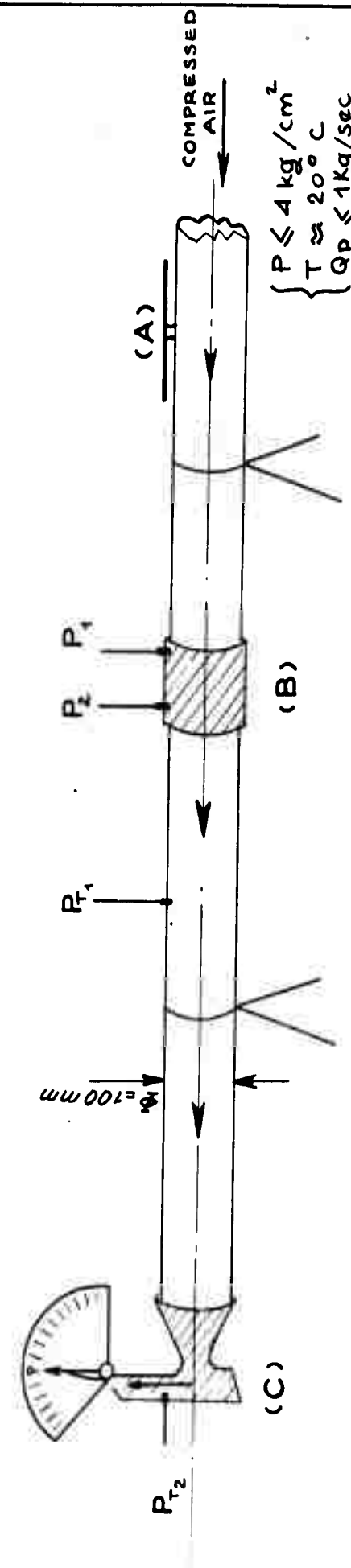
ONERA - Note Technique 4/1727-A.
- M.KADOSCH. "Déviation des jets par adhérence à une paroi convexe".
Journal de Physique et le Radium (Physique appliquée)
Tome 19 - supplément au n°4 - avril 1958.
- M.KADOSCH. "Action d'un jet transversal à un écoulement".

Bulletin de la Société Française des Mécaniciens, 1955, n°18.
- J.BERTIN.et M.KADOSCH "Principes et applications de la striction axiale et directionnelle".

Bulletin de la Société Française des Mécaniciens, 1958, n°24.
- I.M.DAVIDSON "The jet-flap".

B.Sc. A.F.R.Ae.S (National Gas Turbine Establishment)
A lecture given before the Royal Aeronautical Society on 20 th
October 1955 at the Royal Institute, Albemarle Street, London.

JET FLAP PRELIMINARY TESTING INSTALLATION IN THE WIND-TUNNEL OF THE "SERVICE TECHNIQUE AERONAUTIQUE" (S.T.A.)

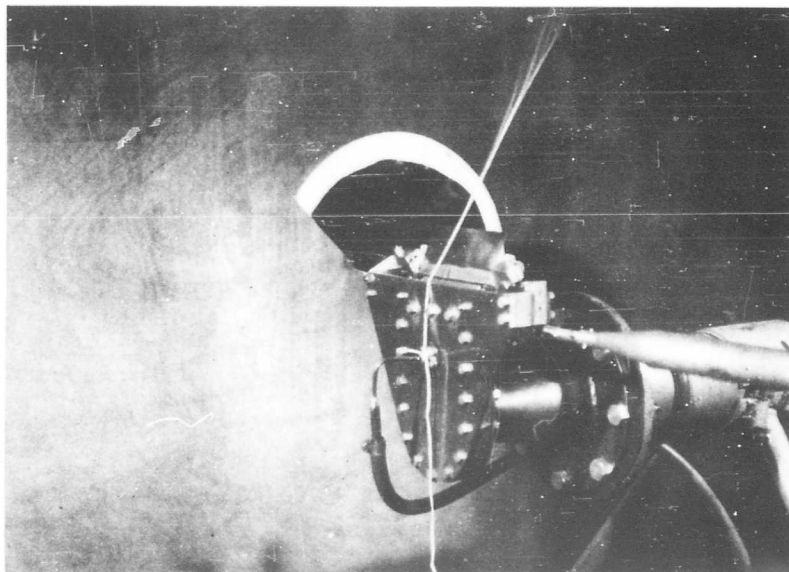


- (A) TOTAL PRESSURE AND AIRFLOW CONTROL (UP STREAM) P_{T_1} : TOTAL PRESSURE IMMEDIATELY BEYOND FLOWMETER.
 - (B) AFNOR FLOWMETER (NOZZLE SYSTEM $D=100$ mm, $D=40$ mm).
 - (C) TEST MODEL ASSEMBLY . (REF. DRAWING F4102-100).
- P_1 { FLOWMETER PRESSURE INTAKES :
 P_2 { P_1 : UP THE RIVER PRESSURE
 P_2 : DOWN STREAM PRESSURE
 $P_{T_1} - P_{T_2}$: PRESSURE LOSSES EVALUATION.
 CJE (CORRECTION COEFFICIENTS.
 Q_1 SPECIFIC WEIGHT (UP STREAM).

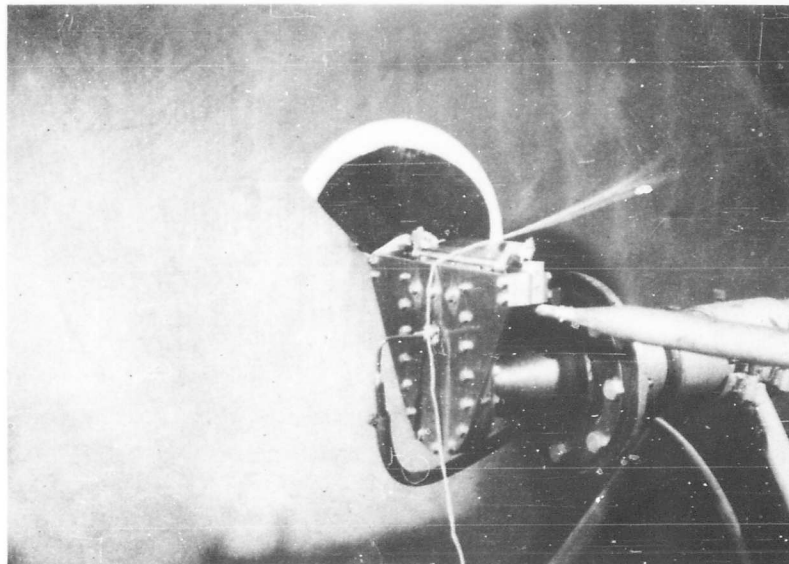
$$Q_p = CJE \sqrt{2g(P_1 - P_2)} \frac{Q_1}{m^2 \frac{m}{s^2} \frac{kg}{m^3}} \rightarrow \frac{kg}{sec}$$

Fig. 1

BLOWING OVER MECHANICAL FLAP



Small deviation

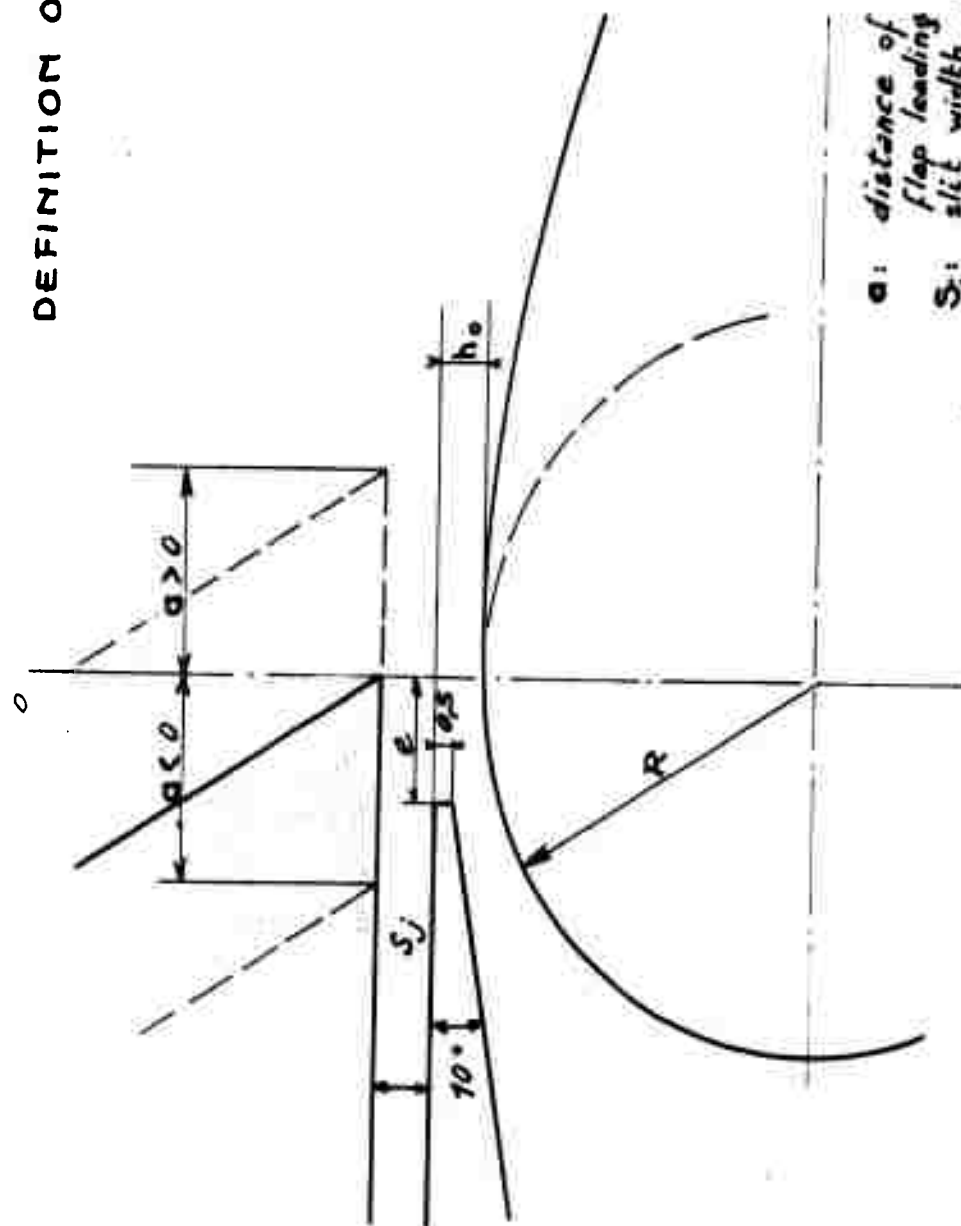


Large déviation

Fig. 2

BLOWING WITH MECHANICAL FLAP

DEFINITION OF ASSEMBLY



- a: distance of slit upper edge to flap leading edge axis
- S_j : slit width, with $L = 100 \text{ mm}$ (length)
- h_0 : initial vertical distance of flap to slit
- e: lateral distance of flap leading edge axis to slit
- R: radius of curvature of leading edge

Fig. 3

EFFECT OF WIDTH OF SLOT s_j
ON JET STREAM MAX.
DEFLECTION ANGLE VERSUS
PRESSURE RATIO $\frac{P_2}{P_0}$

1 - STALLING ON FLAP
LEADING EDGE

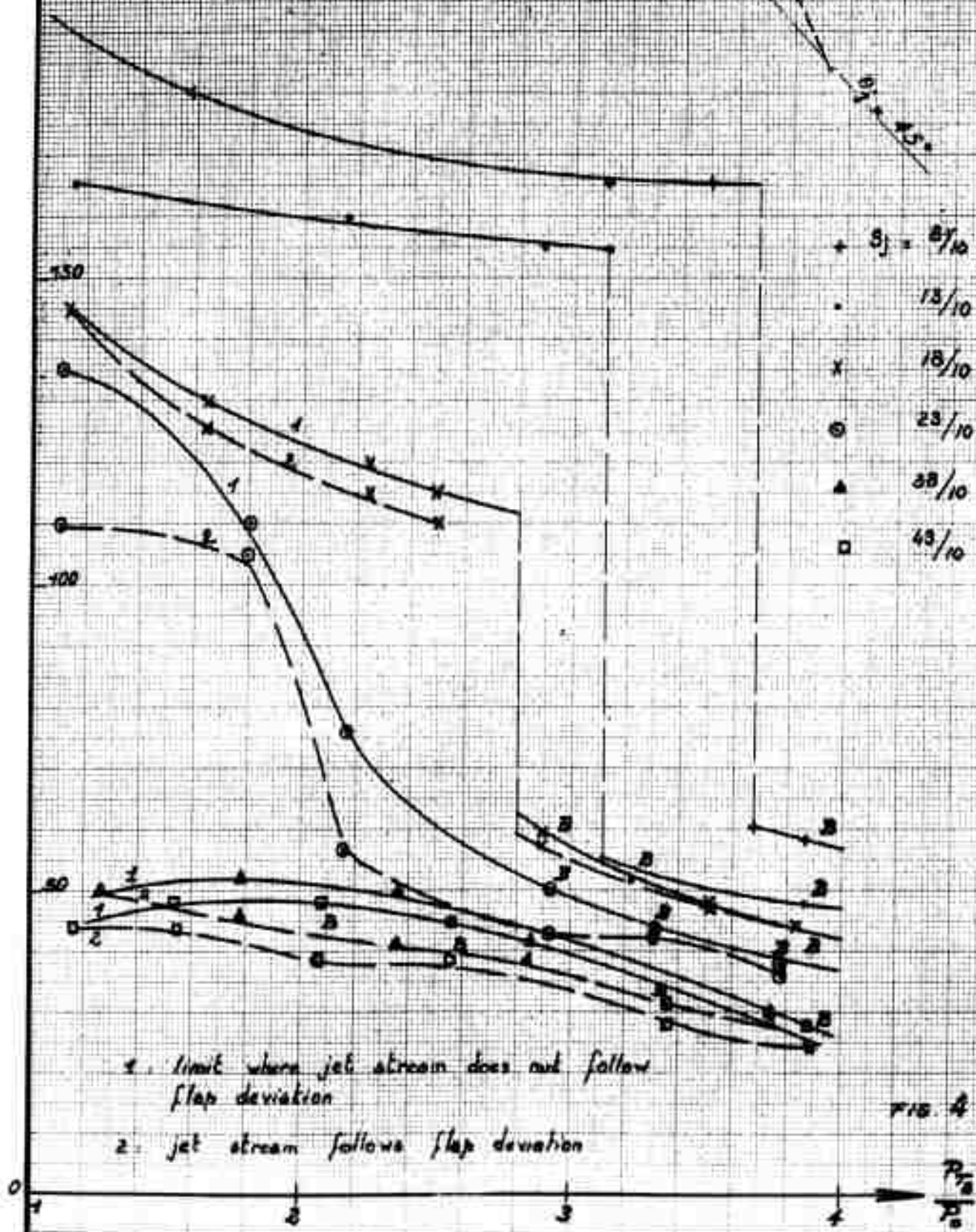
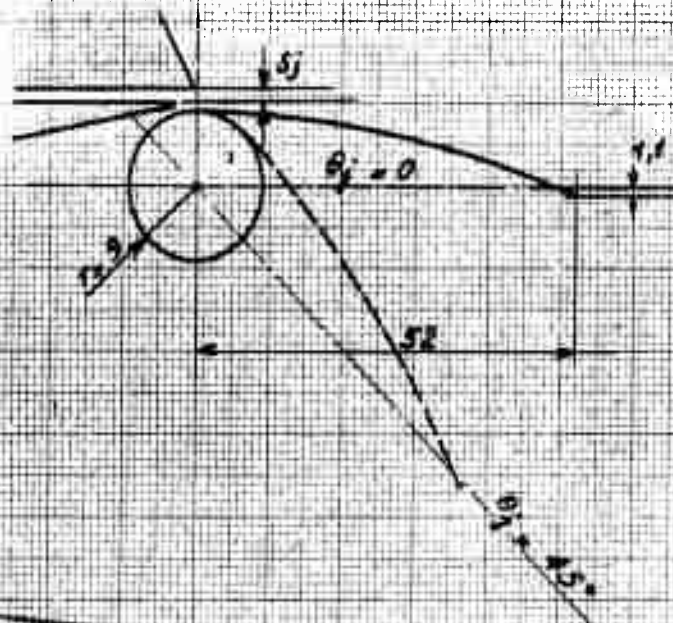
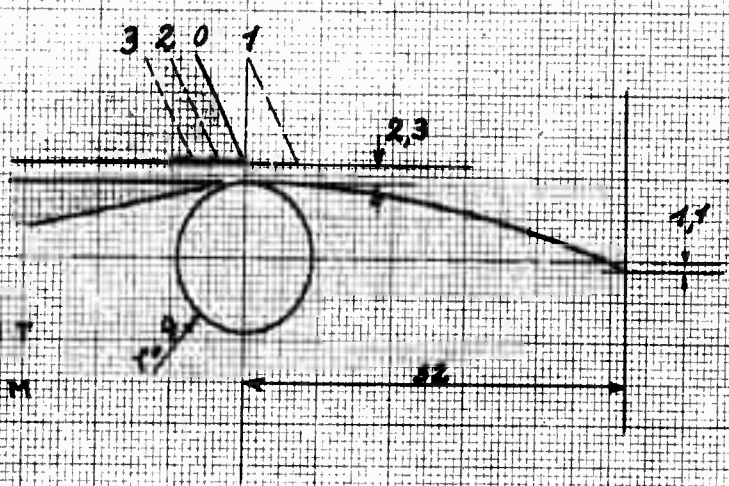


FIG. 4



EFFECT OF SETTING OF SLIT
UPPER EDGE ON JET STREAM
MAX. DEFLECTION.

COMPARISON WITH INITIAL POSITION "0"

$$S_j = 23/10 \quad (\text{AT INITIAL "0" SETTING})$$

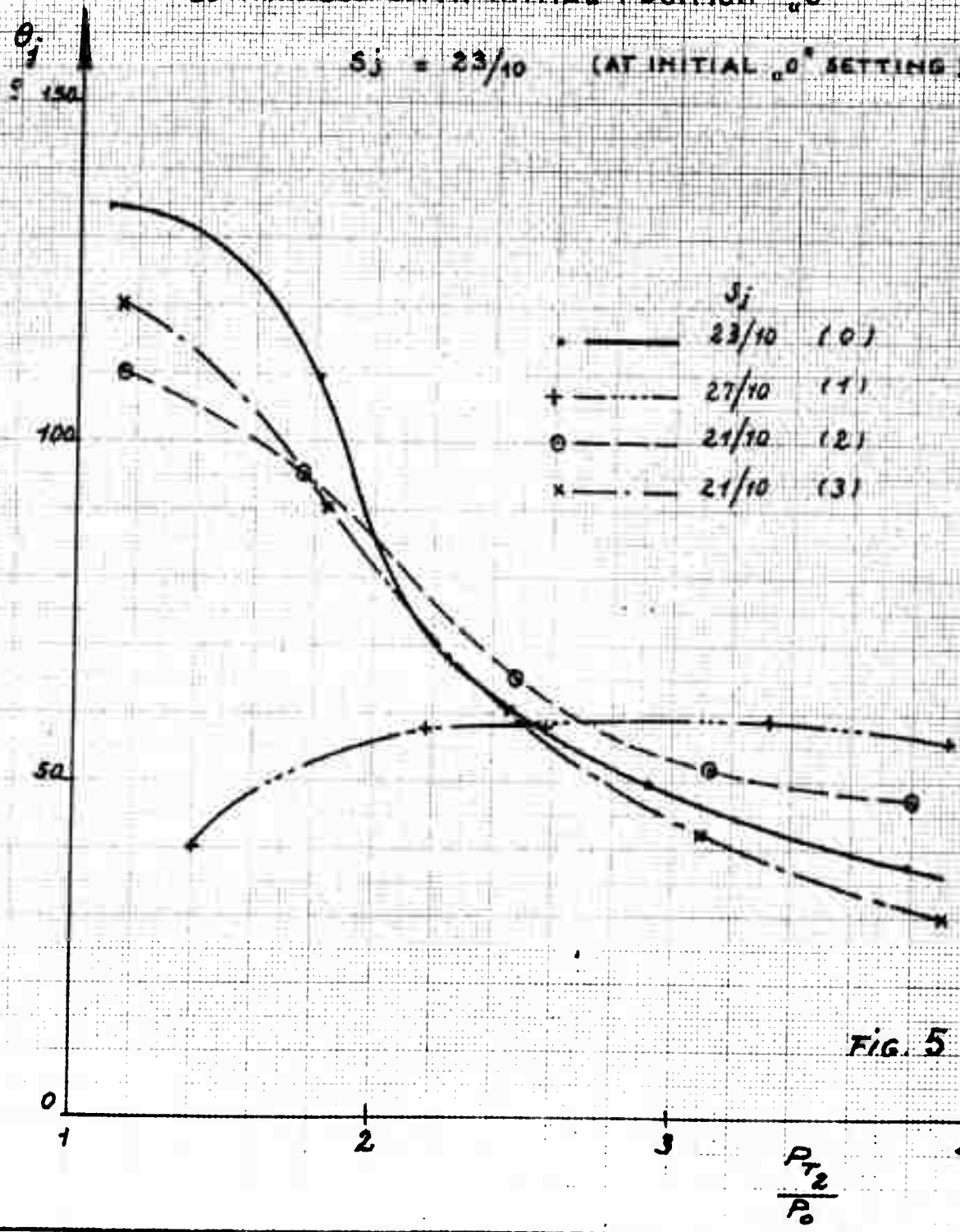
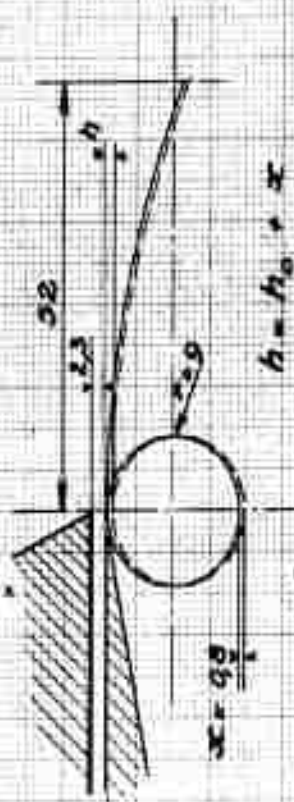


FIG. 5

BLOWING WITH MECHANICAL FLAP



EFFECT OF VERTICAL DISTANCE "h"

OF FLAP TO SLIT ON LIMIT

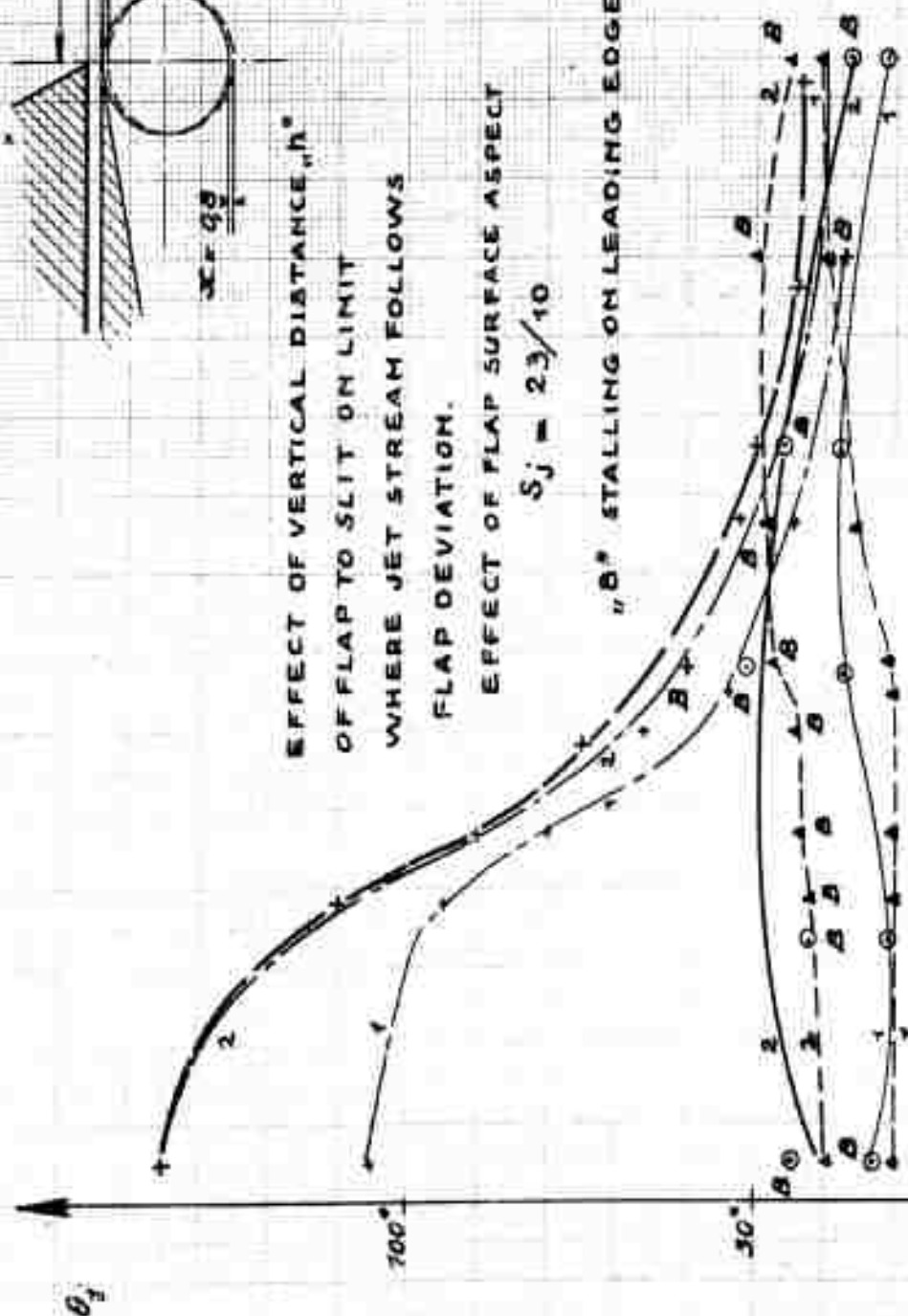
WHERE JET STREAM FOLLOWS

FLAP DEVIATION.

EFFECT OF FLAP SURFACE ASPECT

$S_j = 23/10$

"B" STALLING ON LEADING EDGE



- + initial setting h_0
- x polished flap
- o 5/10 setting $h = h_0 + 5/10$
- triangle 8/10 setting $h = h_0 + 8/10$

FIG. 6

BLOWING WITH MECHANICAL FLAP

EFFECT OF APERTURES FOR COMMUNICATION WITH ATMOSPHERIC PRESSURE ON LIMIT WHERE JET STREAM FOLLOWS FLAP DEVIATION.

COMPARISON WITH INITIAL FLAP

$$S_j = 0.10$$

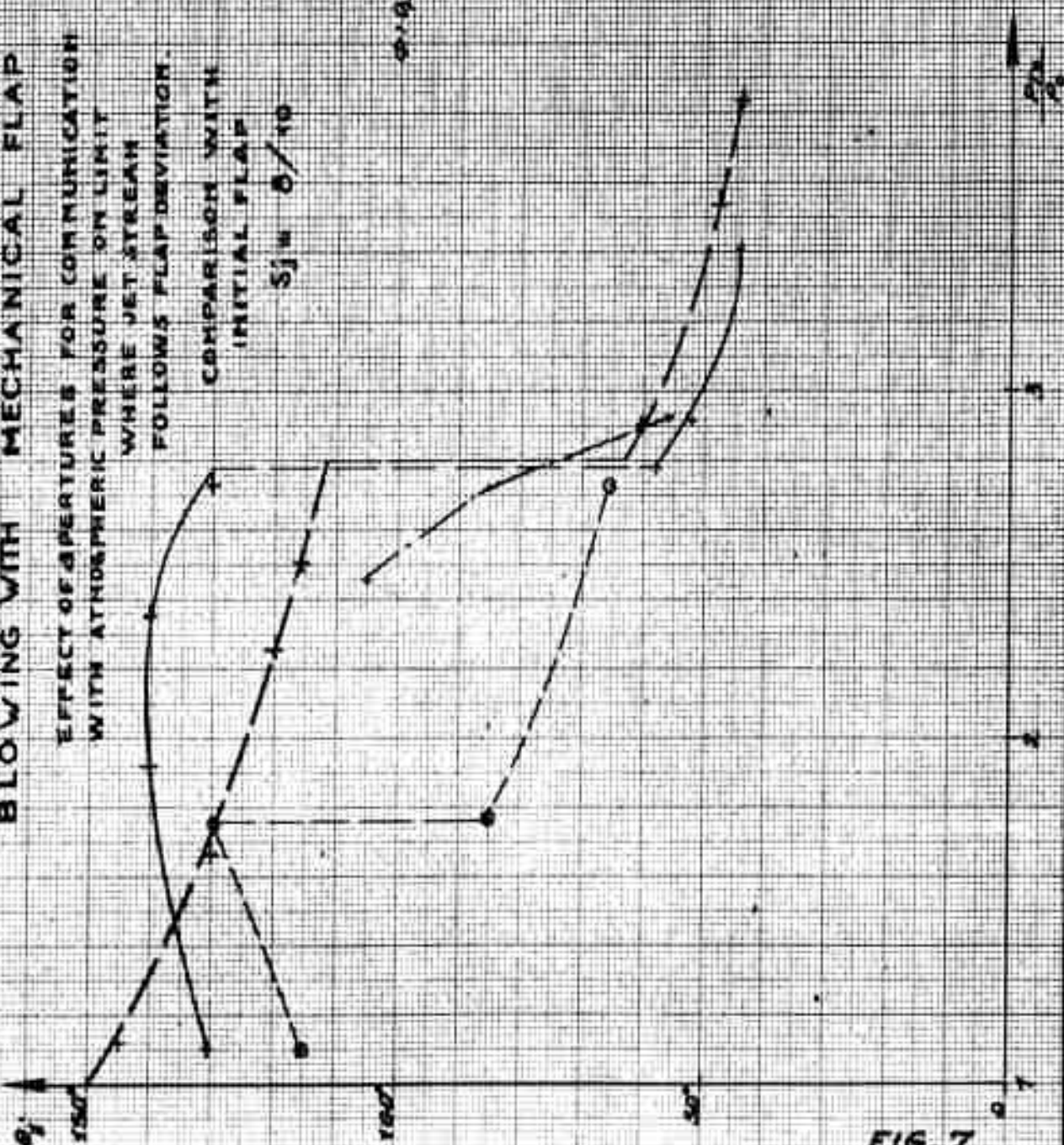
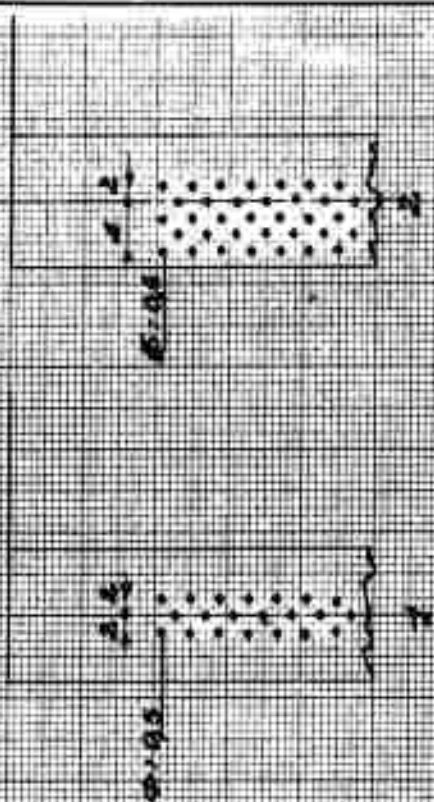


FIG. 7

+ initial flap without aperture
o communication with P_0 blocked

EFFECT OF FLAP AIRFOIL
(SAME LEADING EDGE)
ON LIMIT WHERE JET STREAM
FOLLOWS FLAP DEVIATION.
COMPARISON WITH INITIAL FLAP.

$$S_j = 2.3/10$$

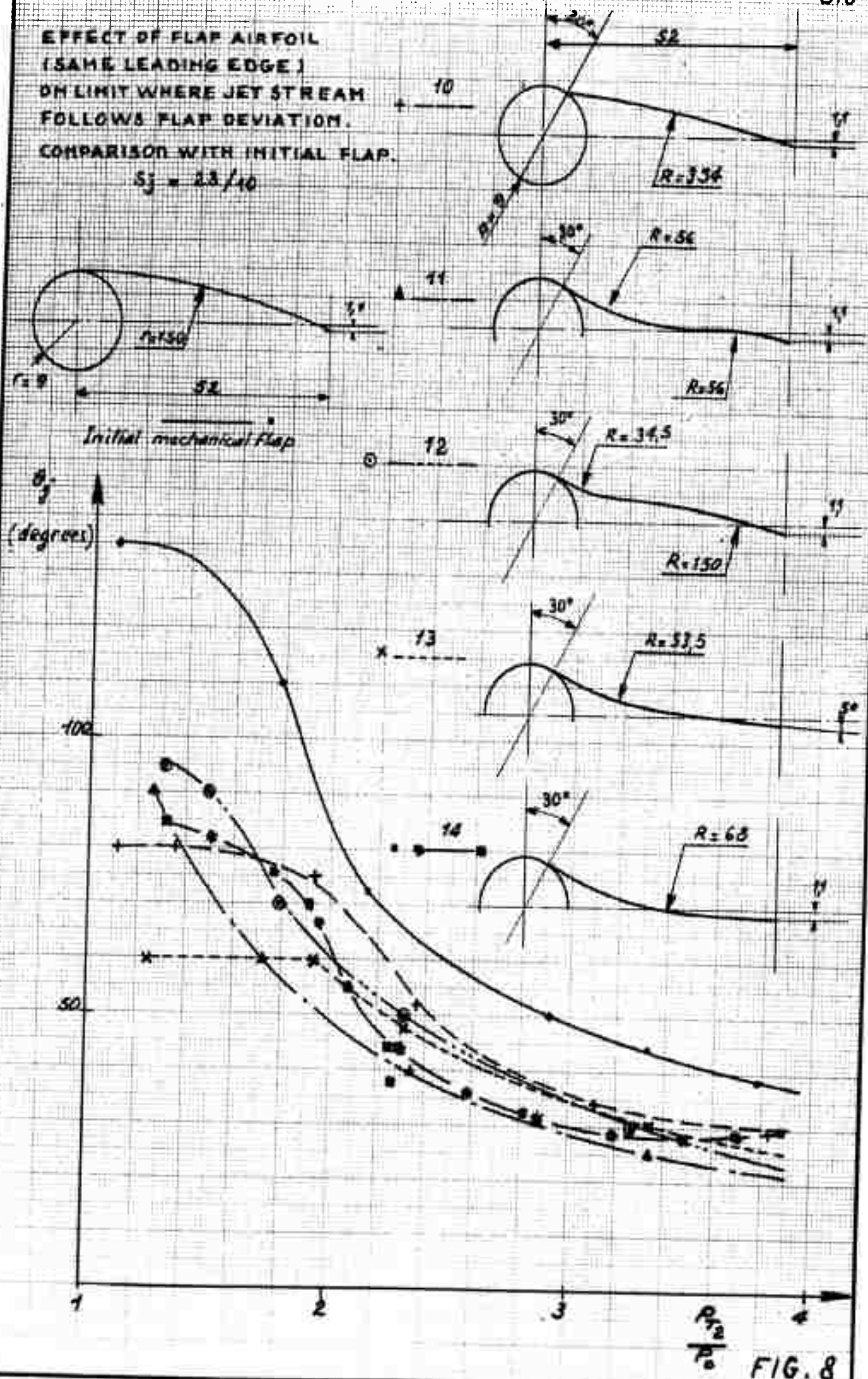
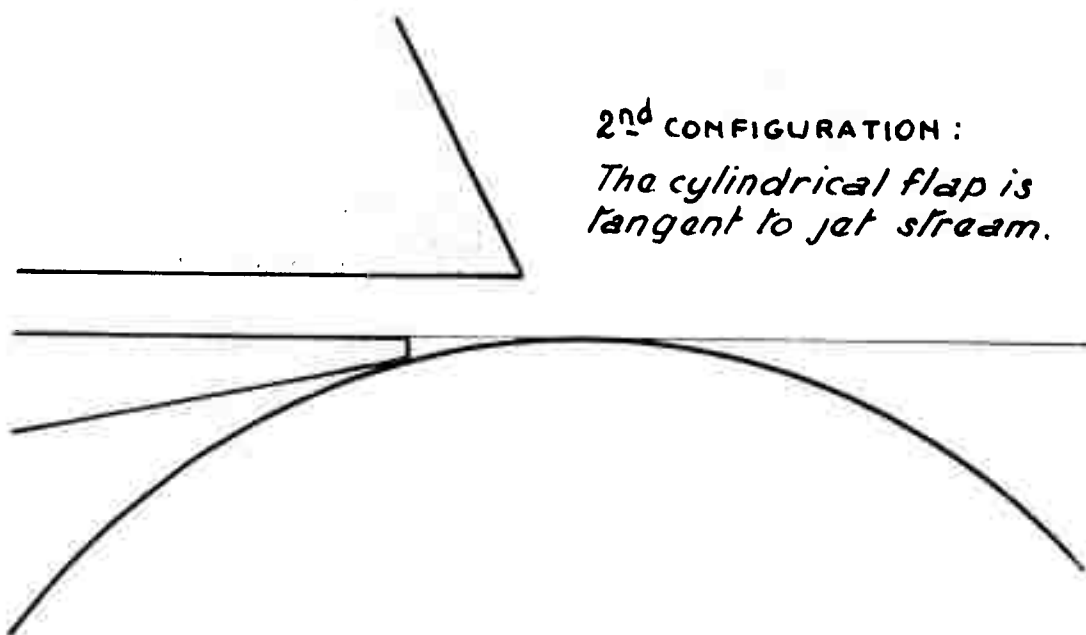
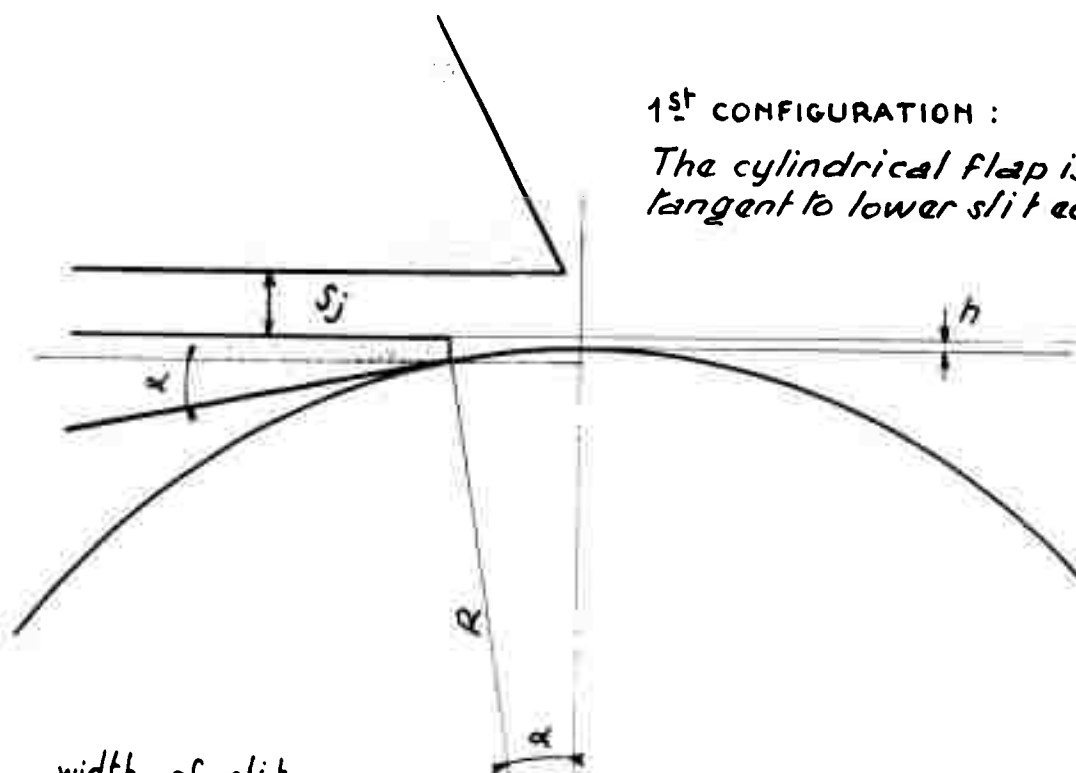


FIG. 8

BLOWING WITH CYLINDRICAL FLAP

DEFINITION OF ASSEMBLY . TWO CONFIGURATIONS :

2nd CONFIGURATION :*The cylindrical flap is tangent to jet stream.*1st CONFIGURATION :*The cylindrical flap is tangent to lower slit edge.* S_j width of slit h distance of cylindrical flap to jet stream (or to slit) α angle of tangent to cylindrical flap at application point R radius of cylindrical flap

$$h = 0,5 - 0,0173 R$$

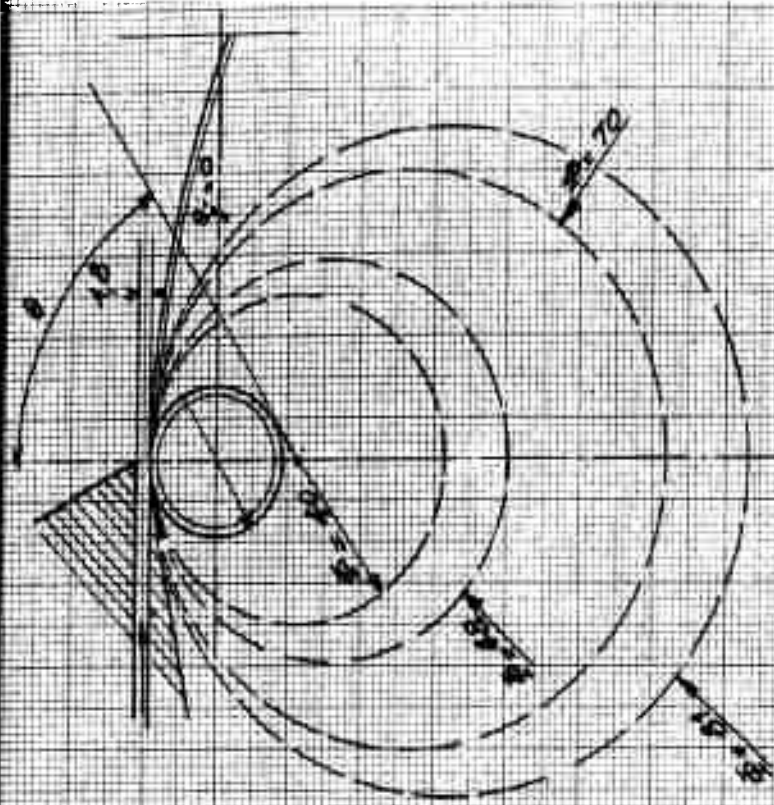
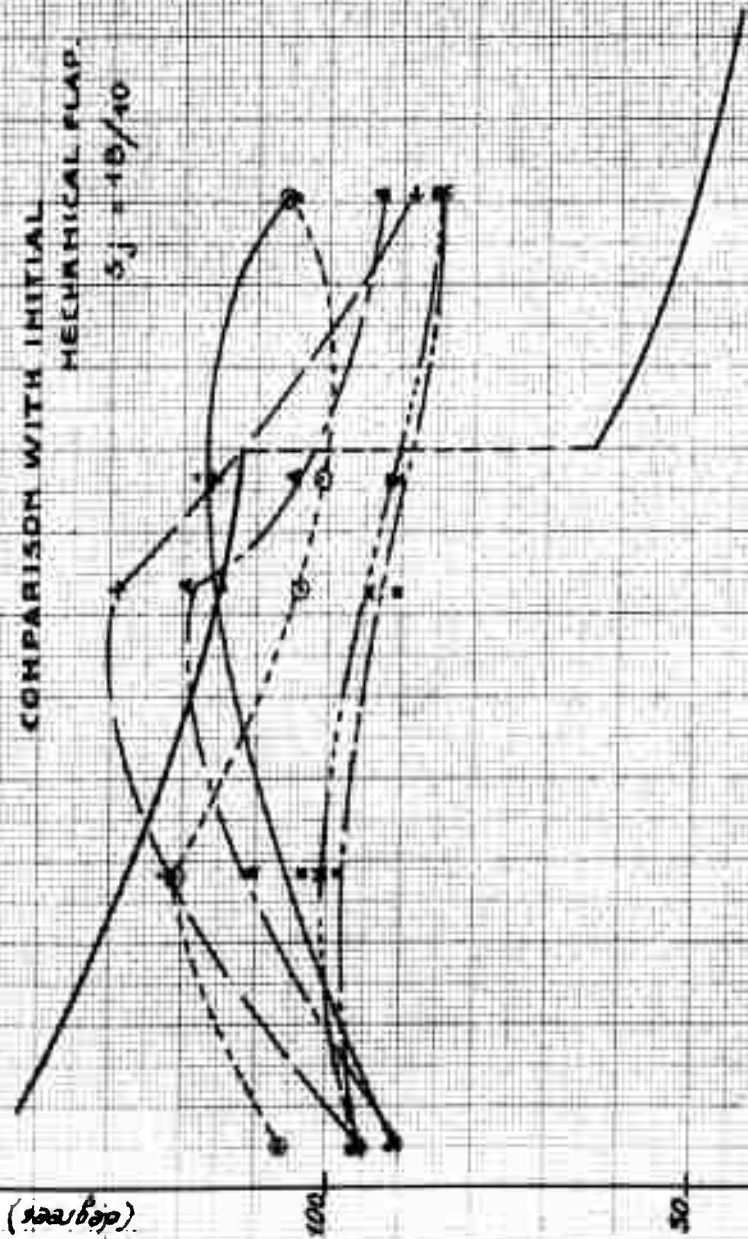
FIG. 9

BLOWING WITH CYLINDRICAL FLAP

EFFECT OF RADIUS OF CYLINDRICAL FLAP
ON MAX. DEVIATION θ

COMPARISON WITH INITIAL
MECHANICAL FLAP.
 $S_j = 10/10$

θ_j (град)



- ϕ 40 mm
- 48
- 70
- 81
- 110
- 126
- Initial mechanical flap

$\frac{P_2}{P_1}$

B.10

FIG. 10

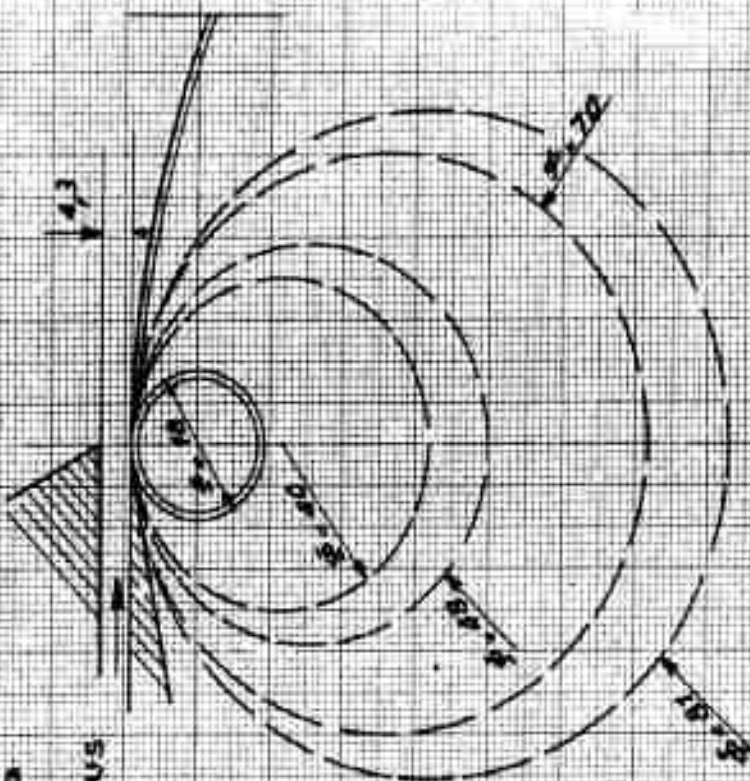
BLOWING WITH CYLINDRICAL FLAP

EFFECT OF CYLINDRICAL FLAP RADIUS
ON MAX. DEVIATION θ_j

COMPARISON WITH INITIAL FLAP

$$S_j = 43/10$$

1) configuration 1
2) configuration 2



initial mechanical flap

θ	
40	
60	
70	
80	
90	
100	
110	
120	

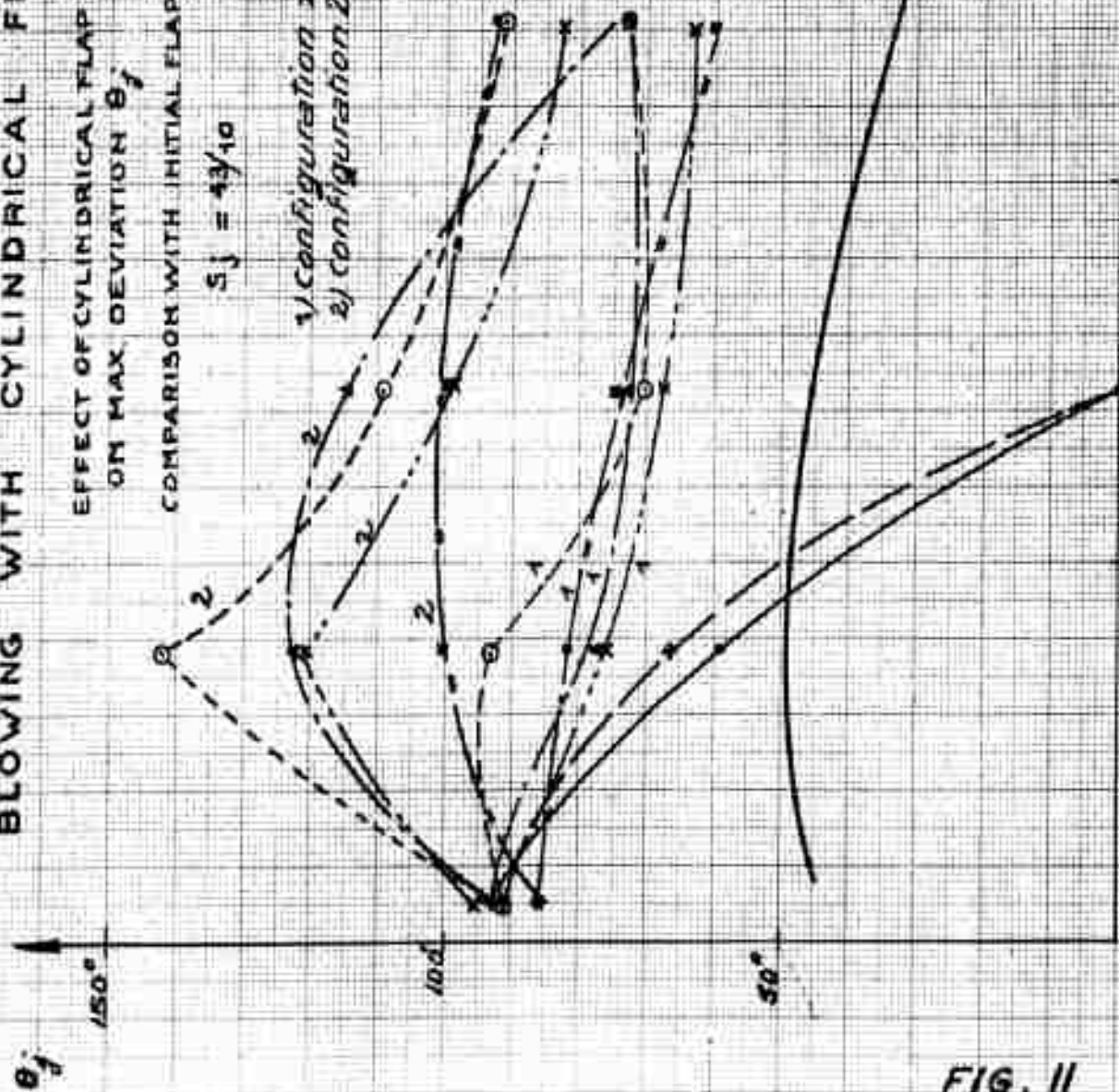


FIG. II

BLOWING WITH CYLINDRICAL FLAP

EFFECT OF CYLINDRICAL FLAP RADIUS
ON MAX. DEVIATION θ_j'

$$S_j = 73/10$$

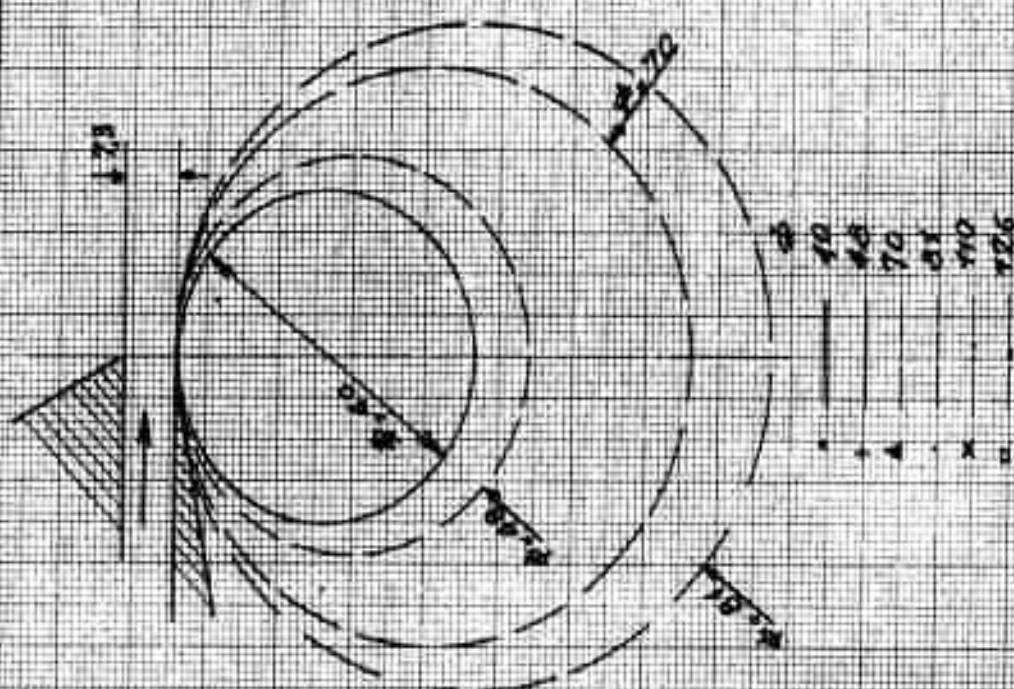
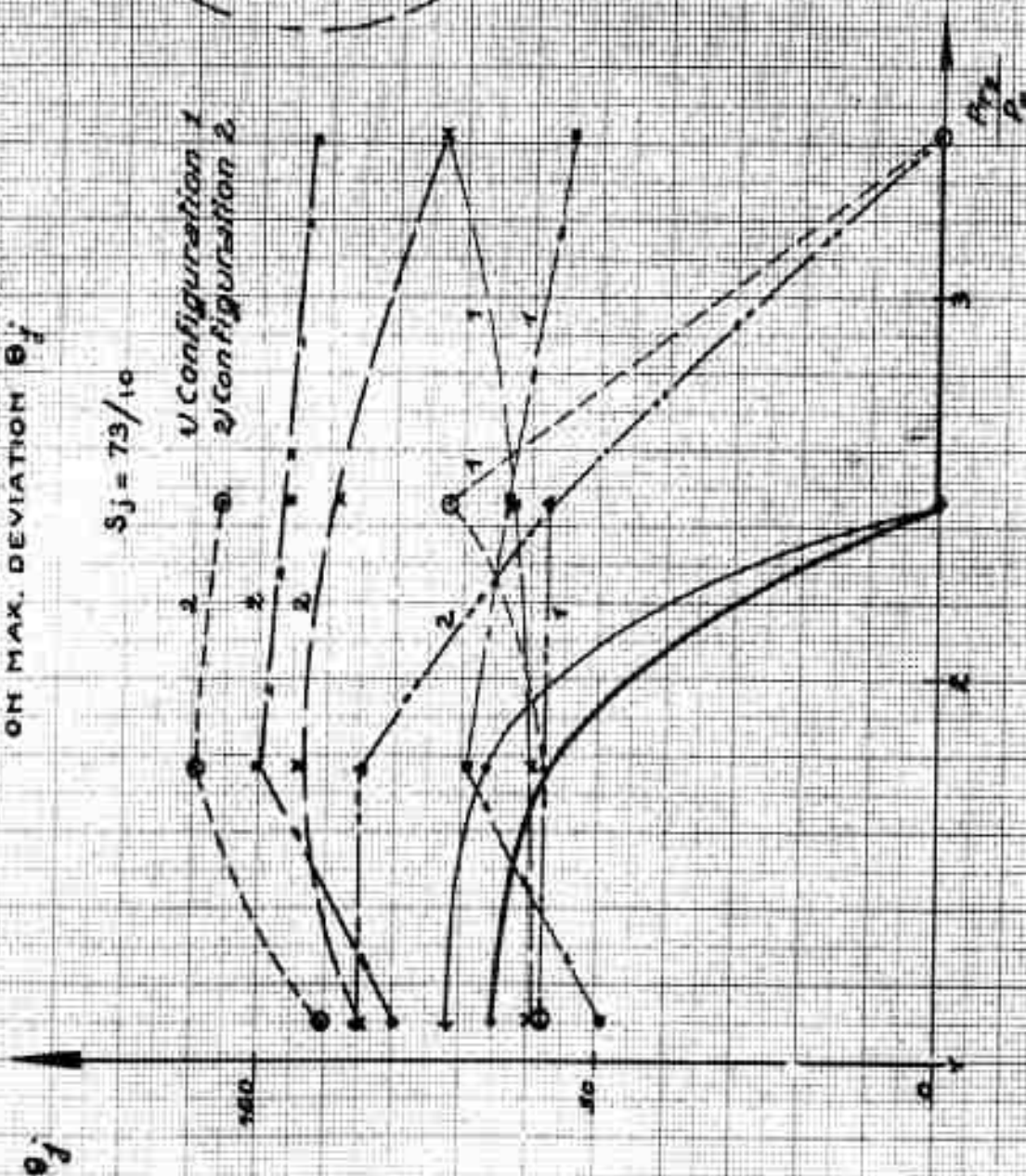
1) Configuration 1
2) Configuration 2

FIG. 12

Required slit width ($\frac{\delta_j}{R}$), plotted against pressure ratio, in order to avoid the 2^d working condition of the jet flow.

(Line of separation between laminar and turbulent flows).

δ_j : slit width

R : flap upper surface radius of curvature.

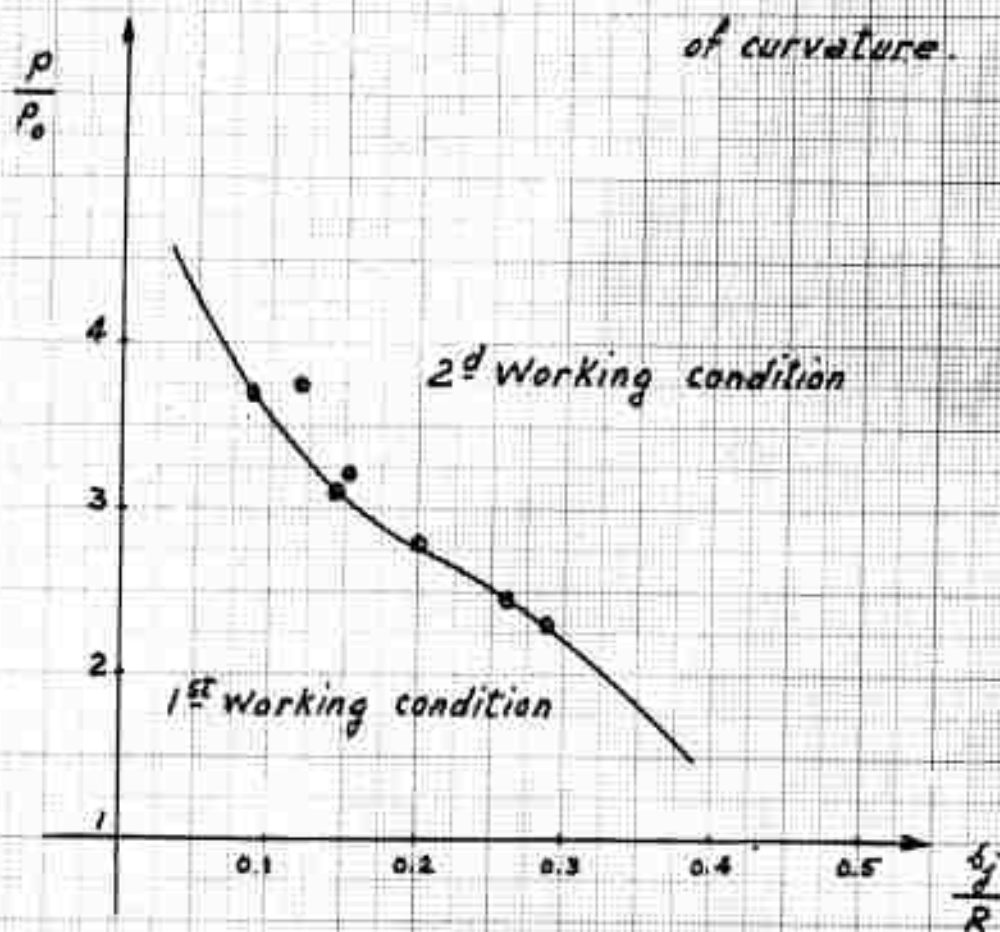
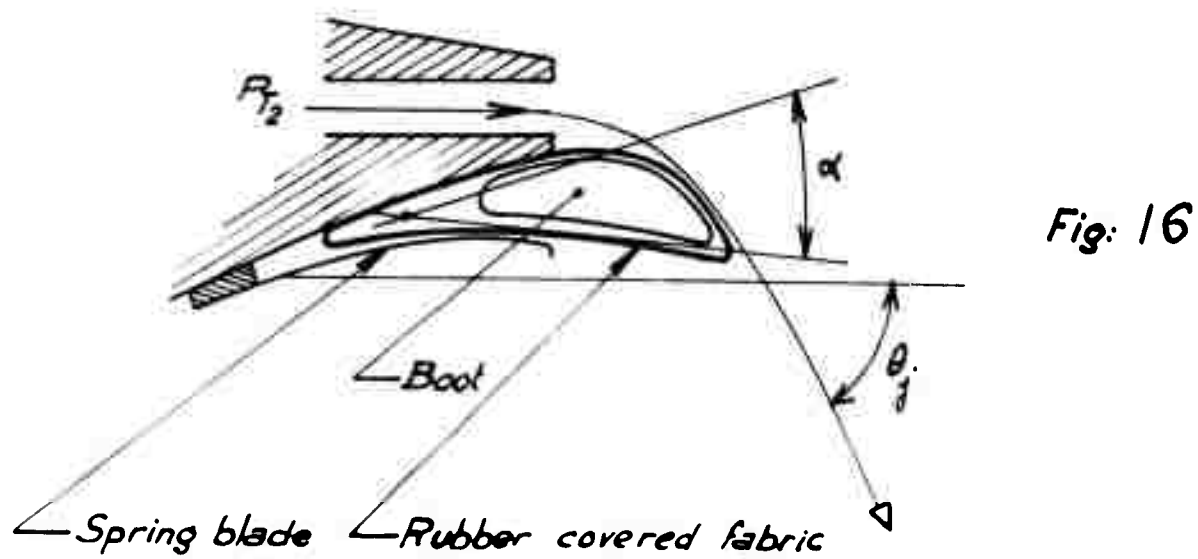
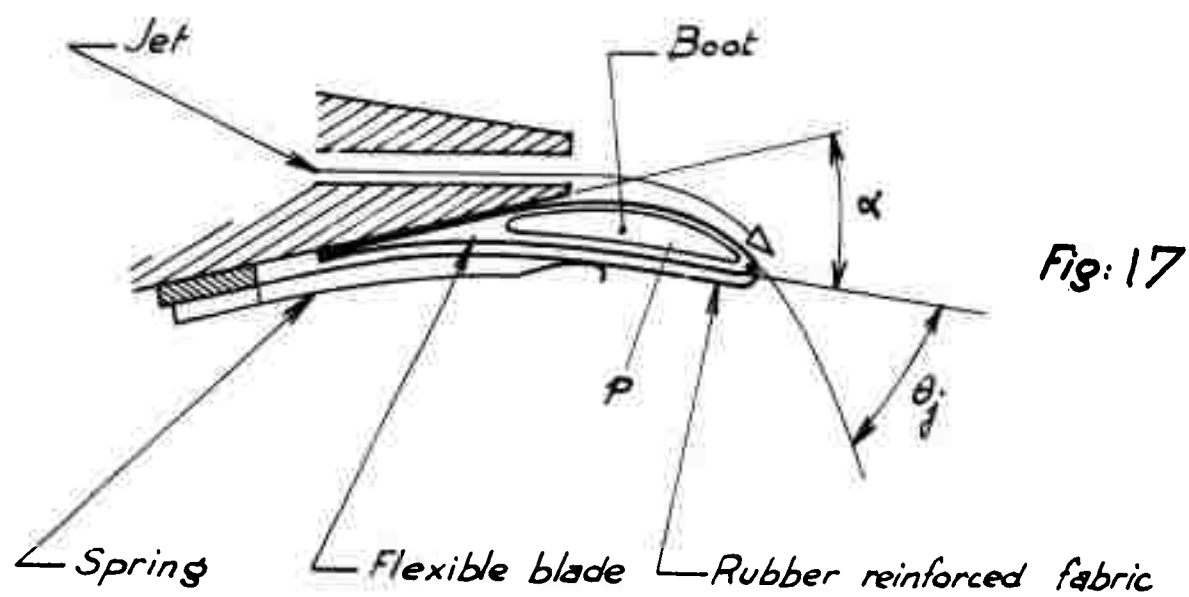
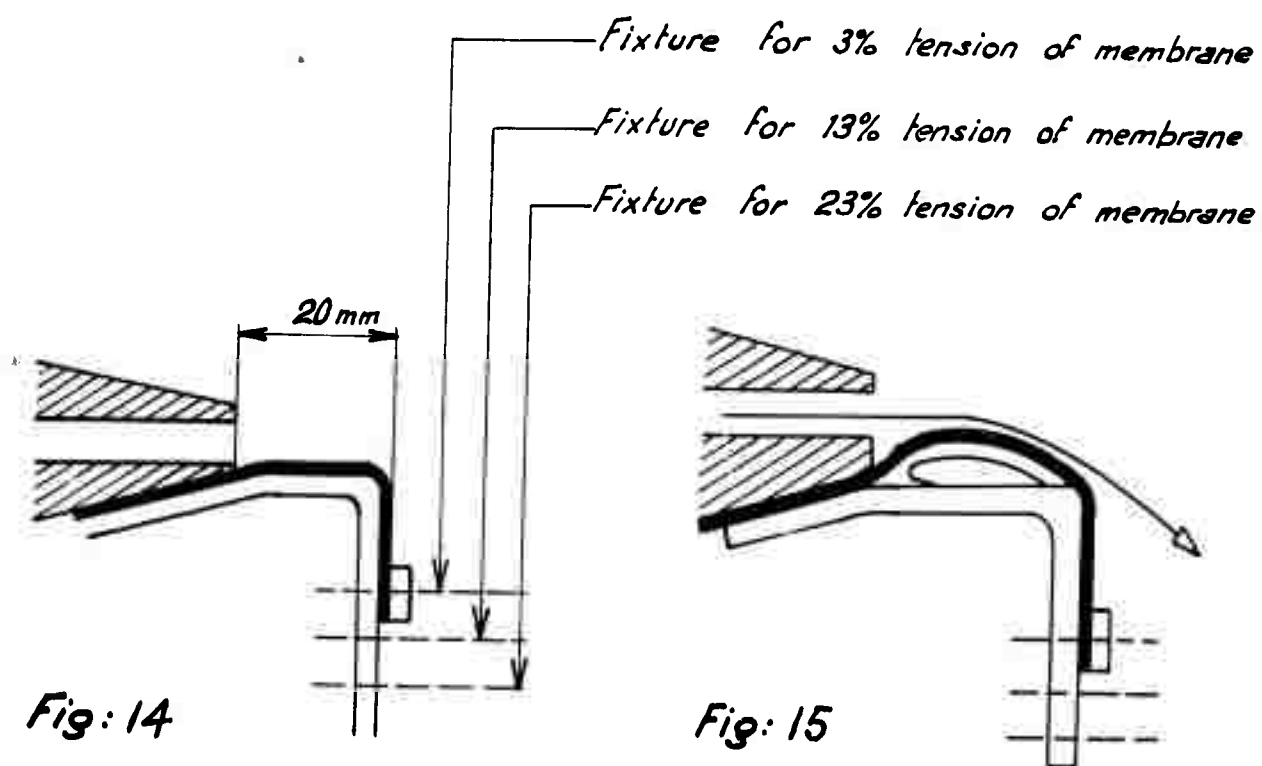


Fig. 13



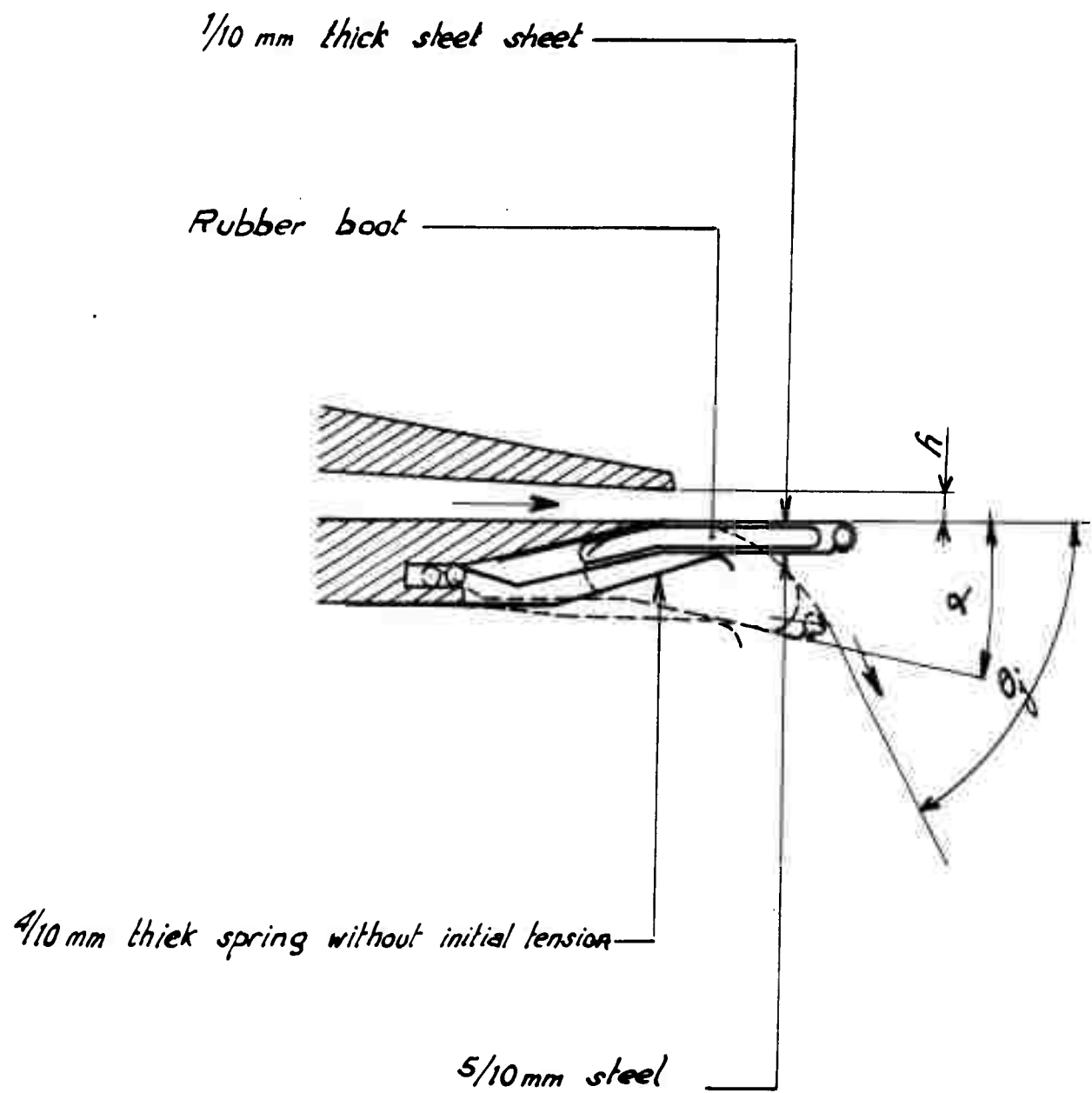
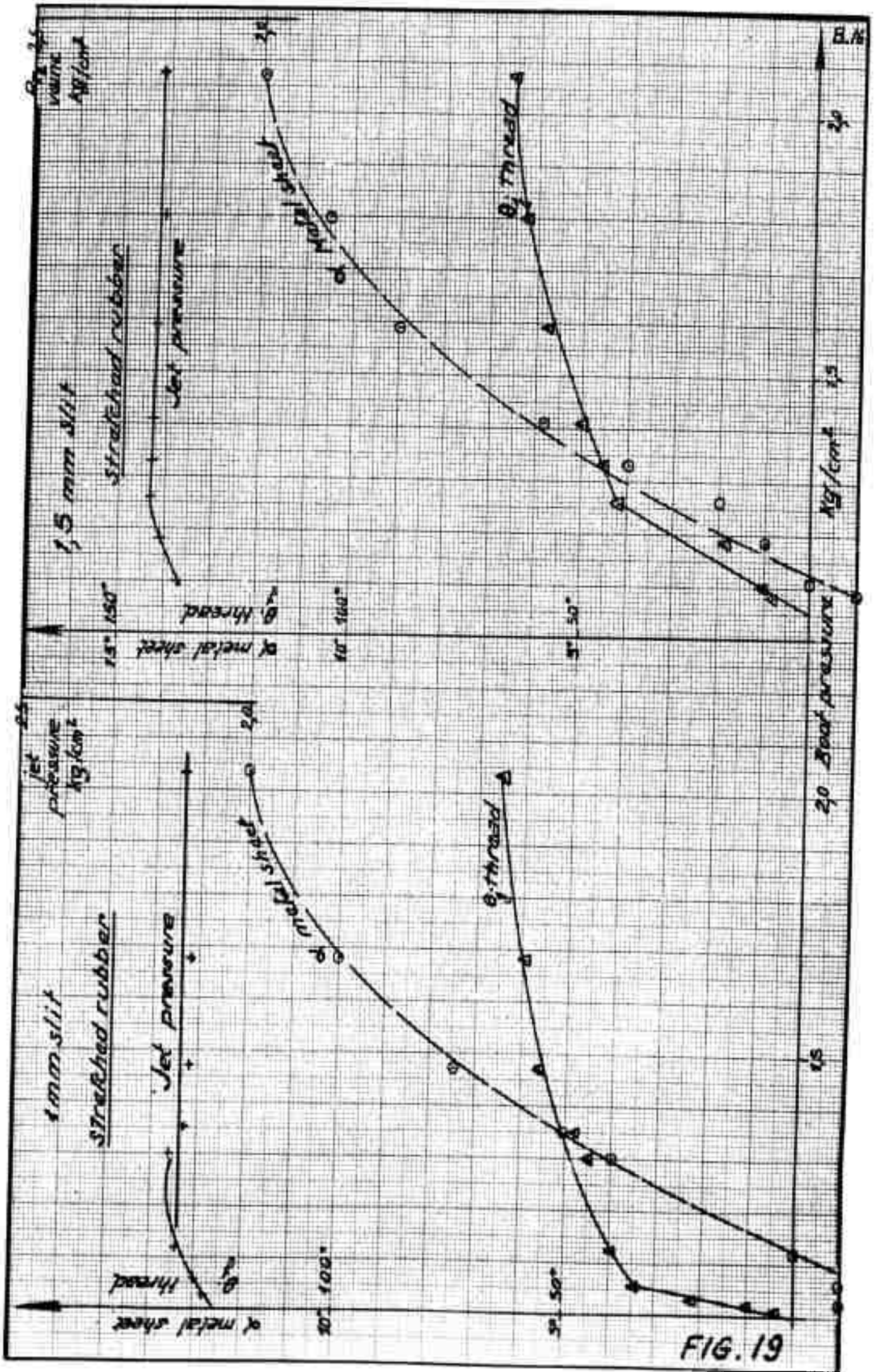
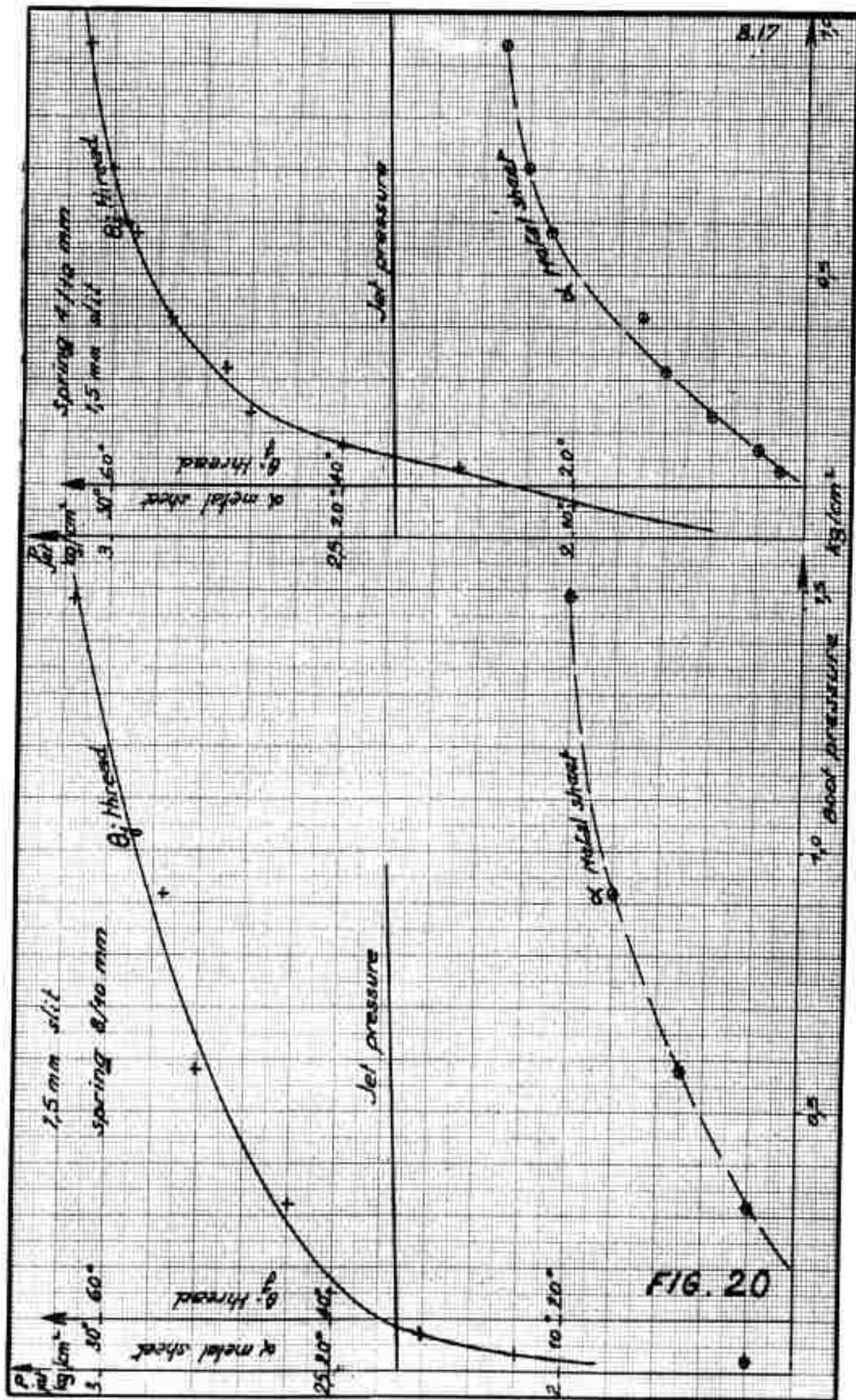


Fig: 18



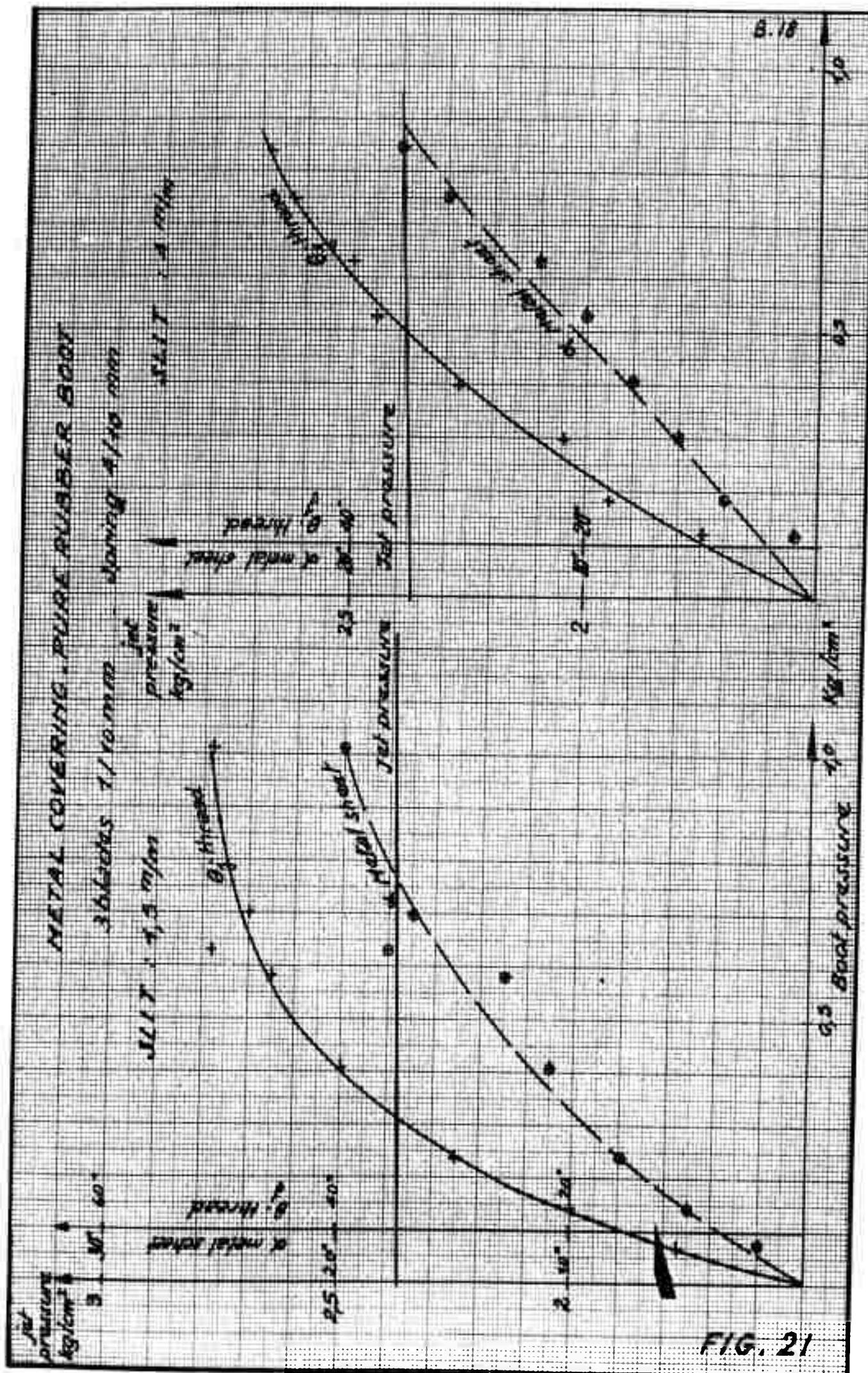


METAL COVERING. PURE RUBBER BOOT

3 blanchas 7/10 m m - morning 8/10 m m

1117 : 4.5 m/100

11/17/2008



METAL COVERING PURE RUBBER BOOT

Slit: 4 m/for Spring: 4/10 mm

2 blades 1/10 mm

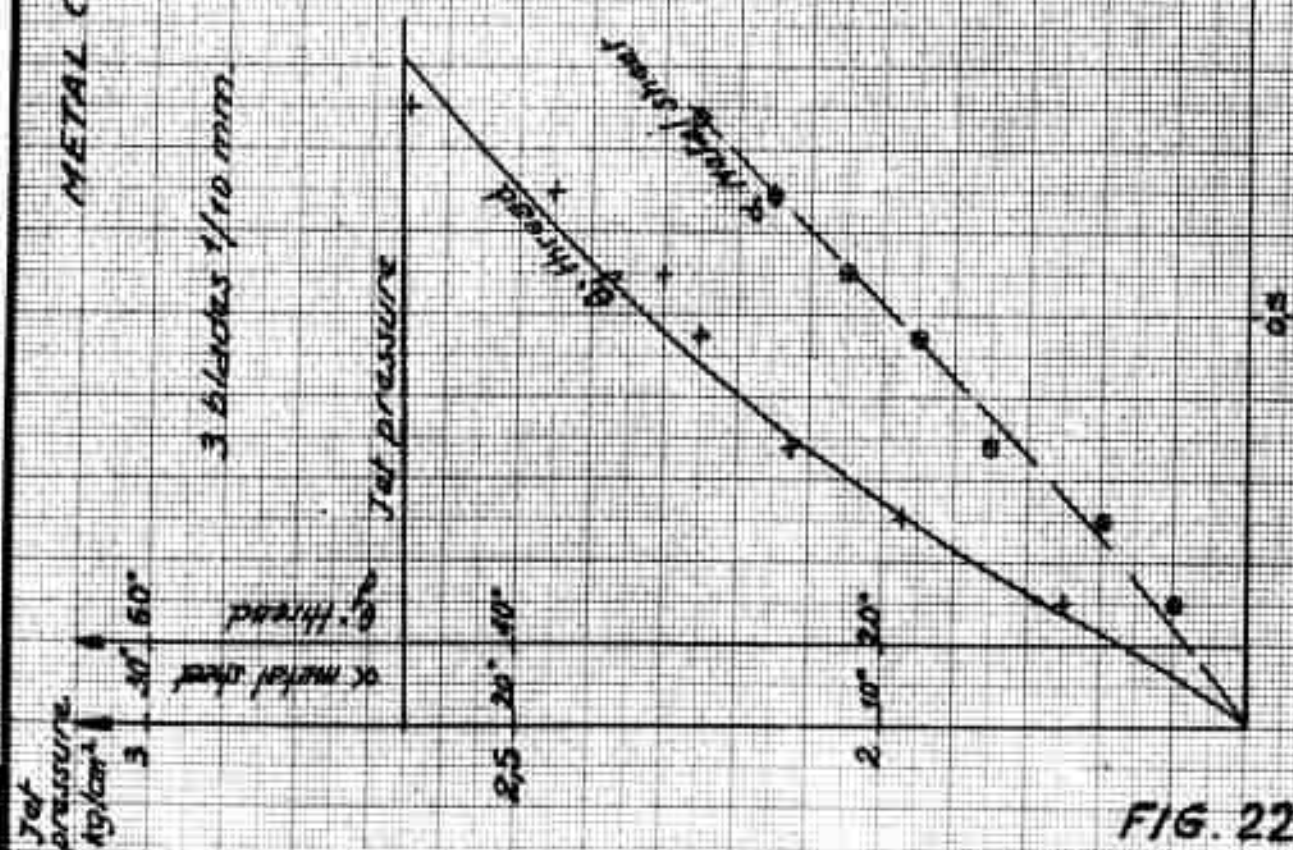
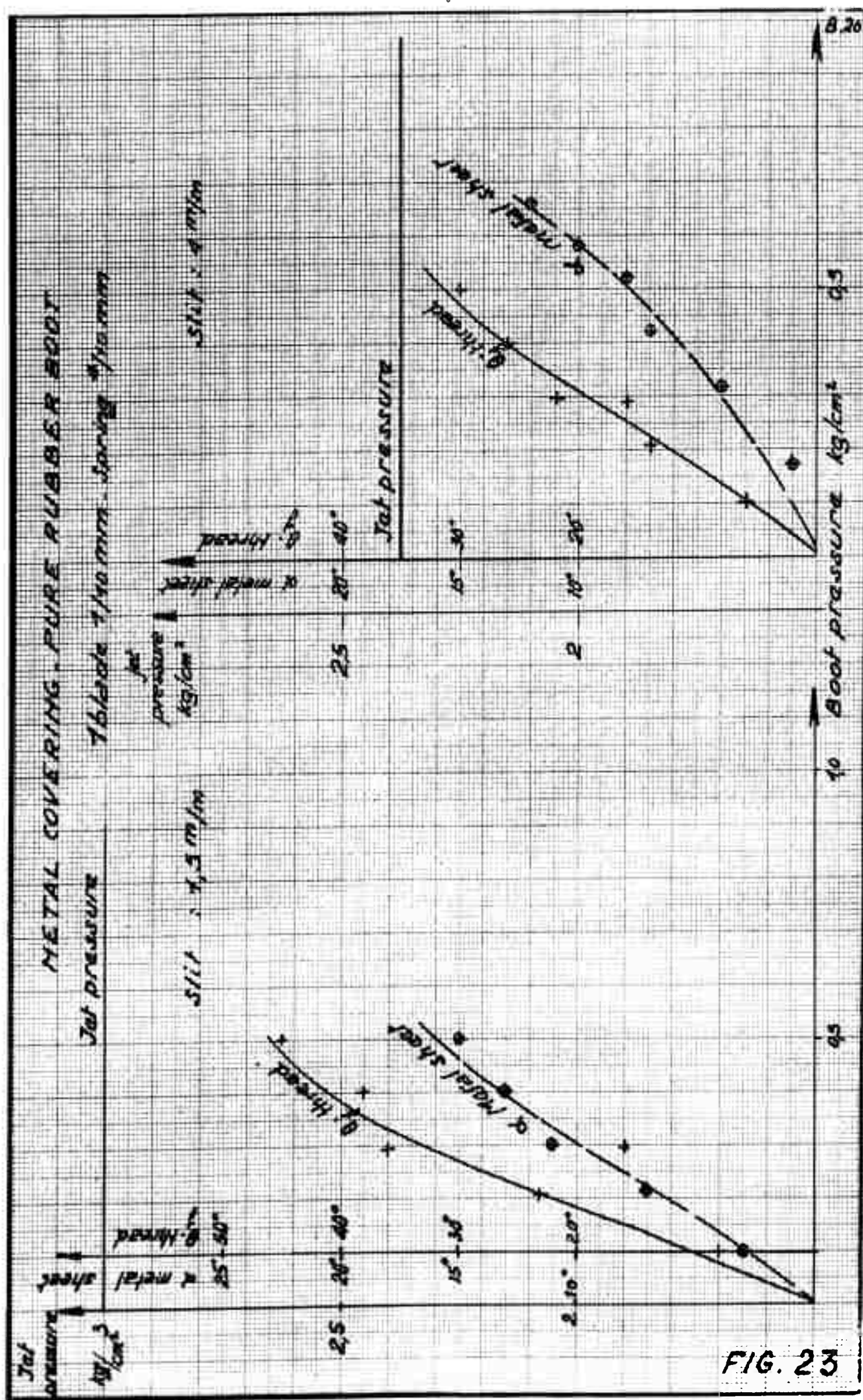


FIG. 22



Schematic configuration of spoiler type jet deflector

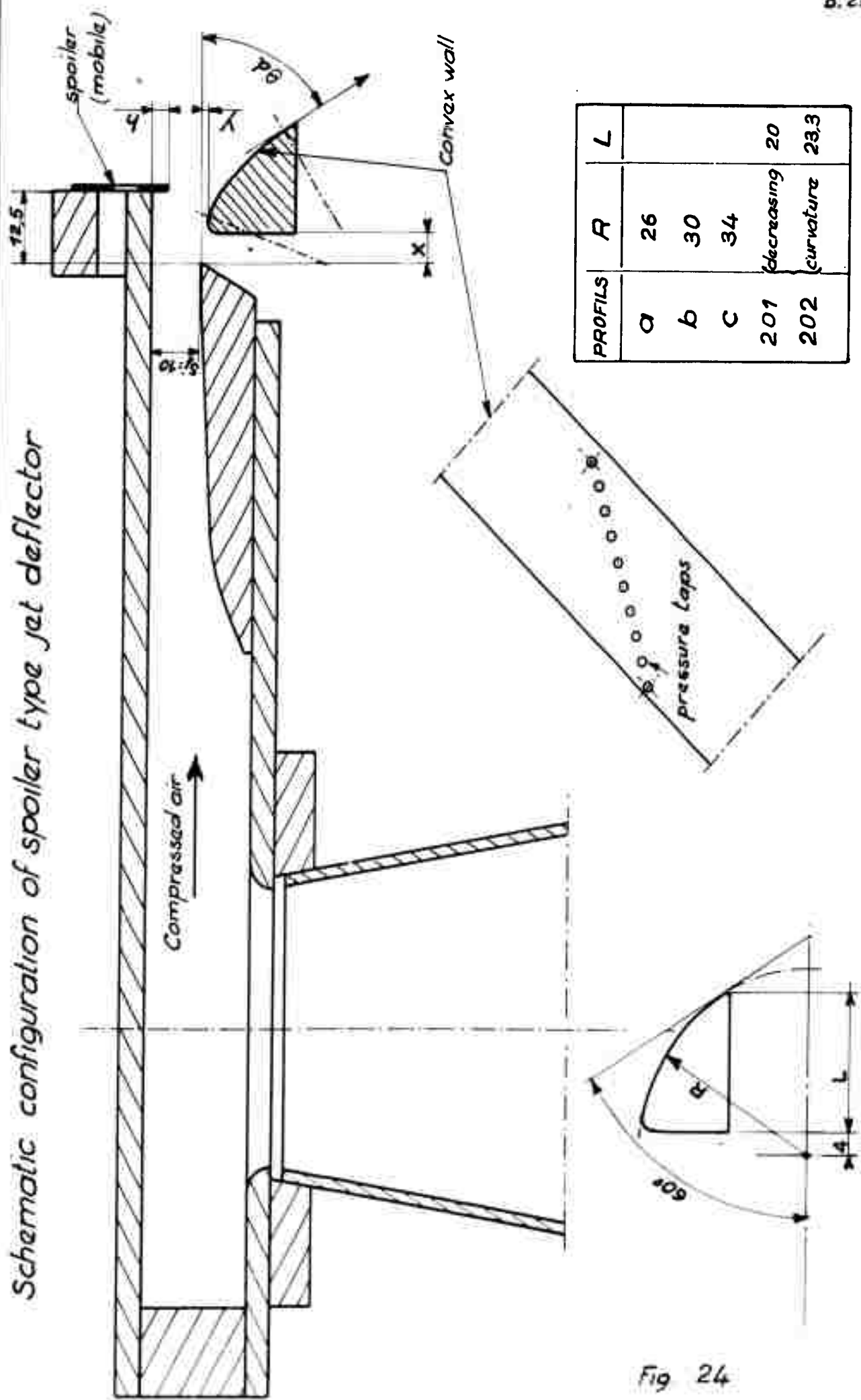
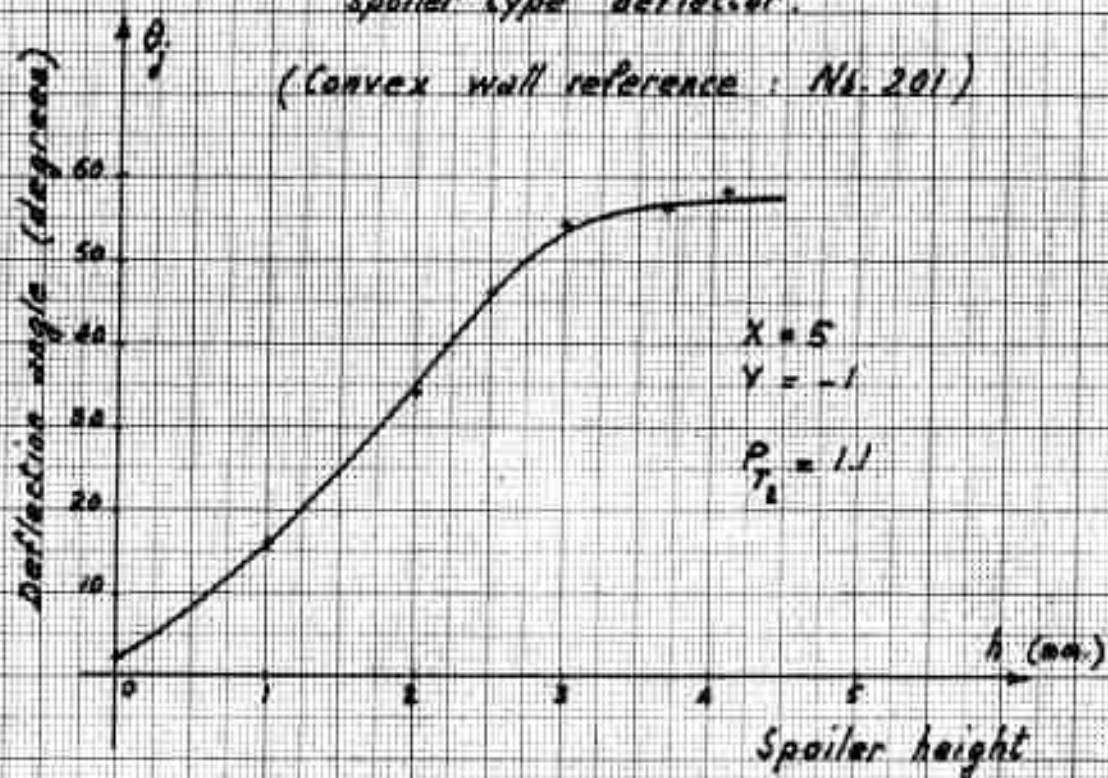


Fig 24

Deflection angles versus spoiler height for
spoiler type deflector.

(Convex wall reference: Nk. 201)



Δp
(cm. Hg)

Pressure distribution along convex wall
for different spoiler heights.

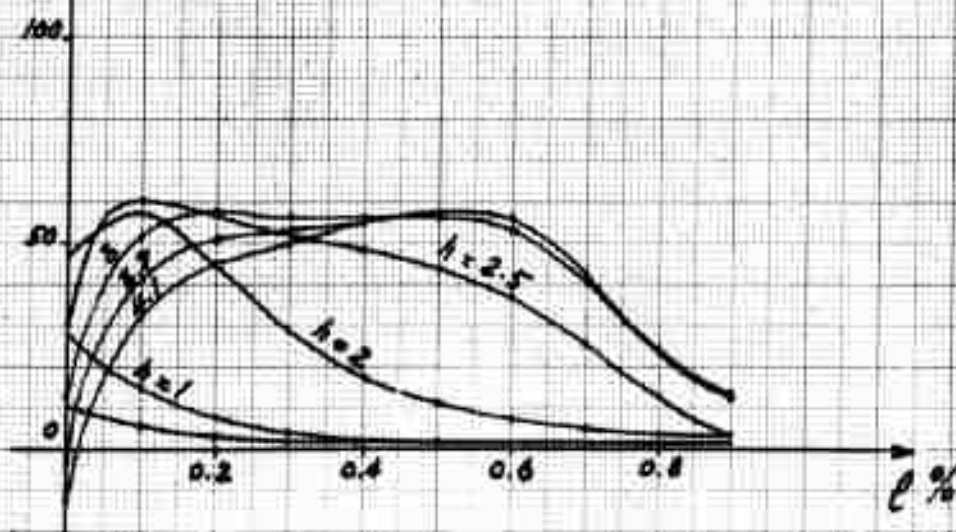


Fig. 25

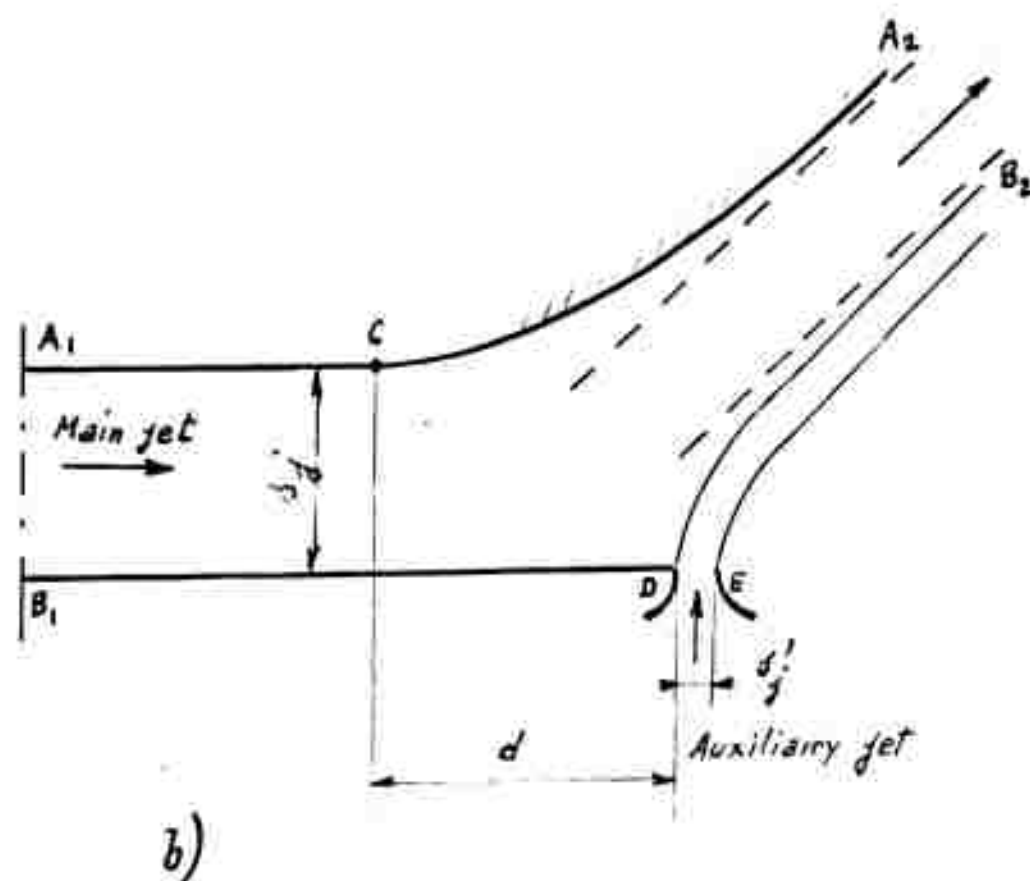
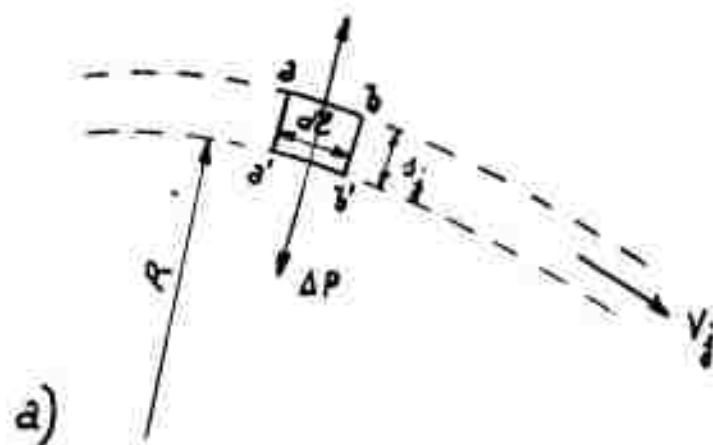


Fig. 26

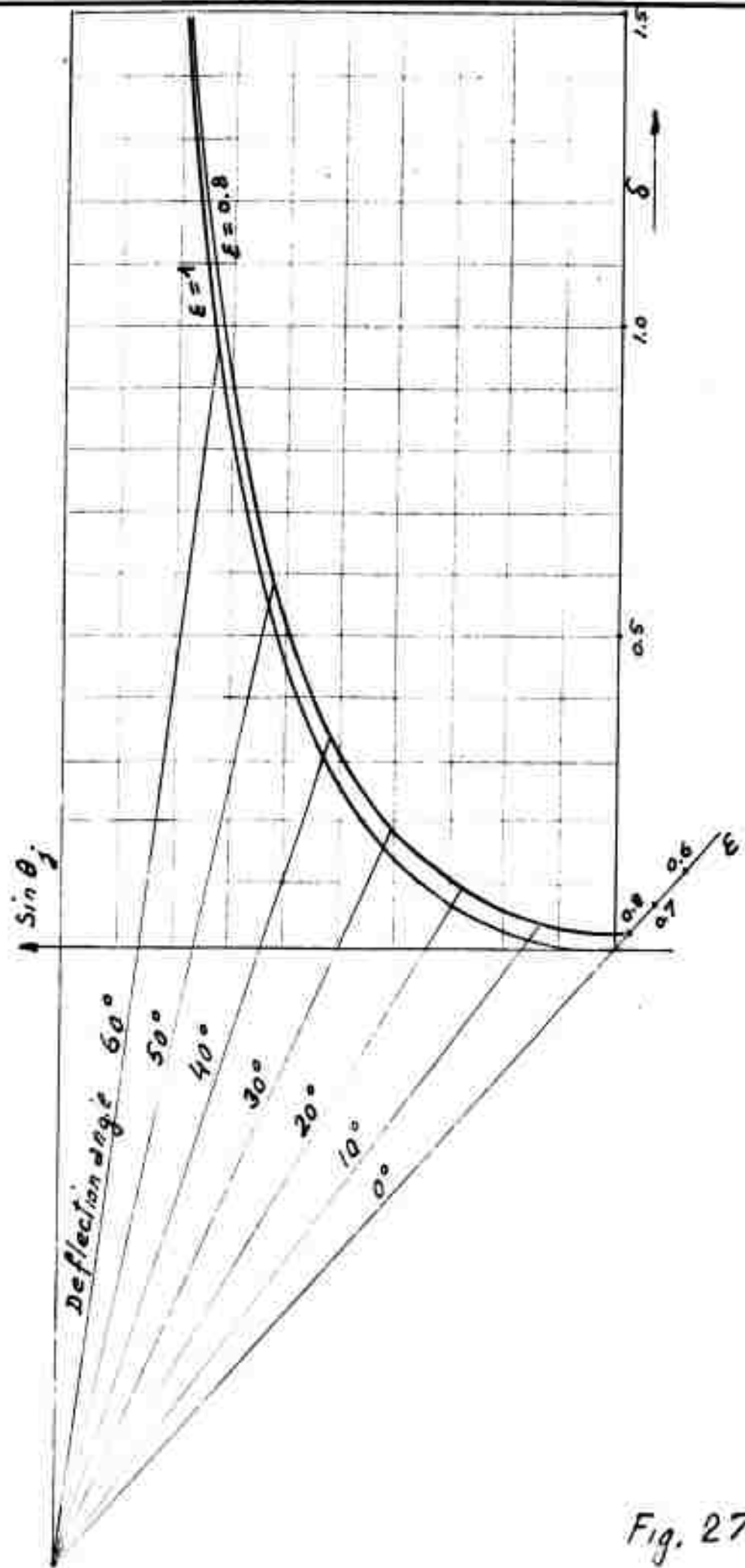


Fig. 27

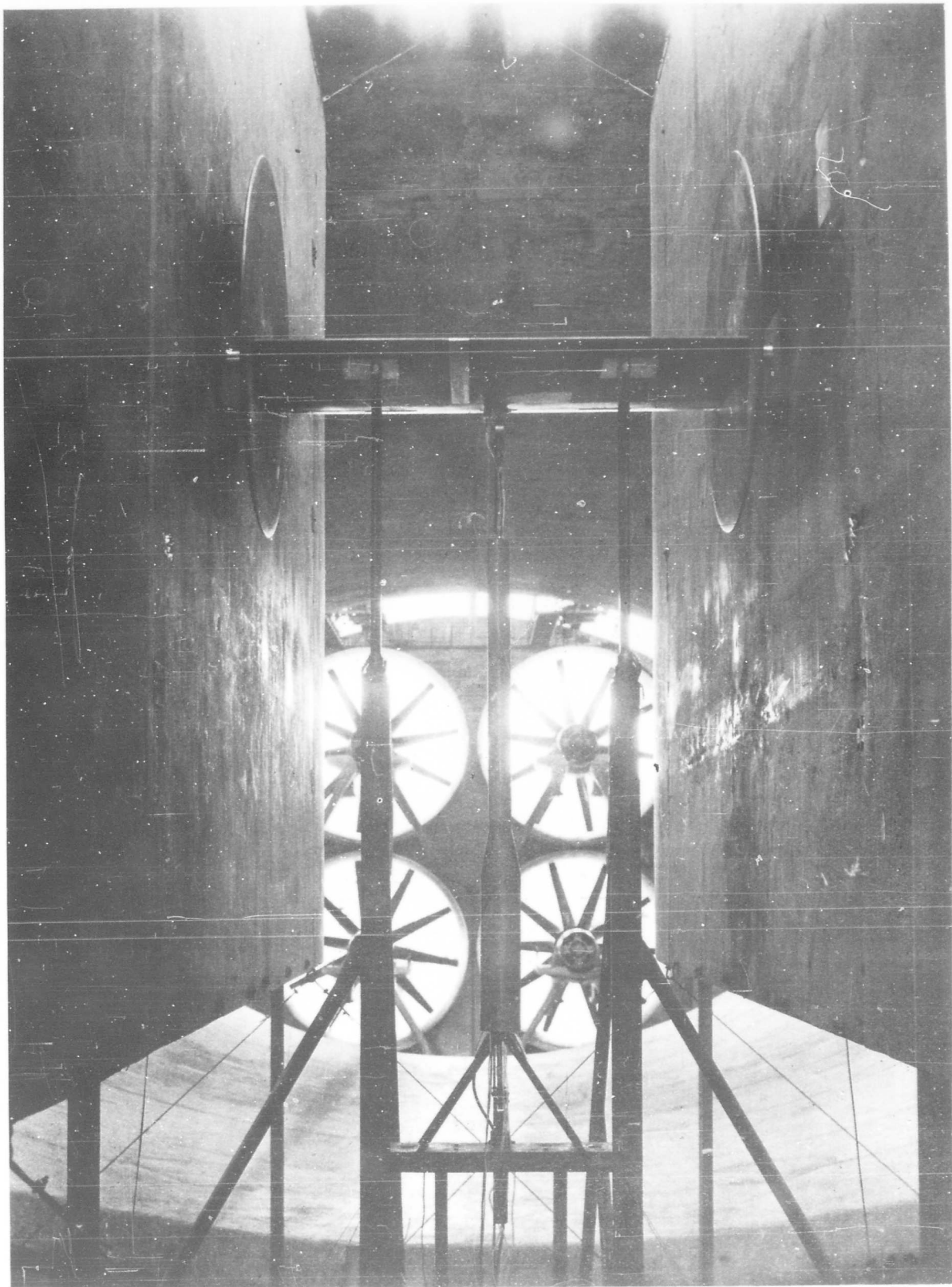
S₁ Wind - tunnel tests

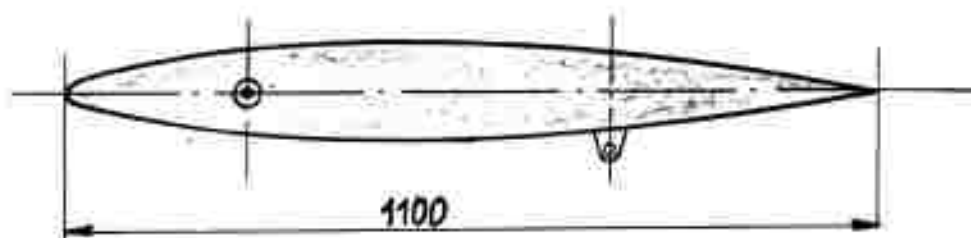
Fig. 28

Allimentation an
air comprimé.
Compressed air
intake.

FIG. 29

Model definition schemeDéfinition de la maquette

Profil NACA 66011
NACA 66011 Airfoil



Vue intrados - view from below

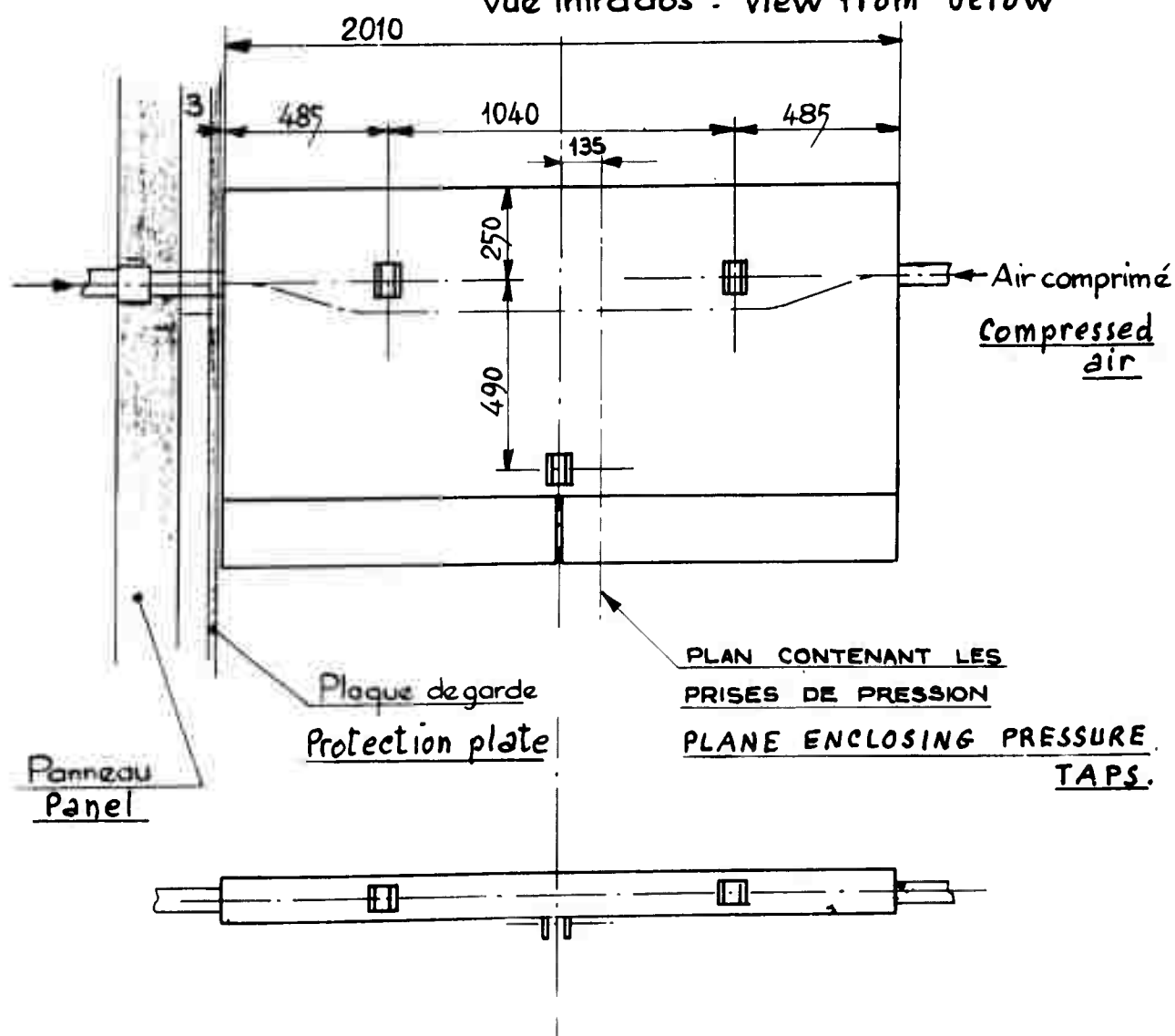


FIG. 30

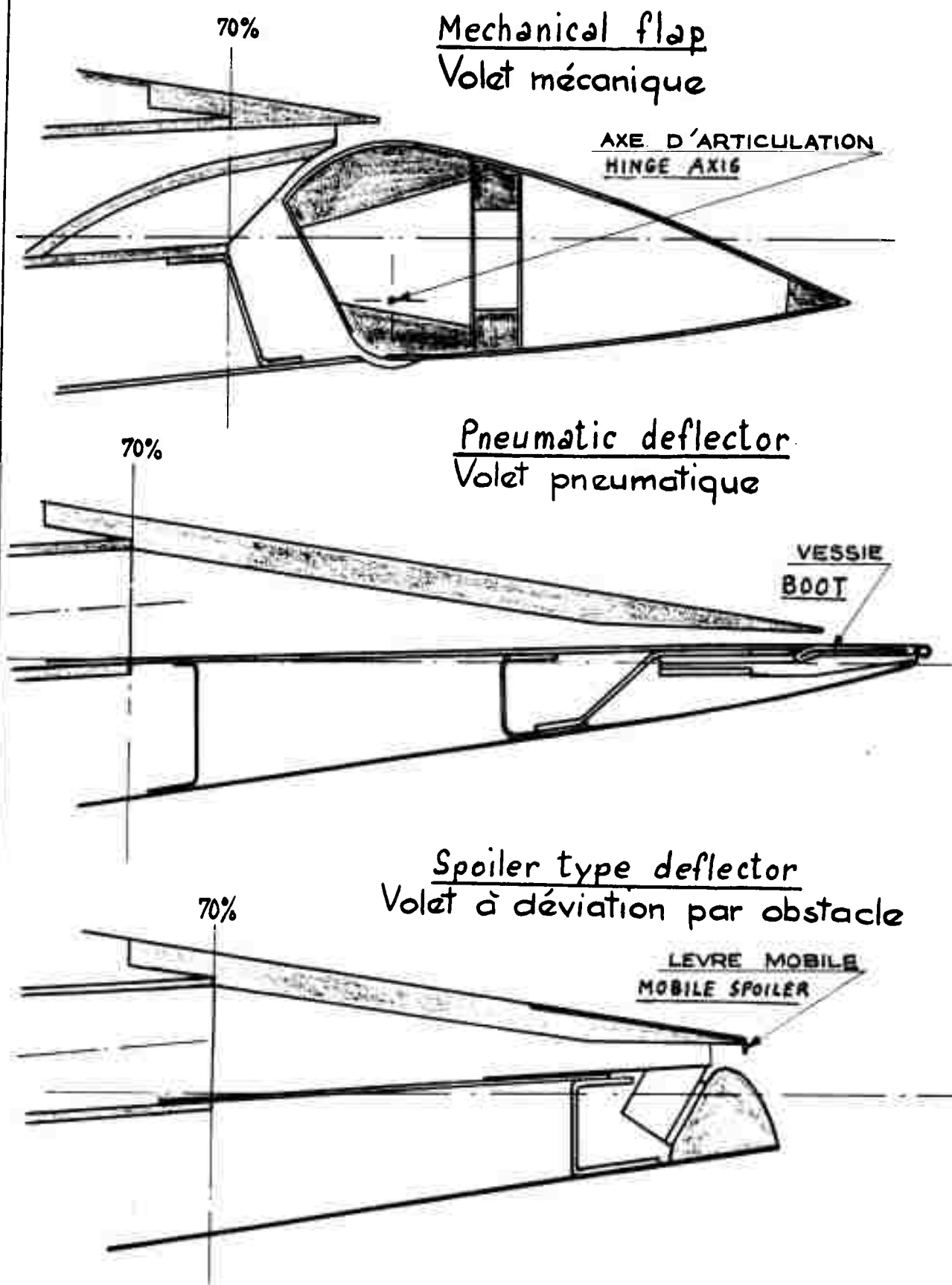
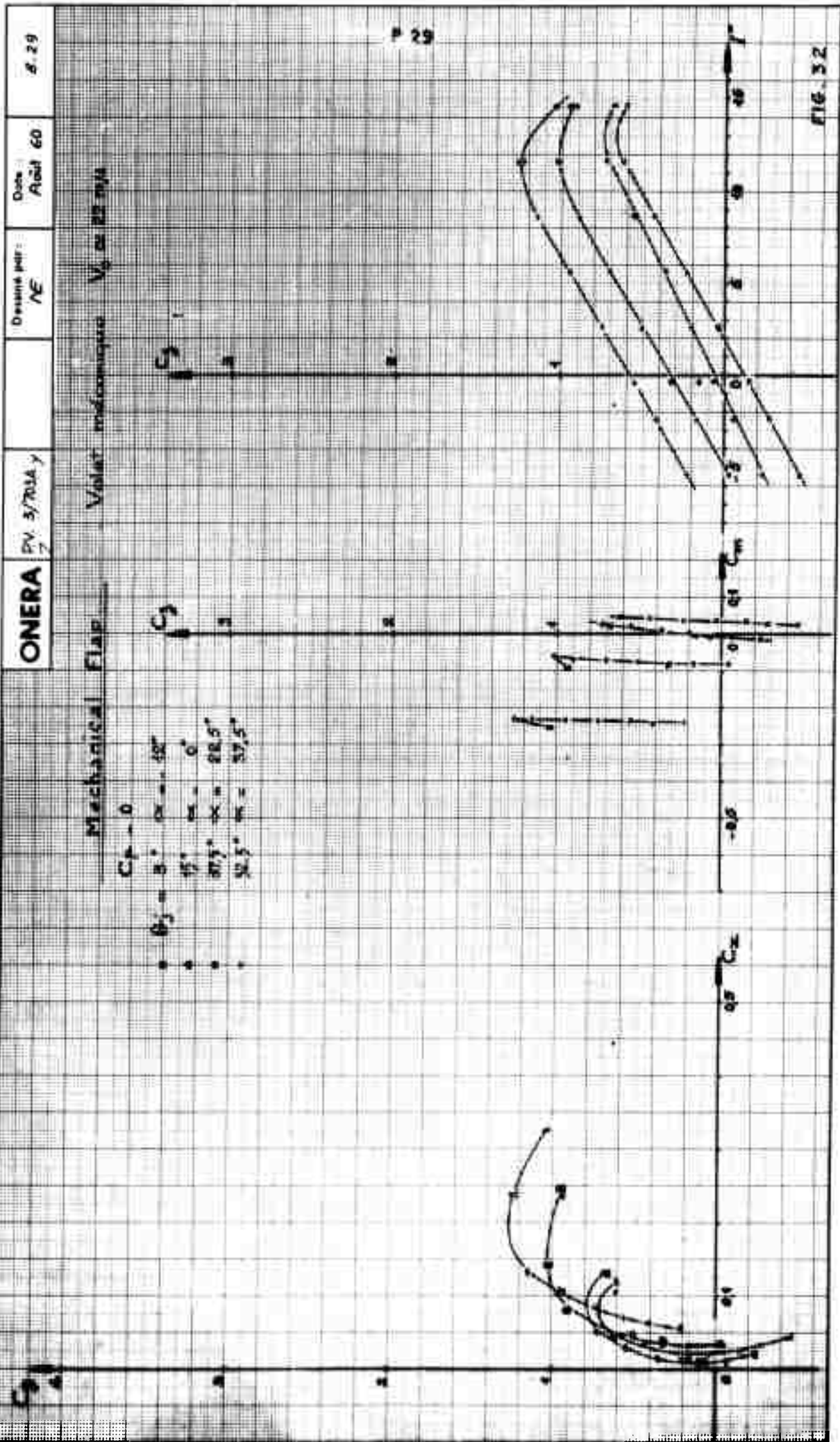


FIG. 31



ONERA

PV 5/703AY

Desiné par
NE

Date
Jul 18 60

8.30

Mechanical Flap

Velocité maximum

$V_0 = 28 \text{ m/s}$

$C_{M} = 0.09$

$\alpha_1 = 3^\circ$
 $\alpha_2 = 6^\circ$
 $\alpha_3 = 12^\circ$
 $\alpha_4 = 18^\circ$
 $\alpha_5 = 28.5^\circ$
 $\alpha_6 = 37.5^\circ$

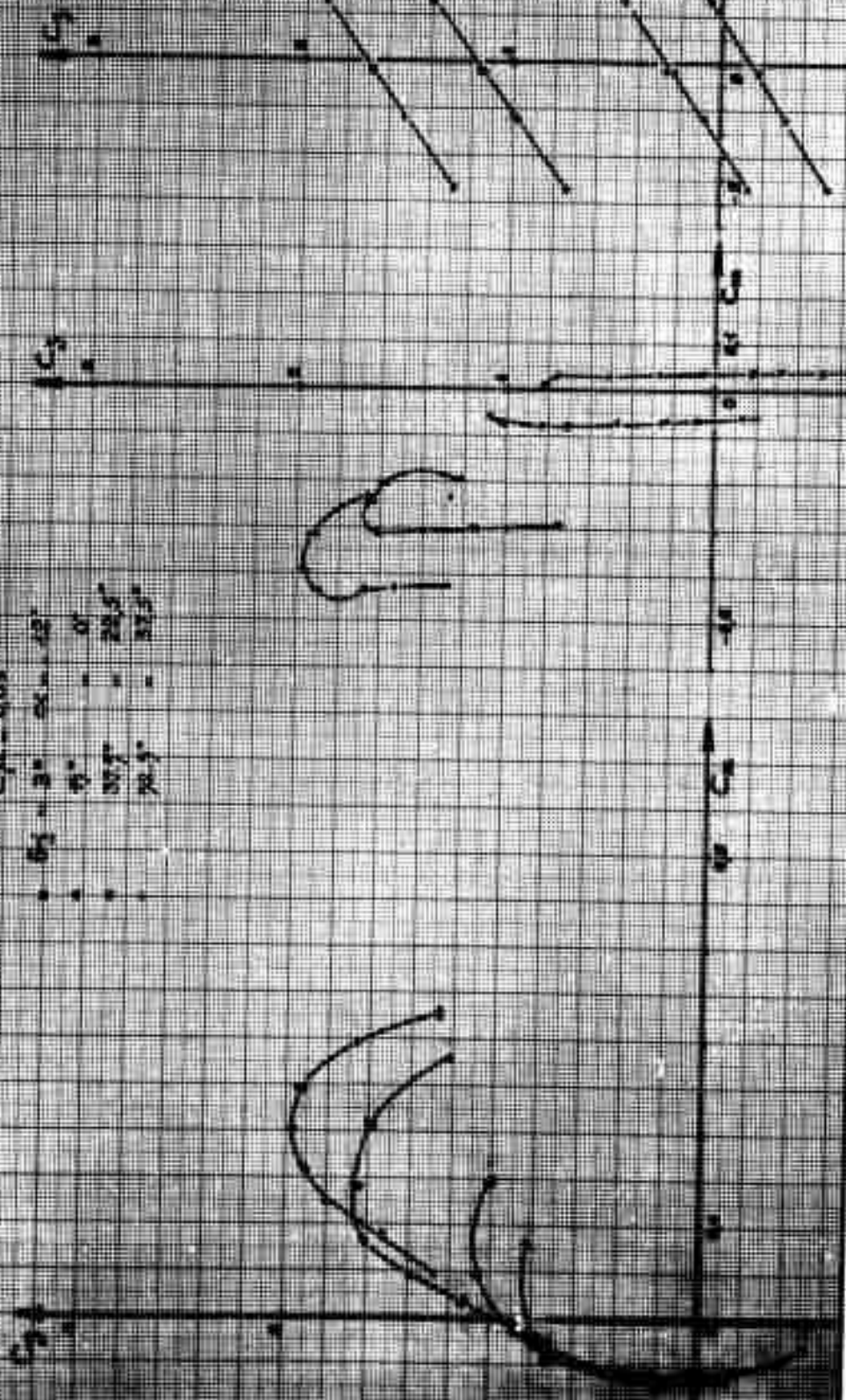
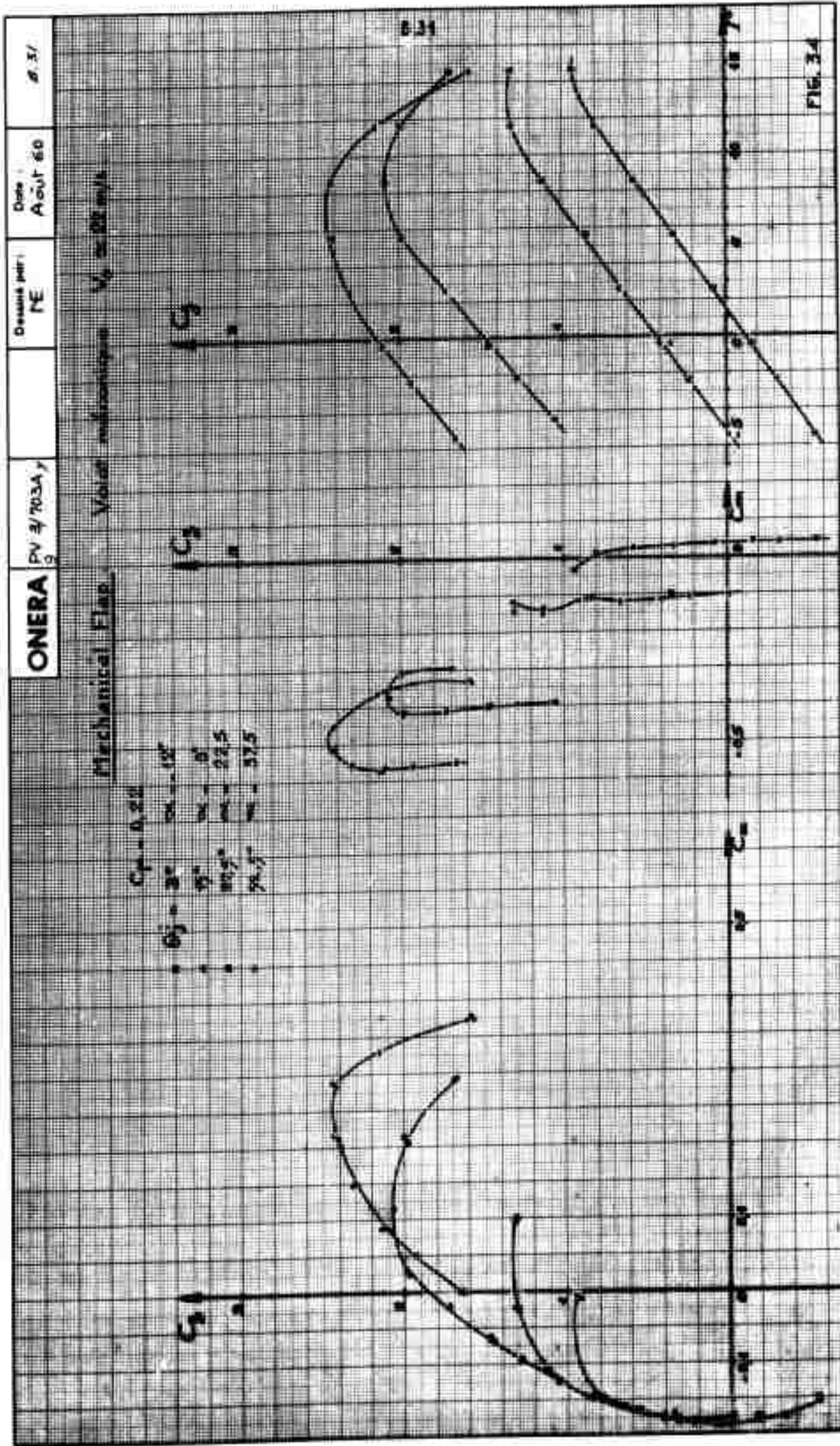


Fig. 53



ONERA

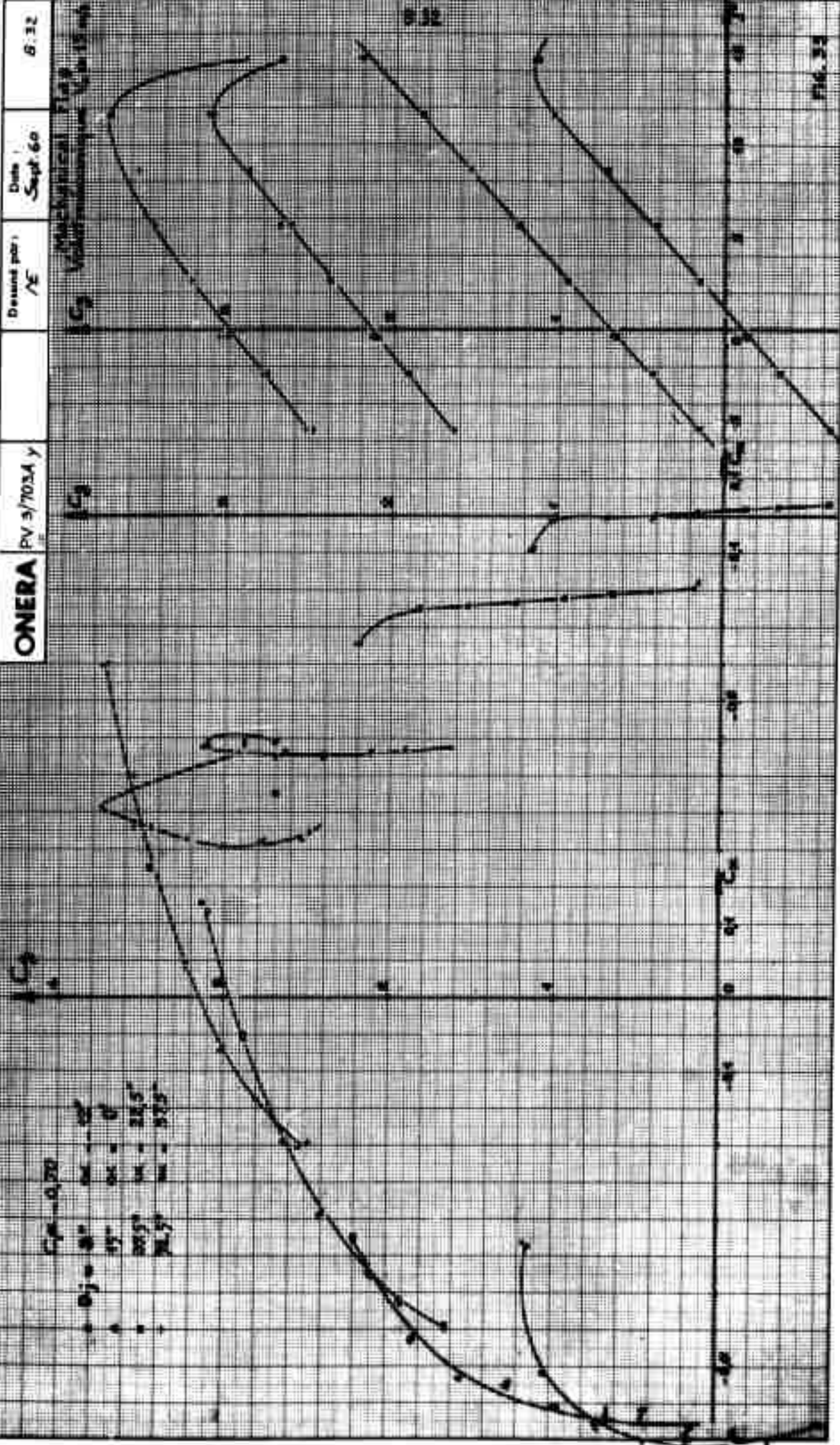
PV 3/7034 y

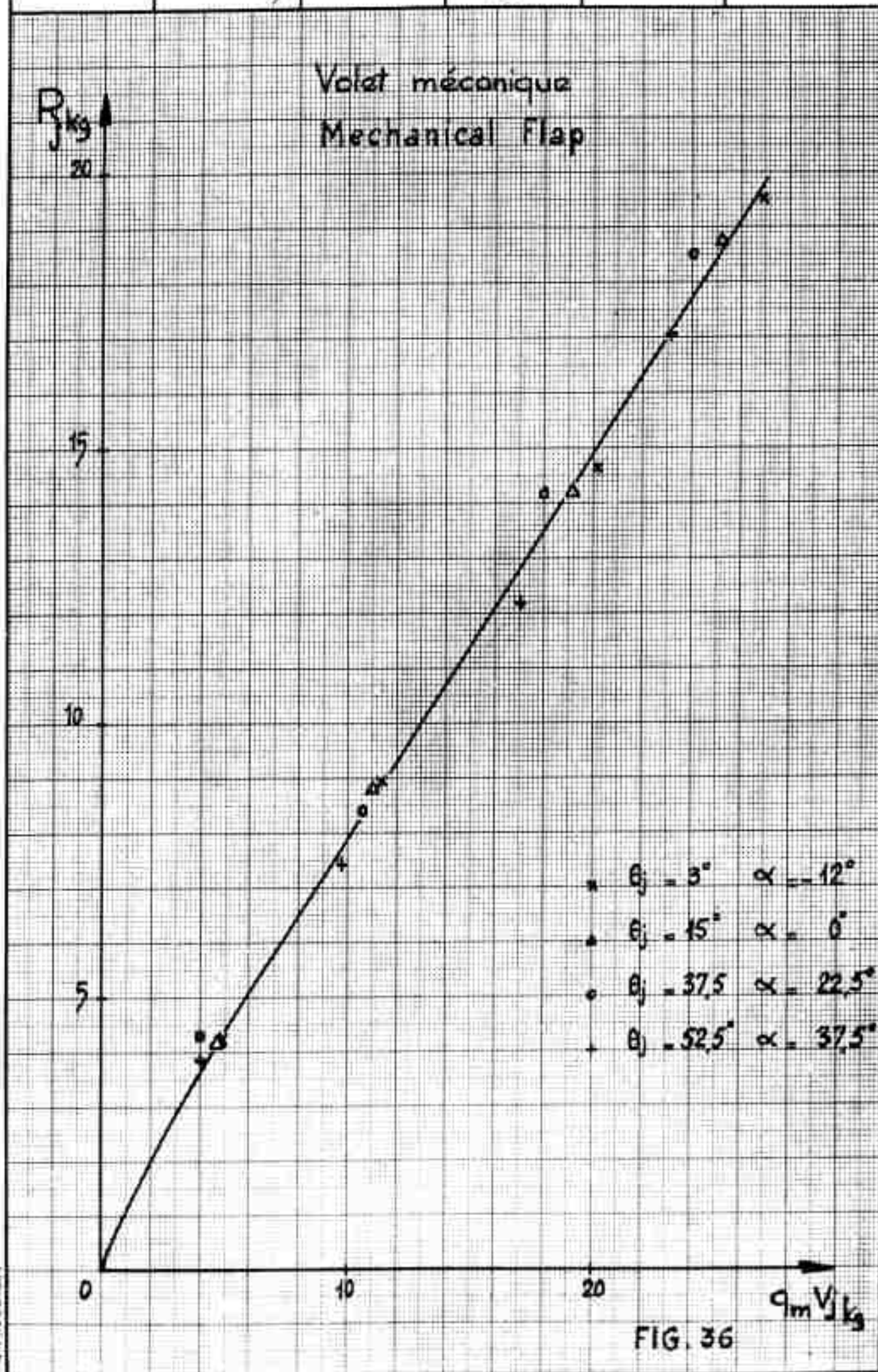
Desand par
/E

Date
Sept 60

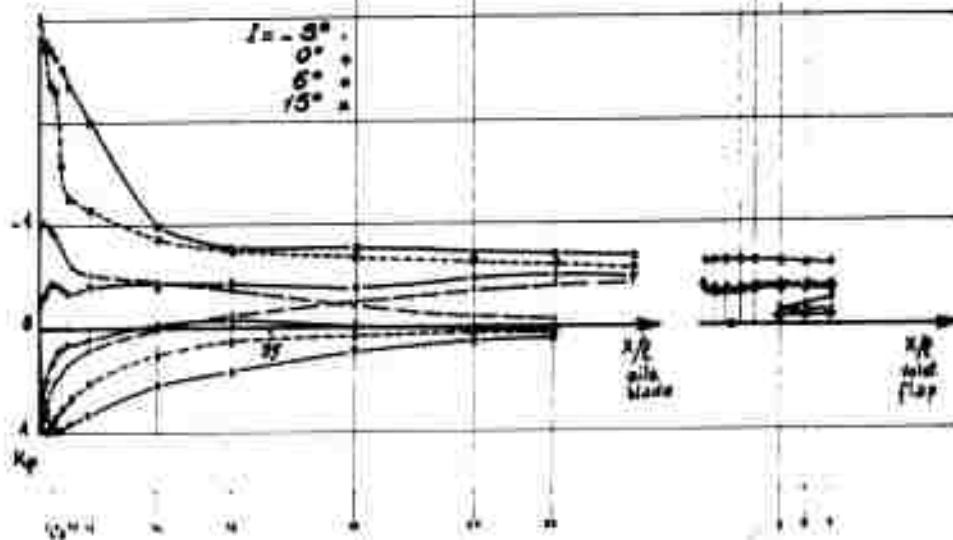
B:32

Mechanical Properties
of Polyethylene
at 15 mb

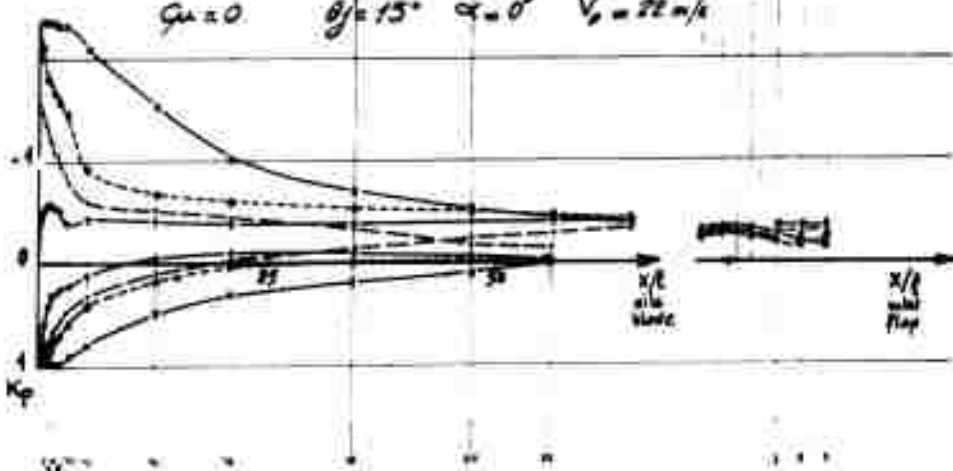




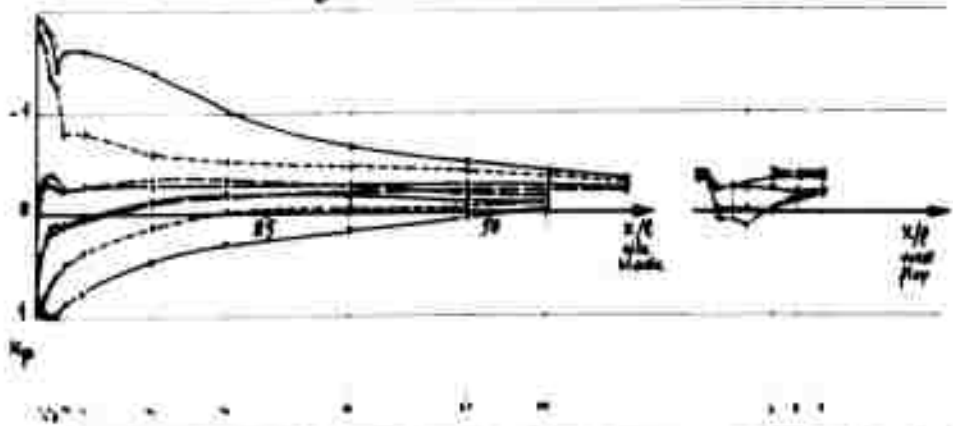
$C_p = 0 \quad \theta_f = 37.5^\circ \quad \alpha = 22.5^\circ \quad V_\infty = 22 \text{ m/s}$



$C_p = 0 \quad \theta_f = 15^\circ \quad \alpha = 0^\circ \quad V_\infty = 22 \text{ m/s}$



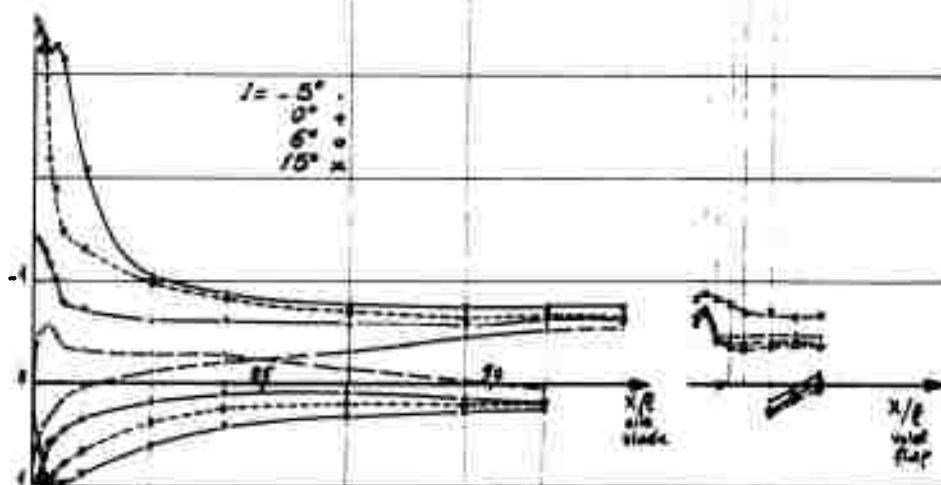
$C_p = 0 \quad \theta_f = 3^\circ \quad \alpha = -12^\circ \quad V_\infty = 22 \text{ m/s}$



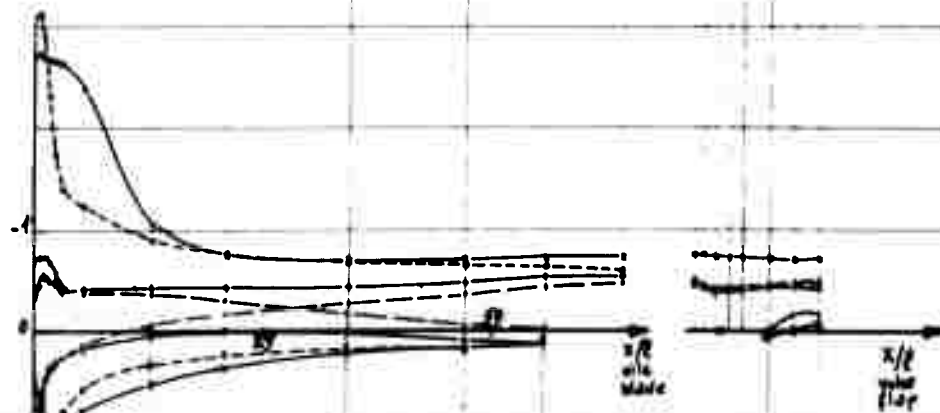
ONERA 19V.3/7632A Y
 DATE 30 Sept 60
 0.34

MECHANICAL FLAP
VOLET MECANIQUE

$Q_v = 0$ $\theta_j = 52,5^\circ$ $\alpha = 37,5^\circ$ $V_o = 28 \text{ m/s}$



$Q_v = 0$ $\theta_j = 45^\circ$ $\alpha = 30^\circ$ $V_o = 22 \text{ m/s}$



B. 35

DATE
Sept 60

DESIGNER
R. E.

BY
3/7/60

ONE RA

MECHANICAL FLAP
VOLET MECANIQUE

Photos 22 23

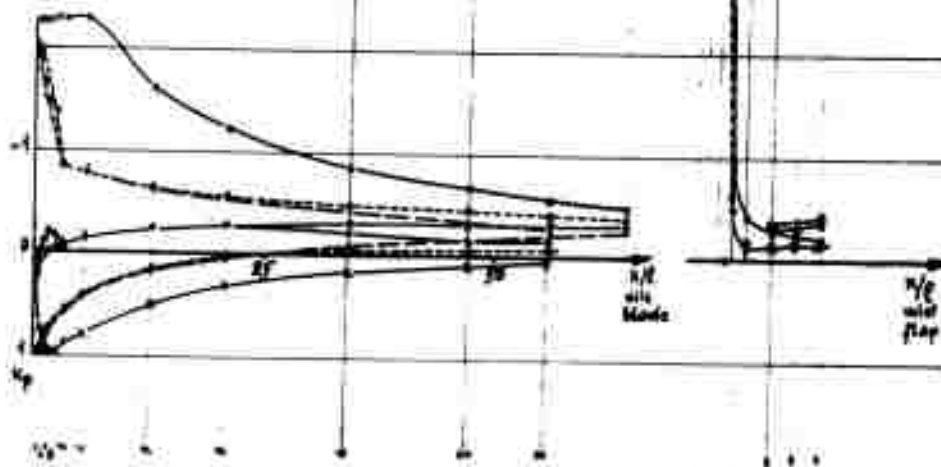
47 48
50 51

B.36

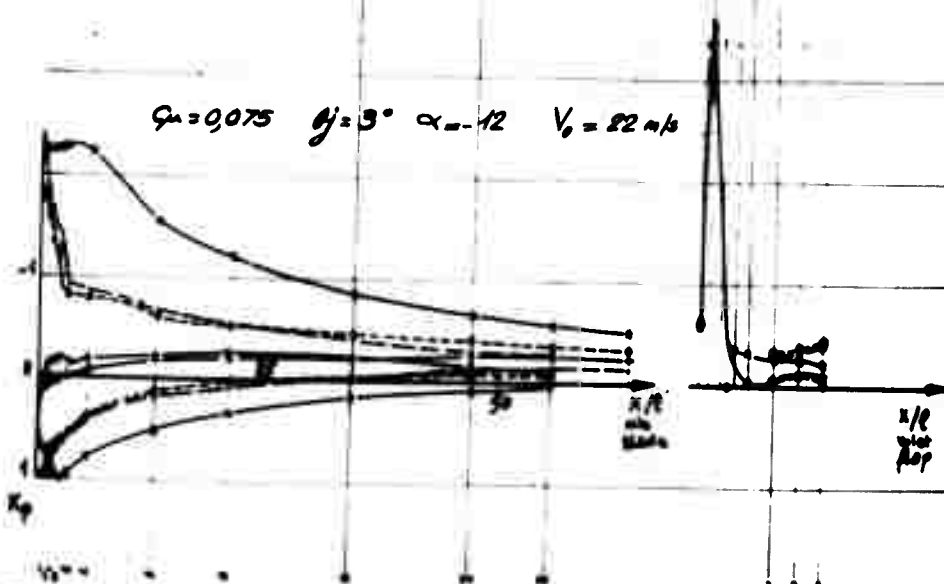
FIG. 39

$C_{\mu} = 0.075$ $\theta_j = 15^\circ$ $\alpha = 0^\circ$ $V_o = 22 \text{ m/s}$

$I = 5^\circ$
 0°
 6°
 15°

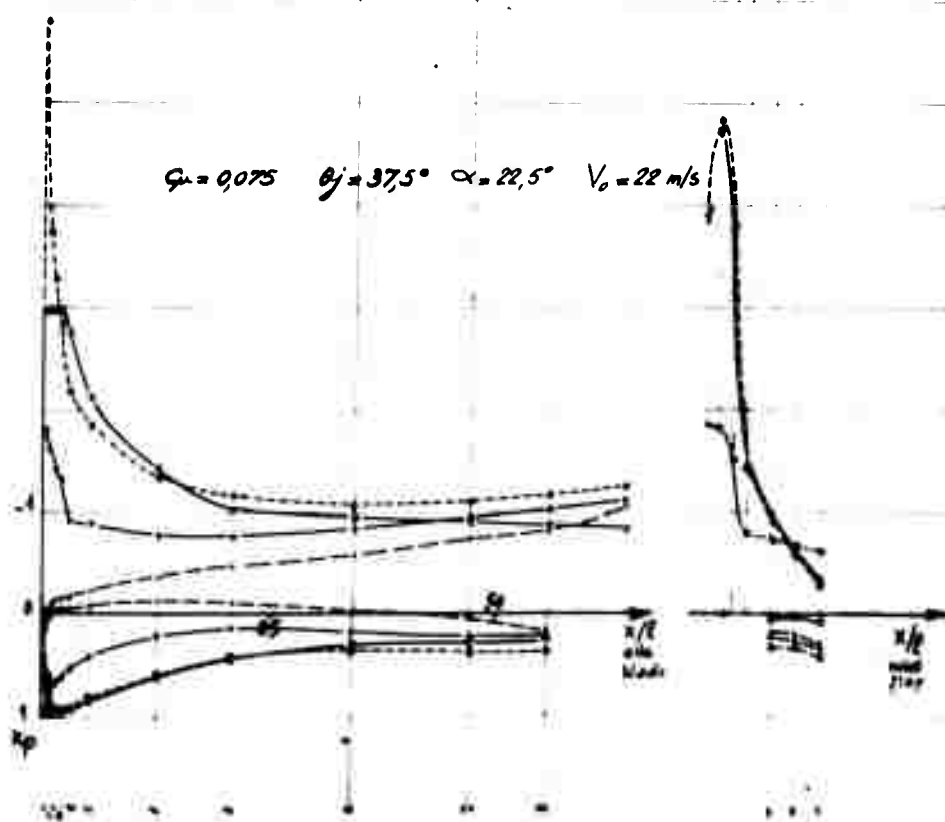
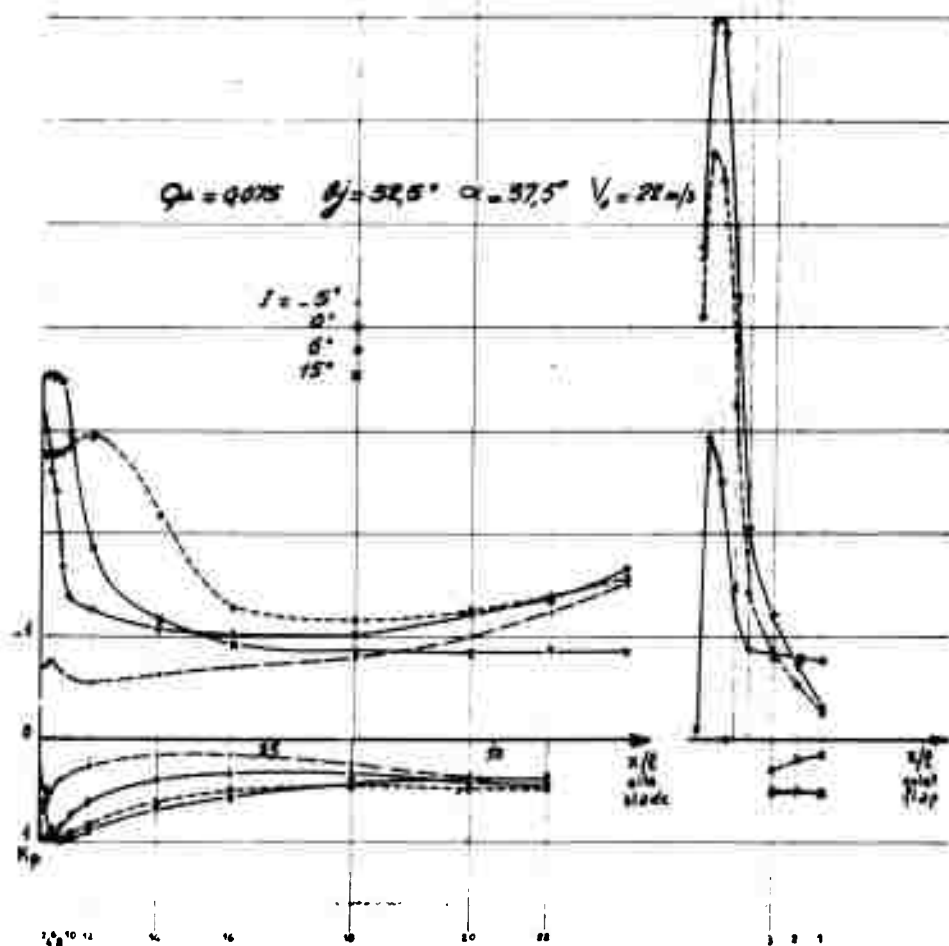


$C_{\mu} = 0.075$ $\theta_j = 3^\circ$ $\alpha = -12^\circ$ $V_o = 22 \text{ m/s}$



ONERA [P.V. 37404] [RESEARCH UNIT] [DATE] [B.36]

MECHANICAL FLAP
VOLET MECANIQUE



Photos 68 69
70 71

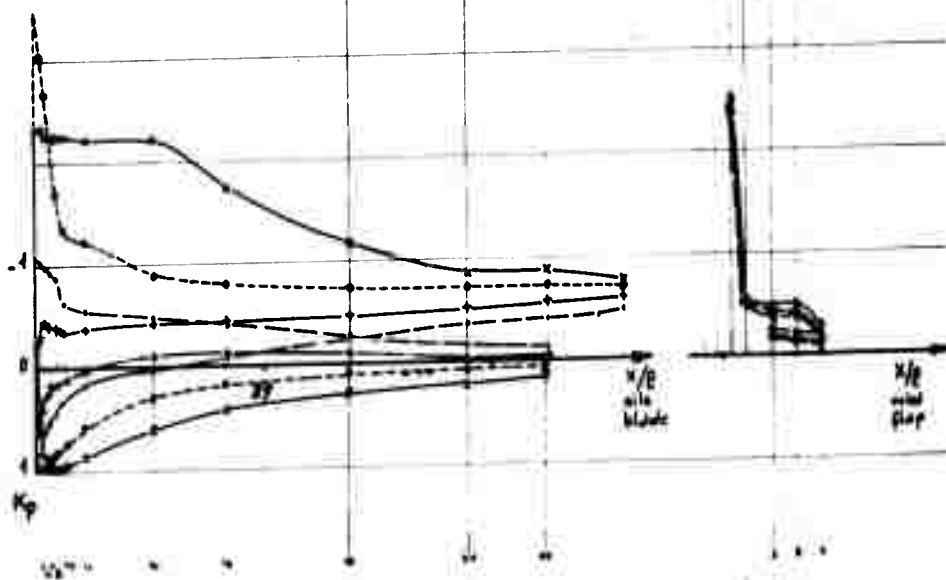
64 65
66 67

B.38

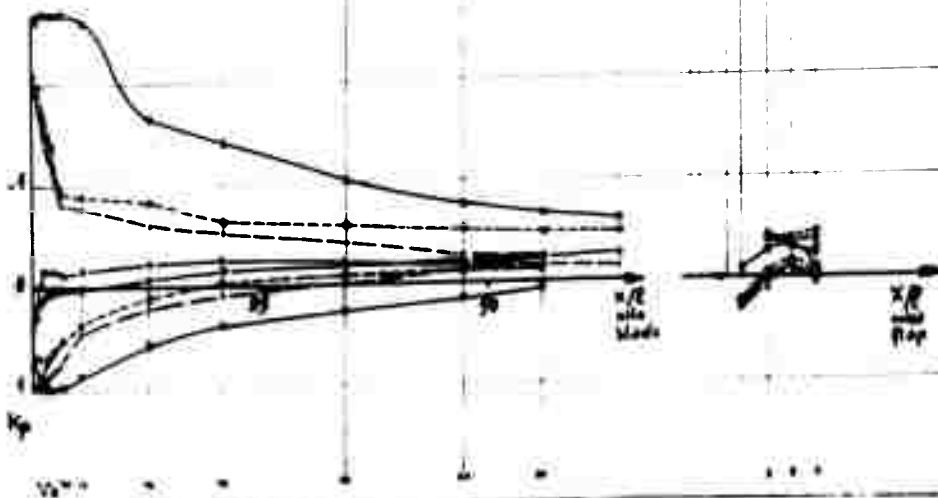
FIG. 41

$$C_{\mu} = 0.22 \quad \theta_j = 15^\circ \quad \alpha = 0^\circ \quad V_o = 22 \text{ m/s}$$

$1 \times -5^\circ$
 $0 \times 0^\circ$
 $6 \times 6^\circ$
 $15 \times 15^\circ$



$$C_{\mu} = 0.22 \quad \theta_j = 3^\circ \quad \alpha = -12^\circ \quad V_o = 22 \text{ m/s}$$



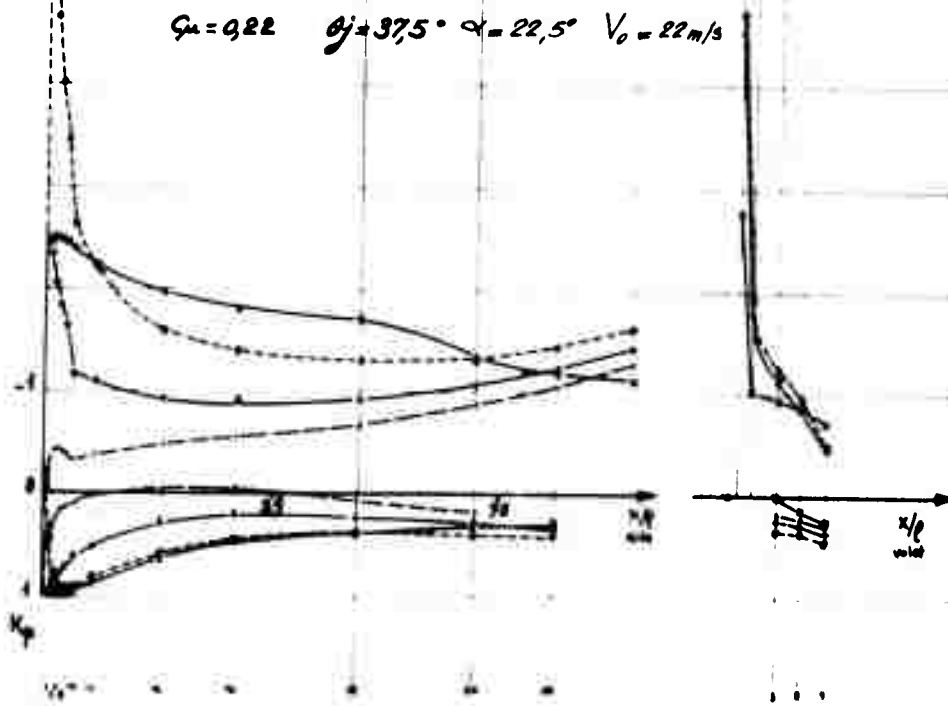
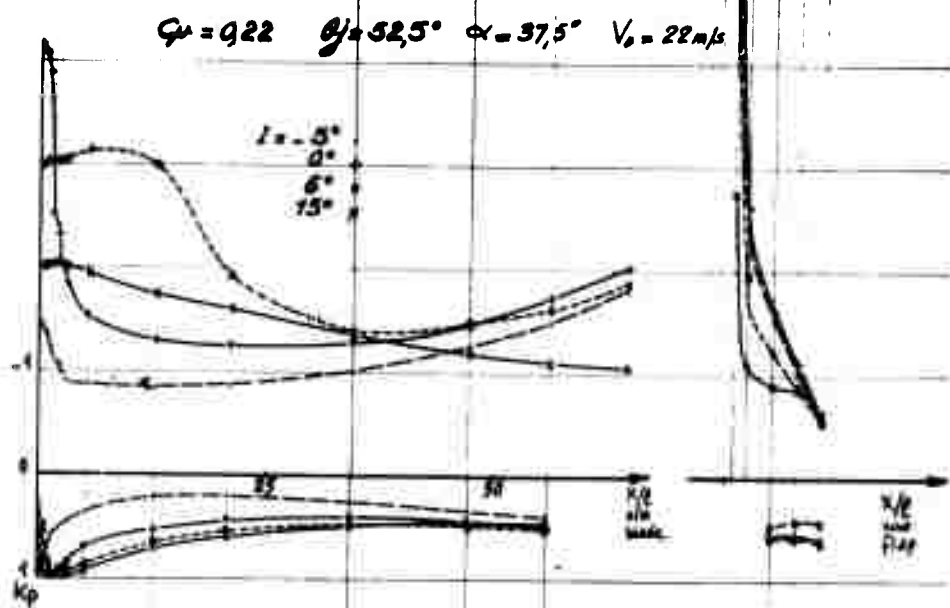
ONERA P.V. 3708 A Y

DESIGNED PAR
N

DATE
Sept. 60

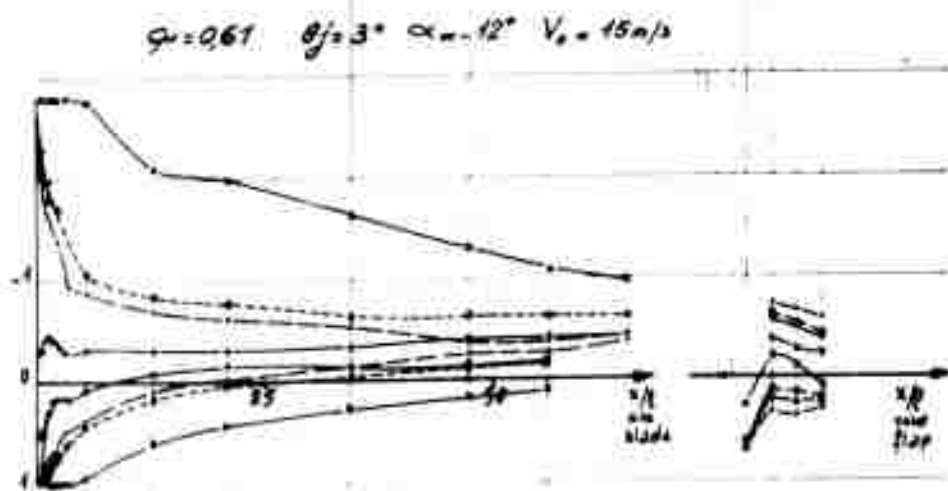
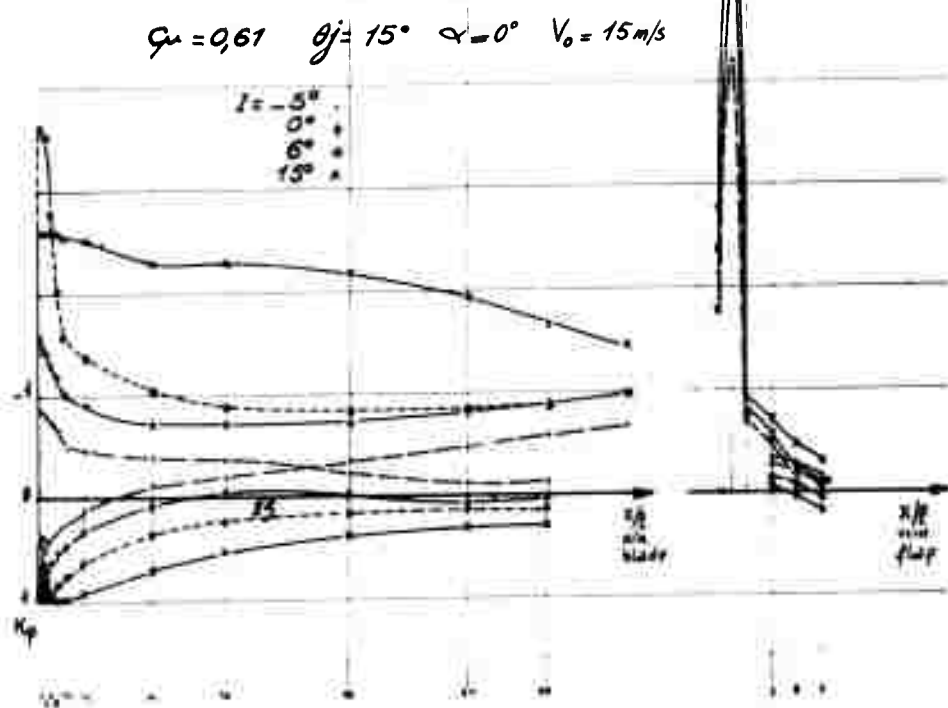
B.38

MECHANICAL FLAP
VOILET MECANIQUE



ONERA PV. 3/703AY
DRESSE MR NE
DATE Sept 60
B.39

MECHANICAL FLAP
VOLET MECANIQUE



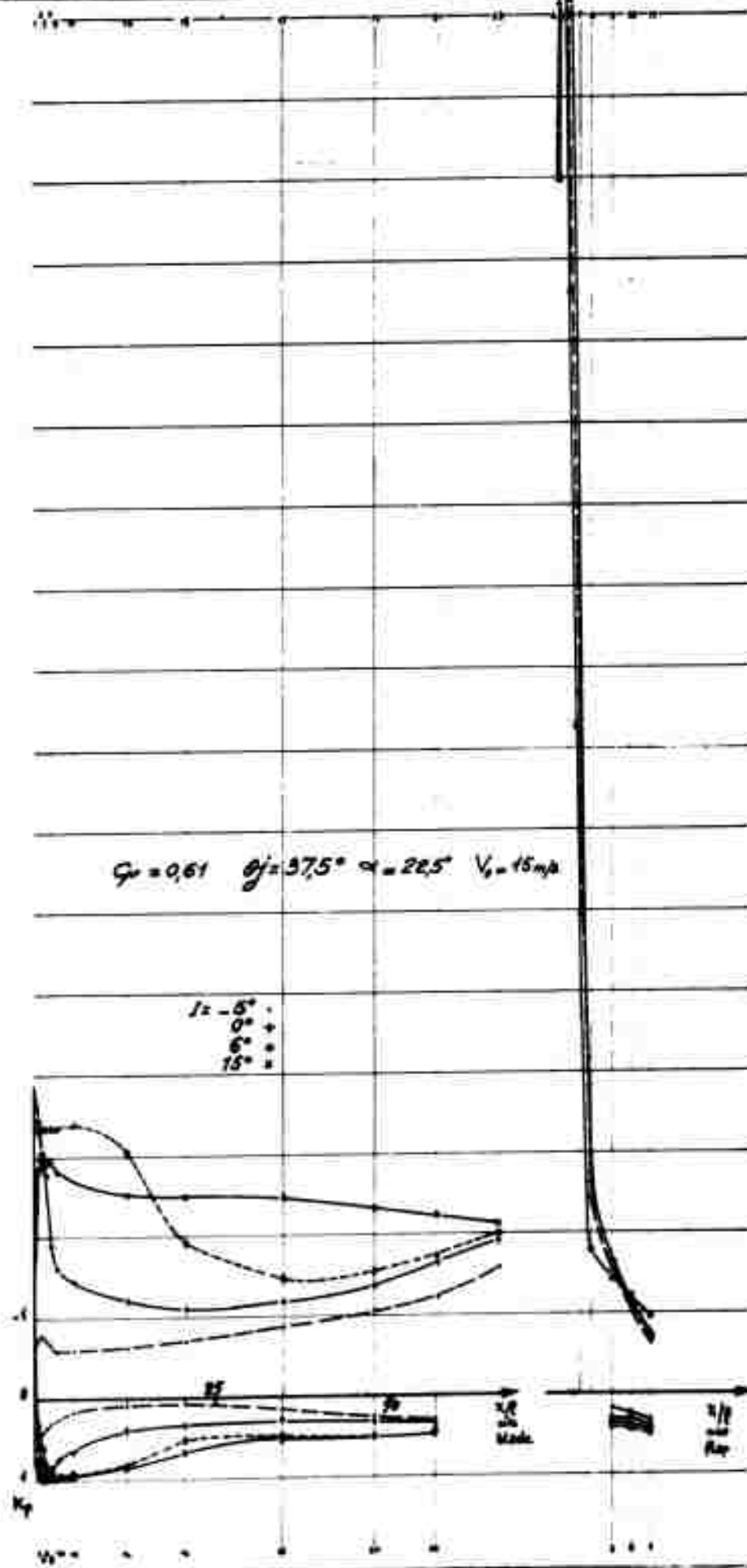
ONERA | REV. 3/703AY | DESIGNER | DATE | 8.40

MECHANICAL FLAP
VOILET MECANIQUE

Photo 40 41
42 43

B.41

FIG. 44



ONERA

B.41

DATE
Sept 60

PROJECT
No

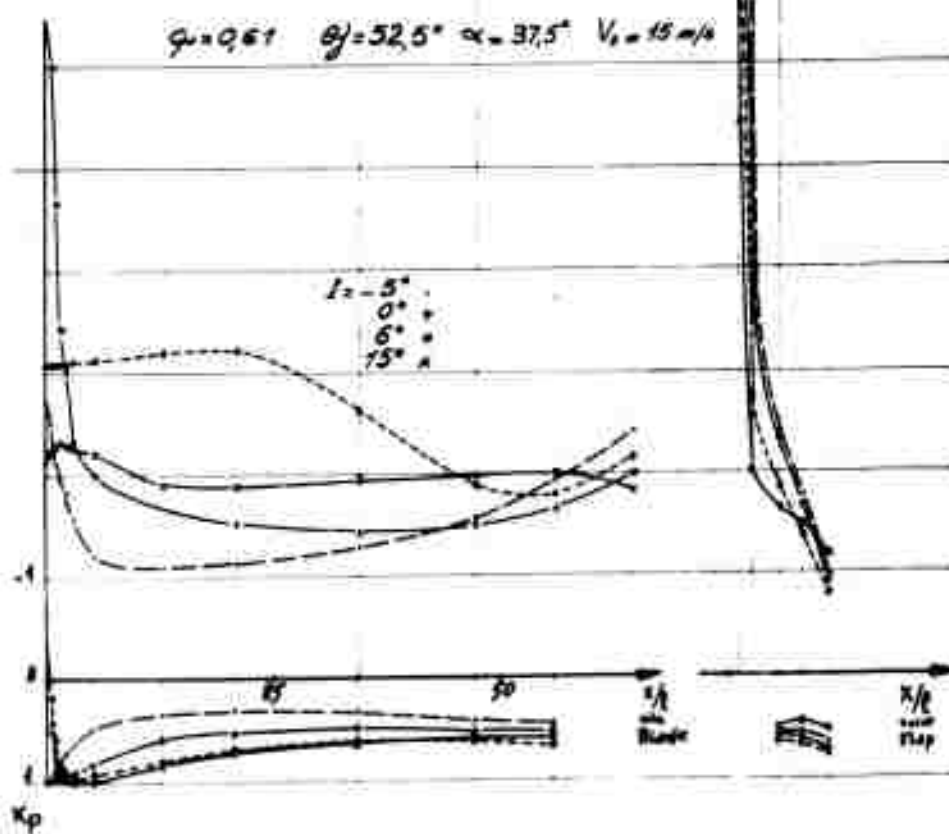
ONERA BY 3/2047

MECHANICAL FLAP
VOLET MECANIQUE

Rehe 45 45

B.42

FIG. 45



V.M.E.N.O

0.42

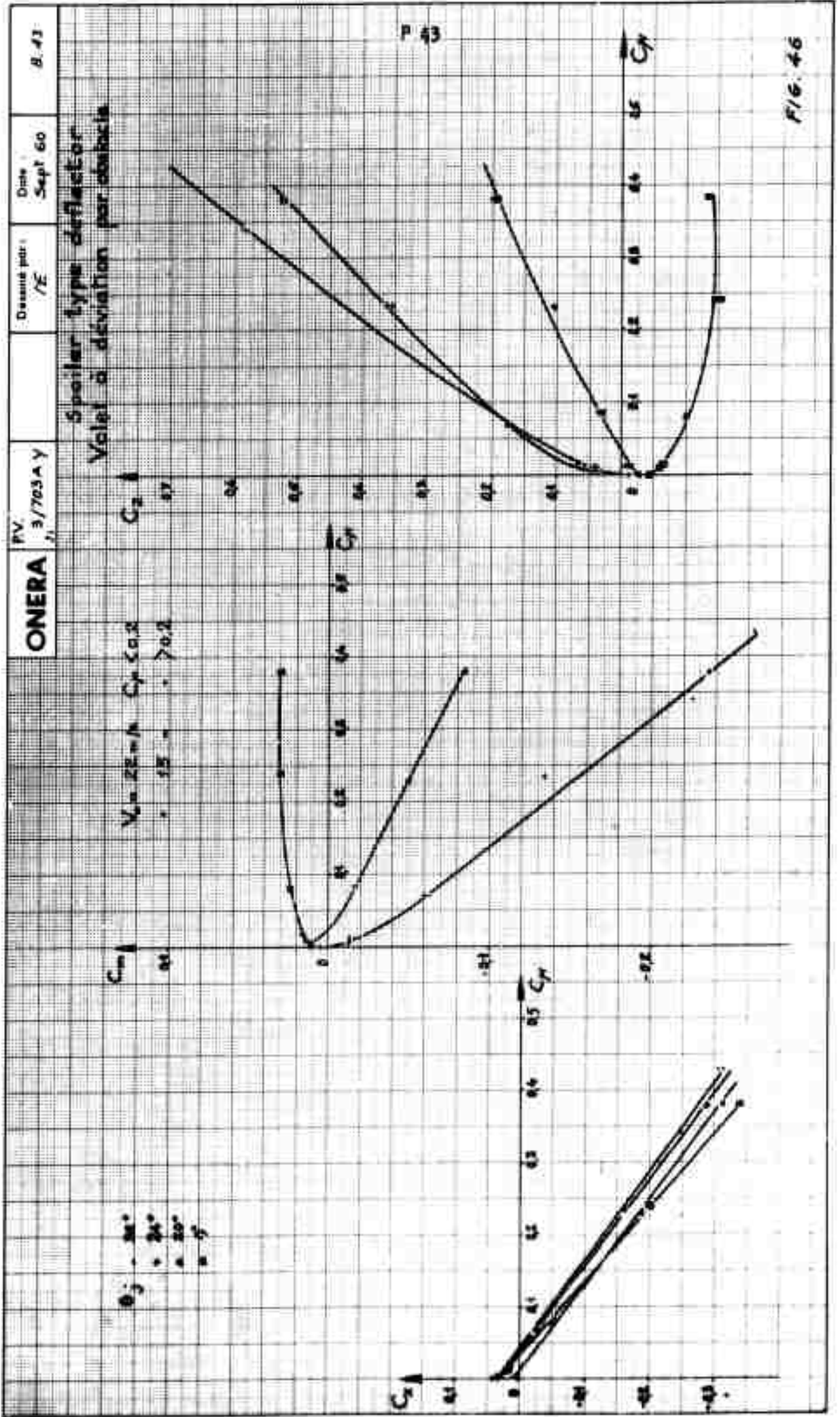
DATE

5 Sep 40

RE

ONERA PV 3123 AY

MECHANICAL FLAP
VOLET MECANIQUE



Voilet à déviation par obstacle

Spoiler type deflector

 R_{log}

15

10

5

0

5

10

 θ
log
kg

- $\theta_j = 0^\circ$
- $\theta_j = 20^\circ$
- $\theta_j = 24^\circ$
- $\theta_j = 30^\circ$

FIG. 47

100-101

ONERA

P.V. 3/703A
23

Dessiné par :
NE

Date :
Sept. 60

B. 45

Spoiler type deflection
Volet à déviation
par obstacle

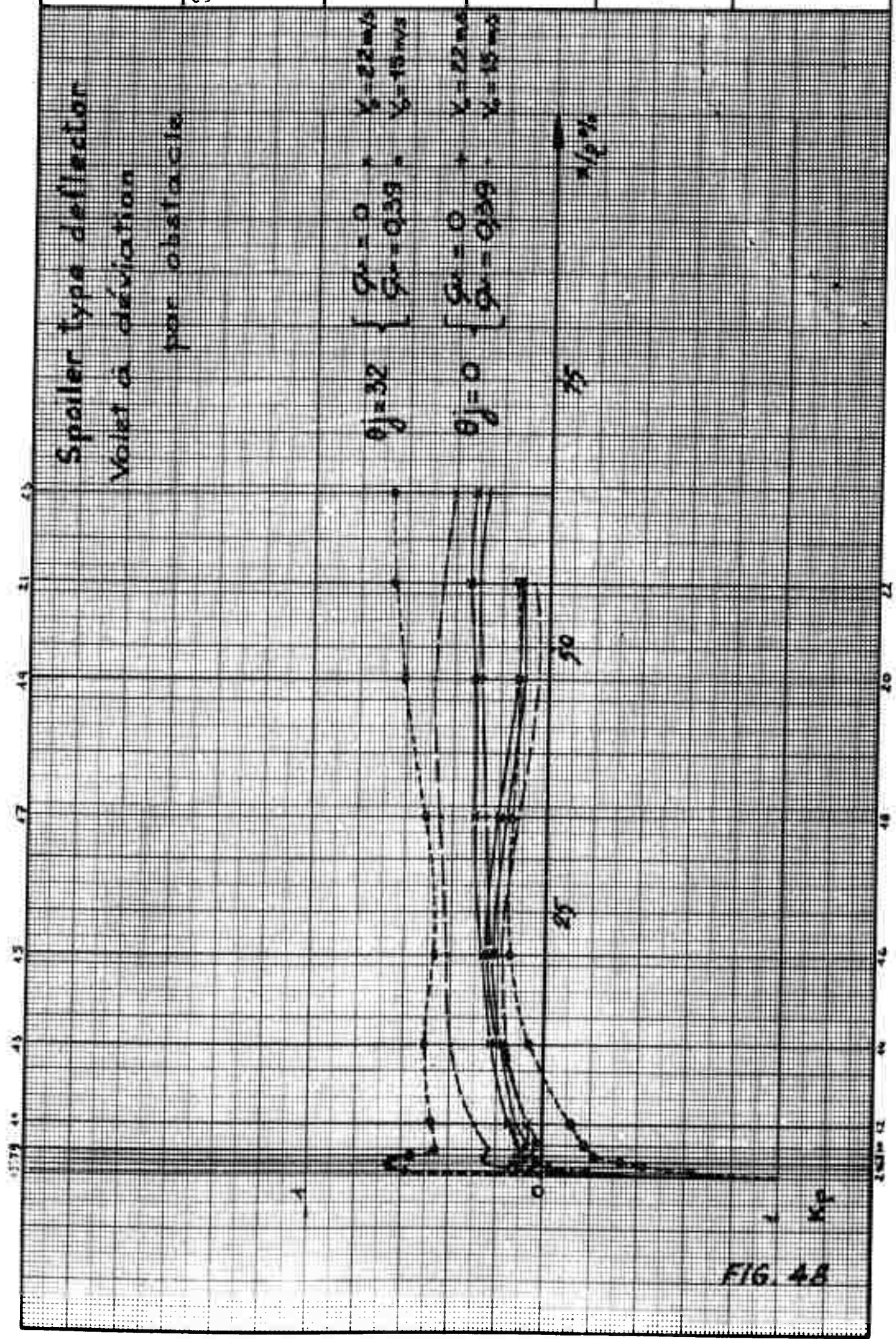


FIG. 4B

ONERA

PV. 3/703A, y

Revised per:
NE

Date:
Sept 68

B. 46

Pneumatic deflector

Valid pneumatic V_0 or 20-40

$C_{D0} = 0$

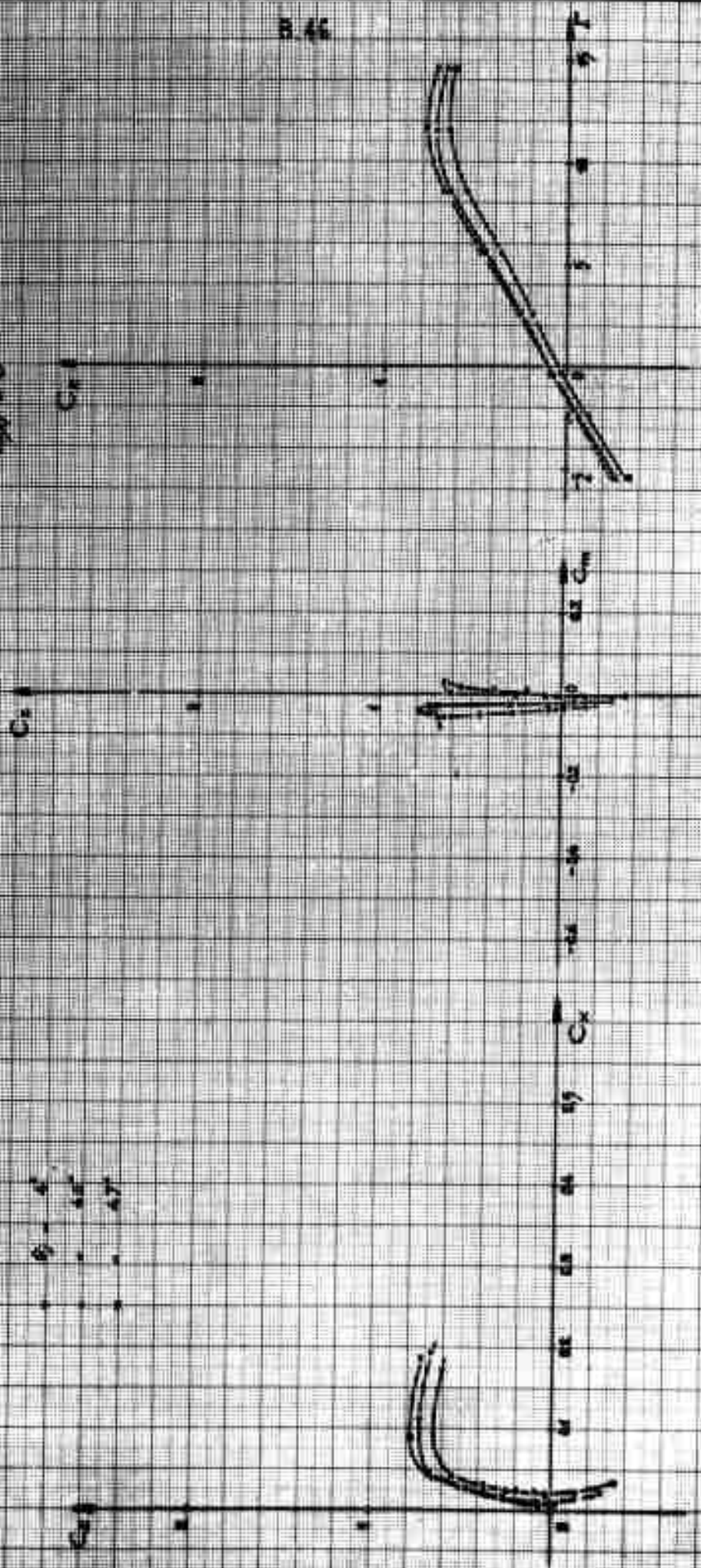
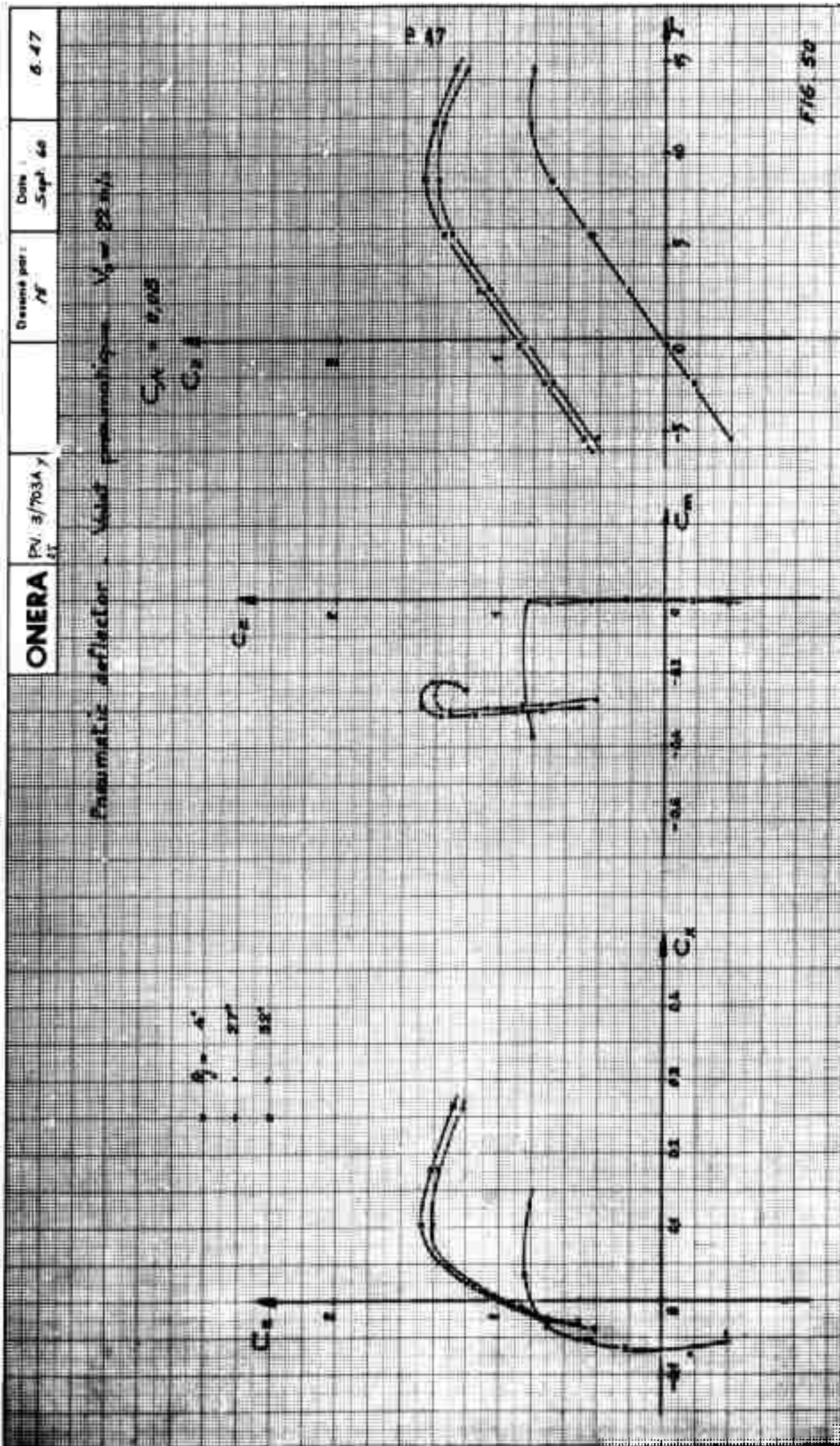
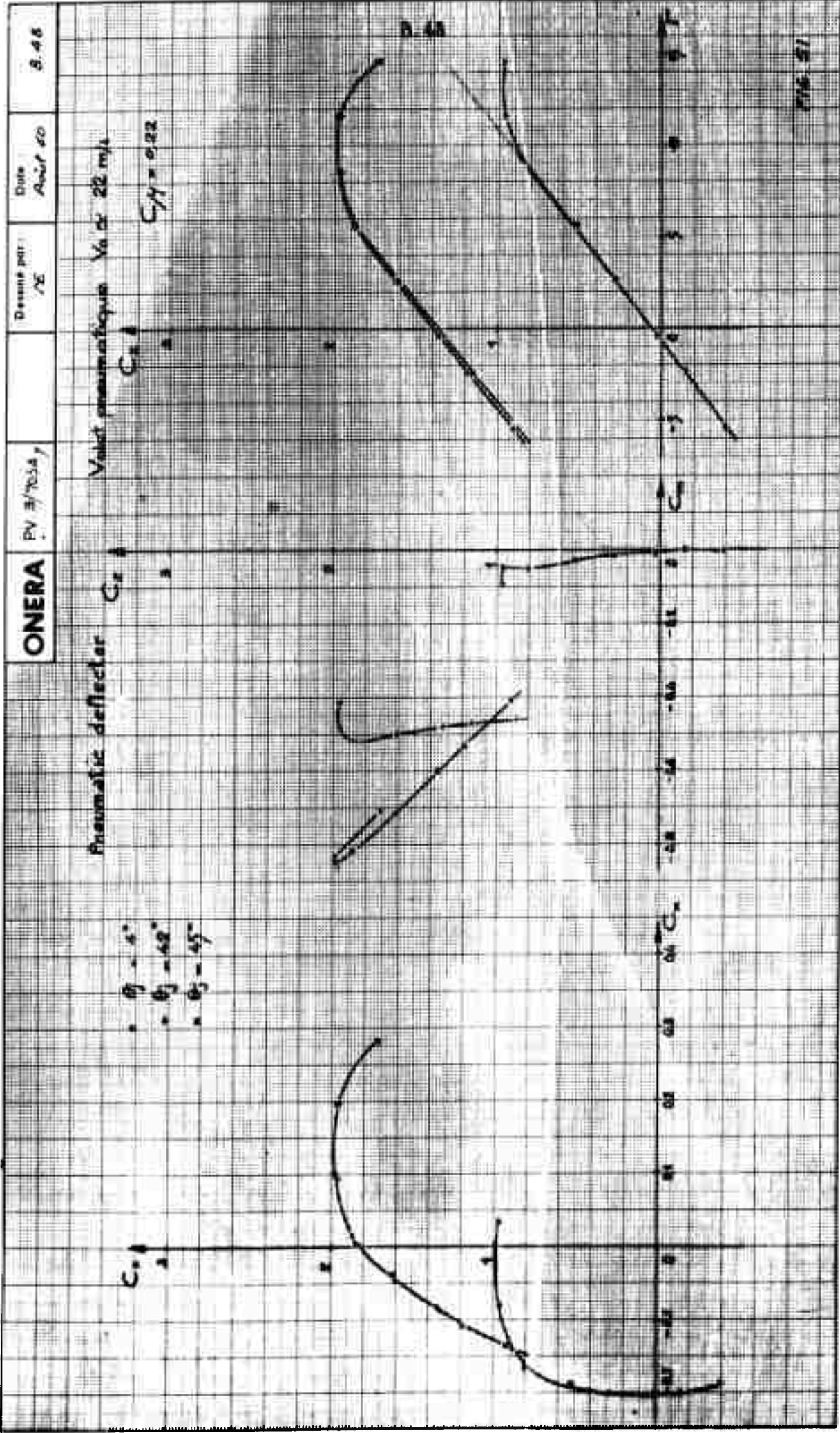
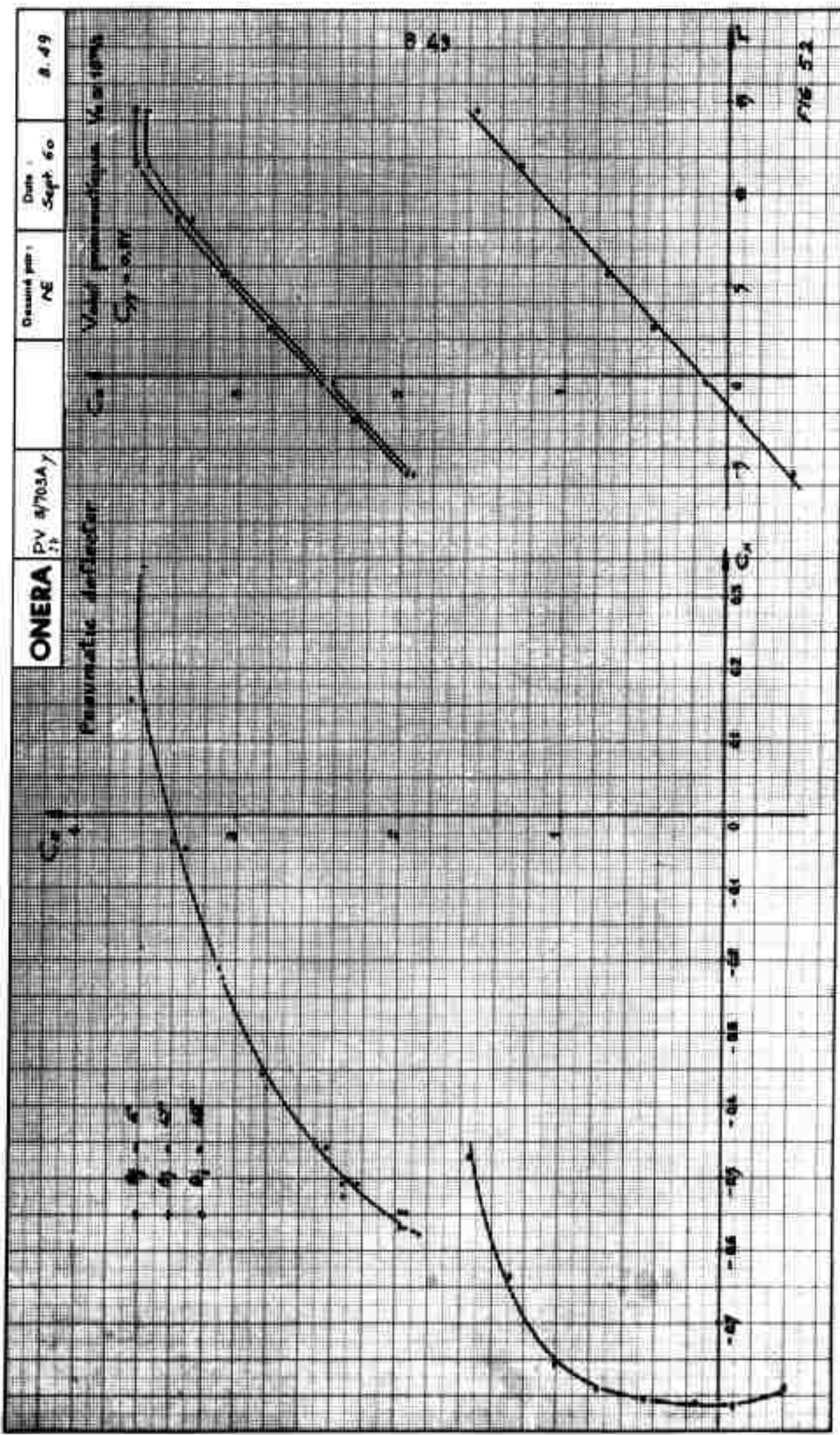
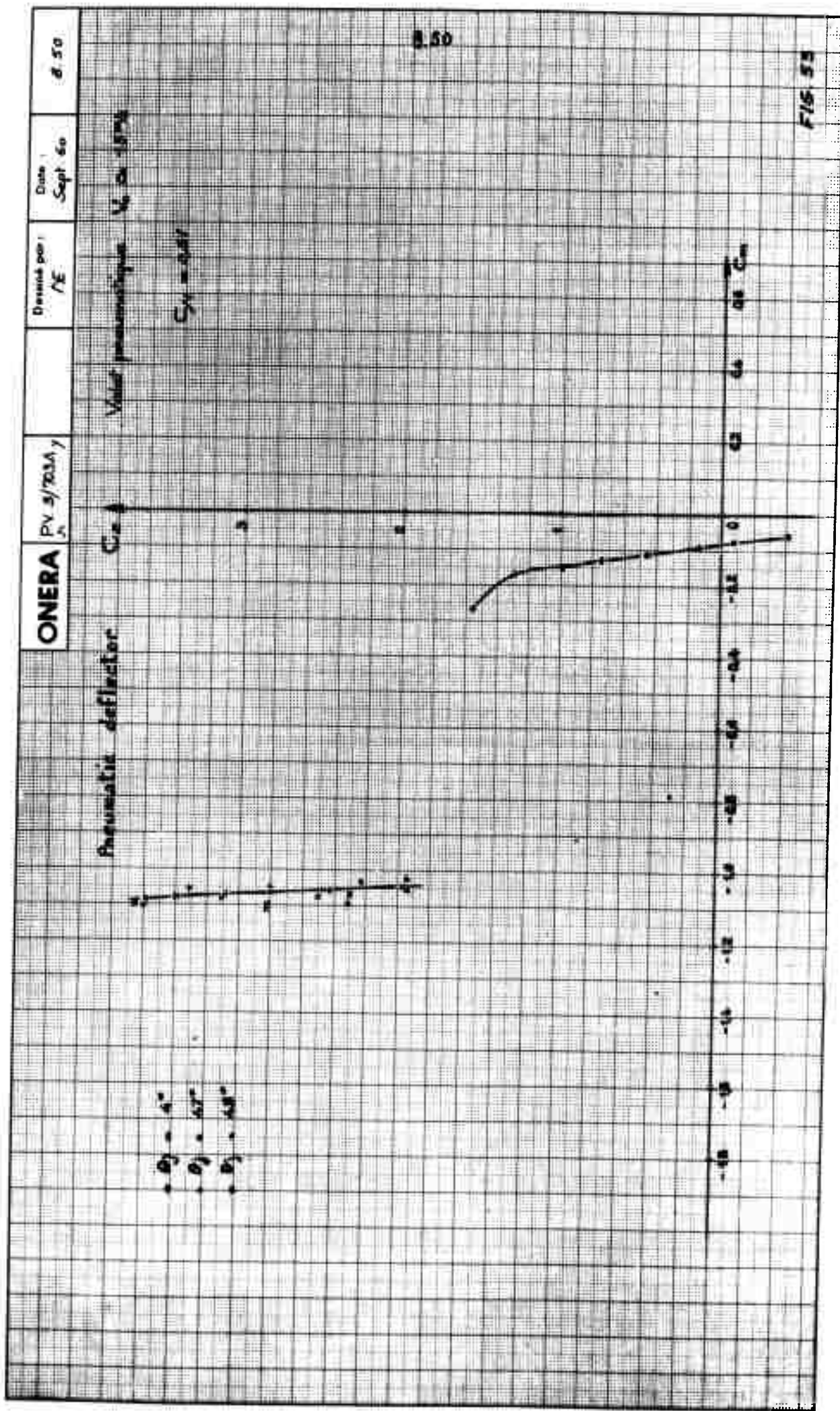


Fig. 49









Pneumatic deflector.
Volet pneumatique.

Les mesures ont été effectuées pour différentes valeurs de la pression statique.

The measurements have been carried out for various static pressures.

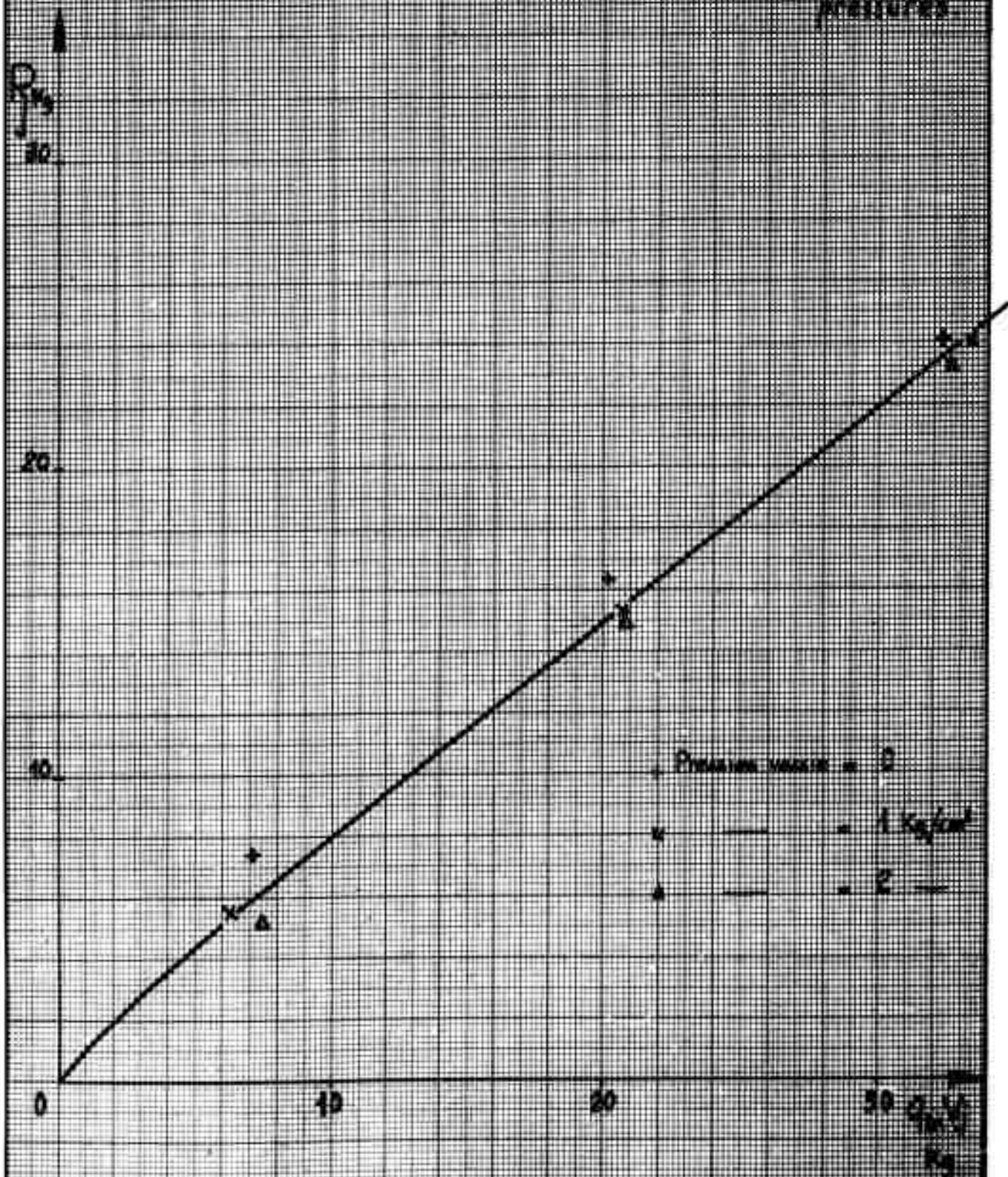
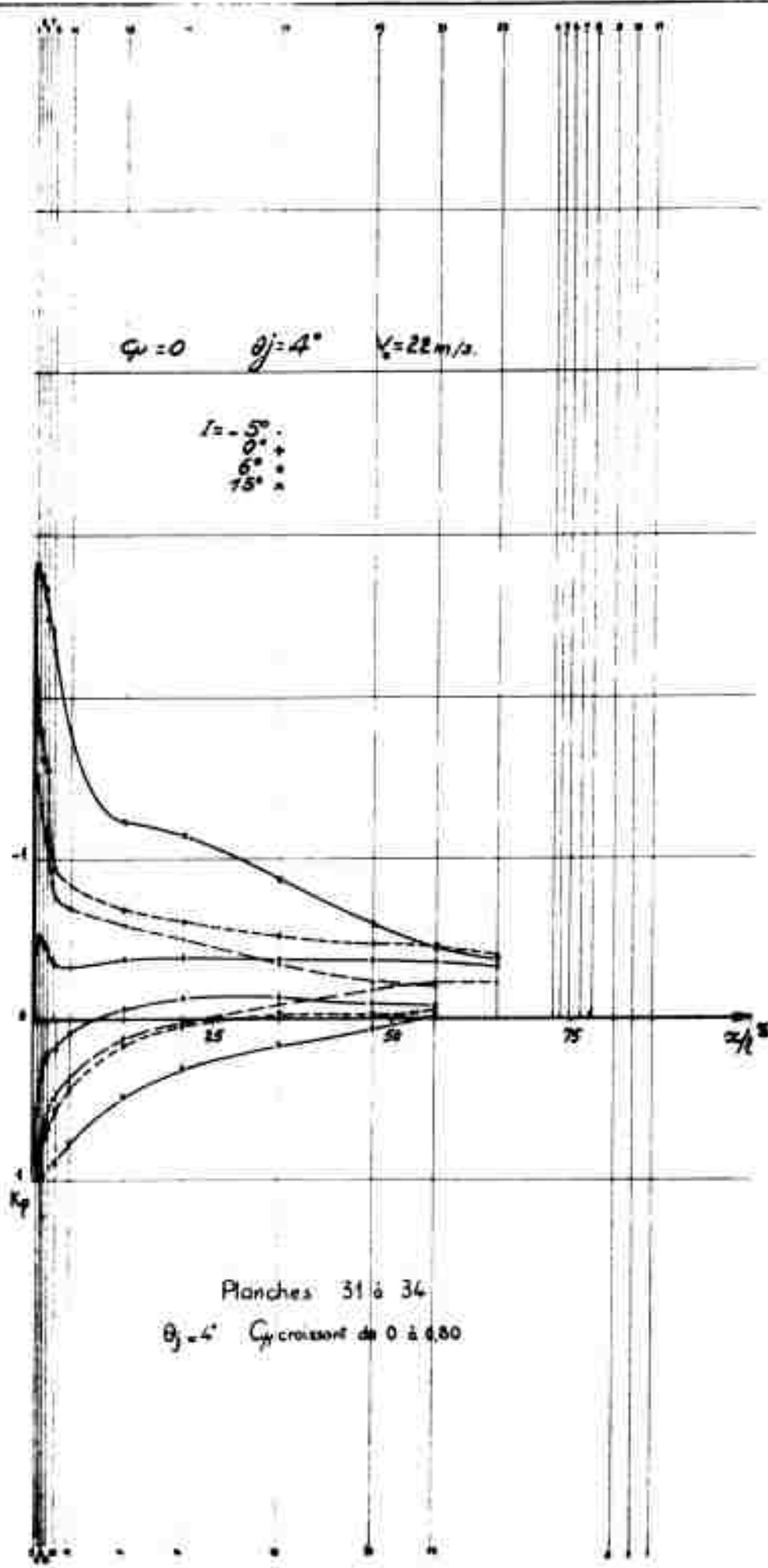


FIG. 55



Planches 31 à 34
 $\theta_j = 4^\circ$ C_p croissant de 0 à 0.80

PNEUMATIC DEFLECTOR - VOILE PNEUMATIQUE

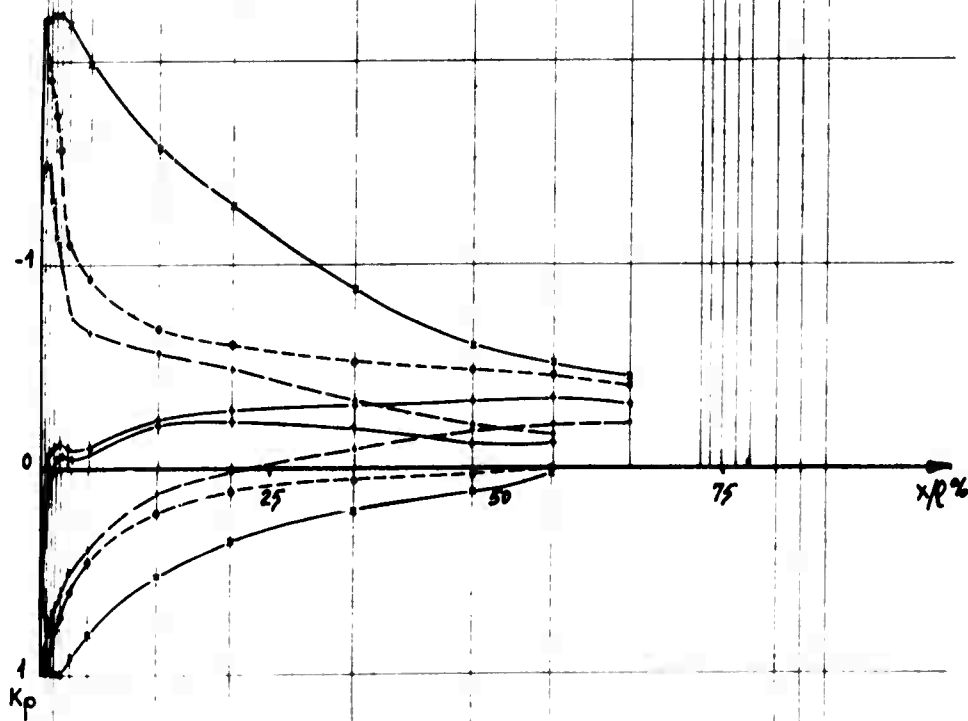
ONERA	ONERA	DATE	8.53
	REV. 5/1934	8.53	

Photos 112 113 114 115

$$C_p = 0,087 \quad \theta_j = 4^\circ$$

$$V_\infty = 22 \text{ m/s.}$$

$I = -5^\circ$
 0°
 6°
 15°



voir Fig. 56
 see Fig. 56

VOLET PNEUMATIQUE

PNEUMATIC DEFLECTOR

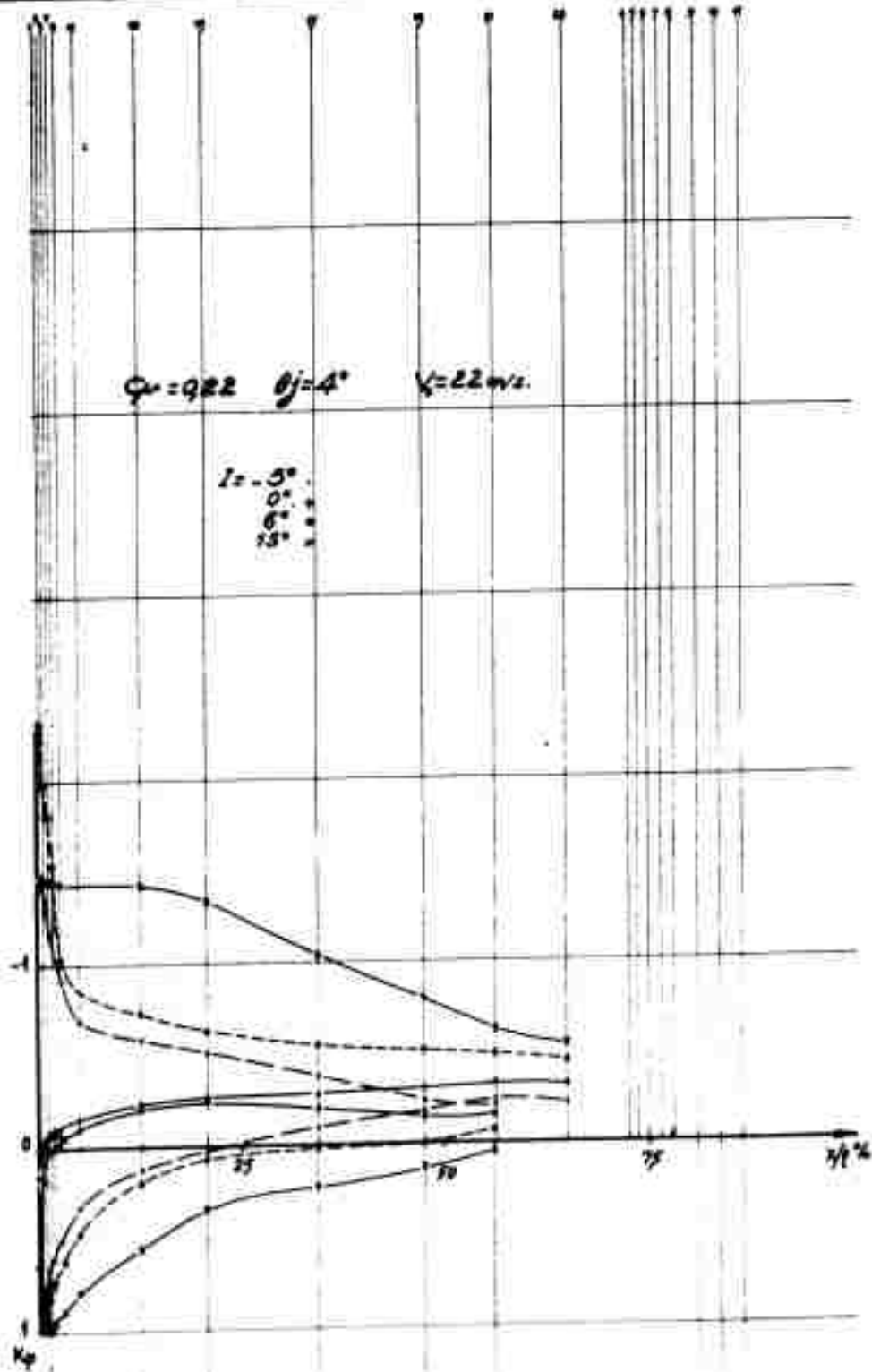
B.54

DATE
Sept. 60

DRAWING
PAR
J.E.

ONERA
EX. 5/105AY

O.N.E.R.A.

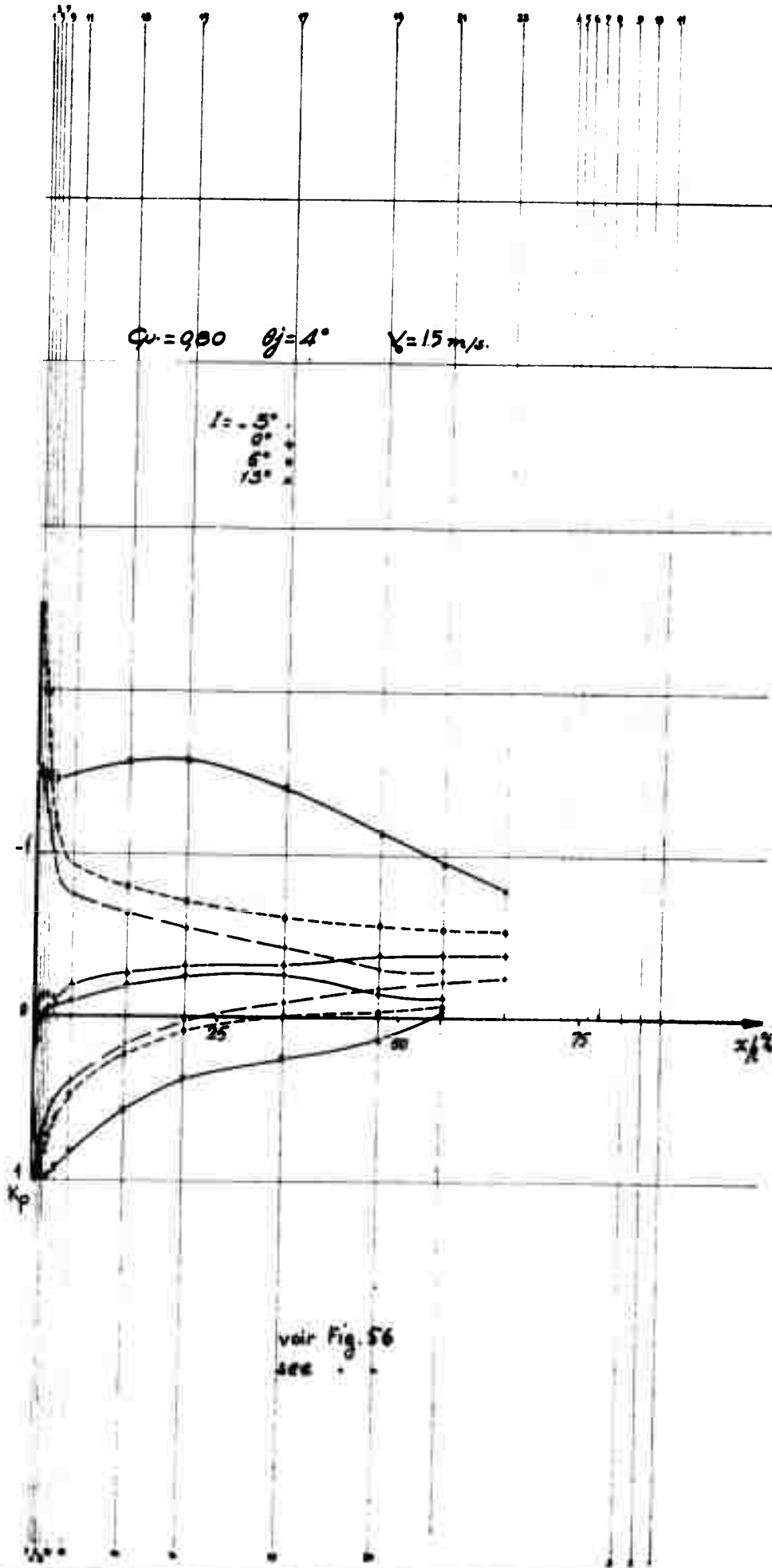


voir Fig. 56
see . . .

VOLET PNEUMATIQUE

PNEUMATIC DEFLECTOR

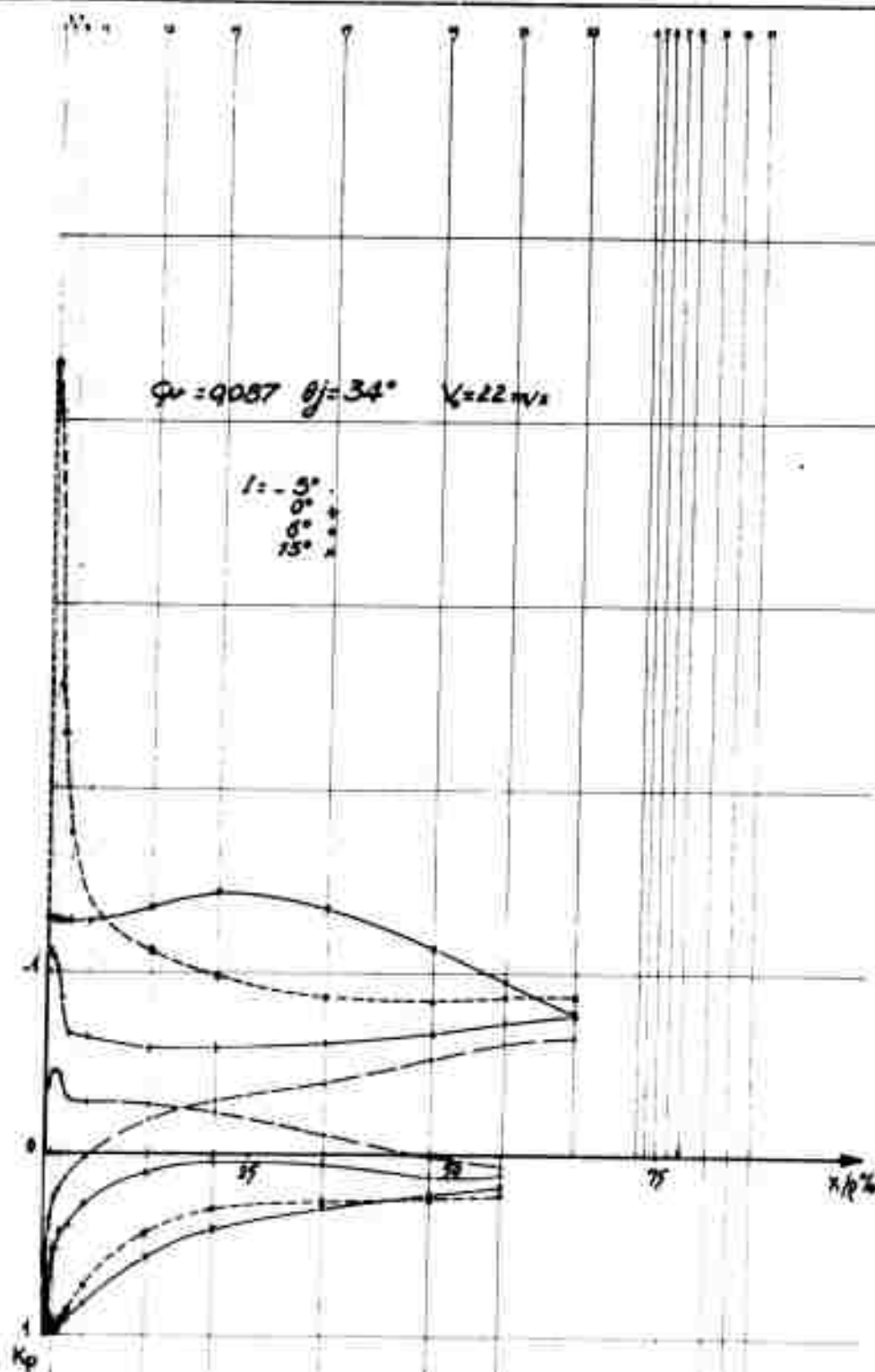
ONERA	EX. 5/283 A Y	RELEVÉ PAR M ^e	DATE Sept. 69	0.55
-------	---------------	------------------------------	------------------	------



voir Fig. 56
see . .

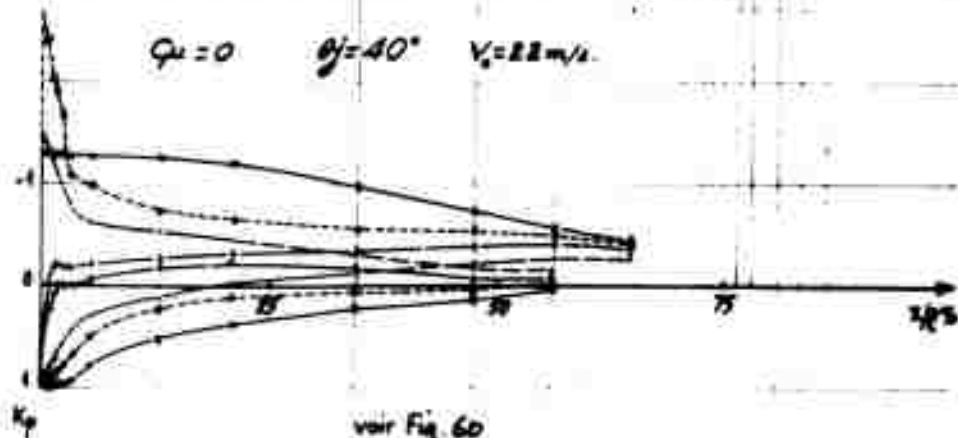
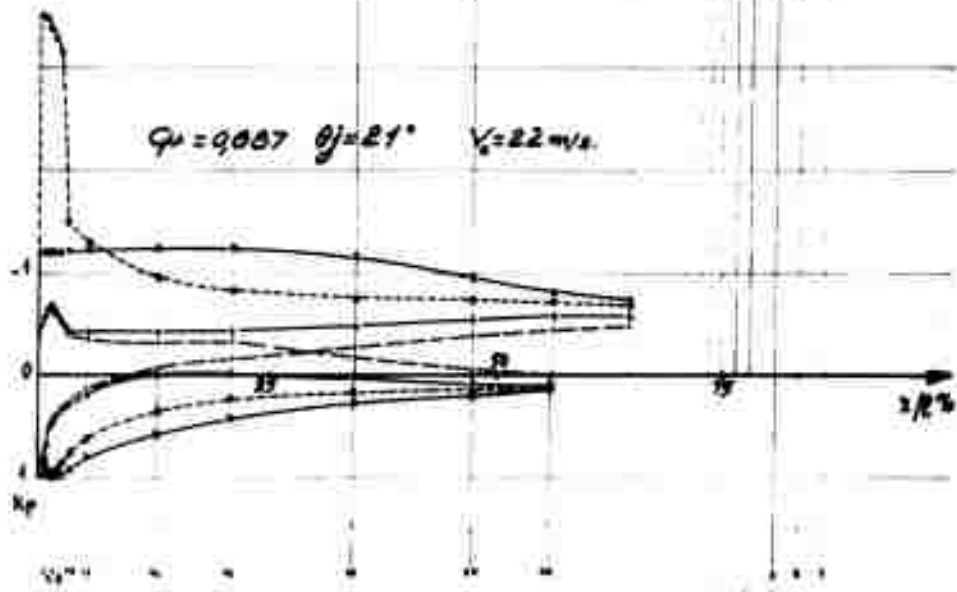
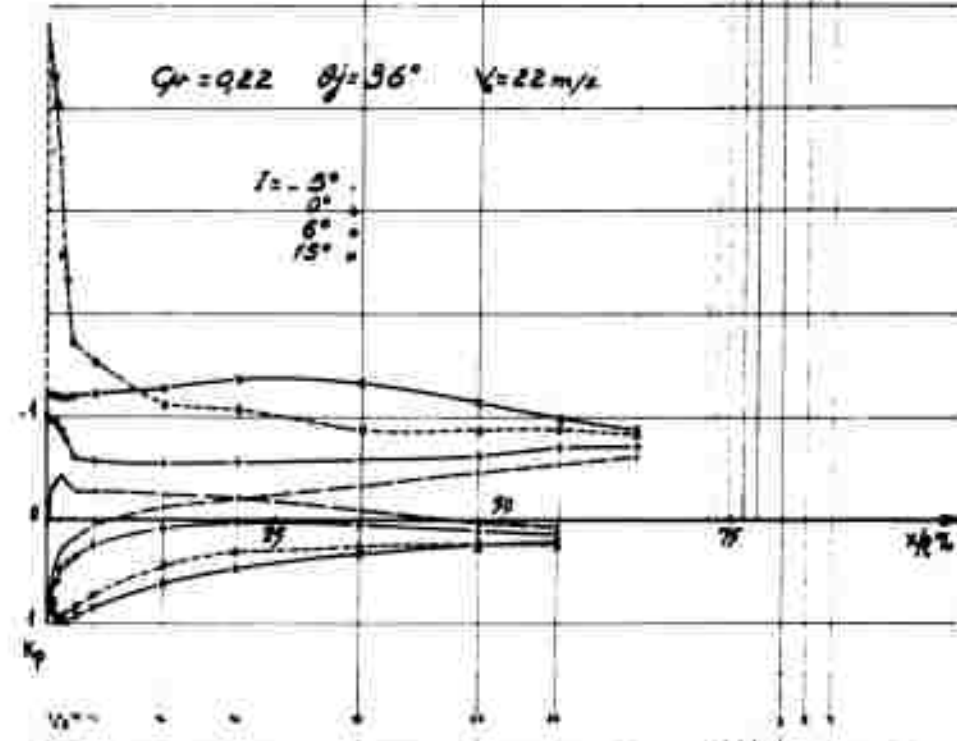
PNEUMATIC DEFLECTOR - VOLET PNEUMATIQUE

ONERA	ONERA	DATE	B.56
3/7/54	NE	Sept 60	



Figures 60 à 66
 $34^\circ < \theta_j < 48^\circ$ pour différentes valeurs de C_μ

Fig. 60 to 66
 $34^\circ < \theta_j < 48^\circ$ for different C_μ values



voir Fig. 60

PNEUMATIC DEFLECTOR VOILET PNEUMATIQUE

ONERA 31/05/60

SAVE

Sept. 60

124

125

126

127

128

129

130

131

132

133

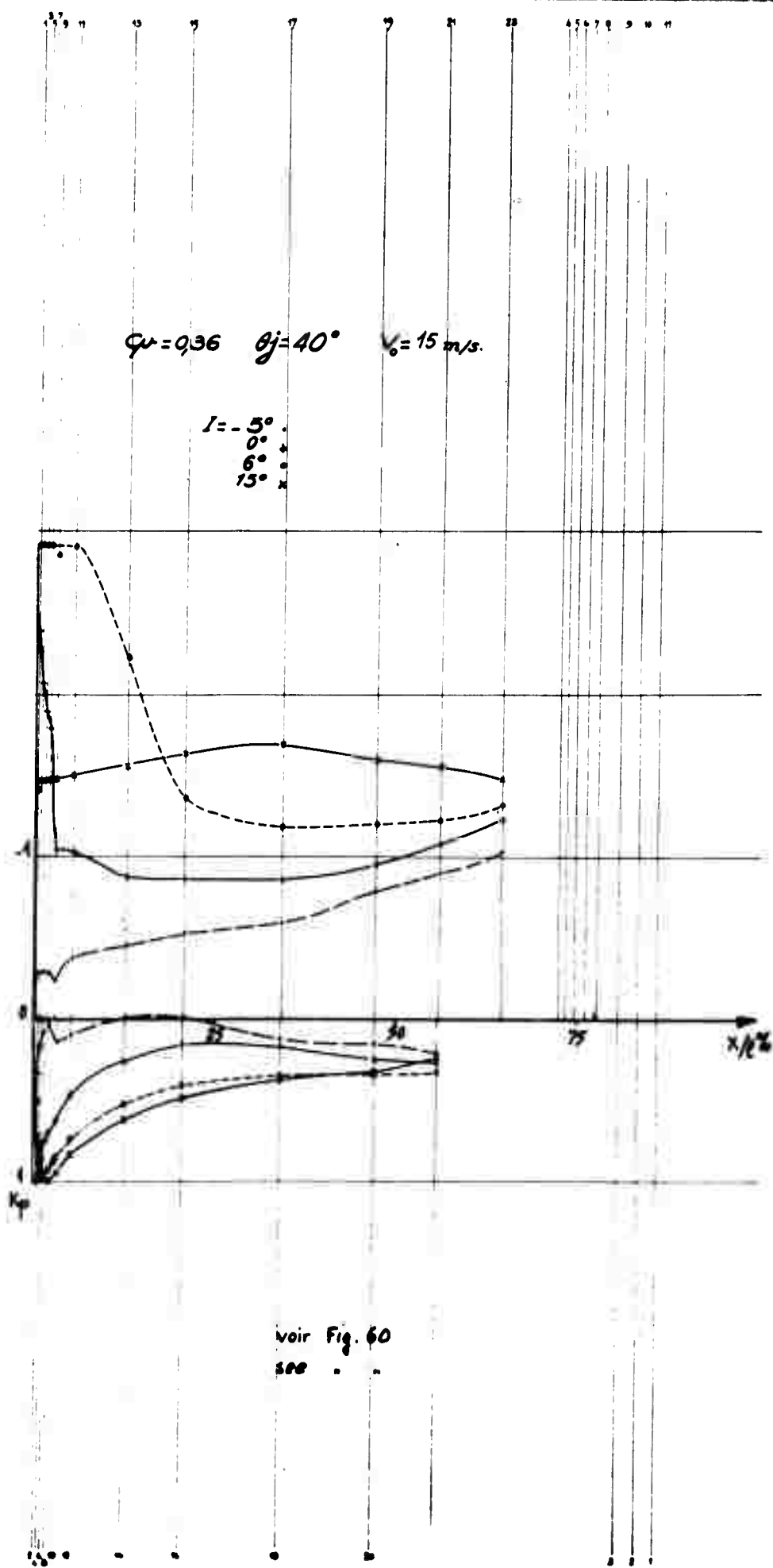
134

135

136

137

138



PNEUMATIC DEFLECTOR . VOLET PNEUMATIQUE

O.N.E.R.A.

ONERA 3/703AY

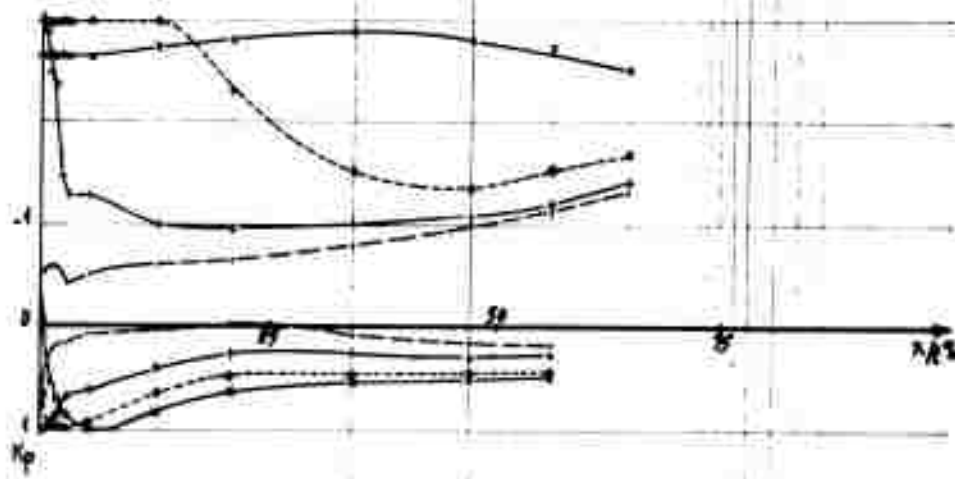
DESSIN PAR
NE

DATE
Sept. 60

B.59

Photo 46 - 47, 48, 49

432, 433, 434, 435

 $Q_\infty = 980$ $\theta_j = 43^\circ$ $V = 15 \text{ m/s.}$ $I = 5^\circ$ 0° 6° 13°  $Q_\infty = 936$ $\theta_j = 43^\circ$ $V = 15 \text{ m/s.}$ 

voir Fig. 60

100

PNEUMATIC DEFLECTOR . VOLET PNEUMATIQUE

ONERA

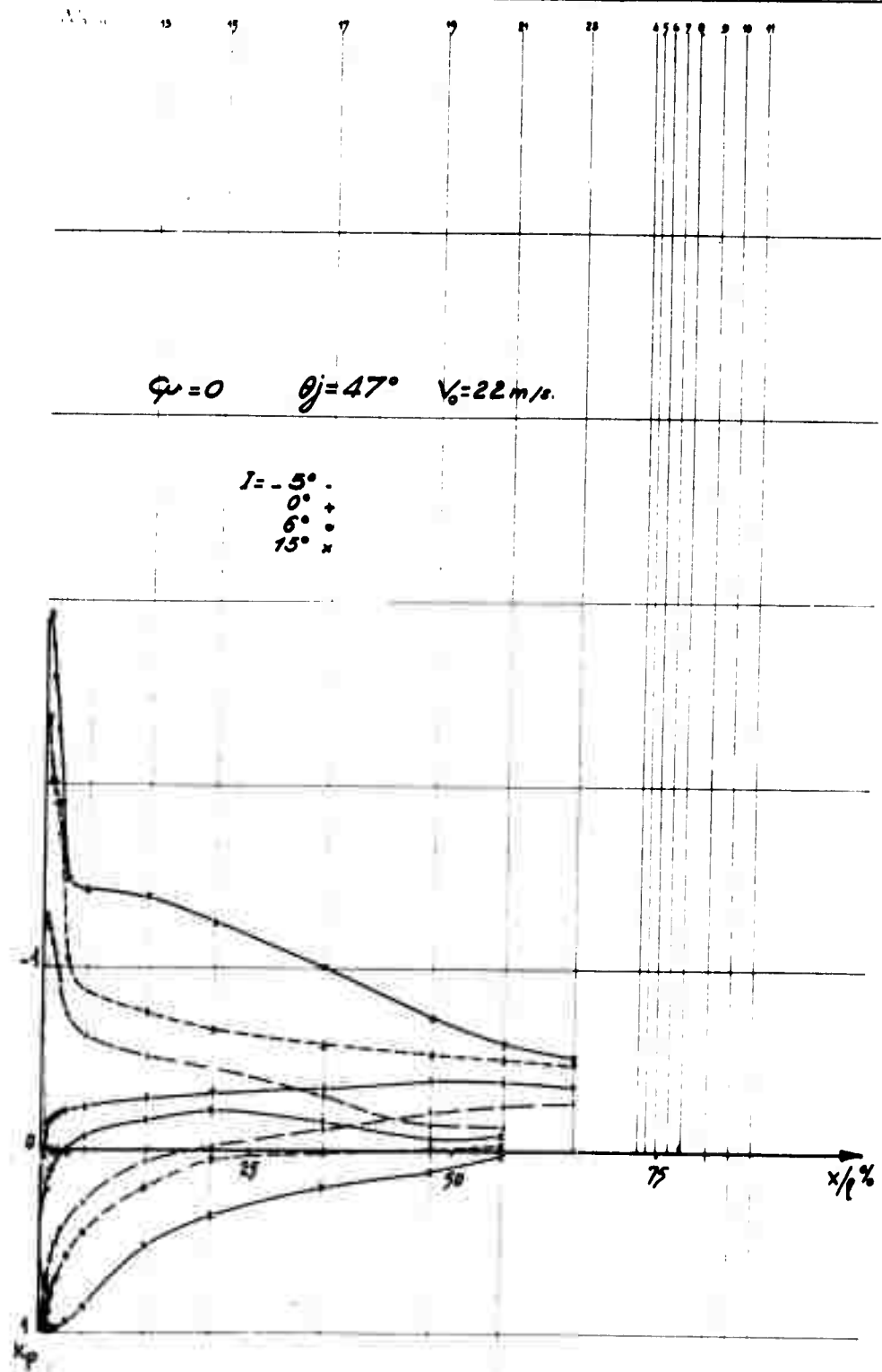
ONERA IV 3/20/57

PREMIER N° 12

DATE 5 sept. 60

B.60

Photos 176 175 176 177



VOLET PNEUMATIQUE

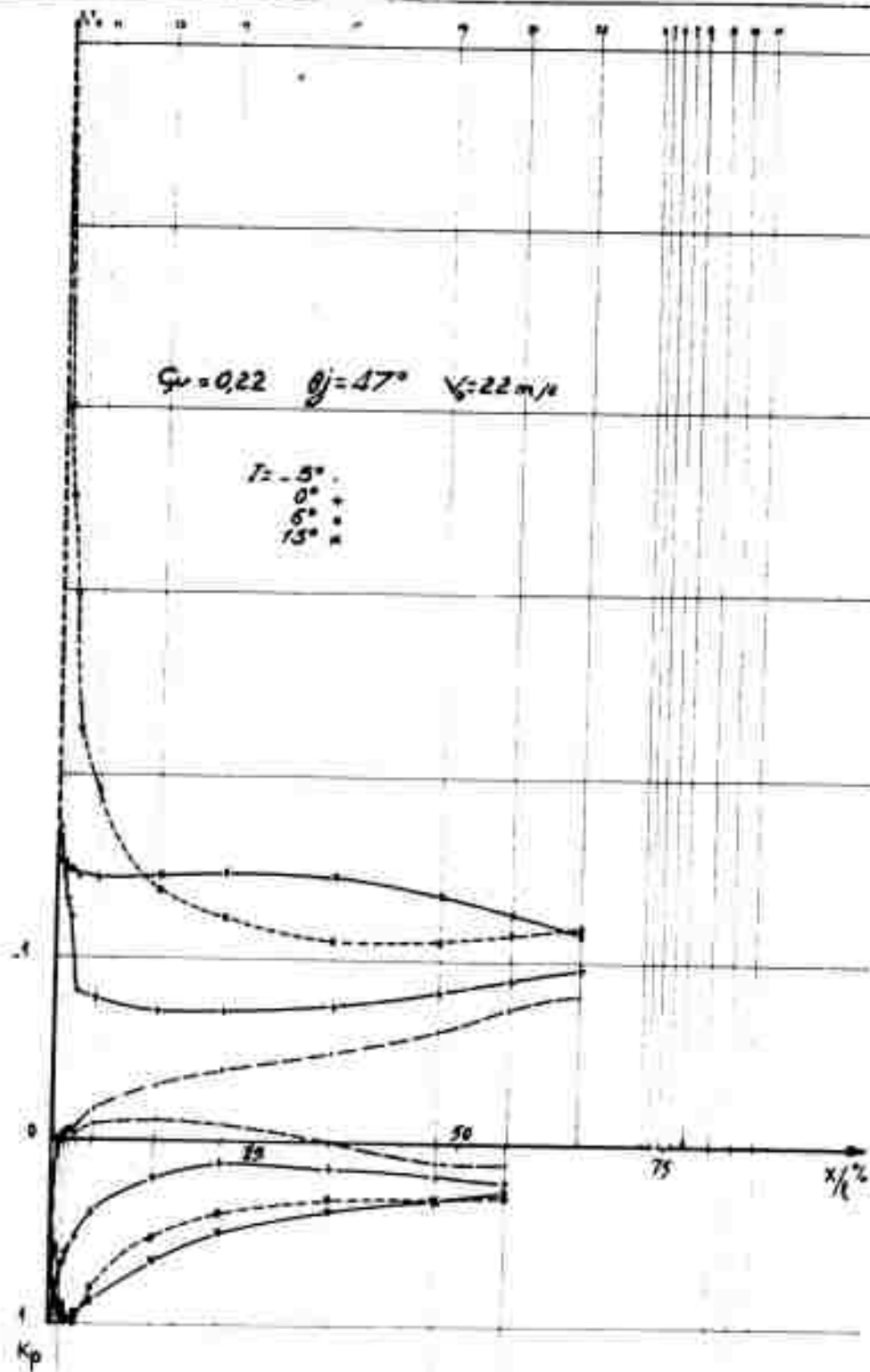
PNEUMATIC DEFLECTOR.

Fig. 64 à 66
 $\theta_j = 47^\circ$ C_p croissant de 0 à 0.80

Fig. 64 to 66
 $\theta_j = 47^\circ$ C_p increasing from 0 to 0.80

B.61

DATE
Sept. 60DRESSING PAR
NEONERA
PV 3/703 AY



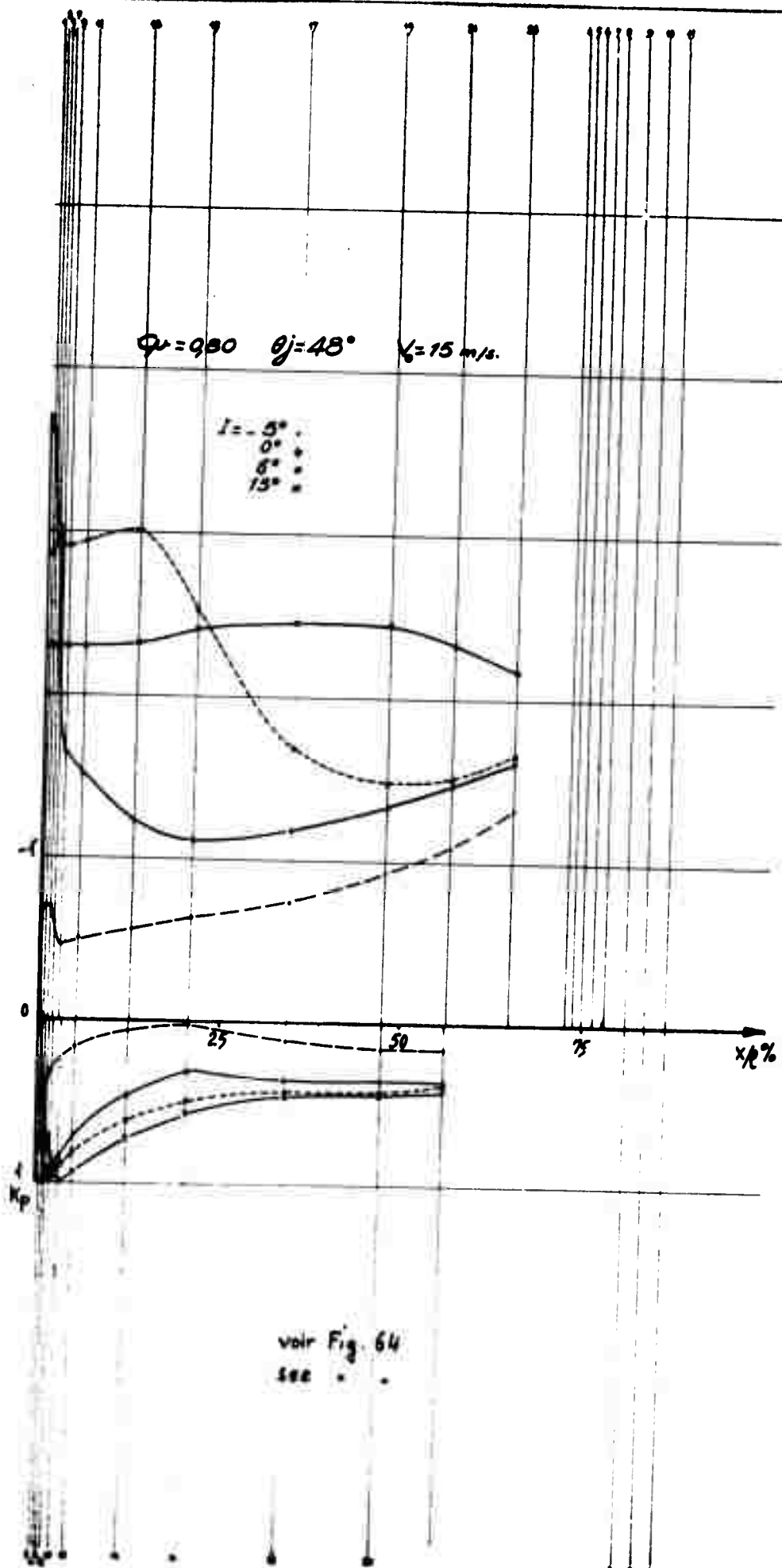
$C_u = 0.22$ $\theta_j = 47^\circ$ $V_\infty = 22 \text{ m/s}$

$T = 5^\circ$
 0°
 6°
 15°

voir Fig. 64
 see . . .

PNEUMATIC DEFLECTOR . VOLET PNEUMATIQUE

ONERA	ONERA	DATE	B.62
	3/70347	Sept. 60	
	NE		



PNEUMATIC DEFLECTOR VOILE PNEUMATIQUE

O.N.E.R.A.

ONERA 3/2004 Y

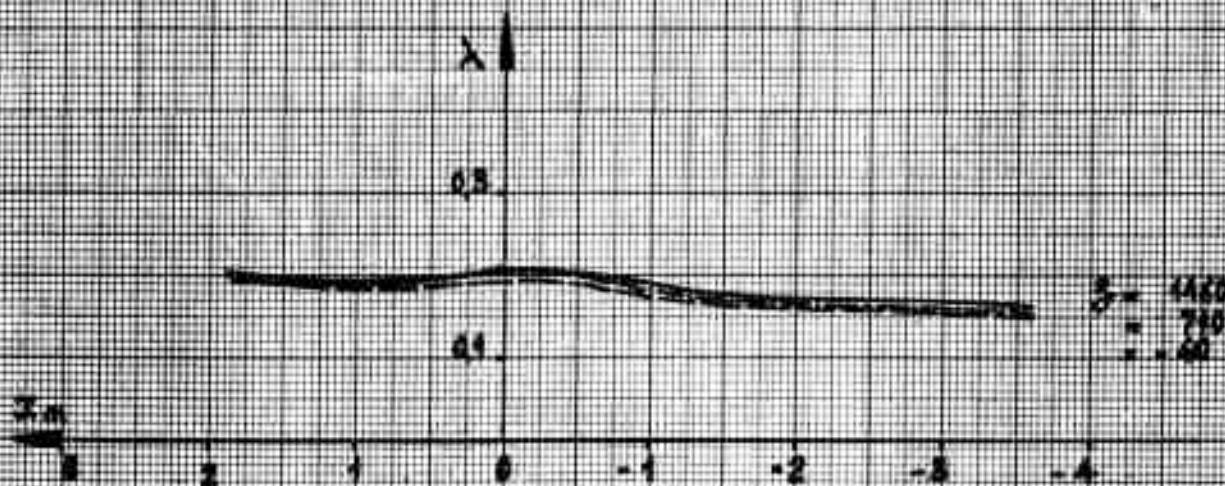
PREMIER 100
 1/2

Sept. 60

B.63

Exploration of the air-flow
Exploration de Veine

$$y = -409$$

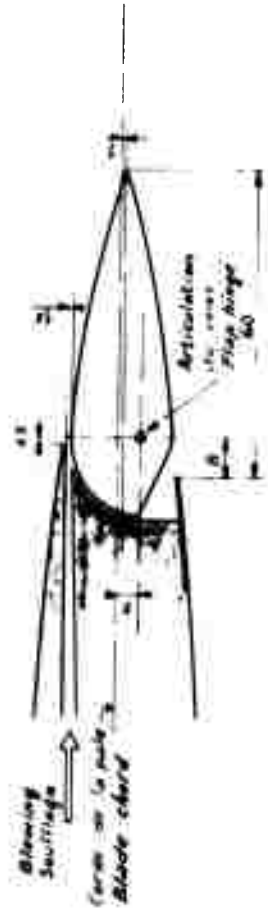
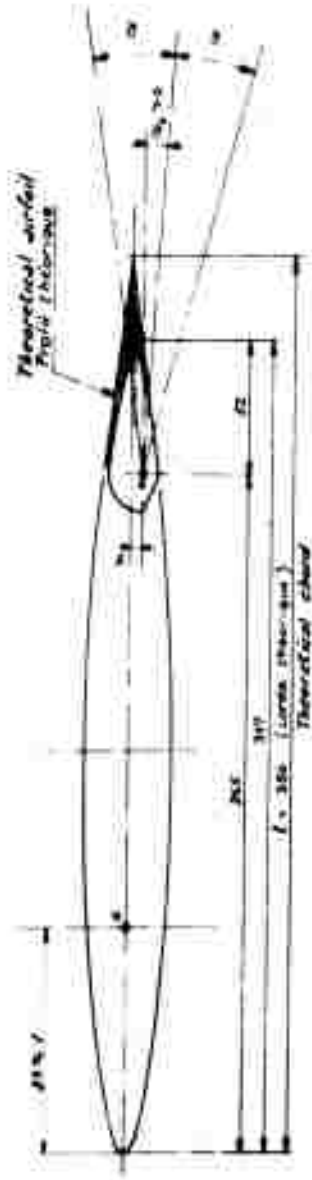


x, y, z , Coordonnées de Référence (voir texte)
 x, y, z , Reference coordinates (see text)

FIG. 67

MECHANICAL FLAP

Volet rigide



Detachable parts: Flap Volet
Elements démontables Matière
N.B. - Les cotes cotées par le responsable de l'essai seront soulignées.

Scale of drawing: 1/4 : 1/2
Echelle du dessin

O.N.E.R.A. O.A.	PV. 1/705AY	Designé par: Louis	Date: 7 9.60	8.65
Wind tunnel: Soufflerie: S3 CE				
Balance:				
Model Maquette				
Echelle: Centrage				
S = 0.350				
References: S = 0.154				
I = 5 x 1 = 0.0522				
I = 5 x 6 =				
Wing AILE				
Span Envergure: 0.440				
Chord (au leading edge): 0.350				
Circles (diamètres): 0.350				
Aspect ratio: 1.25				
Allongement: 1.25				
Paper				
Lift: 0				
Lift coefficient: 0				
Drag coefficient: 0				
Pitch: 0				
Roll: 0				
Yaw: 0				
Airfoil Profil: 55041 K				
Dihedral: 0				
Surface d'aile: 0				
Twist: 0				
EISELAGE				
Longueur: 0				
Maitre-couple: 0				
Allongement: 0				
Volume: 0				
EMPENNAGE HORIZONTAL				
Longueur: 0				
Corde moyenne: 0				
Surface: 0				
Pente: 0				
Bras de levier: 0				
Volume: 0				
DERIVE				
Longueur: 0				
Surface: 0				
Pente: 0				
OBSERVATIONS				

ONERA

P.V. 1/703 AY

P.V. 142 /53Ch

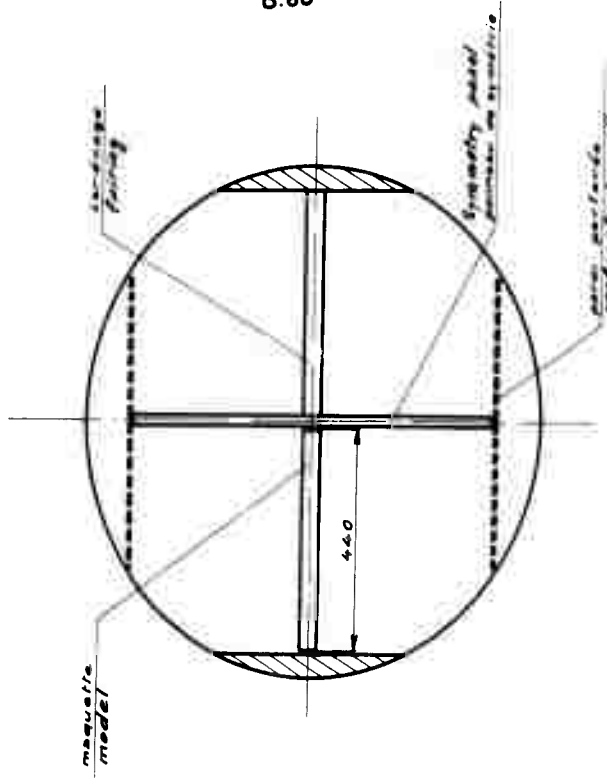
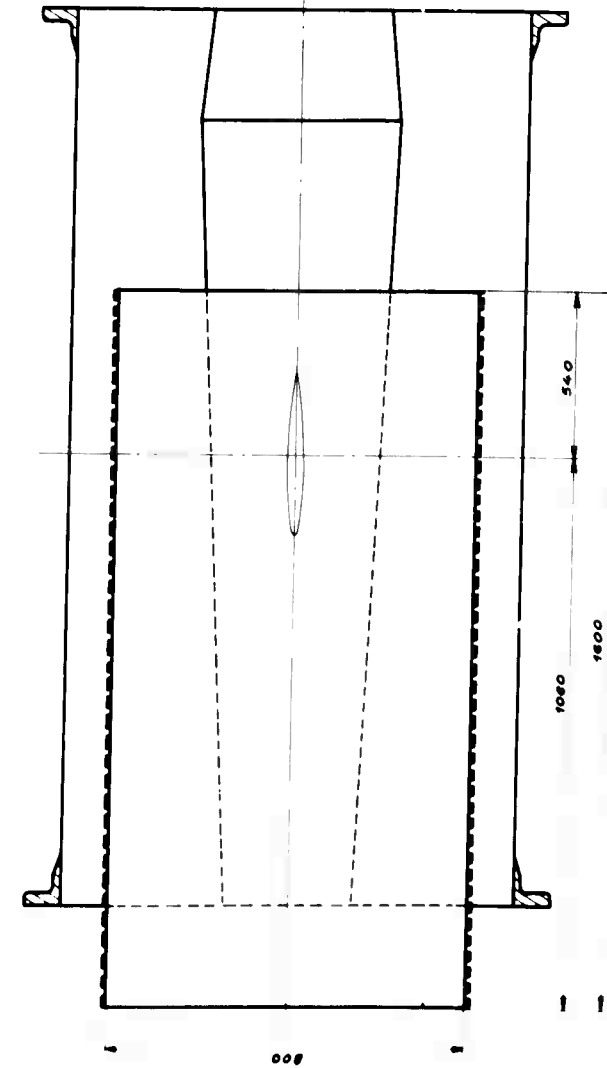
M. F.

12.9.60

B.66

SET-UP IN TUNNEL SECTION

Montage en Veine



B.66

FIG. 69

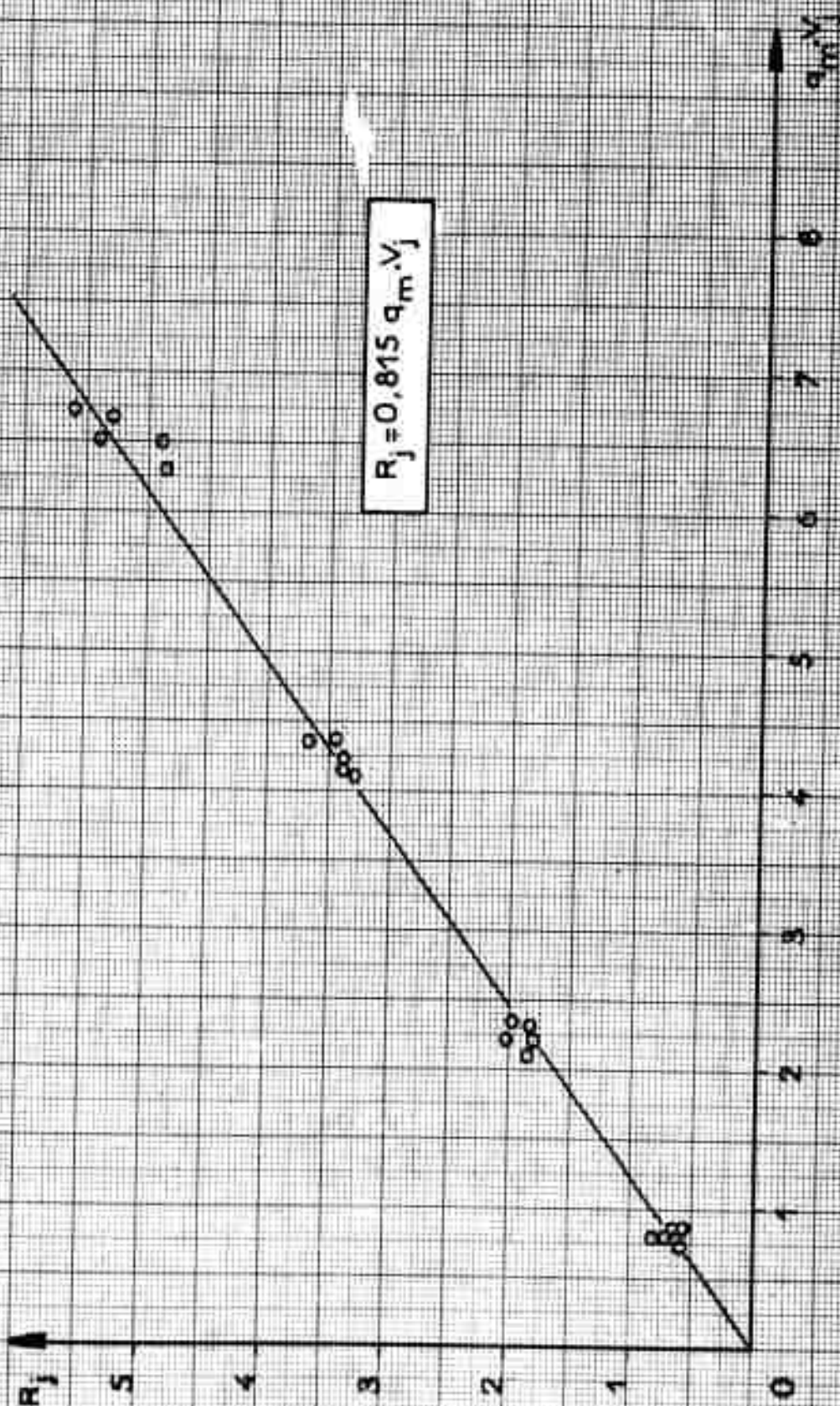
Tests with mechanical flap

FIG. 70

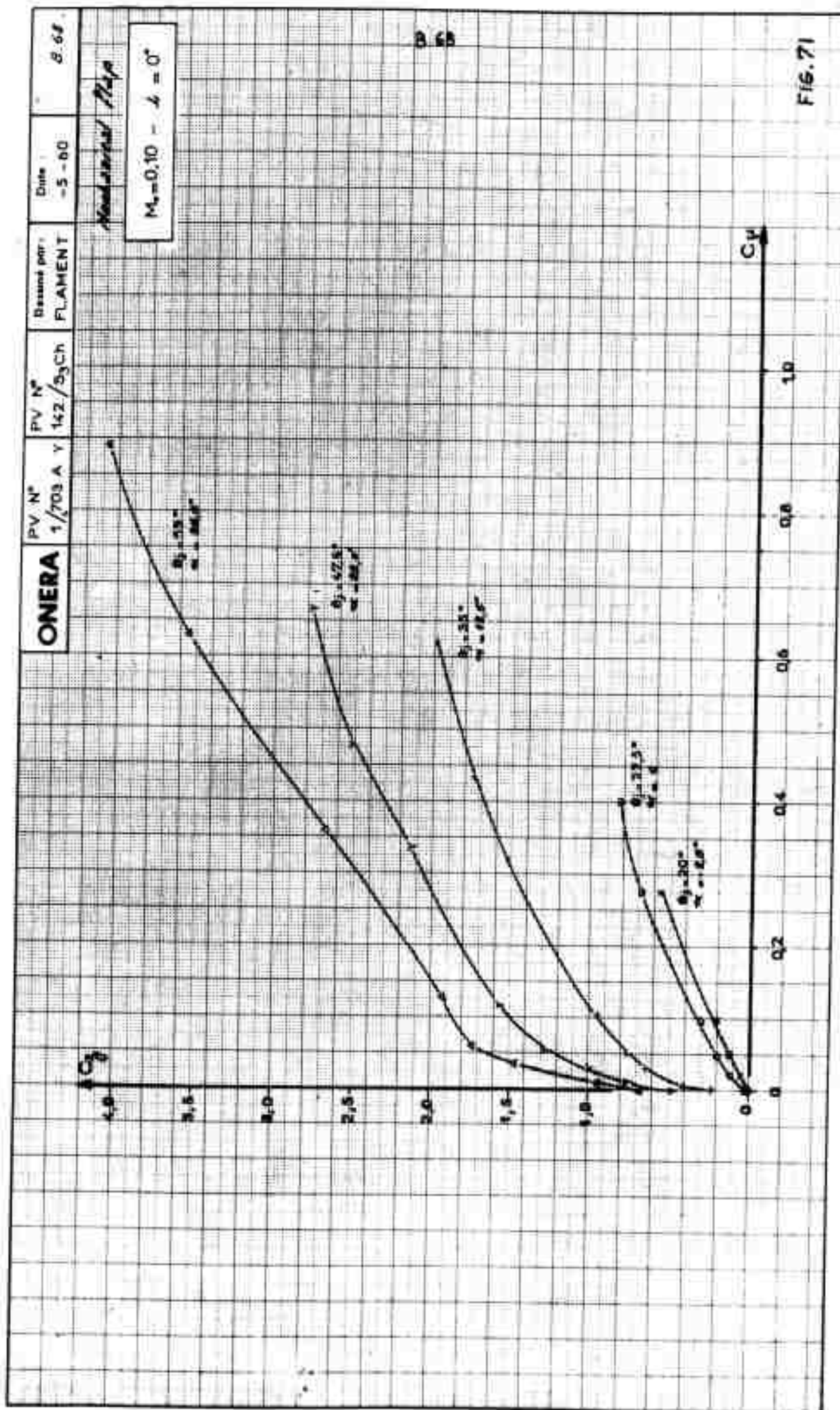


FIG. 71

ONERA	PV N° 1/703 A Y	PV N° 142 / SCh	Design par: FLAMENT	Date: - 5 - 60	B.69
-------	--------------------	--------------------	------------------------	-------------------	------

Mechanical flap

$$M_{\infty}=0,10 - C_{\mu}=0$$

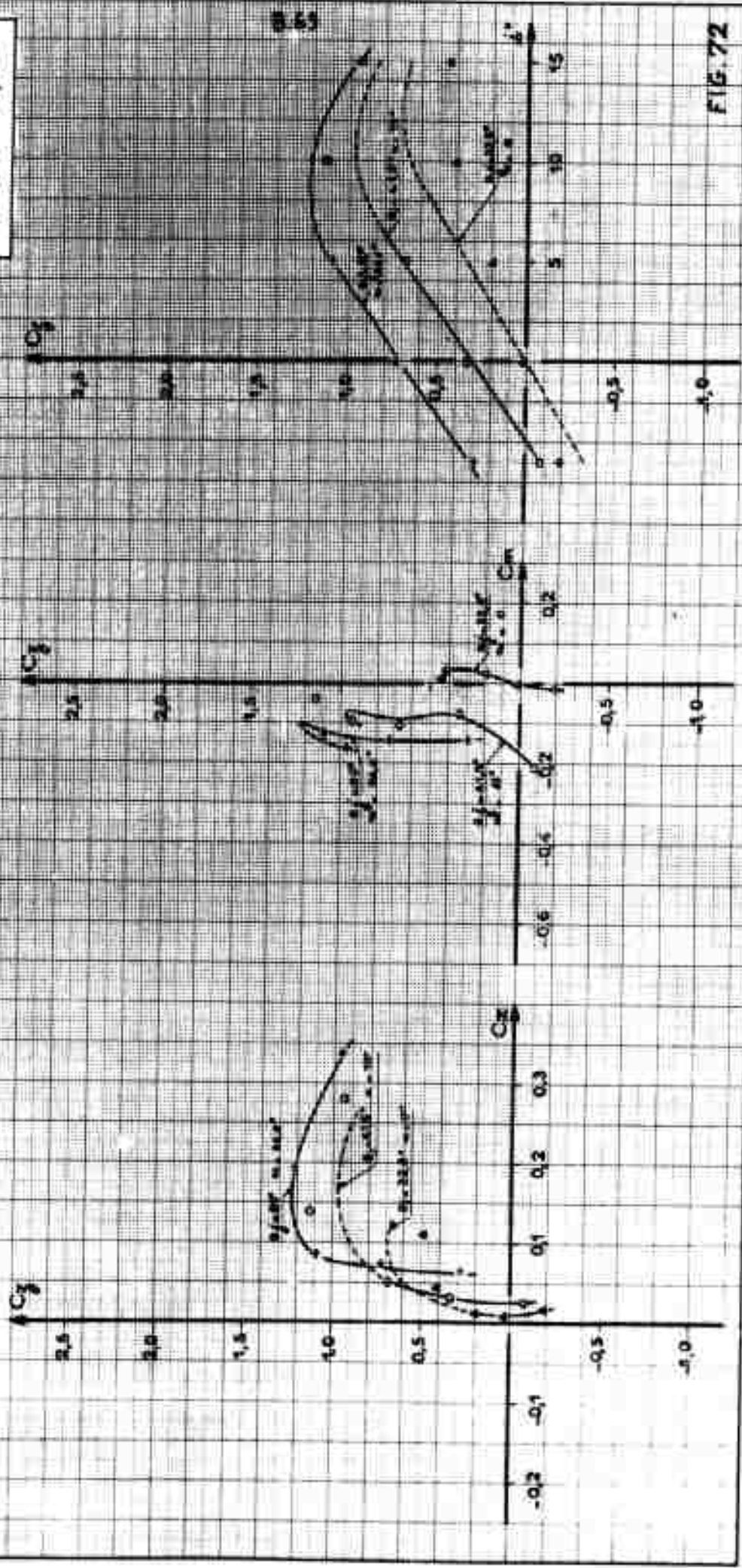


FIG. 72

ONERA	PV N° 1/703A Y	FV N° 142/S3 Ch	Designé par : FERAUNET	Date - 5 - 60	8.70
-------	-------------------	--------------------	---------------------------	------------------	------

Mechanical flap
 $M_0 = 0,10 - C_M = 0,02$

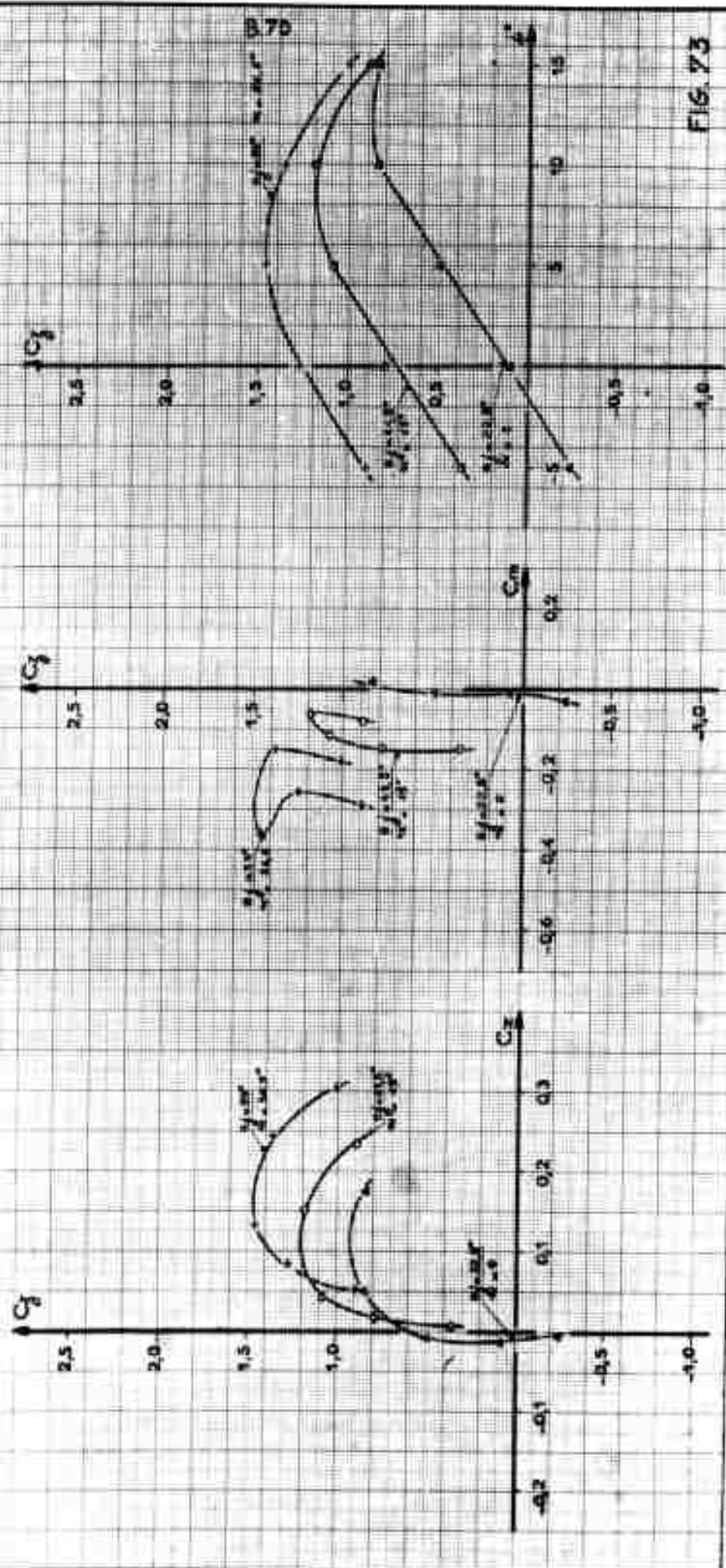


FIG. 73

ONERA

PV N°
1/703 A Y

PV N°
142/SCH

Dessiné par:
FERAUDDET

Date:
- 5 - 60

B. 71

Mechanical Map

$M_\infty = 0,10 - C_\mu = 0,06$

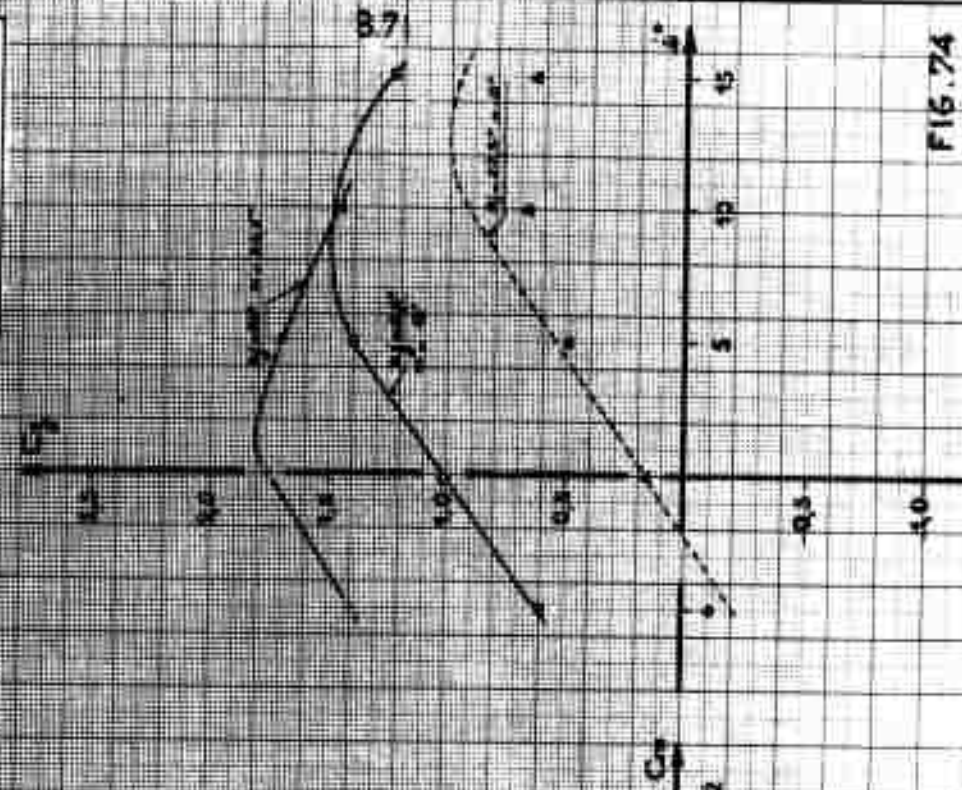
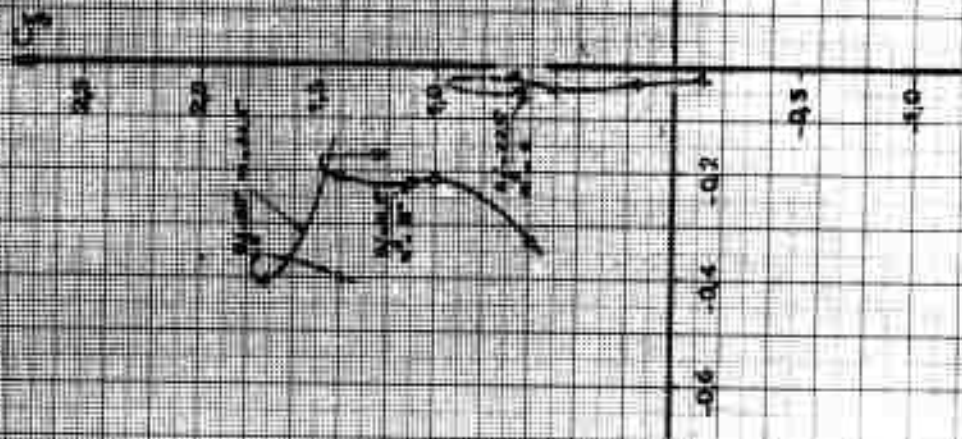
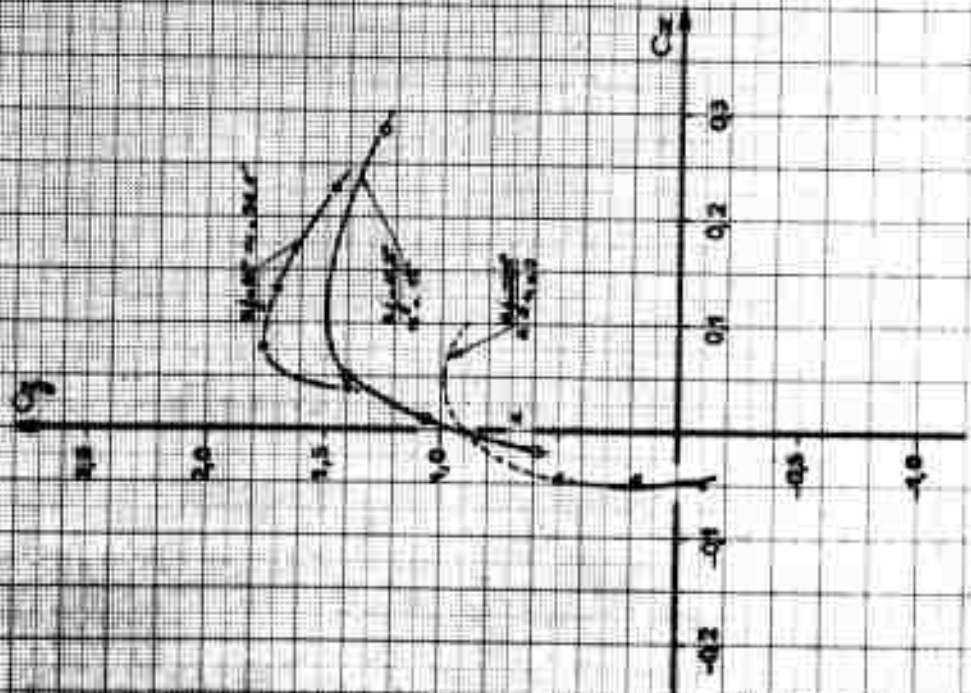


FIG. 74

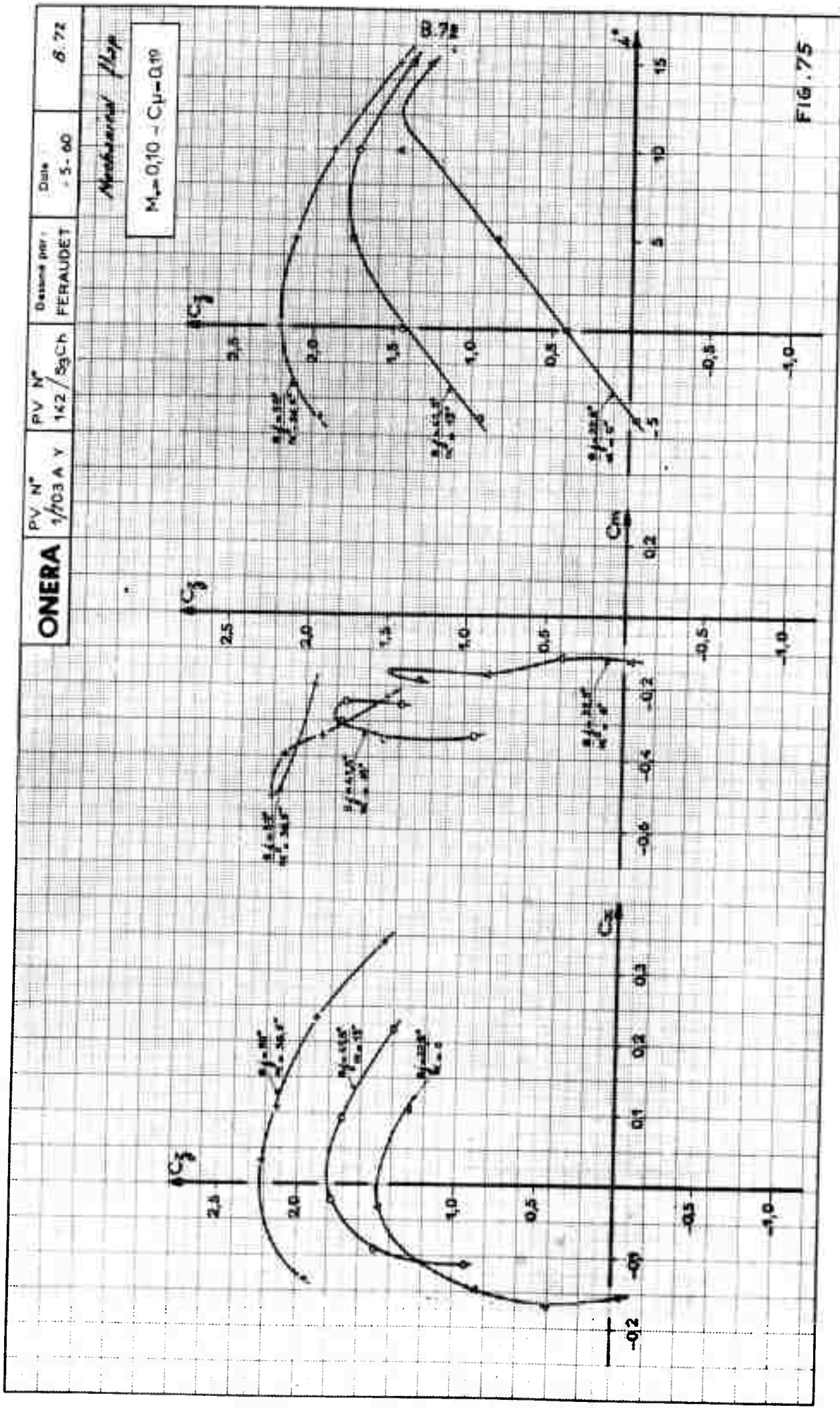


FIG.75

ONERA

PV N°
1/703A Y

PV N°
142/S3CH

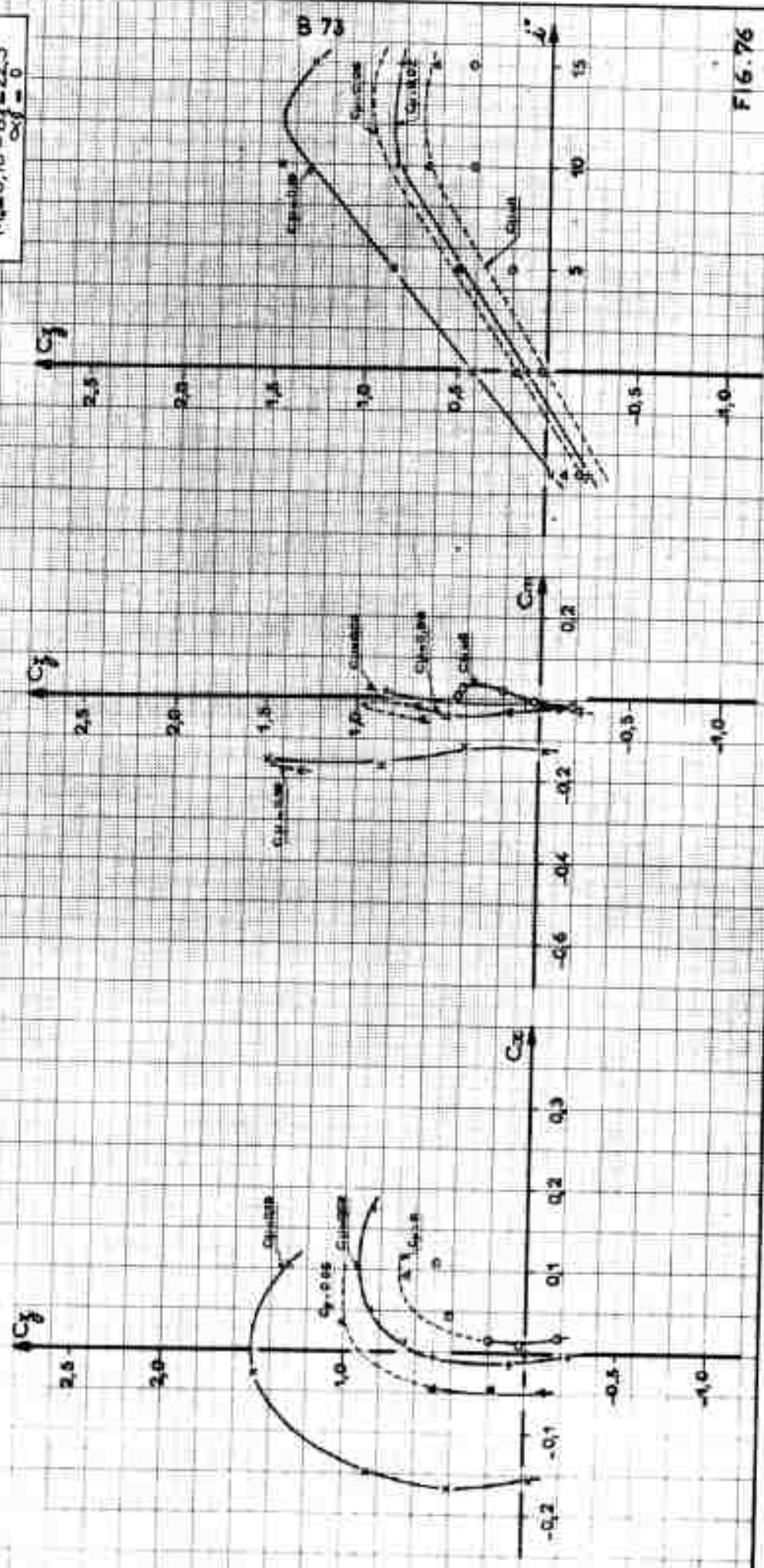
Designé par:
FERAUNET

Date:
- 5 - 60

8.73

Mechanical flap

$M_\infty = 0,10$ - $\theta_f = 22,5^\circ$
 $\alpha_f = 0$



ONERA

PV N°
1/703 A Y

PV N°
142/53 Ch

Devisé par:
FLAMENT

Date
- 5-60

B 74

Mechanical Flap

$M_\infty = 0,10 - \theta_f = 41,5^\circ$
 $\alpha_f = 10^\circ$

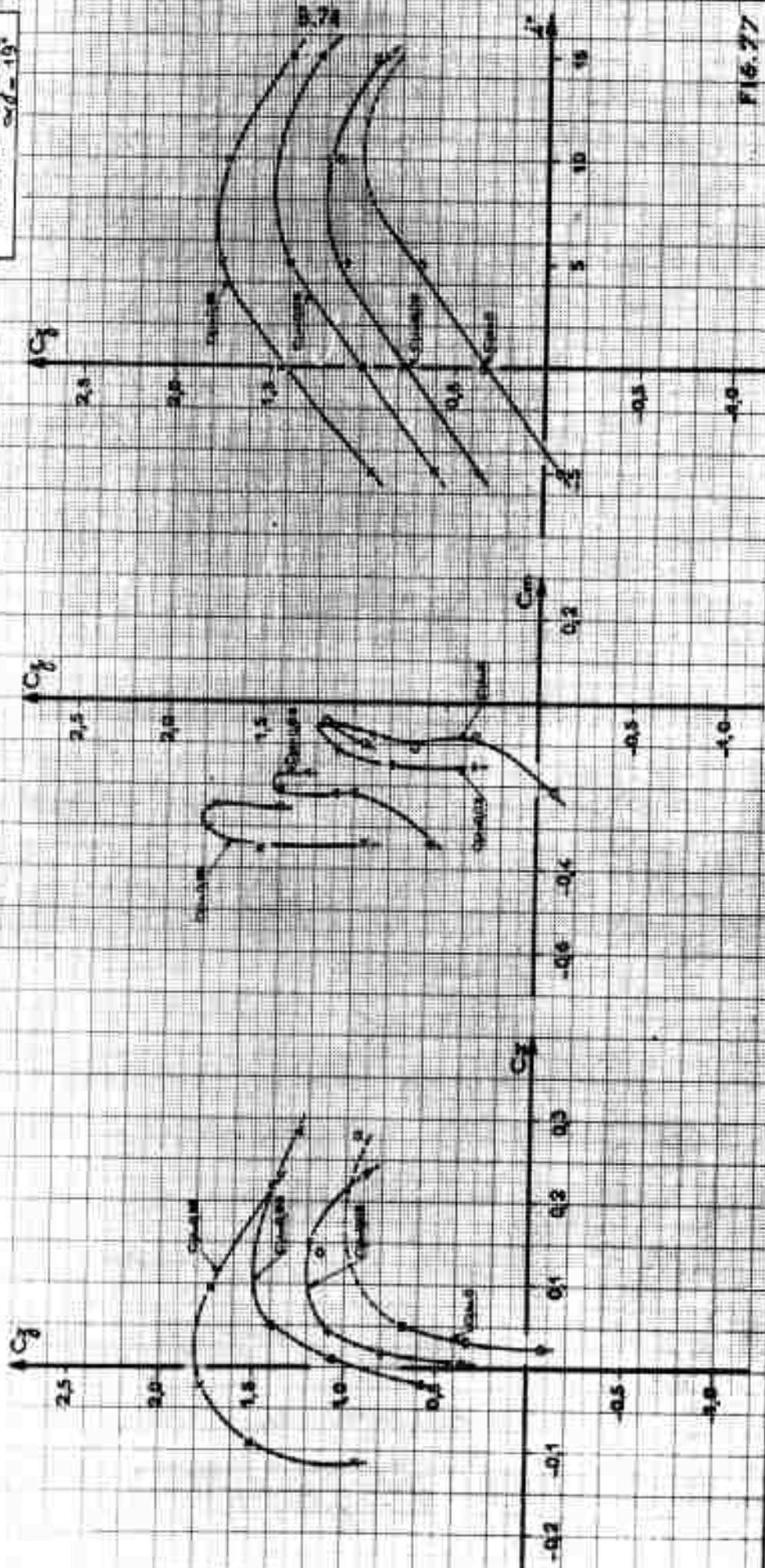


FIG. 27

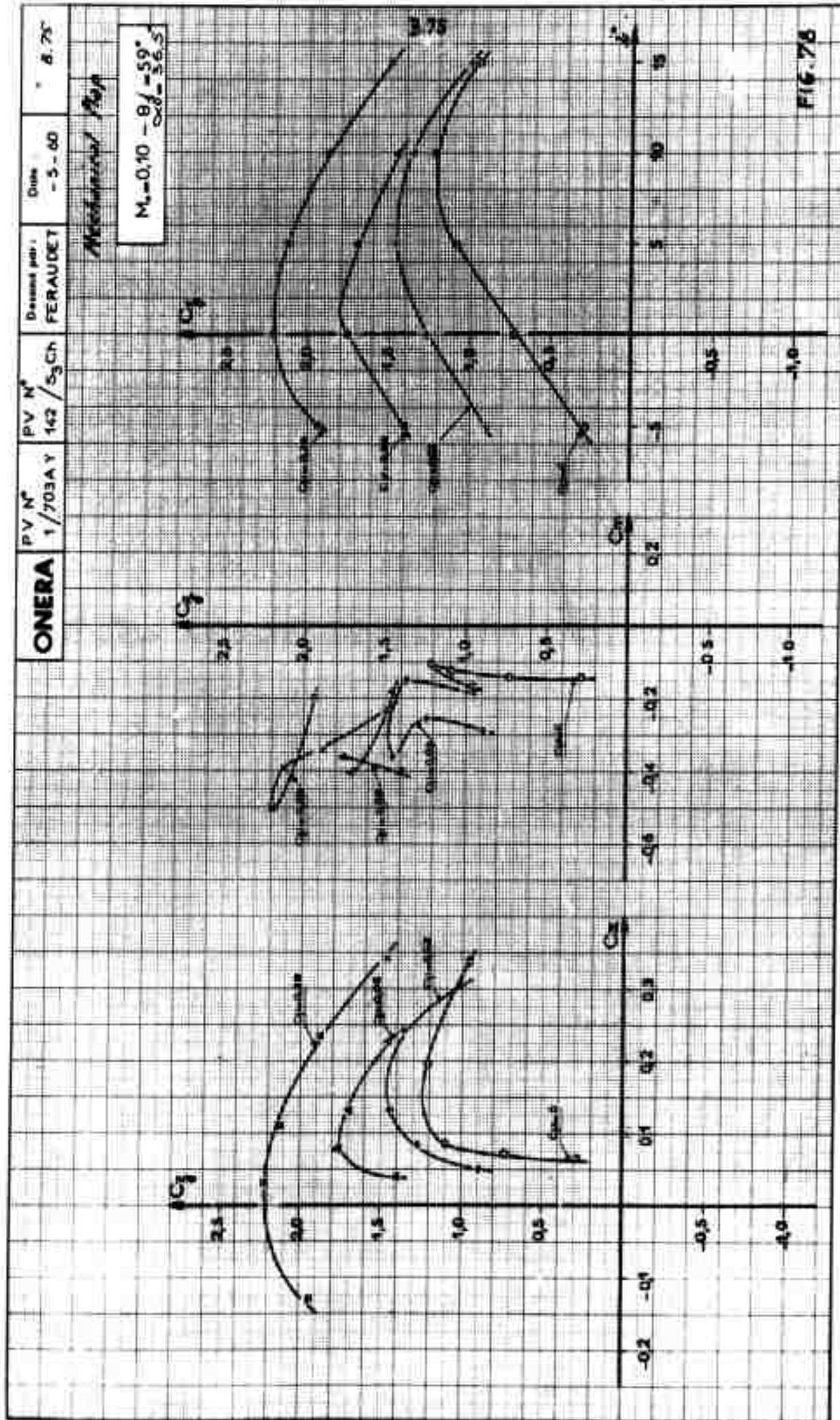


FIG. 78

ONERA

P.V. N°
1/1034 Y

P.V. N°
142 / 53 CH

Design (post):
FERAUADET

Date:
- 5 - 60

8.96

Mechanical flap

$M_0 = 0.60 - B_f = 22.5^\circ$
 $\alpha_f = 0^\circ$

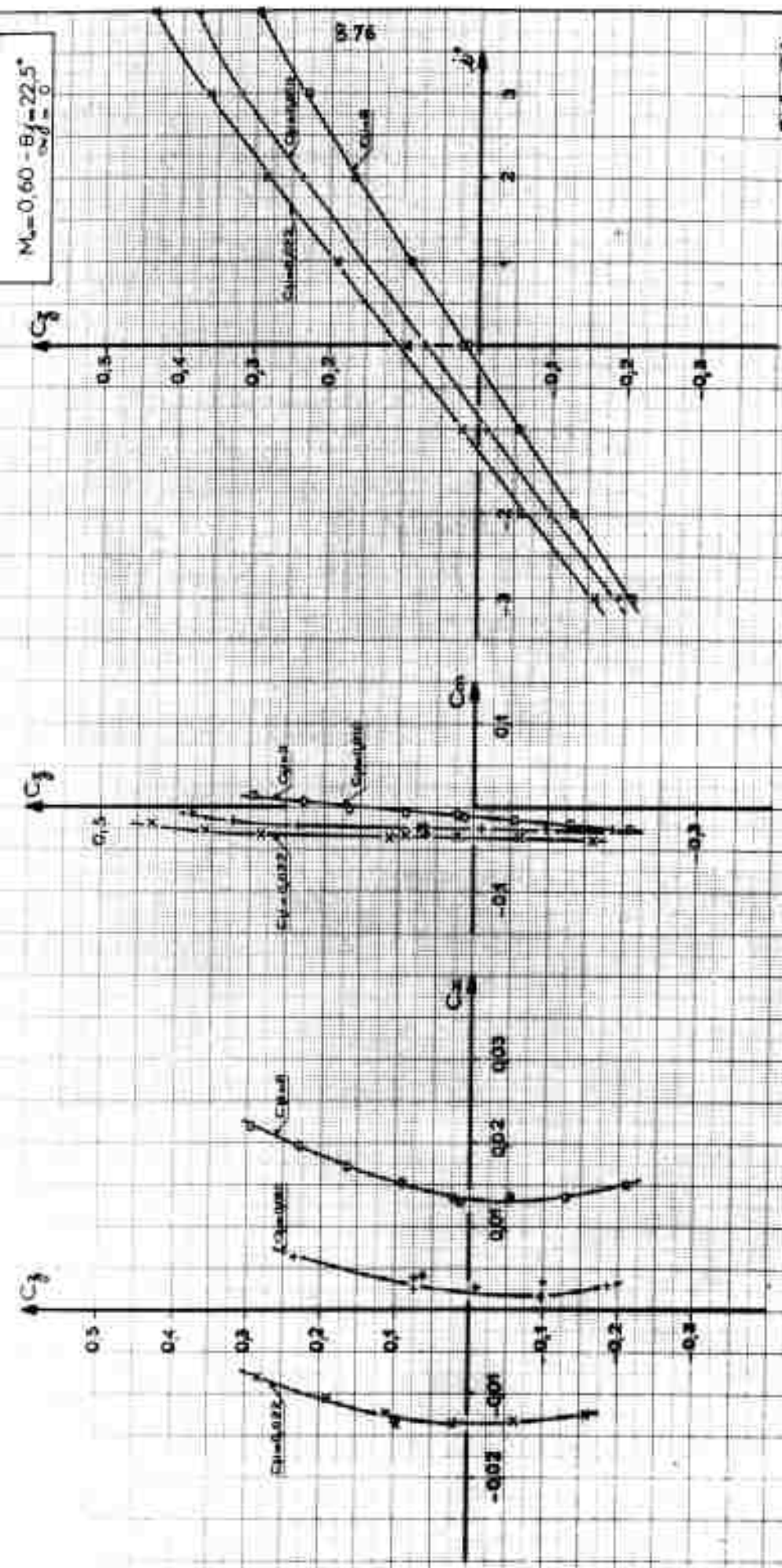
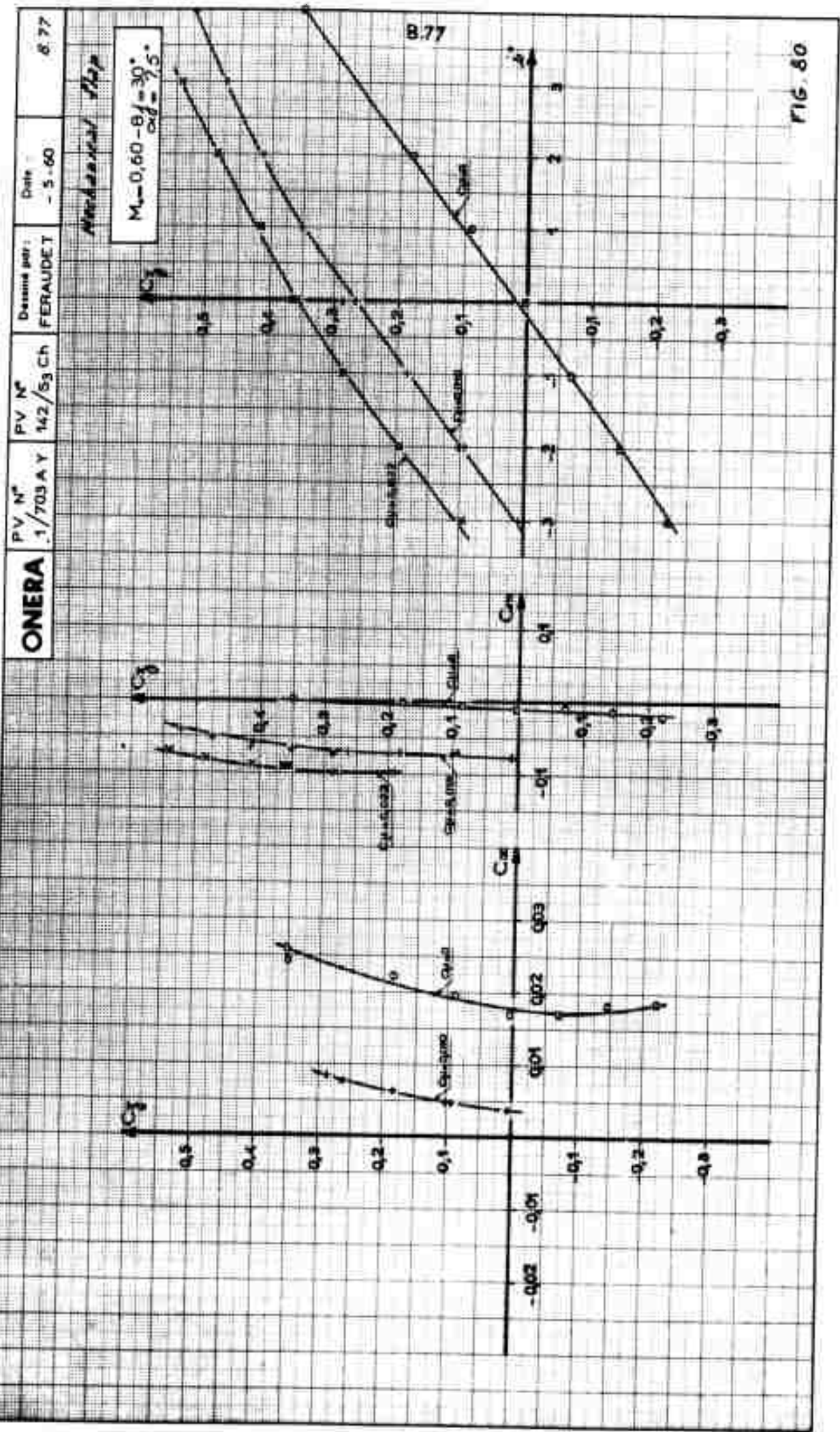


FIG. 79



ONERA

PV N° 1/703 A Y

PV N° 142 / 53 Ch

Dessiné par : FLAMENT

Date : 5 - 60

8.78

Mechanical flap

$$M_0 = 0,60 - B_1 = 37,5^\circ$$

$$\Delta \theta = 1,5^\circ$$

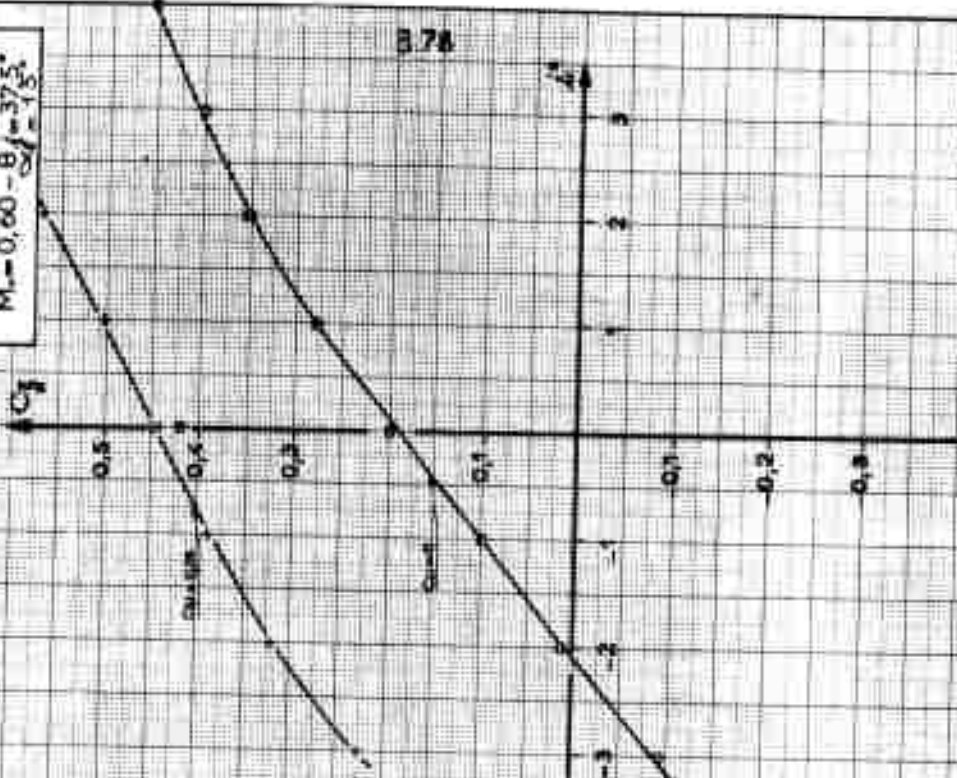
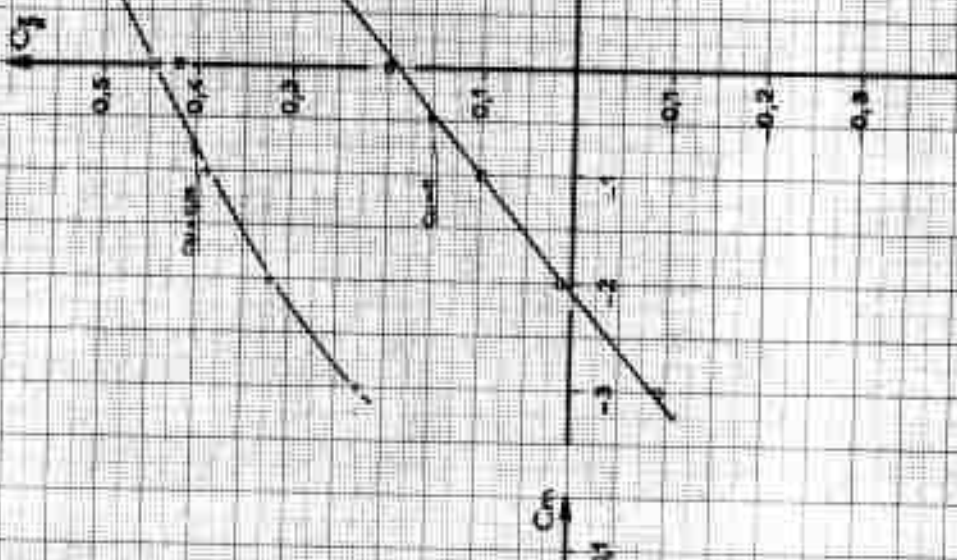
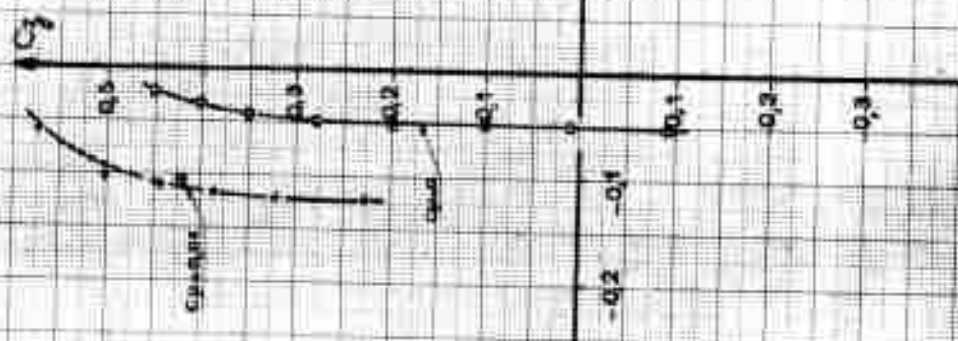
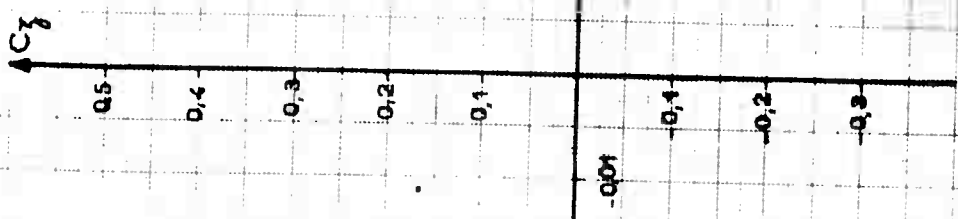


FIG. 81

ONERA	PV N° 1/703 A Y	PV N° 142/S3 Ch	Dessiné par : FERAUDET	Date : - 5 - 60	B.79
-------	--------------------	--------------------	---------------------------	--------------------	------

Mechanical Shop

$$M_1 = 0,70 - \theta_1 = 22,5^\circ$$

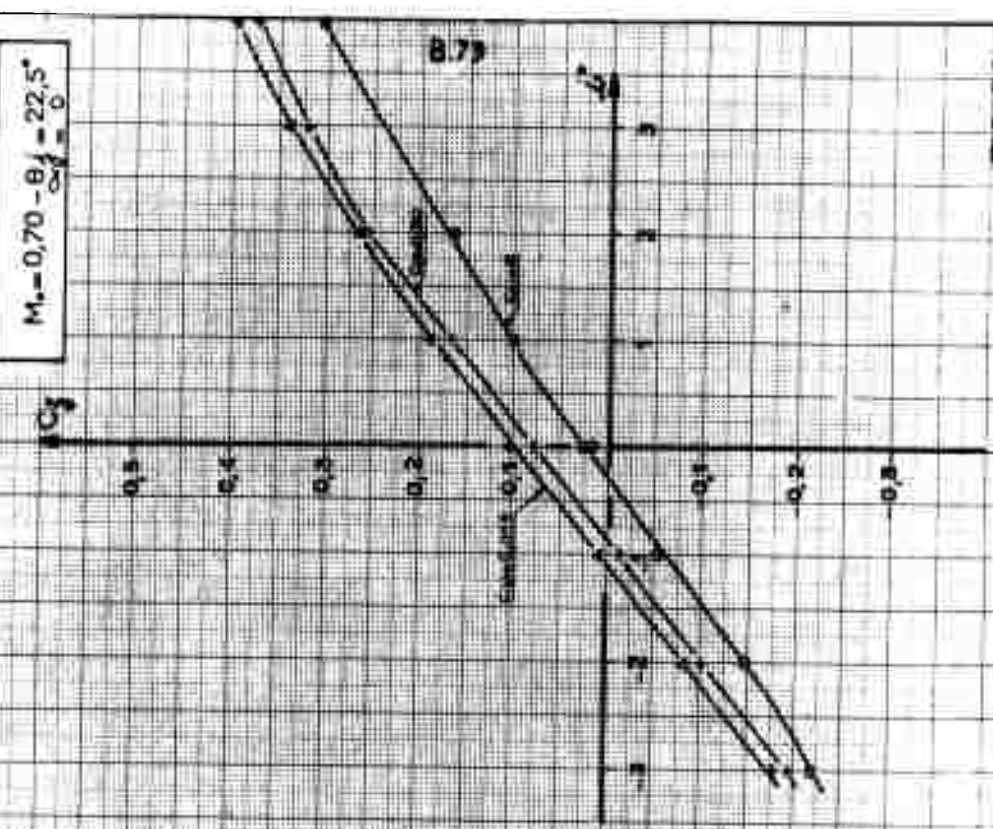
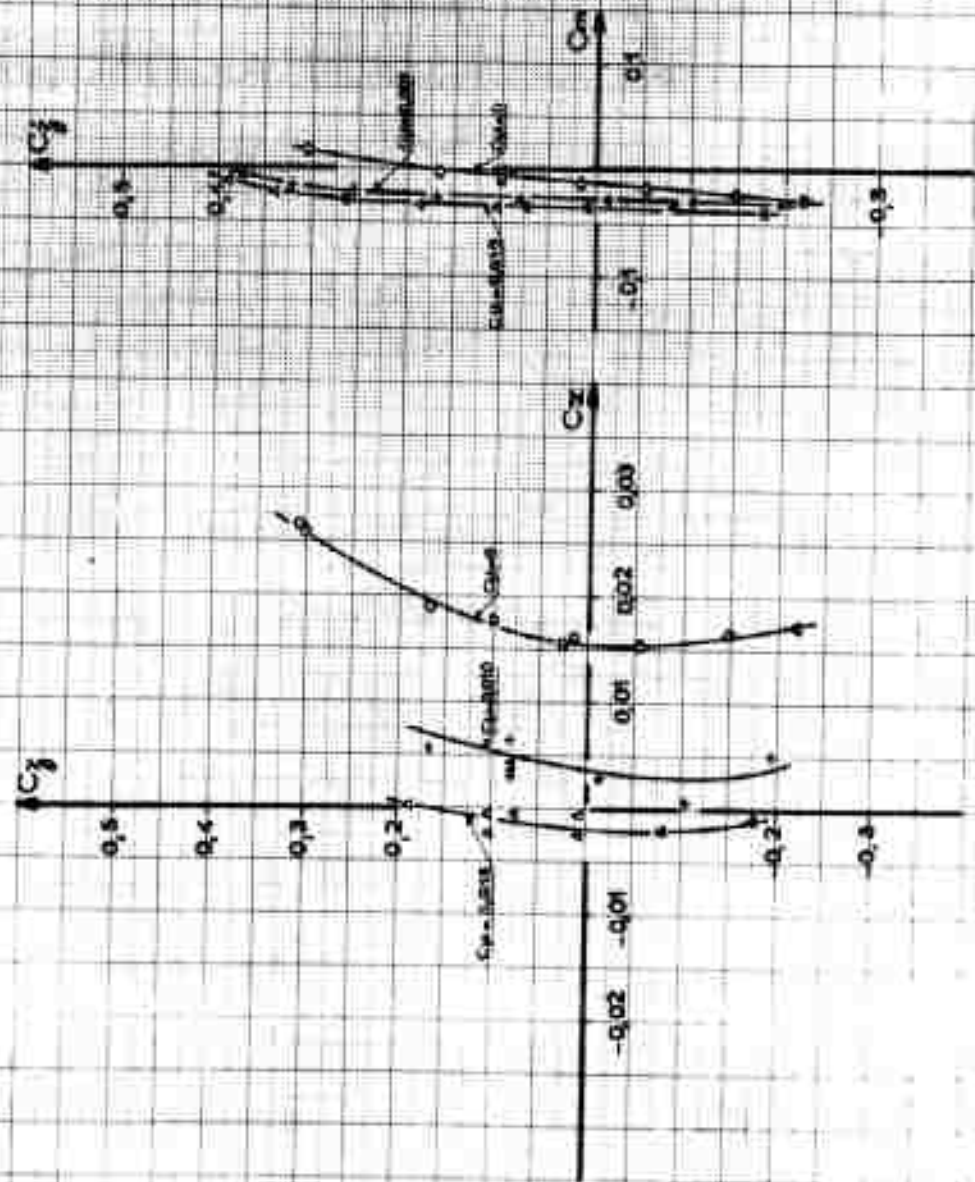


FIG. 82

ONERA

PV N° 1/703A Y

PV N° 142/S3CN

Designé par: FERAUDET

Date: 5-60

8.80

Mechanical flap

$M_\infty = 0.70 - 8.1 - 30^\circ$
 $\alpha_{eff} = 7.5^\circ$

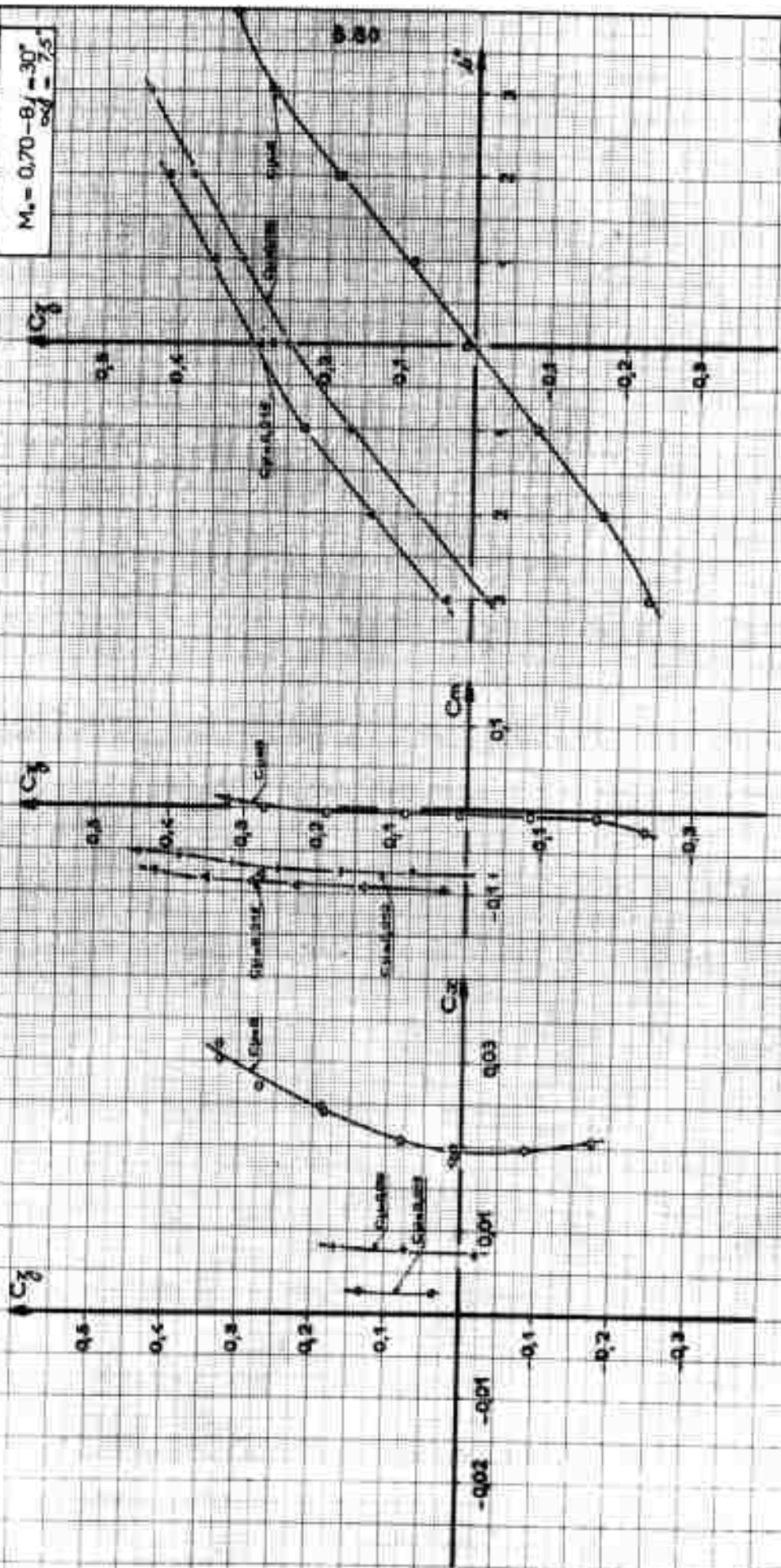


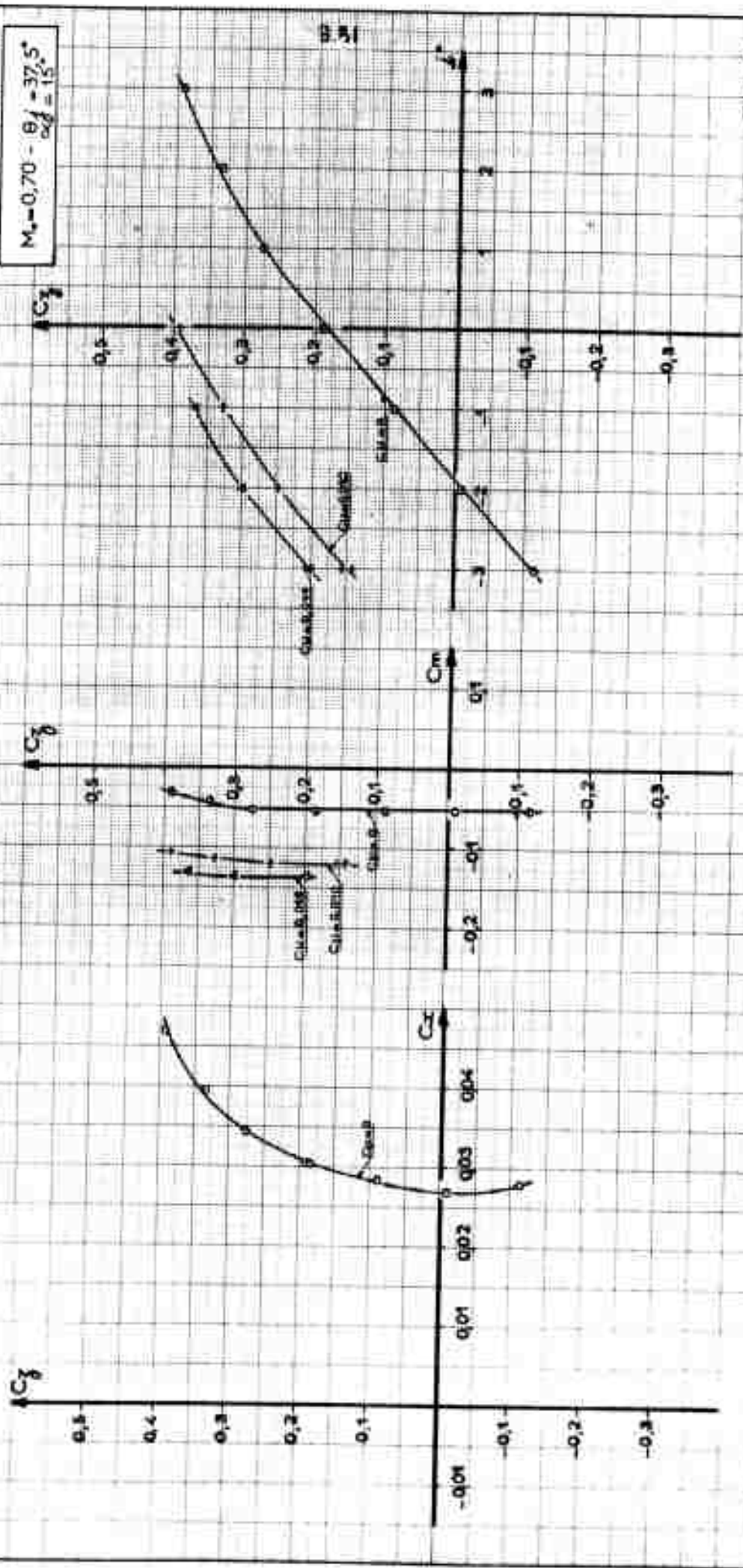
FIG. 83

ONERA	PV N°	PV N°	Date	8.81
	1/703A Y	142/S3 CH	FERAUADET - 5.60	

Mechanical Map

$$M_x = 0.70 - \theta_f - 37.5^\circ$$

$$\alpha_d = 15.5^\circ$$



ONERA

PV N°
1/703 A Y

PV N°
142/53CH

Dessiné par :
FERAIDEY

Date :
- 5 - 60

B.82

Neutrization flap

$M_{\infty} = 0.80 - B_f = 22.5^\circ$
 $\alpha_f = 0$

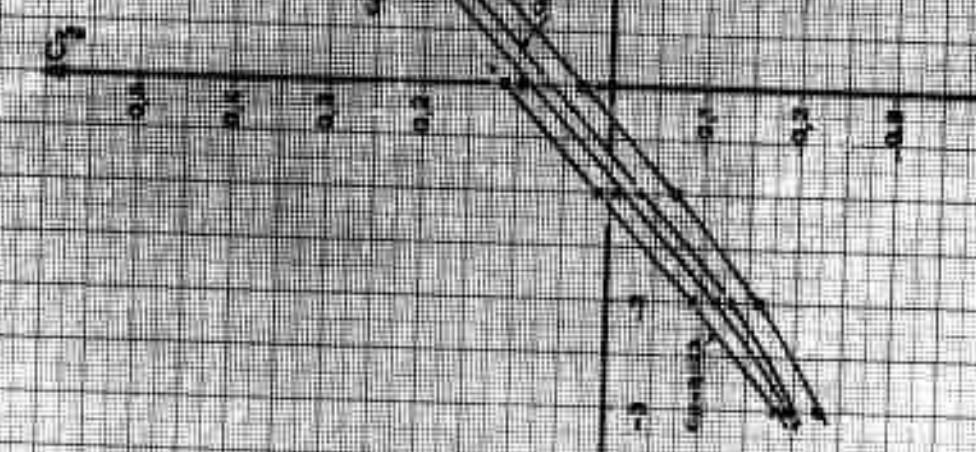
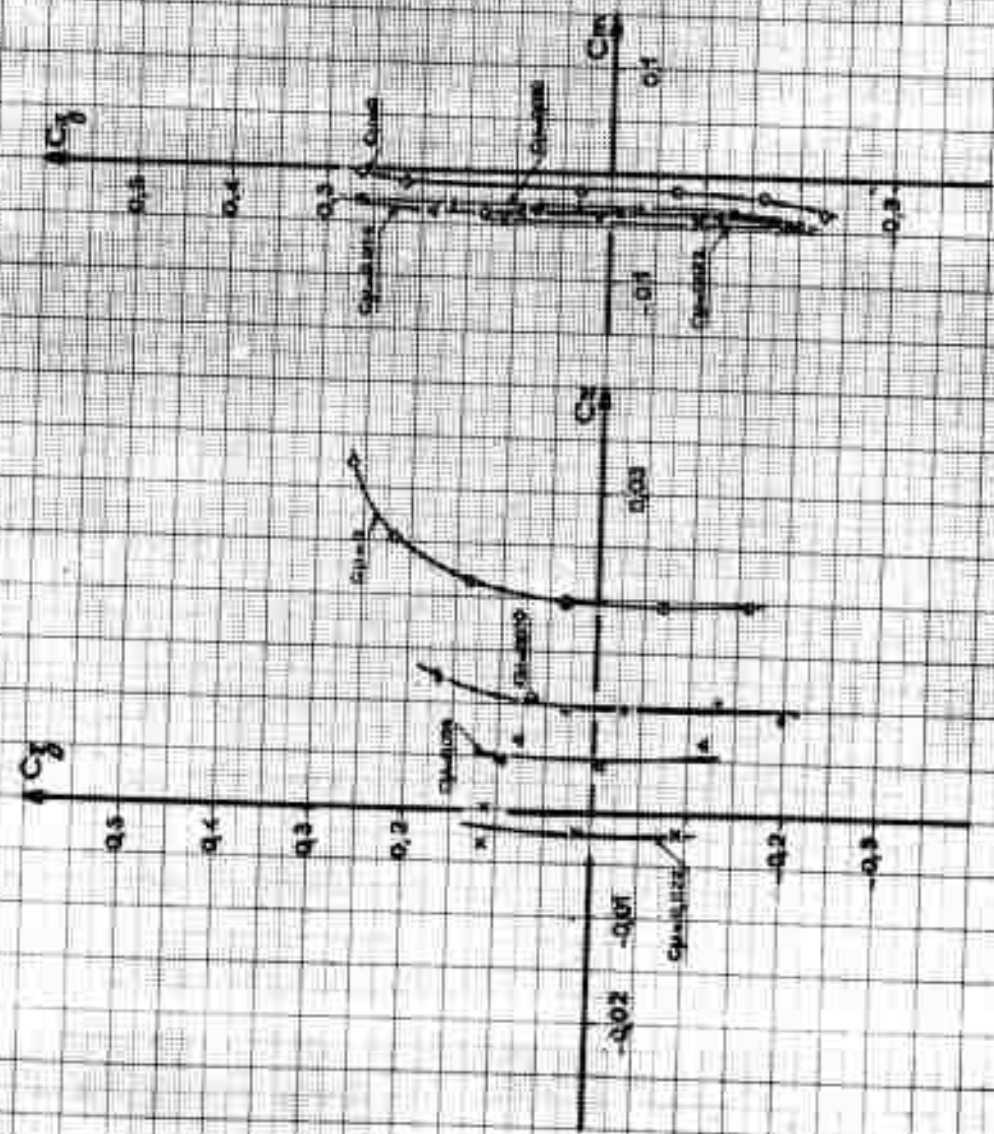


Fig. 85

ONERA	PV N°	PV N°	Design par:	Date	8-83
	1/703 A Y	142/S3CH	FLAMENT	- 5 - 60	

Heckmann/Flap

$$M_{\infty} = 0.80 - \theta / -30^{\circ} - \frac{\alpha}{5^{\circ}}$$

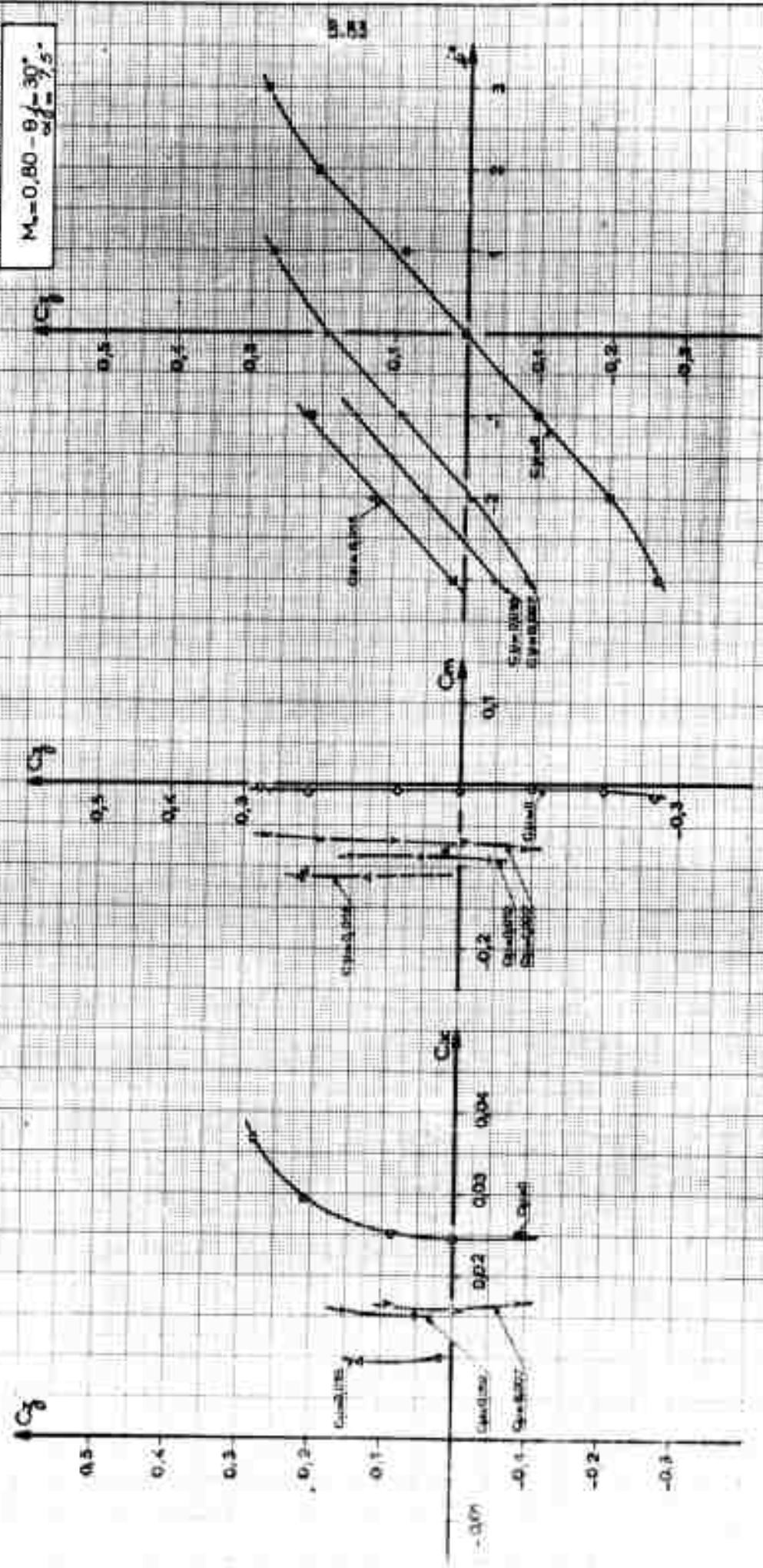


FIG. 86

ONERA

PV N°
1/703 A Y

PV N°
142/53 Ch

Dessiné par :
FERAUDET

Date :
- 5 - 60

3.84

Mathématique

$$M_1 = 0.80 - 8 / -37.5$$

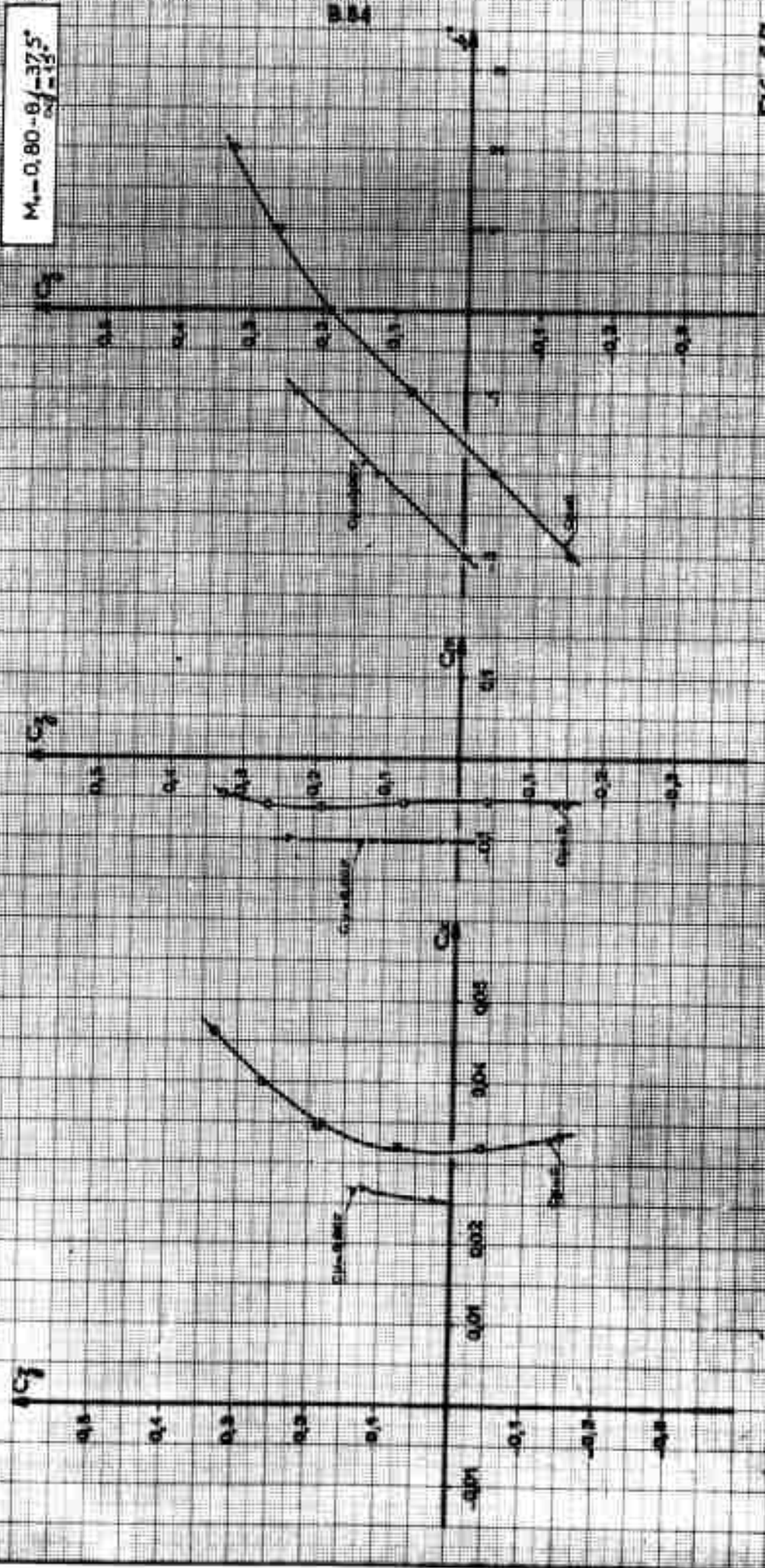


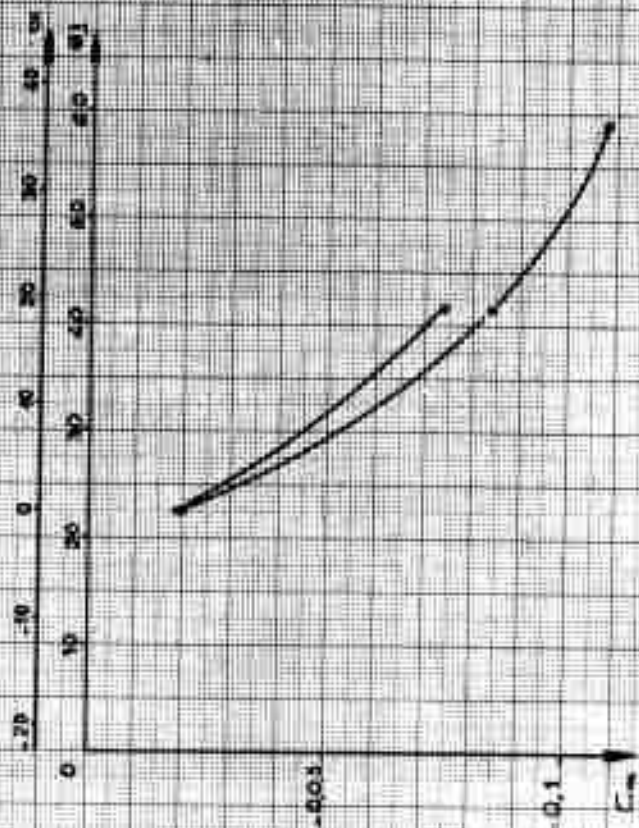
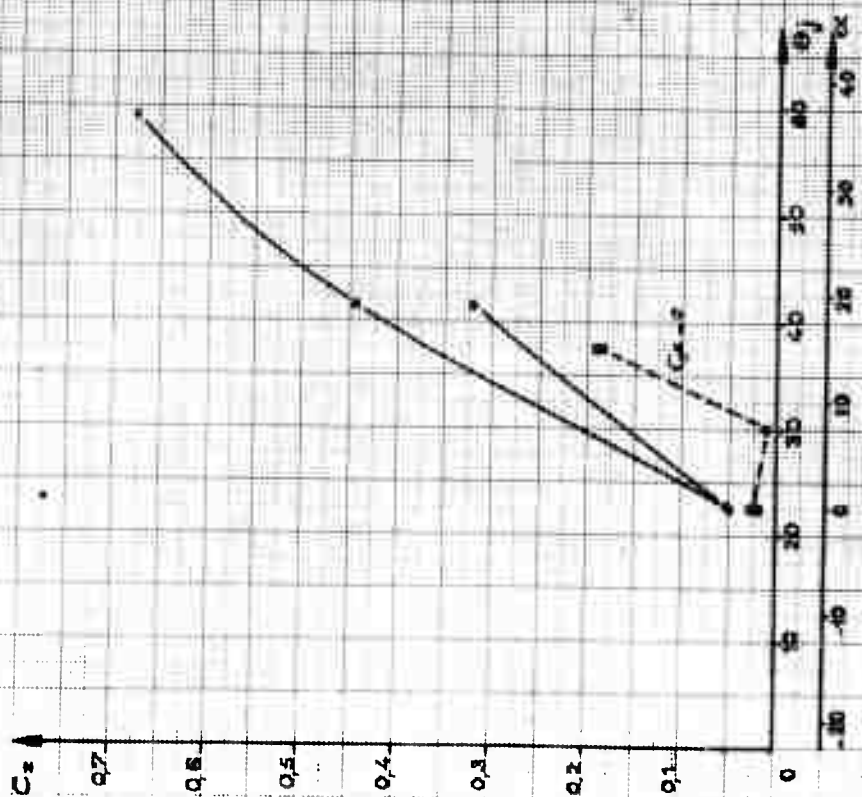
FIG. 87

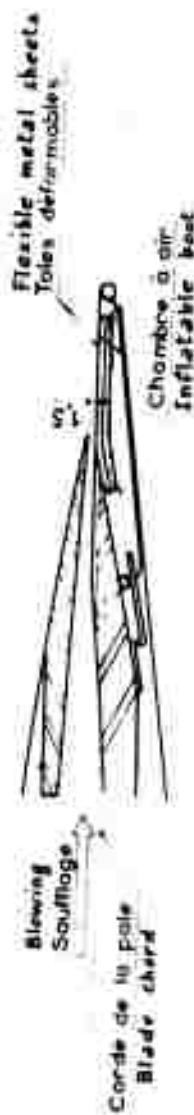
	pression	up stream of jet	mm of water
• $M_0 = 0.0$, pression	an avant de la lante	$P_0 = 4000$ mm d'eau	
• $M_0 = 0.7$, pression	up stream of jet		
	an avant de la lante	$P_0 = 3700$ mm d'eau	
• $M_0 = 0.7$, $C_0 = 0$			

5

Mechanical Step

10



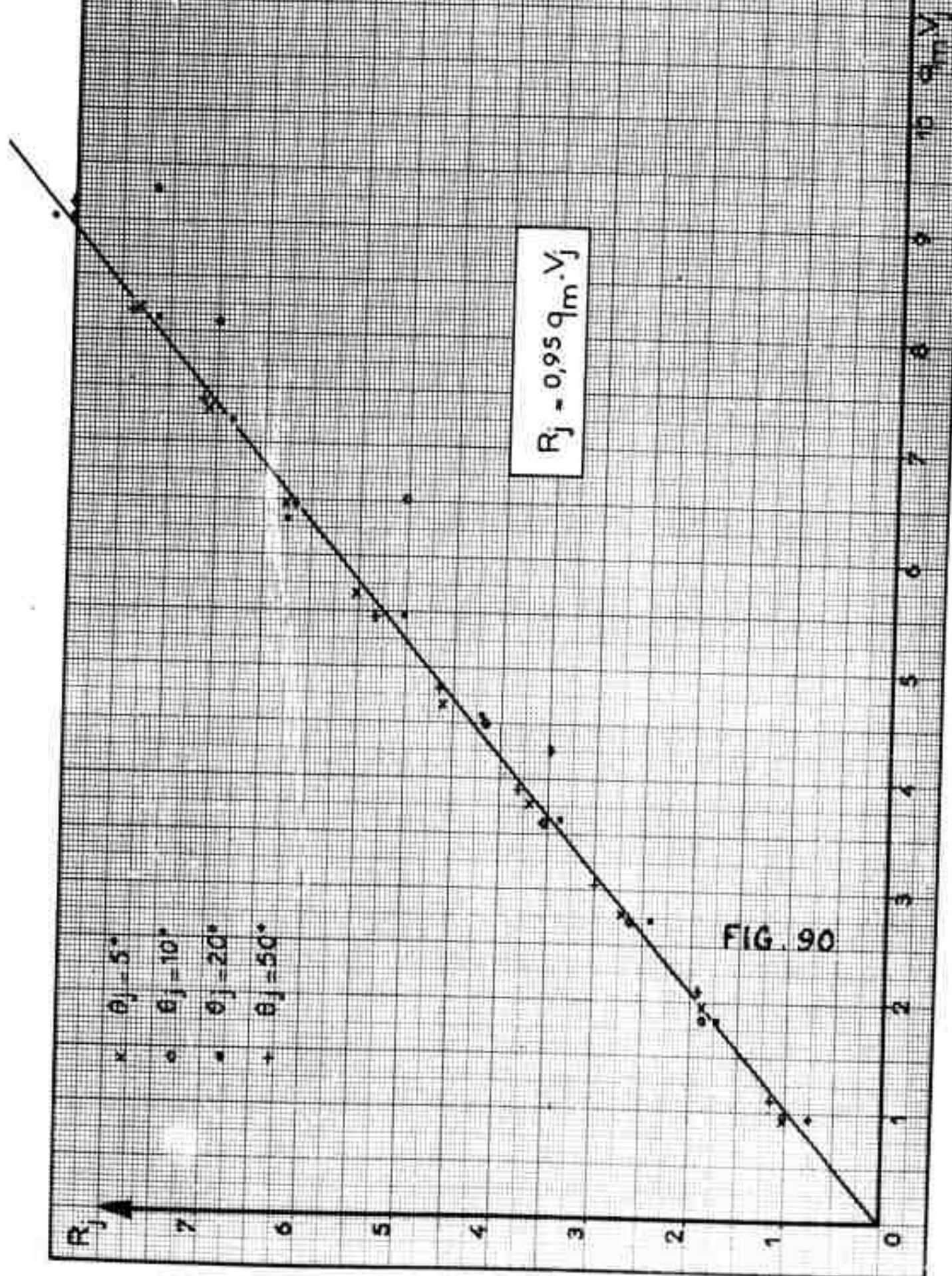


Scale of drawing: 1/2"

[illegible]

PV. N°:	Dessiné par :	Date :
147/S₃Ch	GANNE	5-10-60
Wind tunnel: S₃ Ch.		
Soufflerie		
Balance		m ²
Model Maquette :		
Echelle	Coefficient	% l
(l _m =)	0,350	m
References	(l _r =)	0,154 m
(l _p = S x l _m)	0,539	m ²
(l _f = S x b)		m ²
WING AILE		
Envergure : b	0,450	m
Chord sur l'axe central : c	0,350	m
Cordes d'extrémité : c _e	0,350	m
Aspect ratio		m
Allongement : A = $\frac{b^2}{S}$	0	
Paper	...S	
Effilement : $1 - \frac{l_c}{l_o}$		
Swamp back B.A.: $\gamma_{RA} =$	0	
Fliches ...%		
airfoil	0	
Profile	11% à 45	
Entrée	Vitesse Free	0
		0,86
EXAMEN		
EMPERANCE PERFORMANT		
Longueur		
Surface		
Poids		
Résistance		
Vitesse		
REMARKS		
OBSERVATION		
N° 241 / ECH FIG. 89		

Tests of pneumatic flap



ONERA

PV. 6/703 AY PV. 148/53 Ch

Dessiné par :
NE

Date :
10-60

B. 88

Asymétrique Flap

$M_{\infty} = 0,10$ $\alpha = 0^\circ$

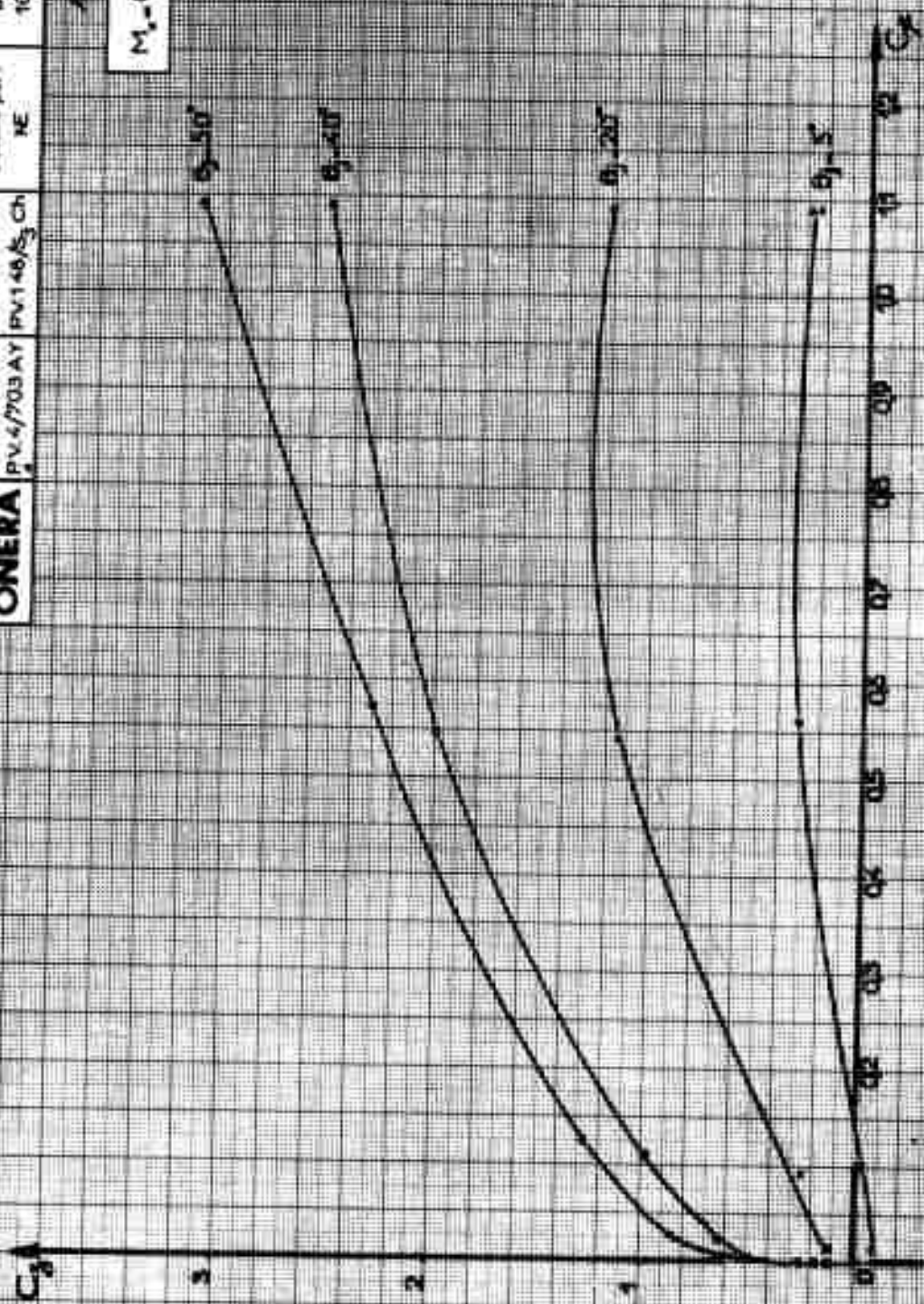


FIG. 91

ONERA	P.V.4/703 AV	PV140/S ₃ Ch	Distance par / NE	Date 10-60	B. 89
--------------	--------------	-------------------------	----------------------	---------------	-------

Parametric Study

$M_\infty = 0.10 \quad C_{\mu} = 0$

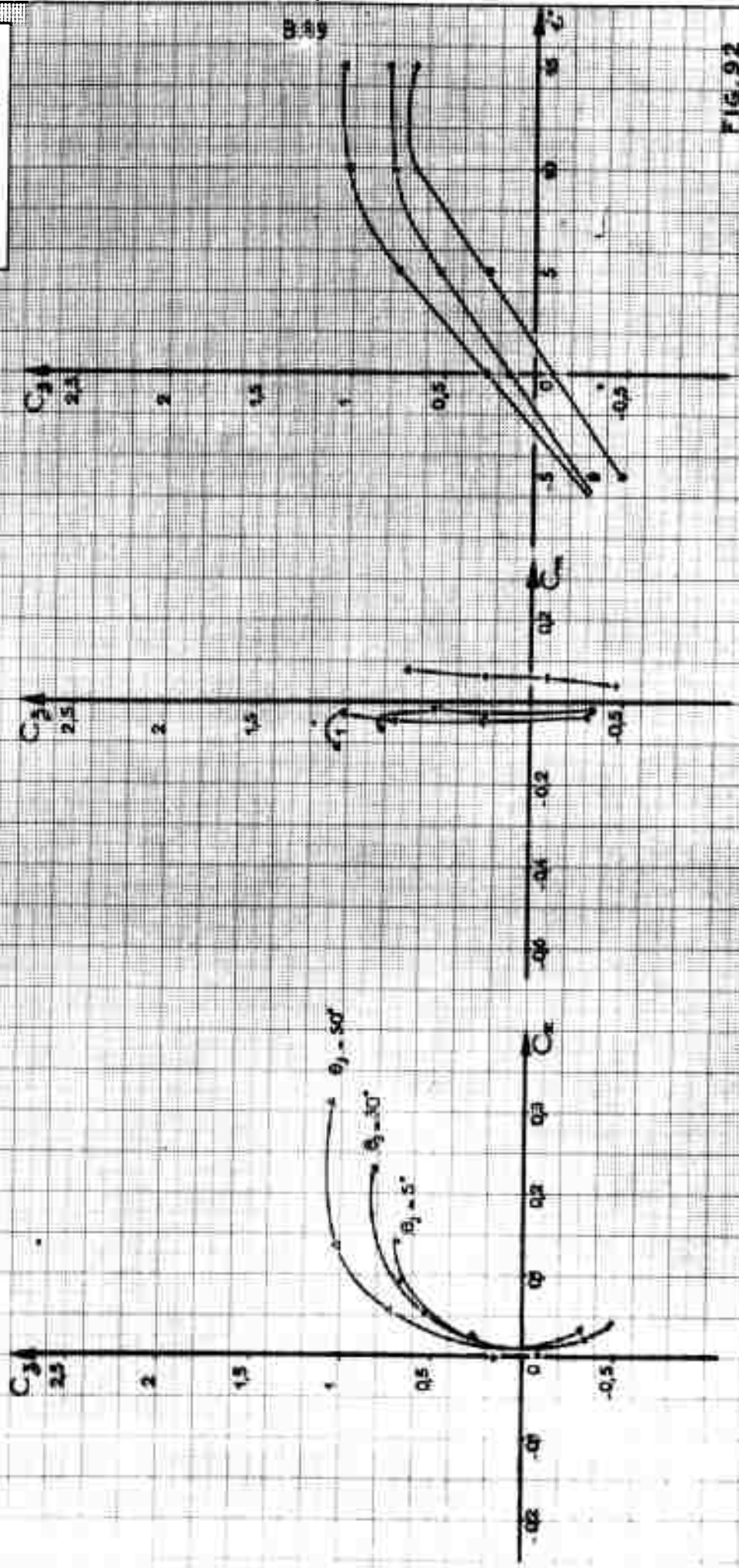


FIG. 92

ONERA

PV6/703AY

PV148/53CH

Desired year:
NE

Date:
10-60

11.90°

Approximate slope

$M_s = 0,10$ $C_{\mu} = 0,03$

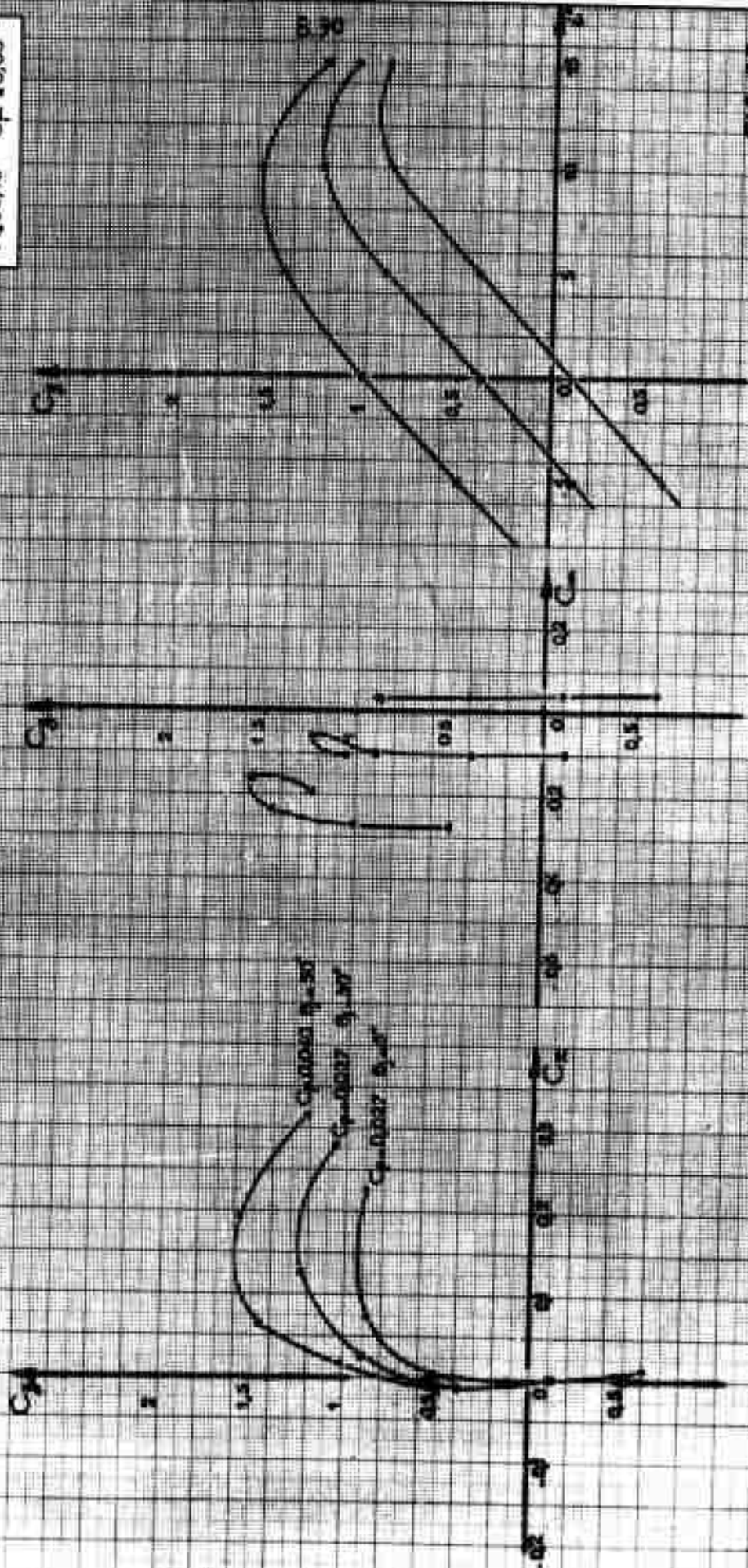


FIG. 93

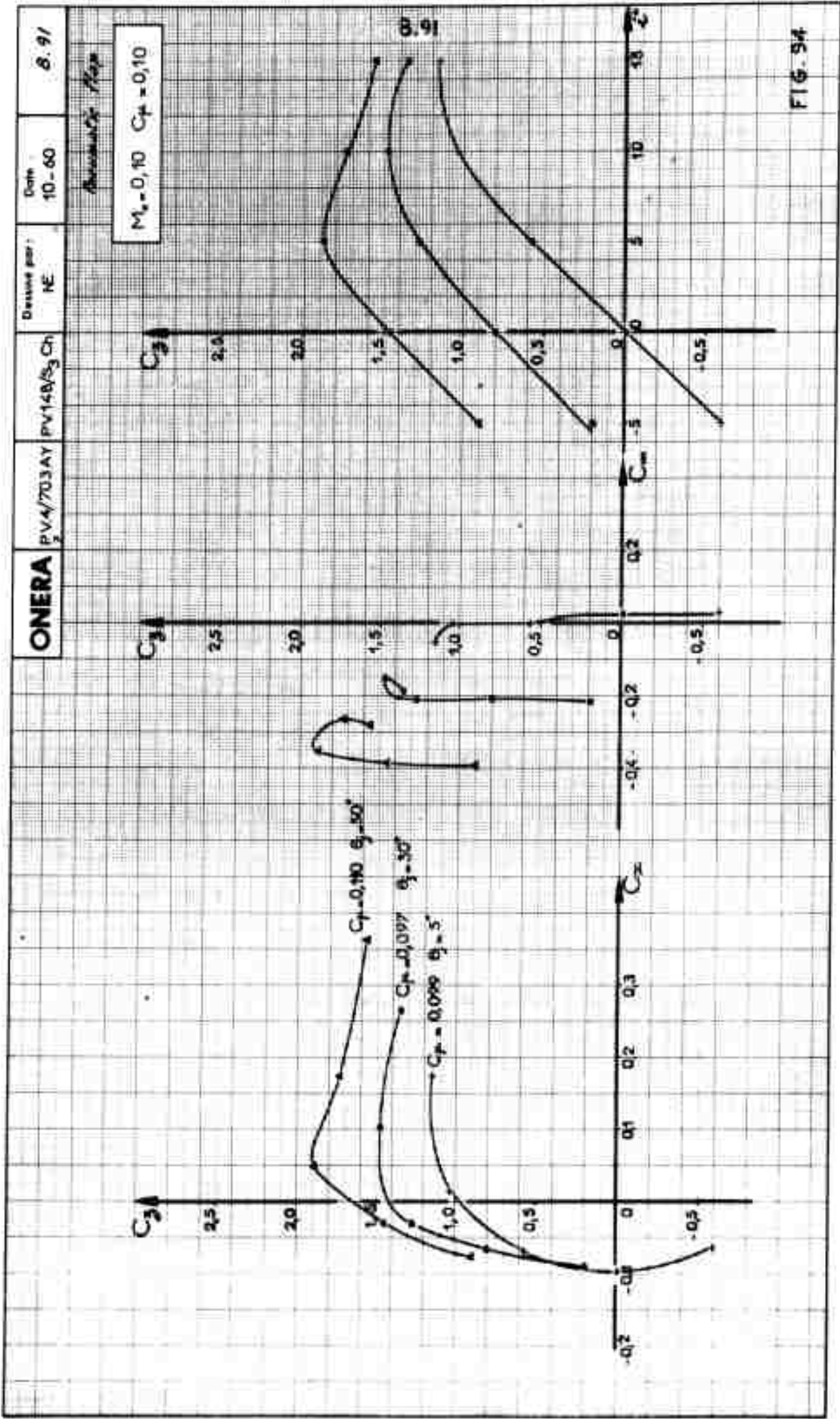
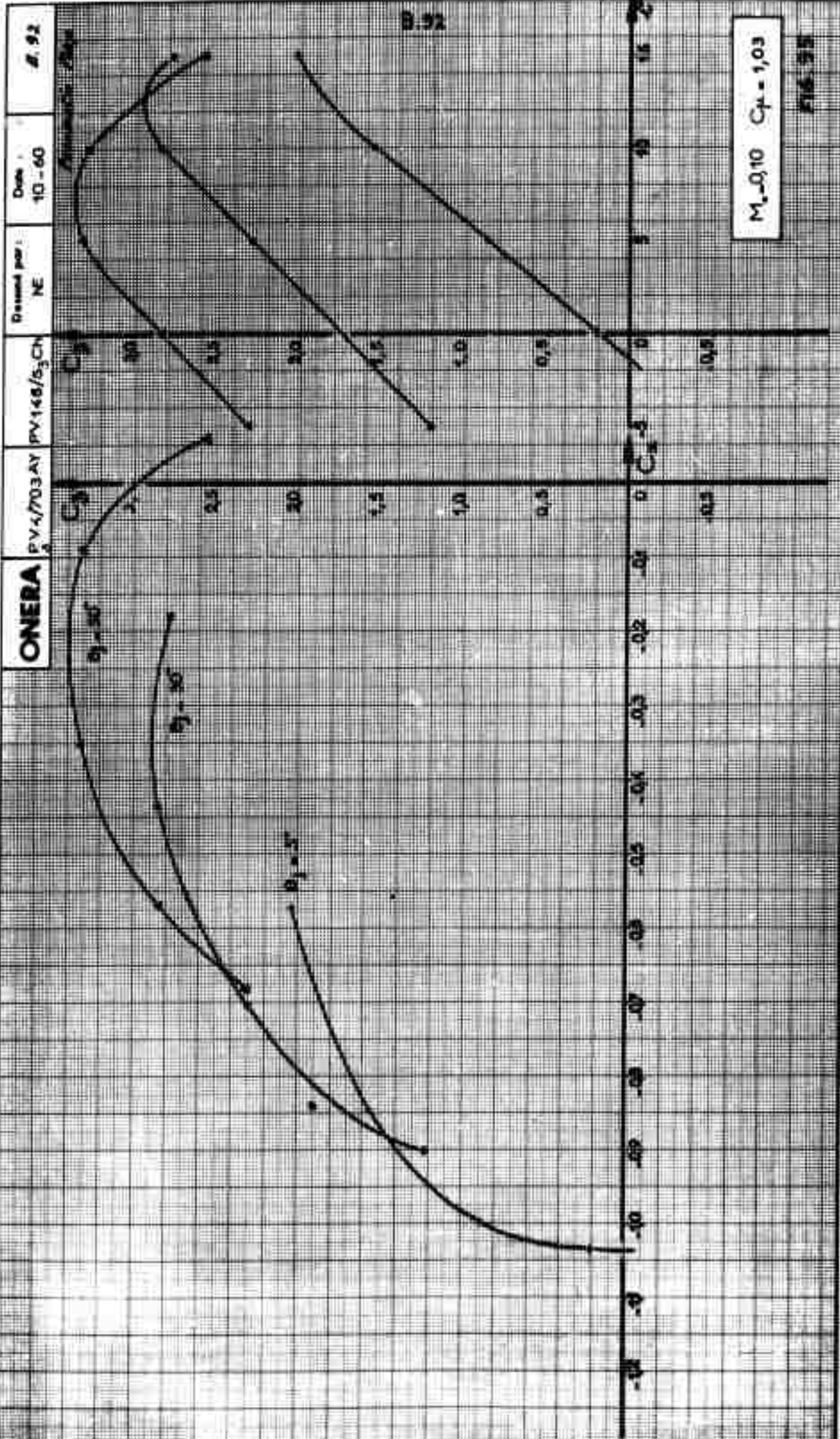


FIG. 94



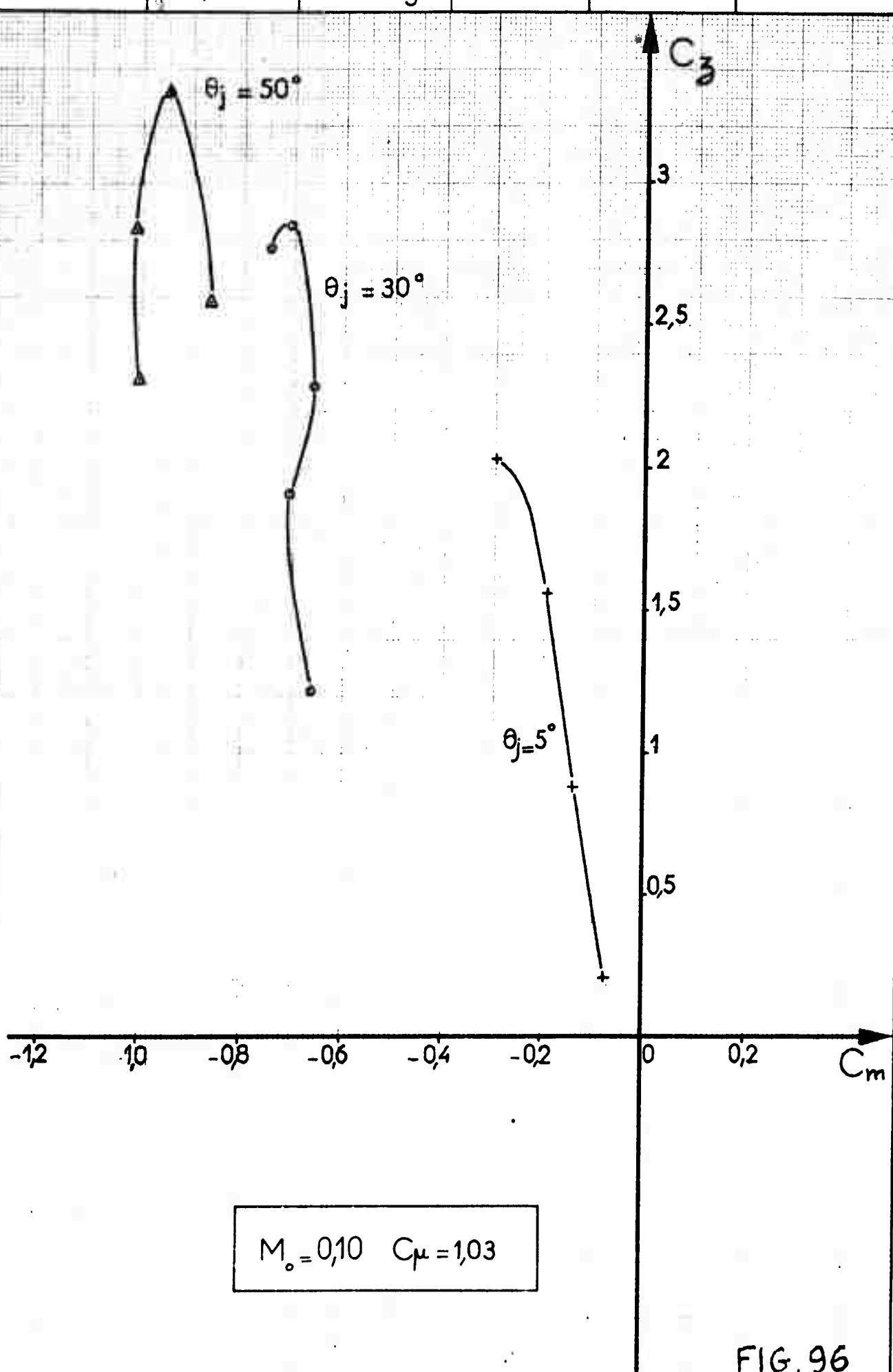


FIG. 96

ONERA

PV 4/703 AY
16

PV 148/53 CH

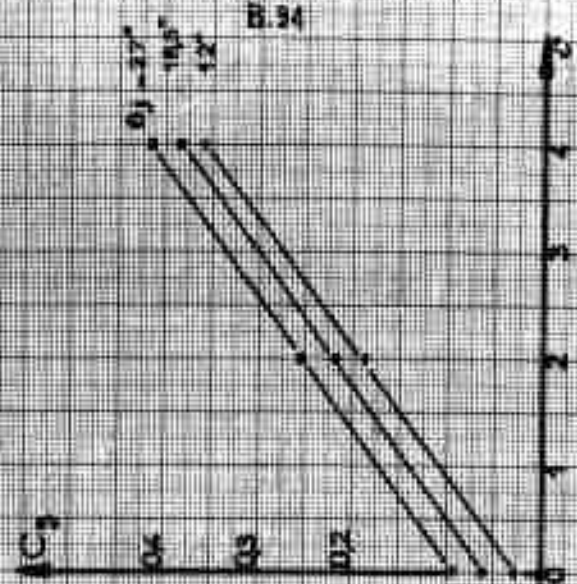
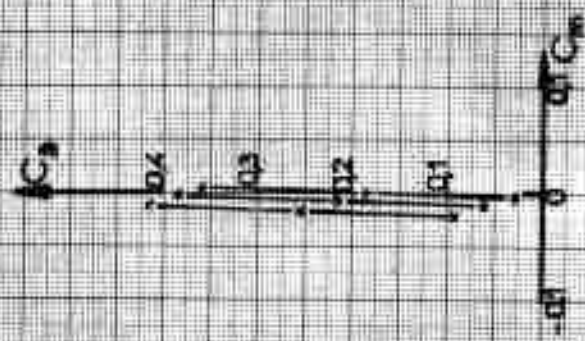
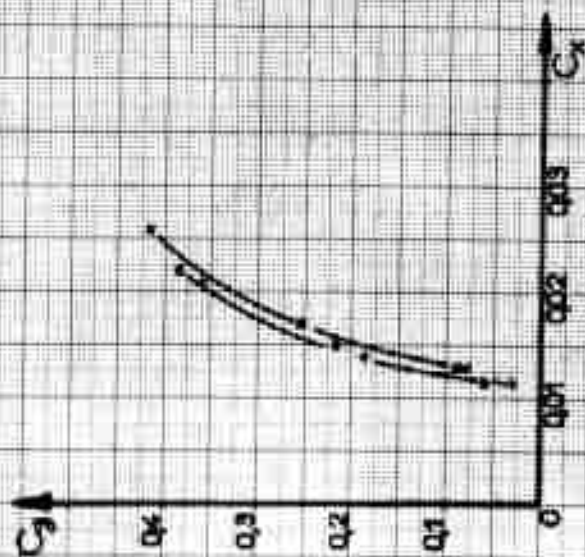
Dessiné par :
NE

Date
10-60

B. 94

Reconnaissance des

$$M_x = 0,50 \quad C_F = 0$$



B. 94

FIG. 97

Remarque: Flap
 $M_c = 0,50 \quad C_{p0} = 0,013$

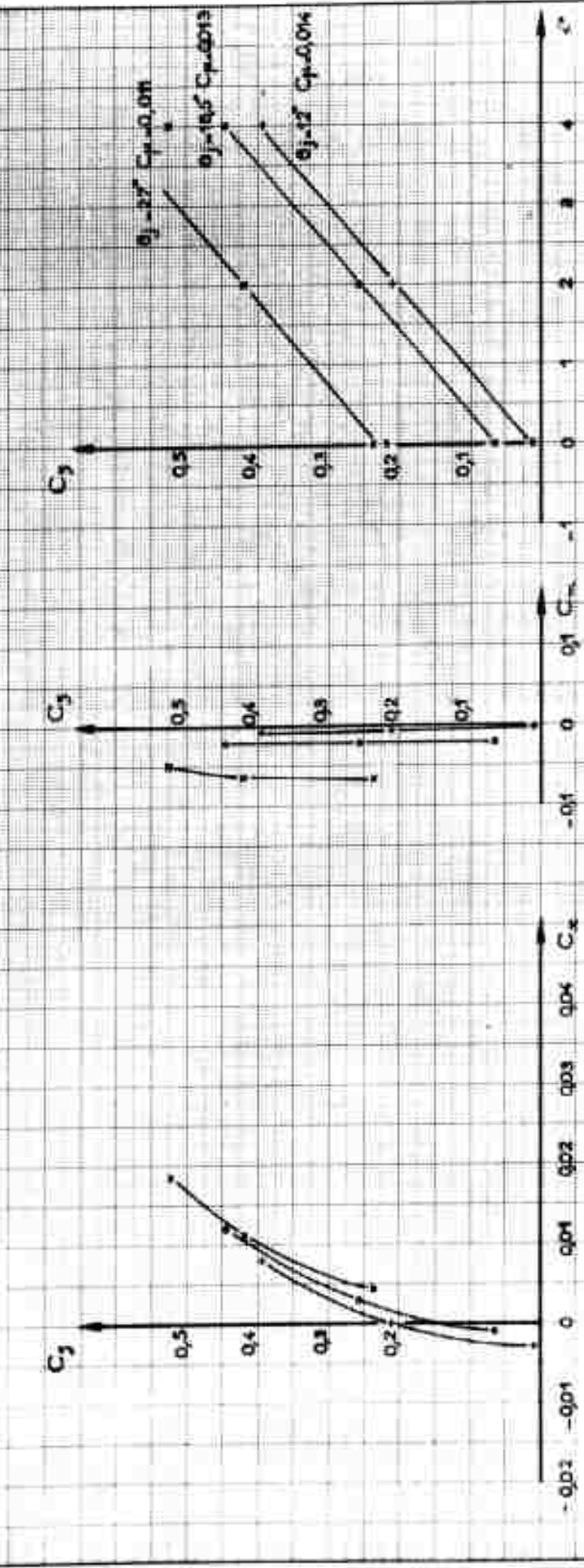


FIG. 98

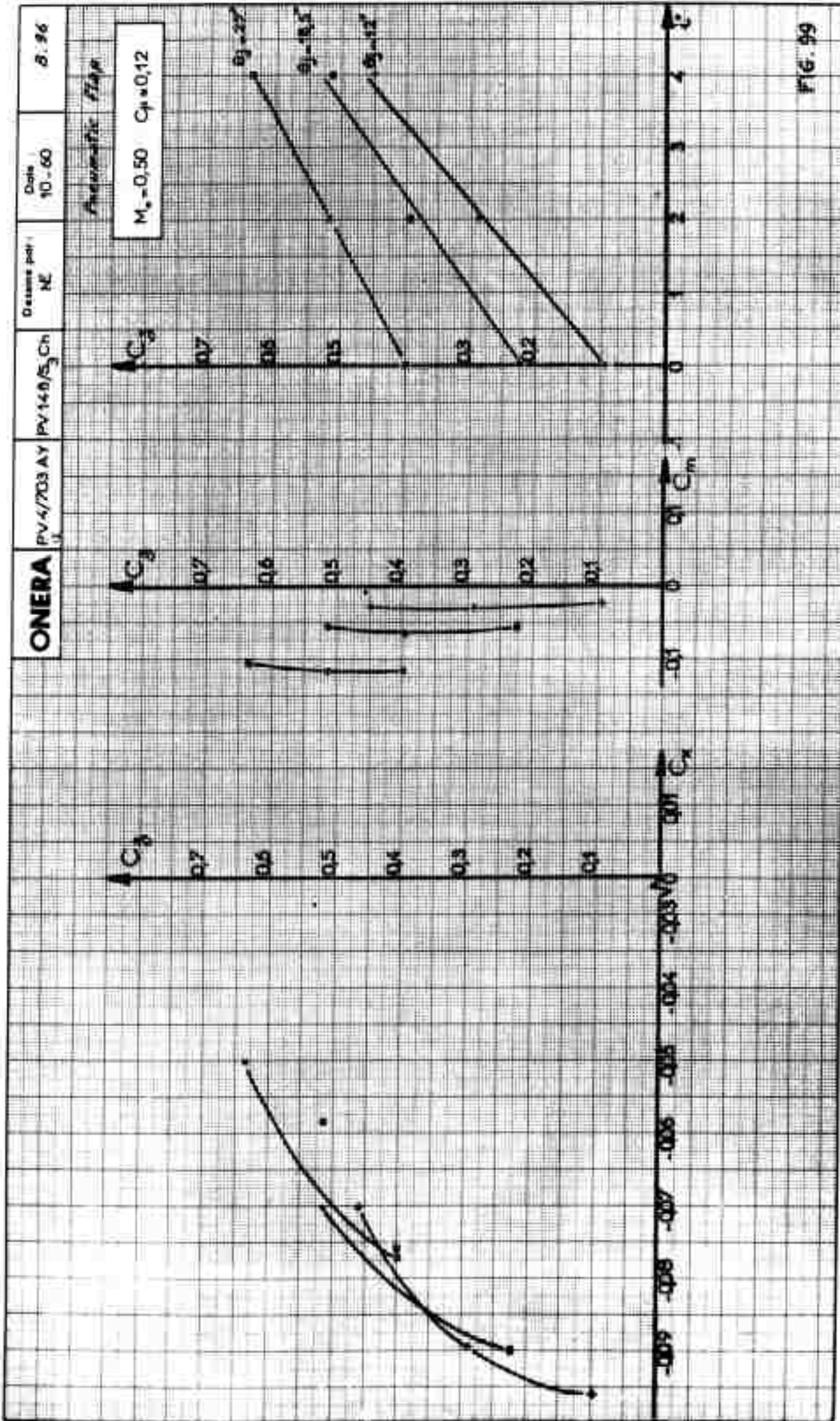


FIG. 99

ONERA

PV 4 / 703 AY

PV 148 / S₃ CH

Dessiné par :

NE

8.9.7

Assimilation des

$M_\infty = 0,60$ $C_{\mu} = 0$



ONERA

PV4/703AY

PV148/S₃CH

Designé par :

PC

Date :

10-60

d. 98

Projet de Plan

$M_\infty = 0,60$ $C_p = 0,012$

B. 98

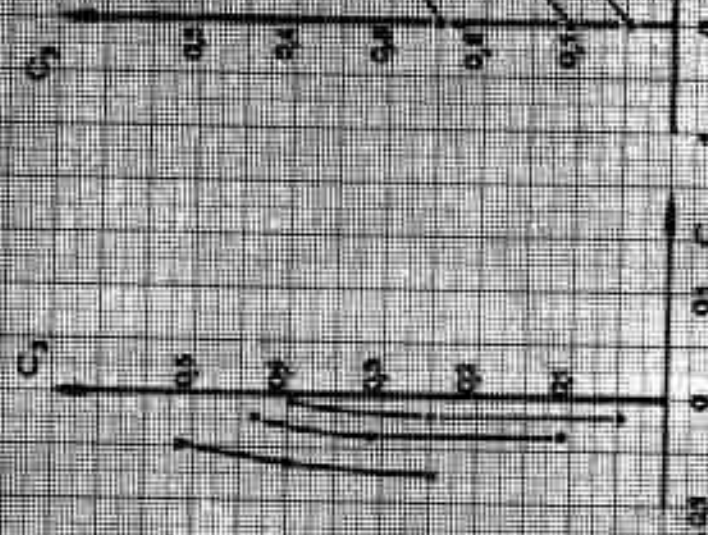
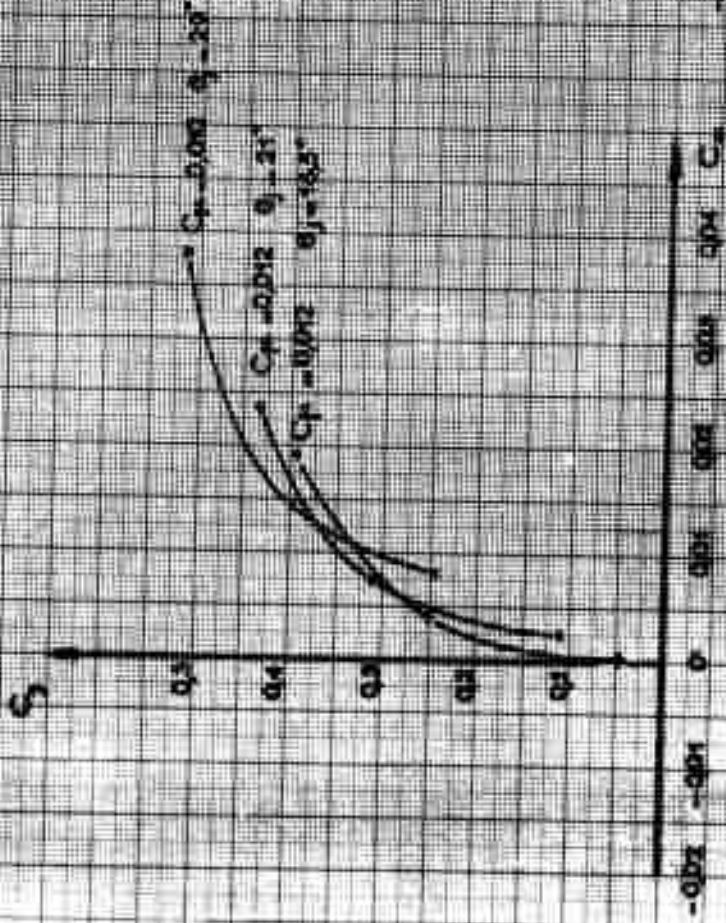


Fig. 101

ONERA

PV 4/703AY

PV 140/S₂Ch

Designé par:

NE

Date:

10 - 60

B. 49

Remarque: Révisé

$M_{\infty} = 0,60$ $C_{\mu} = 0,087$

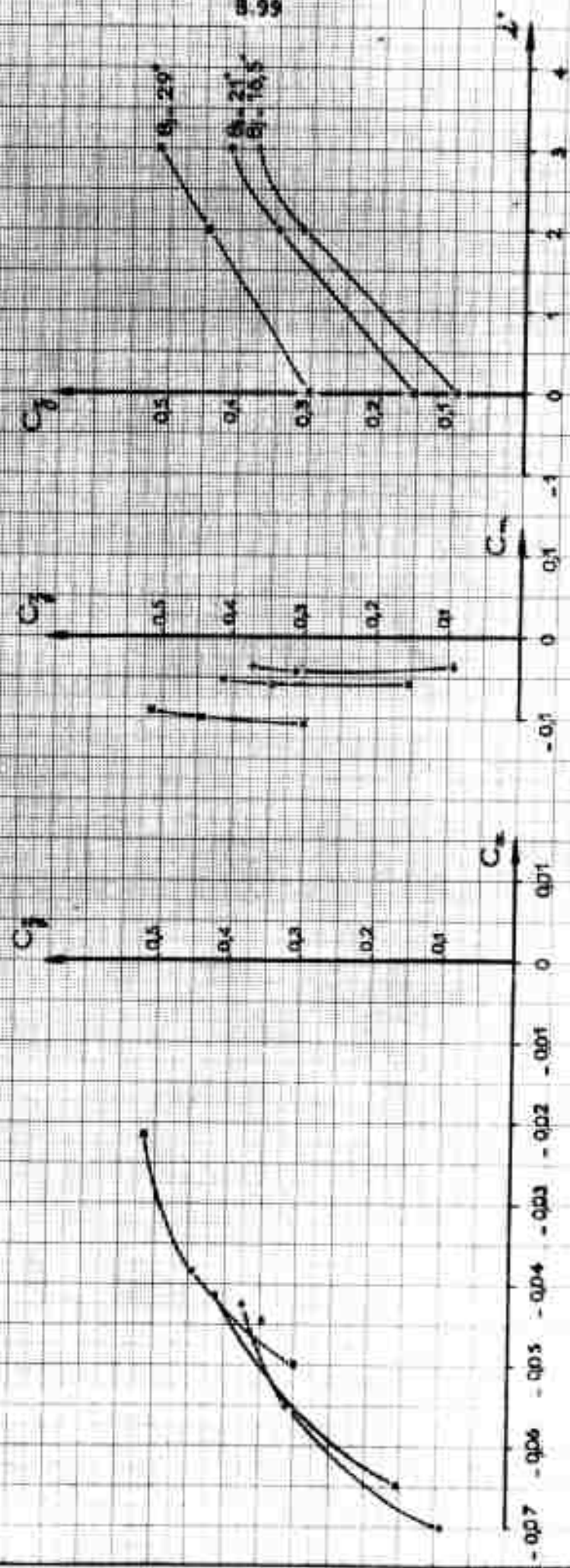


FIG. 102

ONERA

PN 4/703AY

PN 148/S₂CH

Document n°:

F.C.

Date:

10 - 60

8. 100

Remarque: Non

$M_\infty = 0.70$ $C_\mu = 0$

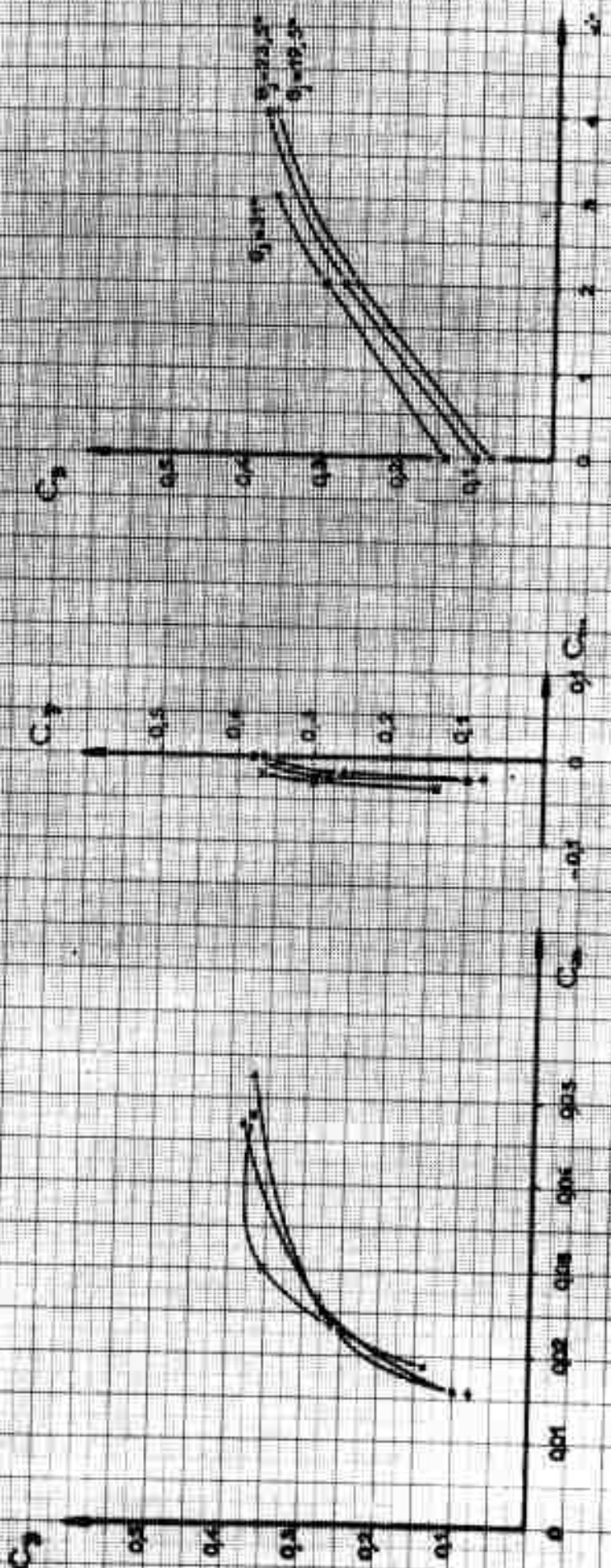
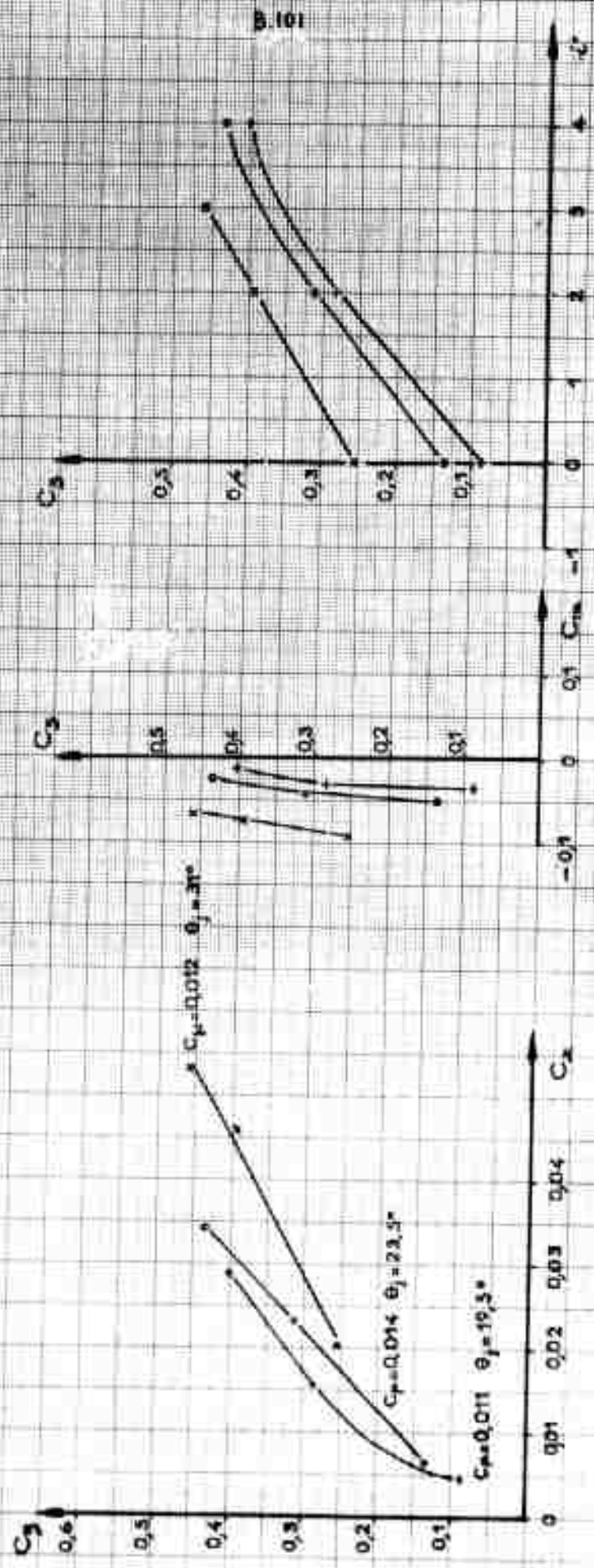


Fig. 103

$M_\infty = 0.70 \quad C_\mu = 0.012$

Phononémie flap



B.101

Automatic flap

$$M_0 = 0,70 \quad C_F = 0,074$$

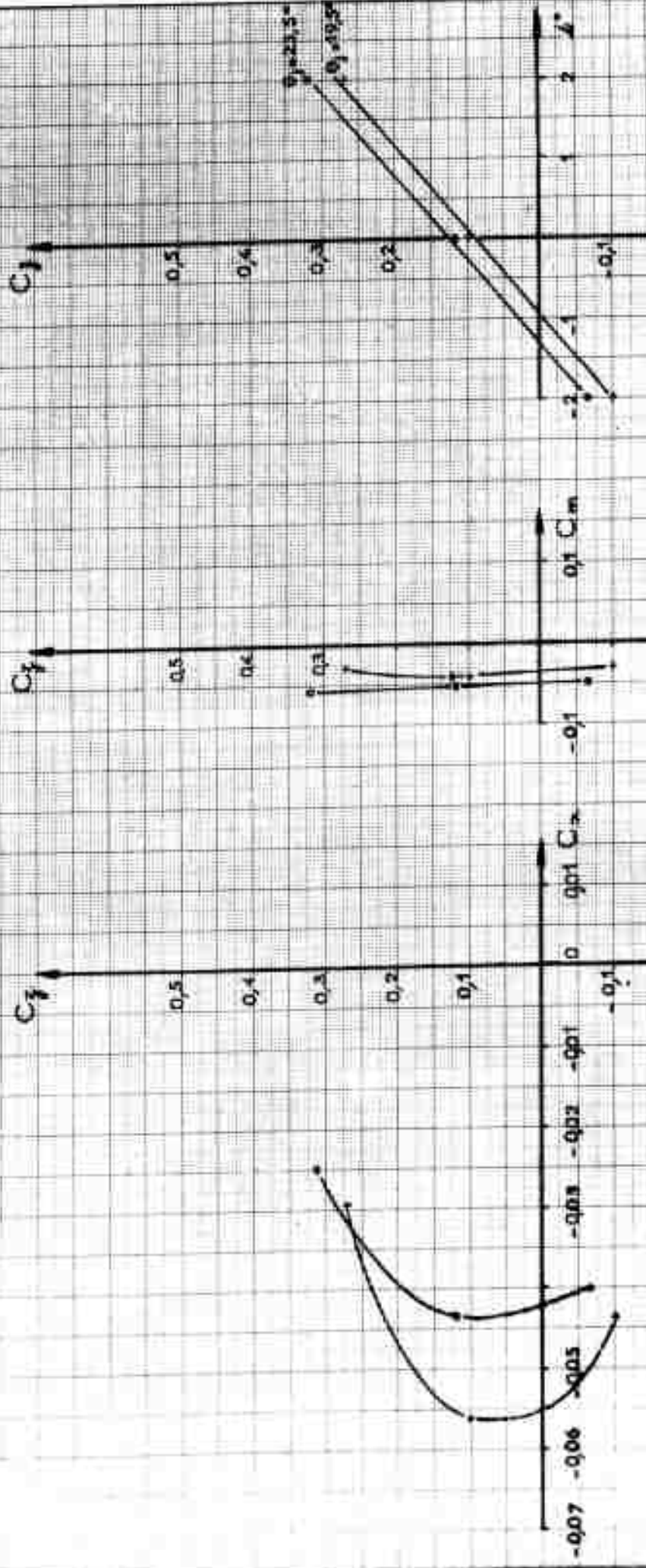


FIG. 108

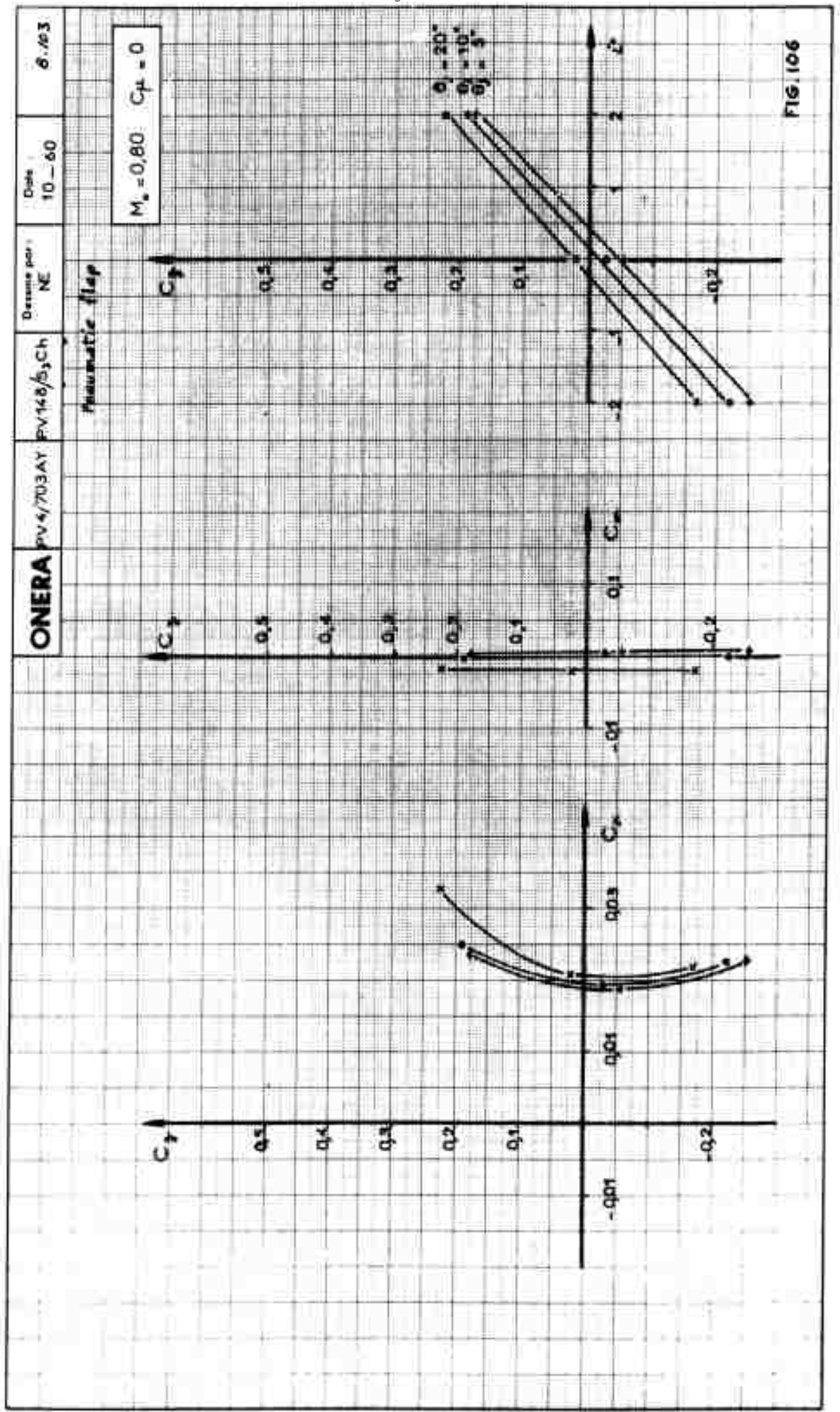


FIG 106

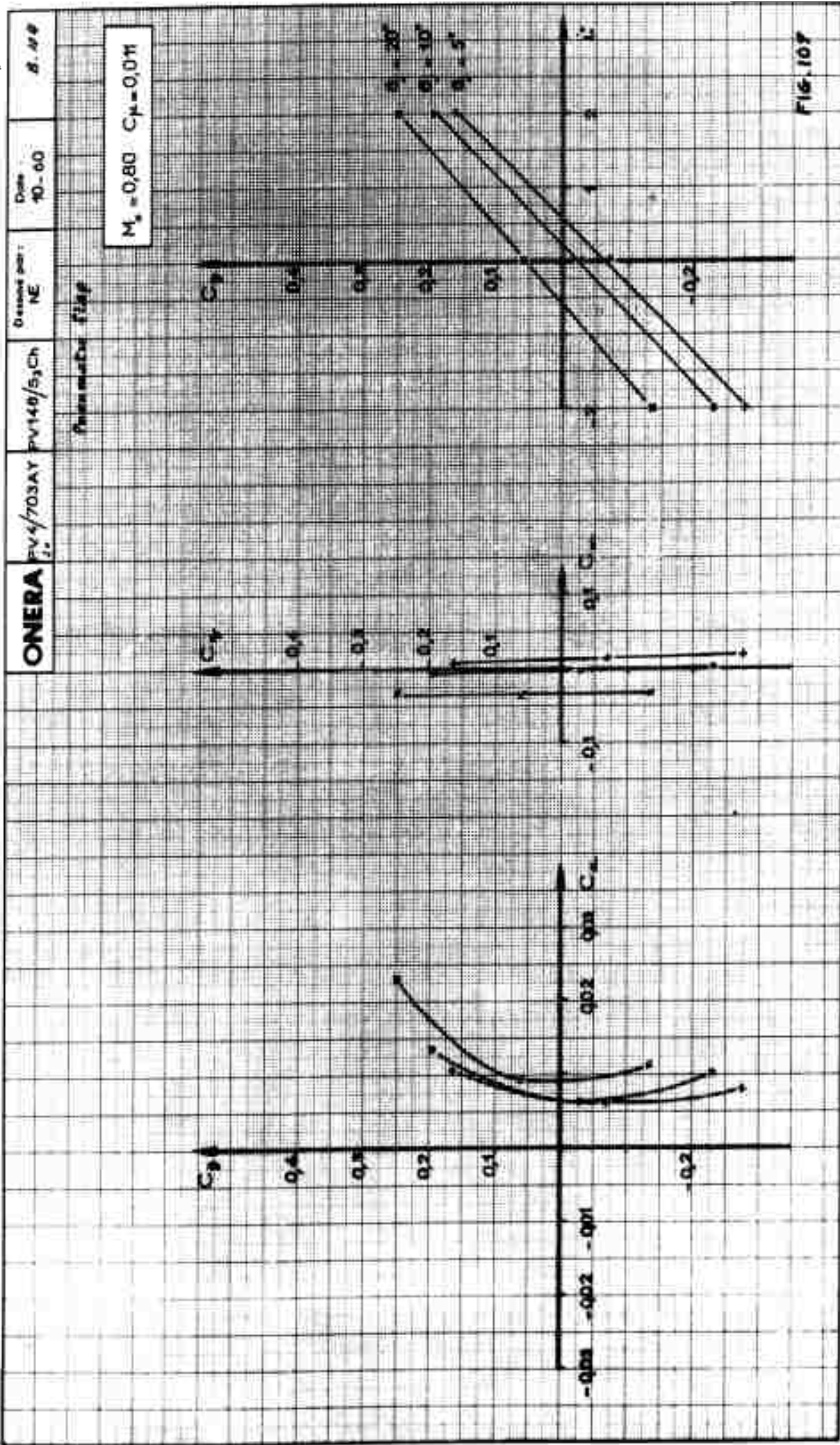


FIG. 107

ONERA PV 4/703AY PV140/S3Ch

Direction: NE

Date: 10-60

8.105

Assessment slip

$M_0 = 0.80$ $C_T = 0.066$

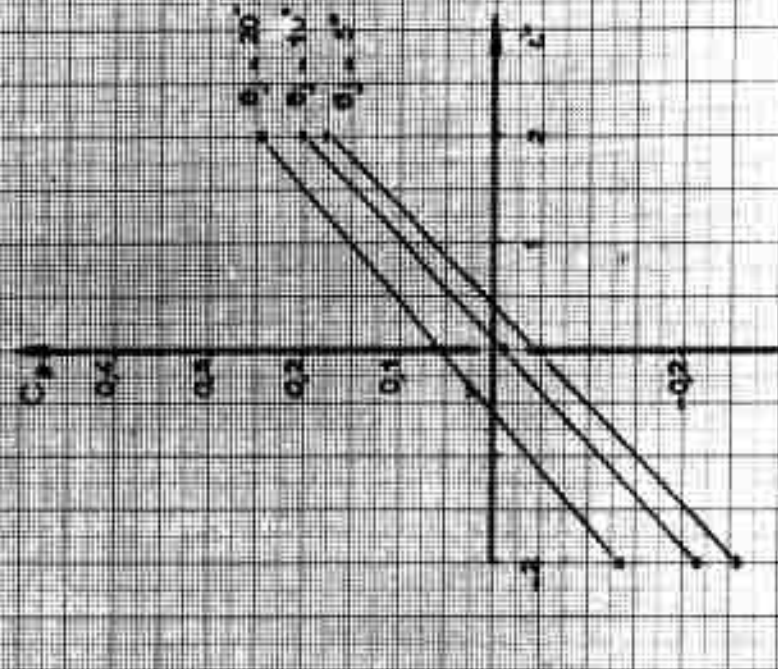
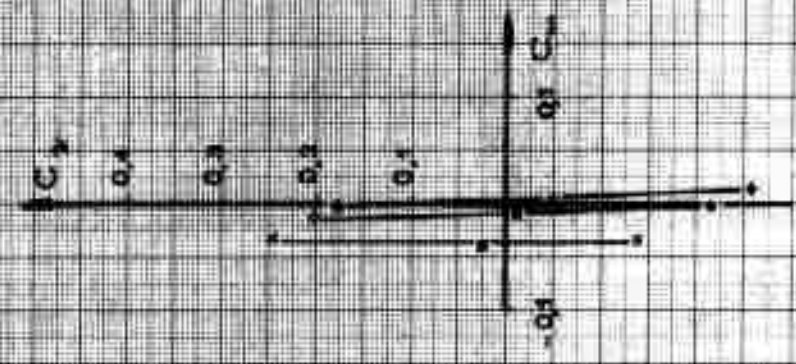
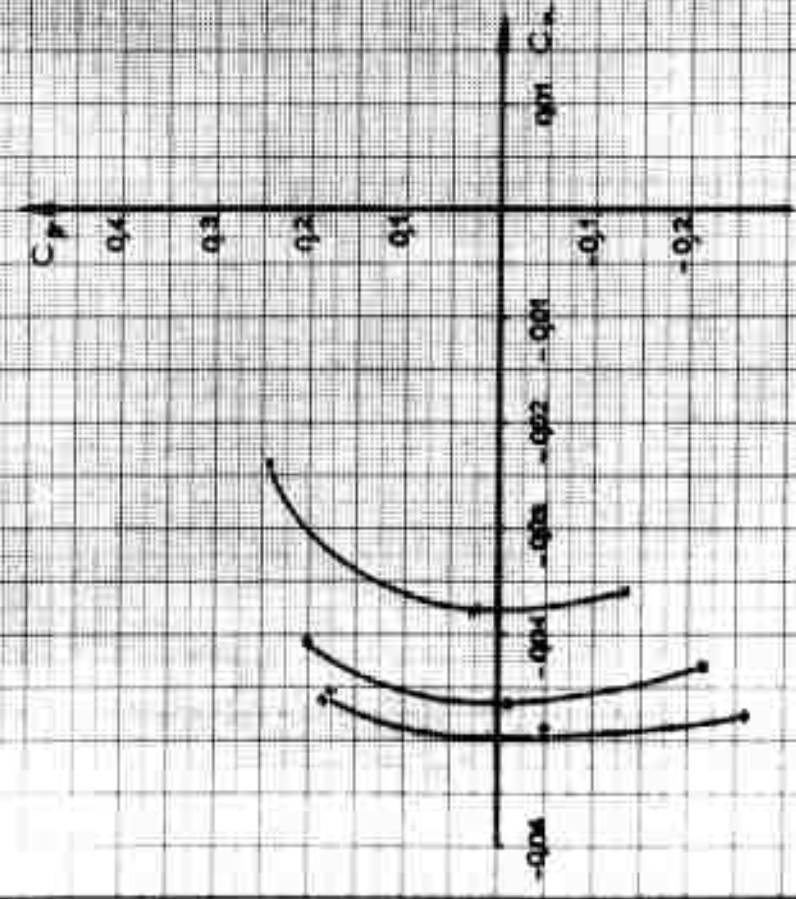


FIG. 108

ONERA

PV 4/703AY PV 140/53CH

Design par :

NE

Date :

10-60

B. 105

Pneumatic flap

 $M_\infty = 0,80$ Ecoulement tridimensionnel
tridimensionnel flow

— $\alpha = 0^\circ$	$\bullet \theta_f = 5^\circ$
- - - $\alpha = 2^\circ$	$\circ \theta_f = 10^\circ$
	$\Delta \theta_f = 20^\circ$

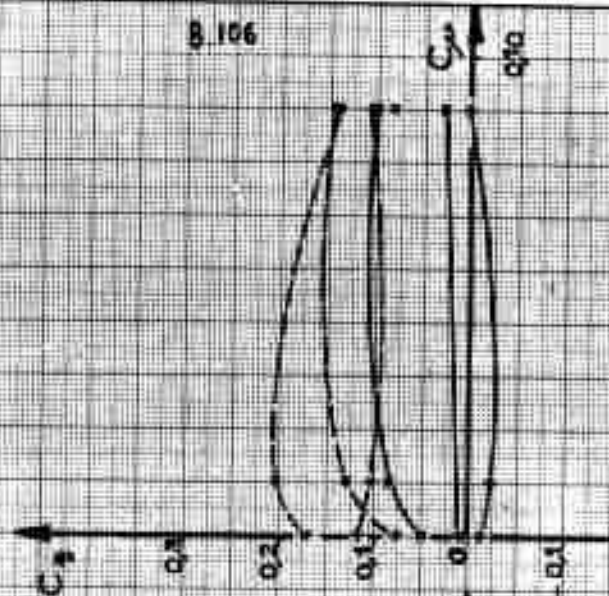
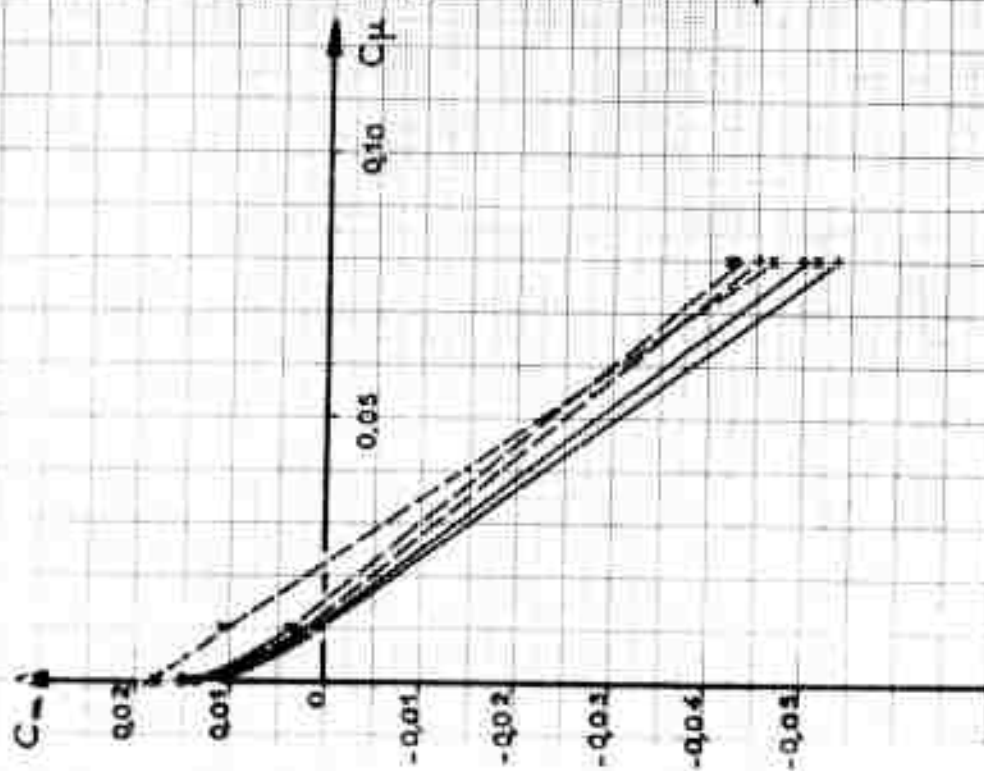


FIG. 105

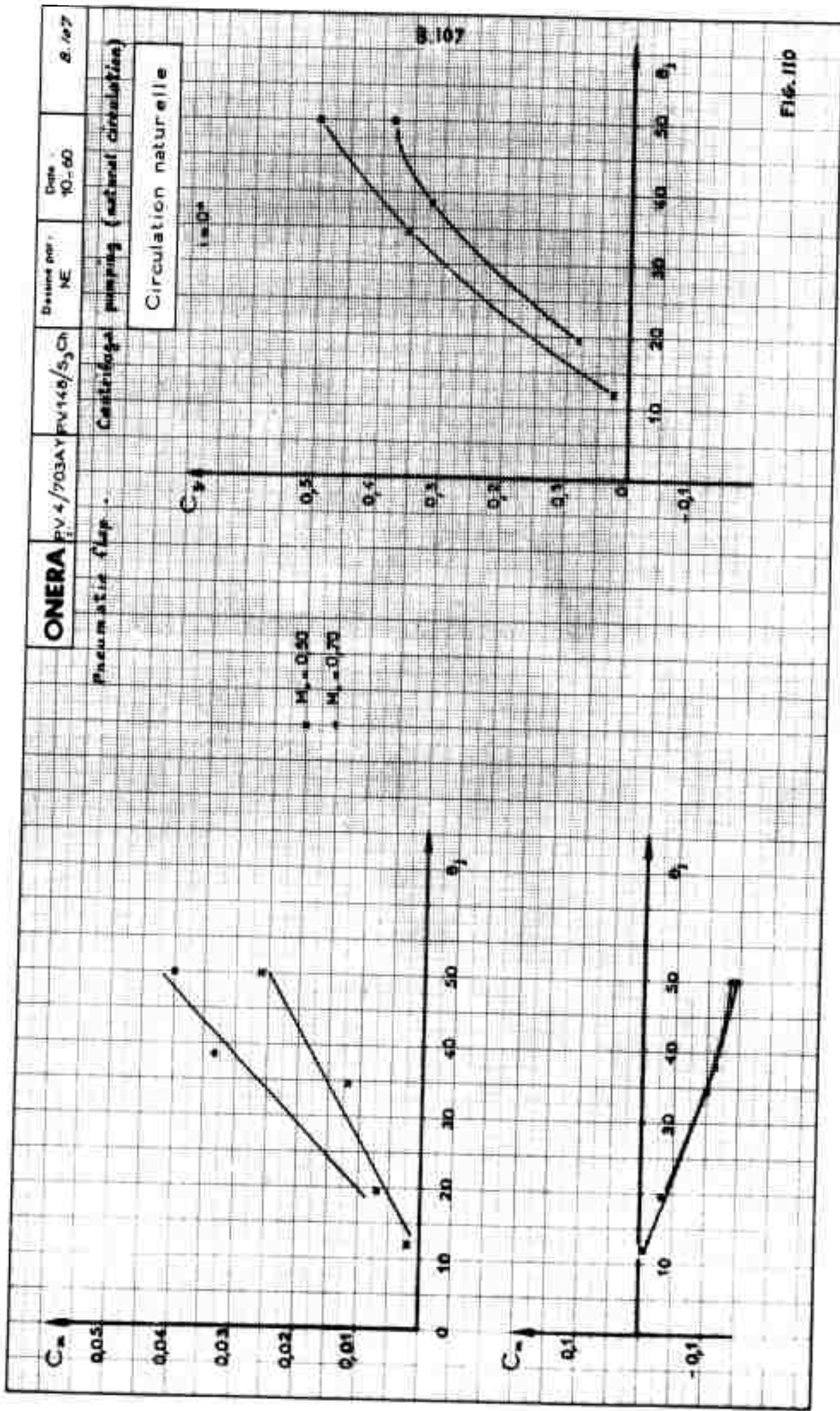


Fig. 110

O.N.E.R.A.
-O.A.-

2/703 A_y

Dessiné par : Louis

Date : 7.9.60

B.108

Wind-tunnel : 2.1.18

Soufflerie : Oscillating flap (velocimétrique)

Model : Maquette :

Echelle : 1 : 0.350

Centrage : 0.154

Relevances : V = S x l = 0.0539

V₁ = S x b =

Span : 3.40

chord : 0.440

Cordes : 0.300

Aspect ratio : 11.33

Alongement : 11.33

Effilement : 1.15

Flèche : 1.15

Swing-back : 1.15

Airfoil : Profil 65.011

Dièdre : 0

Surface d'attaque : 0

Longueur : L =

Maitre-couple : S_F =

Allongement : λ_F =

Volume : V_F =

Envergure : b =

Corde moyenne : l_m =

Surface : S =

Flèche : φ =

Bras de levier : L₀ =

Volume : V₀ = S₀ x L₀ =

Hauteur : h =

Surface : S_d =

Flèche : φ =

OBSERVATIONS :

N° 241 / Ech F16.111

Pressure gauge Manometre ①

Pressure gauge Manometre ②

Theoretical airfoil Profil théorique

Blowing soufflage

Carène du volet

Blade chord

Articulation du volet

Flap hinge

Scale

Echelle du dessin : 9/3 ; 1/2

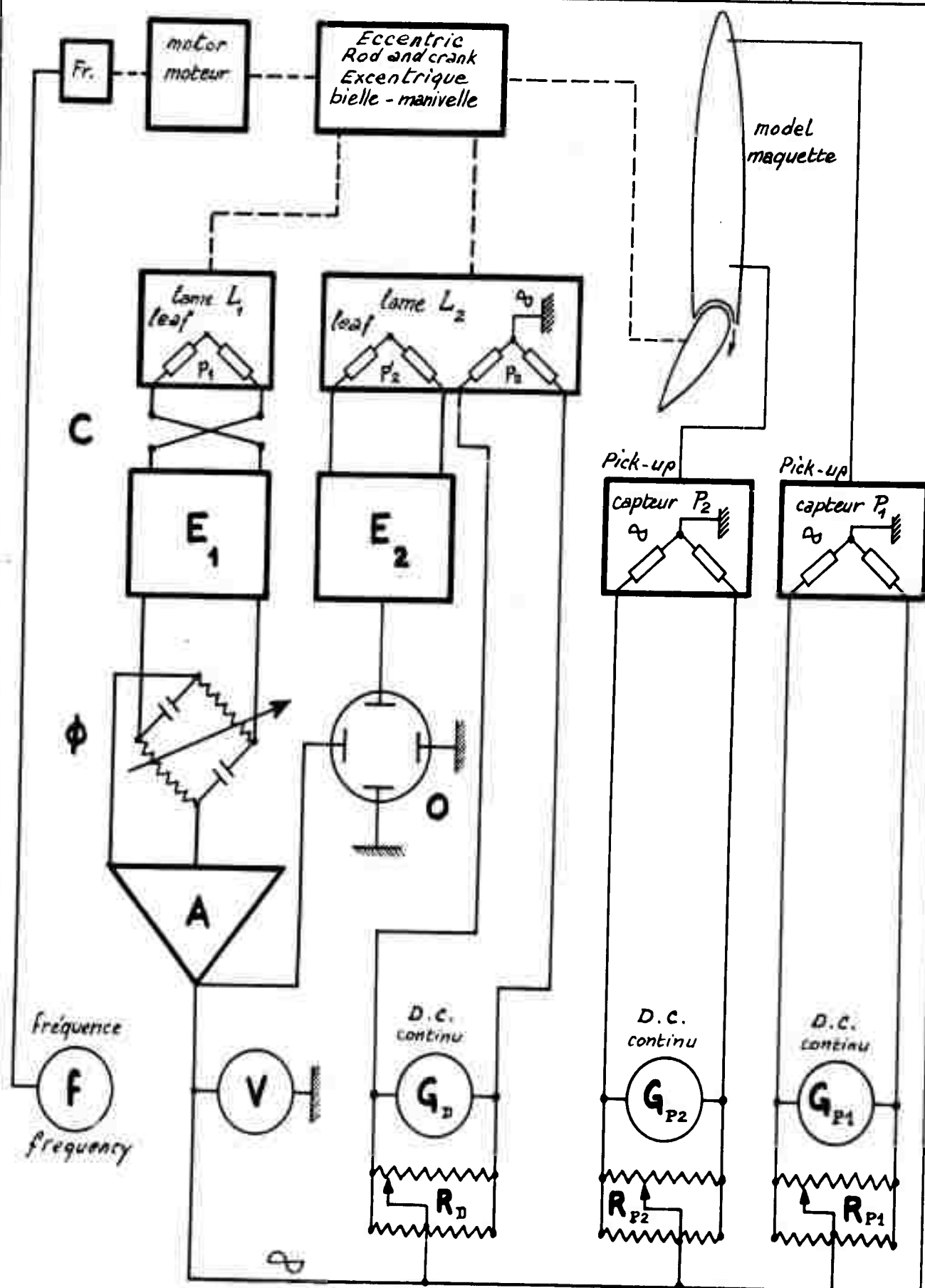
Detachable part : Flap

Éléments démontables : Volet

N.B. - Les cotes complètes par le responsable de l'essai seront fournies.

Matériau :

Matériau :



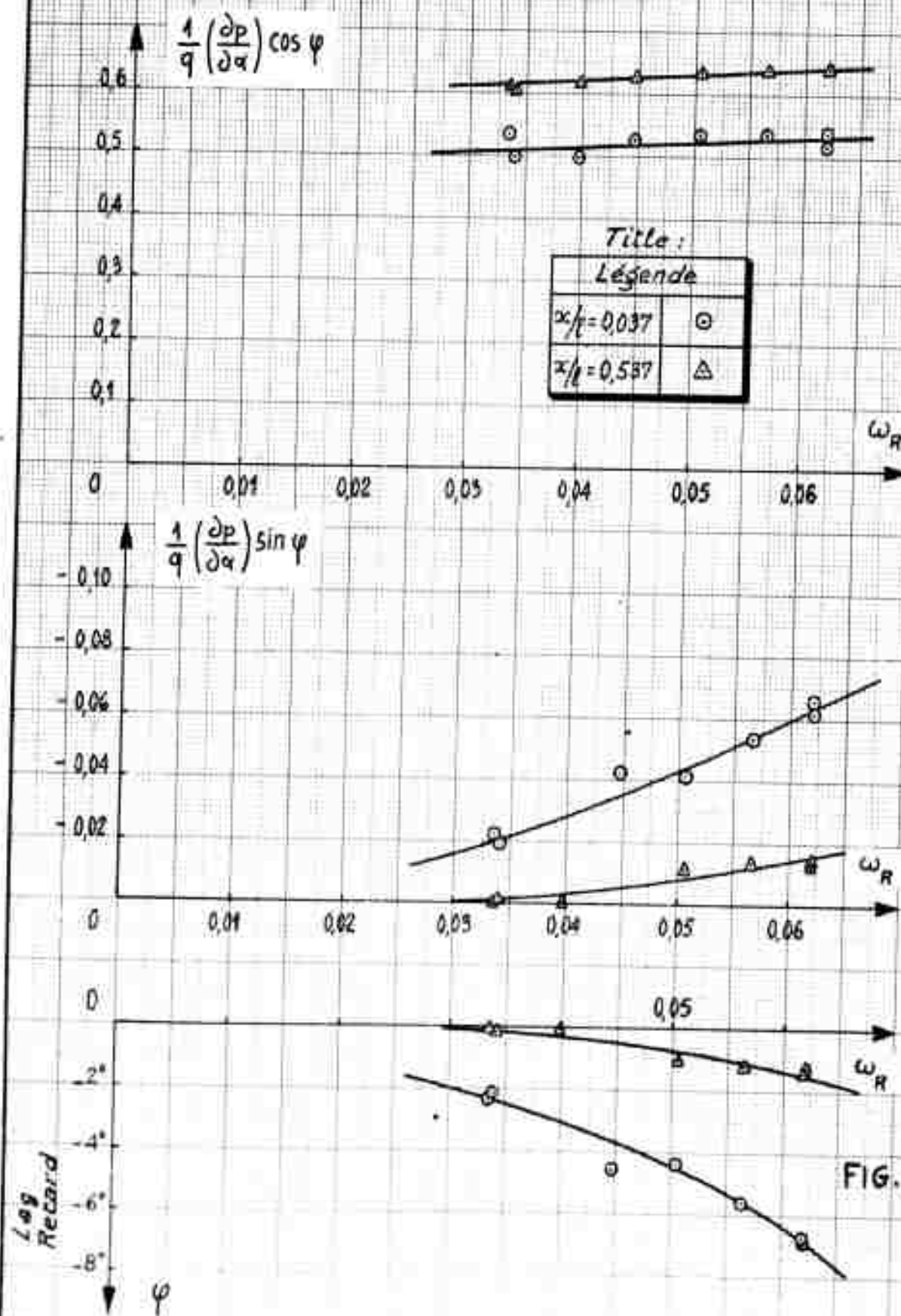
Schematic lay-out of measuring equipment
Disposition de l'équipement de mesure.

FIG. 112

liaisons électriques ———— , liaisons mécaniques - - - -
electrical connections , mechanical connections

$$i = 6^\circ; \alpha = 12,25^\circ; \alpha_0 = 3,25^\circ; C_\mu = 0$$

$$M = 0,5$$

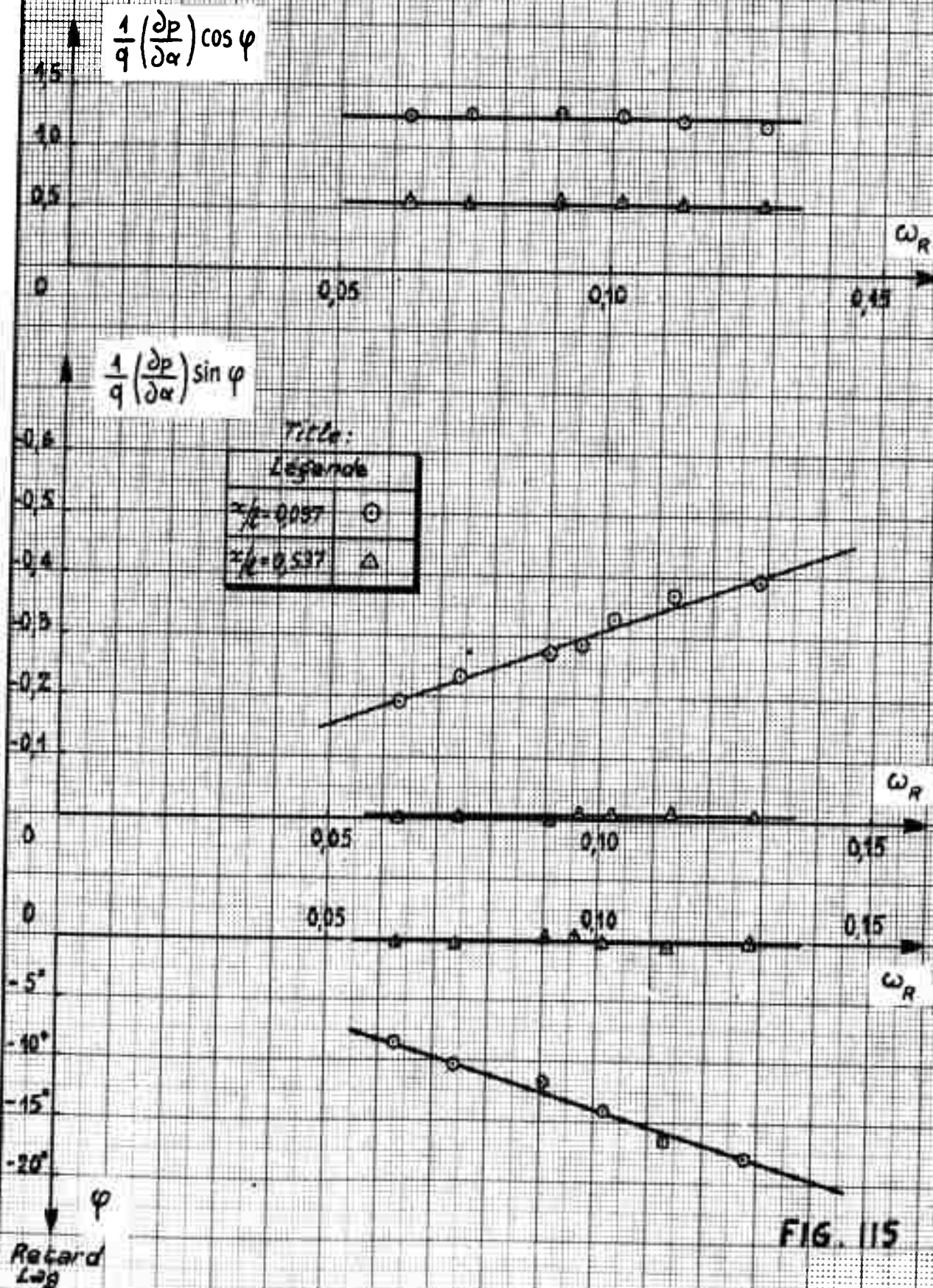


M=0,5



$$i = 6^\circ ; \alpha = 12,25^\circ ; \alpha_0 = -2,5^\circ ; C_M = 0$$

$$M = 0,5$$



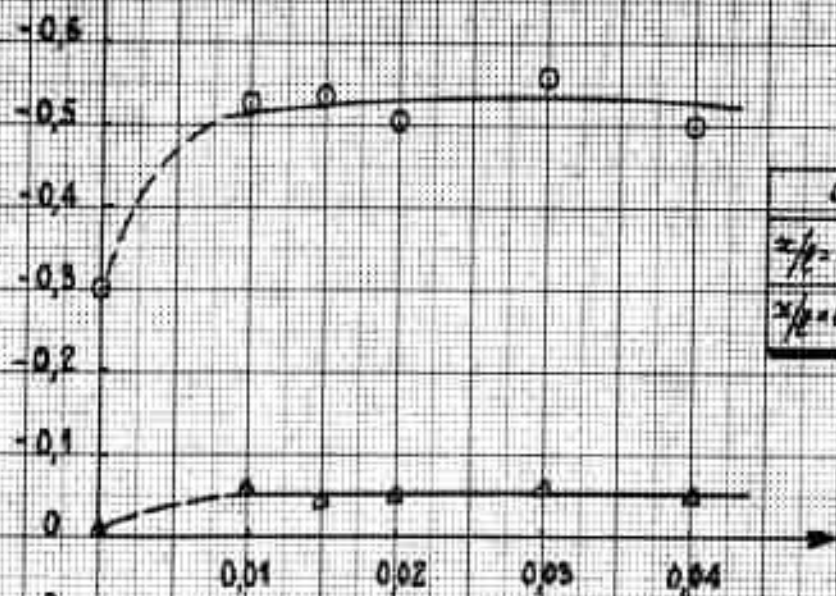
$$i = 6^\circ \quad \alpha = 12,25^\circ \quad \alpha_0 = -2,5^\circ \quad \omega_R = 0,096$$

$$M = 0,5$$

$$\frac{1}{q} \left(\frac{\partial p}{\partial \alpha} \right) \cos \varphi$$



$$\frac{1}{q} \left(\frac{\partial p}{\partial \alpha} \right) \sin \varphi$$



Titré:

Légende

$$x/l = 0,037$$

○

$$x/l = 0,537$$

Δ

φ

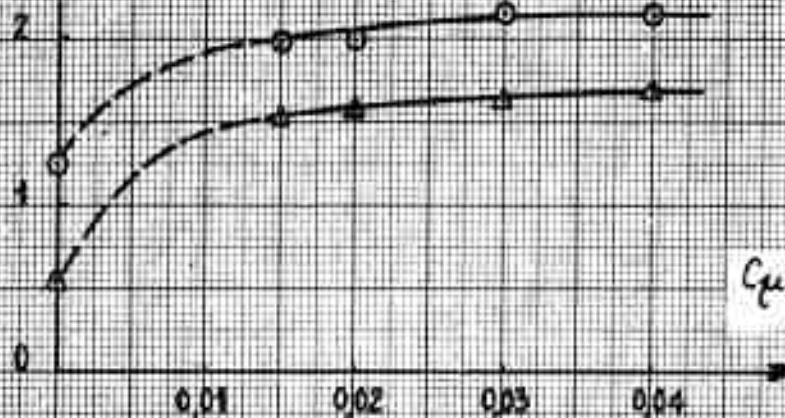
Retard
Log

FIG. 116

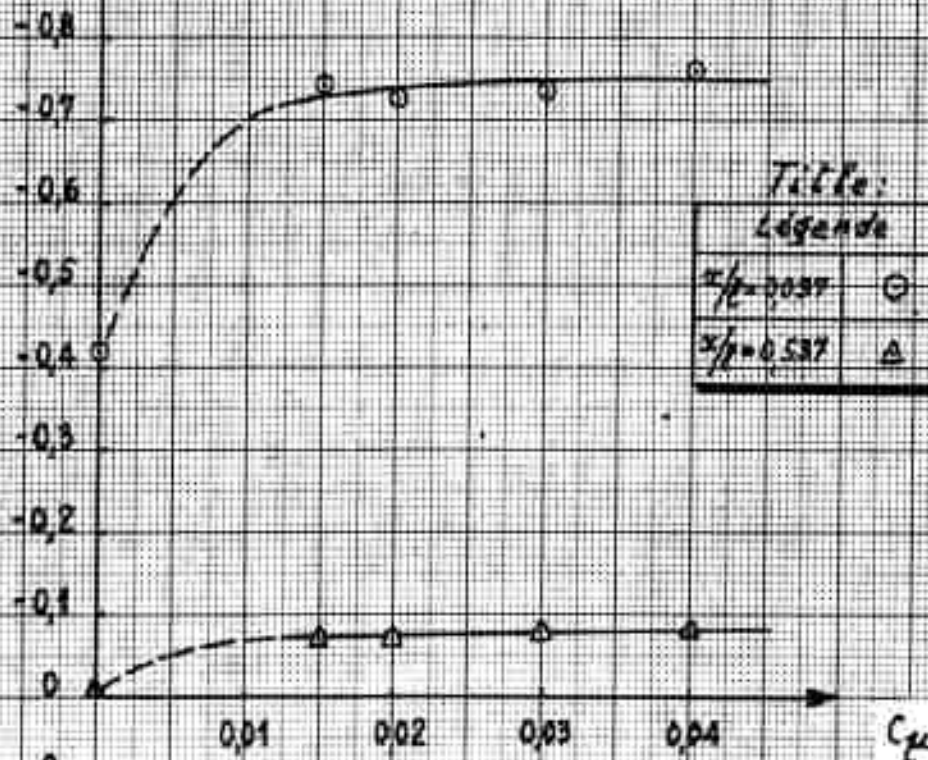
$$i = 6^\circ \quad \alpha = 12,25^\circ \quad \alpha_0 = -2,5^\circ \quad \omega_R = 0,134$$

$$\frac{1}{q} \left(\frac{\partial p}{\partial \alpha} \right) \cos \varphi$$

$$M=0,5$$



$$\frac{1}{q} \left(\frac{\partial p}{\partial \alpha} \right) \sin \varphi$$



Titre:
Légende

$x/\ell = 0,037$	○
$x/\ell = 0,537$	△

φ
Retard
Lag

FIG. 117

$$i = 6^\circ \quad \alpha = 12,25^\circ \quad \alpha_0 = -2,5^\circ \quad \omega_R = 0,192$$

$$M = 0,25$$

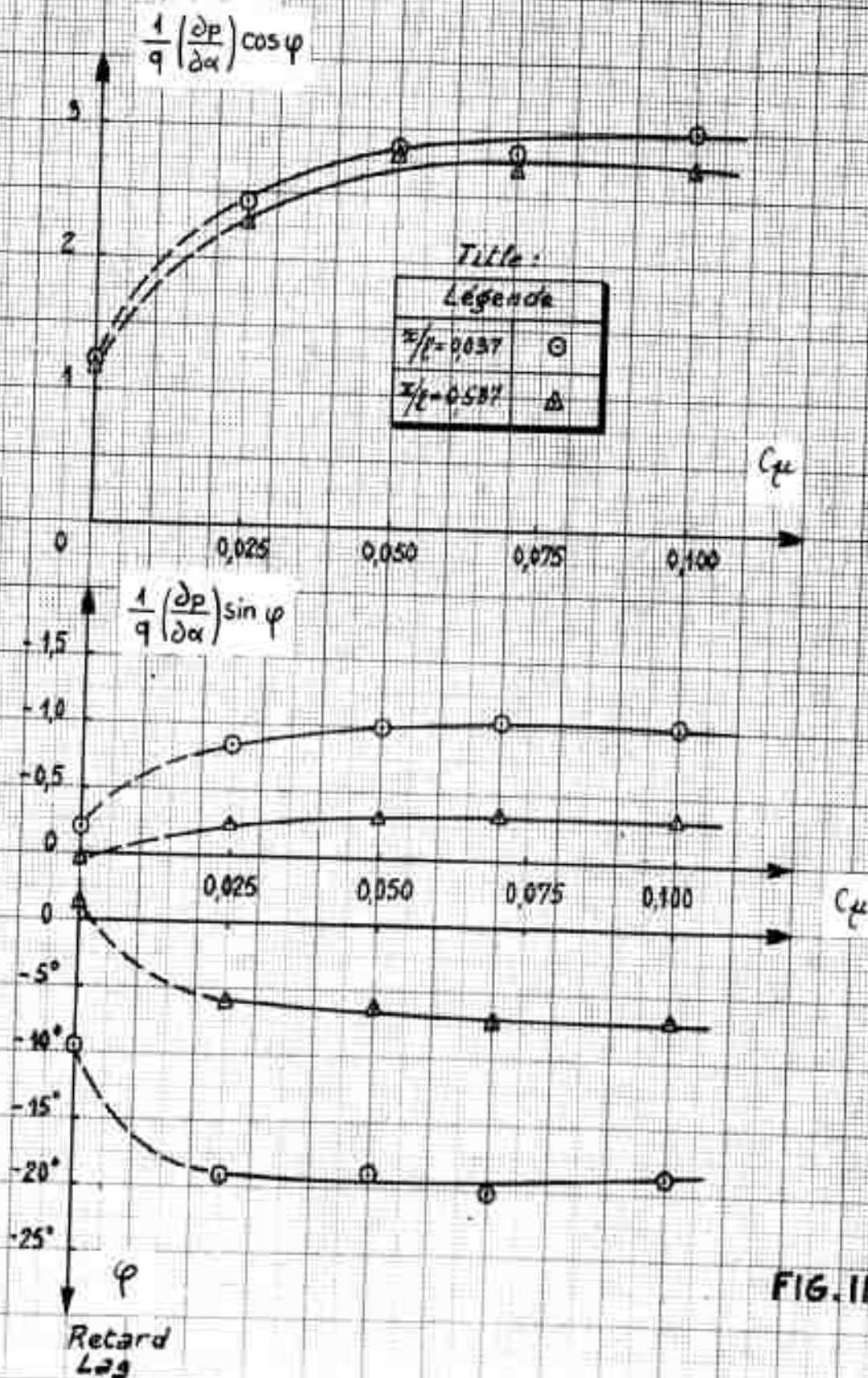


FIG. 118

$$\dot{i} = 6^\circ \quad \alpha = 12,25^\circ \quad \alpha_0 = -2,5^\circ \quad \omega_R = 0,272$$

$$M = 0,25$$

Titre :

Légende

$x/l = 0,037$	⊙
$x/l = 0,587$	△

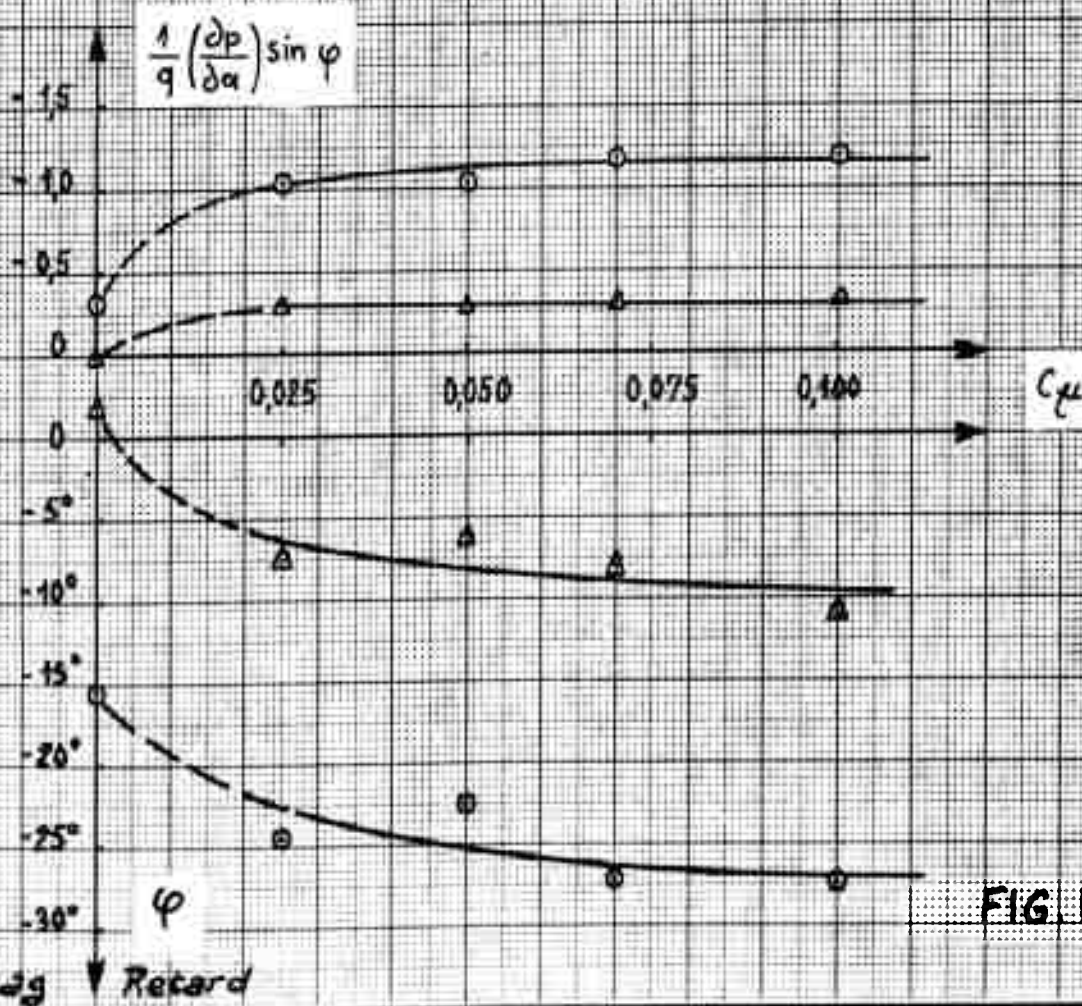
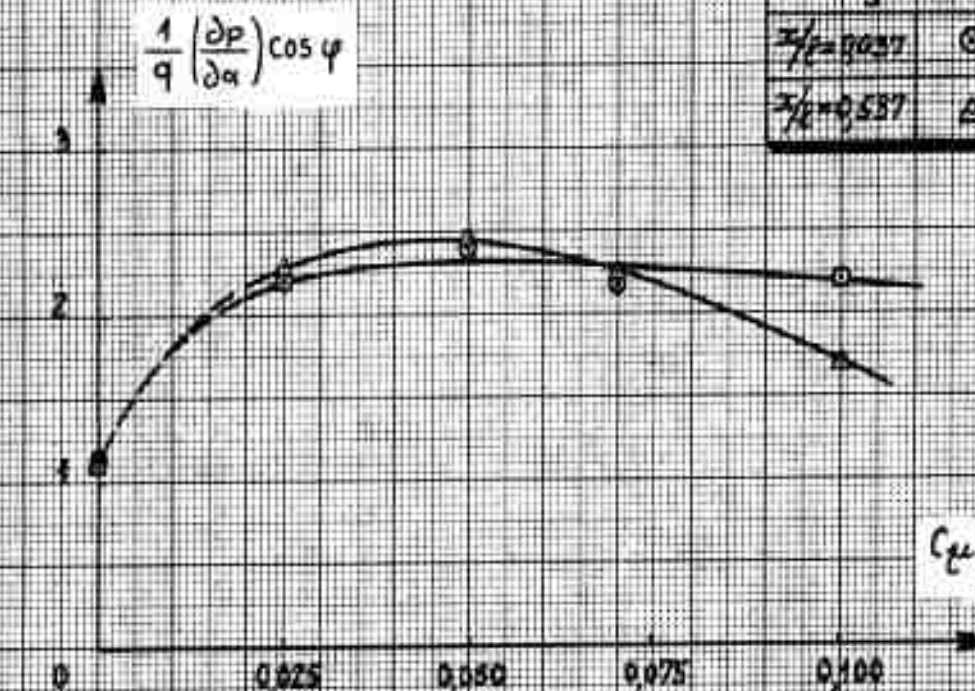


FIG. 119

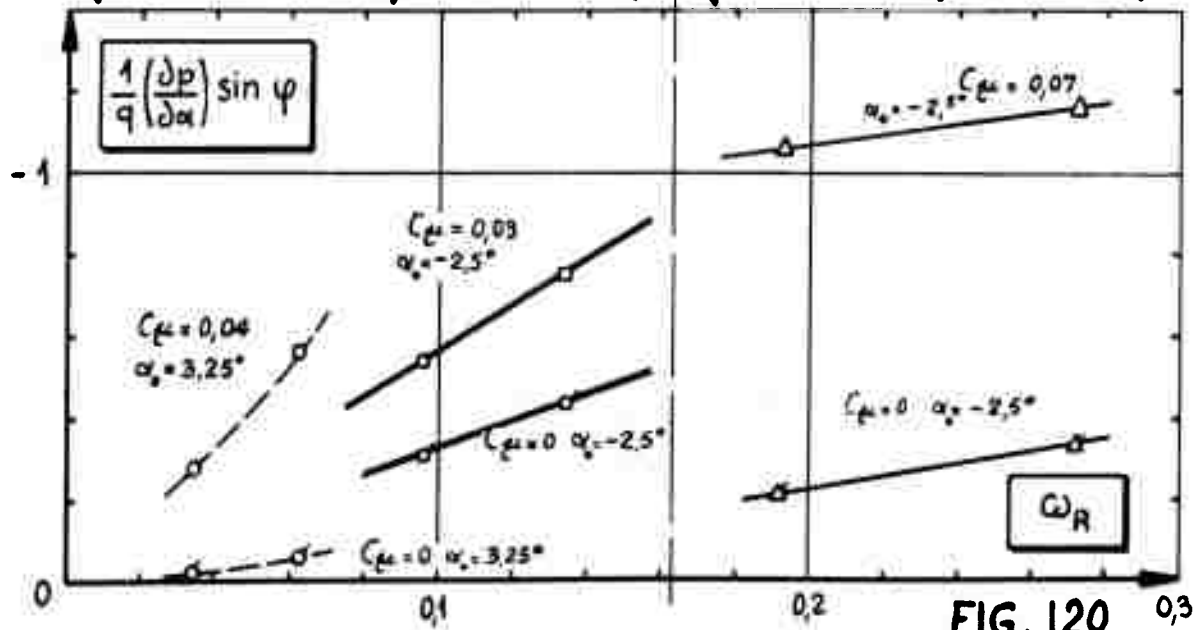
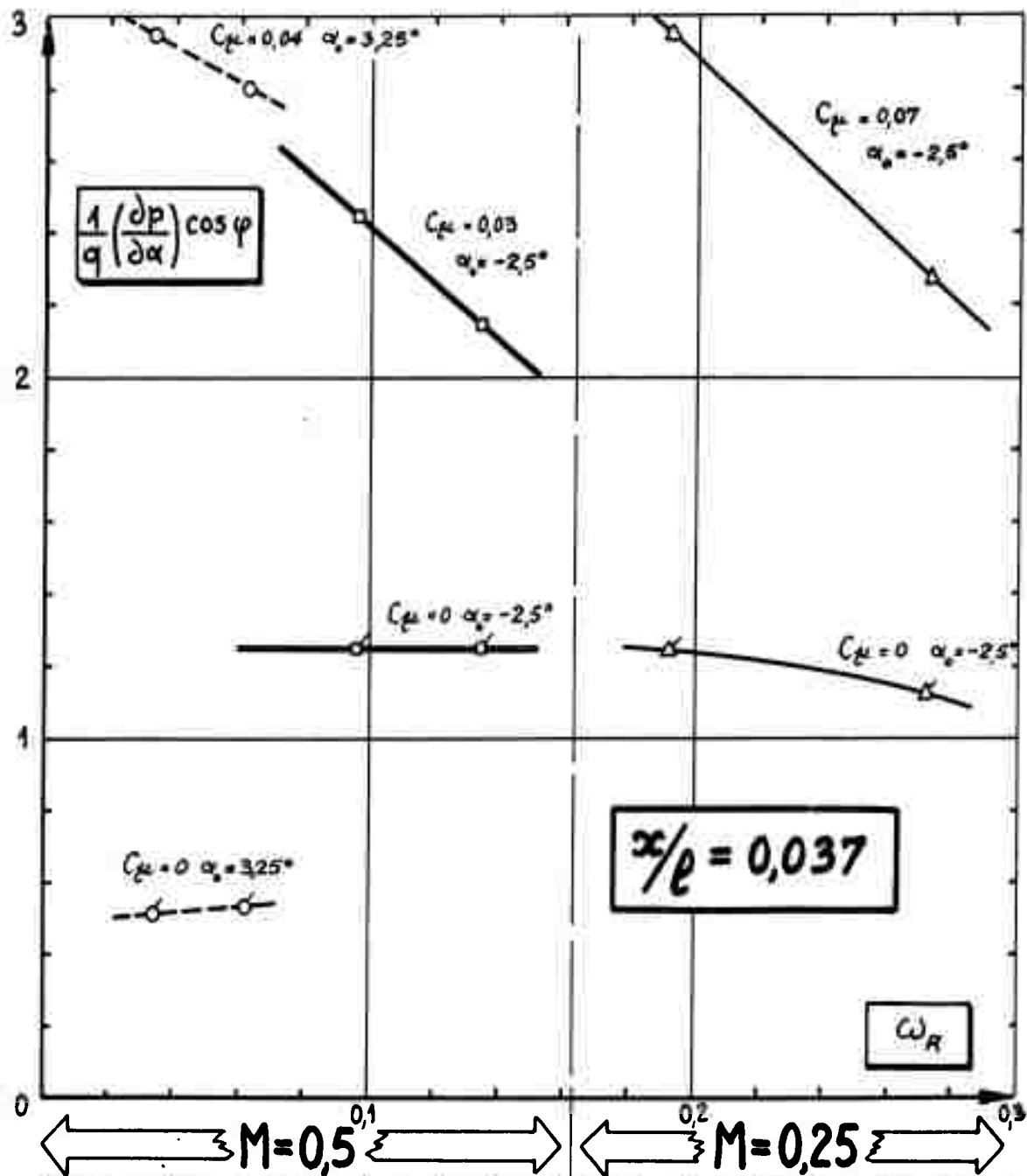
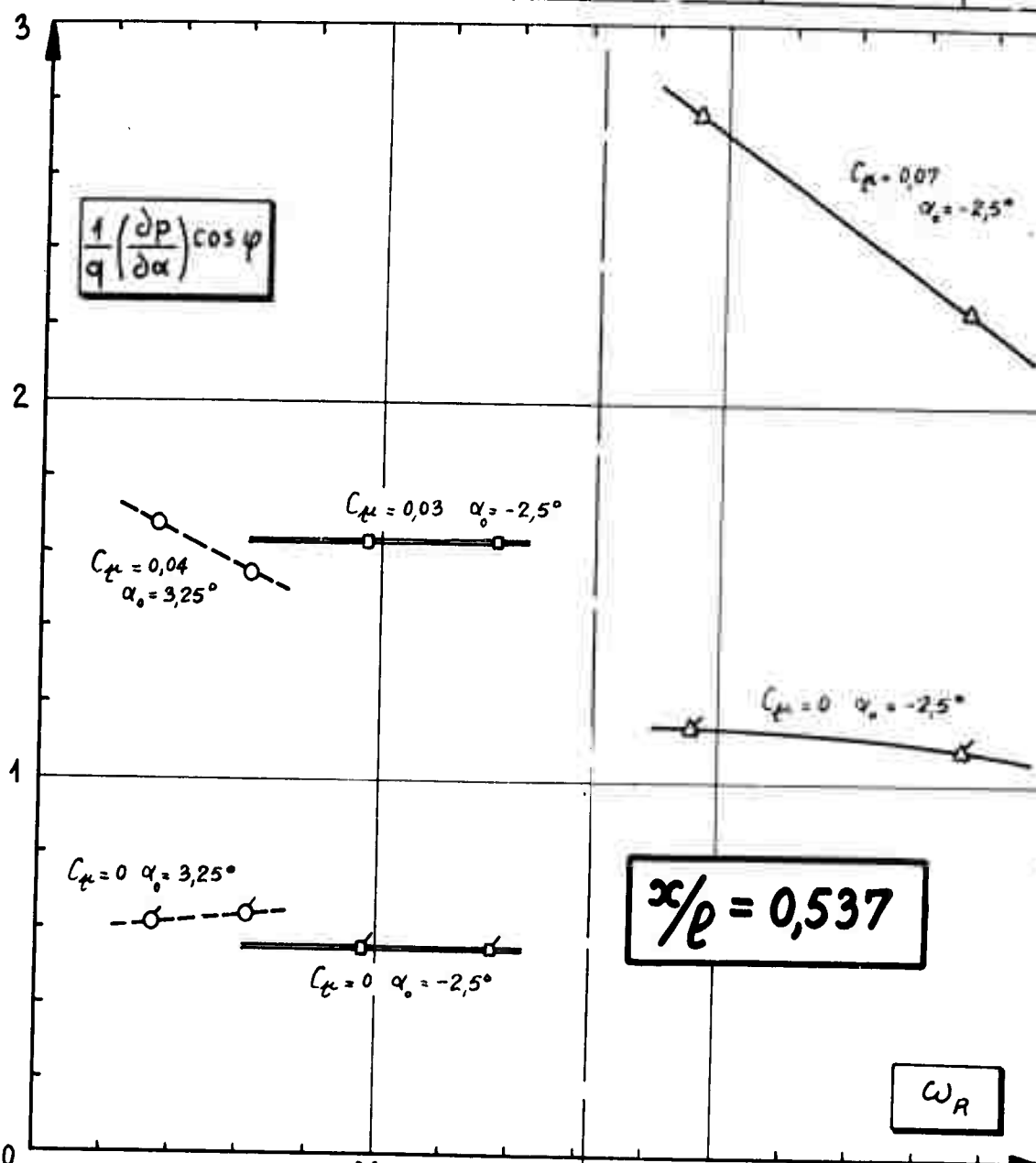


FIG. 120



$$x/l = 0.537$$

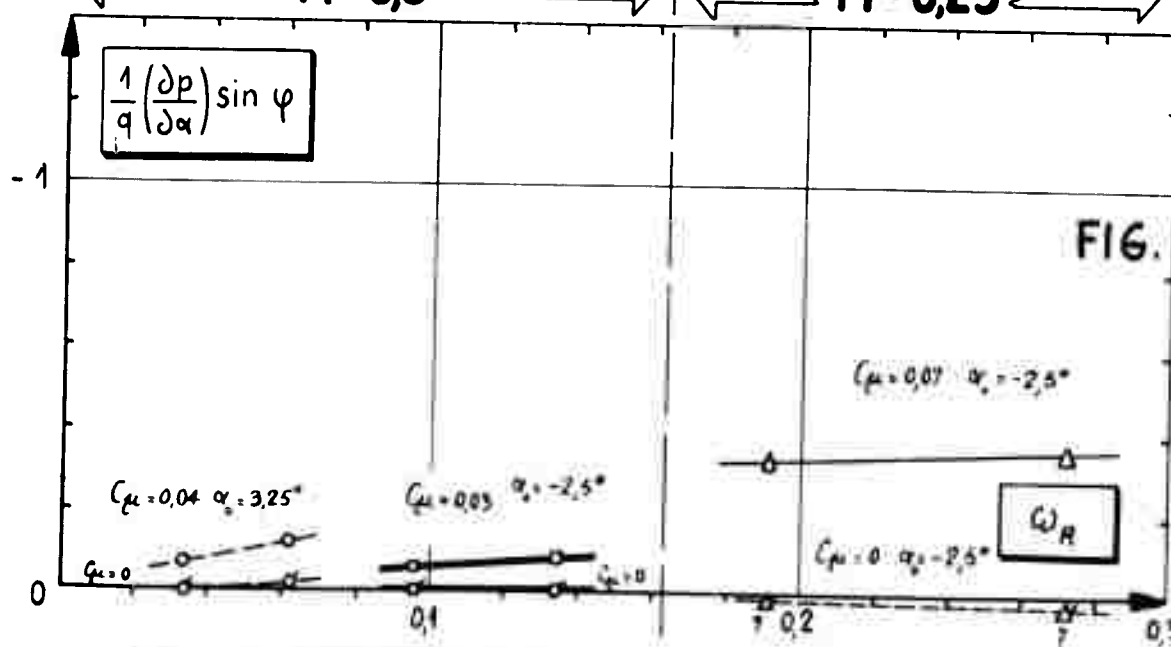
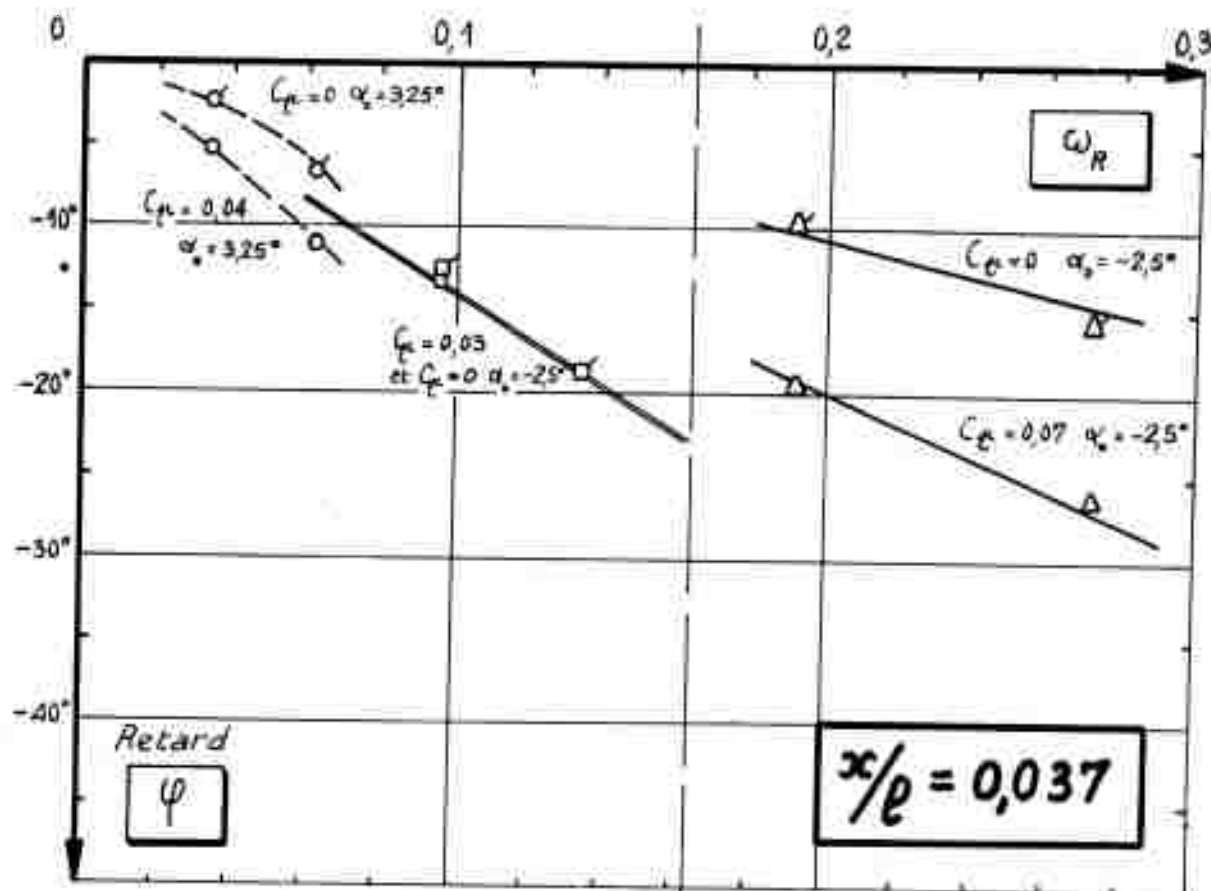


FIG. 121



$\longleftrightarrow M=0,5 \longleftrightarrow \longleftrightarrow M=0,25 \longleftrightarrow$

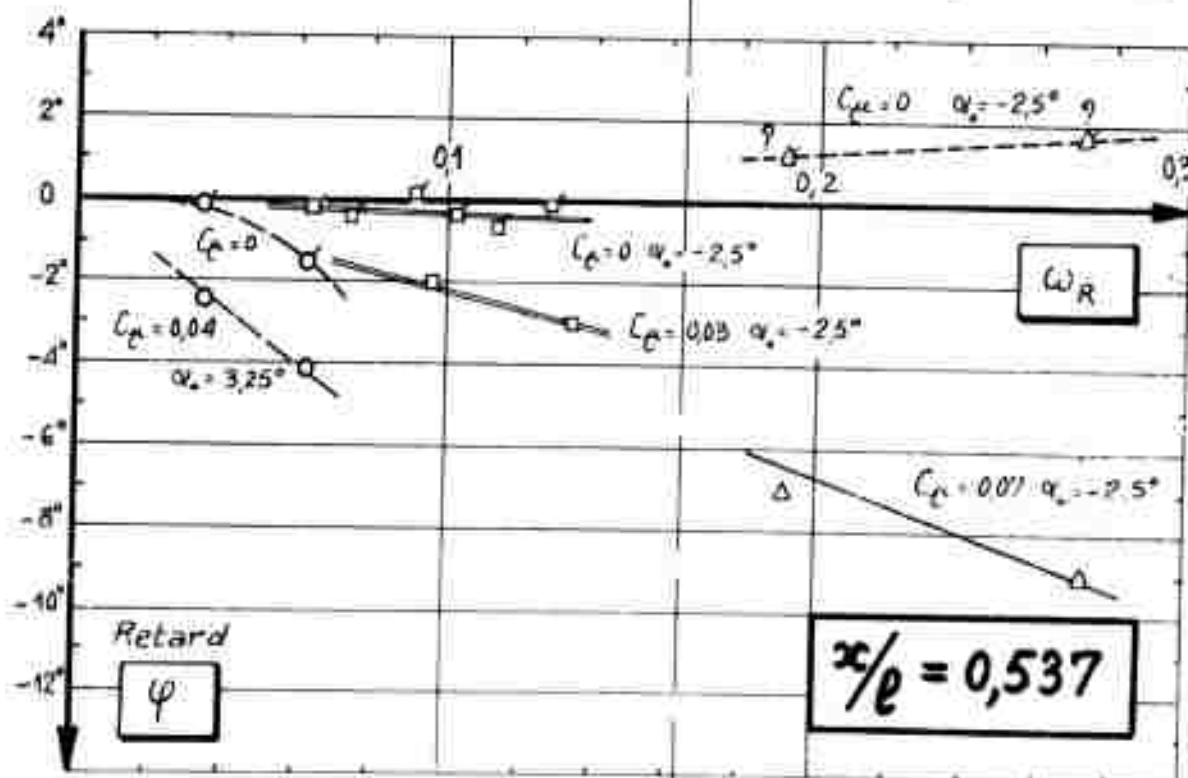
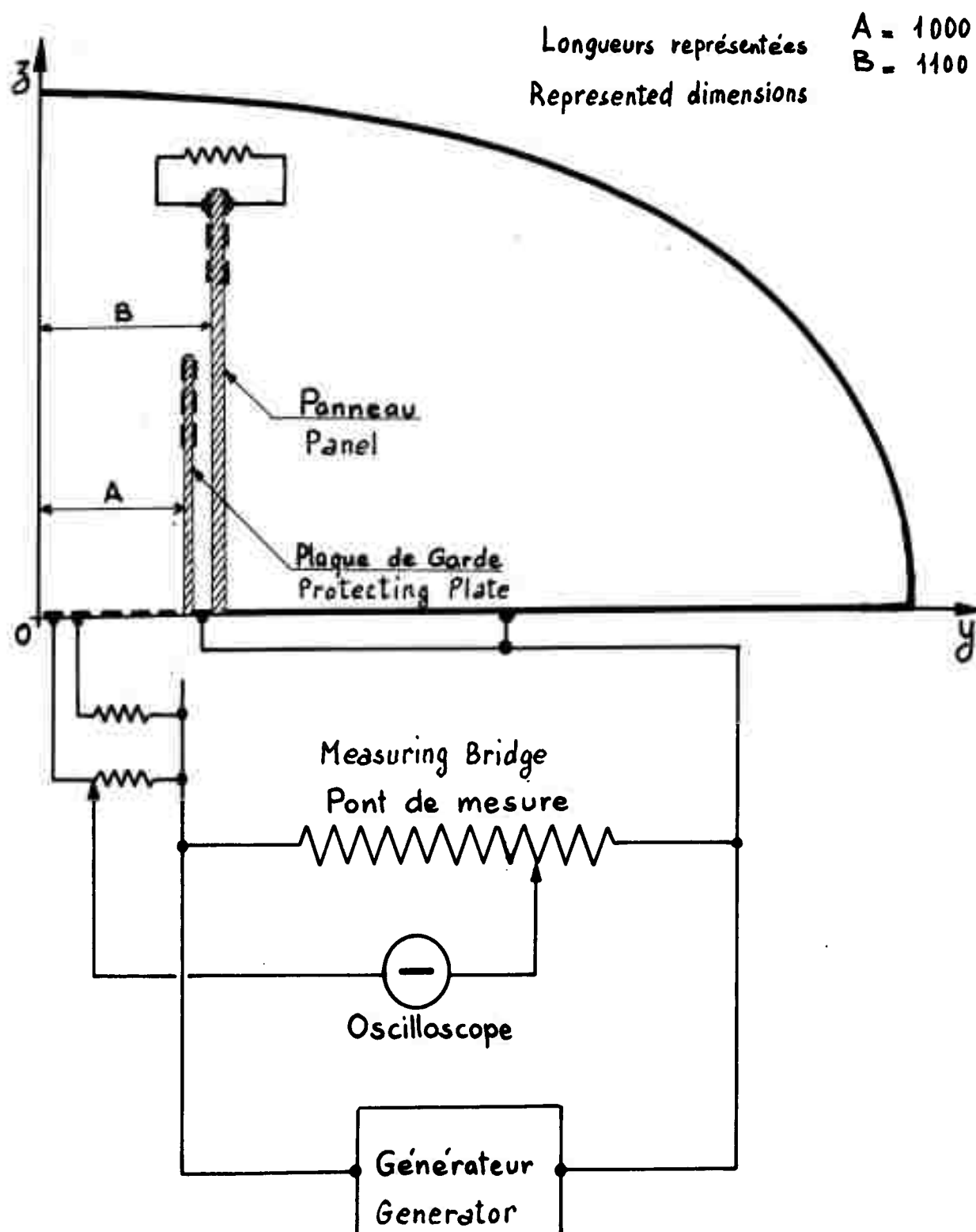
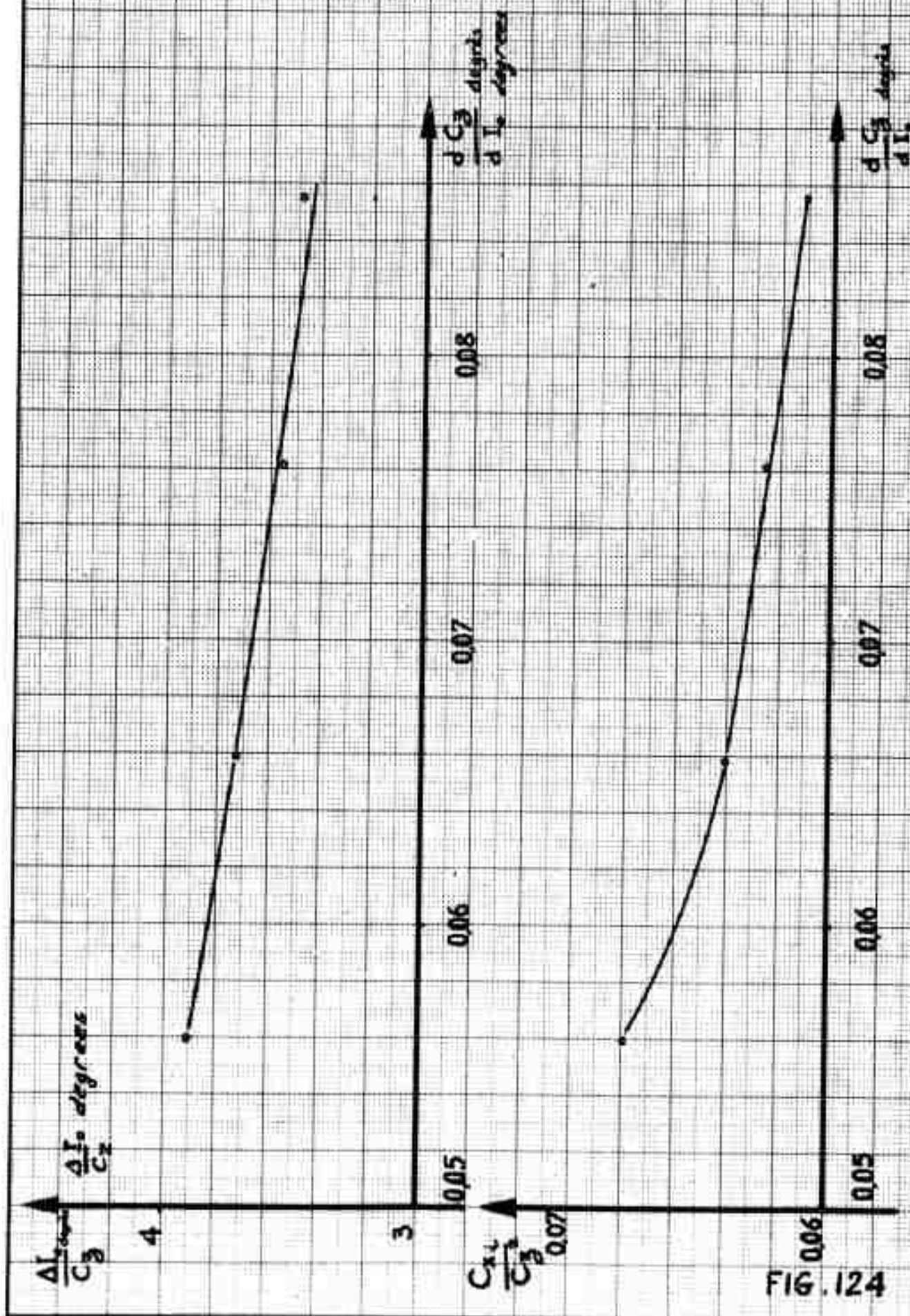


FIG.122



Schematic Assembly for Rheo-electric Analogy
Schéma du montage en cuve rhéoélectrique



ONERA

PV 5/703AY

Dessiné par :
NE

Date :
10-60

B 122

Volet Mécanique $\alpha = 22.5^\circ$
Mechanical Flap

$A = \infty$

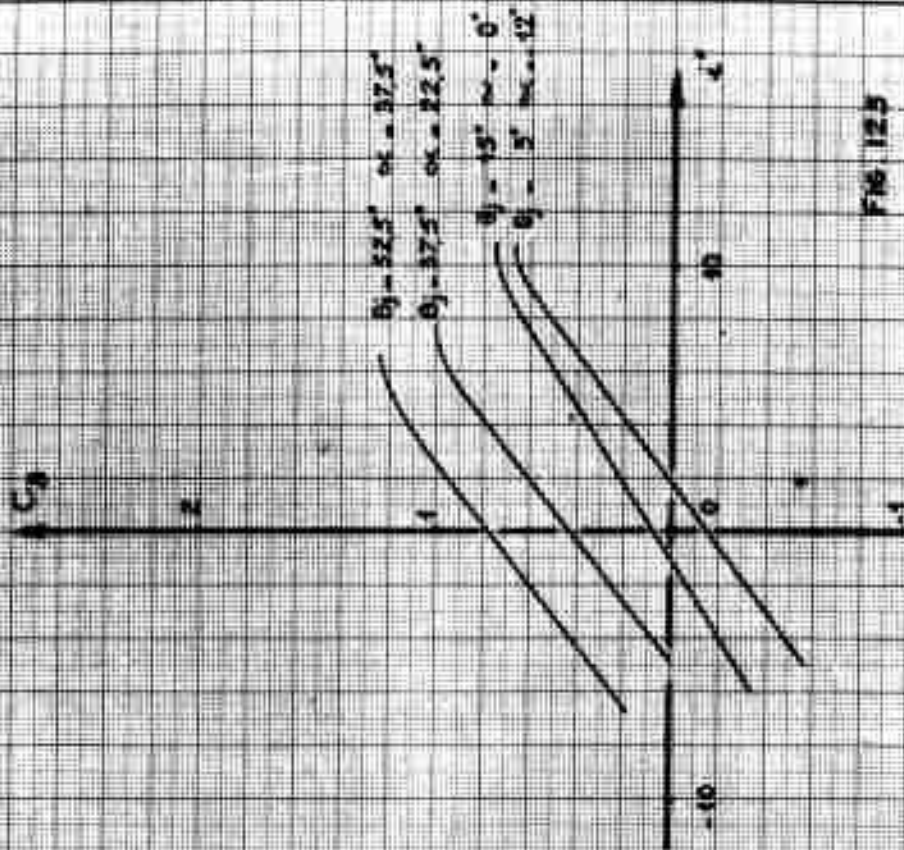
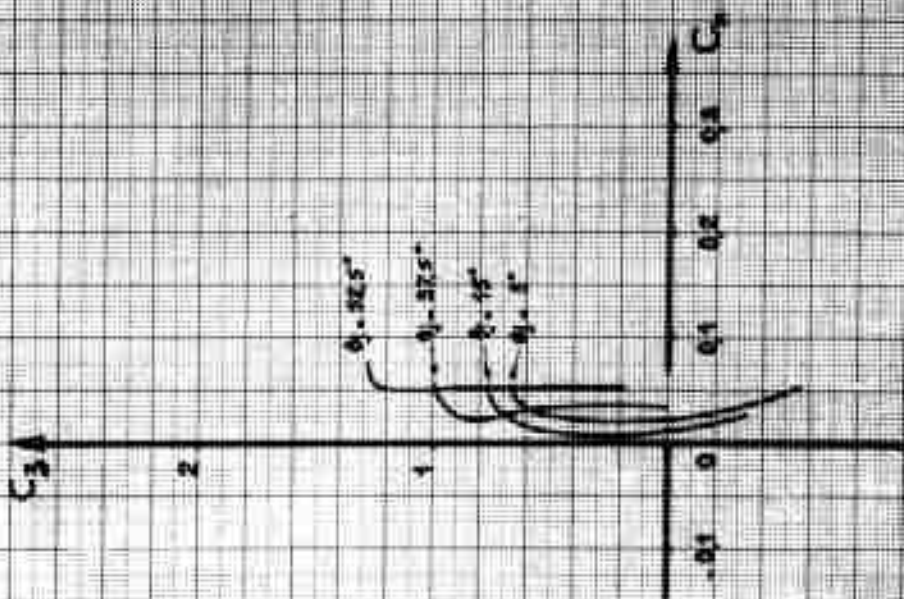


Fig 123

ONERA

PV 5/703AY

Designé par :
NE

Date
10-60

B. 123

Volet Mécanique
Mechanical Flap

$V_c = 22 \text{ m/s}$

$C_p = 0,09$

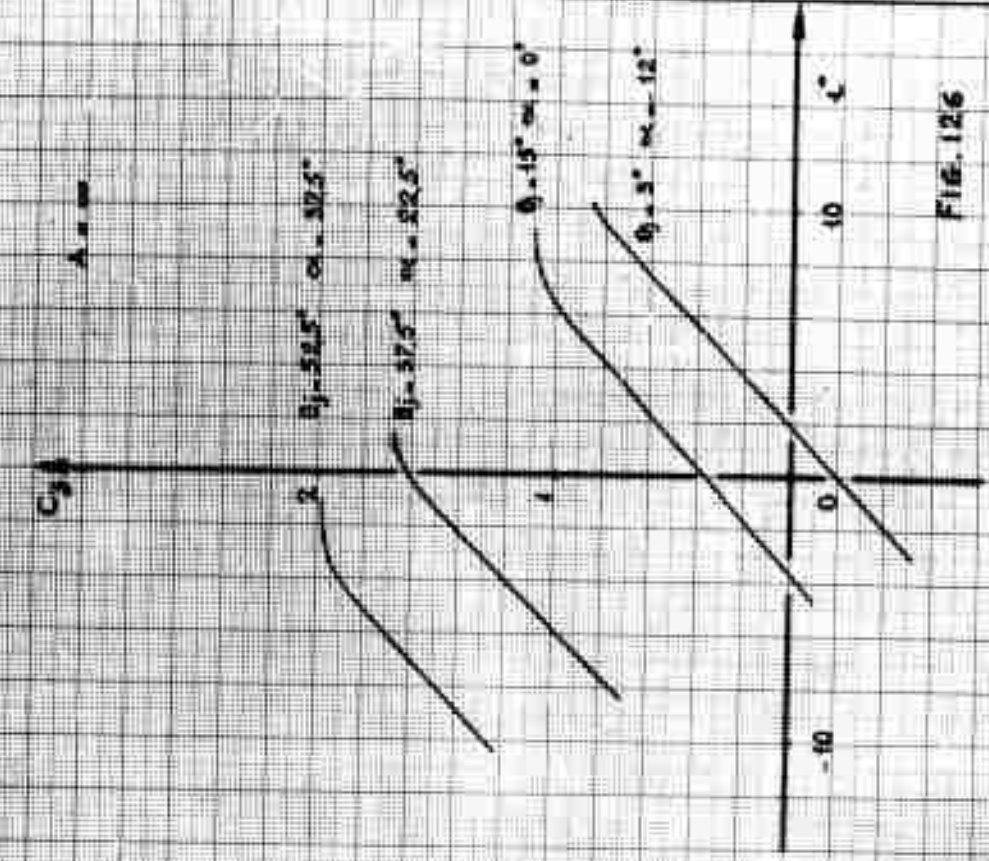
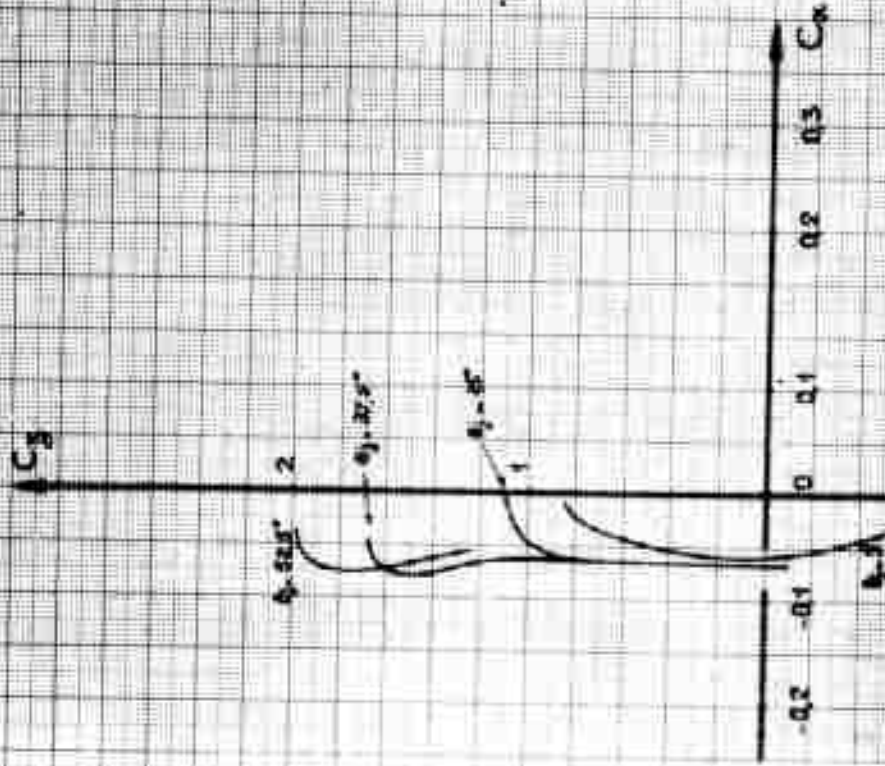
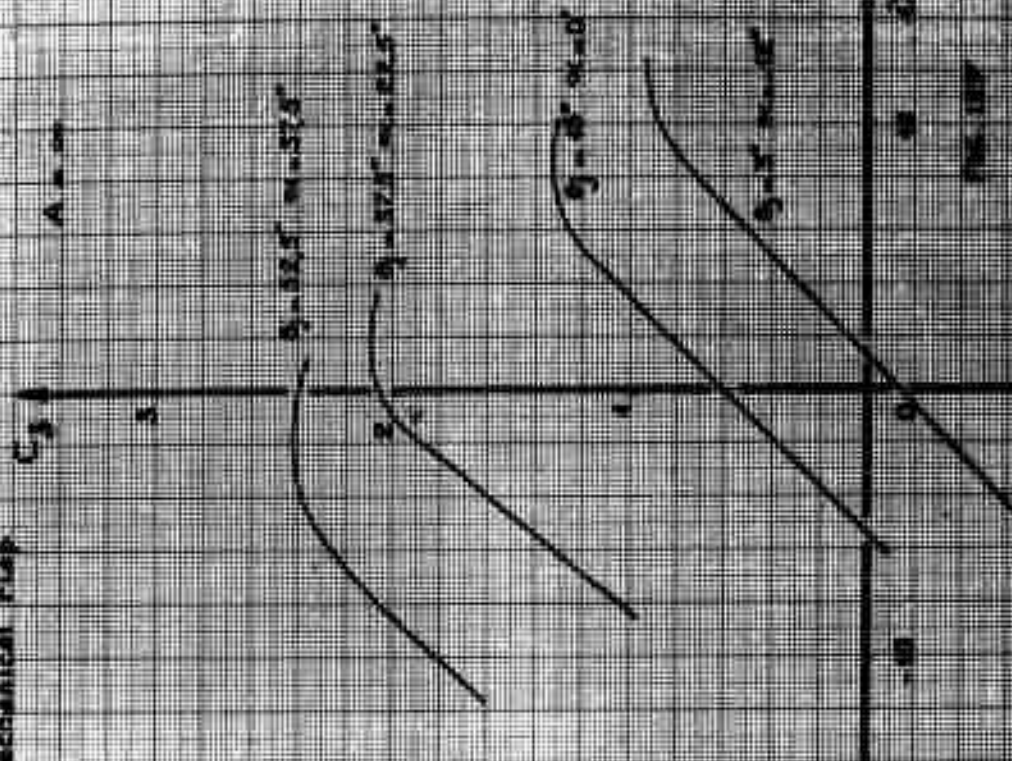
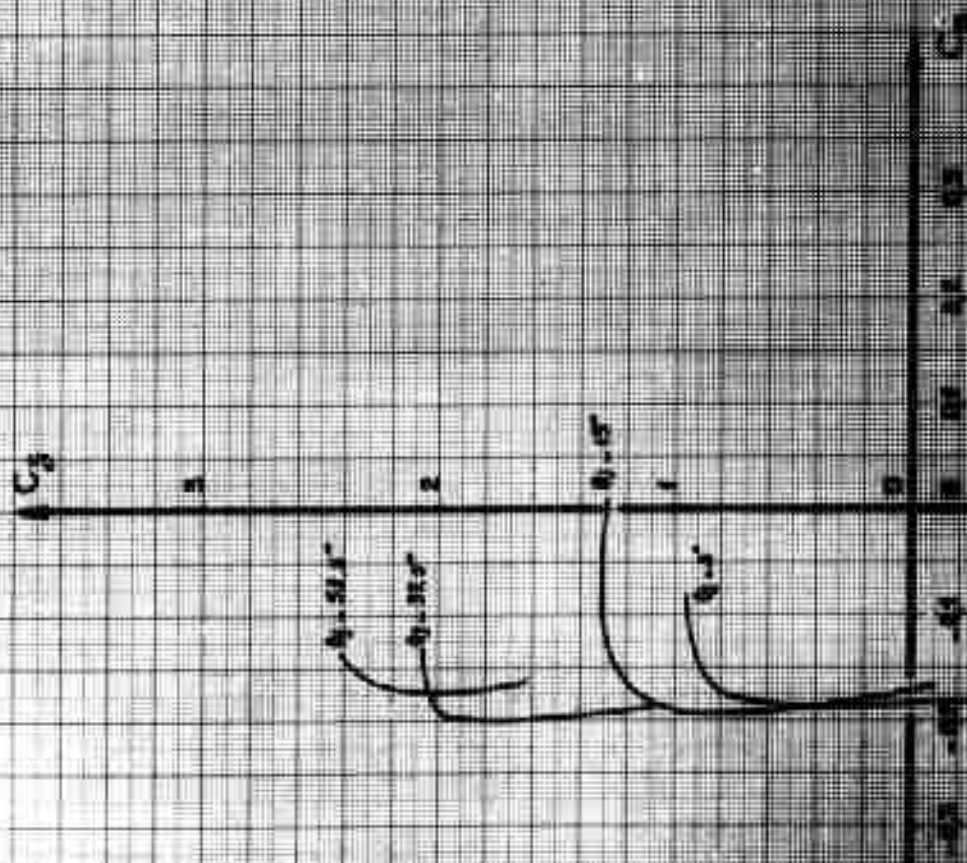
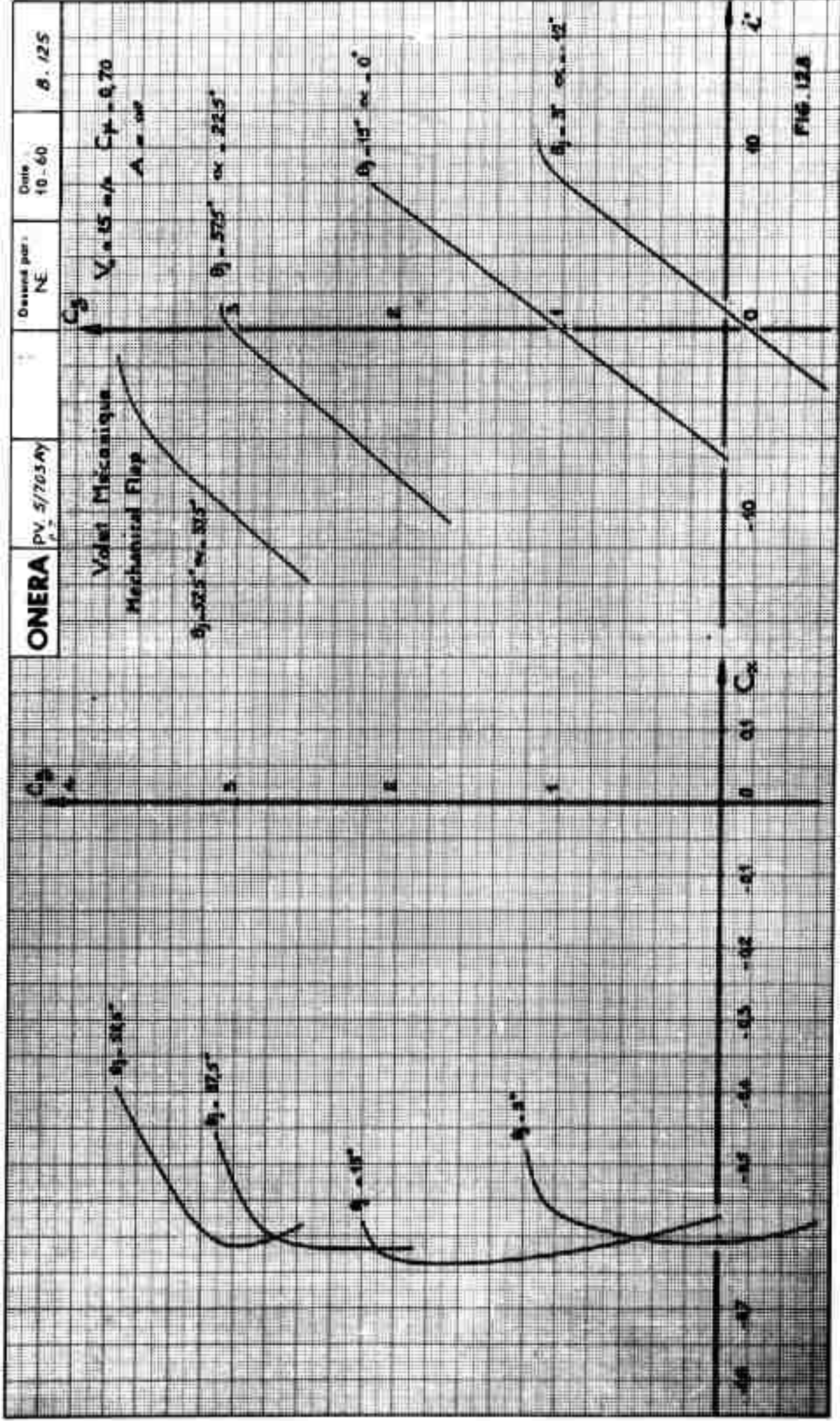


FIG. 126

Volter Mécanique $V_{\text{a}} = 22 \text{ V}$ $C_{\text{p}} = 0.22$
Mechanical Flap



100



ONERA

PV 5/70.8.8V

Designé par:

17E

Date:

10 - 60

B. 126

Volet Pneumatique
Pneumatic Flap

$V_{\infty} = 22 \text{ m/s}$

$C_{pL} = 0$

$\Lambda = \infty$

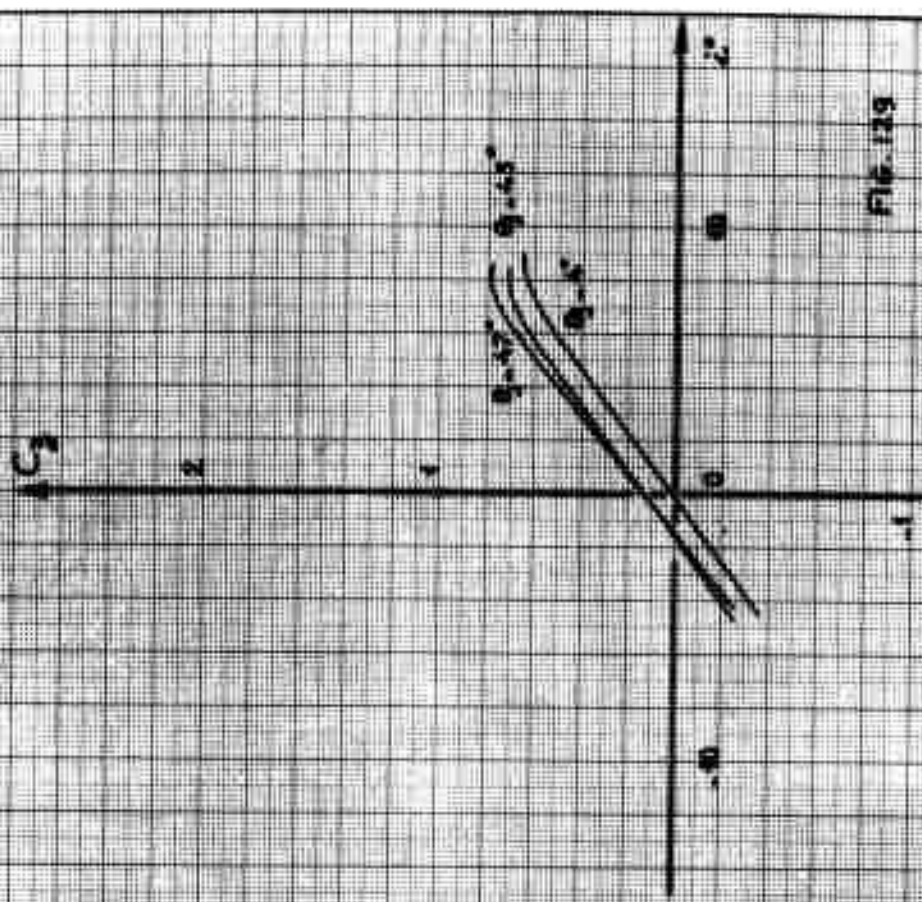
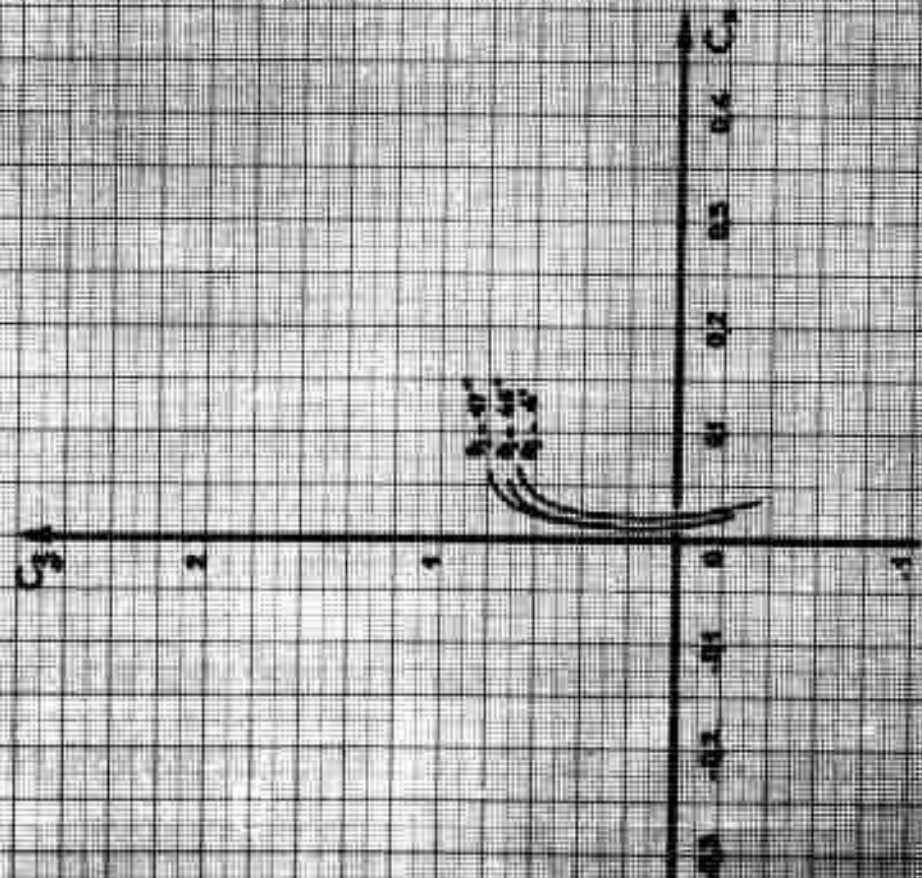


Fig. 129

ONERA

PV 5/703AY

Designé par :
NE

Date :
10-60

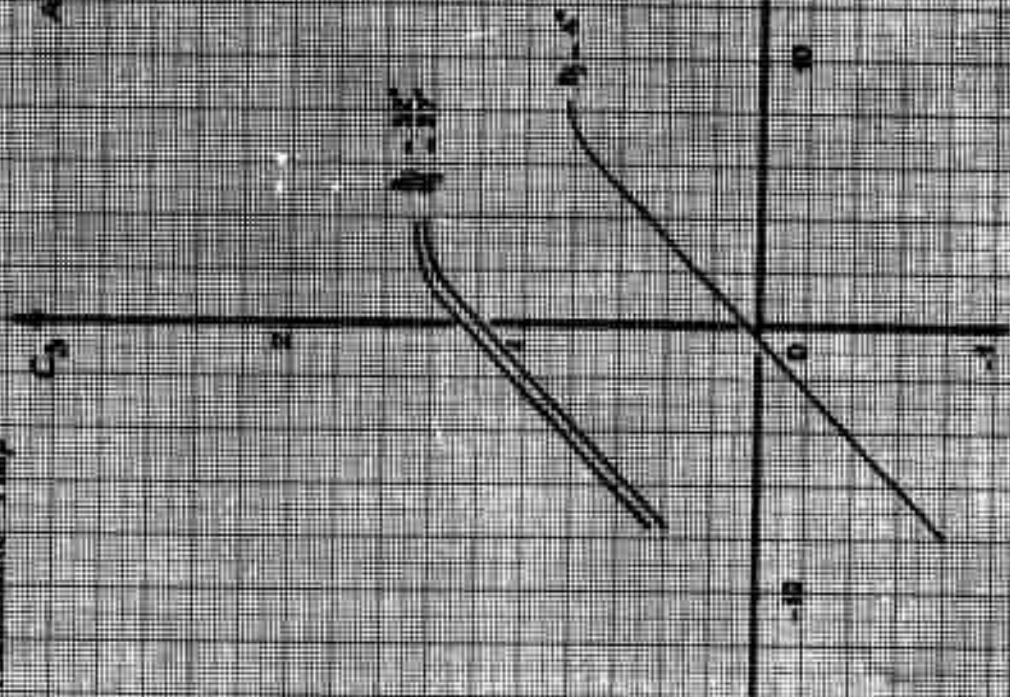
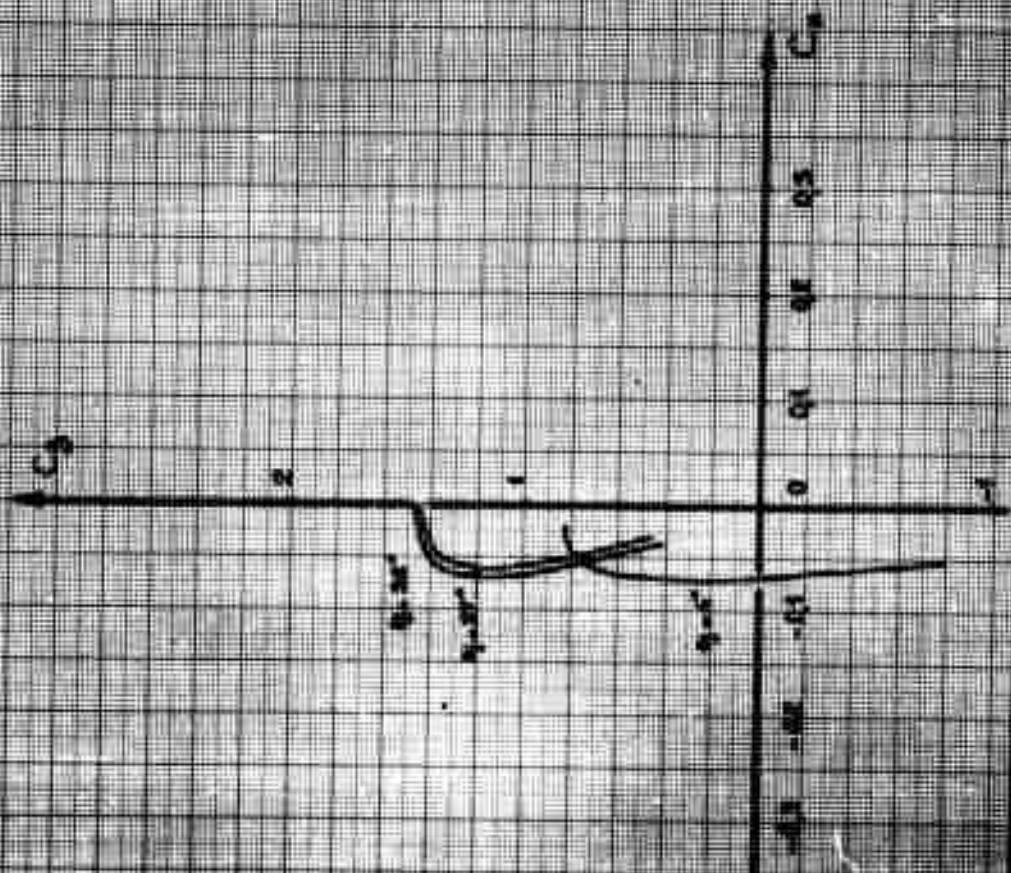
8.127

Volet Pneumatique
Pneumatic Flap

$V_c = 22 \text{ m/s}$

$C_{p0} = 0.08$

$A = 0.00$



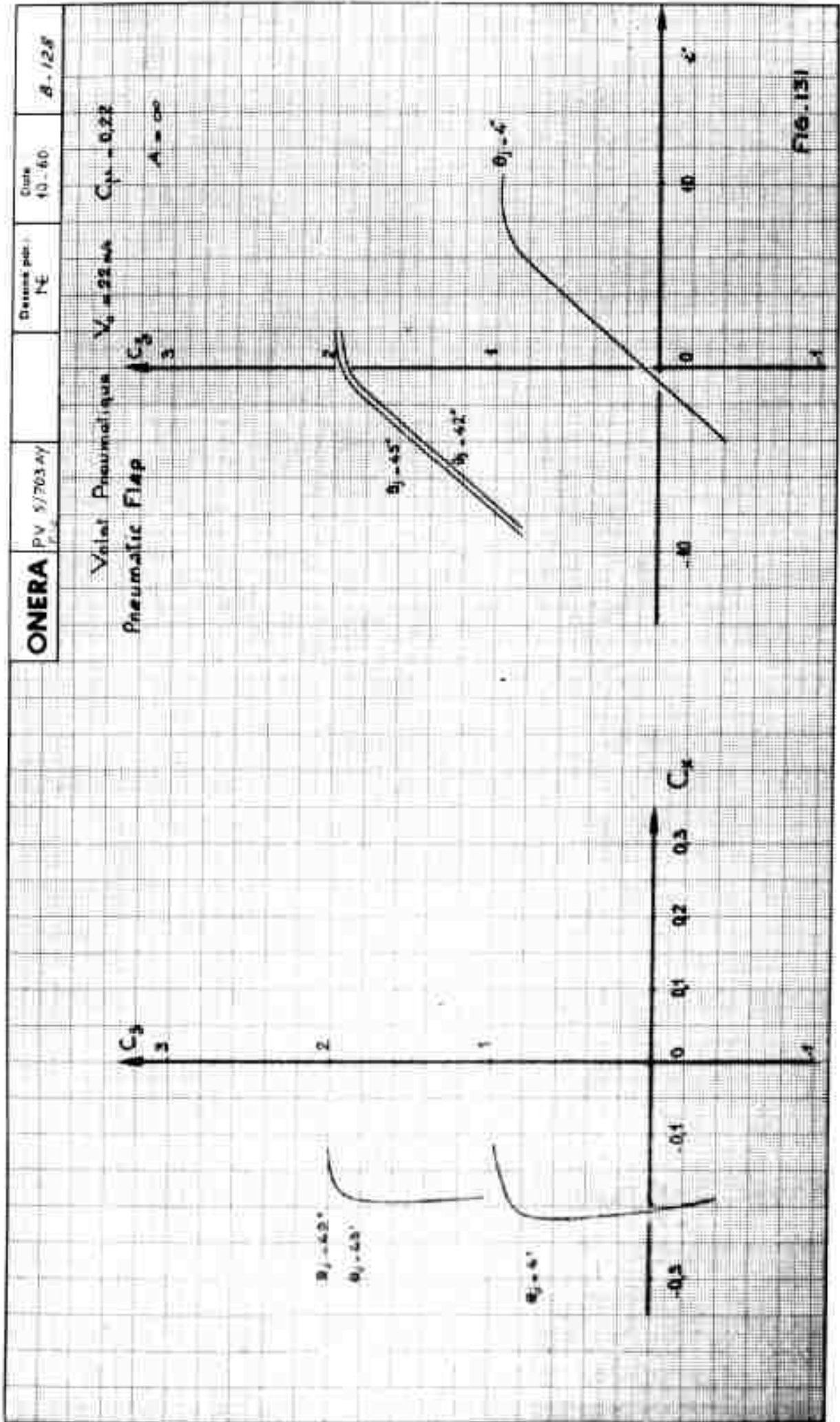
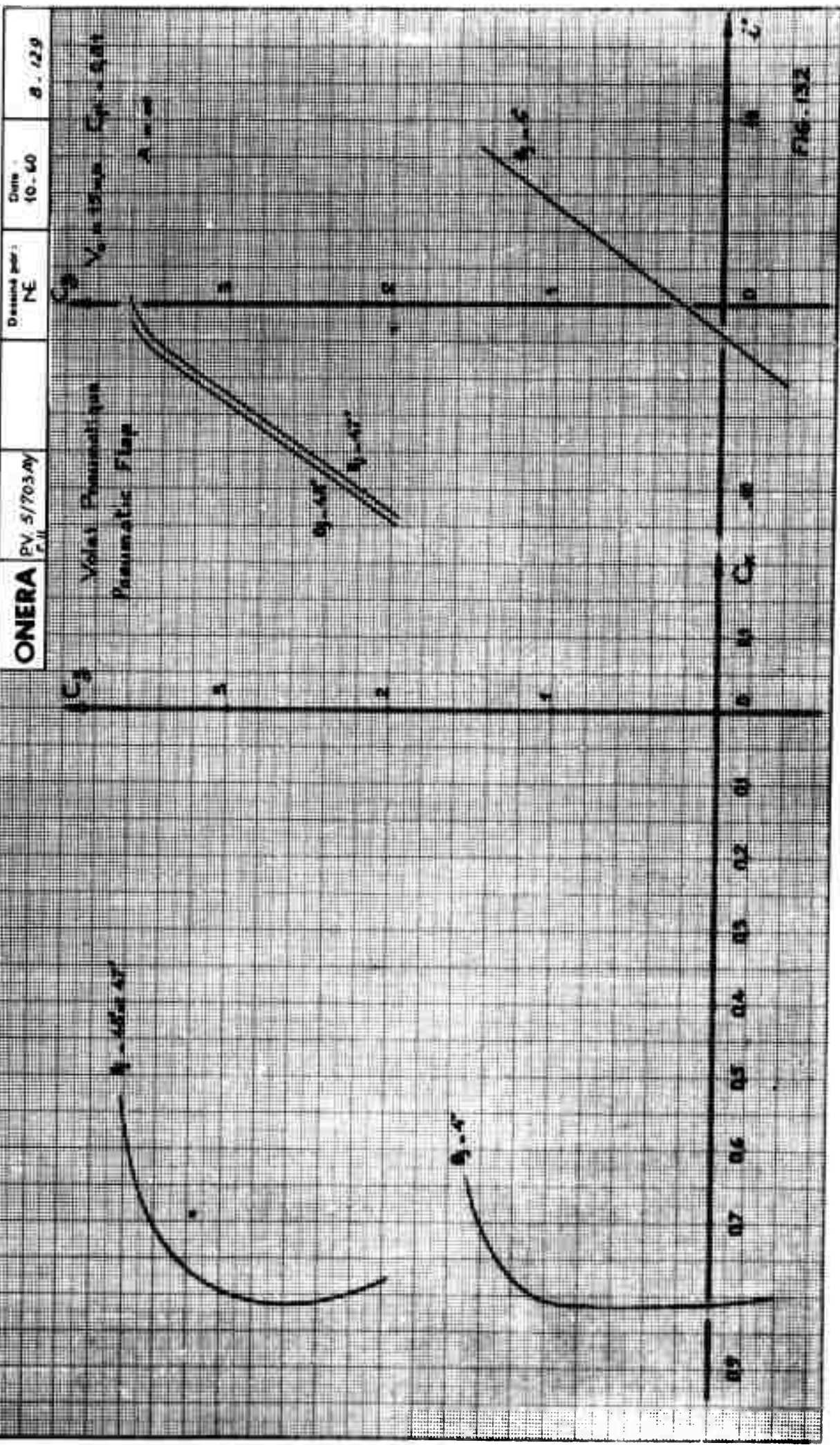
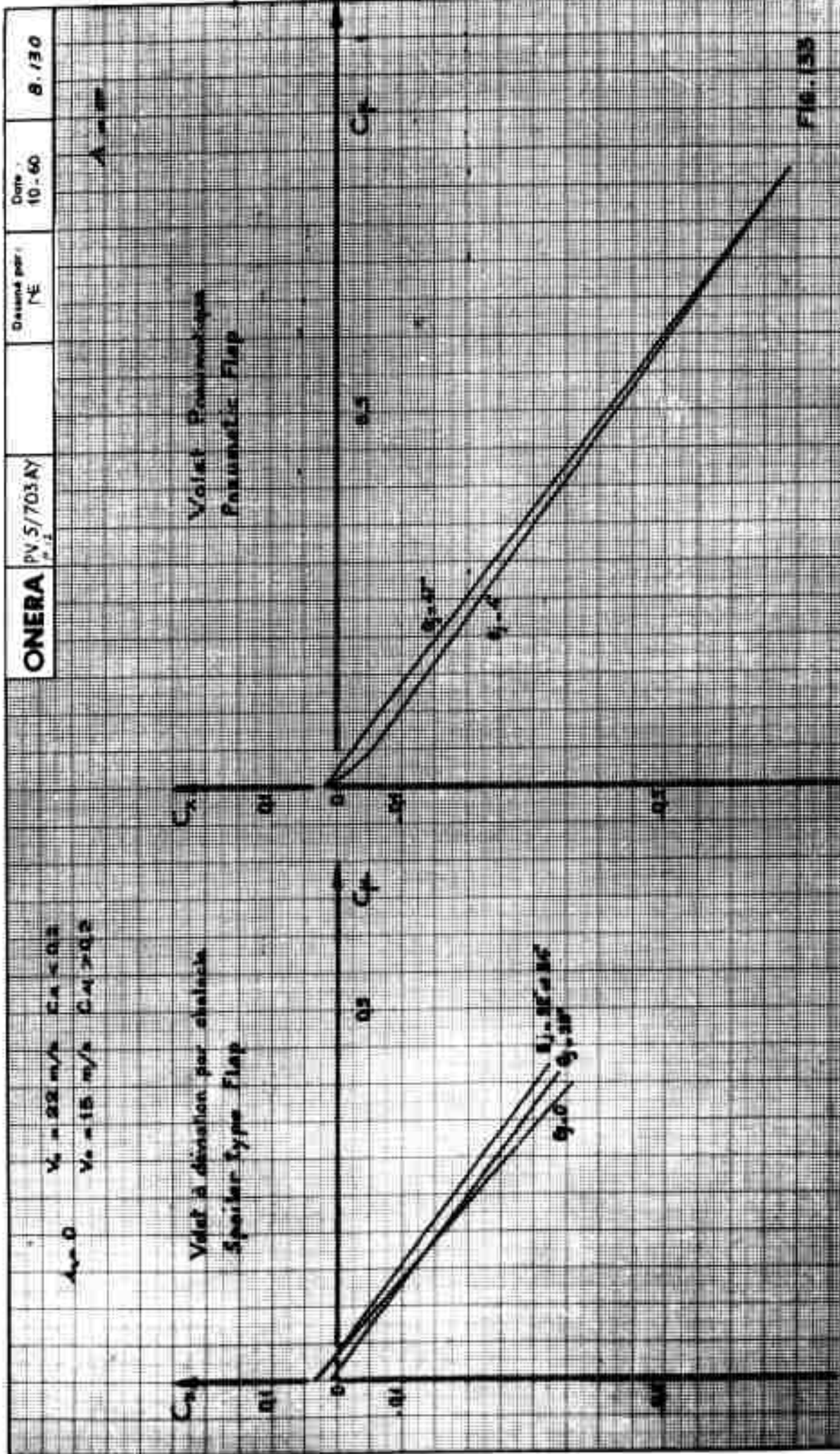
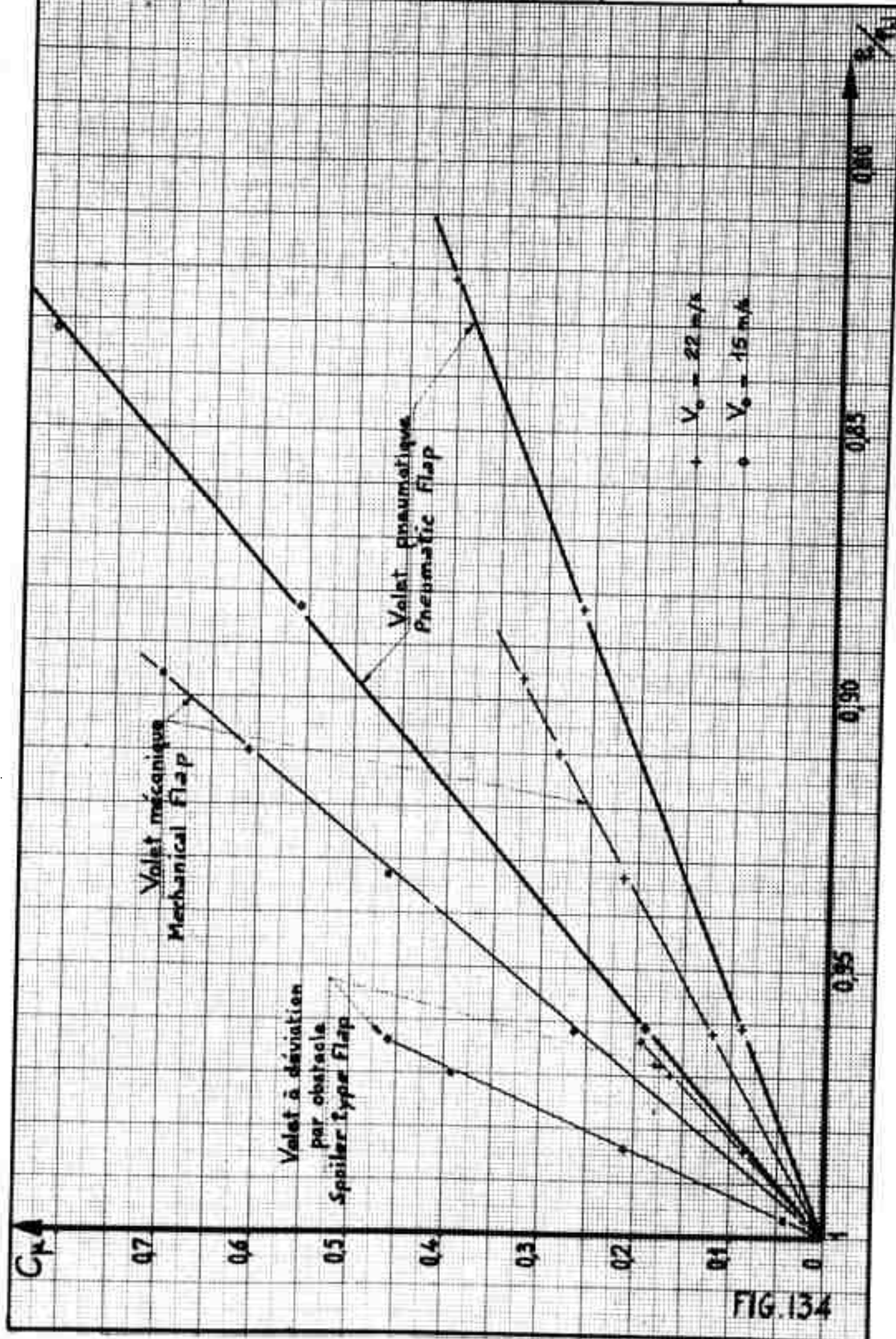


FIG. 131







Tests in S₃ Ch w.E.
(2nd series of tests)

Curves $C_x(i)$ without blowing
Courbes (C_x, i°) sans soufflage

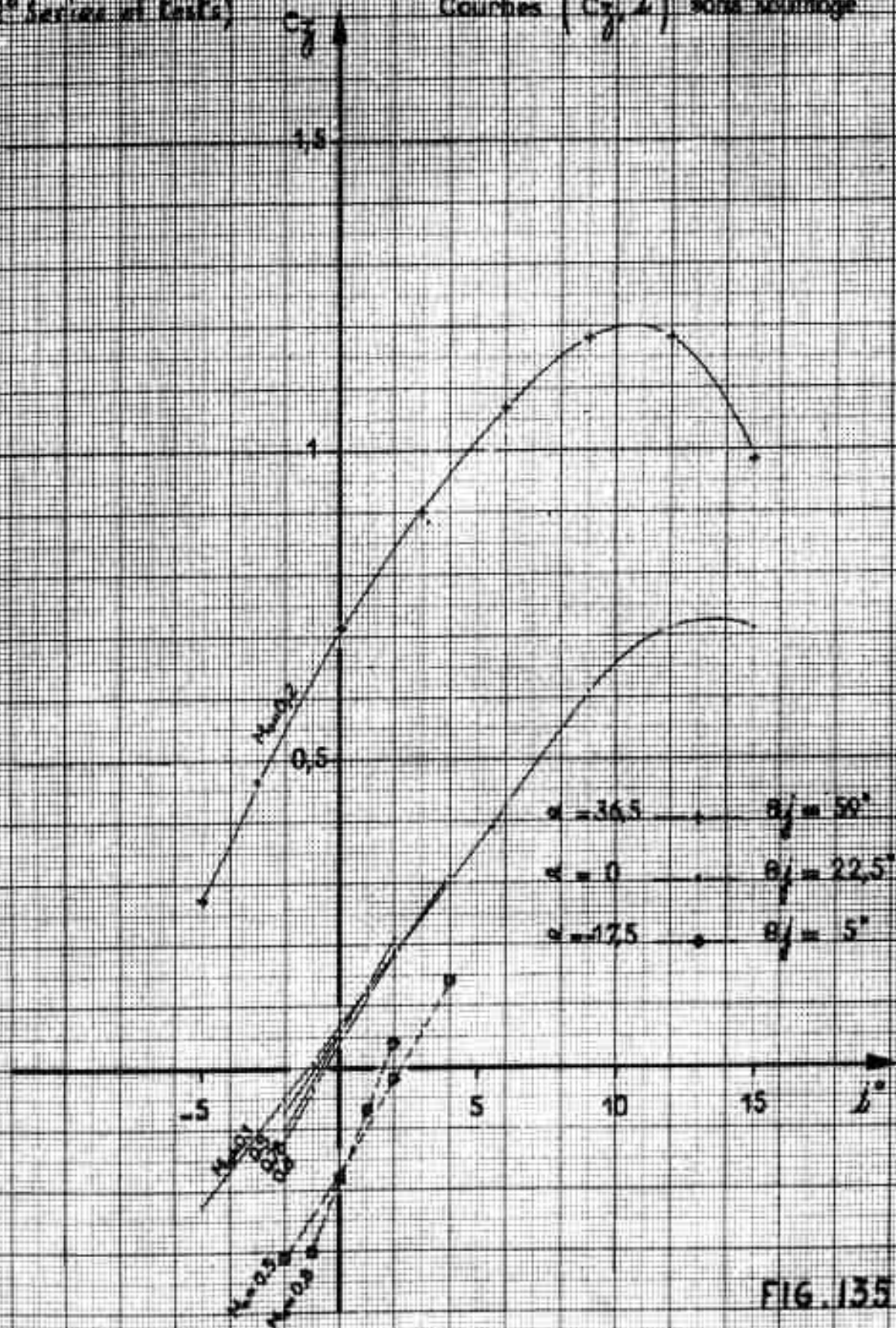
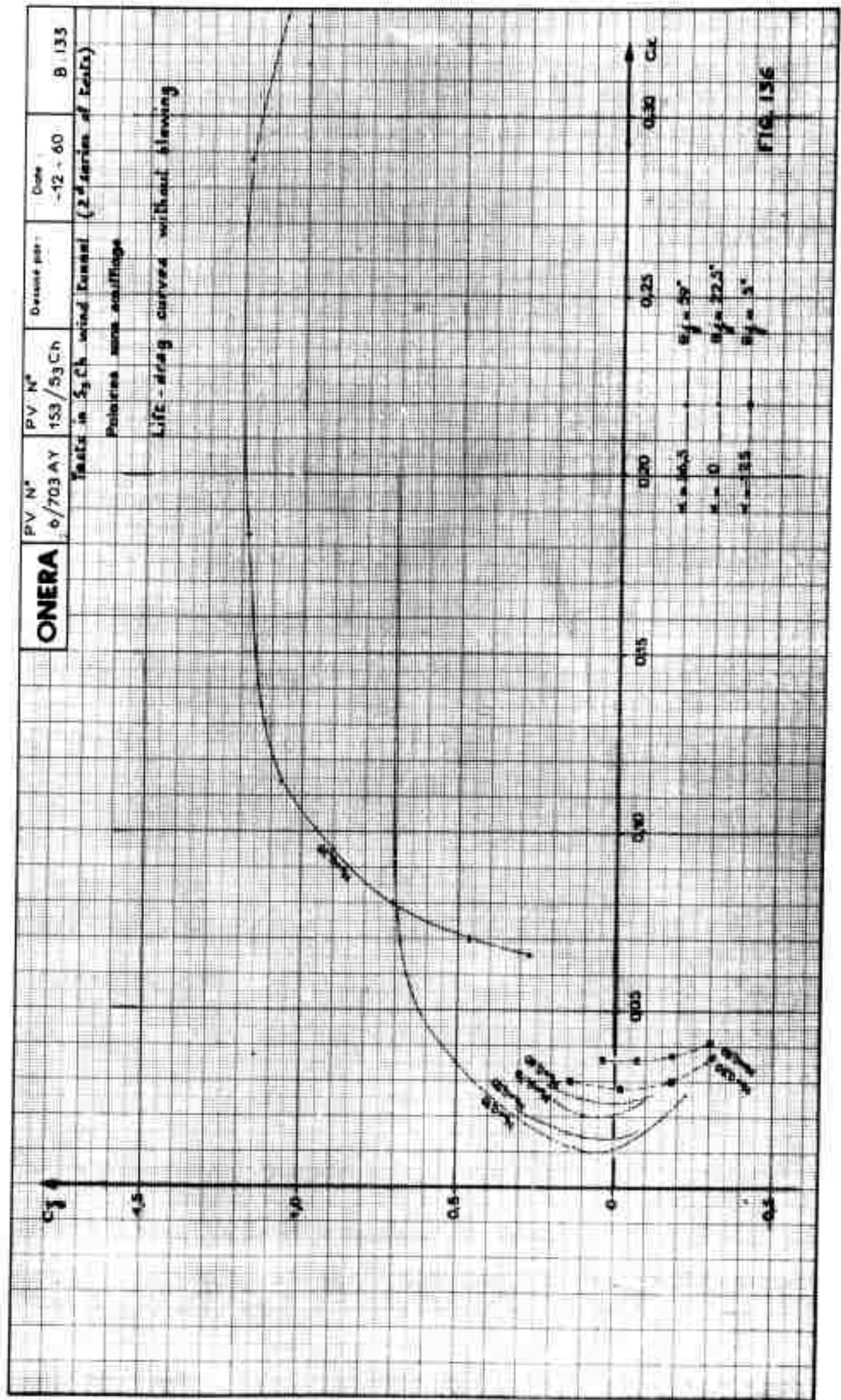
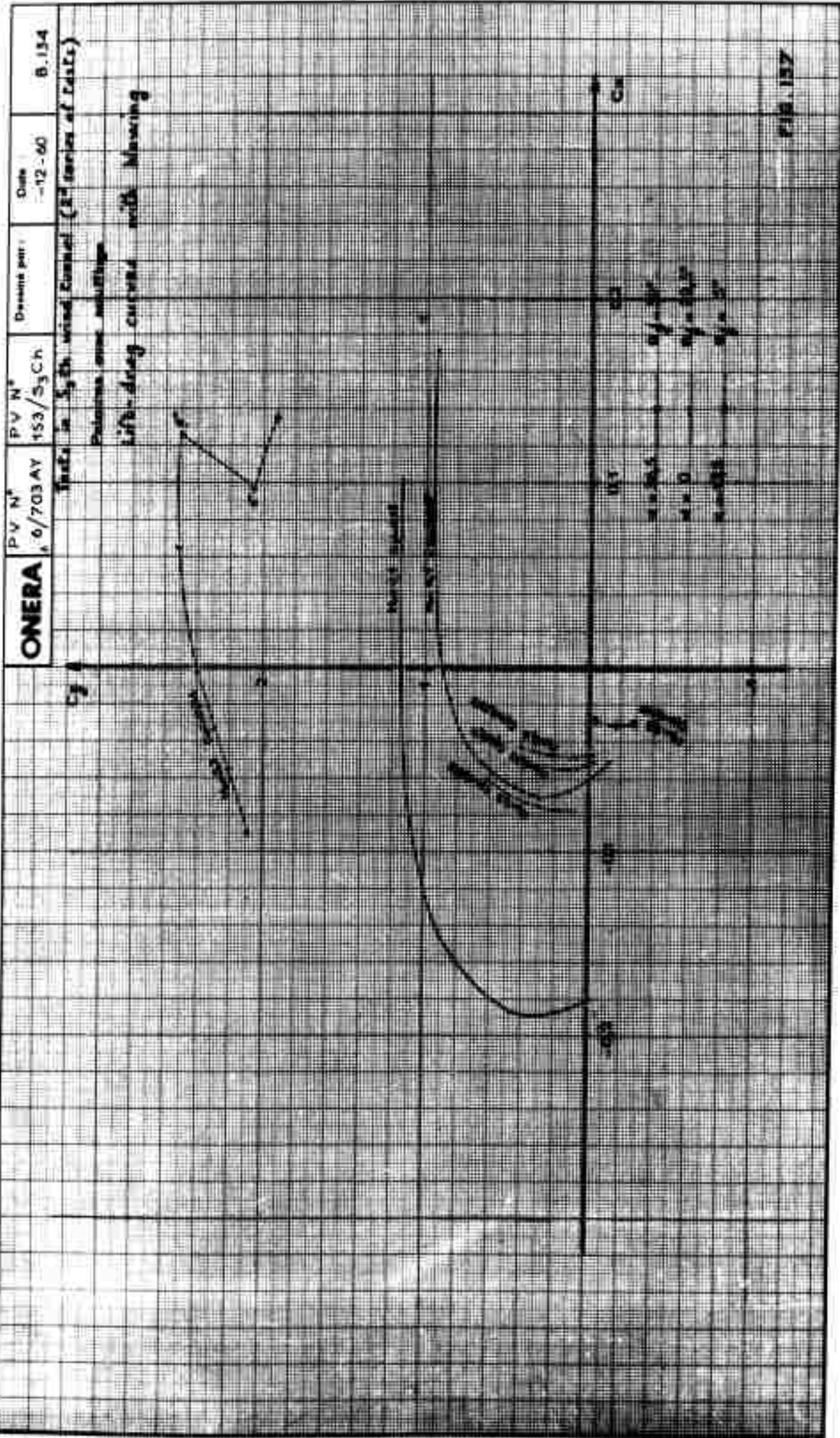
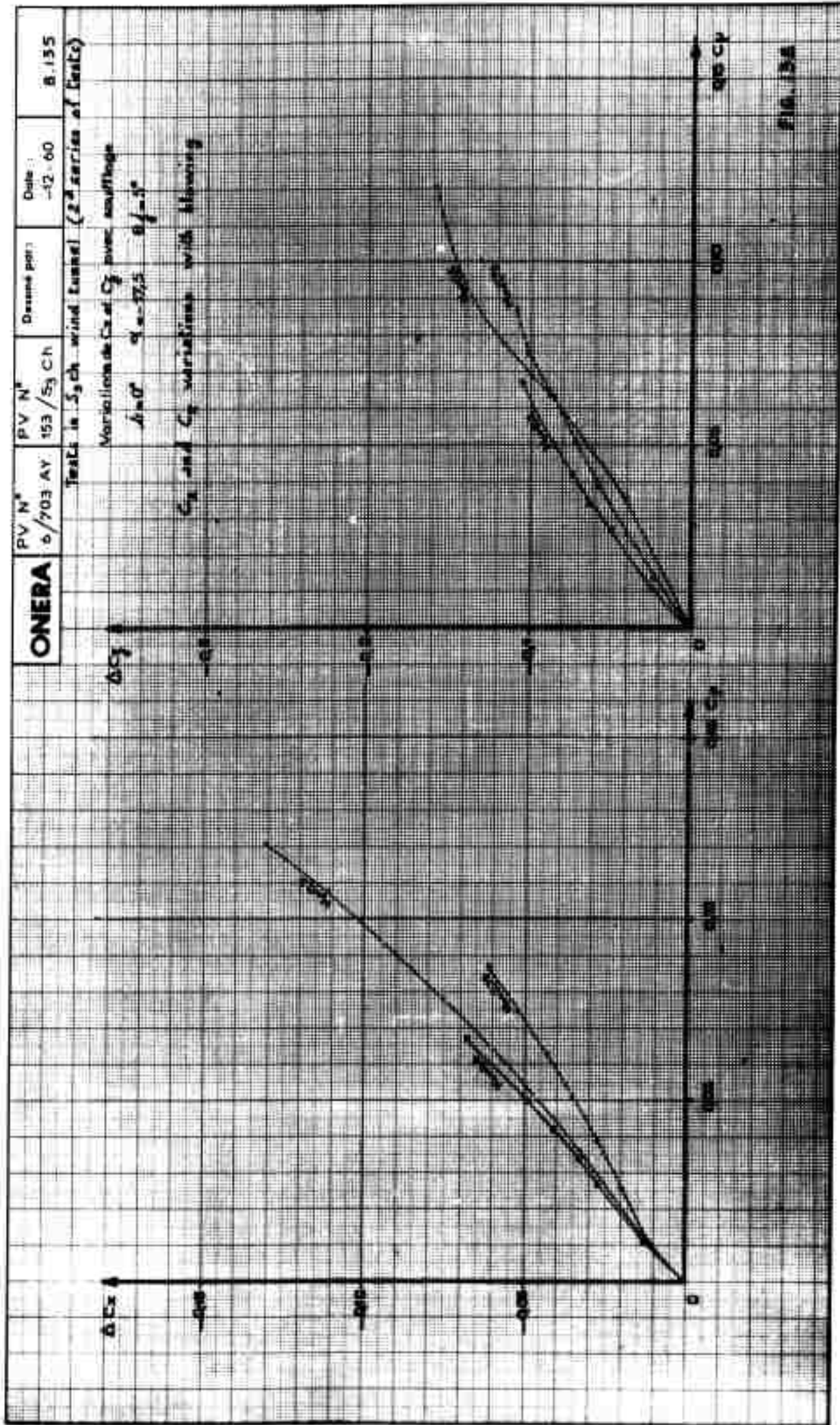


FIG. 135







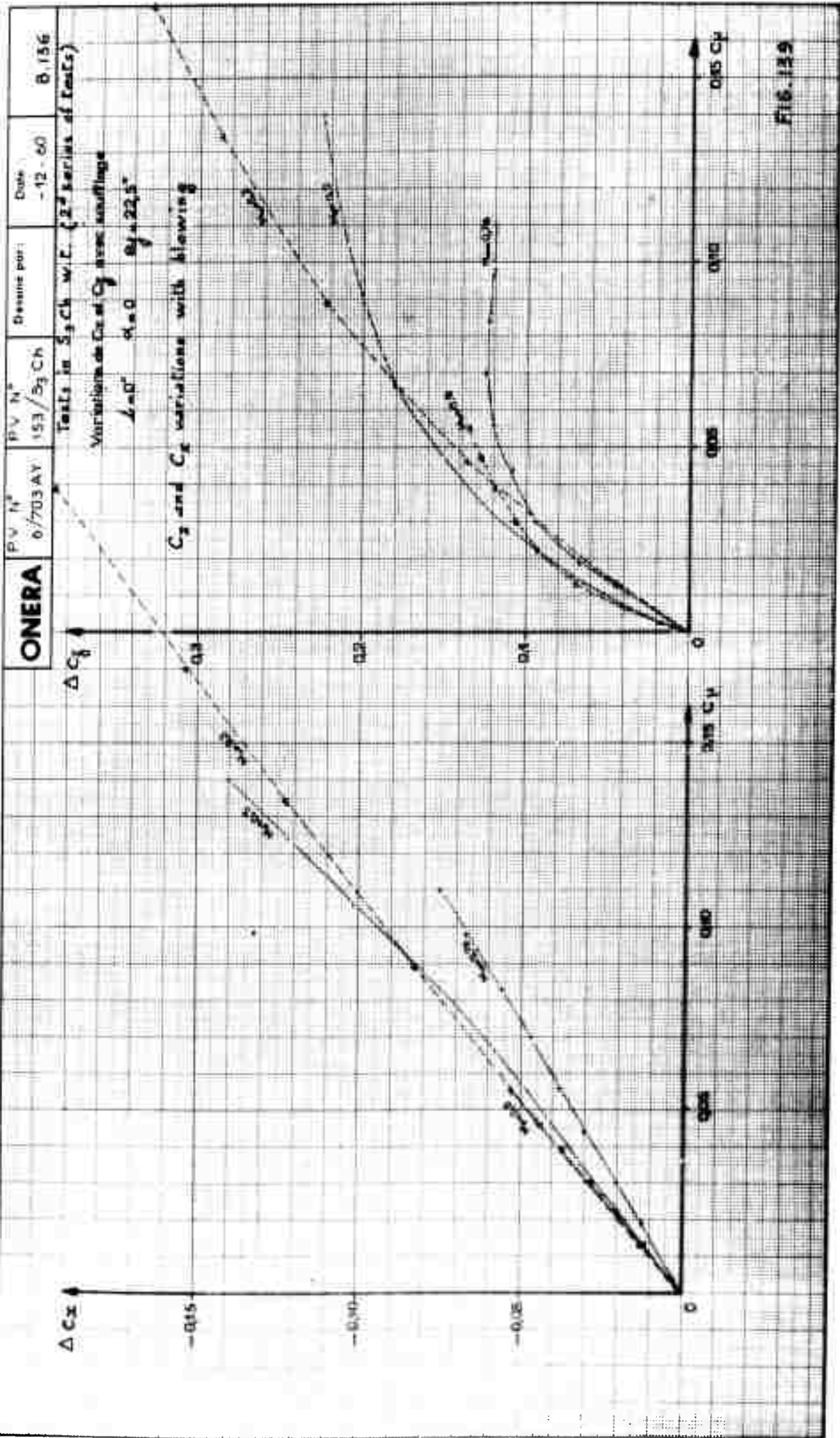


Fig. 139

ONERA

PV N°
6/703 AYPV N°
153/S₃Ch

Dessiné par:

Date :
-12 -60

B.137

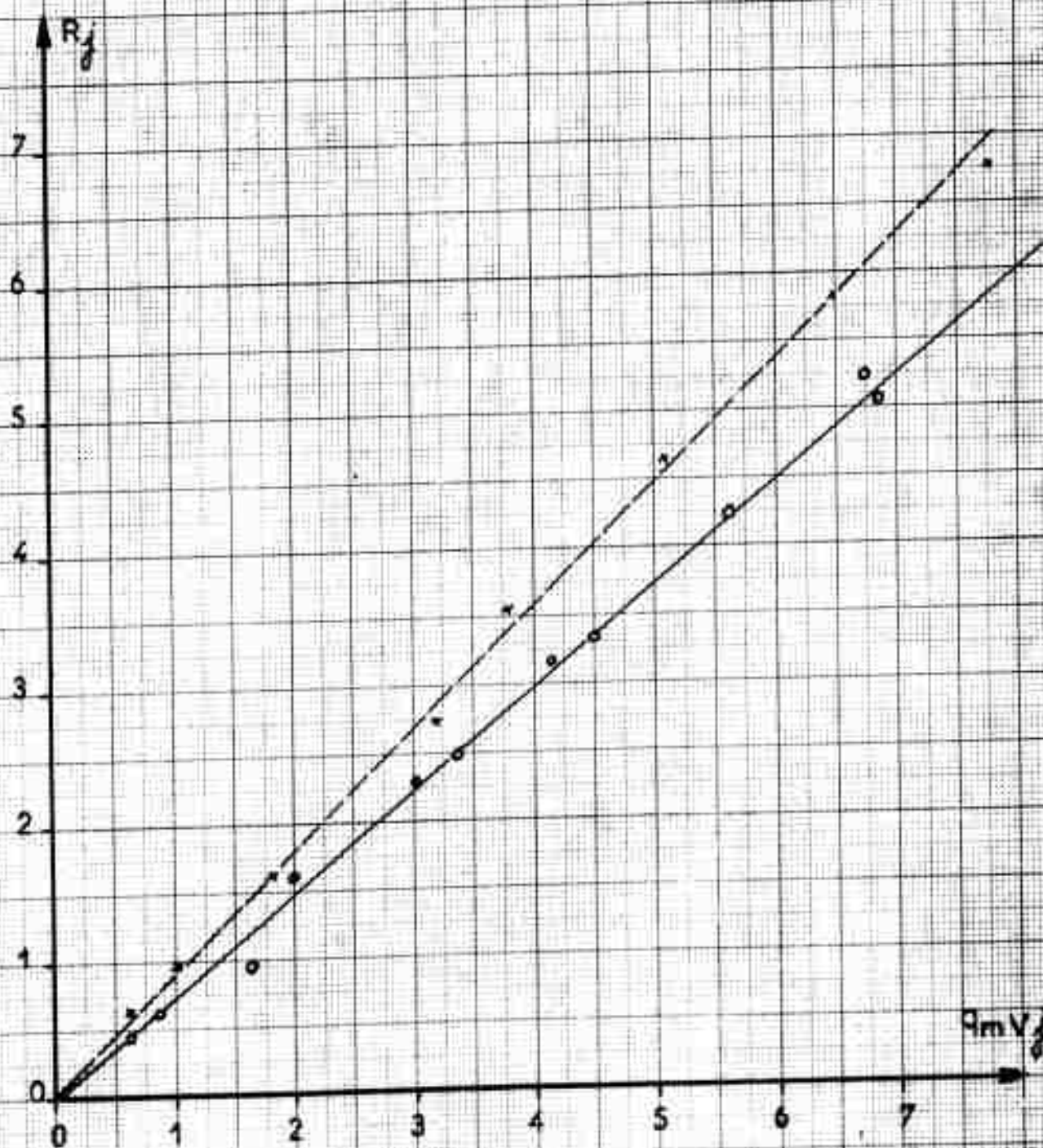
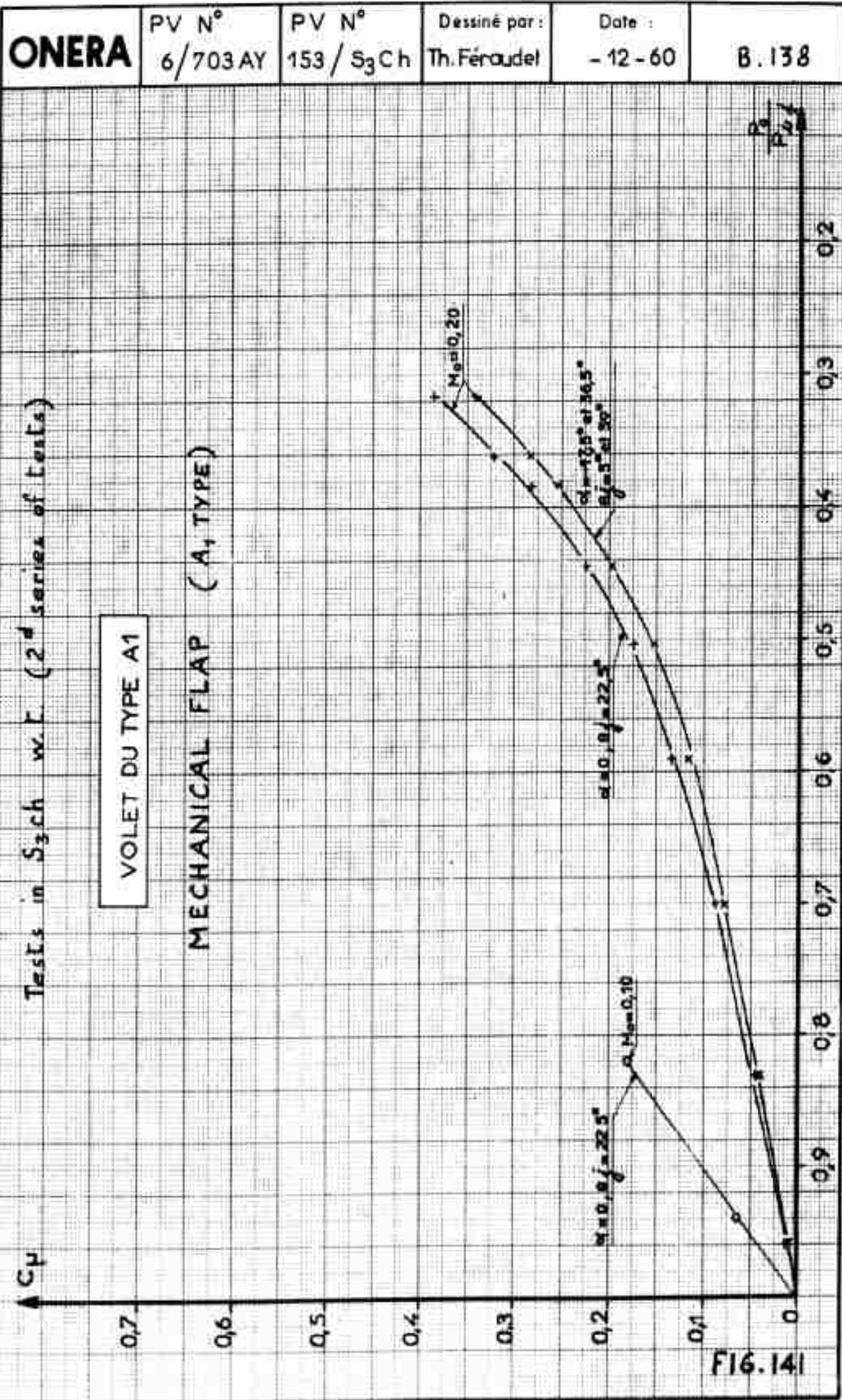
Tests in S₃Ch wind tunnel (2^d series of tests) $\alpha = -17,5^\circ \text{ et } 36,5^\circ$ $\theta_f = 5^\circ \text{ et } 59^\circ$ $R_f = 0,77 q_m V_f$ $\alpha = 0$ $\theta_f = 22,5^\circ$ $R_f = 0,88 q_m V_f$ 

FIG. 140



ONERA

PV N°
6/703 AYPV N°
153 / S₃ Ch

Dessiné par :

Date :
- 12 - 60

B.139

Tests in S₃ ch w.L. (2^d series of tests)

VOILET DU TYPE A1

 $\alpha = 0$ $\theta_f = 22.5^\circ$ $\alpha = -17.5^\circ$ et 36.5° $\theta_f = 5^\circ$ et 59°

MECHANICAL FLAP (A, TYPE)

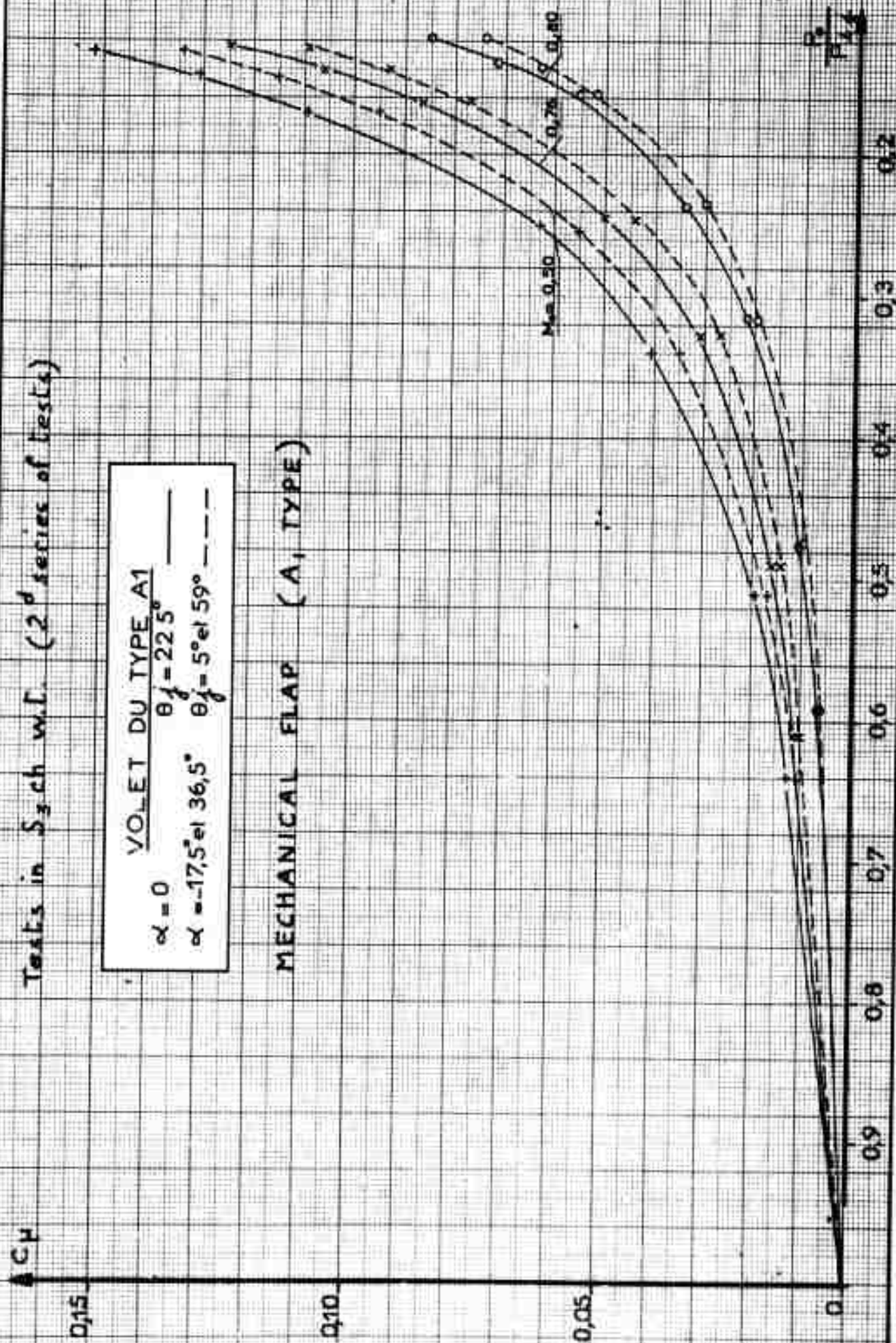
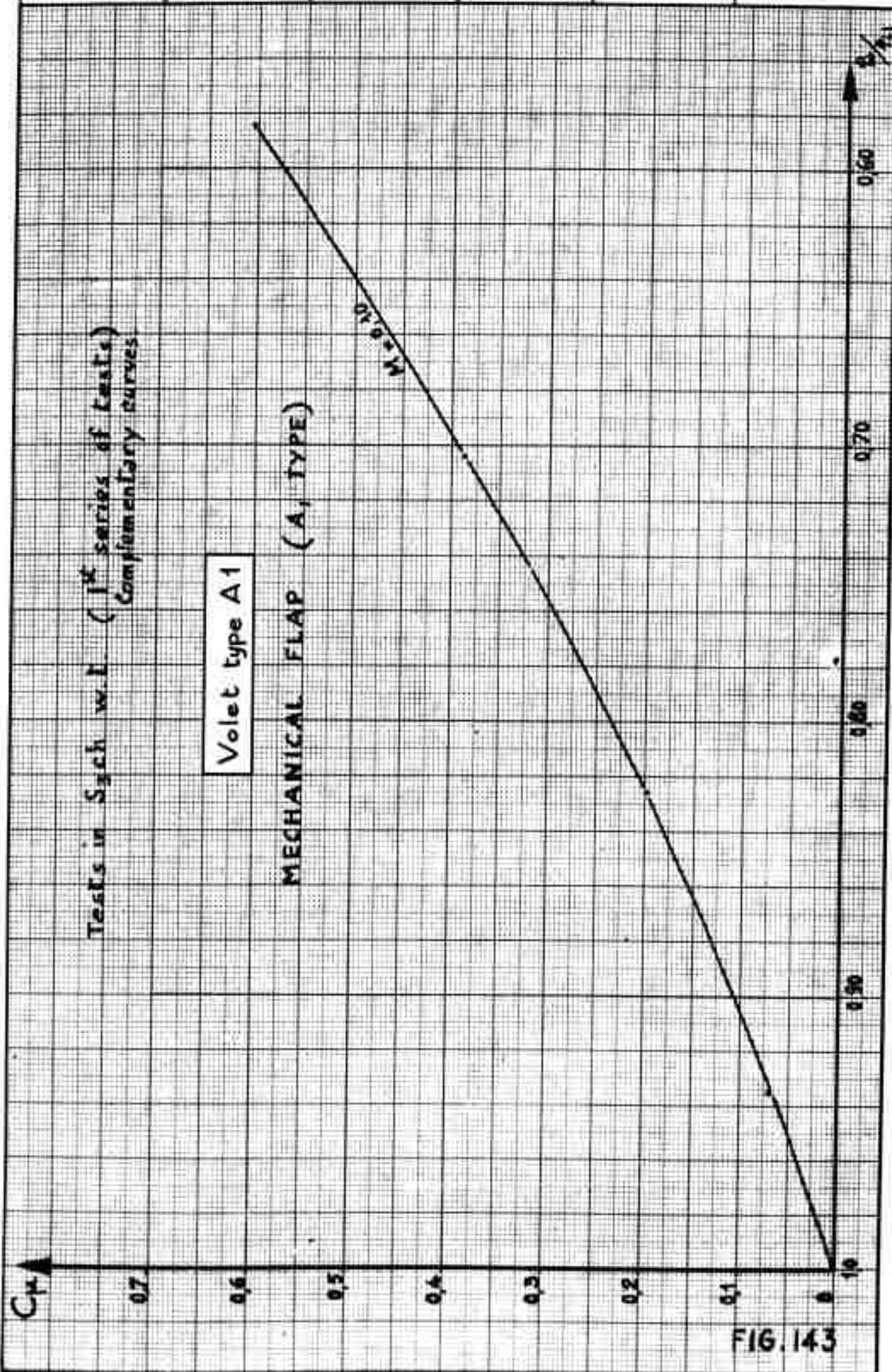
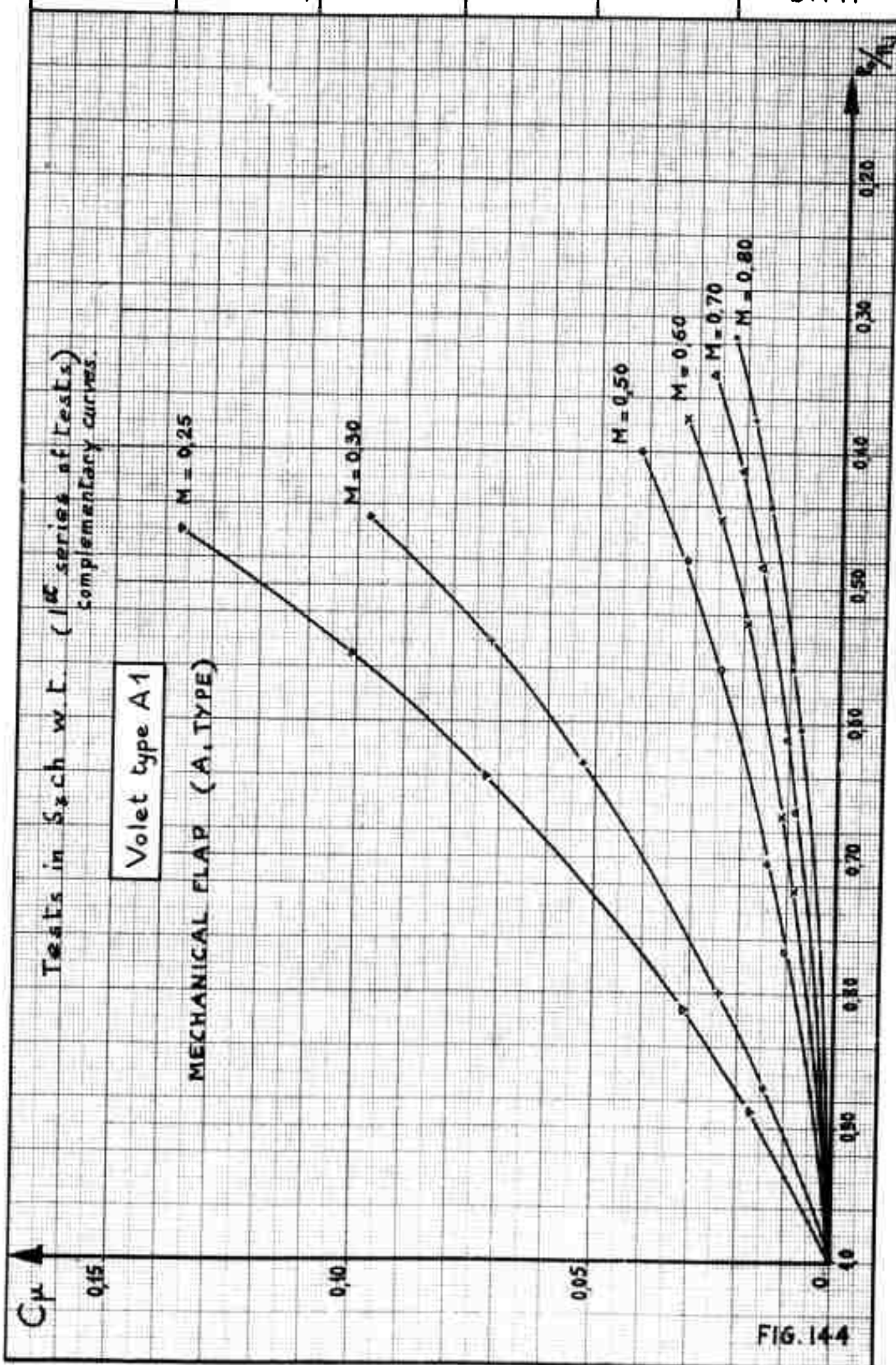
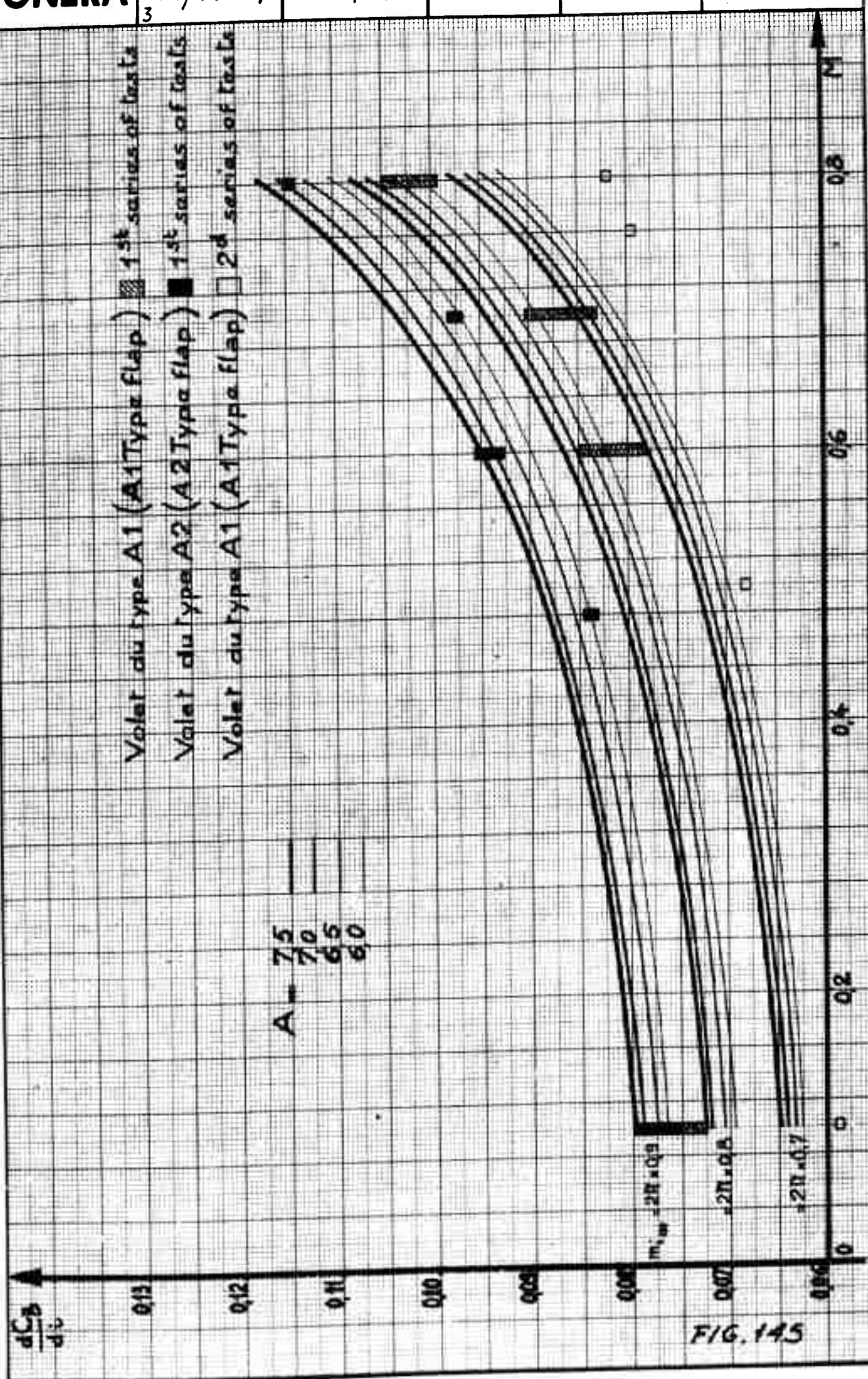
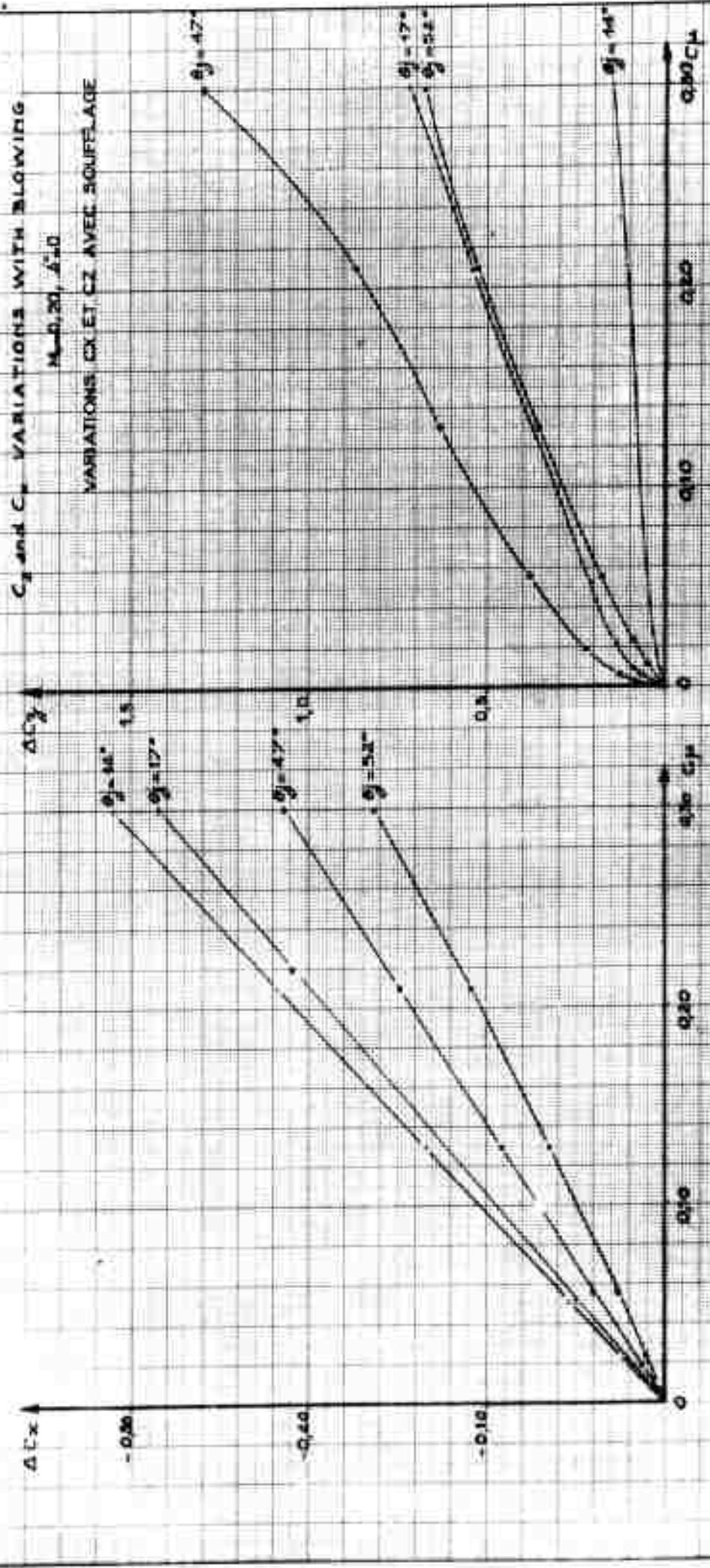


FIG. 142







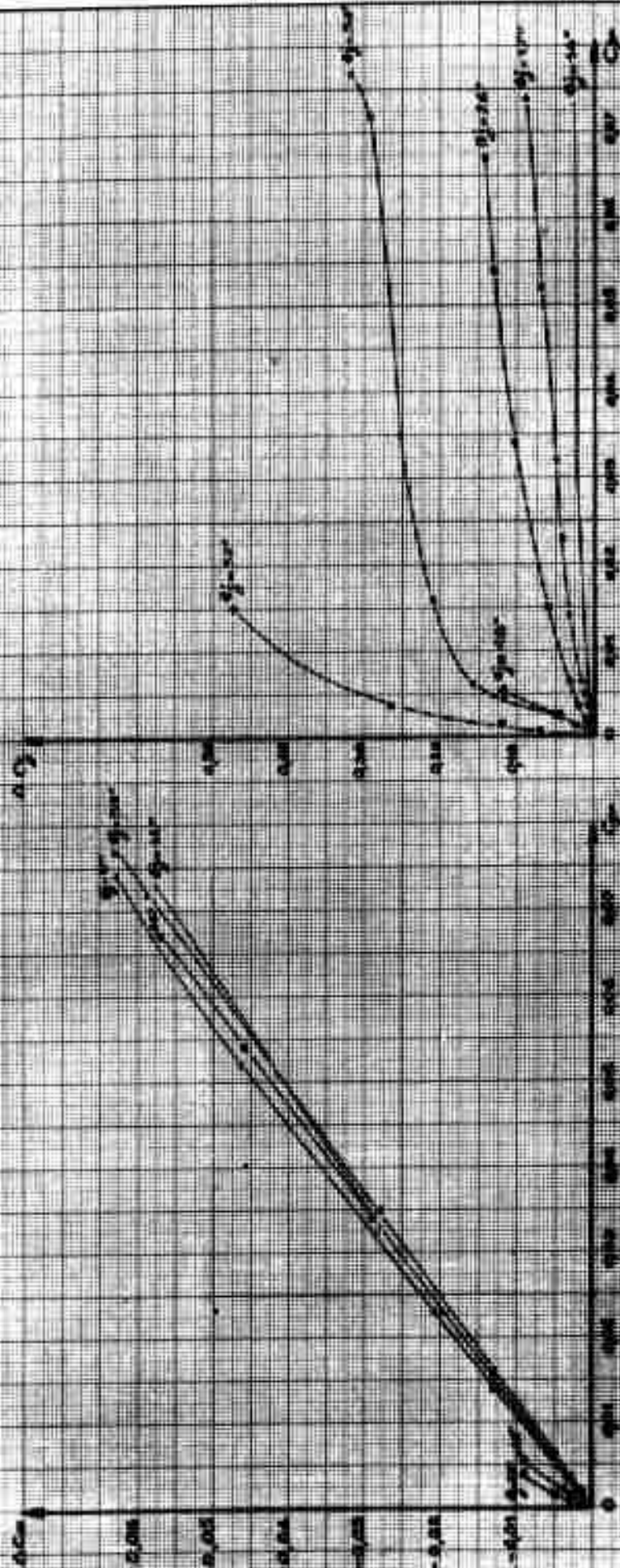


ONERA	PV N°	PV N°	Designe par:	Date	B 144
	7/703 AY	155/S3 Ch		-12-60	

C_L AND C_D VARIATIONS WITH BLOWING

$M_0 = 0.50$ $\beta^* = 0$

VARIATIONS CX ET CZ AVEC SOUFFLAGE



Coefficient C_x et C_z en fonction de θ_j
 $C_\mu = 0$, $\lambda = 0$

C_z AND C_x COEFFICIENTS VERSUS θ_j

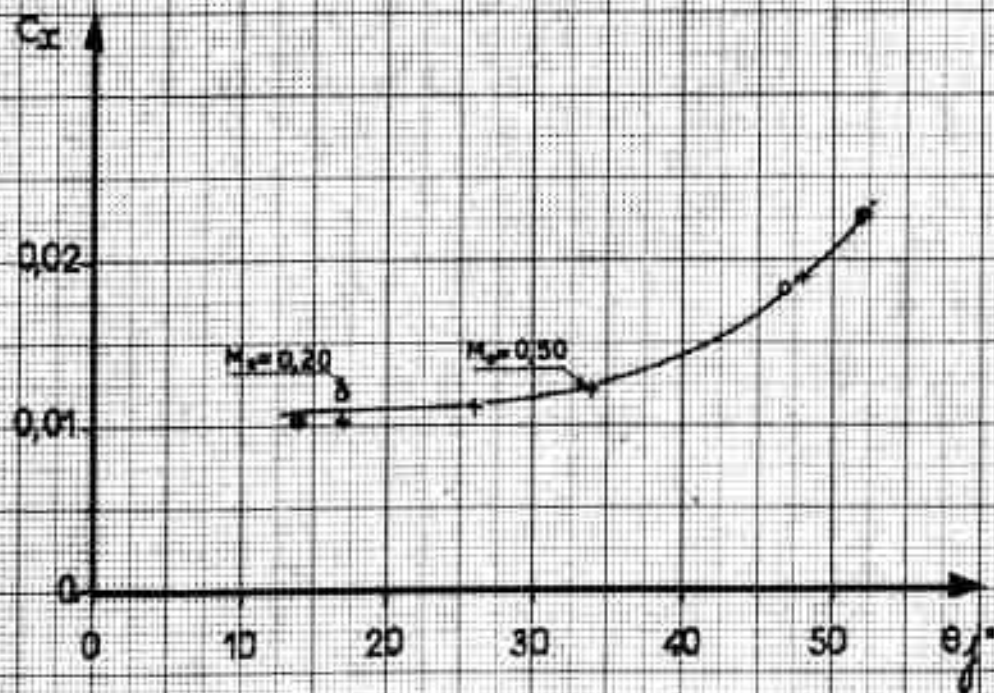
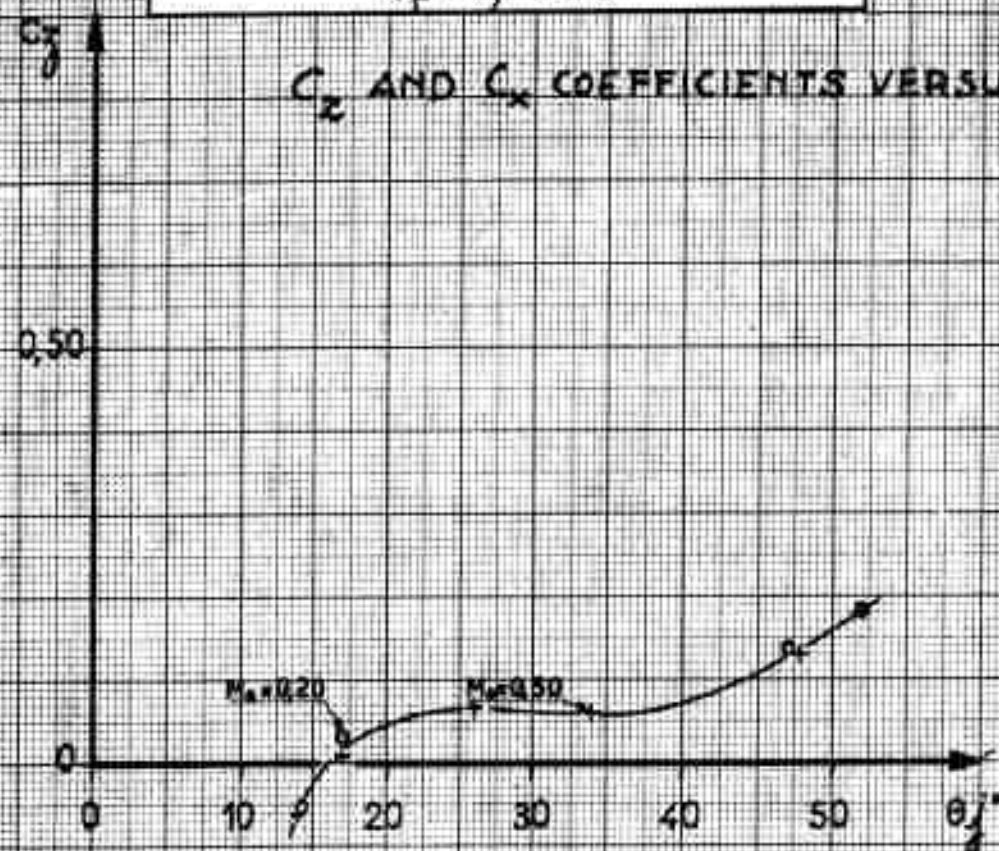
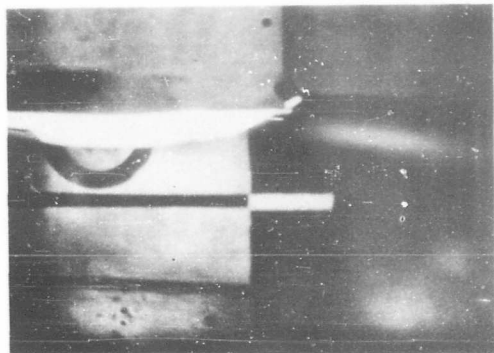
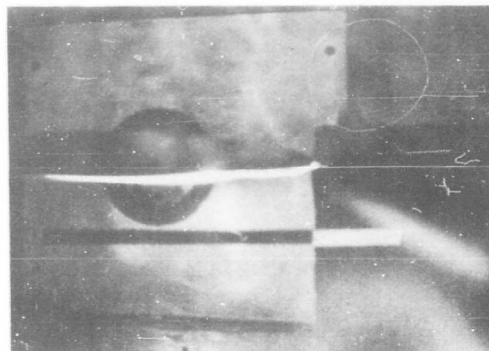
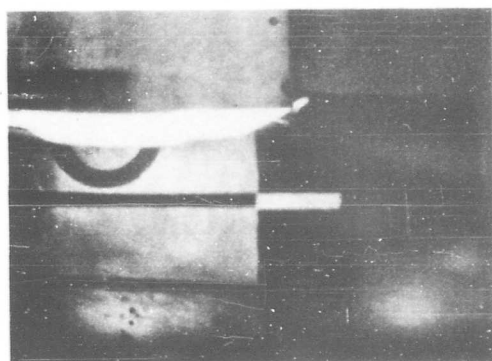
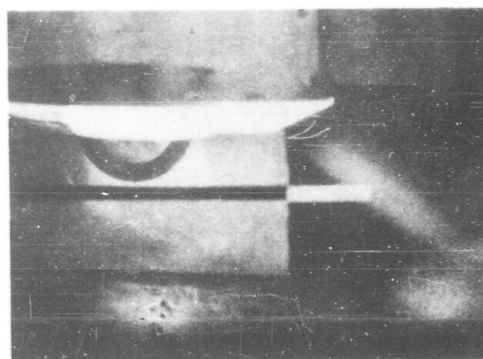
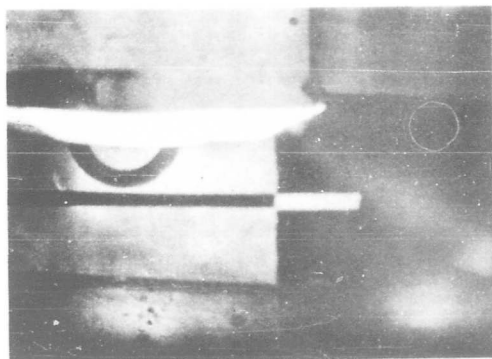
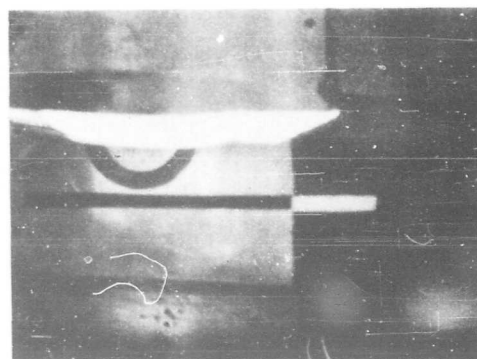
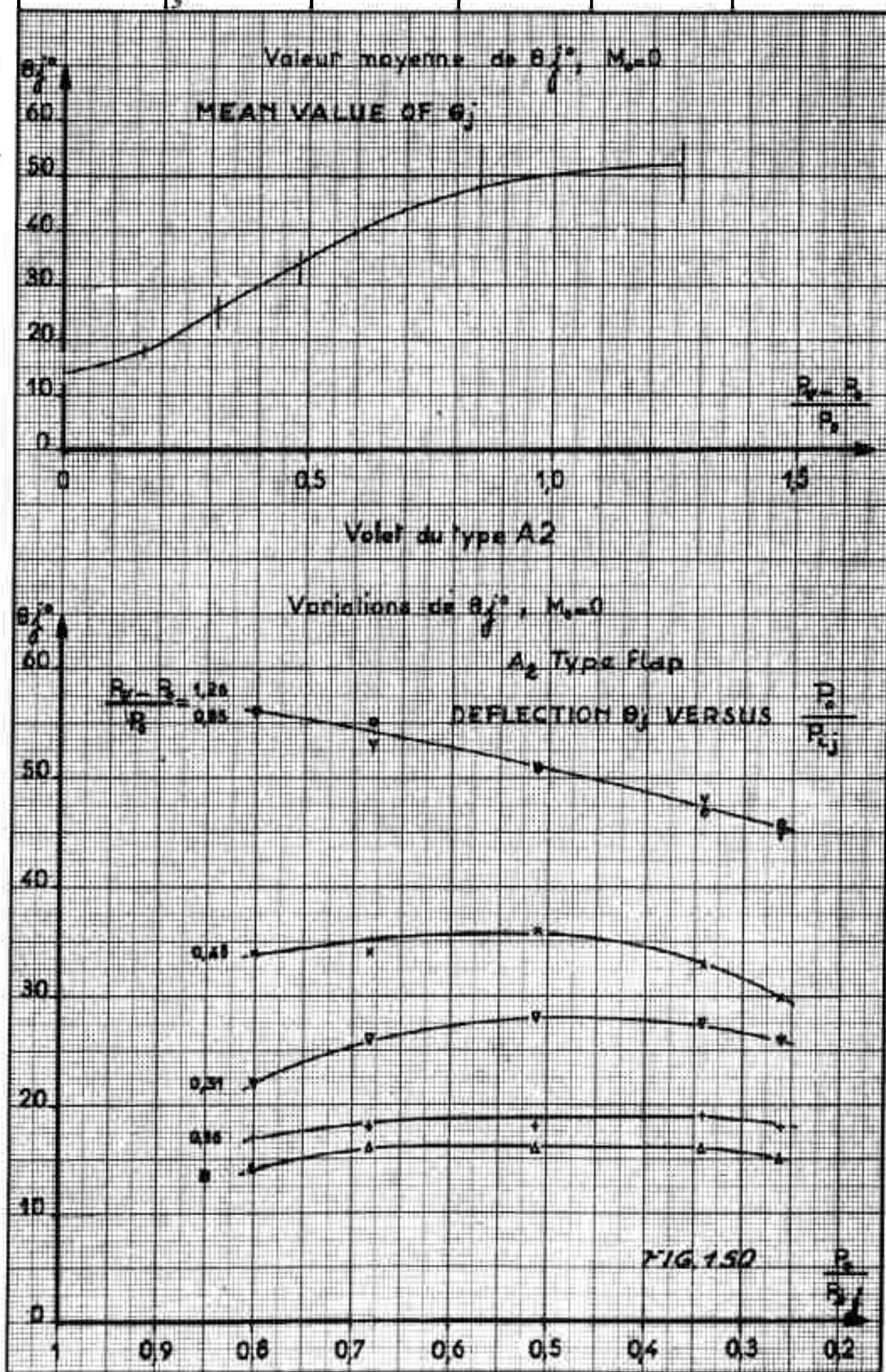


FIG. 14B

DEFLECTED FLOW VISUALIZATION
Tests in S₃Ch Wind Tunnel . Pneumatic Flap. $M_o = 0,10$  $\theta_f = 18^\circ$ $p_{if} = 3 \text{ kg/cm}^2$  $\theta_f = 52^\circ$ $p_{if} = 1 \text{ kg/cm}^2$  $\theta_f = 25^\circ$ $p_{if} = 3 \text{ kg/cm}^2$  $\theta_f = 52^\circ$ $p_{if} = 2 \text{ kg/cm}^2$  $\theta_f = 48^\circ$ $p_{if} = 3 \text{ kg/cm}^2$  $\theta_f = 52^\circ$ $p_{if} = 3 \text{ kg/cm}^2$



ONERA

PV 7/70 JAY

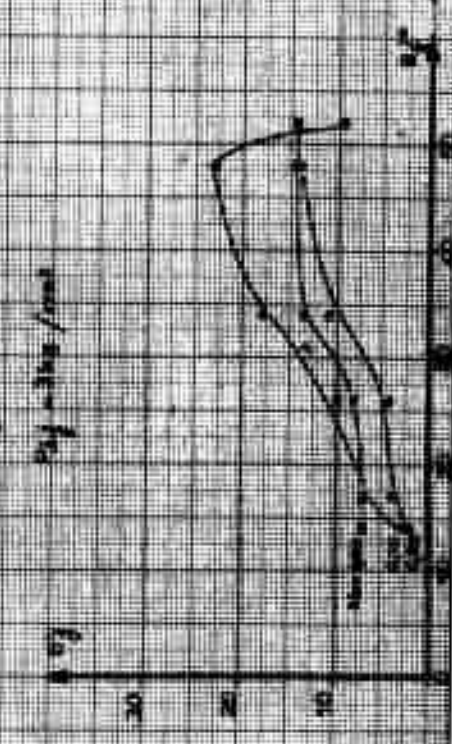
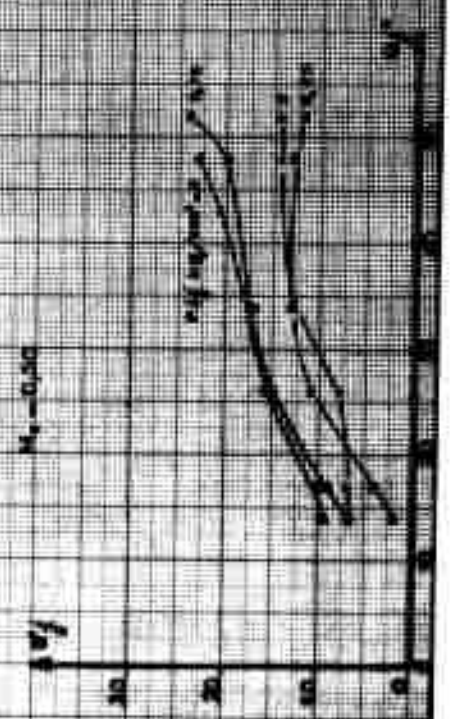
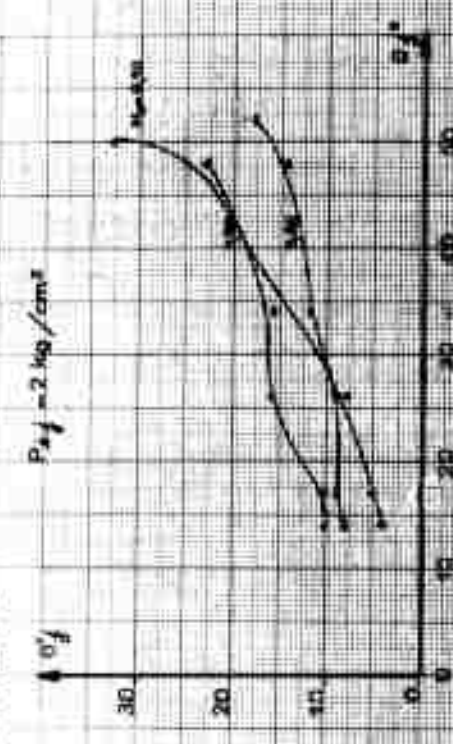
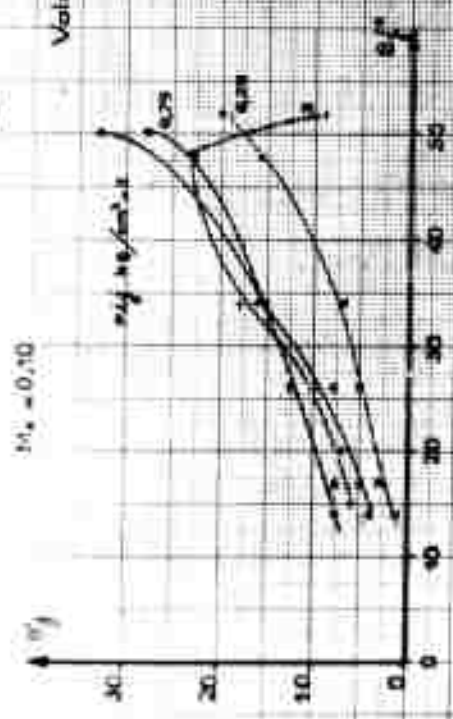
FN 155, S1C1

Destinée par : J. H. J. J. J.

Date : 11-60

B 149

A₂ TYPE FLAP (PNEUMATIC FLAP)



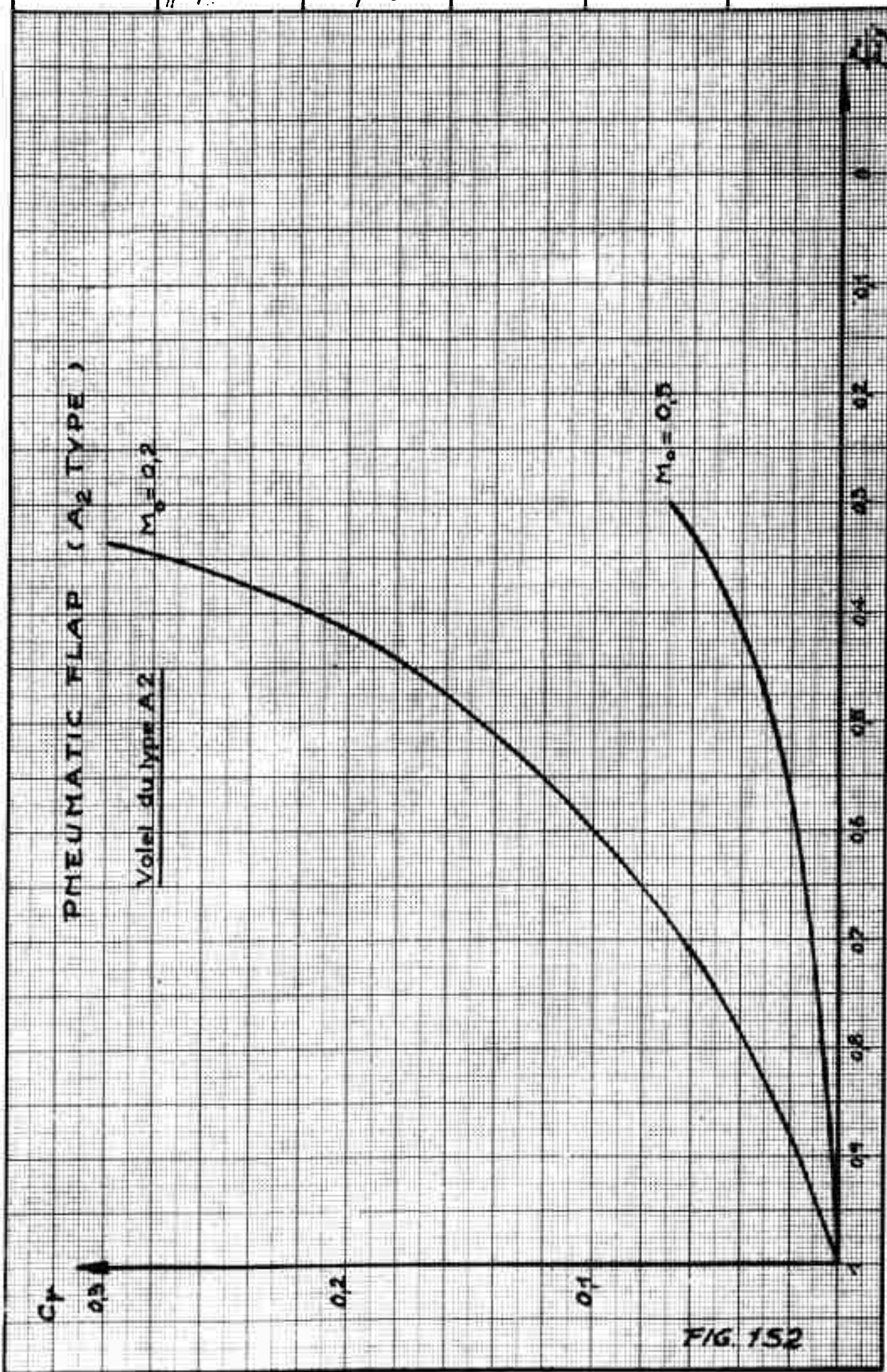
PNEUMATIC FLAP (A₂ TYPE)Volet du type A2 $M_0 = 0,2$ $M_0 = 0,5$ C_F

0,3

0,2

0,1

FIG. 152



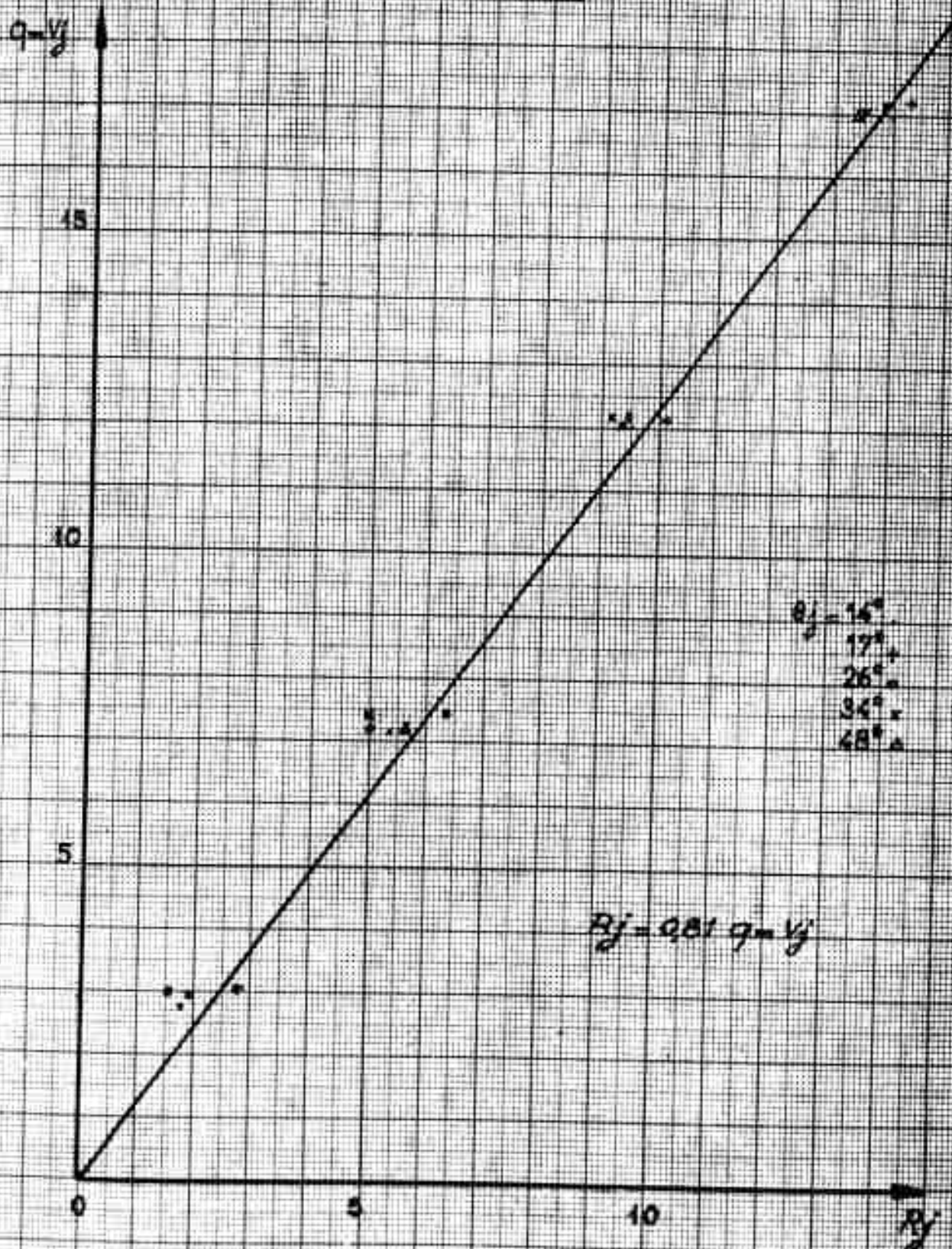
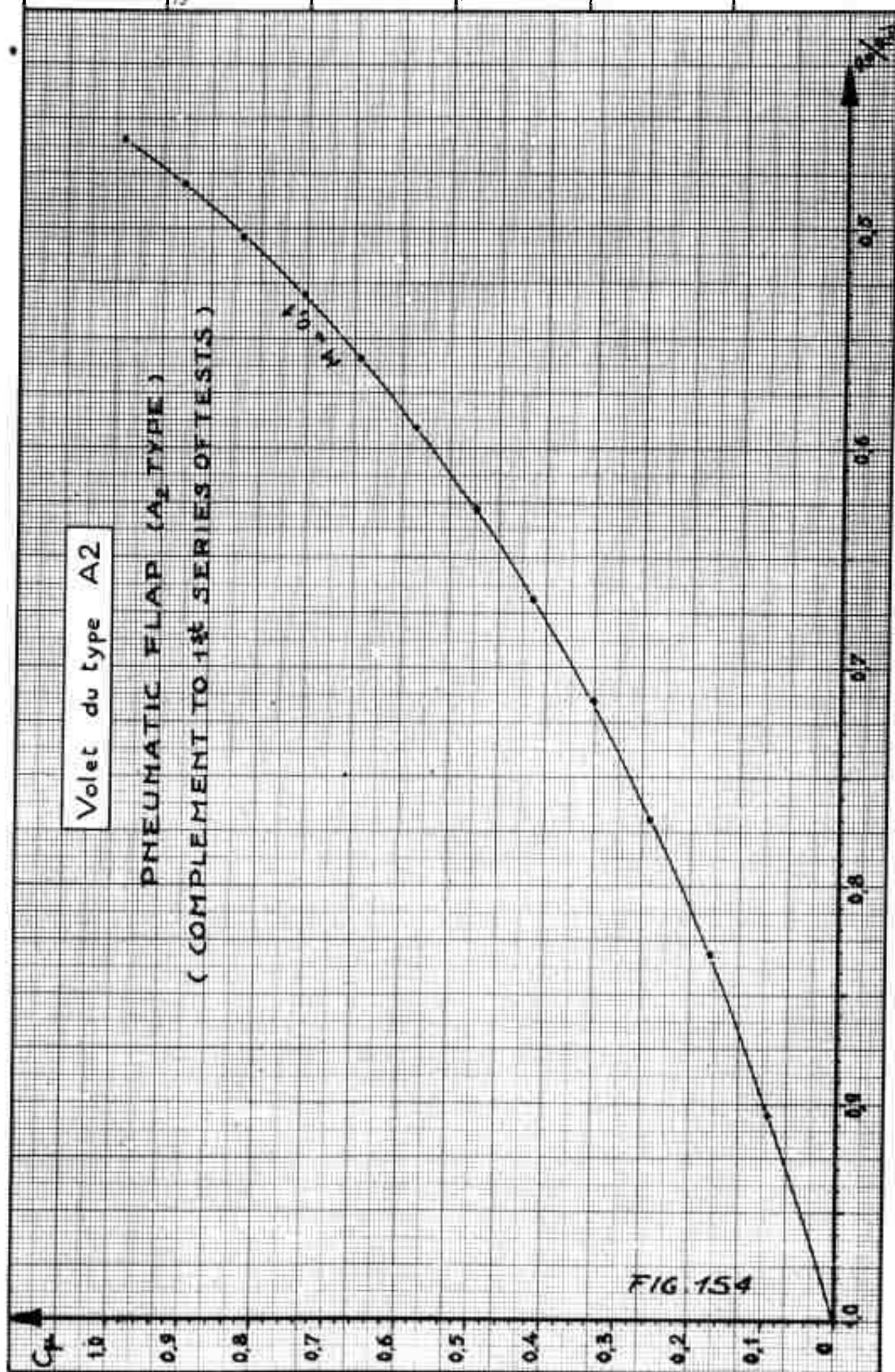
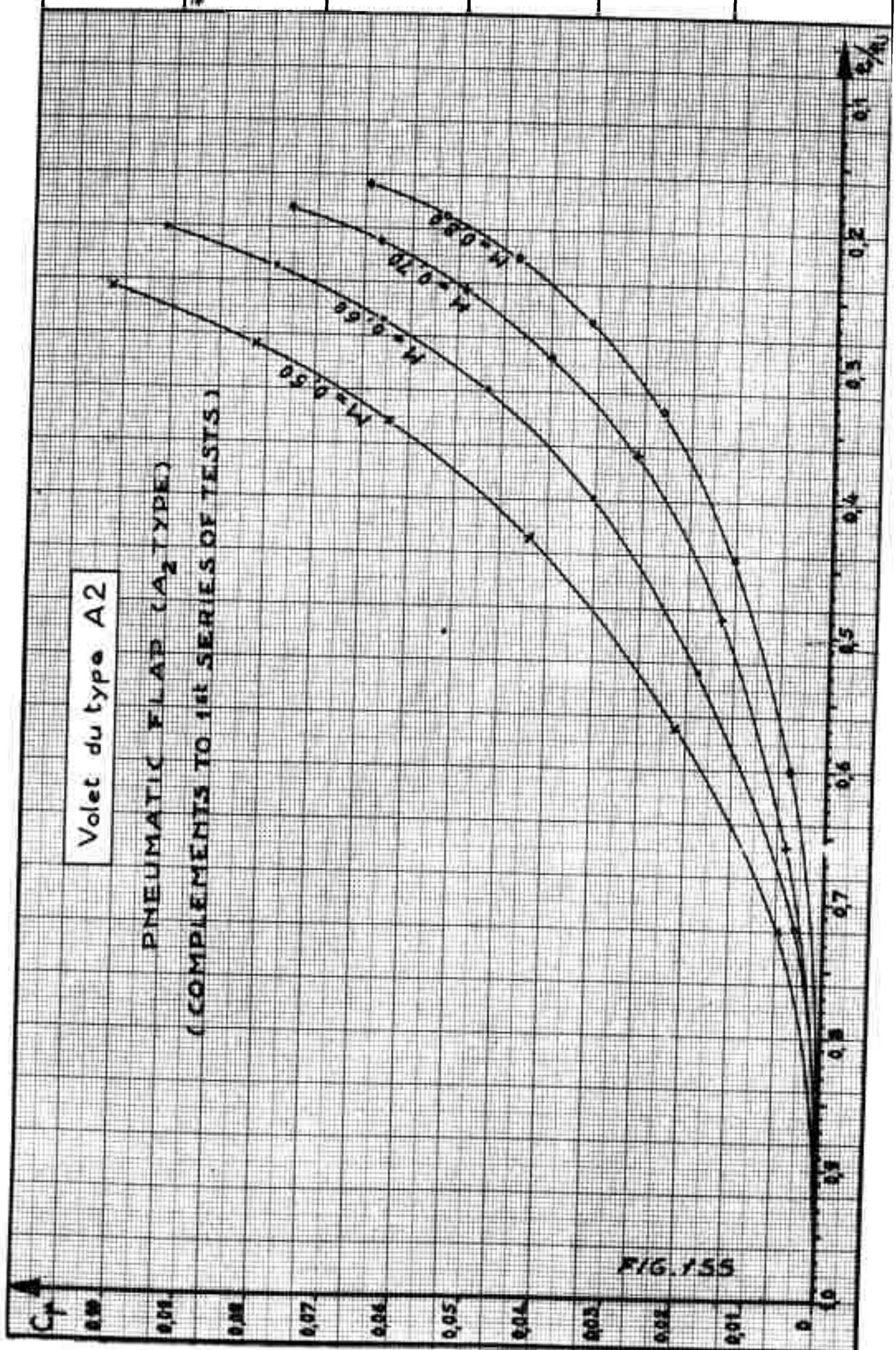
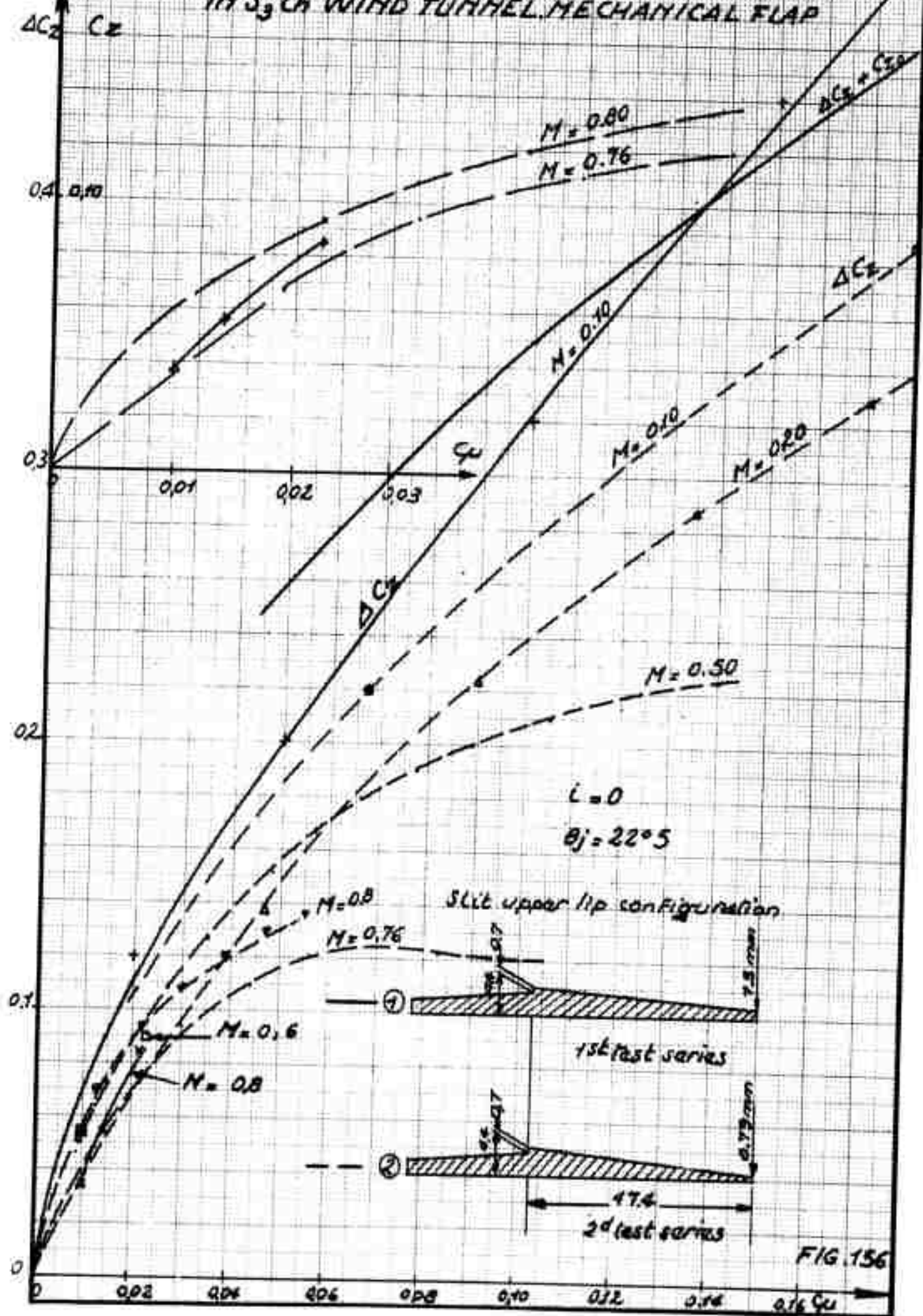
PNEUMATIC FLAP (A₂ TYPE)Volet de type A2

FIG. 153





COMPARISON OF $C_z(q_u)$ CURVES
FOR FIRST AND ADDITIONAL TESTS
IN S_3 CH WIND TUNNEL MECHANICAL FLAP



TESTS IN S₃ CH WIND TUNNEL

B.154

(ADDITIONAL TESTS)

MECHANICAL FLAP

TOTAL SECTION LIFT COEFFICIENT C_L
VERSUS M

$L = 0$

$\theta_j = 22^\circ 5'$

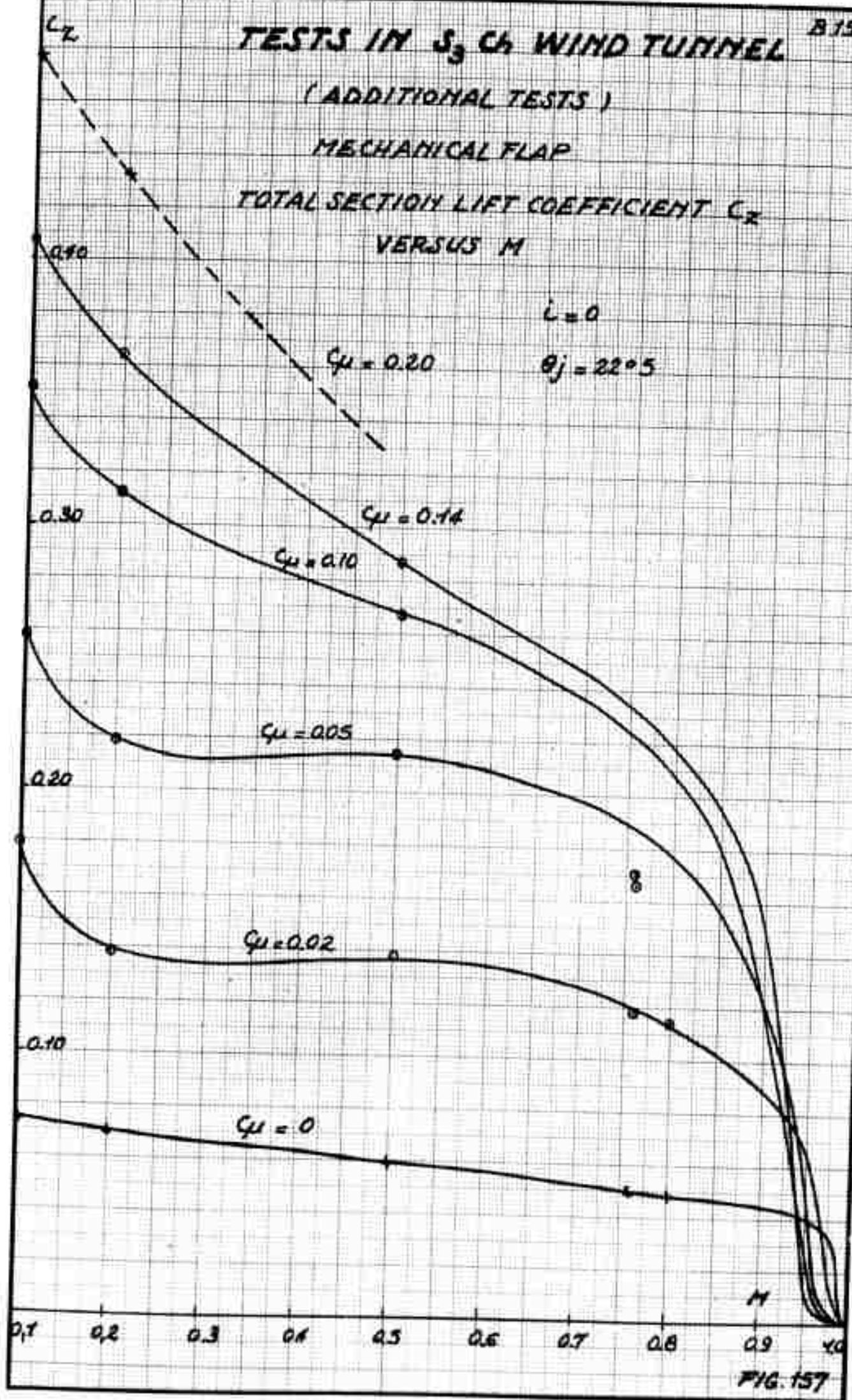


FIG. 157

MECHANICAL FLAP

ADDITIONAL TESTS

A: Mechanically driven rotor with jet flap control

B: Rotor with partial mechanic propulsion and jet flap control.

C: Rotor driven and controlled by jet flaps - cold cycle.

D: Rotor driven and controlled by jet flaps - hot cycle.

E: High speed rotor driven and controlled by jet flaps.

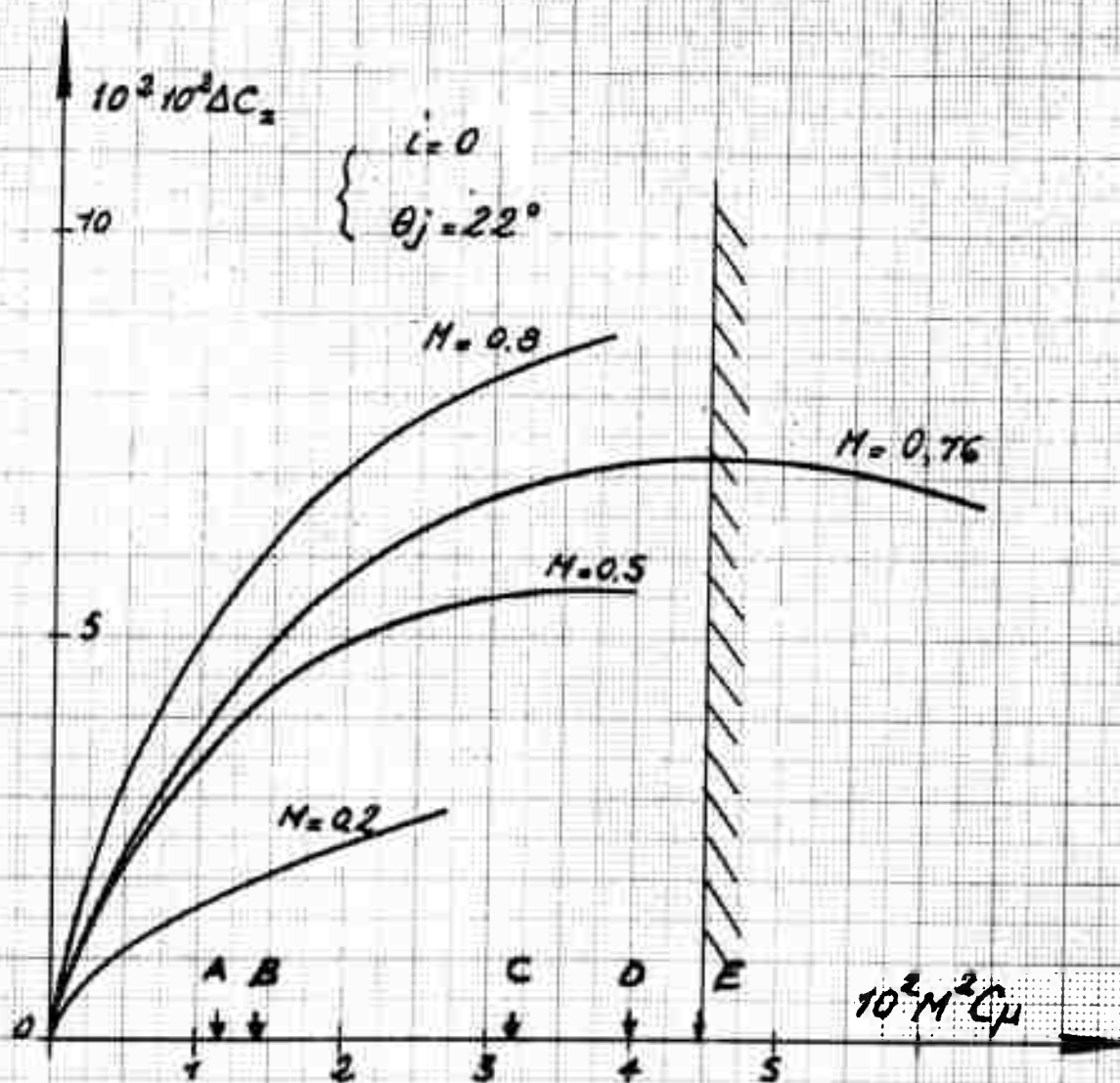


FIG. 138

TESTS IN S₃ Ch WIND TUNNEL PNEUMATIC FLAP

B.156

TOTAL SECTION LIFT COEFFICIENT C_z
VERSUS M

$i = 0$

$\theta_j = 30^\circ$

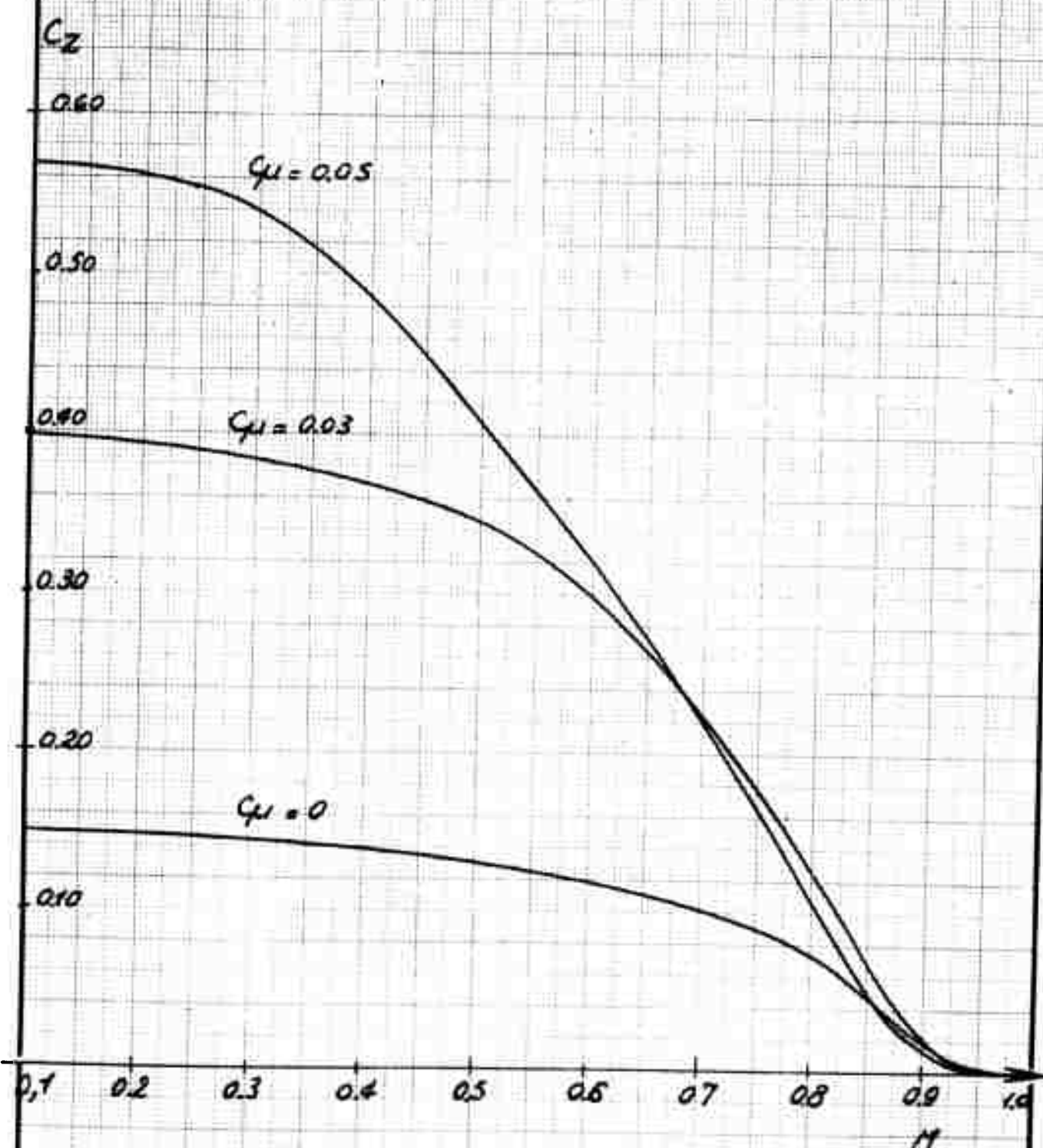


FIG. 159

TESTS IN S_3 CH WIND TUNNEL

PNEUMATIC FLAP

$\left. \begin{matrix} A \\ B \\ C \\ D \\ E \end{matrix} \right\}$ See FIG

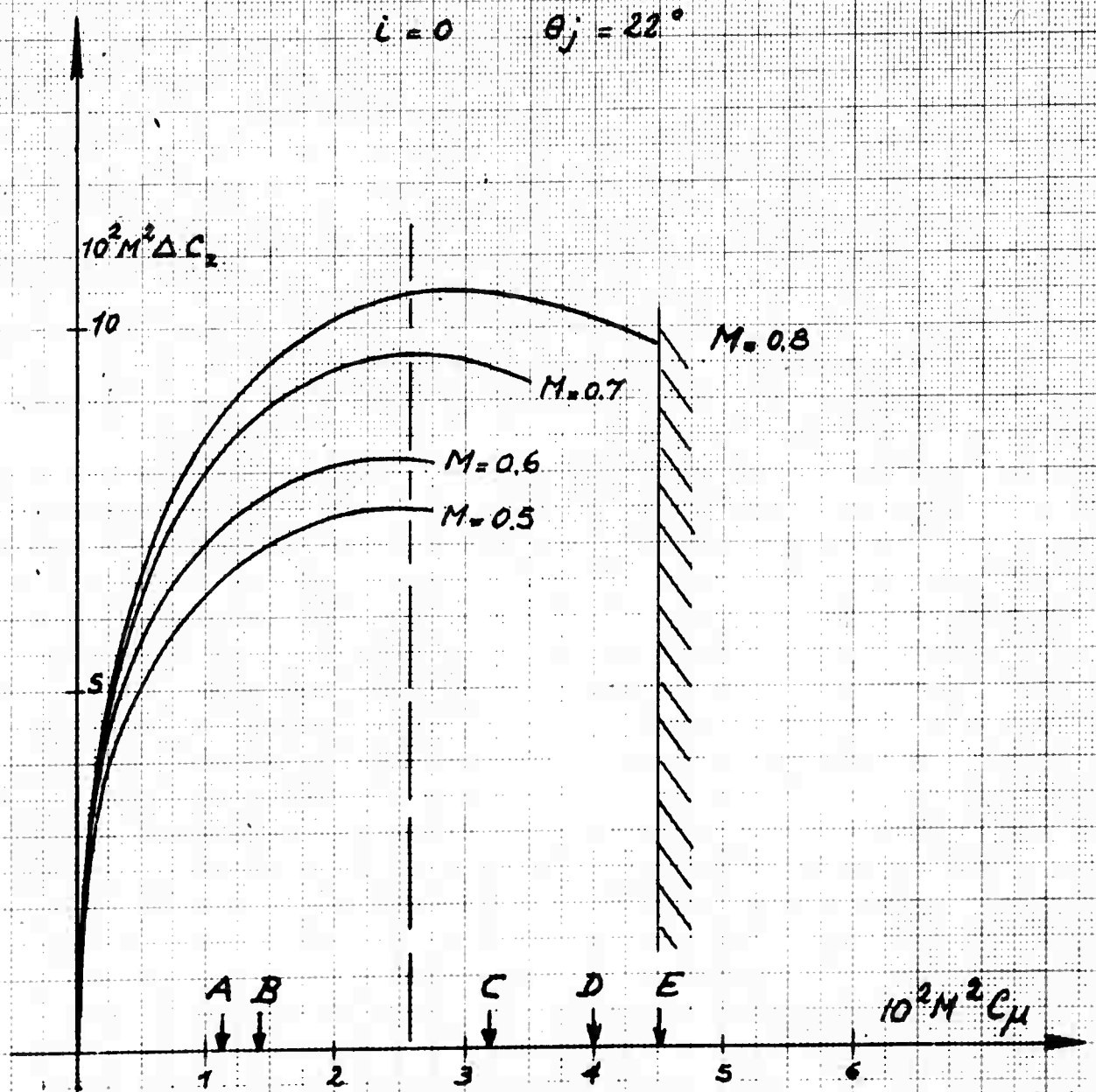


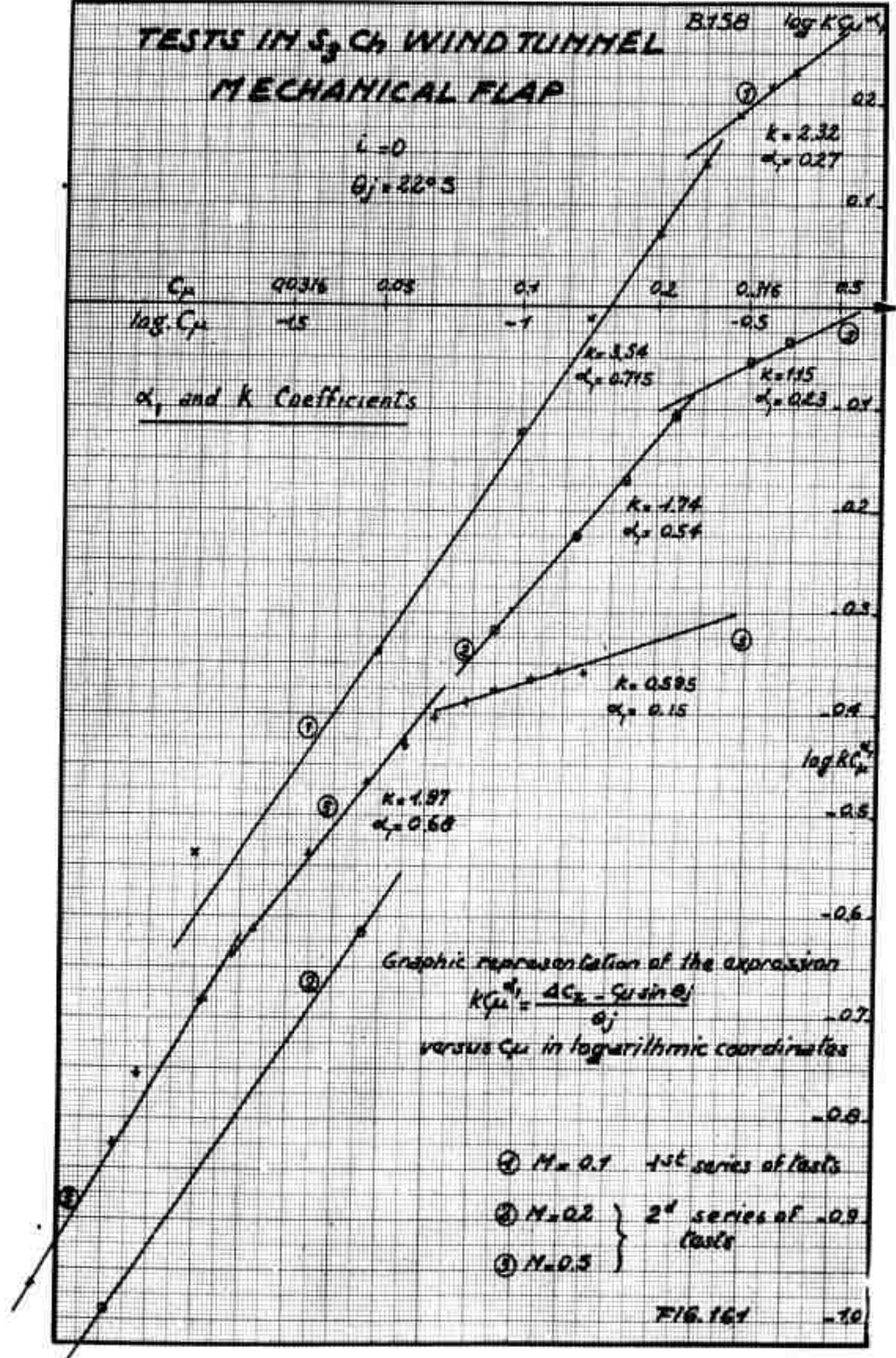
FIG. 160

TESTS IN S₃ CH WIND TUNNEL MECHANICAL FLAP

B158 $\log KC_u K_f$

$i = 0$
 $\theta_j = 22^\circ 3$

C_p 0.0316 0.05 0.1 0.2 0.316 0.5
 $\log C_p$ -1.5 -1 -0.5 0 0.5
 α_j and k Coefficients



TESTS IN S_1 CH WIND TUNNEL MECHANICAL FLAP EFFECT OF C_M

B.159

$i = 0$ $V_0 = 22 \text{ m/s}$

θ_j	α	$\sin \theta_j$	$\frac{dC_z}{d\alpha}$	Δ_2
3	-12	0.0525	0.0157	0.036
15	0	0.259		0.028
37.5	22.5	0.61	0.0292	0.034
52.5	37.5	0.795	0.0276	0.034

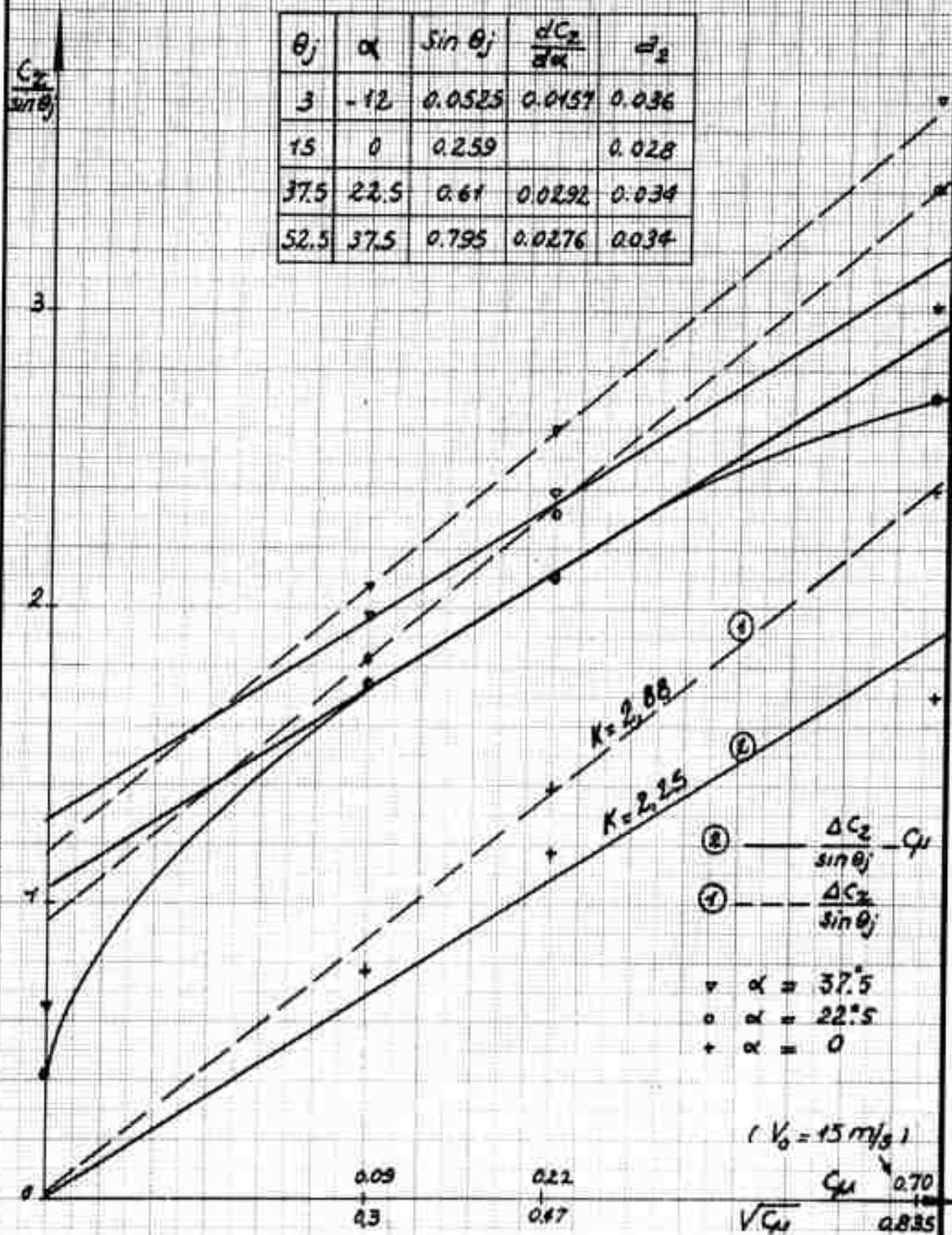


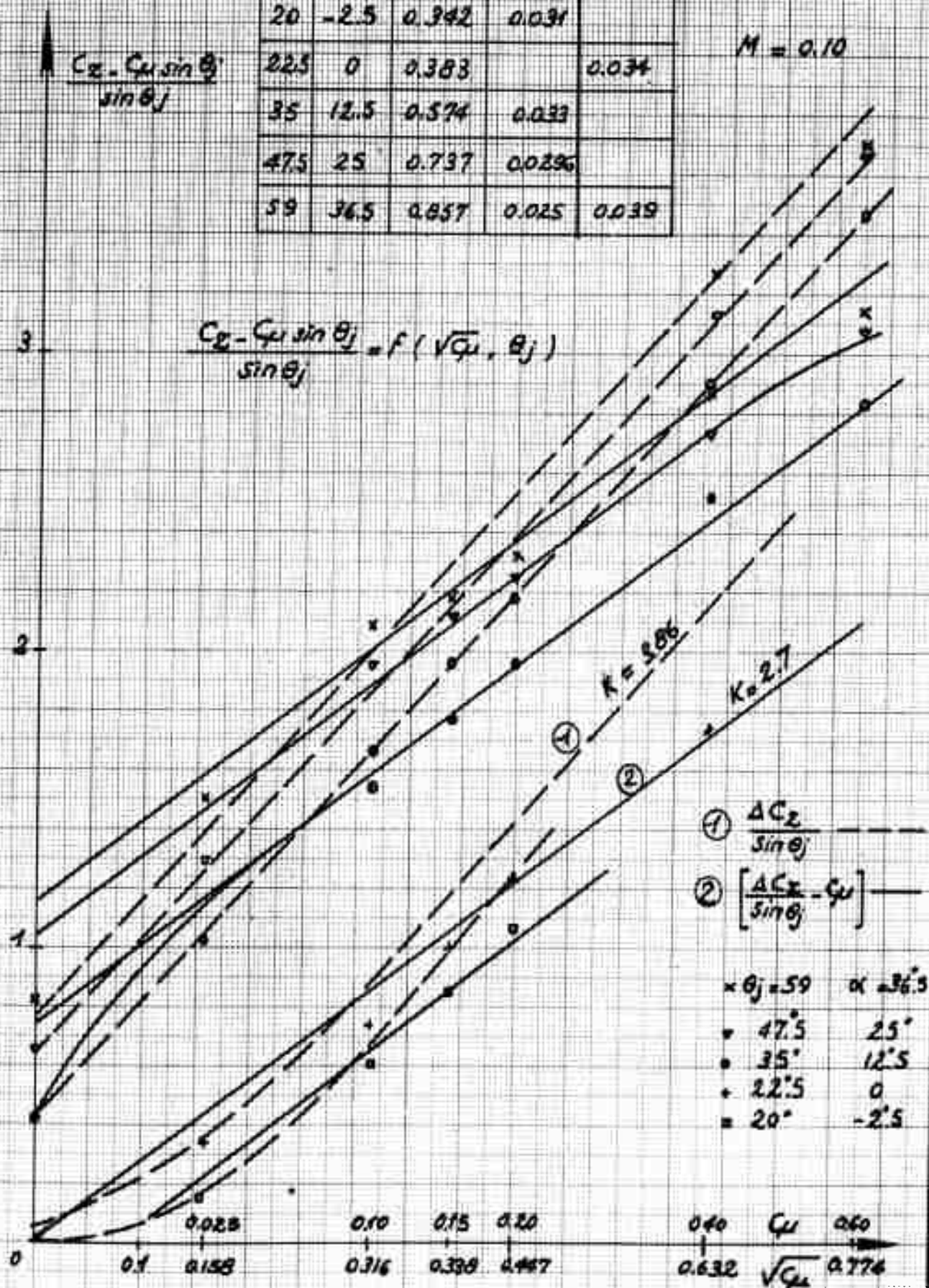
FIG. 162

TESTS IN S_3 CH WIND TUNNEL MECHANICAL FLAP

θ_j°	α°	$\sin \theta_j$	$\frac{\Delta C_z}{\Delta \alpha}$	d_z
20	-2.5	0.342	0.031	
22.5	0	0.383		0.034
35	12.5	0.574	0.033	
47.5	25	0.737	0.0296	
59	36.5	0.857	0.025	0.039

$$i = 0$$

$$M = 0.10$$

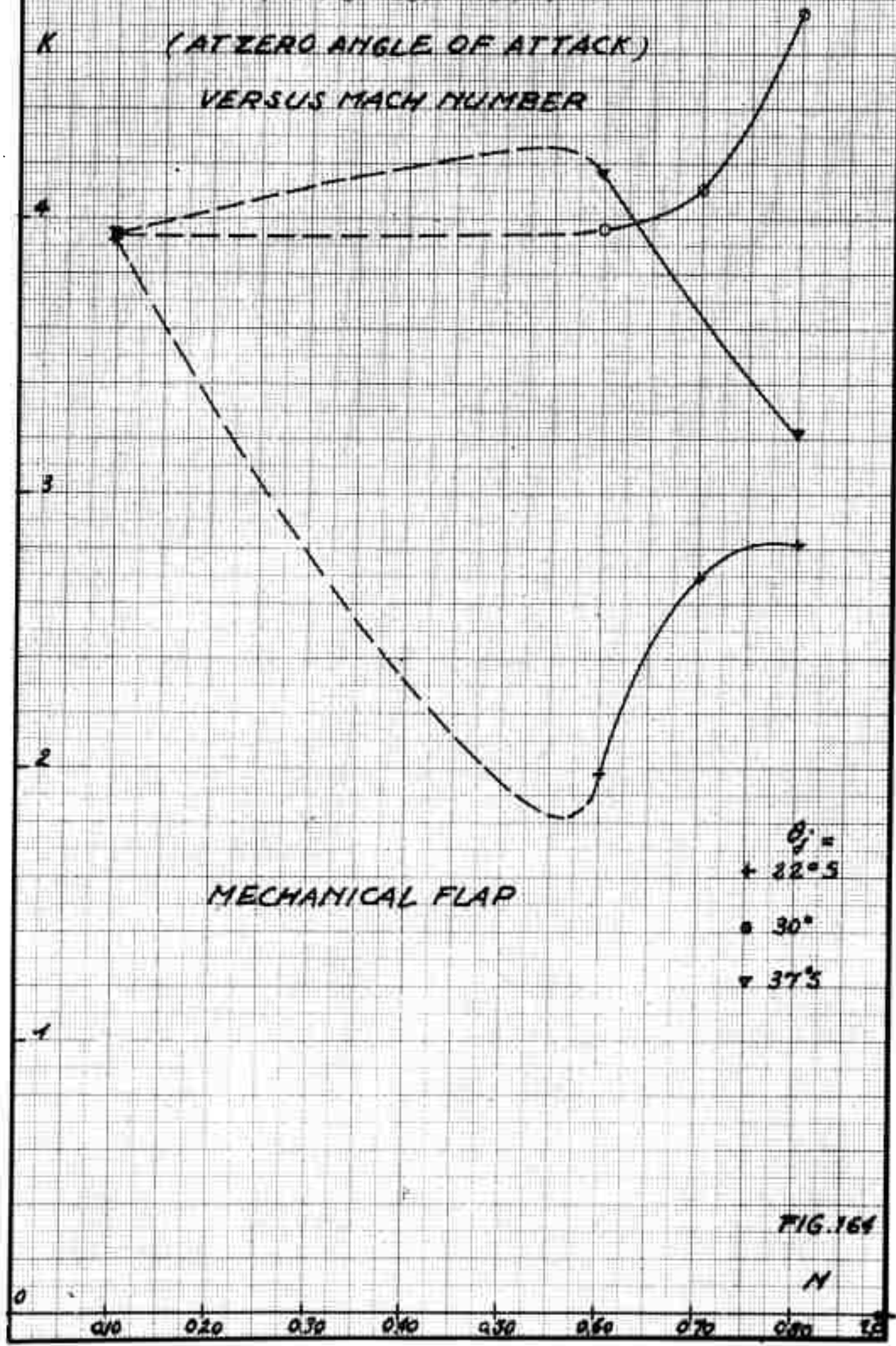


TESTS IN S₃ Ch WIND TUNNEL

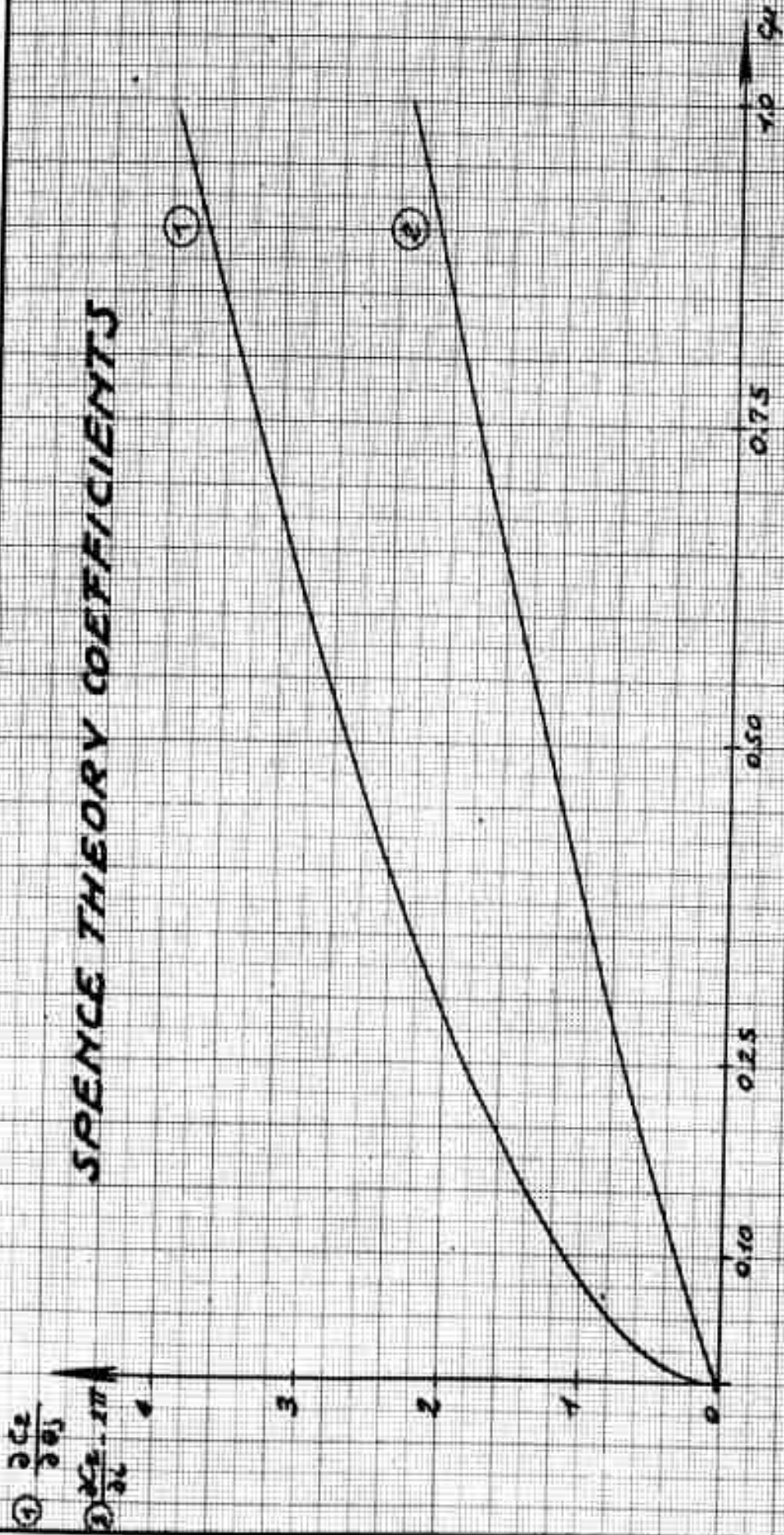
VARIATION OF COEFFICIENT K

(AT ZERO ANGLE OF ATTACK)

VERSUS MACH NUMBER



SPENCE THEORY COEFFICIENTS



$$\frac{\partial C_z}{\partial c} = 2\pi = 1.452 C_\mu^{1/2} + 1.106 C_\mu + 0.054 C_\mu^{3/2}$$

$$\frac{\partial C_z}{\partial \theta_j} = 3.54 C_\mu^{1/2} + 0.325 C_\mu + 0.156 C_\mu^{3/2}$$

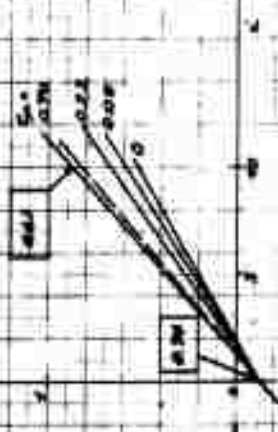
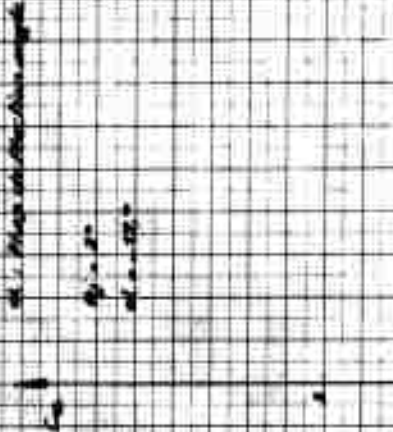
FIG. 165

11/11/2009 11:11 AM

FLAP COPY C11
6-38 6 18 ml

1

100



1000

$\mu = 0.10$
$$\theta_j = 47.5^\circ$$
$$C_{12} = 0.48$$
$$\theta_j = 22.5^\circ$$
$$C_3 \quad \theta_j = 59^\circ$$

Test results

Spurious theoretical slope.

Efficiency of Step compared to:
 Gauss Theory.

B 164

FIG. 163

COMPARISON BETWEEN TEST RESULTS AND SPENCE THEORY FLAP EFFICIENCY

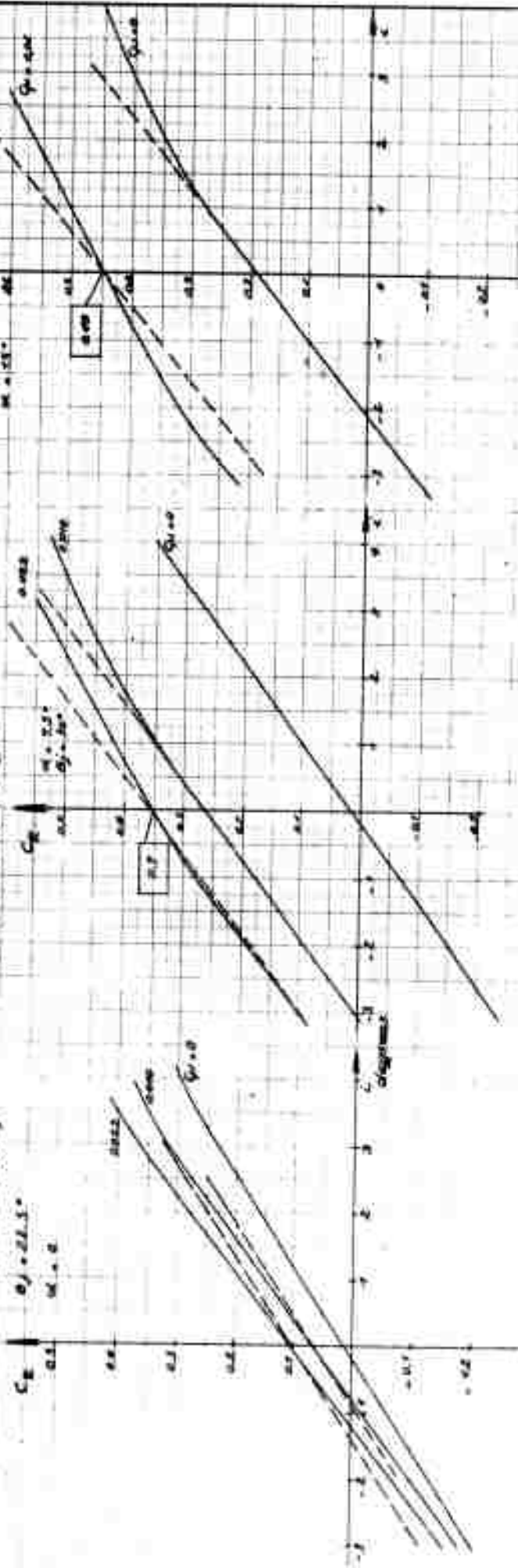
EFFECT OF C_u FOR $N=0.60$

TESTS IN S_3 CH WIND TUNNEL - θ_j : flap deflection angle
 α : flap deflection angle

(1" Test series)
 $\theta_j = 21.5^\circ$
 $\alpha = 0$

$\theta_j = 23^\circ$
 $\alpha = 30^\circ$

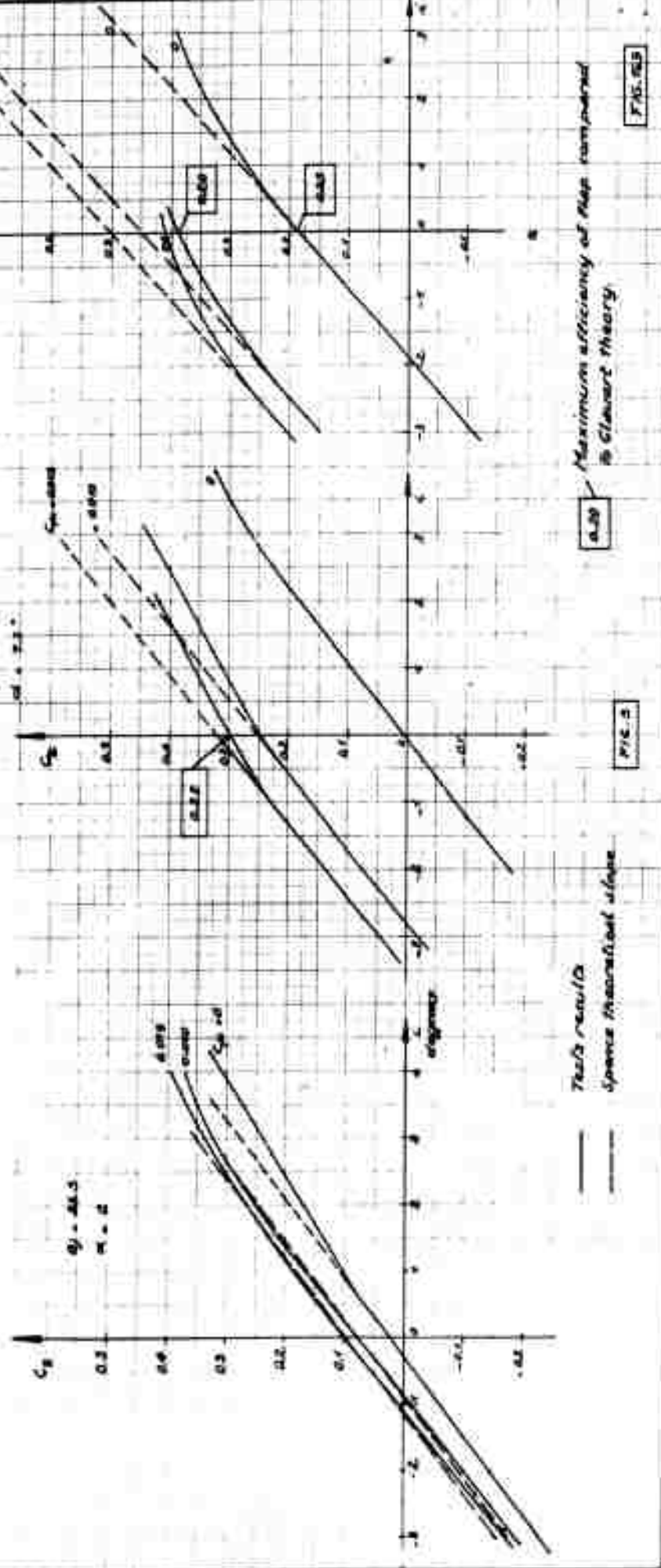
$\theta_j = 22.5^\circ$
 $\alpha = 15^\circ$



— Tests results
 --- Spence theoretical slope

C_u — Efficiency of flap compared to Glauert theory

COMPARISON BETWEEN TEST RESULTS AND SPENCE THEORY EFFECT OF C_H TESTS IN S_3 CH WIND TUNNEL (1st Test series)



Test results
 Spence theoretical slope

Maximum efficiency of flap compared
 to Clamart theory

FIG. 3

COMPARISON BETWEEN TEST RESULTS AND SPENCE THEORY EFFECT OF C_u

TESTS IN S_3 CH WIND TUNNEL
(1st Test series)

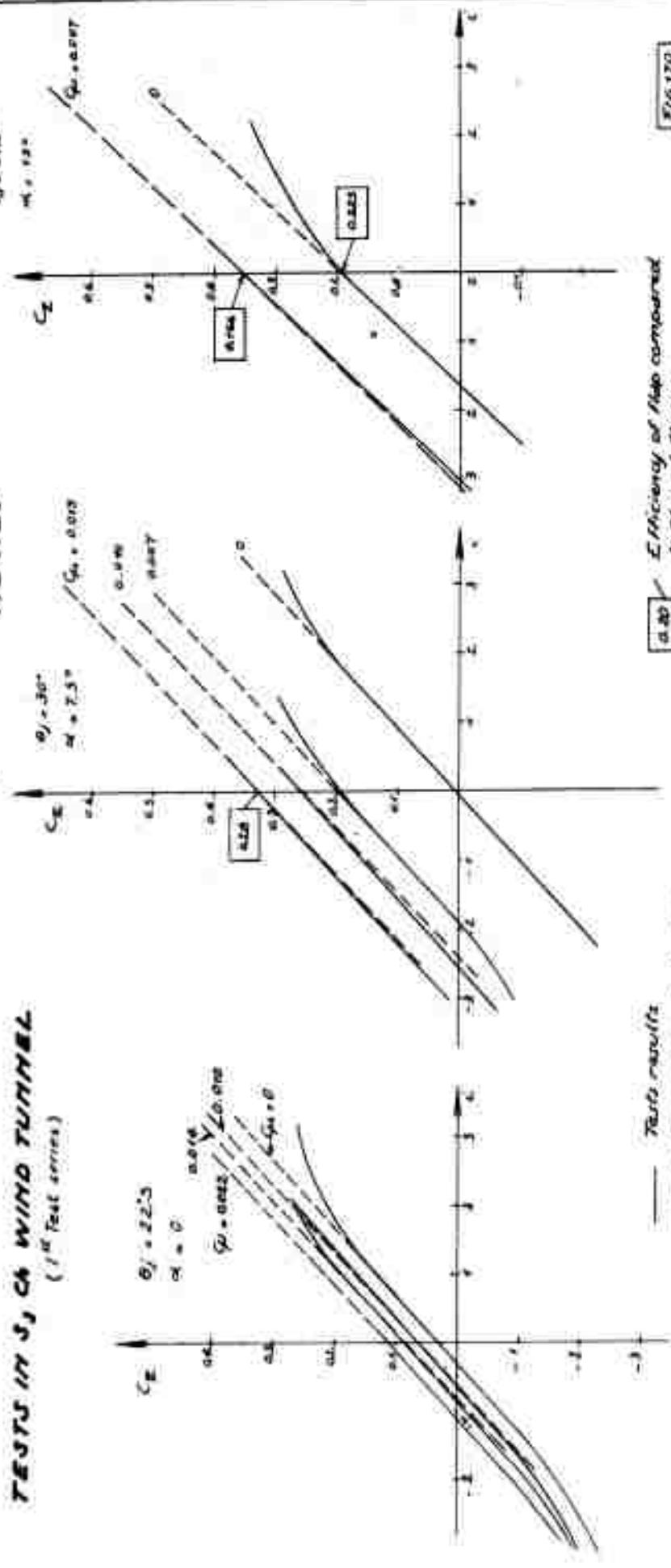
$M = 0.80$

FIGURE

$\theta_j = 27.5^\circ$
 $\alpha = 12^\circ$

$\theta_j = 30^\circ$
 $\alpha = 7.5^\circ$

$\theta_j = 22.5^\circ$
 $\alpha = 0^\circ$



— Tests results
--- Spence theoretical slope

0.20 Efficiency of flap compared to Clavet theory.

FIG. 170

COMPARISON
BETWEEN TEST RESULTS
AND SPENCE THEORY

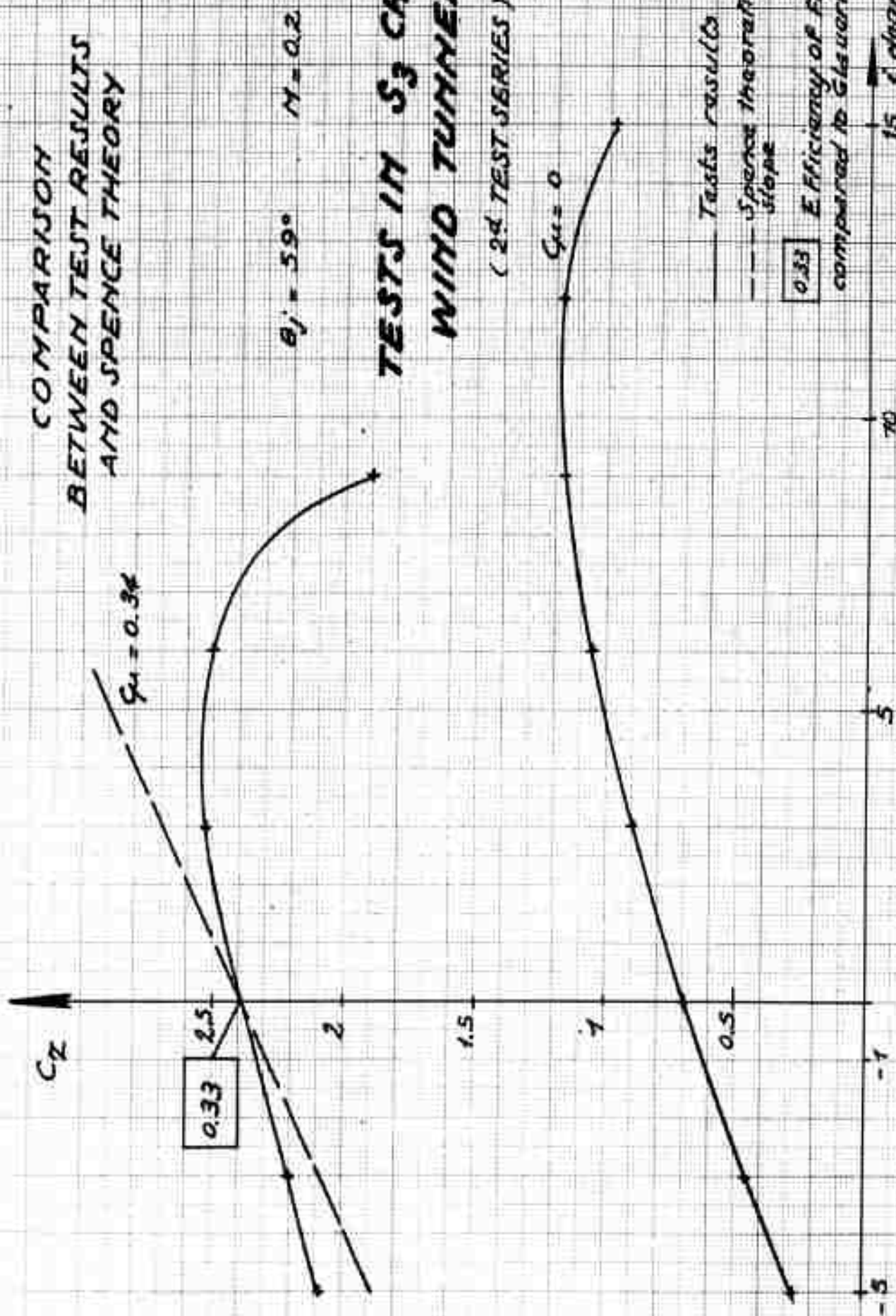


FIG. 171.

**TESTS IN S_3 CH
WIND TUNNEL**
(2^d TEST SERIES)

**COMPARISON BETWEEN TEST RESULTS
AND SPENCE THEORY**

C_x

$\theta_j: 22.5^\circ$

$M = 0.1$

$Q_u = 0.18$

$Q_u = 0.067$

$Q_u = 0$

Tests results

Spence theoretical slope

Efficiency of flow com-
pared to Glauert theory



α
degrees

B 169

FIG. 172

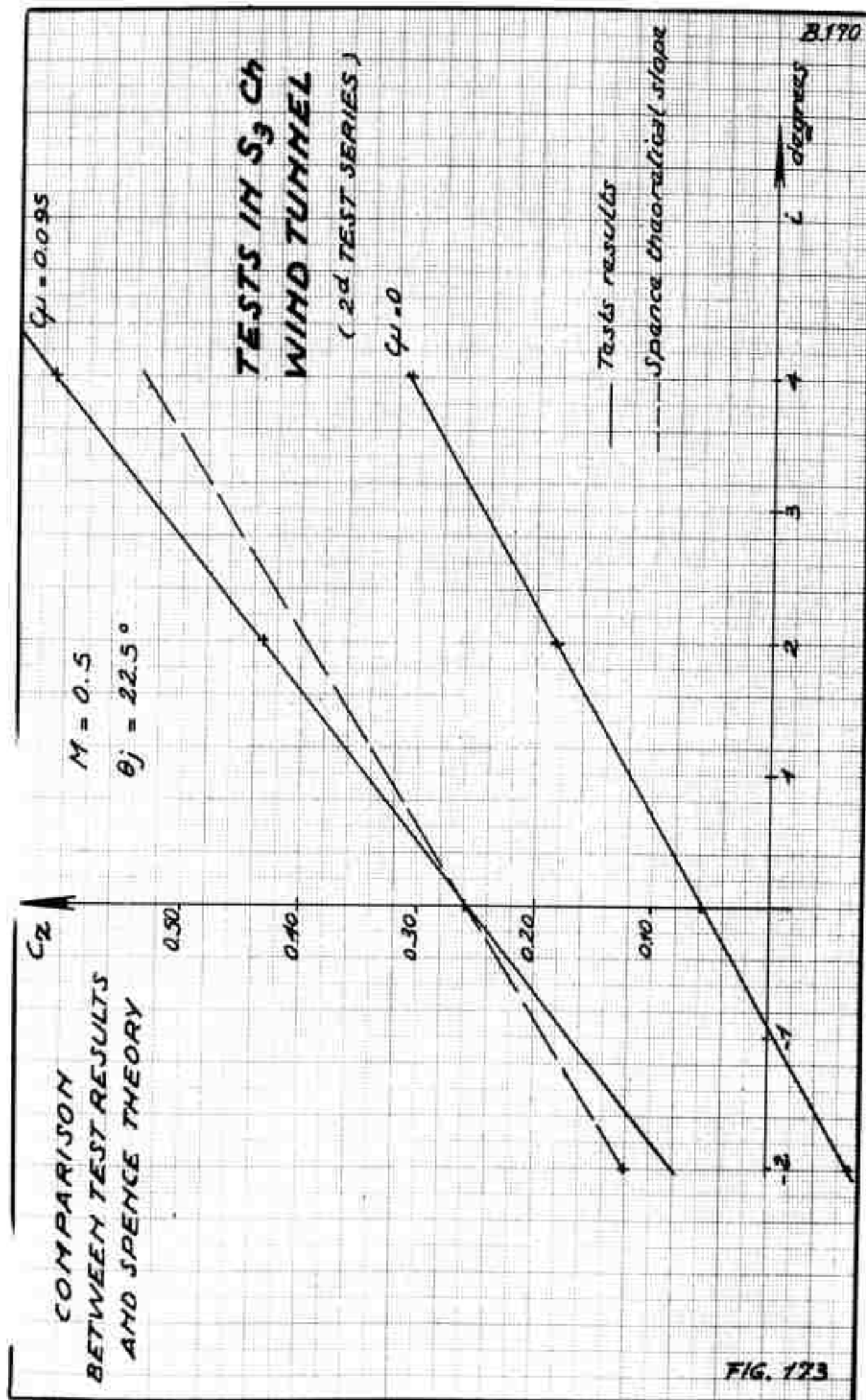


FIG. 173

COMPARISON
BETWEEN TEST RESULTS
AND SPENCE THEO.

TESTS IN S_3 CH
WIND TUNNEL

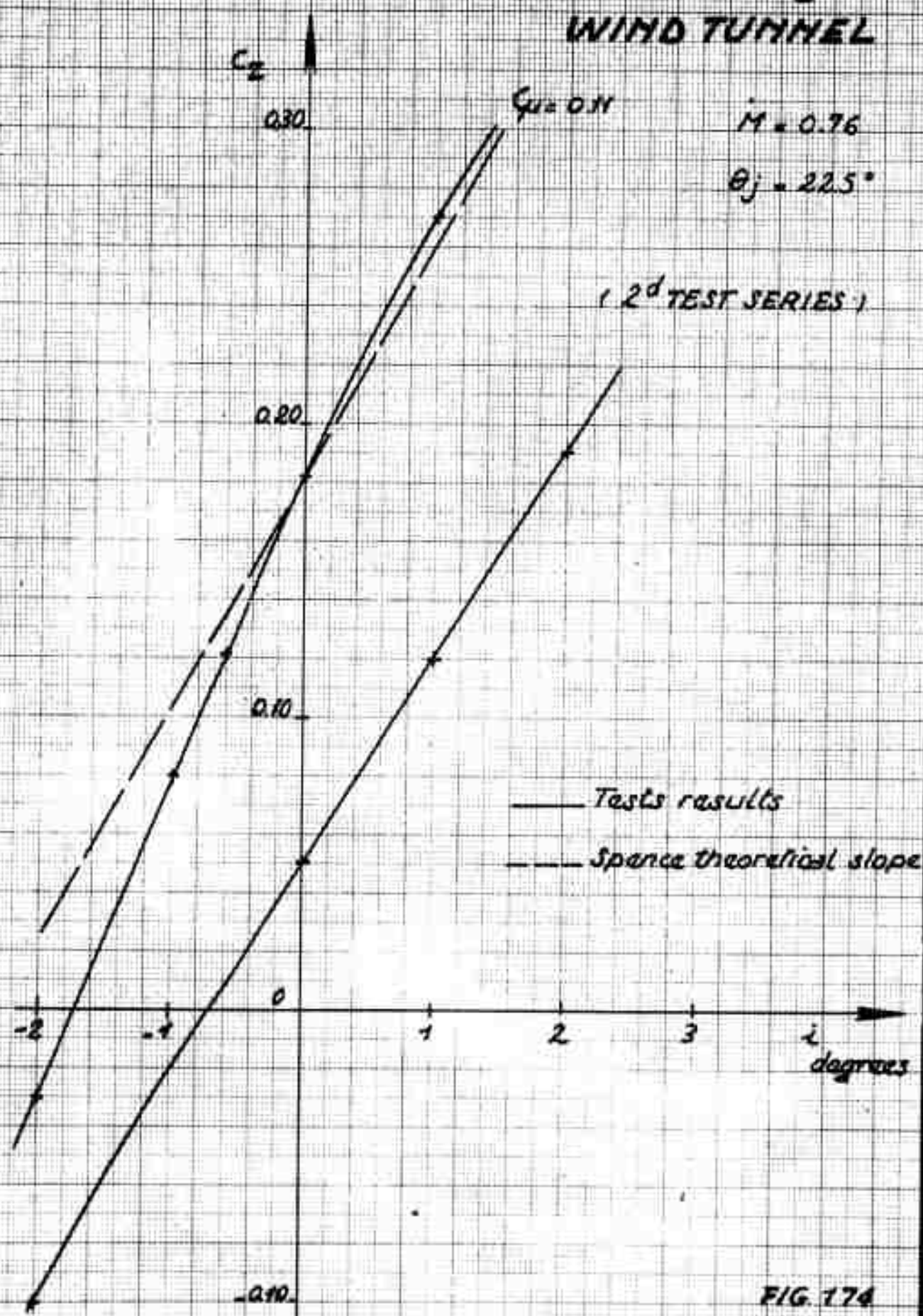


FIG. 174

COMPARISON
BETWEEN
TEST RESULTS
AND SPENCE THEORY

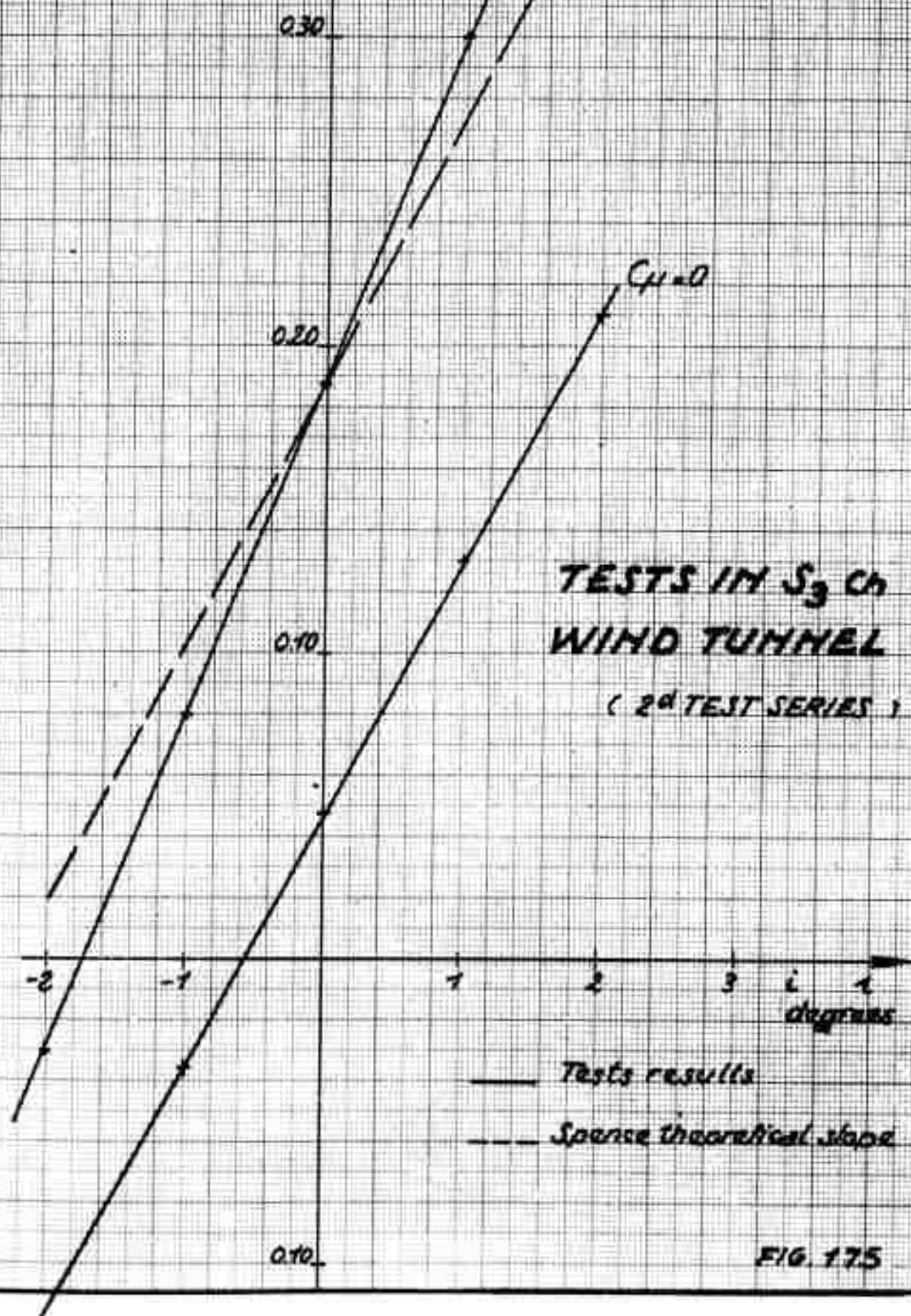
 $M = 0.8$
 $\theta_j = 22.5^\circ$


FIG. 175

TESTS IN S_3 CH WIND TUNNEL

PNEUMATIC FLAP

ASPECT RATIO $A=6$

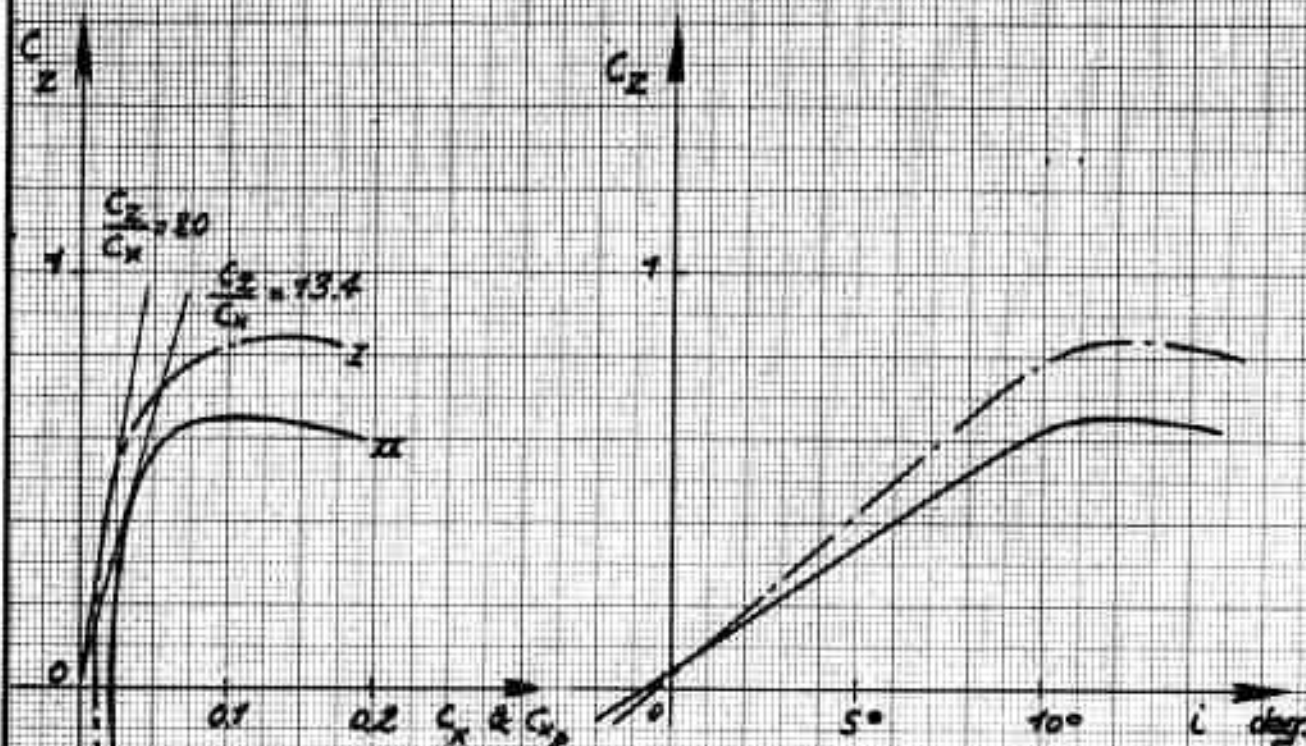


FIG. 176

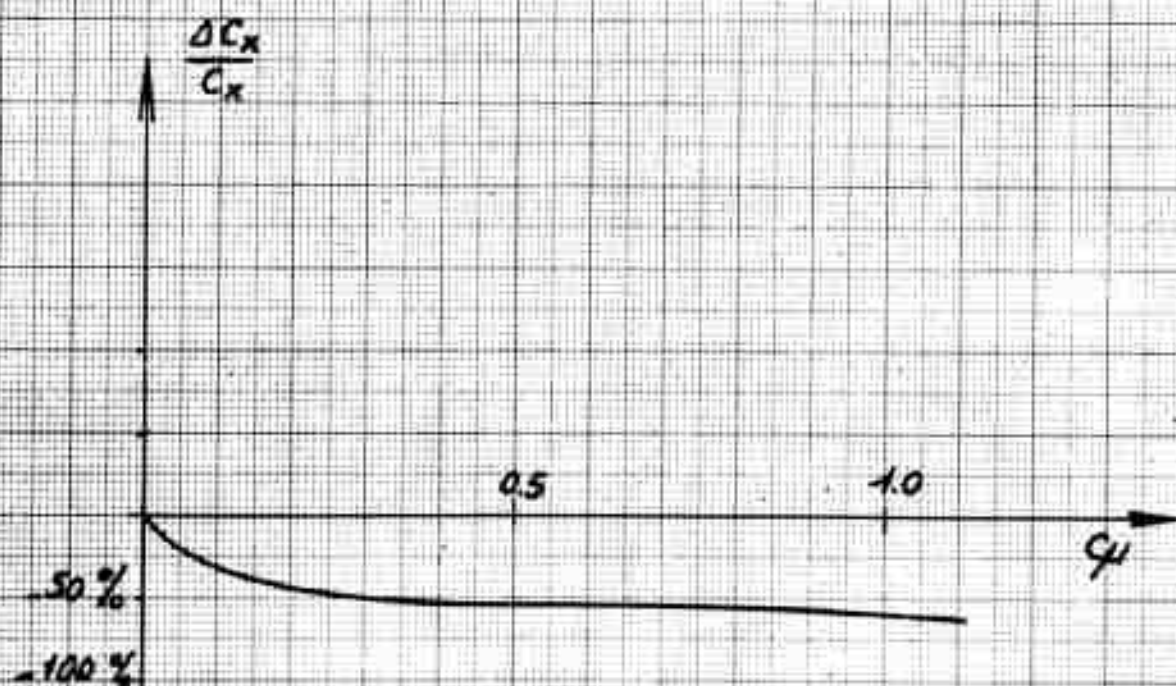
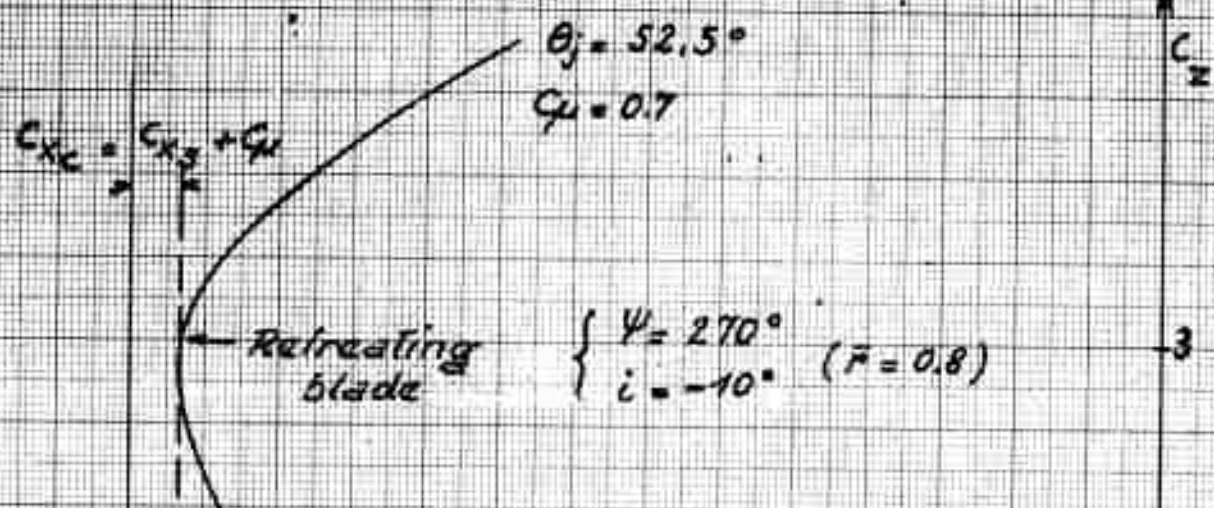


FIG. 177

TESTS IN S_1 CH WIND TUNNEL

MECHANICAL FLAP

ASPECT RATIO $A = \infty$



(Blowing conditions adapted to a jet-driven rotor)

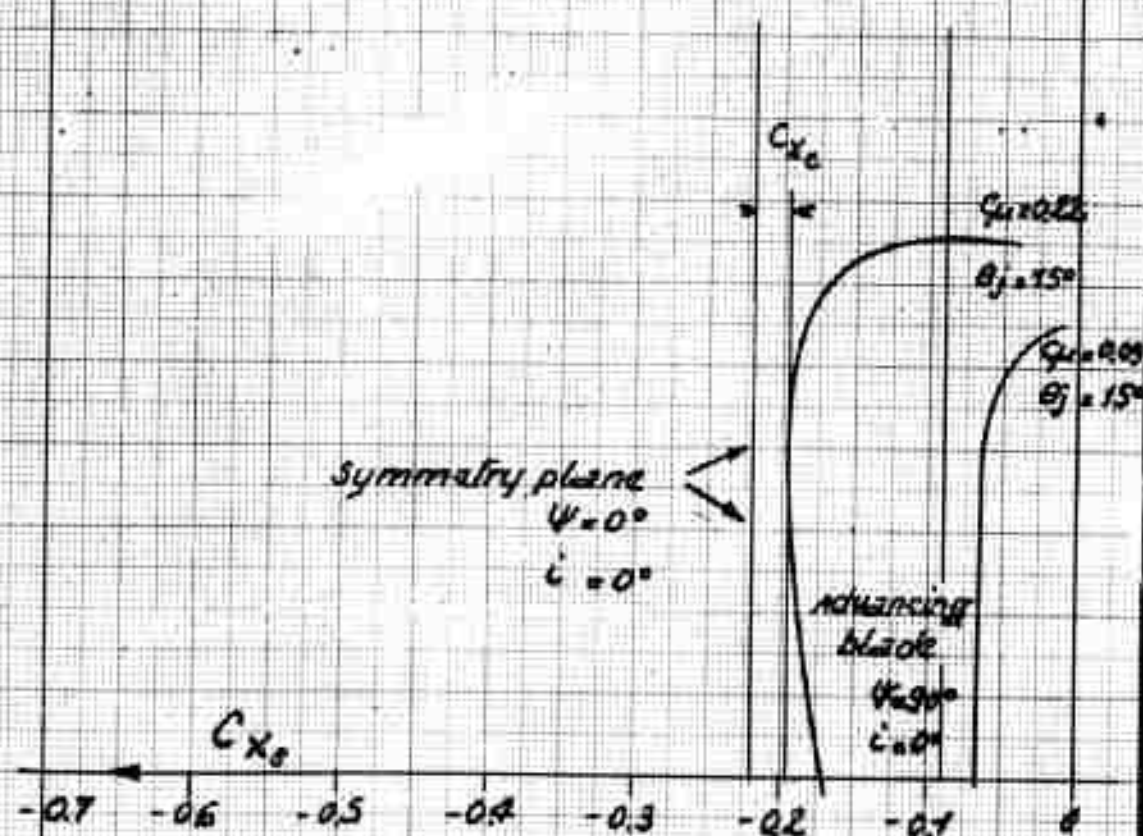


FIG. 176

TESTS IN S_1 CH WIND TUNNEL

PNEUMATIC FLAP

B175

ASPECT RATIO $A = \infty$

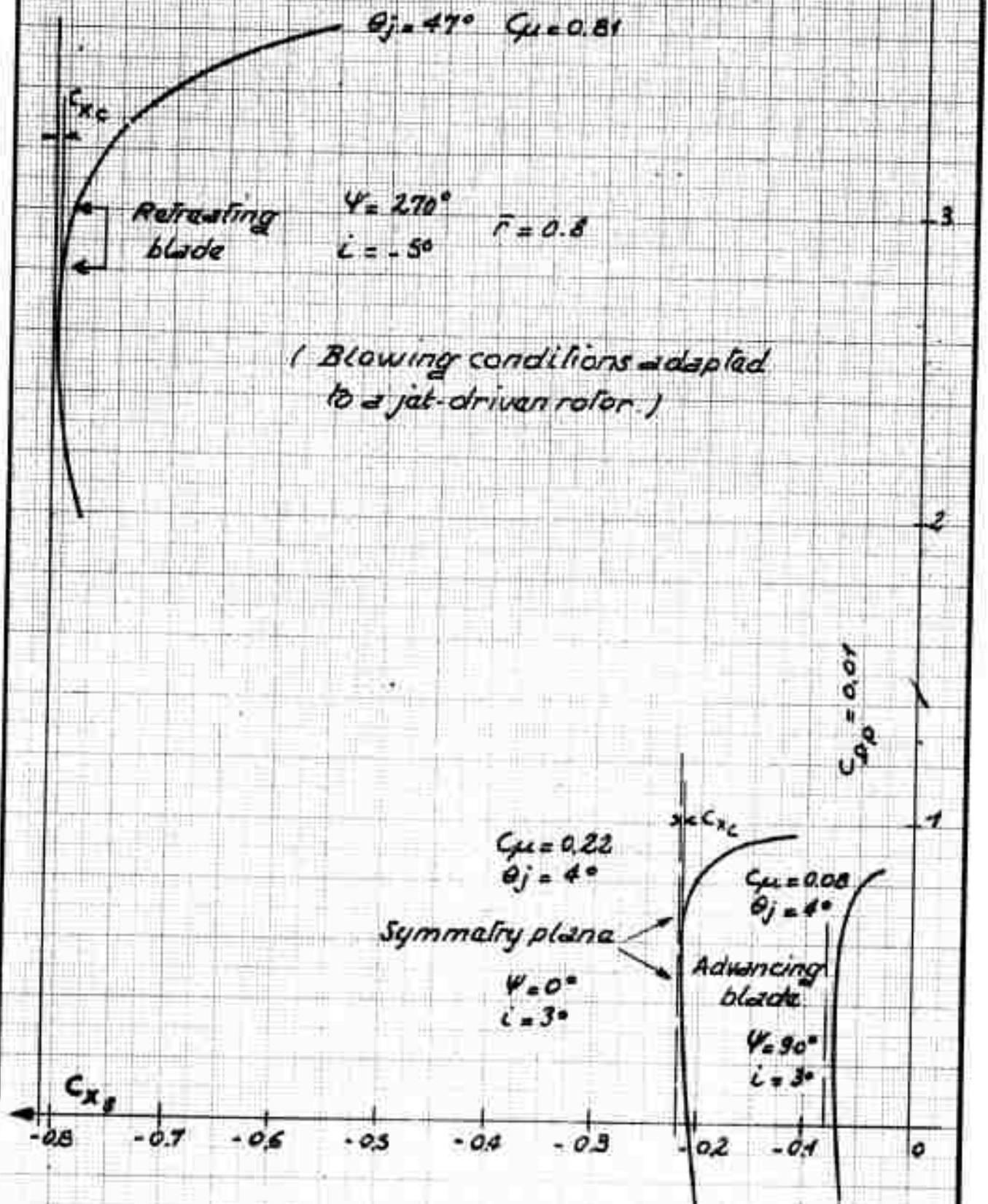


FIG. 179

TESTS IN S, CH WIND TUNNEL

$C_z(C_x)$ curves with constant θ_j and variable i

MECHANICAL FLAP

($A=6$)

PNEUMATIC FLAP

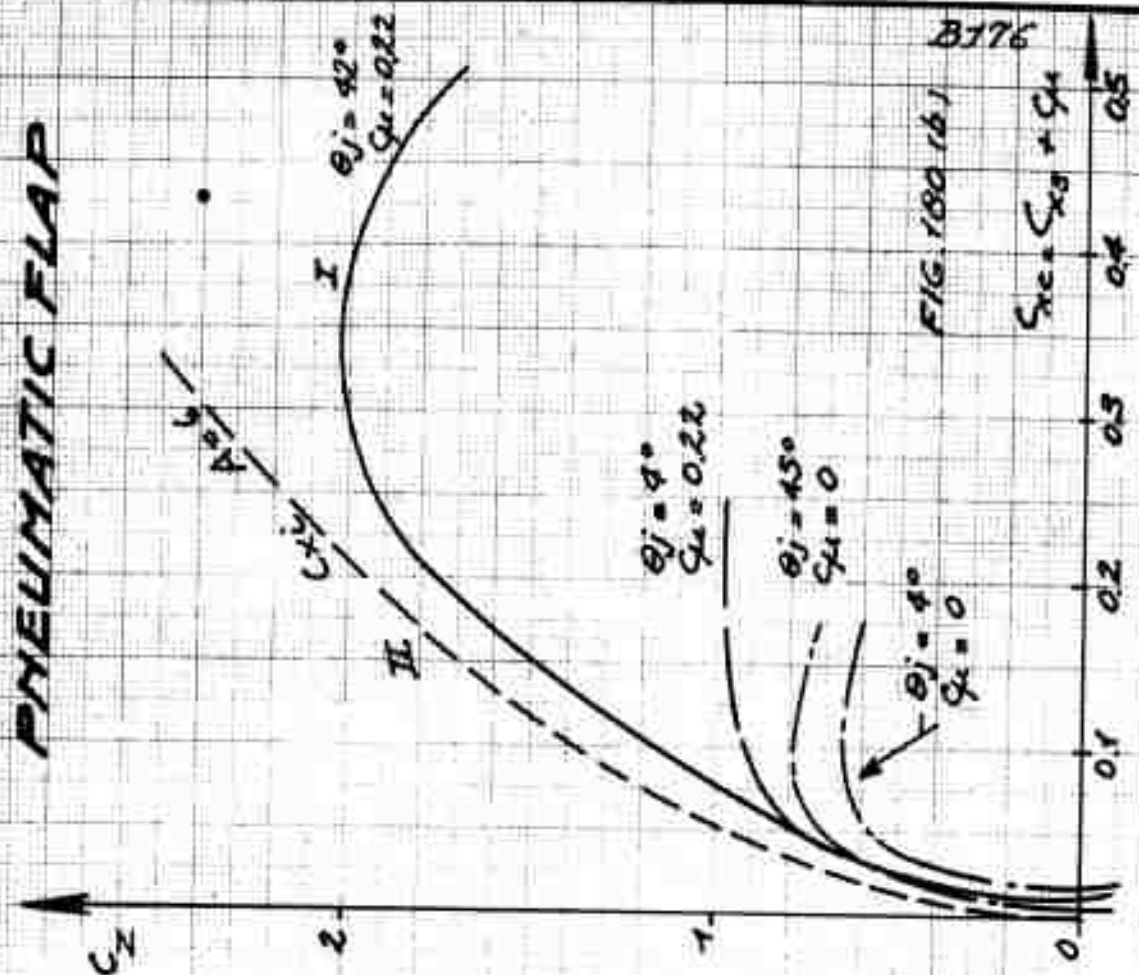


FIG. 180

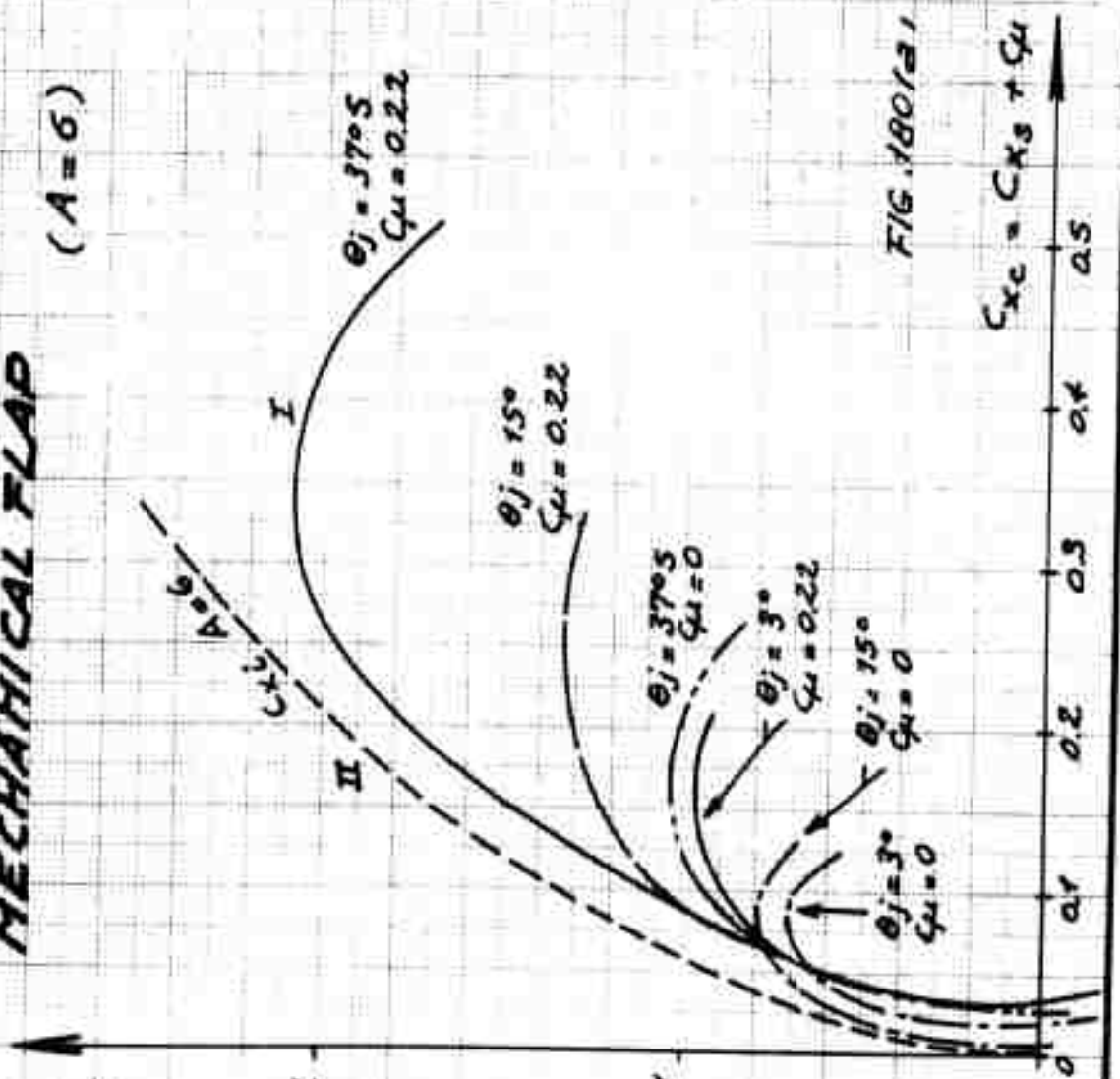


FIG. 180 (a)

FIG. 180 (b)

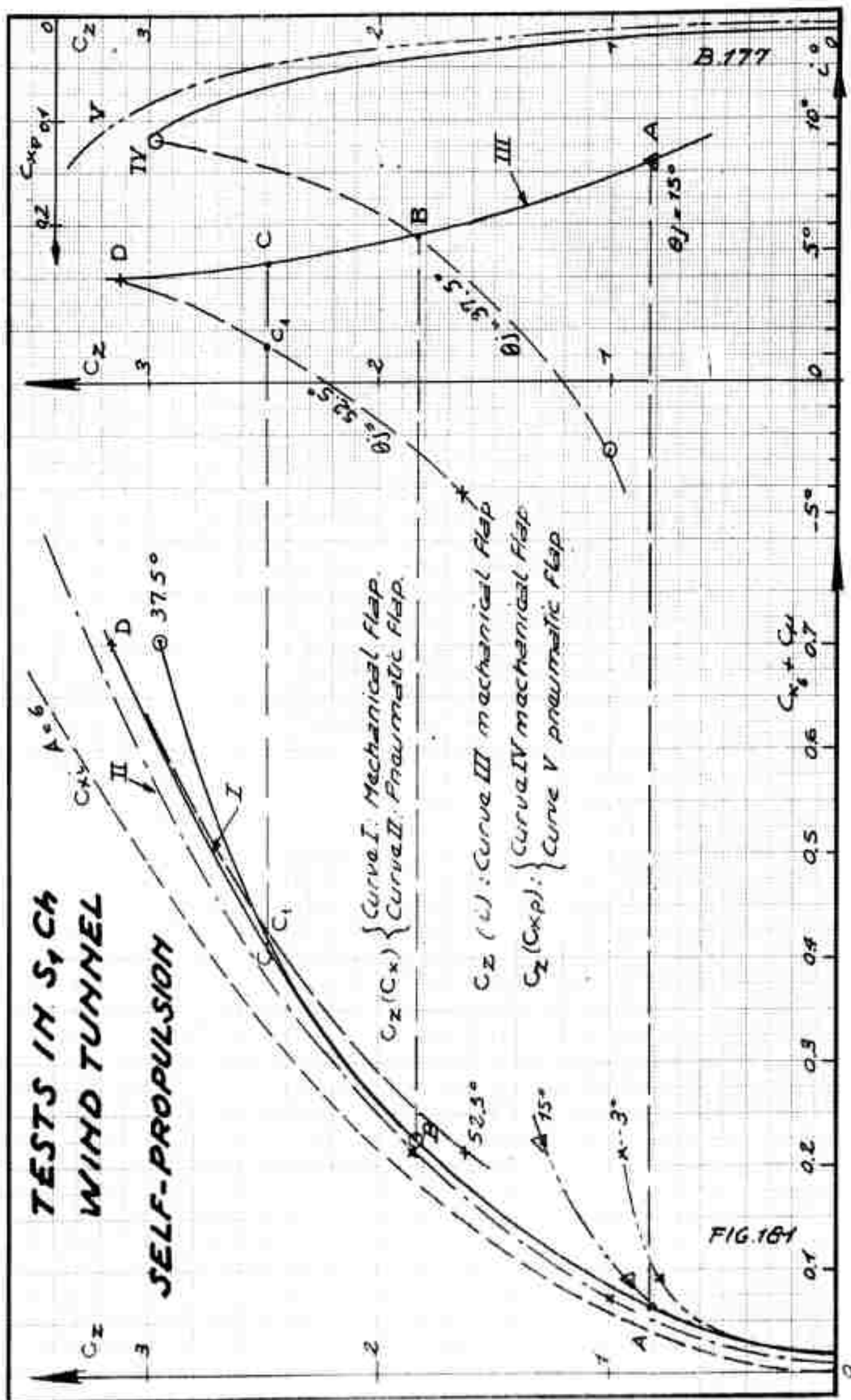
B176

$$C_{xc} = C_{xs} + C_{xi}$$

$$C_{xc} = C_{xs} + C_{xi}$$

TESTS IN S, CH WIND TUNNEL

SELF-PROPULSION



TESTS IN S, CH WIND TUNNEL

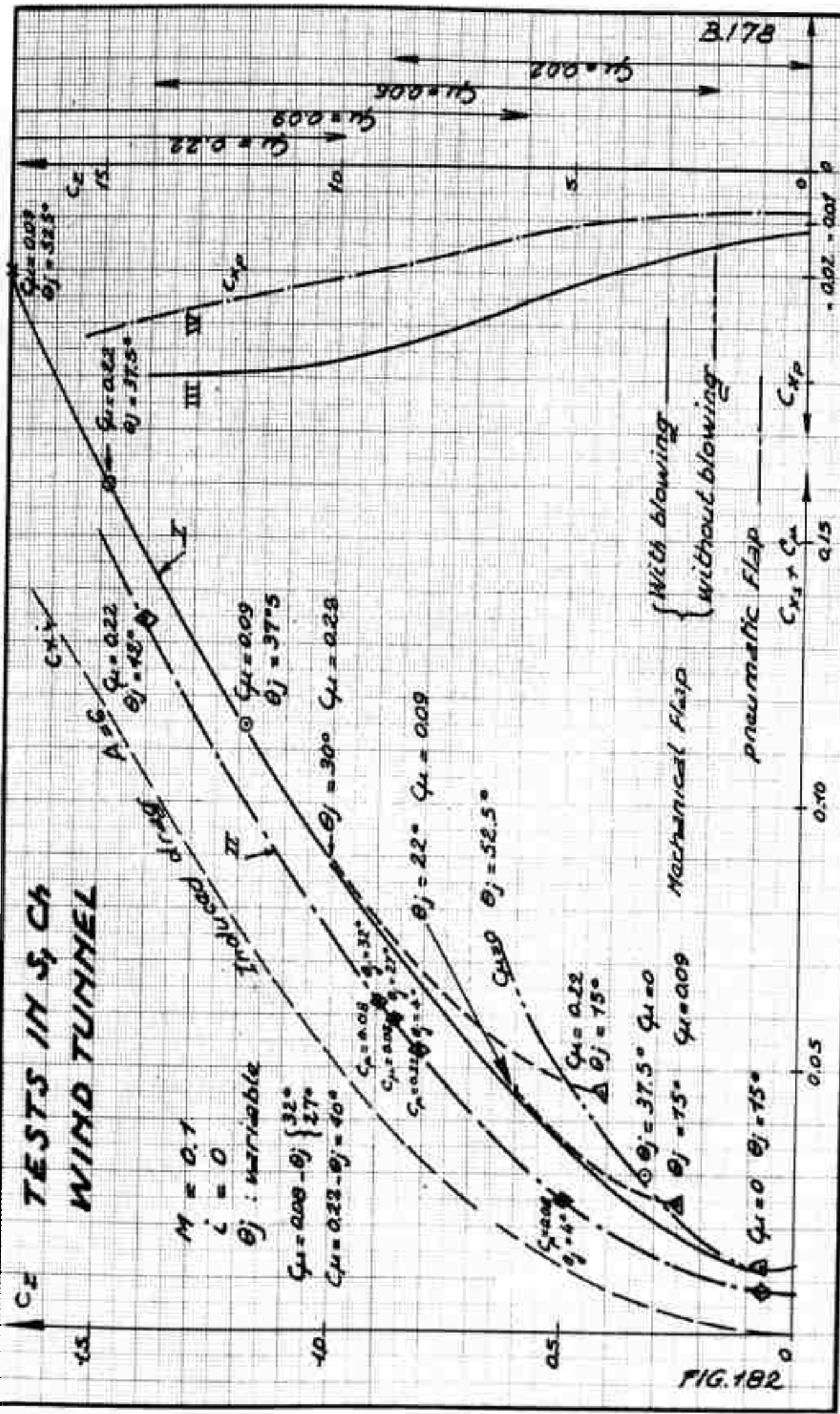


FIG. 182

TESTS IN S_3 CH WIND TUNNEL
PNEUMATIC FLAP
ASPECT RATIO $A=6$

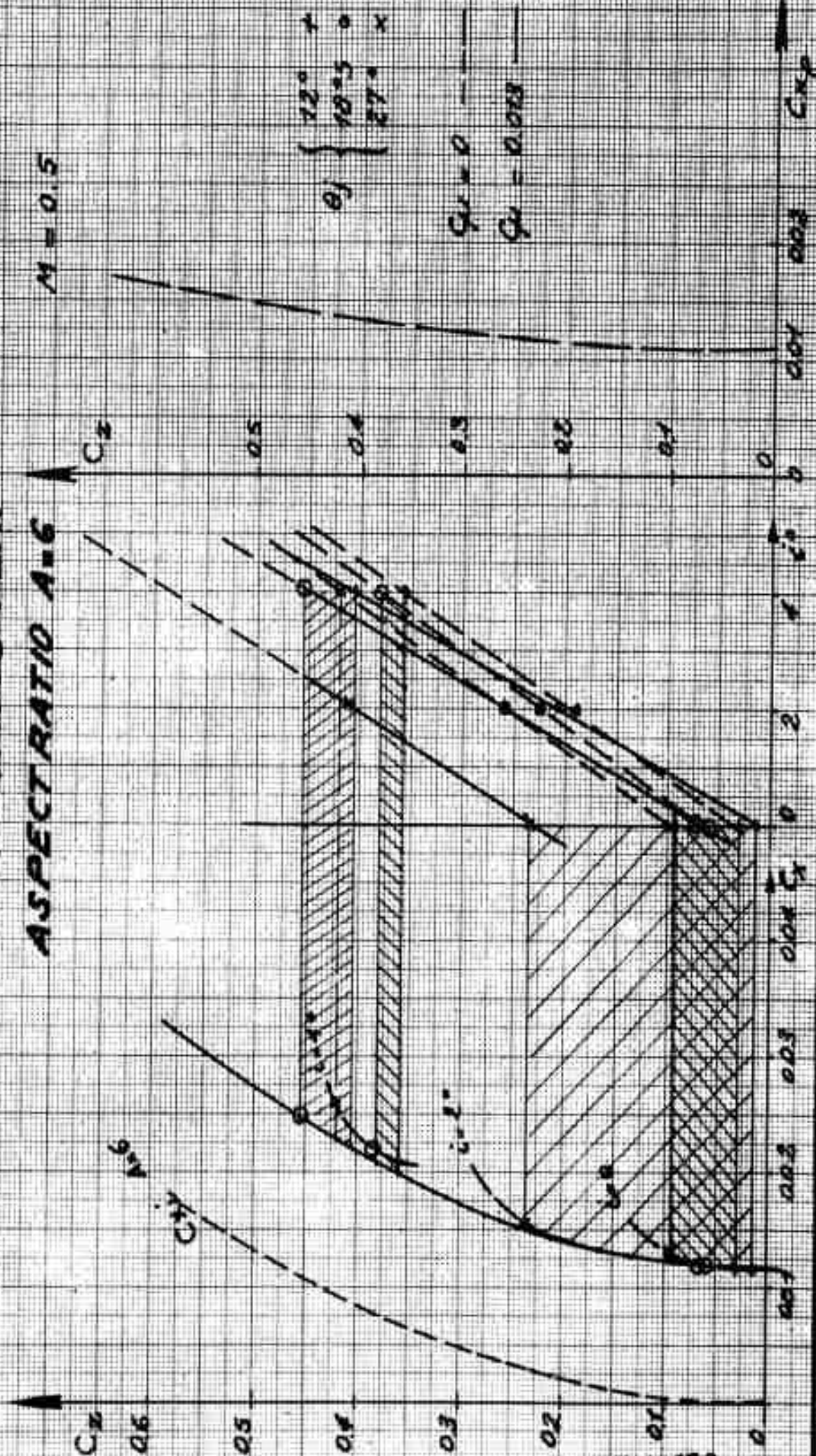
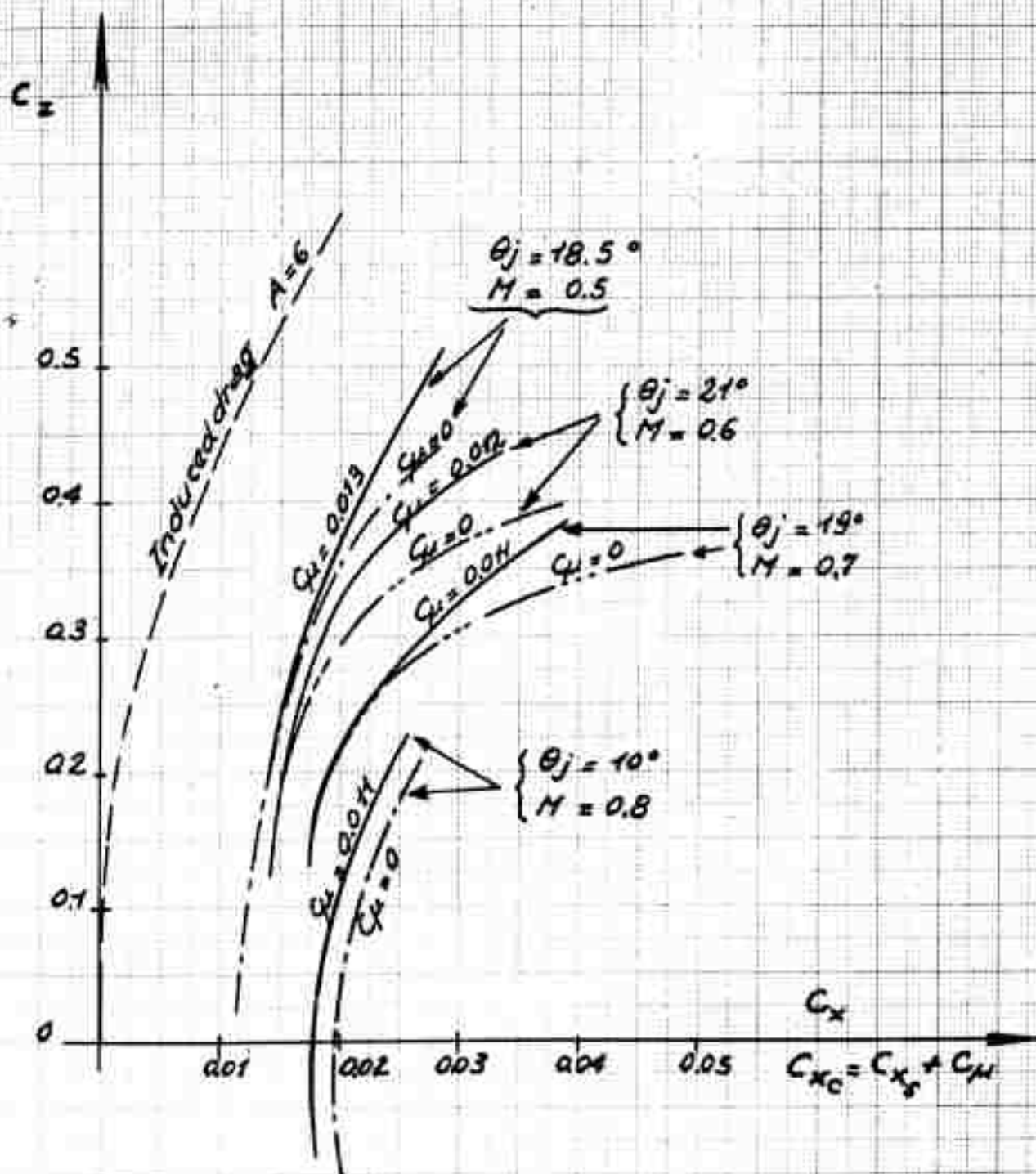


FIG. 183

TESTS IN S_3 CH WIND TUNNEL

PNEUMATIC FLAP

 C_z (C_x) CURVES

C_{xc} — With blowing
 C_x --- Without blowing

FIG 184

TESTS IN S₃ CH WIND TUNNEL

FIG. 184

PNEUMATIC FLAP

$$C_z = 0.2 \quad M = 0.8$$

(ADVANCING BLADE $\bar{r} = 10$)

(A = 6)

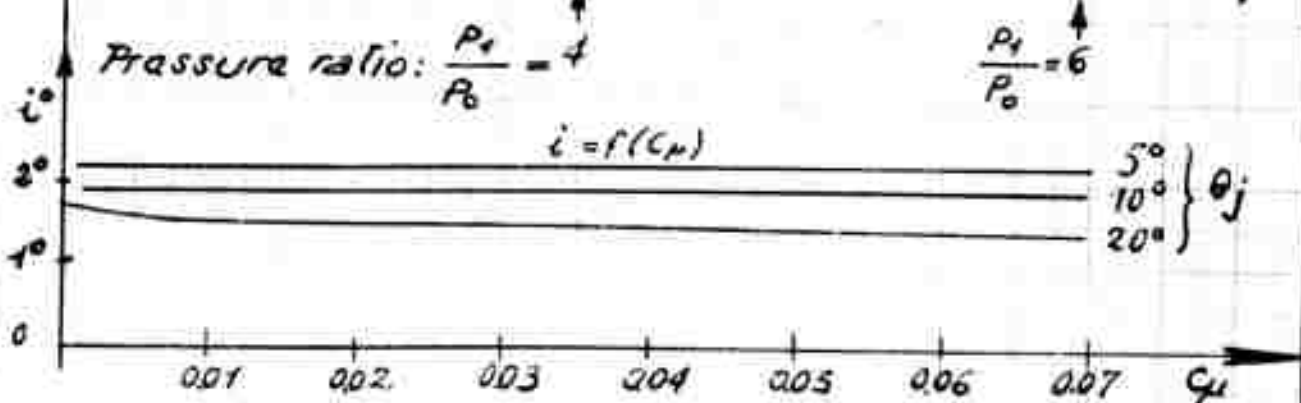
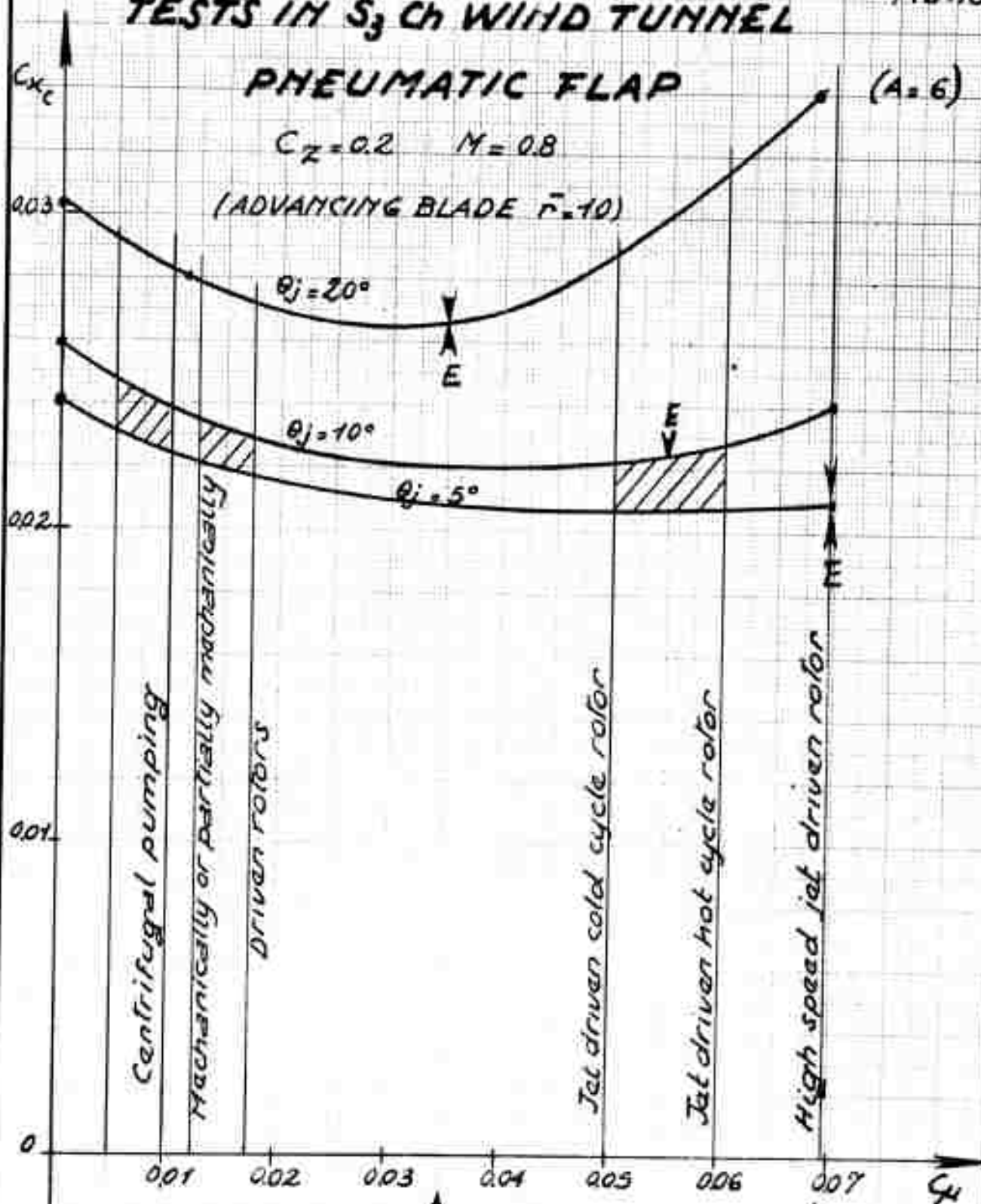


FIG. 185

TESTS IN S_3 CH WIND TUNNEL

B.182

PNEUMATIC FLAP ($A=6$)

$C_z = 0.2$ $M = 0.6$

(ADVANCING BLADE $\tilde{r} = 0.75$)

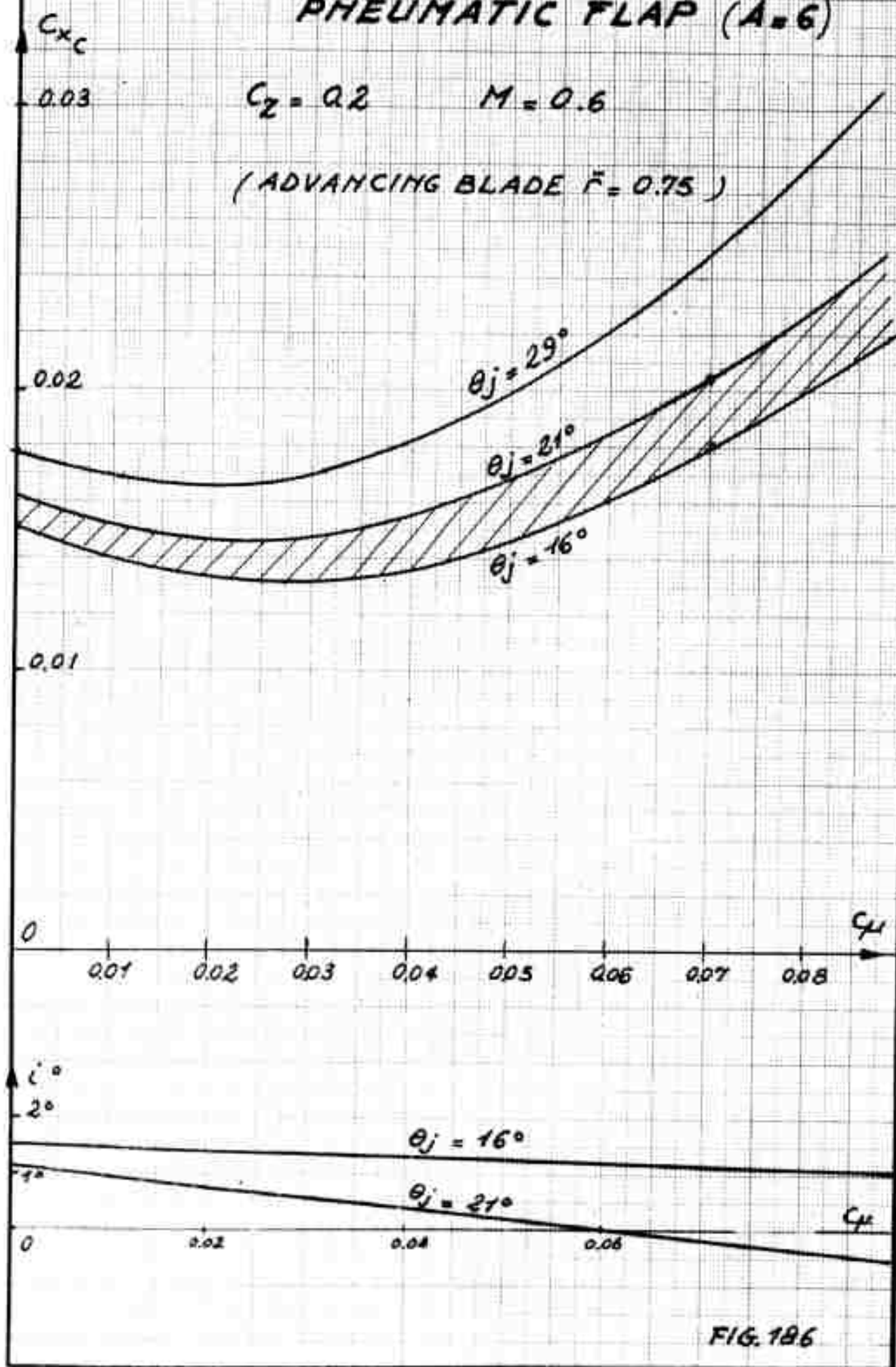


FIG. 186

TESTS IN S_3 CH WIND TUNNEL MECHANICAL FLAP

$\theta_j = 22^\circ 5'$

+ $M=0.5$: Symmetry plane blade
o $M=0.8$: Advancing blade

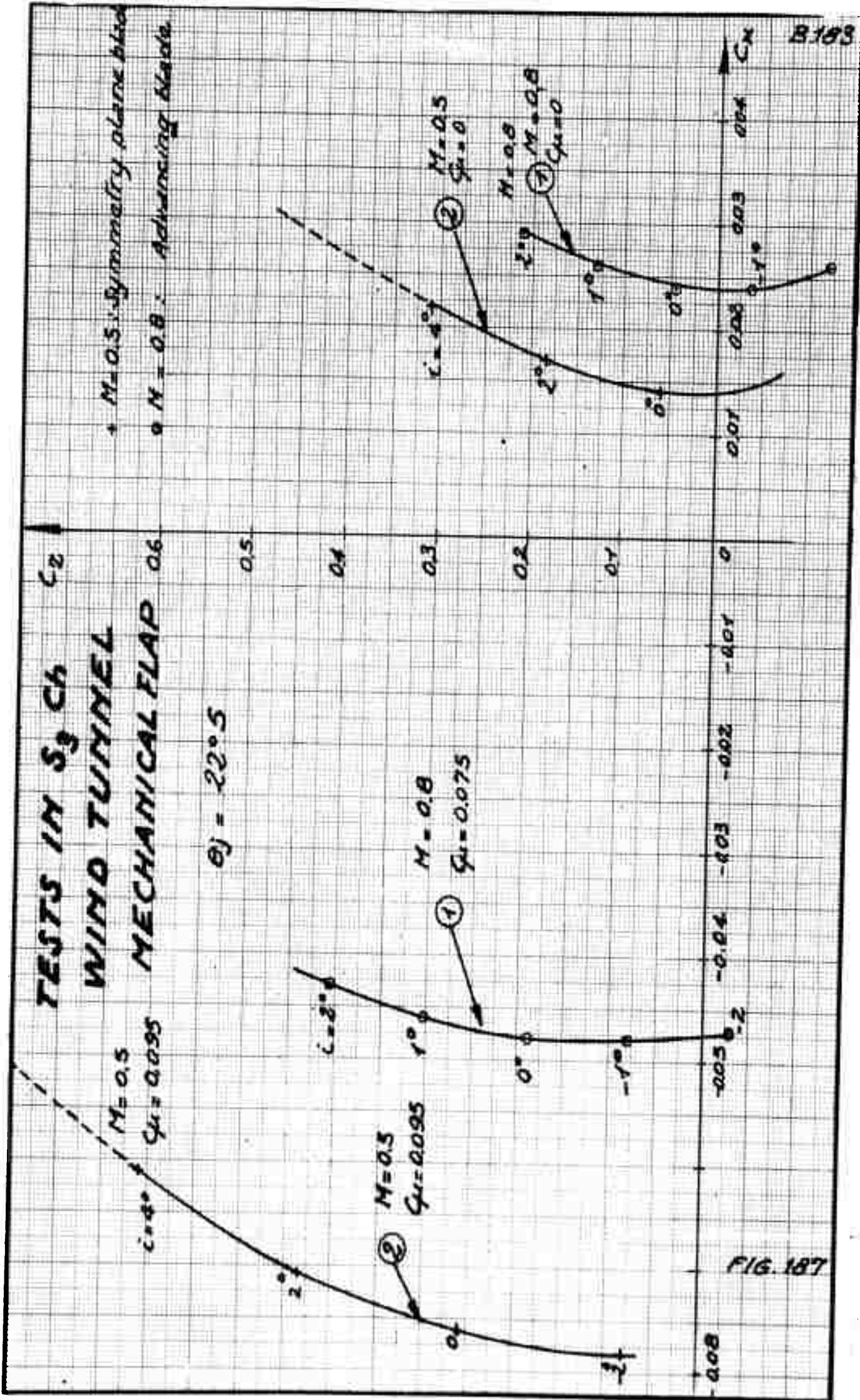
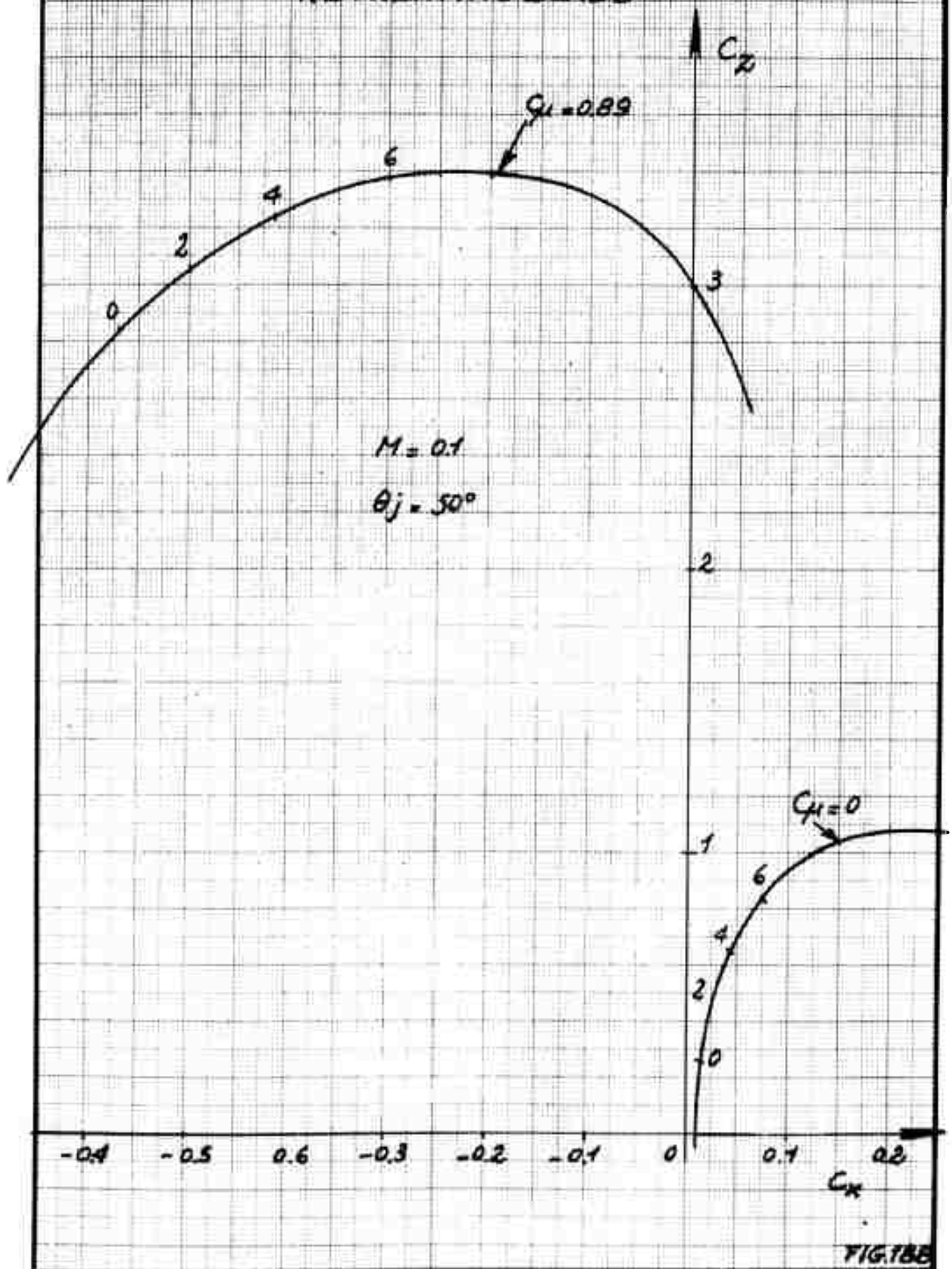


FIG. 187

PNEUMATIC FLAP

RETREATING BLADE



TESTS IN S_3 CH WIND TUNNEL

BLOWING PSEUDO-EFFICIENCY $1+Q$ VERSUS C_M

FOR DIFFERENT MACH NUMBERS

$$1+Q = 1 - \frac{\Delta C_{M0}}{C_M}$$

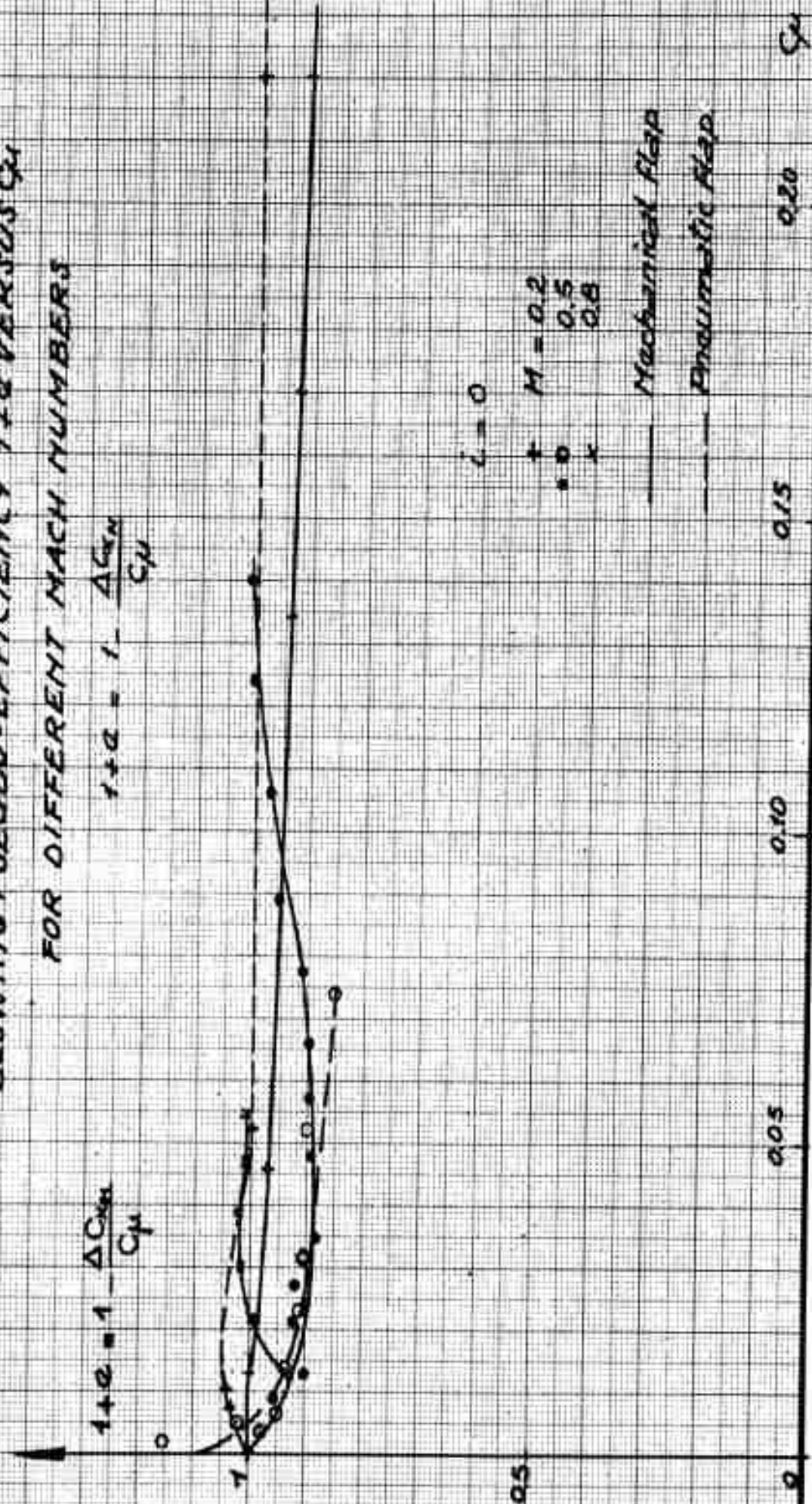


FIG. 189

TESTS IN S, Ch WING TUNNEL

B.186

MECHANICAL FLAP

ASPECT RATIO $A = \infty$

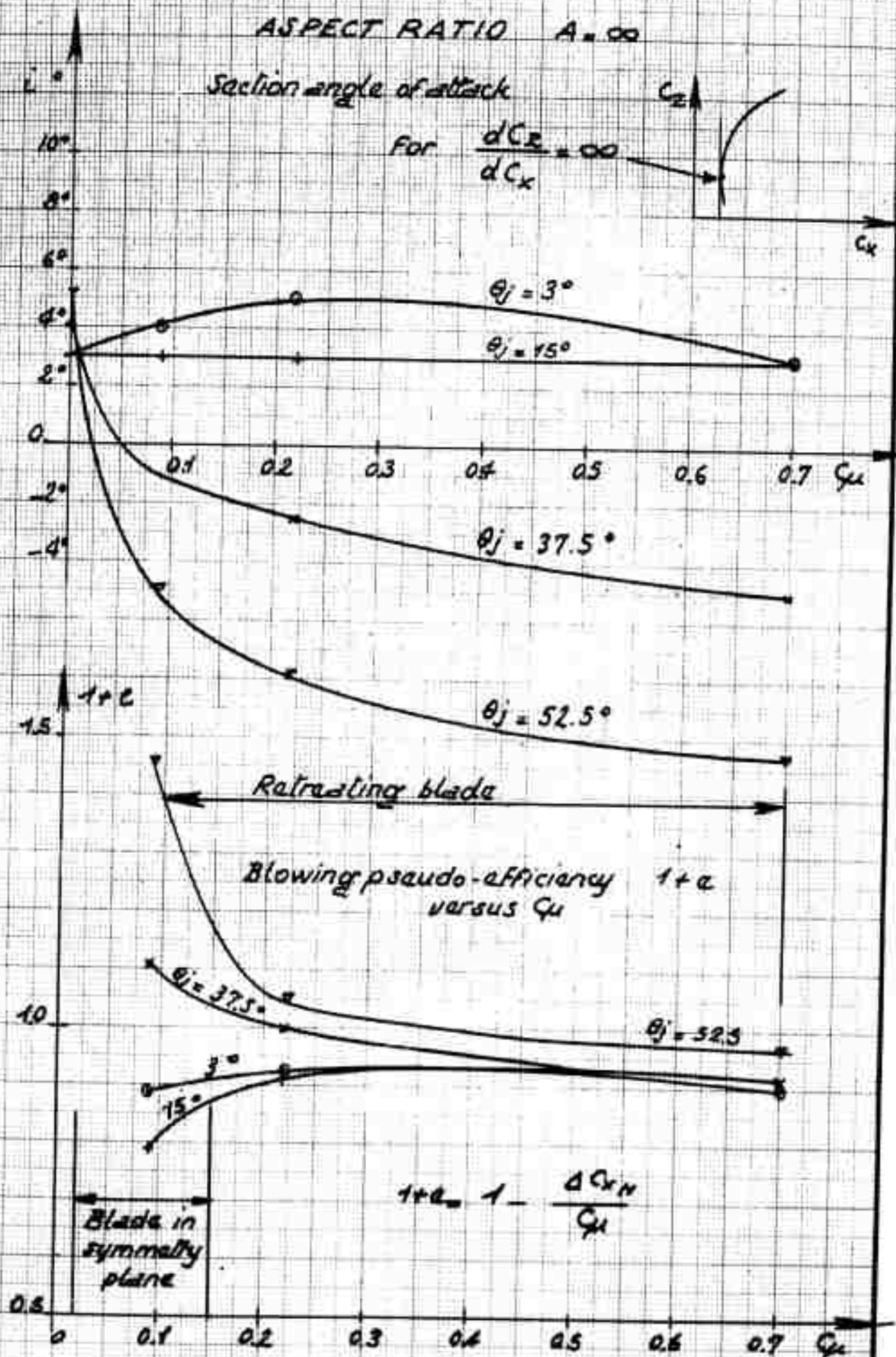


FIG. 190

TESTS IN S, Ch WIND TUNNEL

PNEUMATIC FLAP

ASPECT RATIO $A = \infty$

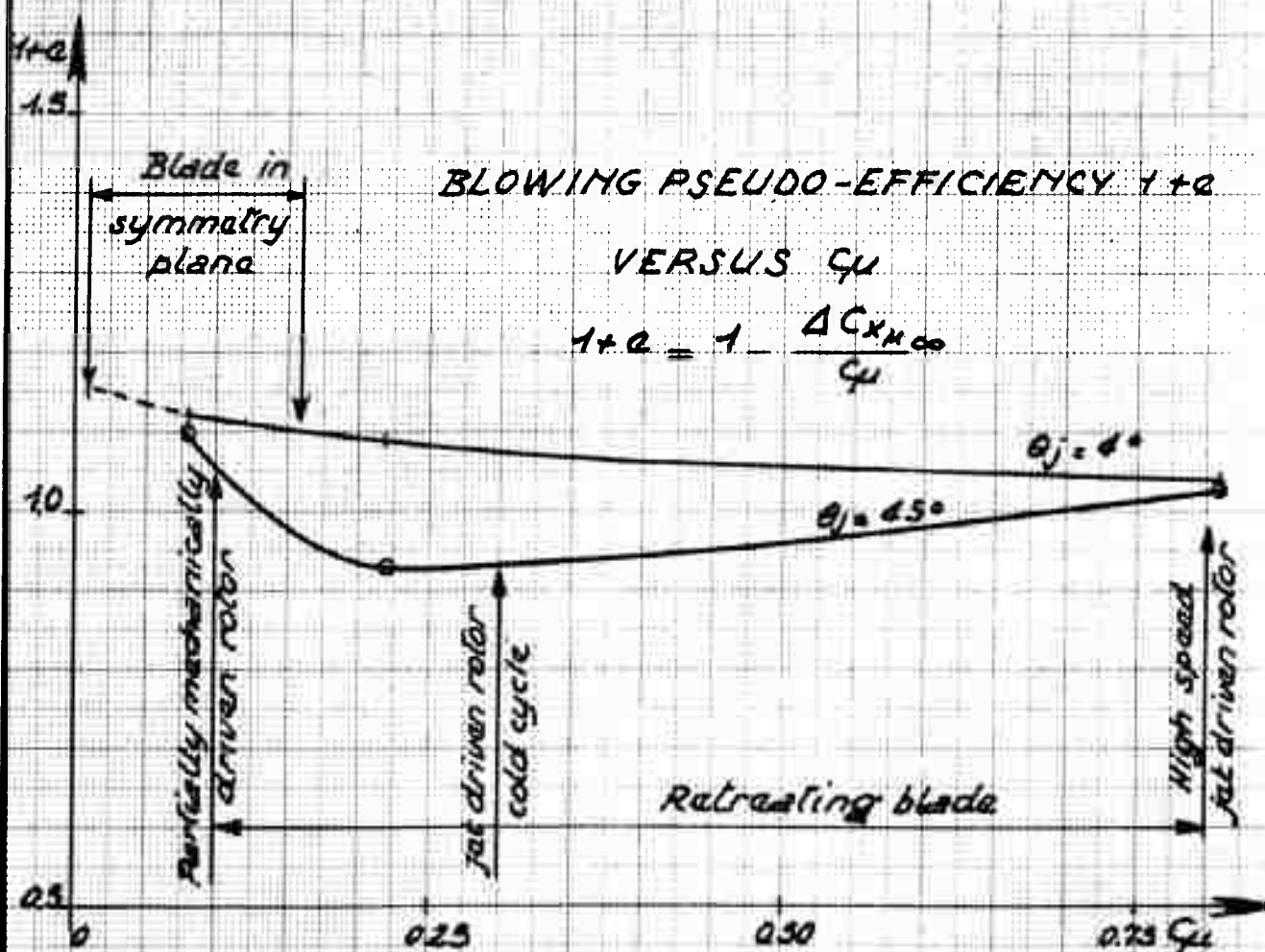
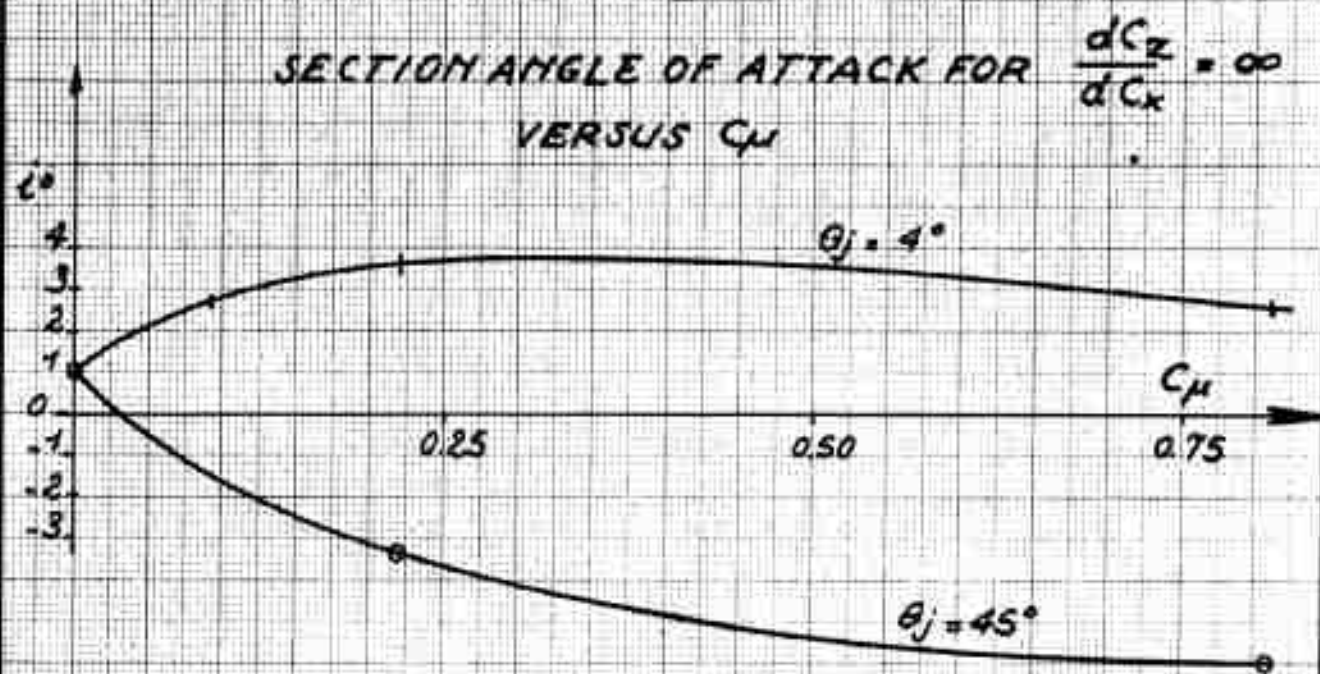
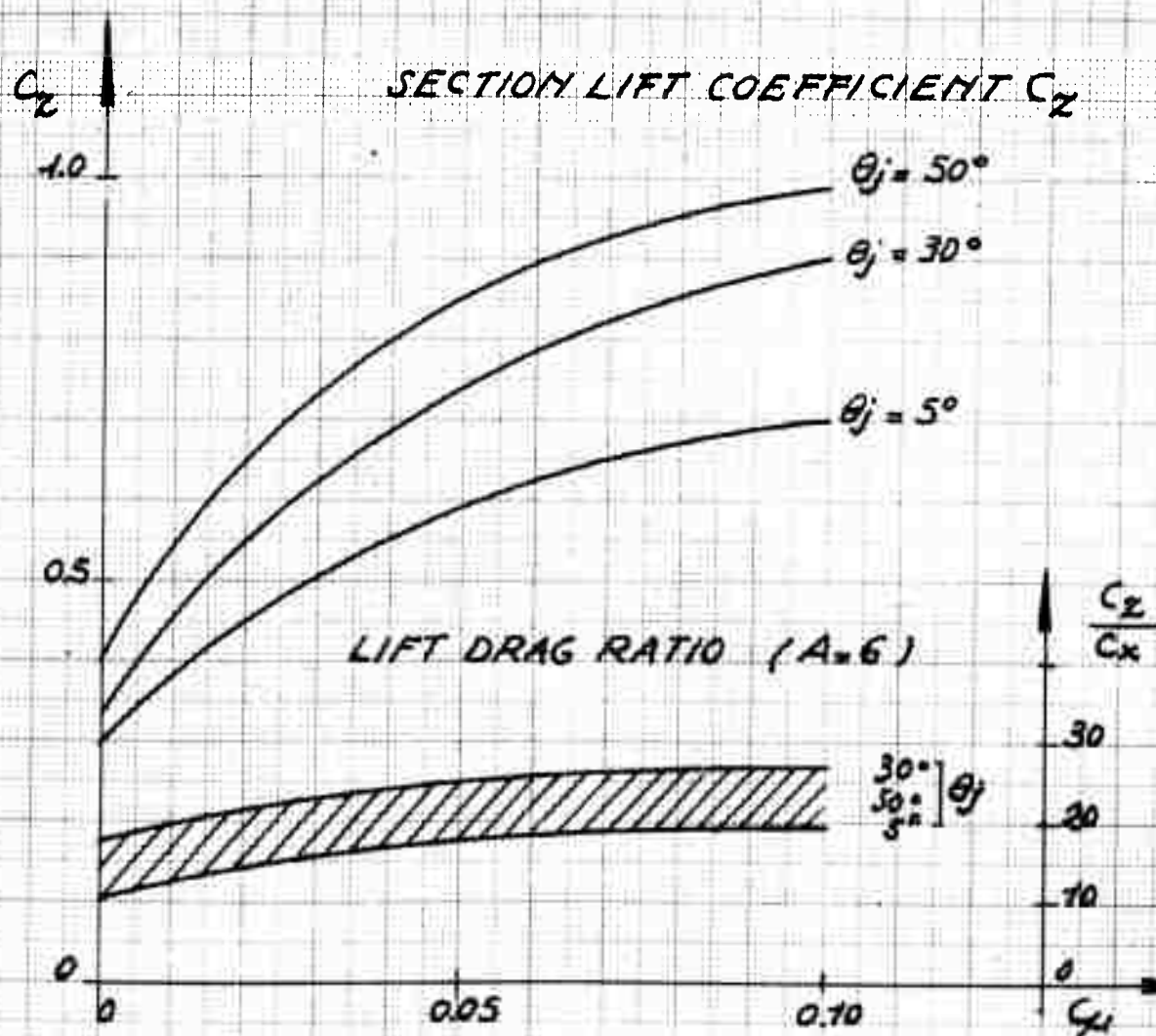
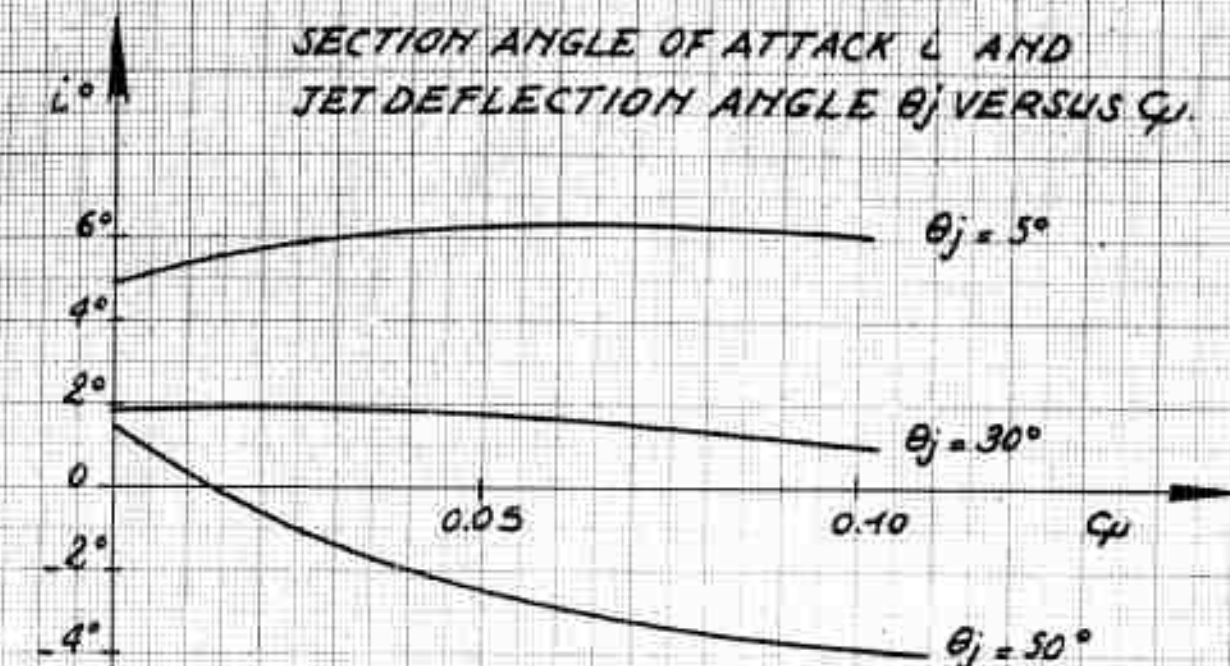


FIG. 194

TESTS IN S₃CH WIND TUNNEL

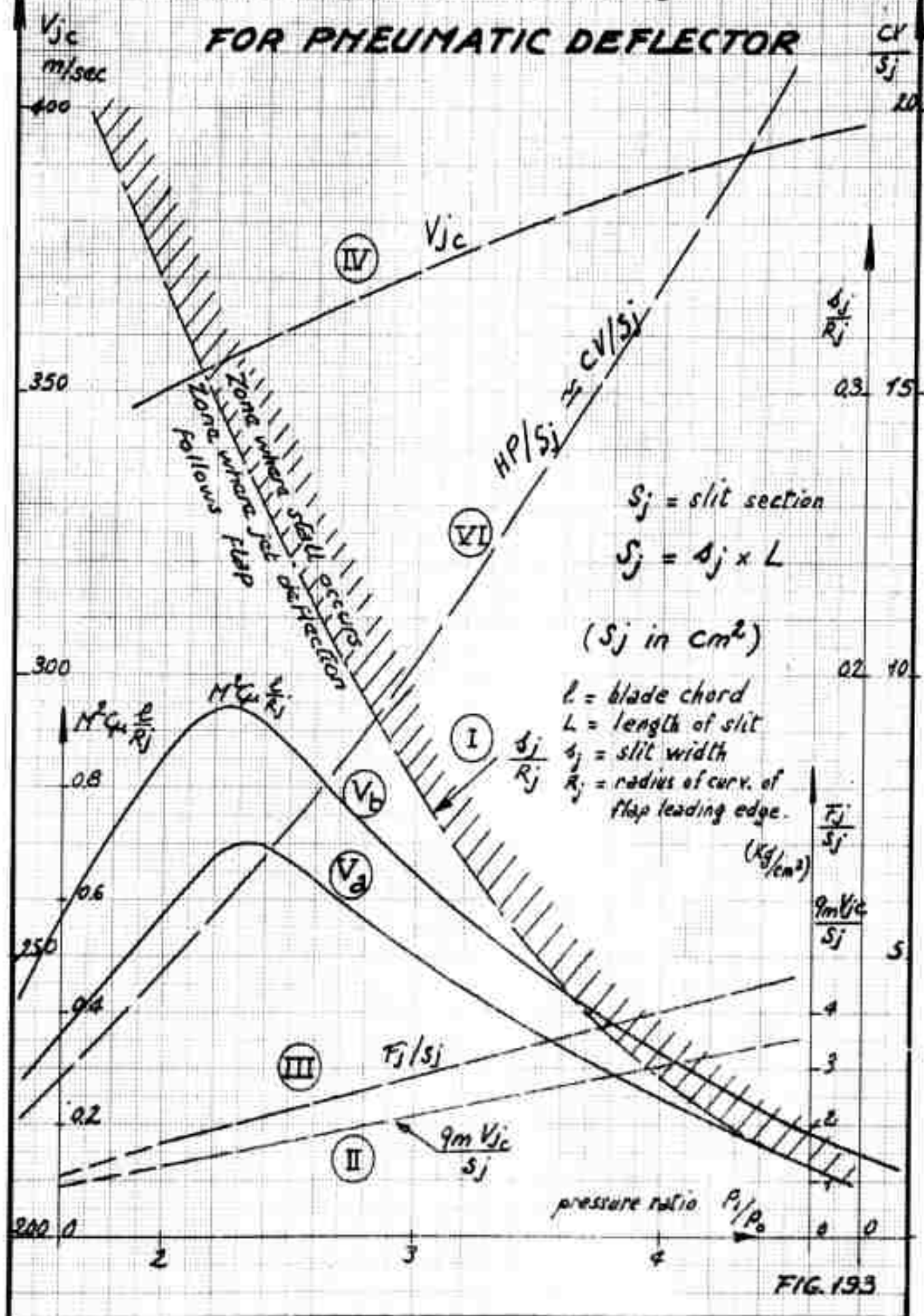
PNEUMATIC FLAP

OPTIMUM COMBINATION BETWEEN
SECTION ANGLE OF ATTACK α AND
JET DEFLECTION ANGLE θ_j VERSUS C_{μ} .



- BOUNDARY OF DEFLECTED JET STALL

ADAPTATION CURVES FOR PNEUMATIC DEFLECTOR



TESTS IN S_3 CH WIND TUNNEL

B.190

Deflection θ_j

$$\frac{P_1}{P_0} = 1.8$$

PNEUMATIC DEFLECTOR

Calibration at $V_0 = 0$
Effective deflection θ'_j
and theoretical deflection θ_j
versus pressure in boot.

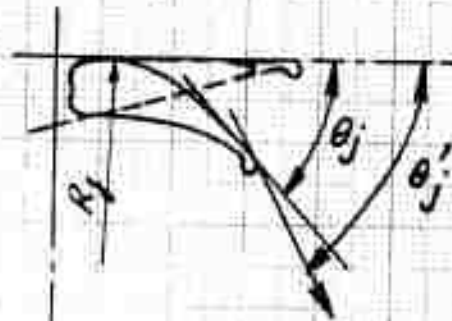
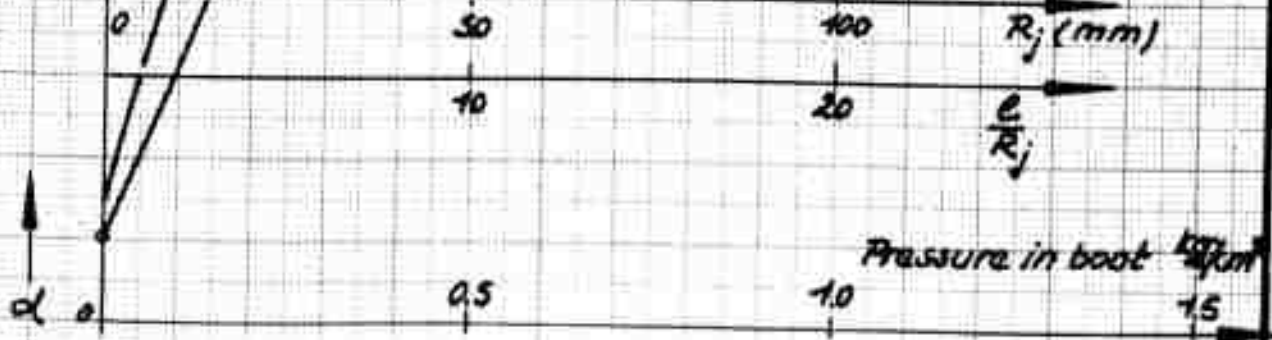


FIG. 194



PNEUMATIC DEFLECTOR TESTED IN S₃CH WIND TUNNEL

Limit values of C_{μ} and pressure ratio
versus θ_j for which jet stream separates
from deflector.

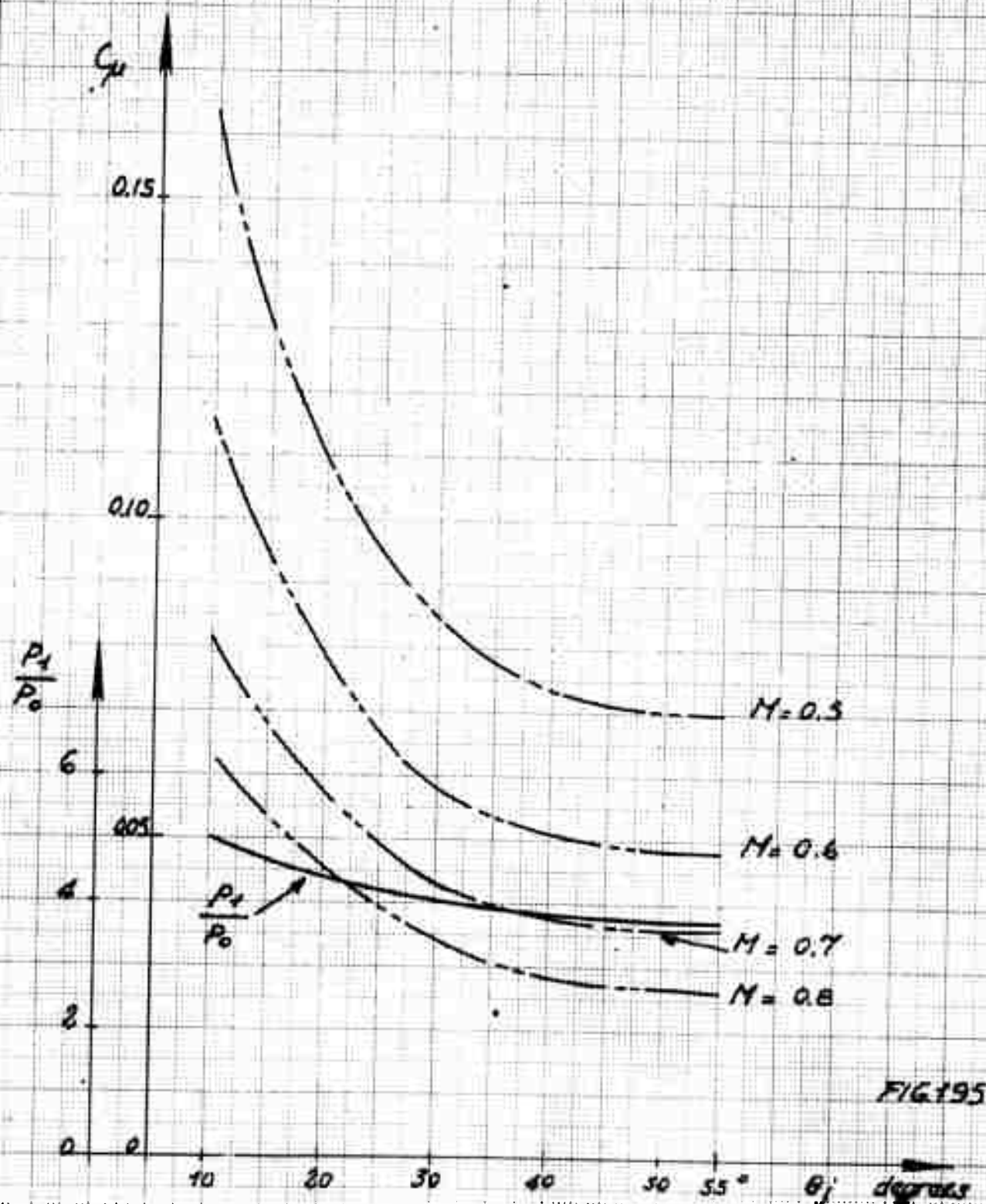


FIG 195

APPLICATION OF PNEUMATIC DEFLECTOR TO HIGH SPEED ROTOR

B.192

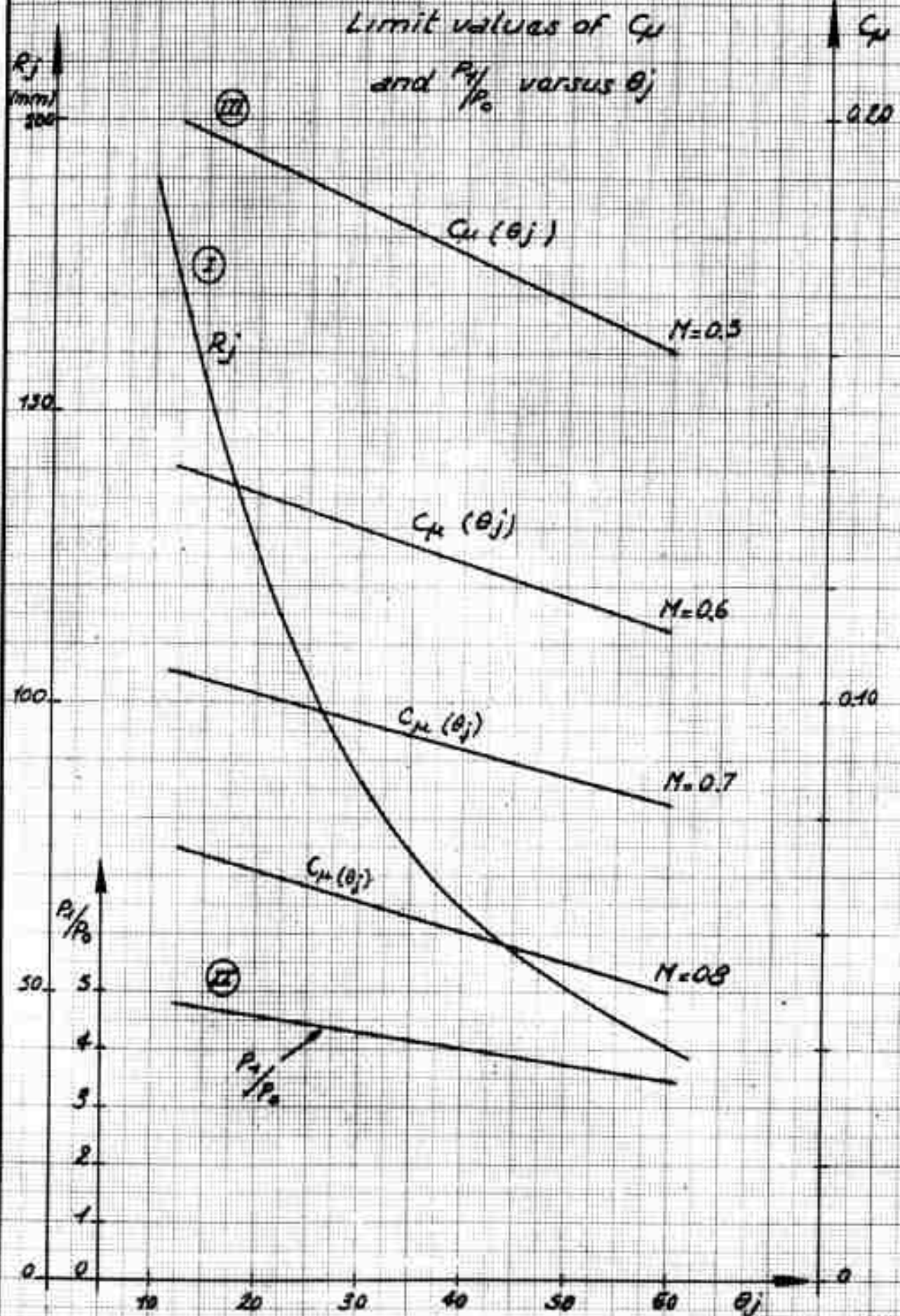


FIG. 196

EFFECT OF JET STALL ON LIFT 8193 **COEFFICIENT AT VARIOUS MACH NUMBERS** **PNEUMATIC DEFLECTOR**

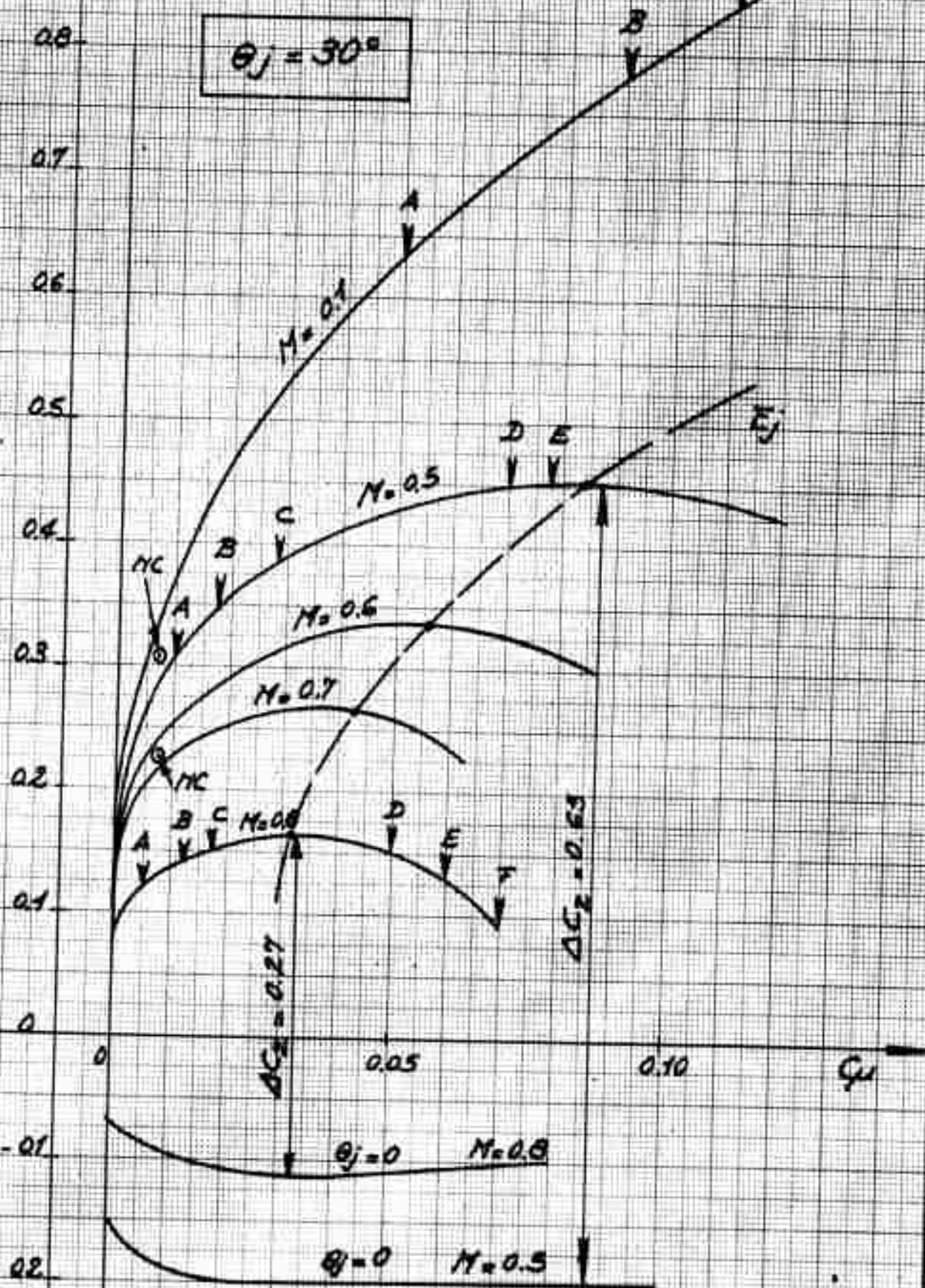
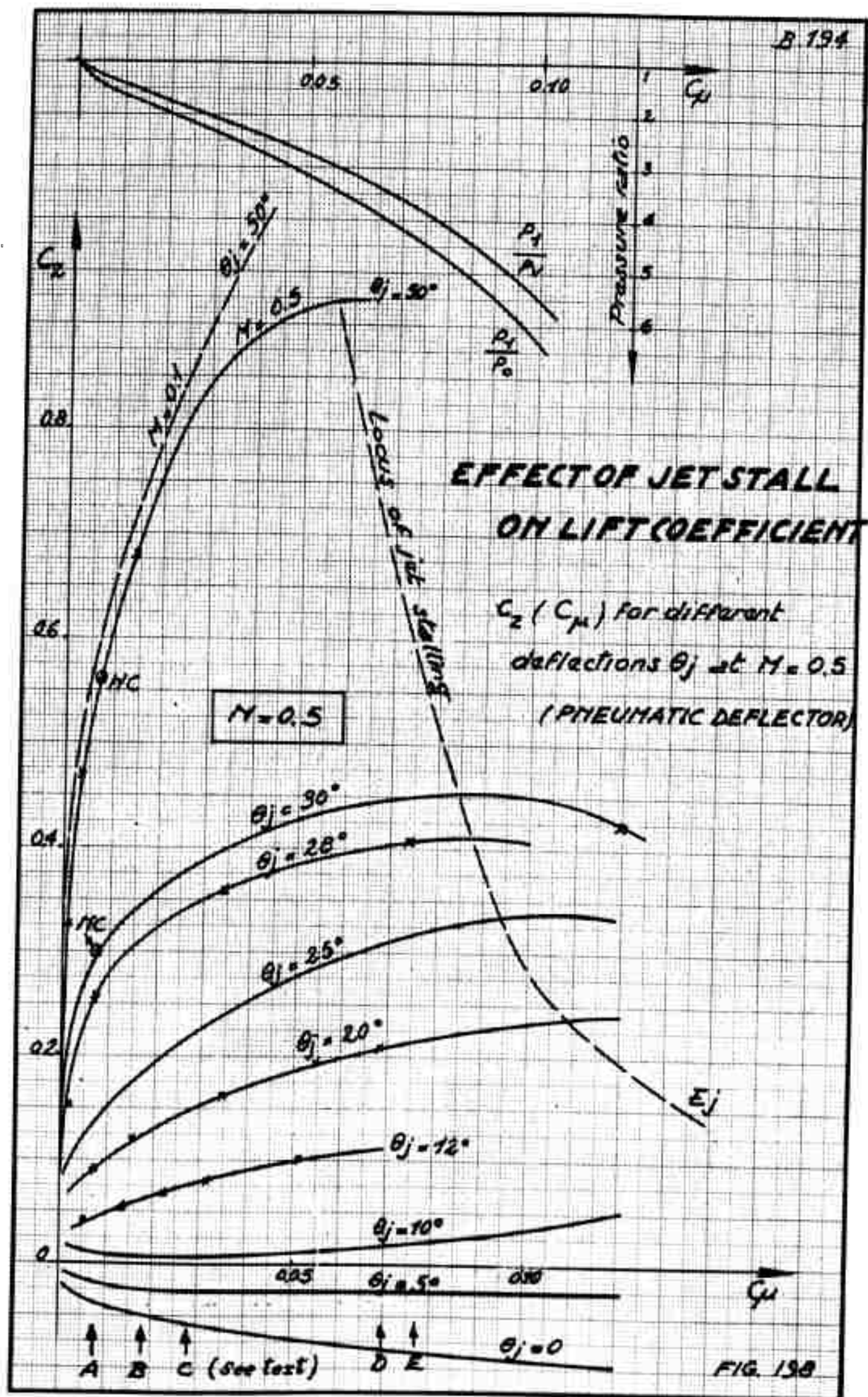


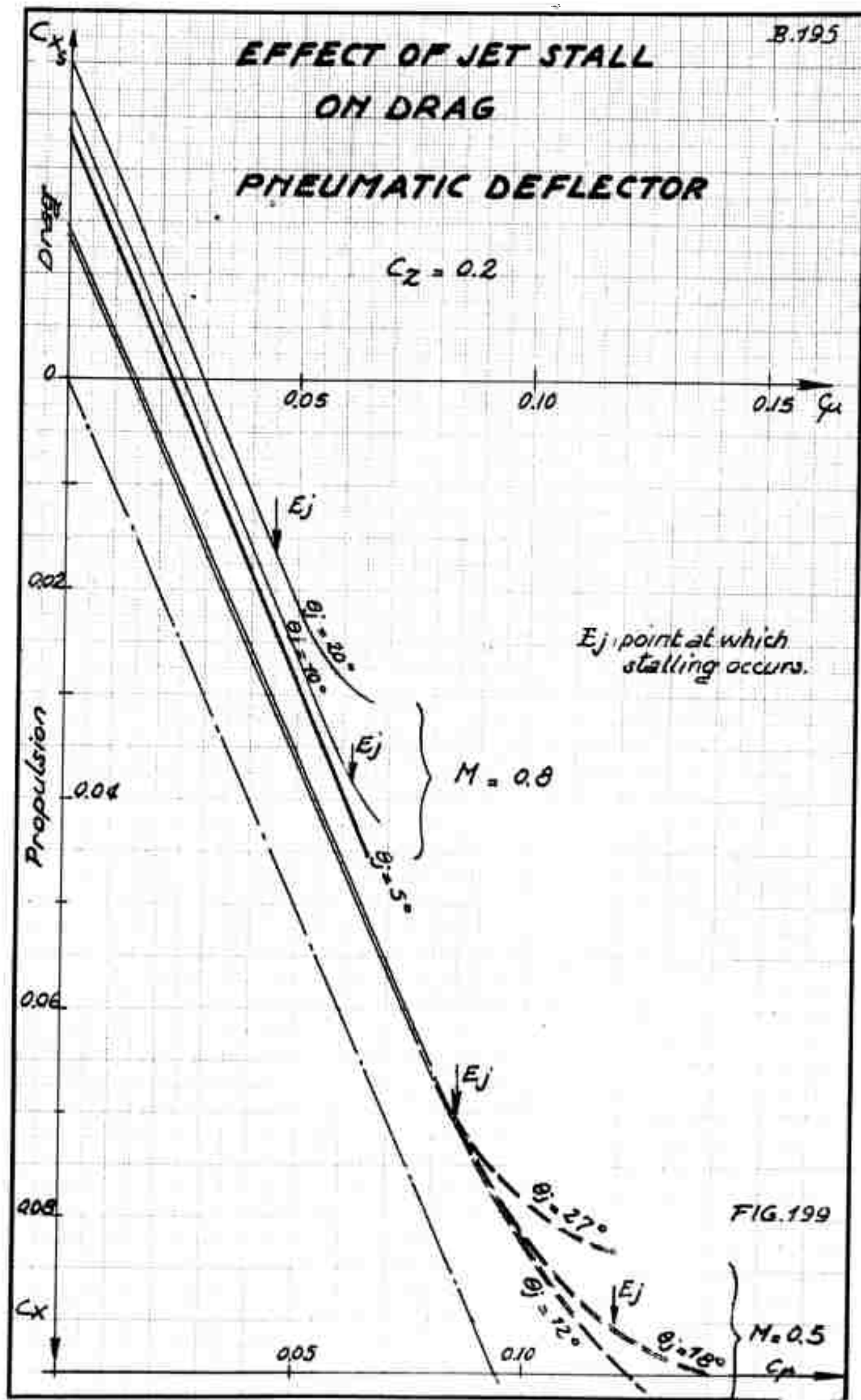
FIG. 197



EFFECT OF JET STALL ON DRAG

PNEUMATIC DEFLECTOR

$$C_z = 0.2$$



EFFECT OF JET STALL ON DRAG PNEUMATIC DEFLECTOR

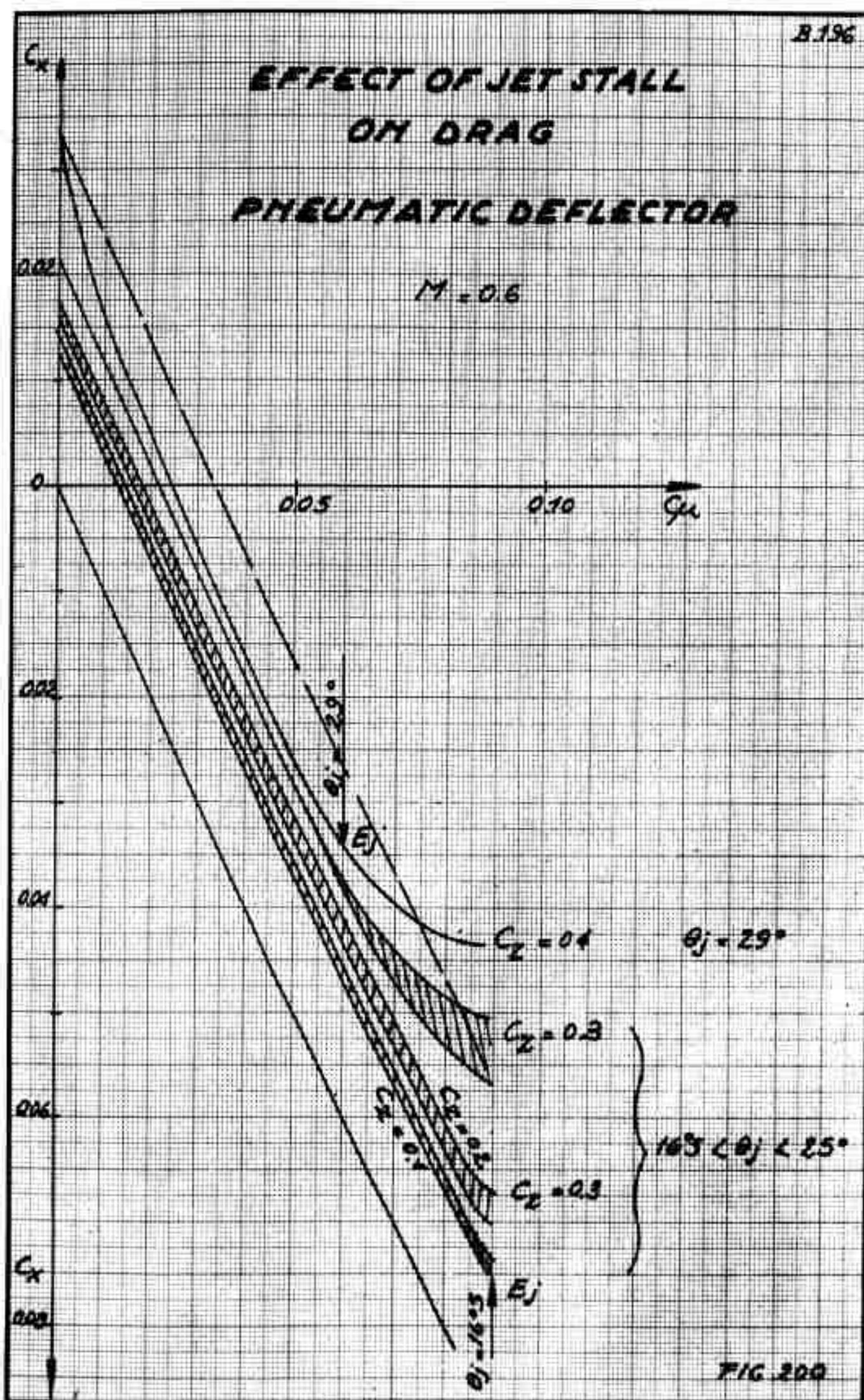
 $M = 0.6$


FIG. 200

PNEUMATIC DEFLECTOR SECTION LIFT COEFFICIENT VERSUS C_{μ}

(FOR LOW C_{μ} VALUES)

$M = 0.1$

$i = 0$

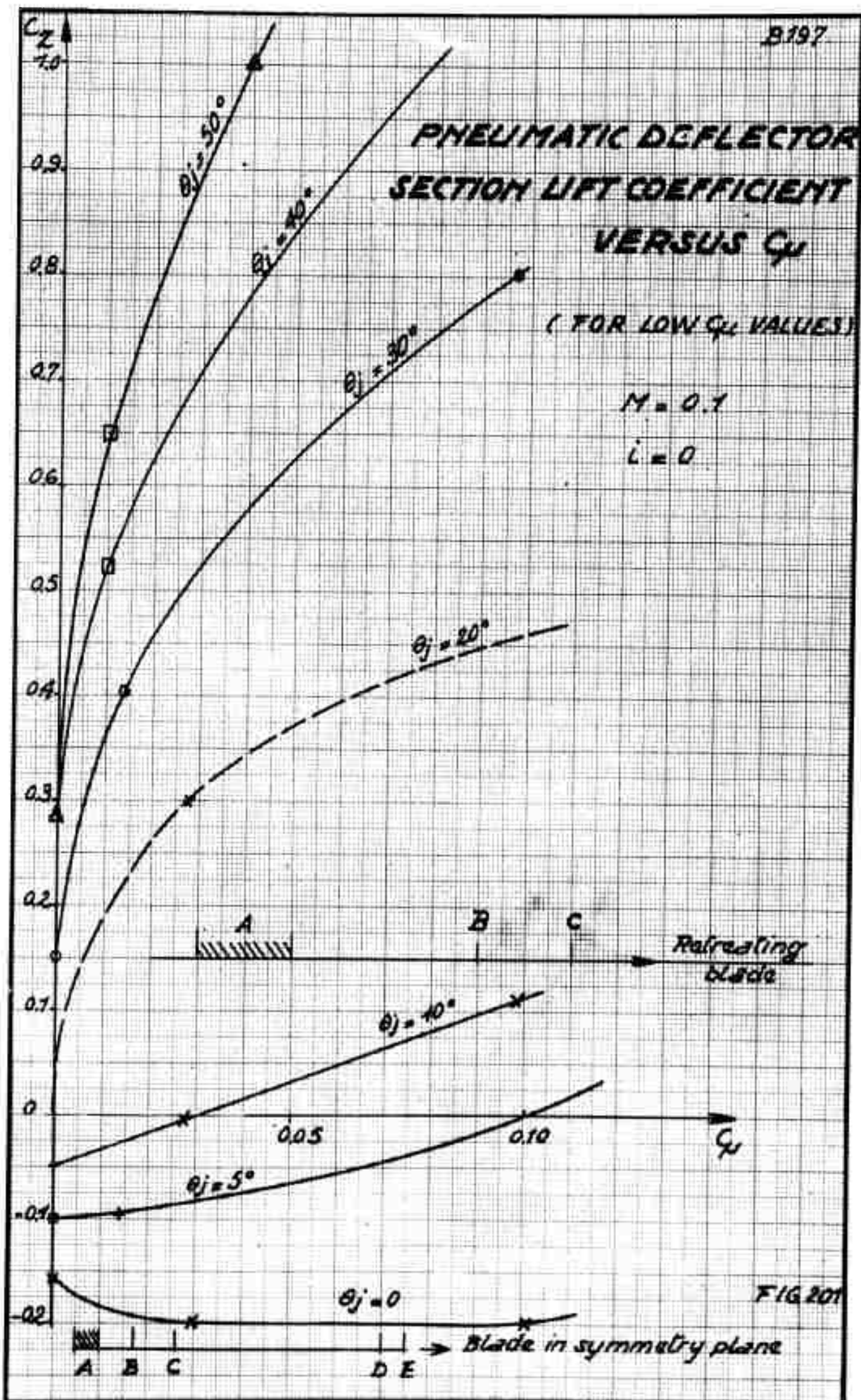
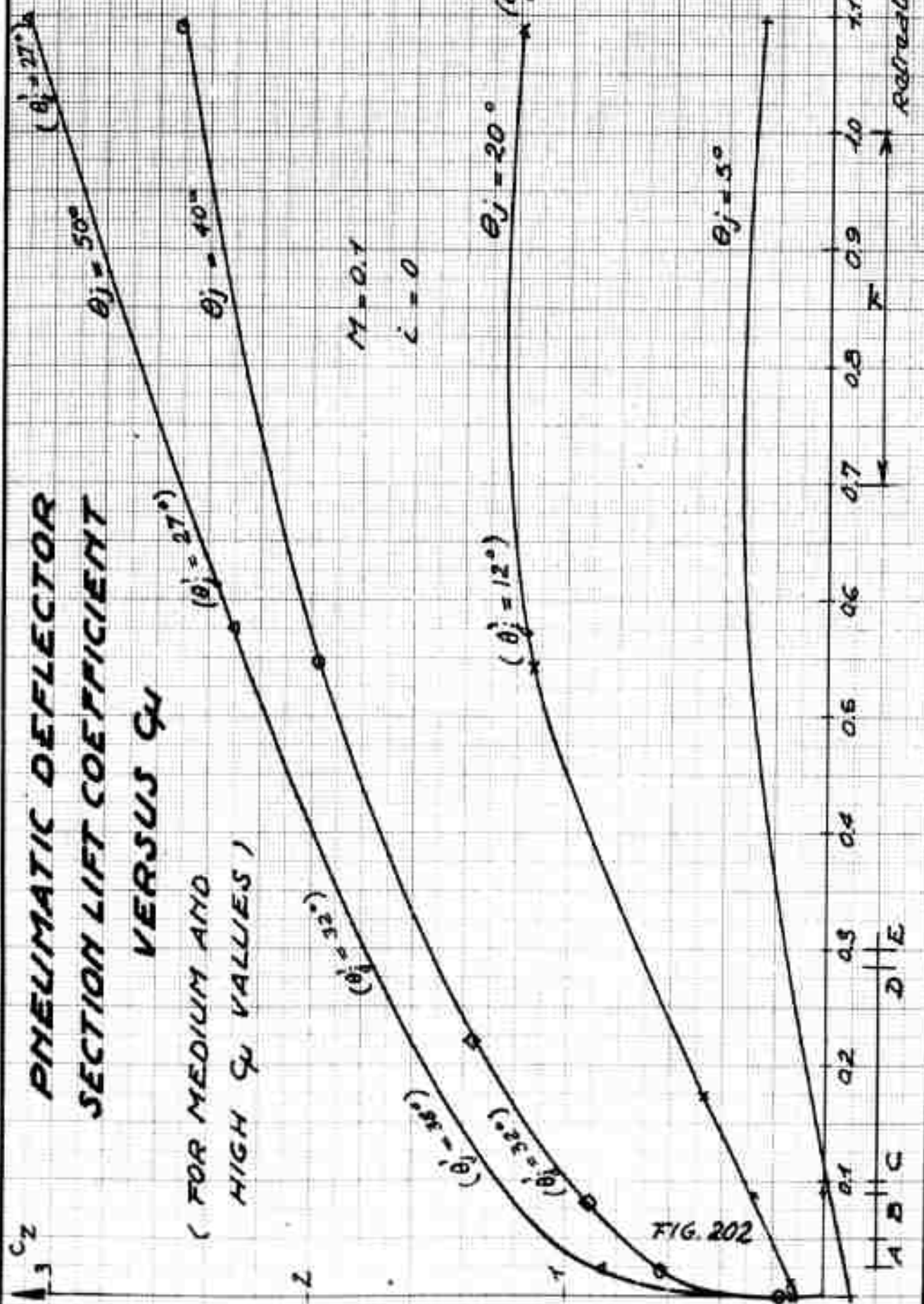


FIG 201



PNEUMATIC DEFLECTOR CONTROL EFFICIENCY $\frac{dC_z}{d\theta_j}$ VERSUS φ

$M = 0.1$

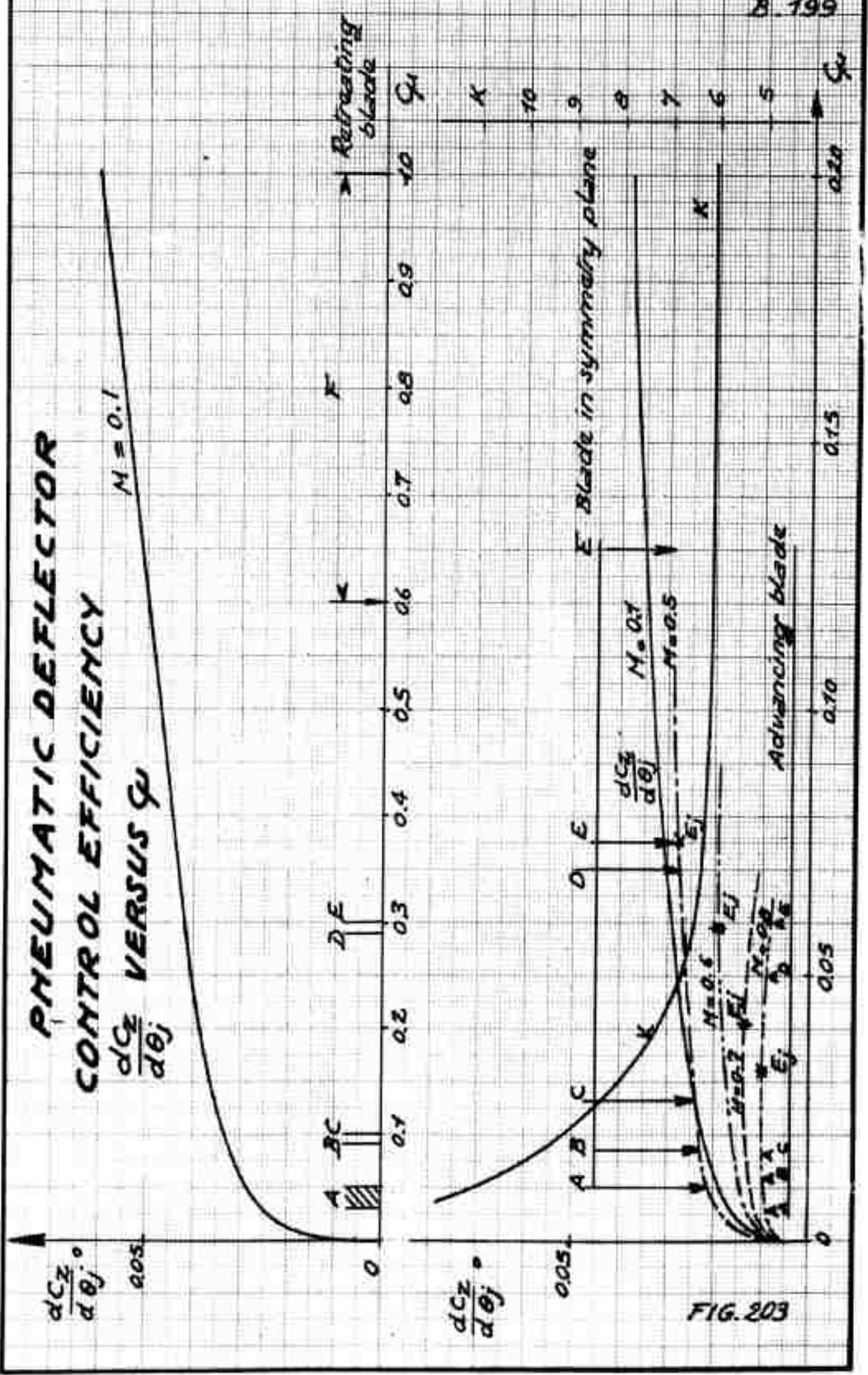


FIG. 203

FLOW CIRCULATION BY CENTRIFUGAL PUMPING

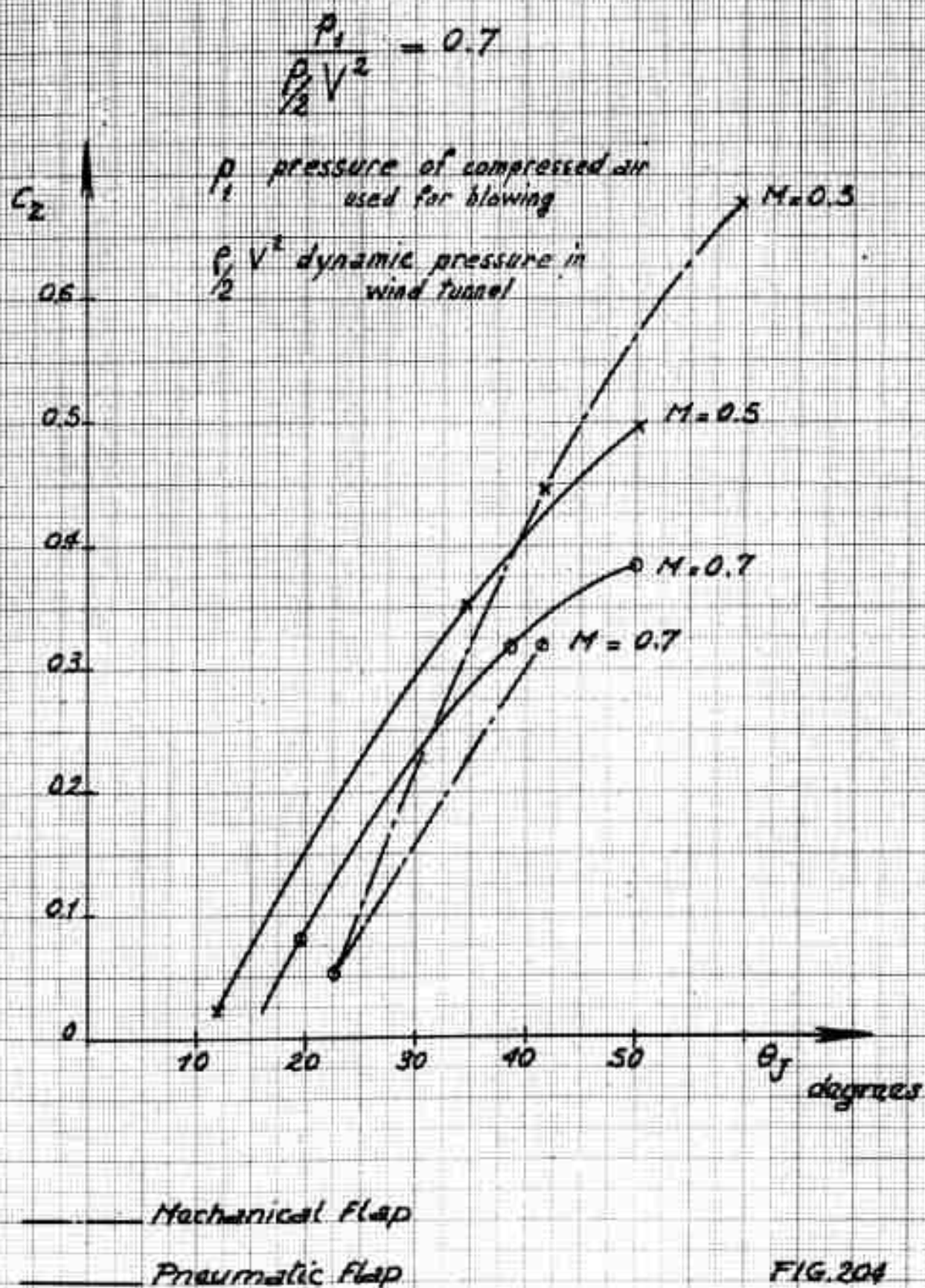


FIG.204

EFFECT OF BLOWING ALONE (WITHOUT FLAP EFFECT)

B.201

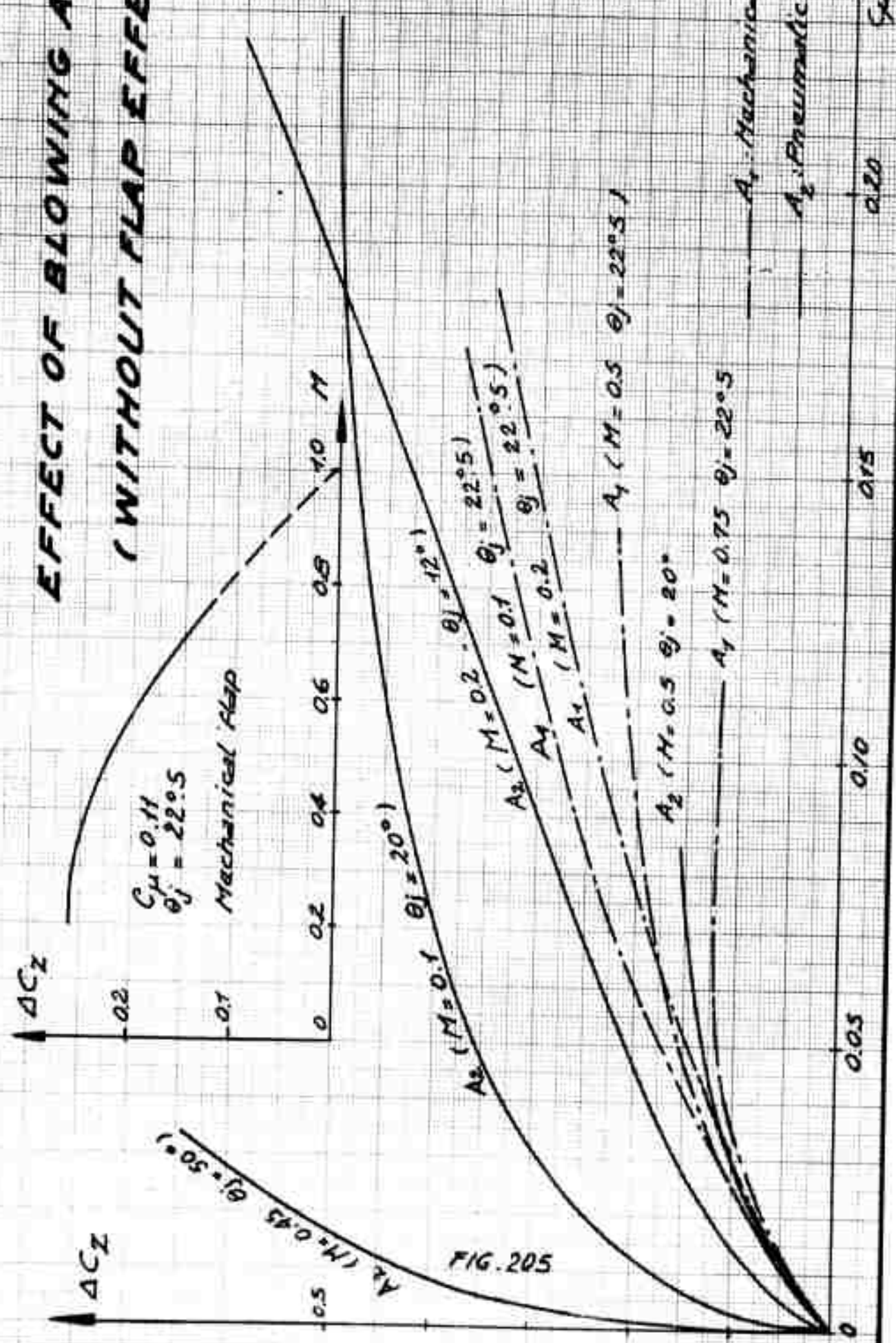
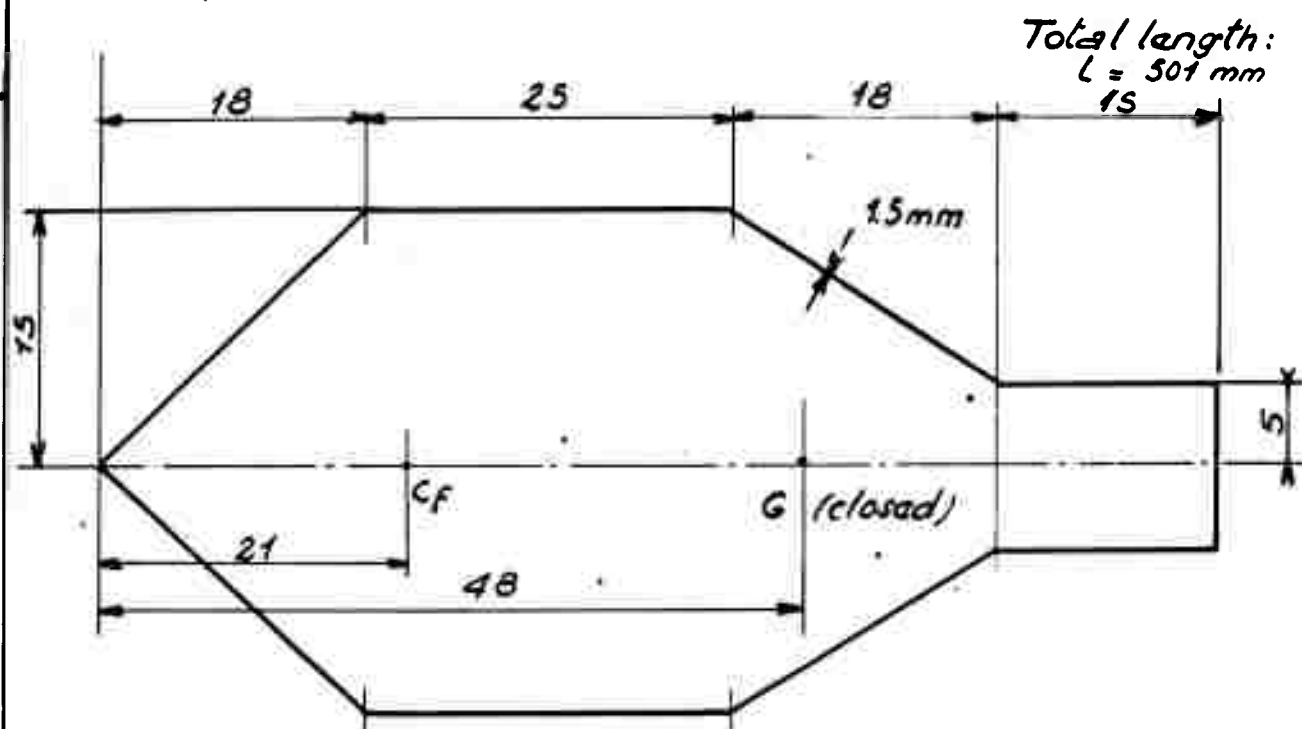


FIG. 205

BLADE MODEL MAIN DUCT
AVERAGE CROSS SECTION. (SCALE 2/1)

B202



BRACES DISPOSITION

$L = 501$

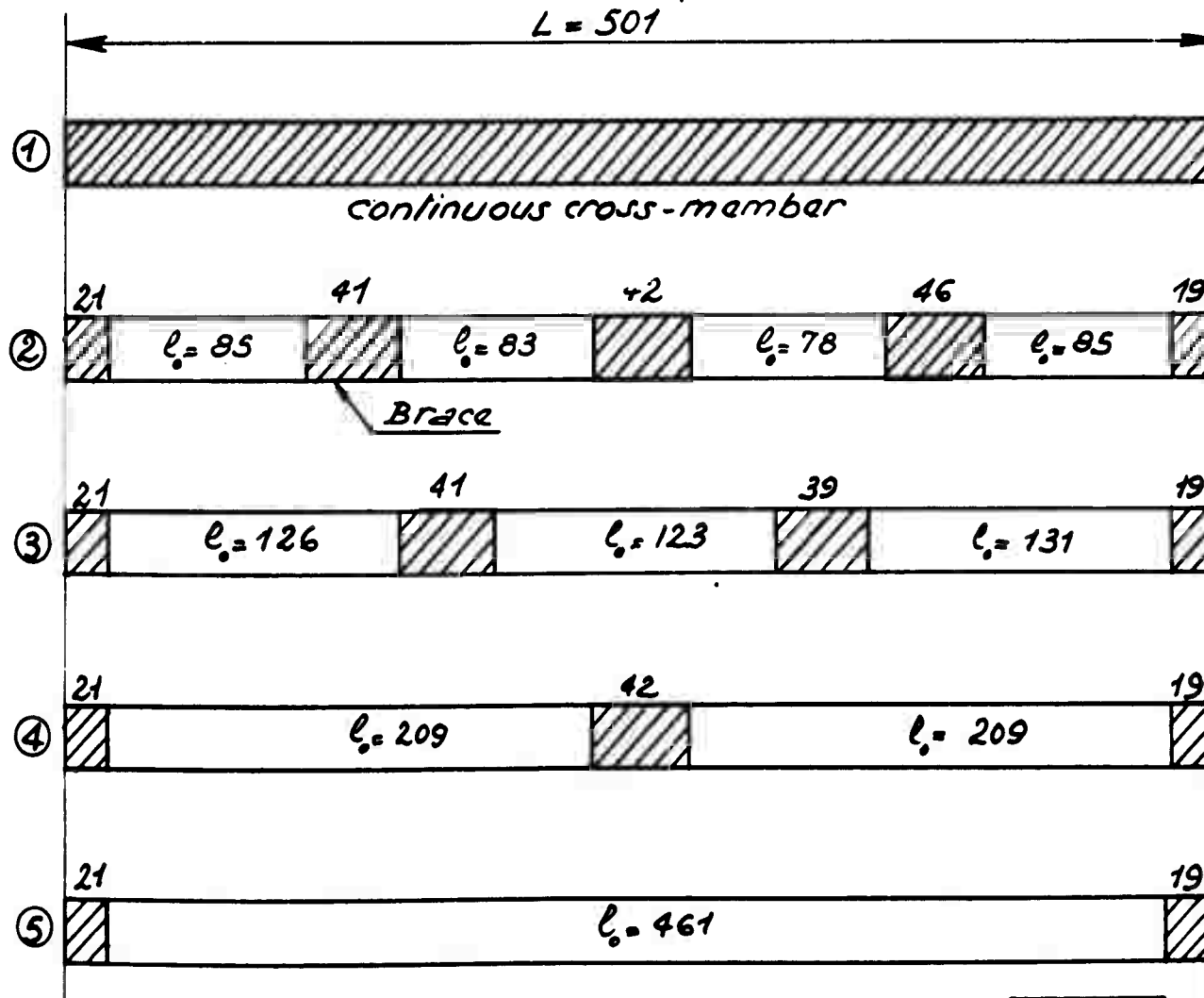


FIG. 206

Clamped end

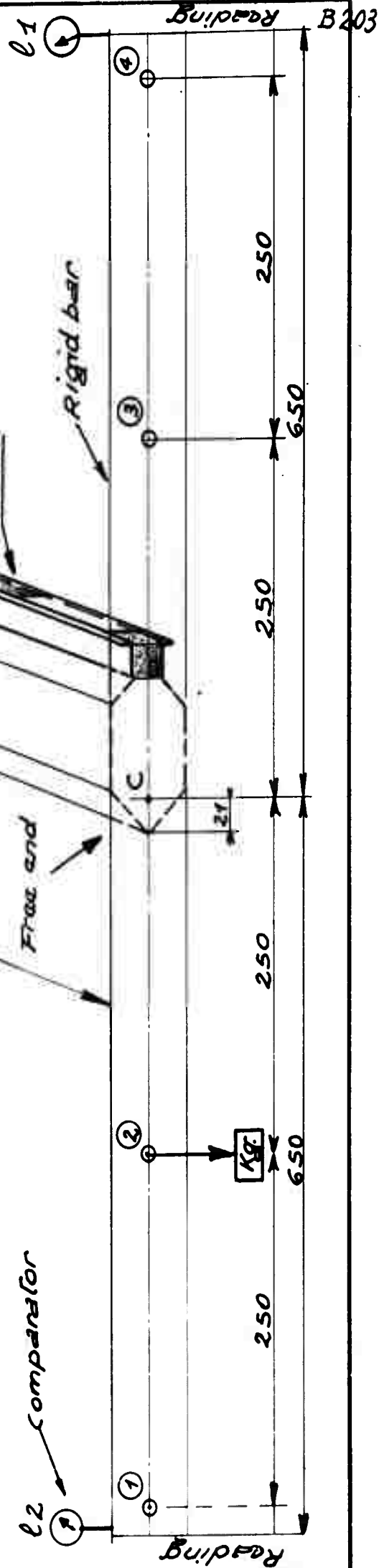
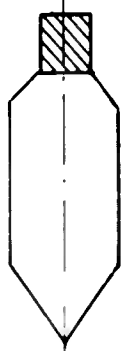



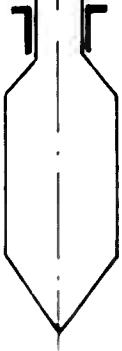







FIG. 207

Cross section	Brace pattern	GK 102 kg.m ²	EI 10 ² kg.m ²	Center of shear (front part)
⑥ 	1	7	1.93	+18 ±3 Theoretical evaluation: +21
④ 	2	6.84	4.16	+10 ±5
② 	2	5.5	2.82	+3.5 ±7.5
③ 	2	5.2	2.6	+7 ±11
	3	3.42	2.34	+2 ±13
	4	2.35	2.08	-18 ±3
	5	0.87	2.32	-27.5 ±8.5
① 	2	4.4	2.77	-1.5 ±2.5
	3	3.66	2.22	-7 ±6
	4	2.42	2.12	-18 ±5
	5	0.63	2.28	-30 ±9

B.204

FIG.208

VARIATION OF CENTER OF SHEAR LOCATION AS A FUNCTION OF β

$$\beta = \frac{EI_c}{EI_o} \times \alpha^3$$

I_c : Bending inertia of beam

I_o : Bending inertia of singly-braced

$\alpha = \frac{S}{L}$: Ratio of average line length between braces to total length

$\frac{CC_o}{CC_o}$: Ratio of distance between section C_o and open section C_o to distance between closed section C_o and open section C_o.

E : Bending elasticity modulus

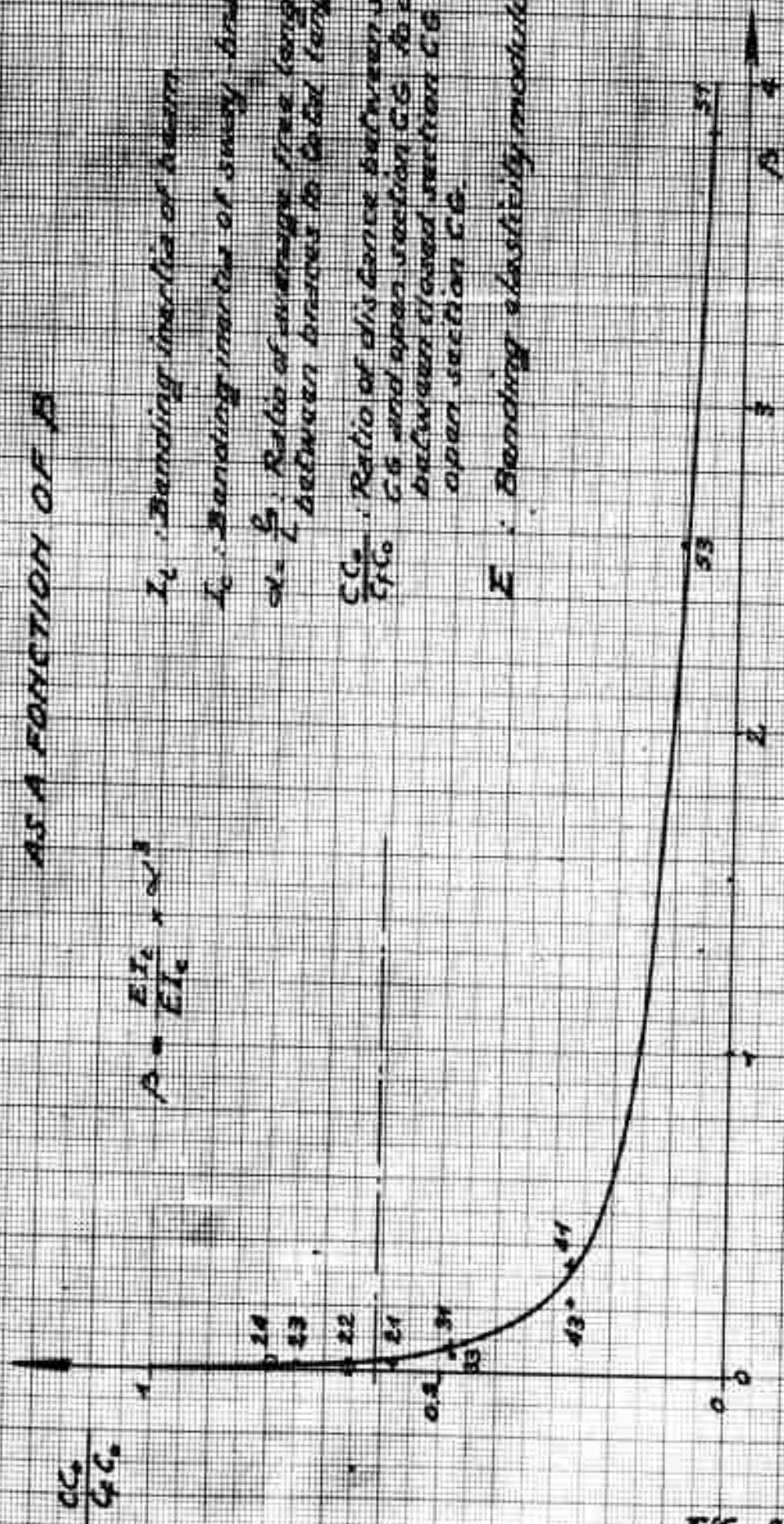


FIG. 210

TESTS IN S, CH WIND TUNNEL - MECHANICAL FLAP

Test result analyses
with A & B methods.

$$C_{\mu} = 0.22$$

$$V_0 = 22 \text{ m/s}$$

--- exp. values

— calculated values



C_x

$$\theta_j = 52^\circ.5$$

$$\theta_j = 37^\circ.5$$

$$\theta_j = 15^\circ$$

A Method

-0.5

C_m

B Method

$$\theta_j = 52^\circ.5$$

$$\theta_j = 37^\circ.3$$

$$\theta_j = 15^\circ$$

-0.5

C_m

B.207

FIG. 211

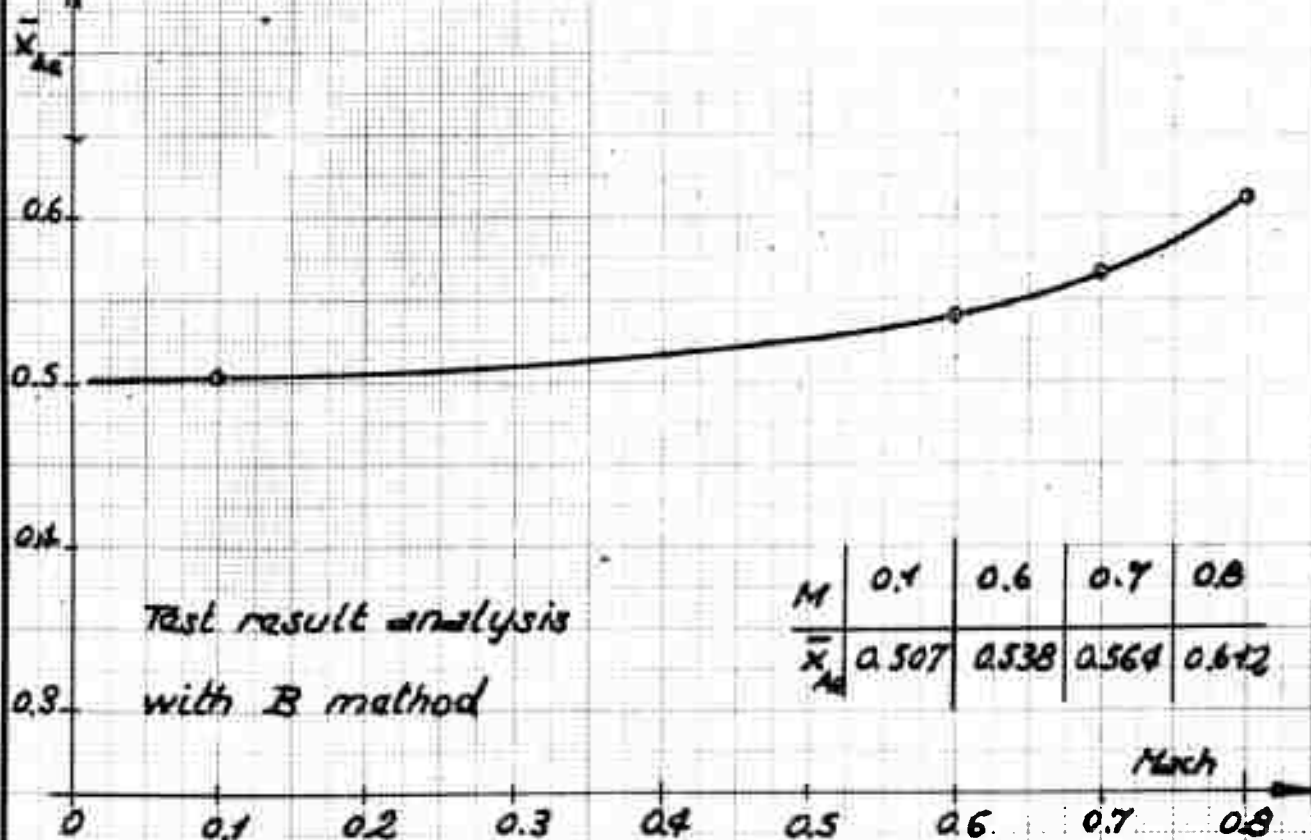
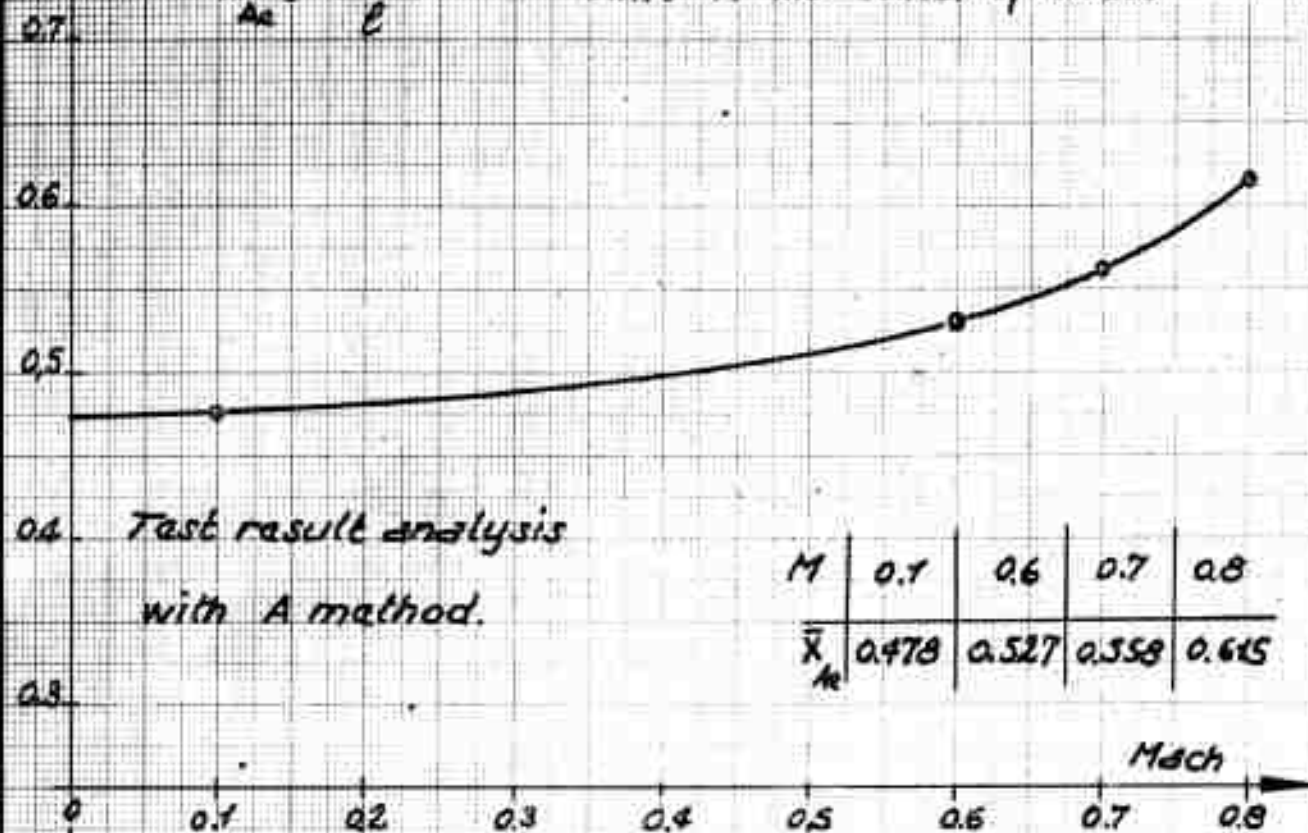
TESTS IN S₃ CH WIND TUNNEL

MECHANICAL FLAP



$$\bar{x}_{Ac} = \frac{x_{Ac}}{l}$$

Shift of the Center of thrust



MECHANICAL FLAP

$C_{\mu} = 0.20$

$C_{\mu} = 0.06$

$C_{\mu} = 0.02$

C_z
2.0
1.5
1.0
0.5

x = exp. values

— calculated values

$\theta_j = 59^\circ$

$M = 0.10$

Test result analysis
with A & B methods.

A Method

-0.6 -0.4 -0.2 0 0.2 0.4 0.6 C_m

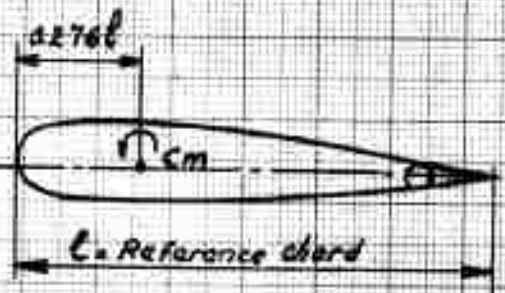
$C_{\mu} = 0.20$

$C_{\mu} = 0.06$

$C_{\mu} = 0.02$

$C_{\mu} = 0$

C_z
2.0
1.5
1.0
0.5



B Method

-0.6 -0.4 -0.2 0 0.2 0.4 0.6 C_m

FIG. 213

TESTS IN S_3 CH WIND TUNNEL

MECHANICAL FLAP

B.210

Test result analyses
with A & B methods.

C_z

$\theta_j = 30^\circ$

$M = 0.70$

Δ exp. values

— calculated values

$C_{\mu} = 0.015$

$C_{\mu} = 0.010$

A Method

-0.2

-0.1

0

0.1

C_m

C_z

0.4

0.3

0.2

0.1

$C_{\mu} = 0.015$

$C_{\mu} = 0.010$

B Method

-0.2

-0.1

0

0.1

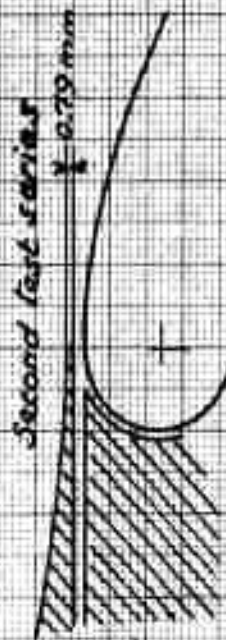
C_m

FIG. 214

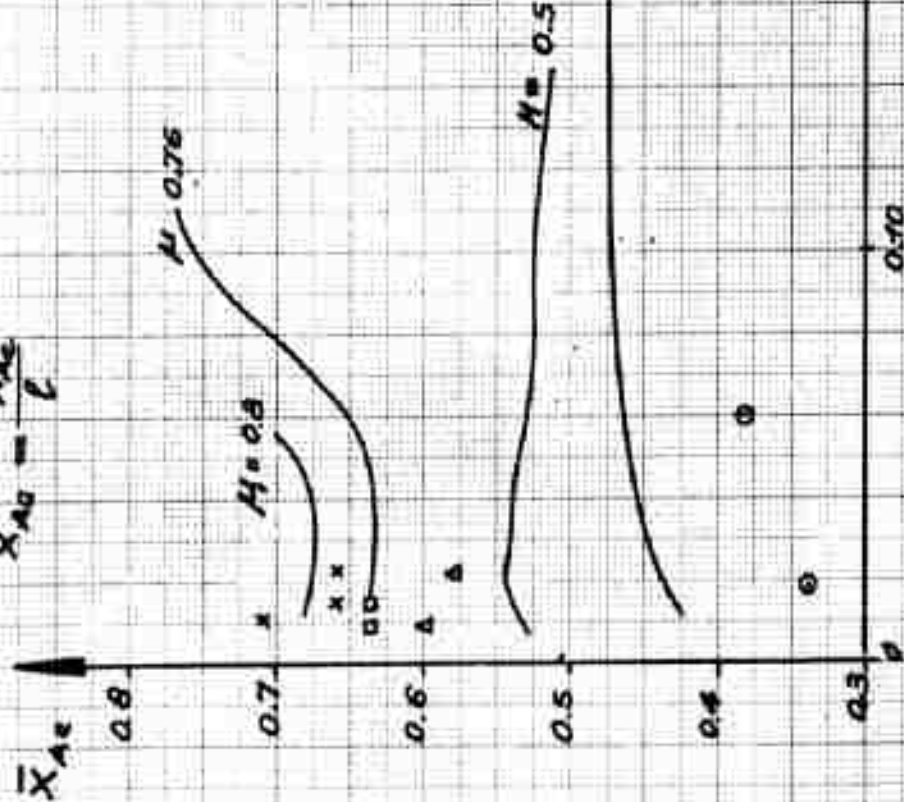
TESTS IN S_3 CH WIND TUNNEL MECHANICAL FLAP

$$\theta_j = 22.5$$

Test points
 ○ Mach 0.10
 △ Mach 0.60
 □ Mach 0.70
 × Mach 0.80



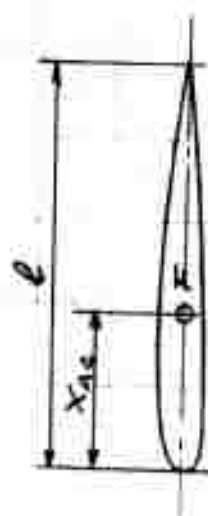
$$\bar{x}_{A0} = \frac{x_{Ae}}{l}$$



Test result analysis with A method

FIG. 215

TESTS IN S_3 CH WIND TUNNEL MECHANICAL FLAP

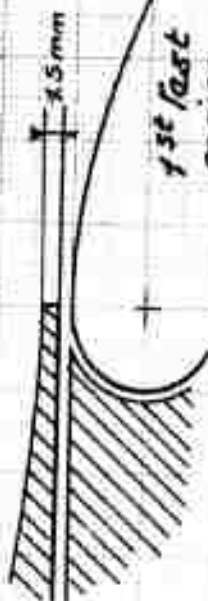


$$\bar{X}_{Ac} = \frac{X_{Ac}}{l}$$

$$\theta_j = 22^\circ 5'$$

Test points
 ○ Mach 0.40
 △ Mach 0.60
 □ Mach 0.70
 × Mach 0.80

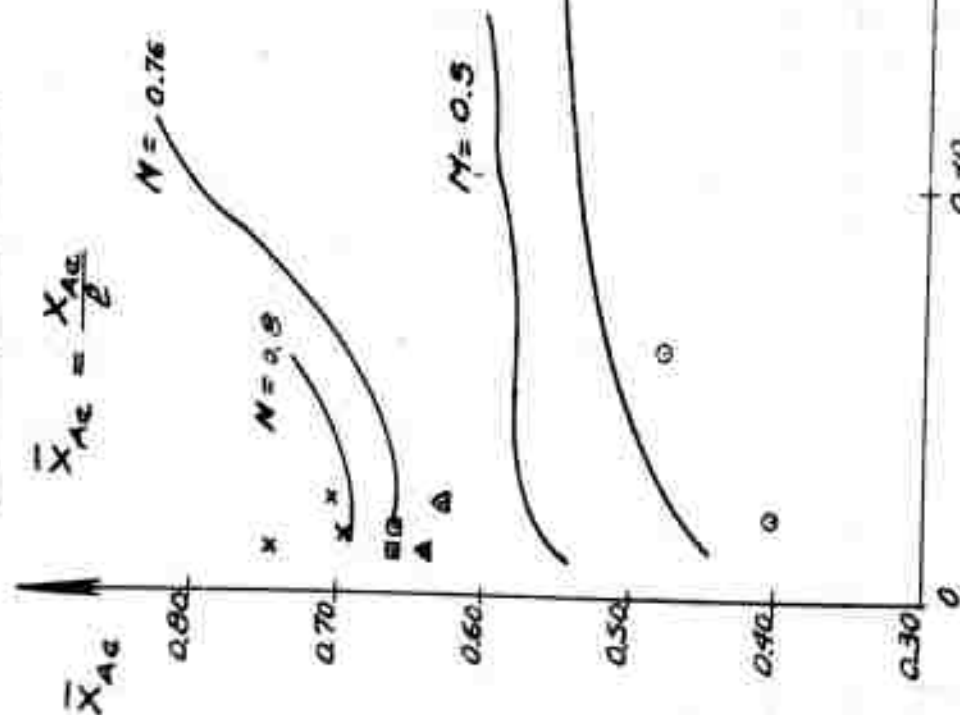
1st test series



Second test series



CURVES



Test result analysis with B method

B.212

FIG. 216

OH.2011 EXPERIMENTAL ROTOR

FLIGHT CONDITIONS AT $V = 300 \text{ km/h}$

A* blade model

$\theta_c = -12^\circ$ (at $\bar{r} = 0.7$)
 $\theta_t = -7^\circ$ } With reference to
 $\theta_p = 1.75^\circ$ } rotor comically axis
 $T_H = 3000 \text{ kg}$ tilted at 10.5° degrees
 $\frac{dC_3}{d\alpha} = 644.040 \text{ MACA Airfoil Section}$
 $K = 3.9$
 $\beta = 0.0453$
 $V = 83.7 \text{ m/sec}$
 $\mu = 0.438$
 $\ell_{\text{rot}} = 0.040 \text{ m}$

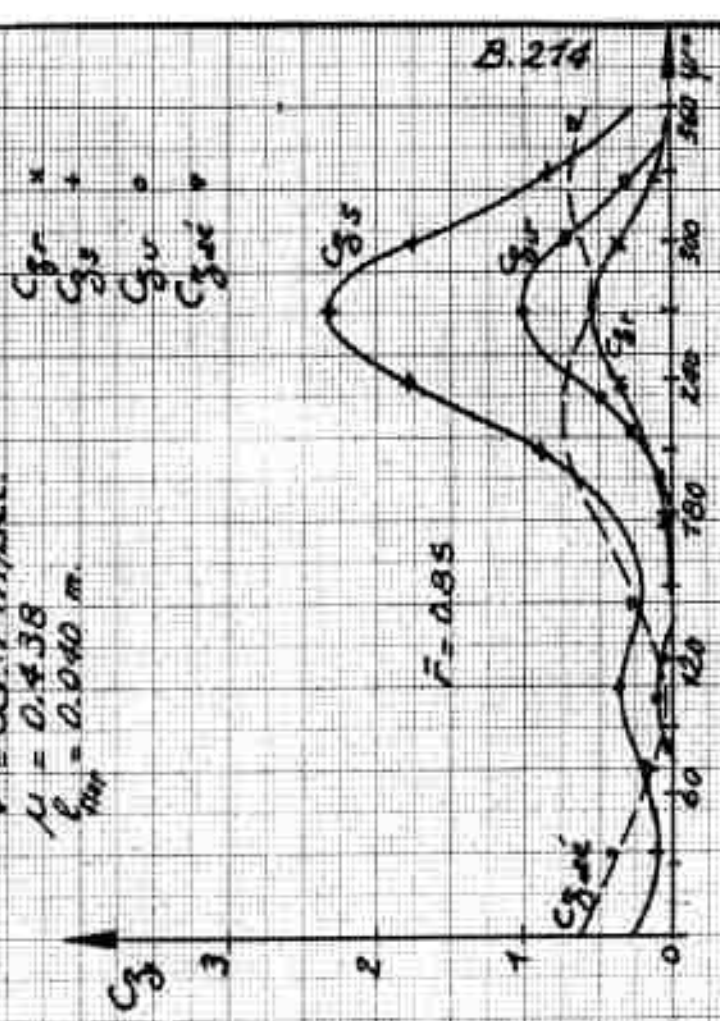
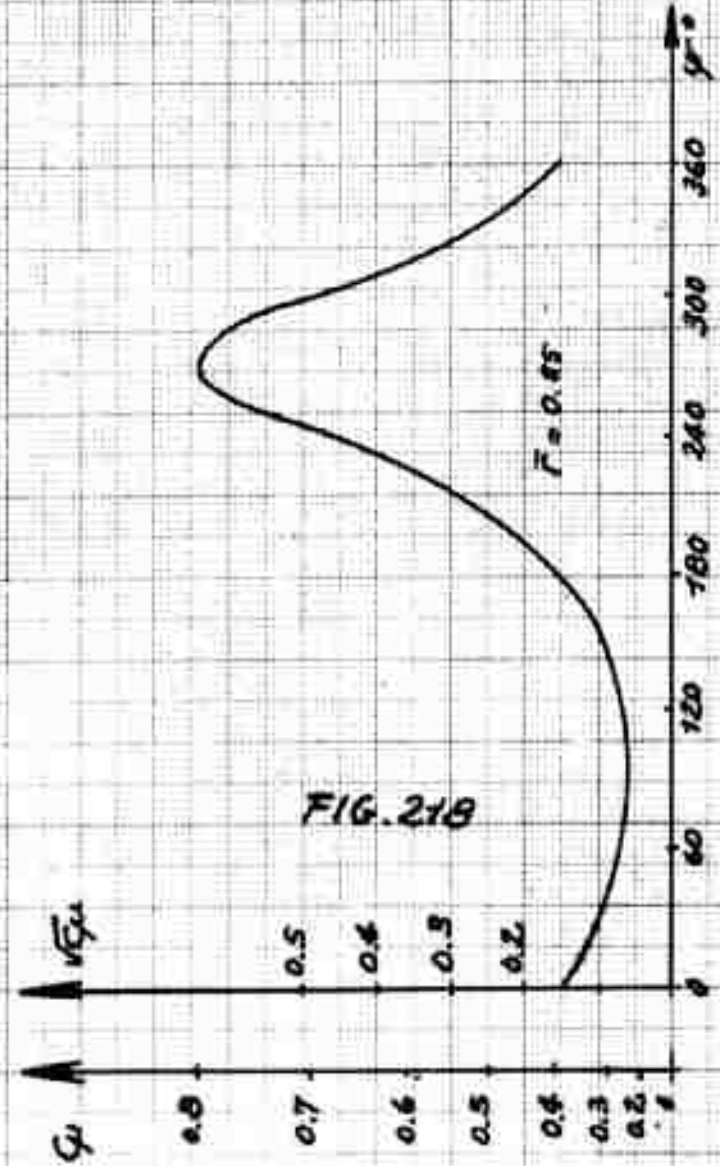
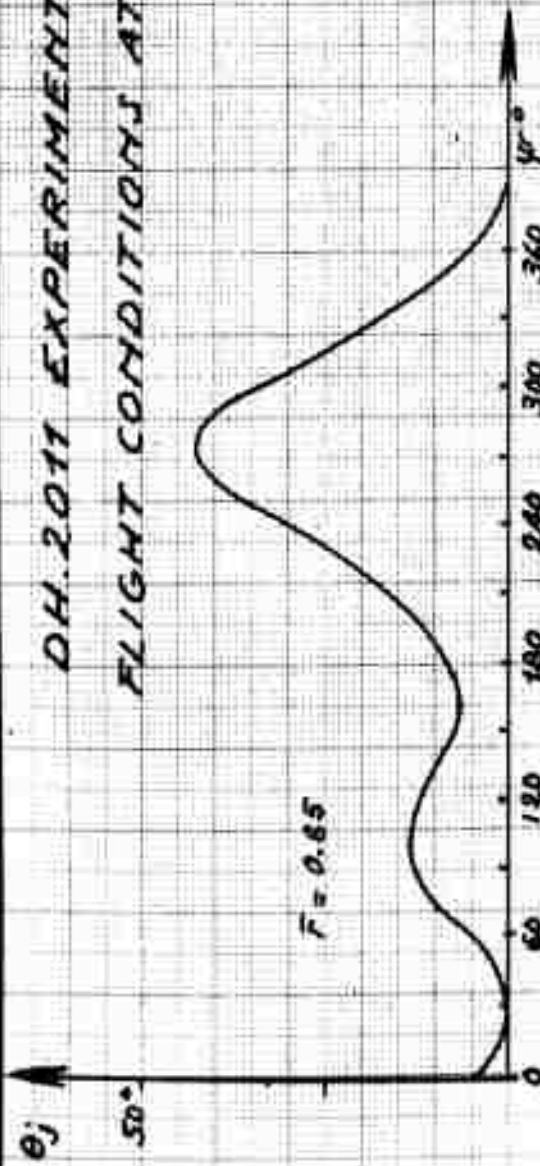


FIG. 218

B.214

DH.2011 EXPERIMENTAL ROTOR FLIGHT CONDITIONS AT $V = 300 \text{ km/h}$

A. blade model:

$\theta_c = 12^\circ$ (at $\bar{r} = 0.7$)
 $\theta_b = -7^\circ$ } With reference to
 $\theta_r = 1.75^\circ$ } rotor conicity axis
 $F_r = 3000 \text{ kg}$. tilted at 10.5° to axis
 $\frac{dC_D}{dC_L} \rightarrow 64 \text{ A 010 NACA Airfoil section}$

$K = 3.9$
 $\beta = 0.0453$
 $V = 83.7 \text{ m/sec.}$
 $\mu = 0.138$
 $C_{\text{hub}} = 0.040 \text{ m}$

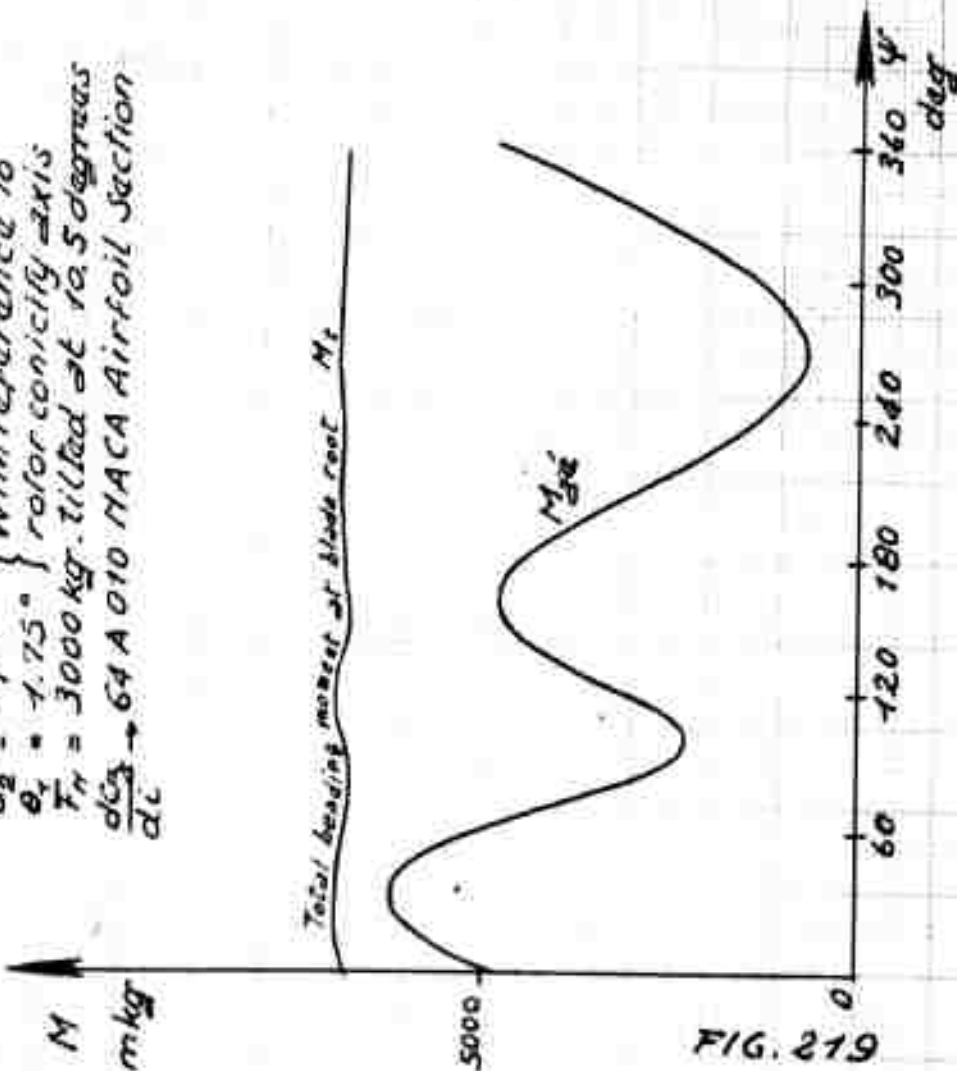
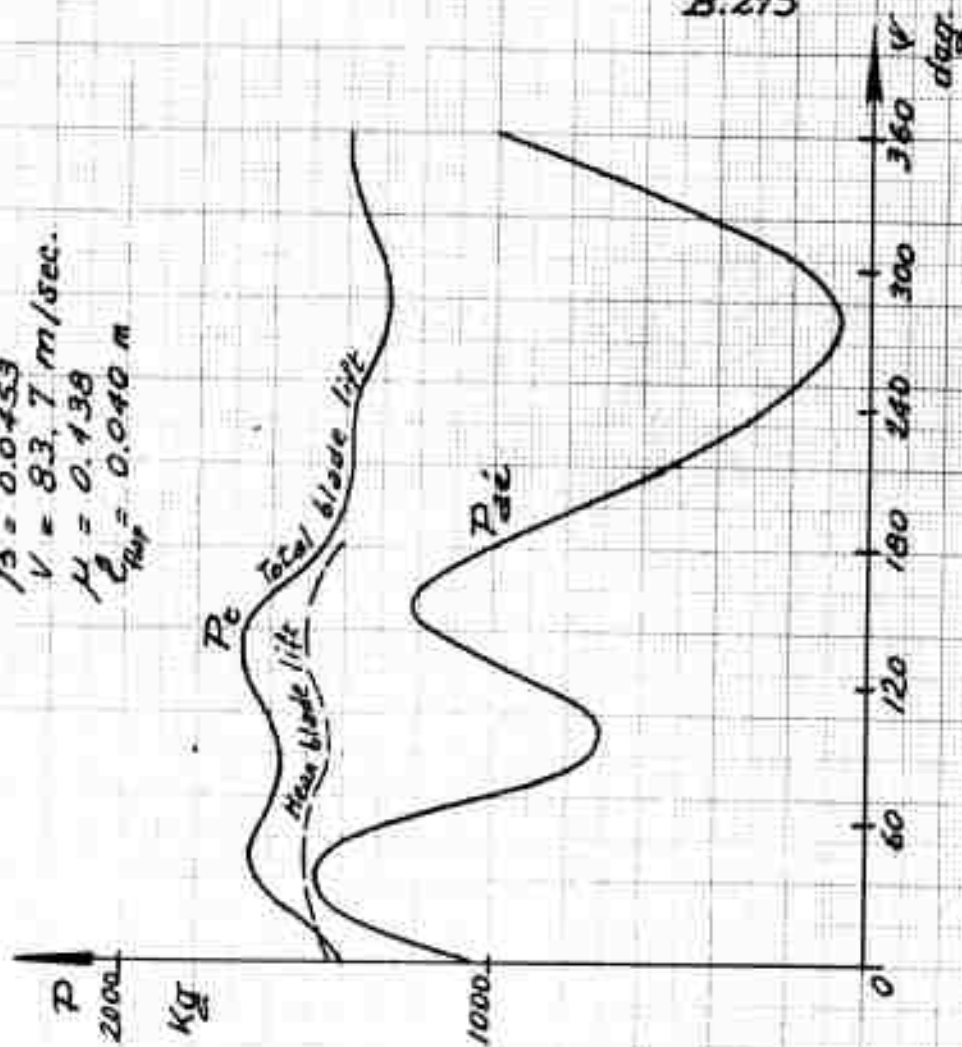


FIG. 219



B.215

DIAGRAM OF AIR LOADS ON BLADE OUTER PORTION

B 215

B.216

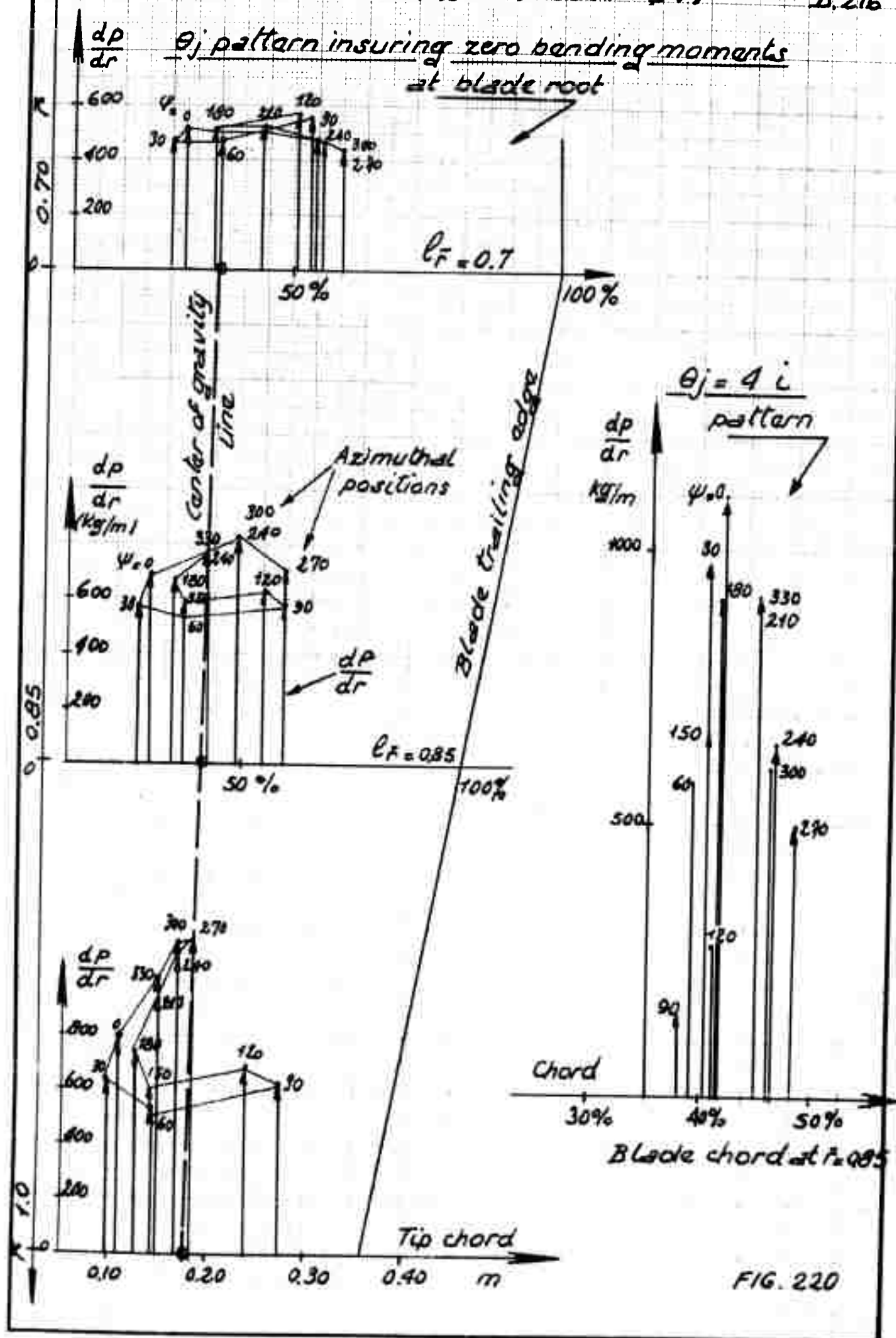
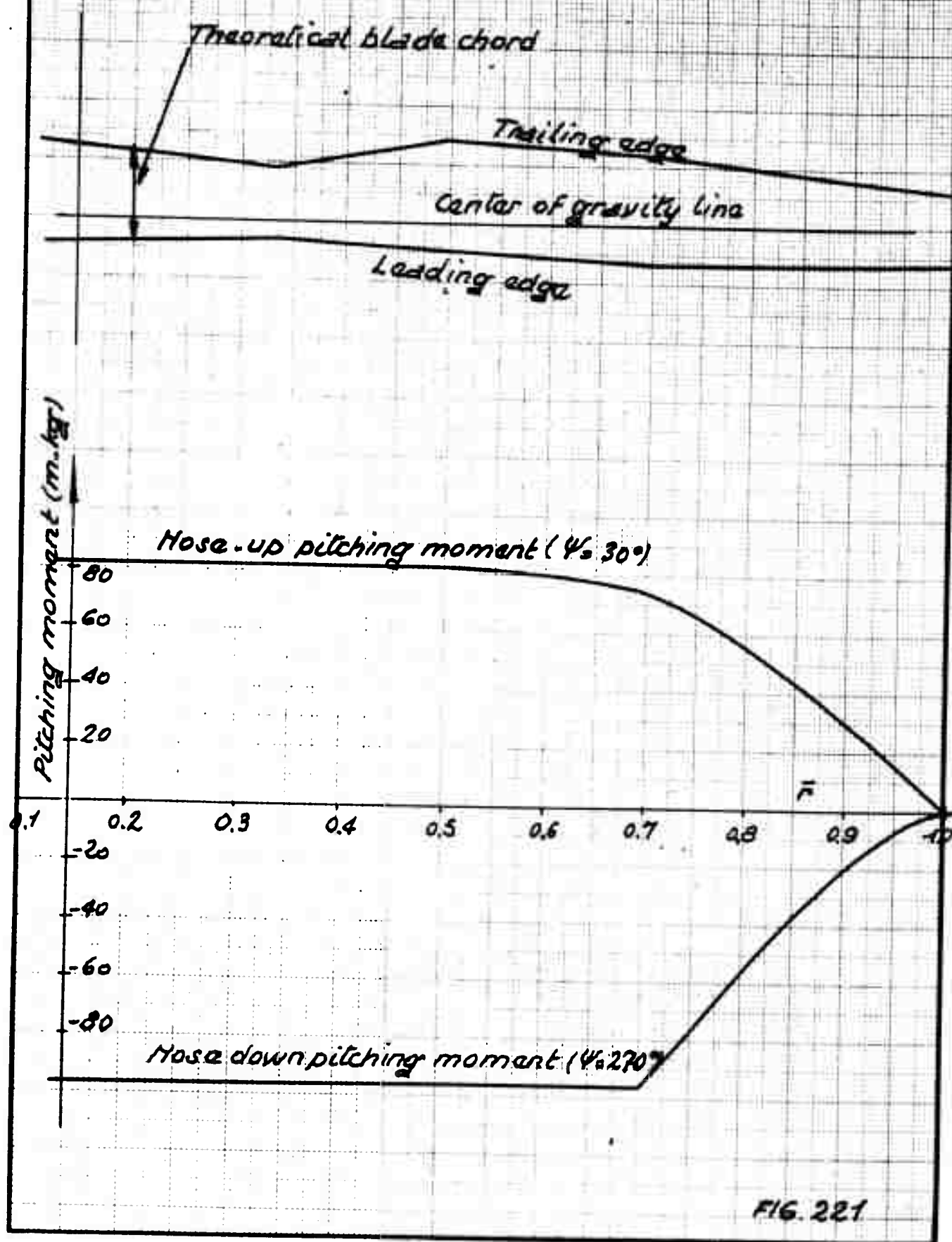


FIG. 220

B.217

MAX. PITCHING MOMENTS DUE TO BLOWING AND THEORETICAL BLADE CHORD VARIATION WITH θ ; PATTERN GIVING ZERO BENDING MOMENTS AT BLADE ROOT



UNCLASSIFIED

UNCLASSIFIED